DISSERTATION

CHARACTERIZING IONIC COMPONENTS OF AEROSOL IN RURAL ENVIRONMENTS: TEMPORAL VARIABILITY, SIZE DISTRIBUTIONS, AND THE FORM OF PARTICLE NITRATE

Submitted by
Taehyoung Lee
Department of Atmospheric Science

In partial fulfillment of the requirements
For the Degree of Doctor of Philosophy
Colorado State University
Fort Collins, Colorado
Spring 2007

COLORADO STATE UNIVERSITY

OCTOBER 31, 2006

WE HEREBY RECOMMEND THAT THE DISSERTATION PREPARED UNDER OUR SUPERVISION BY TAEHYOUNG LEE ENTITLED CHARACTERIZING IONIC COMPONENTS OF AEROSOL IN RURAL ENVIRONMENTS: TEMPORAL VARIABILITY, SIZE DISTRIBUTIONS, AND THE FORM OF PARTICLE NITRATE BE ACCEPTED AS FULFILLING IN PART REQUIREMENTS FOR THE DEGREE OF DOCTOR OF PHILOSOPHY.

Committee on Graduate Work

Adviser

Department Head

ABSTRACT OF DISSERTATION

CHARACTERIZING IONIC COMPONENTS OF AEROSOL IN RURAL ENVIRONMENTS: TEMPORAL VARIABILITY, SIZE DISTRIBUTIONS, AND THE FORM OF PARTICLE NITRATE

Properties of the ambient aerosol were determined at several rural U.S. locations during a series of field studies. Study sites included Bondville, Illinois (February, 2003), San Gorgonio Wilderness Area, California (April and July, 2003), Grand Canyon National Park, Arizona (May, 2003), Brigantine National Wildlife Refuge, New Jersey (November, 2003) and Great Smoky Mountains National Park, Tennessee (July/August, 2004). Daily $PM_{2.5}$ aerosol and trace gas samples were collected using a URG cyclone/annular denuder/filter pack sampling system. Additionally, semi-continuous measurements of $PM_{2.5}$ aerosol composition were made at 15 minute intervals using a Particle Into Liquid Sampler (PILS) coupled to two ion chromatographs. A Micro Orifice Uniform Deposition Impactor (MOUDI) was used to collect 48 hr size-resolved aerosol samples in 10 particle size categories from < 0.18 μm to >18 μm. Measured aerosol species included Cl^-, SO_4^{2-}, NO_3^-, Na^+, NH_4^+, K^+, Mg^{2+} and Ca^{2+}. Measured trace gases included HNO_3, NH_3 and SO_2.

The aerosol measured at most locations was neutral, although acidic aerosol was observed on most days at Great Smoky Mtns NP and occasionally seen at Bondville, IL. Aerosol concentrations and composition observed at many of the study sites varied strongly in time, especially at elevated locations where mountain-valley winds frequently advected polluted air masses from lower elevations to the study site during day and

returned cleaner air to the site in drainage flows at night. Ammonium and sulfate were found predominantly in submicron particles (mode peak typically 0.3 – 0.5 μm) at all sites. Nitrate was sometimes found in submicron particles and sometimes in coarse particles, with a mode peak at several micrometers. Formation of submicron ammonium nitrate was favored when temperatures were low and more than sufficient ammonia was present to neutralize fine particle sulfate, consistent with thermodynamic expectations. A predominance of ammonium nitrate was observed at Bondville, IL in winter and at San Gorgonio, CA in spring. Coarse mode nitrate was more important at Great Smoky Mtns NP in summer and at Grand Canyon in spring, similar to previous observations made at Big Bend and Yosemite National Parks in summer. During fall at Brigantine, NJ and during summer at San Gorgonio, CA, a mix of fine and coarse particle nitrate was observed. Formation of coarse particle nitrate occurs as a result of reaction of nitric acid or its precursors with sea salt or soil dust and is favored when conditions are hot and dry and/or ammonia availability is limited. The traditional 2.5 μm aerodynamic size cut used in routine monitoring networks to define a division between fine and coarse particle modes unfortunately results in frequent inclusion of the lower tail of a coarse particle nitrate mode into fine particle aerosol samples ($PM_{2.5}$), confusing understanding of mechanisms controlling formation of aerosol nitrate. A division at 1 μm would provide a more natural division between these two distinct populations of particles.

The relatively frequent occurrence of coarse particle nitrate observed in this study indicates a need to more closely examine common assumptions regarding the importance of ammonium nitrate at rural locations, to include pathways for coarse mode nitrate

formation in regional scale air quality models, and to consider impacts of coarse particle nitrate on visibility, nitrogen deposition, and other issues.

Taehyoung Lee

Department of Atmospheric Science

Colorado State University

Fort Collins, CO 80523

Spring 2007

ACKNOWLEDGMENTS

I wish I could find the perfect words to express my full respect and thanks to my advisor, Dr. Jeffrey L. Collett, Jr. He provided me with all I needed at the right times and places. I could have not fulfilled my work without his guidance and encouragement. His guidance, encouragement and the excellent example of a scholar will live on in my heart throughout my professional career in the future. Also I would like to give my special thanks to Dr. Sonia M. Kreidenweis for reviewing my thesis and her excellent comments and suggestions. My thanks also go to my committee members, Dr. A. Scott Denning in the Atmospheric Science department and Dr. Charles S. Henry in the Chemistry department, for their time and energy spent providing helpful comments for my thesis.

Dr. Xiao-Ying Yu, Dr. Jackie Carrillo, Benjamin Ayres, and Connie Hale deserve my special thanks for assistance with field campaign planning and preparations and accompanying me to the field work. My great thanks are also given to various researchers and colleagues for their help and advice critical to the results of my work, including Dr. William C. Malm, Dr. Kip Carrico, Dr. Pierre Herckes, Dr. Guenter Engling, Gavin McMeeking, and the rest of the atmospheric chemistry group.

I am grateful to numerous individuals working at each of the field sites for providing site access and/or logistical assistance, including M. Snider in Bondville, H. Abreu at Grand Canyon NP, M. Arbough and D. Jones at San Gorgonio, S. Perchetti at Brigantine, and J. Renfro and B. Stroik at Great Smoky Mountains NP. Chuck McDade and the IMPROVE team at UC Davis are gratefully acknowledged for outstanding support in field preparation and study logistics.

I want to give my unmeasurable thanks to my wife, Jiyean Lee, for her support and patience. Without her love and sincere care, I could not finish this work smoothly. Numerous members of our families also deserve my thanks.

This work was funded by the National Park Service, grant # CA238099001 TO 03-56.

TABLE OF CONTENTS

LIST OF FIGURES

LIST OF TABLES

LIST OF ACRONYMS AND SYMBOLS

AGL	above ground level
CASTNET	clean air status and trends network
CCN	cloud condensation nuclei
CD20	conductivity detector 20
CE	capillary electrophoresis
CV	coefficient of variation
DMS	dimethylsulfide
FTIR	fourier transform infrared spectroscopy
GR	gas ratio
GRSM	Great Smoky Mountains
HPAEC	high performance anion exchange chromatography
HYSPLIT	hybrid single-particle lagrangian integrated trajectory
IMPROVE	interagency monitoring of protected visual environments
MDL	minimum detection limit
MOUDI	micro-orifice uniform deposit impactor
MSA	methanesulfonic acid
NIST	national institute of standards and technology
PAD	pulsed amperometric detection
PCF	principal component factoring
PILS	particle into liquid system
$PM_{2.5}$	particulate matter with an aerodynamic diameter less than 2.5 μm
QA	quality assurance

QC	quality control
READY	real-time environmental applications and display system
RH	relative humidity
RSD	relative standard deviation
SOP	standard operating procedure
TOC	total organic carbon
UV	ultraviolet
VOC	volatile organic compound

1. Introduction

Atmospheric aerosols are comprised of suspensions of liquid and/or solid particles with particle sizes typically ranging from tens of nanometers to tens of micrometers (Hinds, 1999; Wayne, 2000). Aerosols play important roles in many environmental processes including various biogeochemical cycles (Dentener et al., 1996), formation of photochemical smog and associated health effects (Nel, 2005), indirect and direct forcing of Earth's climate (Adams et al., 2001; Anderson et al., 2003; Charlson et al., 1992; Haywood and Boucher, 2000; Jacobson, 2001; Martin et al., 2004), and visibility degradation (Hand et al., 2005; Malm et al., 2000; Seinfeld and Pandis, 1998). Aerosol particles are produced both by natural processes and anthropogenic activities. Particles emitted directly to the atmosphere are referred to as primary aerosol particles. Additional, secondary particles can be formed in the atmosphere as a result of gas-to-particle conversion of volatile precursors, typically involving chemical reactions that produce lower volatility products.

The process by which a particle forms is a primary determinant of its size. Particles larger than approximately 1 μm tend to be formed mainly by mechanical processes (e.g., sea spray, erosion), while submicron particles are most often emitted from combustion processes or produced by gas-to-particle conversion processes in the atmosphere (Hinds, 1999; Seinfeld and Pandis, 1998). Many U.S. and international air quality monitoring networks focus on a division of "coarse" and "fine" particle size at 2.5 μm aerodynamic diameter, despite the existence of a more *natural* break in particle type at approximately 1 μm (Allen et al., 2001; Cabada et al., 2004; Carrico et al., 2004; Lee et al., 2004). The artificial division at 2.5 μm can lead to collection of mixtures of

particle types during "fine" particle sampling. This can be especially problematic for aerosol nitrate, which comprises a substantial fraction of total aerosol mass in many environments. For example, we previously demonstrated that $PM_{2.5}$ aerosol samples collected in Big Bend National Park, Texas, were comprised mainly of acidic, submicron ammoniated sulfate particles but also contained supermicron calcium and sodium nitrate particles present in the lower tail of a coarse particle nitrate mode with a mode diameter of several micrometers aerodynamic diameter (Lee et al., 2004).

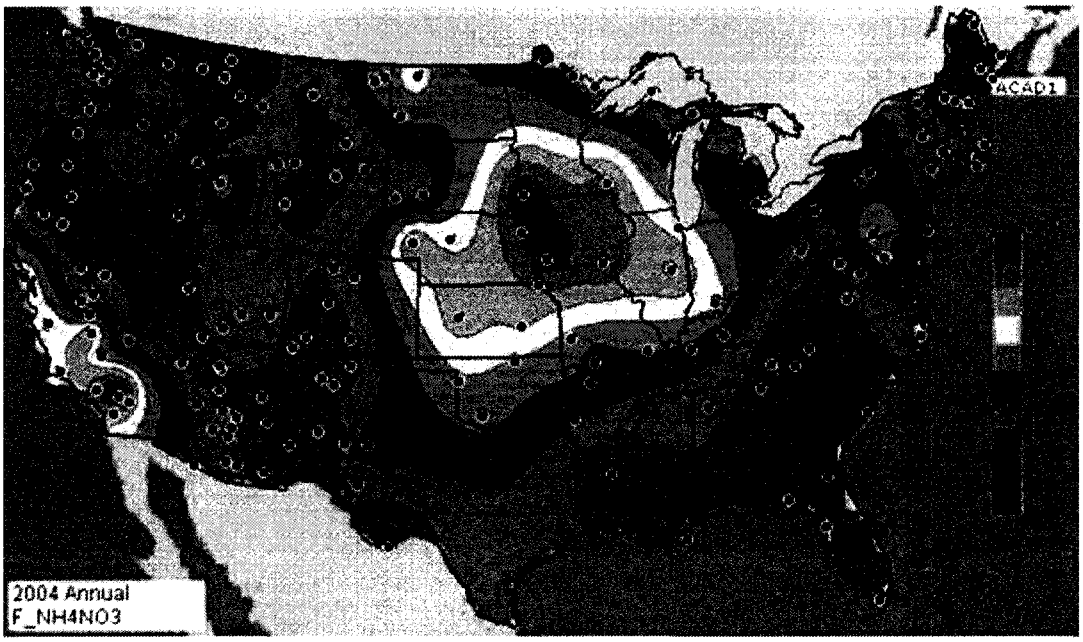

Figure 1.1 Ammonium nitrate percent of fine mass measured in 2004 by the IMPROVE network. Spatial patterns in other years look similar.

$PM_{2.5}$ sampling of an external aerosol mixture like this can be misleading. Fine particle nitrate, for example, is typically assumed to be present as ammonium nitrate. The nitrate concentration map in Figure 1.1 illustrates this approach in presenting fine

particle nitrate data obtained by the Interagency Monitoring of PROtected Visual Environments (IMPROVE) aerosol monitoring program. Note that the IMPROVE data for $PM_{2.5}$ nitrate is presented as ammonium nitrate, despite the fact that IMPROVE does not determine the chemical form of the aerosol nitrate nor measure concentrations of particulate ammonium.

Both the chemical form and the size of aerosol nitrate particles influence their behavior in the atmosphere and their environmental effects. The size of an aerosol particle is a key factor influencing its residence time in the atmosphere and composition can influence a particle's ability to scatter radiation and interact with atmospheric water vapor and clouds (Finlayson-Pitts and Pitts, 2000; Seinfeld and Pandis, 1998).

Particles are removed from the atmosphere by one of three mechanisms: dry deposition, wet deposition, or occult deposition (deposition of cloud/fog drops to surfaces). Dry deposition involves the movement of a particle to a collection surface. Large scale particle motion in the atmosphere typically occurs in turbulent eddies, but once a particle is very near a surface it must penetrate a quiescent laminar sublayer. Large particles tend to have high deposition velocities because of their appreciable terminal settling velocity. Very small particles ($D_p < 0.1\mu m$) also have high deposition velocities because of their high diffusion rates through this laminar sublayer. Particles of intermediate size (roughly 0.1 to 2 μm diameter) have much lower deposition velocities, because they are too large to diffuse quickly and too small to have a large settling velocity. Because of their low removal rate, particles in this size range tend to accumulate in the atmosphere, hence the convention of referring to particles in this size range as the "accumulation mode." The atmospheric lifetime of accumulation mode

particles is governed mainly by wet deposition processes. Particles in this size range that are hygroscopic in character are more likely to act as cloud condensation nuclei (CCN) and, consequently, more likely to be incorporated into precipitation through in-cloud scavenging processes. While accumulation mode particle scavenging also occurs below cloud, this mechanism tends to be less efficient because of the low collection efficiency of raindrops for particles in this size range (Seinfeld and Pandis, 1998).

1.1 Primary aerosols and gas species as precursors to aerosols

Particles in the atmosphere can be directly emitted from natural sources (e.g. soil dust, sea salt and volcanoes) and anthropogenic activities (e.g. biomass burning and vehicle/industrial emission), or they can be formed in the atmosphere through gas to particle conversion. Table 1.1 summarizes the main source of aerosols.

1.1.1 Sea salt

Sea salt particles are one of the main natural aerosol types. Sea salt particles are formed in association with the generation of sea spray by mechanical wave action and the bursting of air bubbles at the ocean's surface (Allen et al., 1996; de Leeuw et al., 2001; Odowd et al., 1997). High winds tear drops from the wave crests and emit larger sea water drops into the atmosphere directly. Most sea salt particles are found in the coarse mode with a diameter greater than 1μm, although the sea salt particle size distribution can extend from submicron to several hundred microns diameter (Allen et al., 1996; de Leeuw et al., 2001; O'Dowd et al., 1997; Roth and Okada, 1998). Sea salt particle composition is dominated by Na^+ and Cl^- with smaller concentrations of SO_4^{2-}, Ca^{2+},

Table 1.1 Estimated global emission rates of particles

	Anthropogenic source (Tg/yr)	Natural source (Tg/yr)
Primary	Industrial Dust (100)	Mineral Dust (< 1μm (48) and 1-10 μm (1442)
	Black Carbon (Biomass burning (5.6)[a] and Fossil fuel (6.6)[a]	Volcanic Dust (30)
	Organic carbon (Biomass burning (54.3)[a] and Fossil fuel (28.8)[a]	Biological debris (50)
		Sea salt (10,100)
Secondary	Sulfate from SO_2 (48.6)[b]	Sulfate from DMS (12.4)[b] Sulfate from volcanic SO_2 (20)[b]
	Nitrate from NO_x (21.3)[c]	Nitrate from NO_x (15)[c]
	Ammonium (33.6)	Organic aerosol (11.2)[a] from biogenic VOC

Source : (Aneja et al., 2000; Raes et al., 2000; Seinfeld and Pandis, 1998; Seinfeld and Pandis, 2006)
[a]:Tg C
[b]:Tg S
[c]:[a]:Tg C
[b]:Tg S
[c]:Tg NO_3^-

Mg^{2+}, and K^+. A small amount of organic material may also be incorporated into sea salt particles. Table 1.2 presents key ion ratios for sea water as reported by several investigators (Cheng et al., 2000; Choi et al., 2001; Wilson, 1975). Sea salt particles provide a non-acidic reactive surface for various chemical reactions with many gaseous species such as HNO_3, H_2SO_4, NO_3 and others (Finlayson-Pitts and Pitts, 2000). Reaction of sea salt with acids provides a source of HCl to the atmosphere through acid displacement. Sea salt particles enriched in sulfur and nitrogen (as sulfate and nitrate, respectively) are considered to be atmospherically aged by reaction with sulfuric or nitric acids or their precursors.

Table 1.2 Ionic concentration ratios in sea water

Ion Pair (μeq)/(μeq)	Ratio (Cheng et al, 2000)	Ratio (Wilson, 1975)
Cl^- / Na^+	1.164	1.16
K^+ / Na^+	0.0218	0.0218
Mg^{2+} / Na^+	0.223	0.227
Ca^{2+} / Na^+	0.0415	0.0439
SO_4^{2-} / Na^+	0.121	0.121

1.1.2 Mineral dust

Mineral dust particles are formed by natural erosion processes and by other anthropogenic sources, including traffic on unpaved roads and fugitive emissions from industrial operations. Mineral dust particles have received considerable attention as a sink for nitric acid, sulfur dioxide, and other species via heterogeneous chemical reactions on their surfaces (Dentener et al., 1996; Goodman et al., 2000; Hanisch and Crowley, 2001c; Tabazadeh et al., 1998). It has been estimated that global emissions are in the range of 1000 to 3000 Tg/yr (Dentener et al., 1996; Grassian, 2002). The shape, chemical composition, and size of dust particles vary widely, depending in part upon regional geology (Choi et al., 2001; Chun et al., 2001). Typical species ratios in crustal material are shown in Table 1.3. Table 1.4 shows the average elemental compositions from different dust source regions by Krueger et al (2004).

Table 1.3 Ratios in the earth's crust

Units	K	Ca	Mg	Na
Weight percent	2.59	3.63	2.09	2.83
	K/Na	**Ca/Na**	**Mg/Na**	**Na/Na**
μeq/μeq	0.54	1.47	1.42	1

Source : (Finlayson-Pitts and Pitts, 2000)

Table 1.4 Average chemical compositions of four different dust source regions

	% Si (Si:Si)	% Al (Al:Si)	% Mg (Mg:Si)	% Ca (Ca:Si)	% Na (Na:Si)	% Fe (Fe:Si)	% K (K:Si)
Sarahan Dust	69 (1)	15 (0.22)	3 (0.04)	2 (0.03)	2 (0.02)	5 (0.07)	2 (0.02)
Coastal Saudi Dust	31 (1)	7 (0.23)	13 (0.42)	39 (1.25)	4 (0.14)	3 (0.10)	1 (0.04)
Inland Saudi Dust	53 (1)	22 (0.41)	7 (0.14)	3 (0.06)	2 (0.03)	9 (0.17)	3 (0.05)
China Dust	45 (1)	17 (0.37)	6 (0.12)	17 (0.37)	2 (0.05)	7 (0.15)	3 (0.07)

Source: (Krueger et al., 2004)

1.1.3 SO_2

Sulfur dioxide (SO_2) is the predominant, anthropogenically emitted sulfur-containing air pollutant and is an important precursor to fine particle sulfate. The global total amount of sulfur emitted into the atmosphere from various natural and anthropogenic sources is estimated at 98-120 Tg(S)/yr, with anthropogenic emissions accounting for about 67 – 75 % (Berresheim et al., 1995; Seinfeld and Pandis, 2006). The total mass of volcanic sulfur emissions is estimated at 9.3 – 11.8 Tg(S)/yr. Table 1.5 summarizes estimated global sulfur-containing compounds emission from different sources.

As shown in Figure 1.2 SO_2 can be formed in the atmosphere through the oxidation of CS_2, dimethylsulfide (DMS) and H_2S by $OH\cdot$ and $NO_3\cdot$. SO_2 is oxidized to form H_2SO_4 mainly in the liquid phase (generally, inside cloud droplets) by H_2O_2 and/or O_3 (Finlayson-Pitts and Pitts, 2000; Seinfeld and Pandis, 2006).

Table 1.5 Global sulfur-containing compound emissions from different sources

Source	H_2S	DMS	CS_2	OCS	SO_2	SO_4	Total
Combustion					70	2.2	71 – 77
Biomass burning	< 0.01		< 0.01	0.075	2.8	0.1	2.2 – 3.0
Oceans	< 0.3	15 - 25	0.08	0.08		40 - 320	15 – 25[a]
Wetlands	0.006 – 1.1	0.003 – 0.68	0.0003-0.06				0.01 – 2
Plants and Soil	0.17 – 0.53	0.05 – 0.16	0.02 – 0.05				0.25 – 0.78[b]
Volcanoes	0.5 – 1.5			0.01	7 - 8	2 - 4	9.3 – 11.8
Anthropogenic							**73 - 80**
Natural (without sea salt and soil dust)							**25 - 40**
Total							**98 - 120**

unit : Tg(S)/yr
Source : (Berresheim et al., 2002; Berresheim et al., 1995)
[a]: Excluding sea-salt contributions
[b]: Excluding soil dust contributions

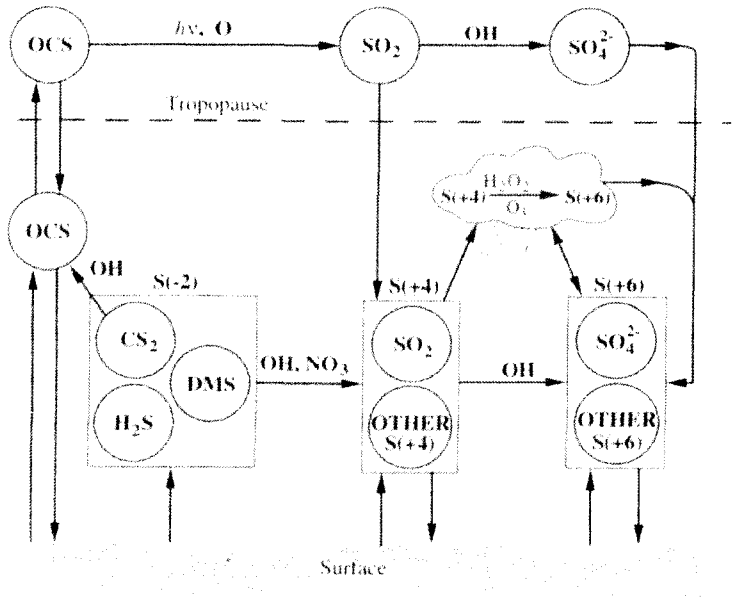

Figure 1.2 Major pathways of sulfur-containing compounds in the atmosphere Source : (Seinfeld and Pandis, 2006).

1.1.4 Nitrogen-containing compounds

Important nitrogen-containing compounds in the troposphere include N_2, nitric oxide (NO), nitrogen dioxide (NO_2), nitric acid (HNO_3) and ammonia (NH_3).

Ammonia is the most prevalent gas phase base in the atmosphere. Emissions of NH_3 originate mainly from animal waste, fertilizer, biomass burning, soil and vegetation. Some ammonia is also emitted by industrial processes and by automotive catalysts. Total global ammonia emissions are estimated at 75 Tg(N)/yr (Aneja et al., 2000; Aneja et al., 2001), with 43% of total global emissions produced by domestic animal waste (Table 1.6).

Table 1.6 Global atmospheric budget for NO_x and NH_3

Source or Sink	NO_x (Tg(N)/yr)	NH_3 (Tg(N)/yr)
Fossil fuel combustion	21	2
Biomass burning	8.0	5
Sea Surface	< 1.0	13
Domestic animal waste		32
Human excrement		4
Lightning	8	
NH_3 oxidation by OH	1	
Stratospheric input	0.5	
Soil emissions	20.2	19
Total sources	**59**	**75**
Wet deposition	12 - 42	46
Dry deposition	12 - 22	10
NH_3 oxidation by OH		1
Total sinks	**59**	**57**

Source : Aneja et al. (2001)

Nitric acid is a major atmospheric oxidation product of nitrogen oxides (NO_x = $NO + NO_2$). Major emissions of NO_X are associated with fossil fuel combustion and natural sources. As shown in Table 1.6, fossil fuel combustion produces approximately 21Tg (N)/yr; other major sources include biomass burning, soil emissions, and lightning. Figure 1.3 illustrates major processes in the atmospheric cycling of nitrogen-containing compounds.

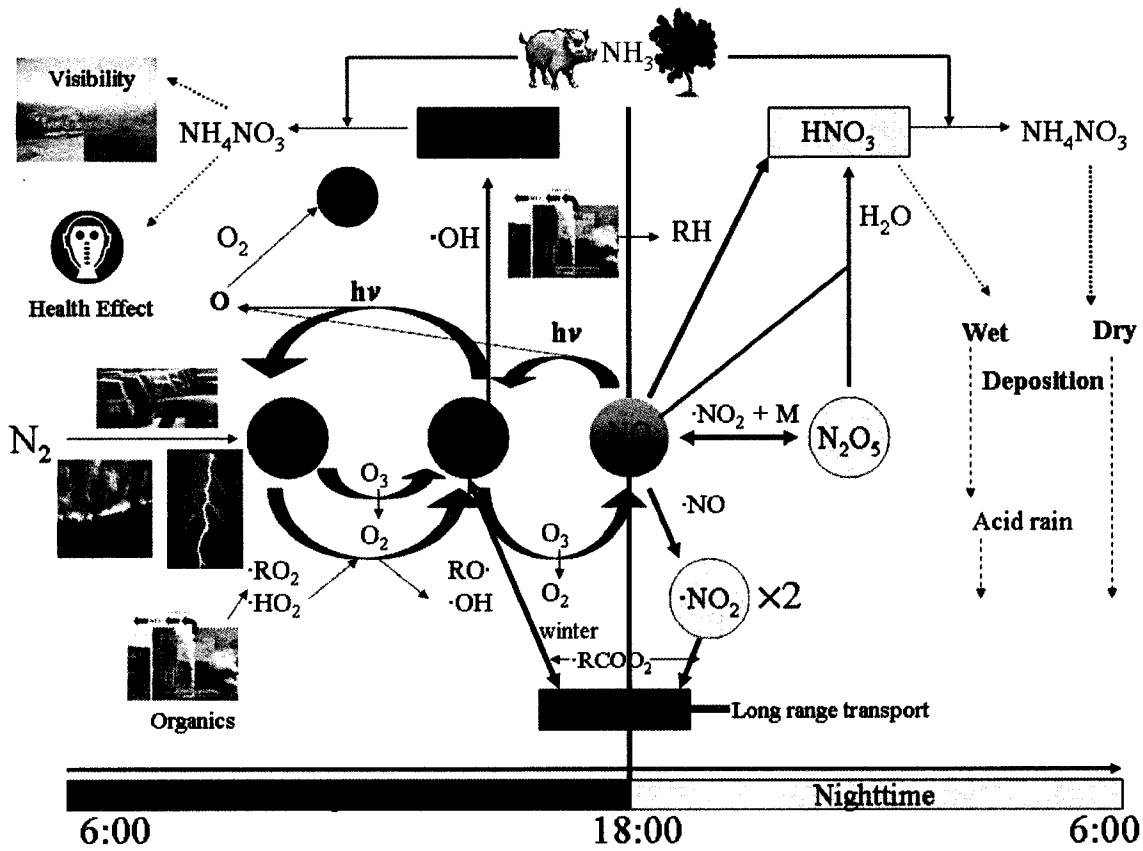

Figure 1.3 Processes in the atmospheric cycle of nitrogen-containing compounds.

1.2 Secondary aerosol formation: NH_4^+, SO_4^{2-}, NO_3^- particles

Although conventional wisdom suggests that $PM_{2.5}$ nitrate is mainly comprised of submicron ammonium nitrate particles, there are actually multiple important pathways for aerosol nitrate formation. These include reaction of gaseous nitric acid with gaseous ammonia to form ammonium nitrate and reaction of gaseous nitric acid with precursor sea salt or soil dust particles to form coarse mode nitrate in forms such as sodium nitrate or calcium nitrate. While ammonium nitrate and ammonium sulfate are typically observed in a fine particle mode, sodium (or calcium) nitrate and sulfate occur mainly in

coarse mode particles. This is because the precursor soil dust or sea salt particles are themselves typically coarse mode particles, having formed from mechanical generation processes.

NH_4NO_3 and ammoniated SO_4^{2-} Particles

In a typical polluted atmosphere, the presence of NH_3, H_2SO_4, and HNO_3 can lead to formation of particulate ammonium nitrate (NH_4NO_3) and/or various forms of ammoniated sulfate, including ammonium sulfate ($(NH_4)_2SO_4$) and ammonium bisulfate (NH_4HSO_4) (Seinfeld and Pandis, 1998). Ammonium nitrate and ammonium sulfate formation are illustrated in equations 1.1 and 1.2 (Spurny, 2000)

$$\mathbf{HNO_3(g) + NH_3(g) \leftrightarrow NH_4NO_3(p)} \quad \textbf{(Eqn. 1.1)}$$

$$\mathbf{H_2SO_4(g) + 2NH_3(g) \leftrightarrow (NH_4)_2SO_4(p)} \quad \textbf{(Eqn. 1.2)}$$

Ammonium nitrate is generally considered the predominant form of nitrate in the inorganic fraction of submicron aerosol particles (Adams et al., 1999; Allegrini et al., 1994). Ammonium nitrate formation is reversible with an equilibrium constant that is dependent on temperature and relative humidity (Appel, 1993; Spicer, 1977; Stelson and Seinfeld, 1982). High humidities and low temperatures favor ammonium nitrate formation. The formation of particulate nitrate in equation 1.1 can be limited by the concentrations of HNO_3 or NH_3. Ammonia limitation is common in many environments because ammonia reacts preferentially with H_2SO_4 to form ammonium sulfate ($[NH_4]_2SO_4$), letovicite ($[NH_4]_3H[SO_4]_2$), or ammonium bisulfate (NH_4HSO_4). Within a

given particle, ammonium nitrate formation is not thermodynamically favored until all sulfate present is fully neutralized.

NO_3^- and SO_4^{2-} in sea salt particles

Freshly emitted sea salt particles are mainly composed of sodium and chloride(Laskin et al., 2002). In the presence of sea salt (symbolized here by NaCl), H_2SO_4 can react to form particulate sulfate (Na_2SO_4) as shown in Equation 1.3 (De Haan and Finlayson-Pitts, 1997; ten Brink, 1998) and HNO_3 and NO_2 can also react with NaCl to form particulate nitrate including $NaNO_3$ (De Haan and Finlayson-Pitts, 1997; Dentener et al., 1996; Gard et al., 1998; John et al., 1990; Lee and Collett, 2002; Padgett and Bytnerowicz, 2001; Pakkanen, 1996; Pakkanen et al., 1996; Prospero and Savoie, 1989; Spurny, 2000; Wolff, 1984) as shown in equations 1.4 and 1.5.

$$H_2SO_4(g) + 2NaCl(p) \rightarrow Na_2SO_4(p) + 2HCl(g) \quad \textbf{(Eqn. 1.3)}$$

$$HNO_3(g) + NaCl(p) \rightarrow NaNO_3(p) + HCl(g) \quad \textbf{(Eqn. 1.4)}$$

$$2NO_2(g) + NaCl(p) \rightarrow NaNO_3(p) + NOCl(g) \quad \textbf{(Eqn. 1.5)}$$

As mentioned above reaction of strong acids, such as sulfuric or nitric acid, with sea salt particles can release hydrochloric acid to the gas phase and leave behind nitrate and sulfate salts. The amount of chloride lost during replacement by nitrate or sulfate can be estimated as shown in Equation 1.6 if the aerosol Na^+ and Cl^- content comes only from sea salt.

$$\textbf{Cl}^{-}\textbf{ depletion (\%)} = \frac{(1.164[Na^{+}]-[Cl^{-}])}{(1.164[Na^{+}])} \times 100\ \% \quad \textbf{(Eqn. 1.6)}$$

The reaction of gaseous HNO_3 with sea salt (modeled as NaCl) has been studied experimentally. Uptake coefficients (molecules/cm^3) for HNO_3 on NaCl ranged from $\gamma = 10^{-4}$ to 10^{-2} (Abbatt and Waschewsky, 1998; Beichert and FinlaysonPitts, 1996; De Haan and Finlayson-Pitts, 1997; Grassian, 2002; Guimbaud et al., 2002; Laux et al., 1994; ten Brink, 1998). These studies also indicate that the availability of surface water on NaCl plays an important role in the uptake of HNO_3.

NO_3^- and SO_4^{2-} in mineral dust particles

Mineral dust influences not only climate (Martin et al., 2004; Tegen et al., 2000) and biogeochemical cycles but also the chemistry of the atmosphere by uptake of gas species. Several studies show heterogeneous removal of HNO_3 on cirrus cloud crystals, sulfate and soot particles (Abbatt, 1997; Rogaski et al., 1997; Zondlo et al., 1997). However, modeling studies indicate that another removal process needs to be considered for reducing global HNO_3 concentrations (Singh et al., 1996; Wang et al., 1998). It has been suggested that mineral aerosols can effectively remove gas-phase HNO_3 from the atmosphere.

Reactions between HNO_3 (and other gaseous species) and mineral dust have been reported based on observations (Dentener et al., 1996; Evans, 2003; Evans et al., 2004; Jordan et al., 2003; Laskin et al., 2005; Maxwell-Meier et al., 2004; Ooki and Uematsu, 2005; Pakkanen, 1996; Sullivan et al., 2006; Umann et al., 2005; Underwood et al., 2001;

Zhang et al., 2003). Included are observations of reaction between H_2SO_4 and/or SO_2 and mineral dust (Dentener et al., 1996; Jordan et al., 2003; Usher et al., 2002). A series of laboratory studies has also been conducted to investigate reactions between various gases (including HNO_3, NO_2, SO_2 and O_3) and mineral dust containing $CaCO_3$, using a variety of techniques including transmission FTIR spectroscopy, diffuse reflectance UV-visible spectroscopy, transmission electron microscopy and Knudsen cell reactor coupled to a mass spectrometer (Borensen et al., 2000; Goodman et al., 2000; Grassian, 2002; Hanisch and Crowley, 2001a; Hanisch and Crowley, 2001b; Hanisch and Crowley, 2003; Krueger et al., 2004; Laskin et al., 2005; Michel et al., 2003; Seisel et al., 2004; Underwood et al., 2000; Underwood et al., 2001; Usher et al., 2002; Usher et al., 2003). Both field observations and laboratory study results indicate that mineral dust particles provide an important sink for acidic gaseous species such as HNO_3 and SO_2.

Generally, mineral dust is comprised of insoluble metal oxides (e.g. SiO_3 and Al_2O_3) with a fraction of an alkaline component such as $CaCO_3$ and $MgCO_3$ and including a small fraction of K_2CO_3 and Na_2CO_3. Calcium carbonate, typically a major constituent in the alkaline component, is especially interesting due to possible reactions with acidic gaseous species (e.g. HNO_3, SO_2 and H_2SO_4) as shown in Equations 1.7, 1.8 and 1.9. Although often less abundant, $MgCO_3$ can also react with nitric acid. Irreversible reactions between gaseous species and mineral dust particles can provide important sinks for HNO_3 and NO_2.

$$\mathbf{2HNO_3(g) + CaCO_3 \rightarrow Ca(NO_3)_2(p) + CO_2(g) + H_2O(aq)} \quad \textbf{(Eqn. 1.7)}$$

$$\mathbf{SO_2(g) + CaCO_3 \rightarrow CaSO_3(p) + CO_2(g)} \quad \textbf{(Eqn. 1.8)}$$

$$\mathbf{H_2SO_4(g) + CaCO_3 \rightarrow CaSO_4(p) + CO_2(g) + H_2O(aq)} \quad \textbf{(Eqn. 1.9)}$$

Goodman et al (2000) and Grassian (2002) indicated that particle water content played an important role in uptake of gaseous HNO_3 by $CaCO_3$. HNO_3 reacted little with solid $CaCO_3$ particles under dry conditions. Reaction to form $Ca(NO_3)_2$ started in the presence of 20 % relative humidity and increased at higher humidities as more water was adsorbed onto the $CaCO_3$ particle surface.

For reaction of HNO_3 with $CaCO_3$, the heterogeneous uptake coefficient, "simply a measure of how likely the molecule will be taken up by the surface on a per collision basis" (molecules/cm^3) (Grassian, 2002), has been determined experimentally and estimated from atmospheric data. Goodman et al (2000) and Grassian (2002) measured uptake coefficient values of $\gamma = 2.4 \times 10^{-4}$ and $\gamma = 0.025$ under dry and 20% relative humidity conditions, respectively. However, Hanisch et al (2001) determined higher uptake coefficients ranging from $\gamma = 0.9 \times 10^{-2}$ to 18.3×10^{-2}. Underwood et al (2000) found uptake coefficients between $\gamma = 2.3 \times 10^{-3}$ and 4×10^{-4}. Umann et al (2005) estimated uptake coefficient values in the range of $\gamma = 0.017$ - 0.054 (RH; 17 – 44%, Mean: 23%) from atmospheric observations.

A competitive partitioning of nitric acid between NaCl and $CaCO_3$ at 78 % RH was examined numerically by Evans (2003) and Evans et al. (2004). Particulate nitrate formation increased with an increase in sodium and/or calcium in the system. Nitric acid reacts more quickly with soil dust ($CaCO_3$) than with sea salt (NaCl), because calcium (Keq = 6.9×10^{16} – 9.2×10^{30}) has an equilibrium constant many orders of magnitude greater than sodium (Keq = 1.4 – 48).

1.3 Previous observations of coarse particle nitrate

Although ammonium nitrate is generally considered the predominant form of nitrate in aerosol particles, various forms of coarse particle nitrate have been identified in a variety of previous atmospheric observations. Savoie et al. (1982), examining marine aerosols, and Wolff (1984) examining continental aerosols found the majority of particle nitrate associated with particles larger than approximately 2.0 μm diameter. Similarly, Wu et al. (1994) and Pakkanen (1996) observed coarse particle nitrate associated with sea salt and/or soil dust, suggesting several formation mechanisms of coarse particle nitrate. Formation of coarse particle sodium nitrate has been observed several times in marine conditions (Evans et al., 2004; Gard et al., 1998; Kerminen et al., 1997; Pakkanen et al., 1996; Savoie and Prospero, 1982; ten Brink, 1998; Zhuang et al., 1999), while coarse particle nitrate has been observed as forms of calcium and magnesium nitrate over continental areas (Evans et al., 2004; Hodzic et al., 2006a; Krueger et al., 2004; Pakkanen, 1996; Umann et al., 2005; Wolff, 1984; Wu and Okada, 1994; Zhang et al., 2005).

The formation of coarse particle nitrate by reaction of nitric acid with soil dust has been confirmed in several studies during Asian ("Kosa" or "China loess") and North African dust events (Aymoz et al., 2004; Chen et al., 2004; Ooki and Uematsu, 2005; Zhang et al., 2003) and in measurements conducted in northern Italy (Umann et al., 2005) and near Paris (Hodzic et al., 2006b). Mineral nitrate formation was also observed during the TRACE-P (Jordan et al., 2003) and ACE-Asia (Arimoto et al., 2006; Maxwell-Meier et al., 2004; Sullivan et al., 2006) field campaigns.

As discussed above, particulate nitrate comprises a significant fraction of aerosol mass in many locations. The forms of nitrate present can be a complex mixture of ammonium nitrate, reacted sea salt and reacted soil dust. Routine monitoring networks, including the IMPROVE (Interagency Monitoring of PROtected Visual Environments) network, often assume that $PM_{2.5}$ nitrate is present in the form of ammonium nitrate. More detailed investigations of aerosol composition at two IMPROVE monitoring locations, Big Bend National Park, Texas and Yosemite National Park, California, indicate that a significant fraction of summertime particle nitrate was actually present as reacted sea salt or mineral dust nitrate (Carrico et al., 2004; Lee et al., 2004; Malm et al., 2005a).

In Big Bend National Park, the dominant fine particle constituents were usually acidic ammoniated sulfate (Lee et al., 2004), while nitrate had a strong correlation in particle size with sodium as shown in Figure 1.4. The acidic nature of the fine sulfate particles, along with the high summer temperatures and relatively low to moderate humidity levels observed in Big Band National Park, do not favor particulate ammonium nitrate formation thermodynamically. High concentrations of gaseous HNO_3 were often available, however, to react with sea salt and soil dust transported to the measurement site. Comparisons between daily $PM_{2.5}$ Na^+, Cl^- and NO_3^- in Figure 1.5 are consistent with nitric acid reaction with sea salt to form particulate $NaNO_3$, simultaneously displacing chlorine from the particle as HCl. In the figure one notices that the ratio of Cl^- to Na^+ is consistently smaller than the ratio found in sea water, indicating a loss of chloride from the aerosol. When the sum of chloride and nitrate is plotted against Na^+, many points fall close to the expected sea water Cl^-/Na^+ ratio, indicating stoichiometric

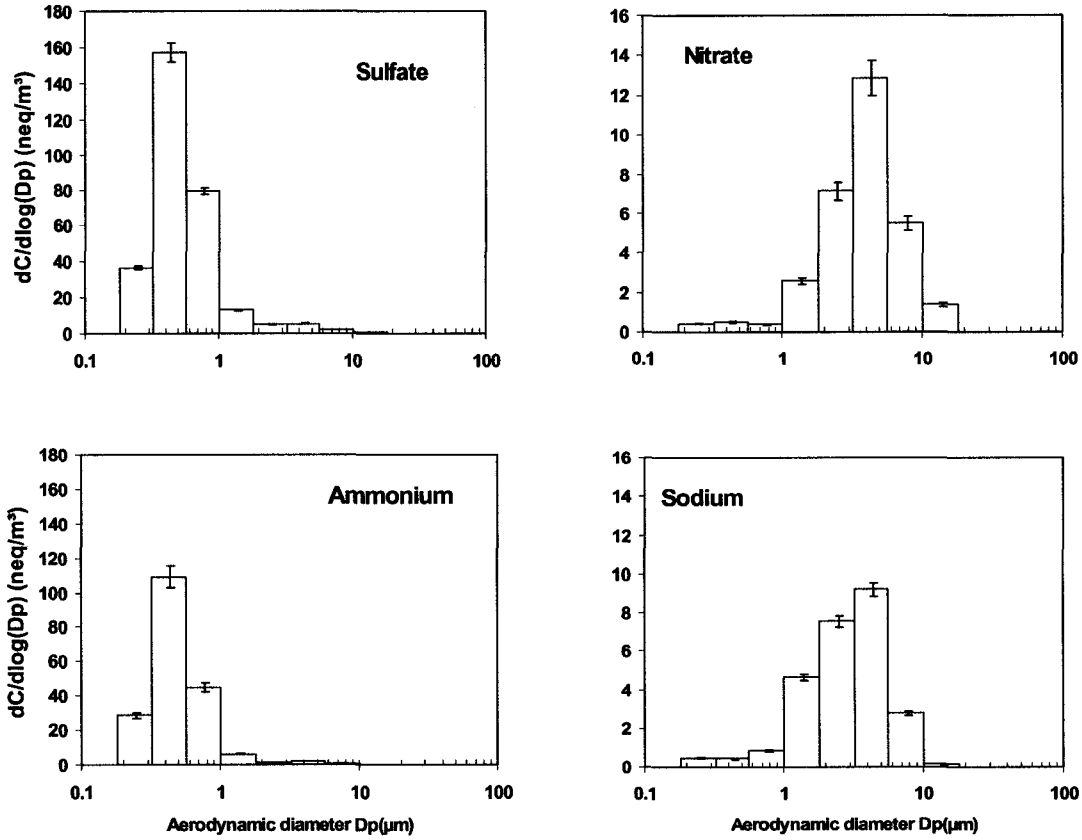

Figure 1.4 The average measured size distributions of sulfate, ammonium, nitrate and sodium at Big Bend National Park, July – October, 1999.

replacement of chloride by nitrate. On some days when the ratio of the sum of nitrate and chloride to Na^+ far exceeds the sea water Cl^-/Na^+ ratio, there is separate evidence from particle species' size distributions that a fair amount of nitrate is present in reacted mineral dust particles (Lee et al., 2004).

Detailed measurements of aerosol composition were made at the IMPROVE monitoring site in Yosemite National Park, California, in the summer of 2002. Yosemite aerosol during the study was dominated by carbonaceous material, derived mainly from

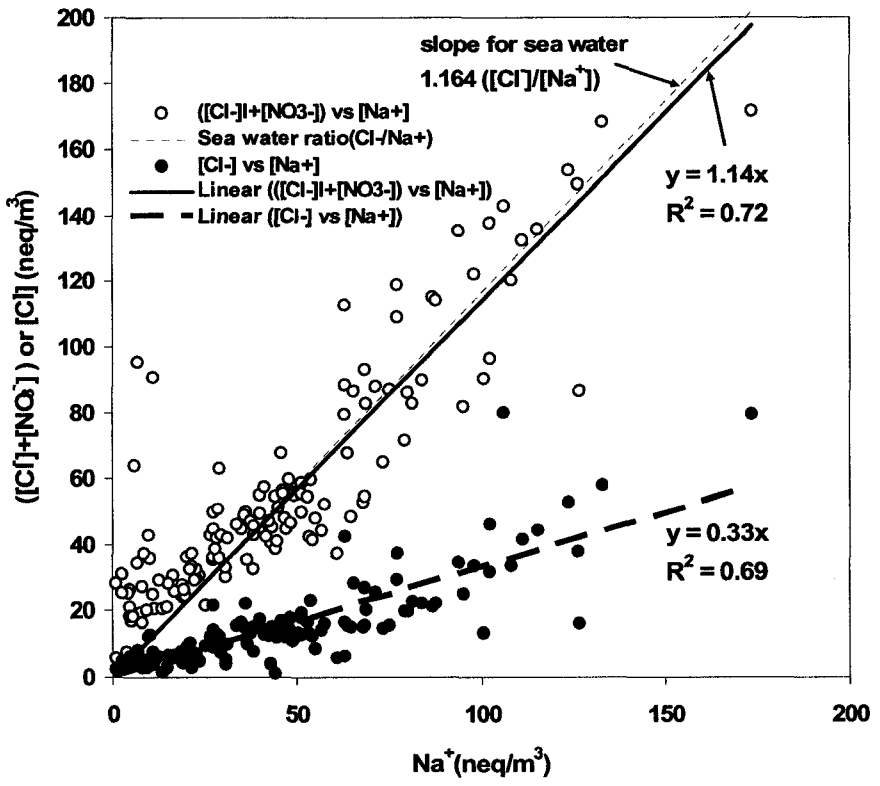

Figure 1.5 Relationship between Na^+ and Cl^- and between Na^+ and the sum of NO_3^- and Cl^- in daily $PM_{2.5}$ samples collected at Big Bend National Park, July – October, 1999.

biomass combustion (Engling et al., 2006; McMeeking et al., 2006). $(NH_4)_2SO_4$ was the main inorganic aerosol component. Particulate nitrate measured during the study was generally present in the form of $NaNO_3$, resulting from reaction of gas phase HNO_3 with sea salt particles (Carrico et al., 2004; Malm et al., 2005a). The importance of reacted sea salt nitrate is clearly illustrated in the $PM_{2.5}$ composition timeline included in Figure 1.6. These high time resolution (15 min) measurements were made using a Particle into Liquid Sampler (PILS) coupled to two ion chromatographs. Further information about

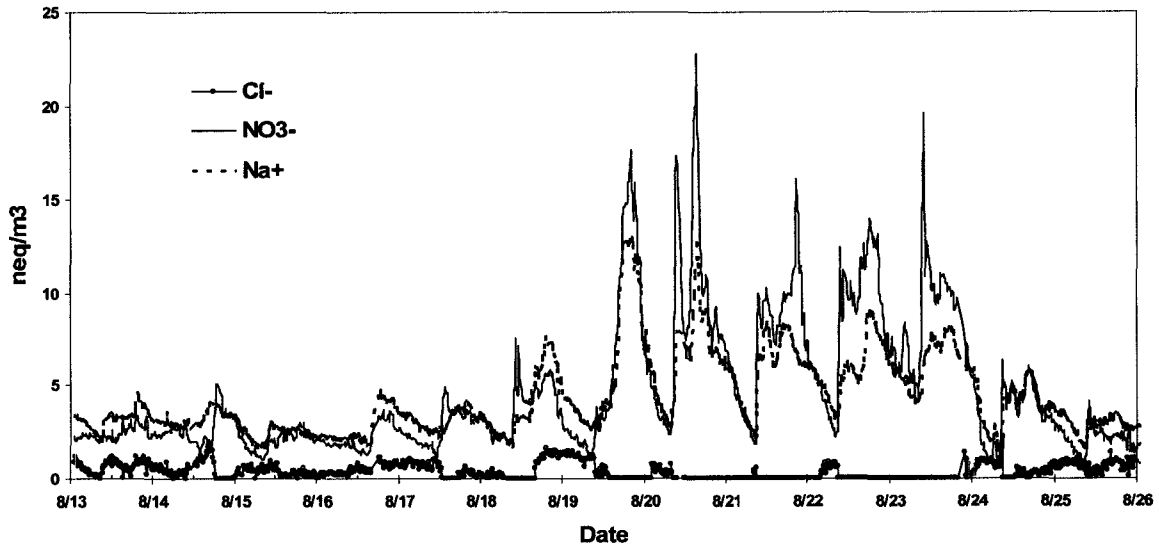

Figure 1.6 Cl^-, NO_3^-, and Na^+ ion concentration measured from Aug 13-26, 2002

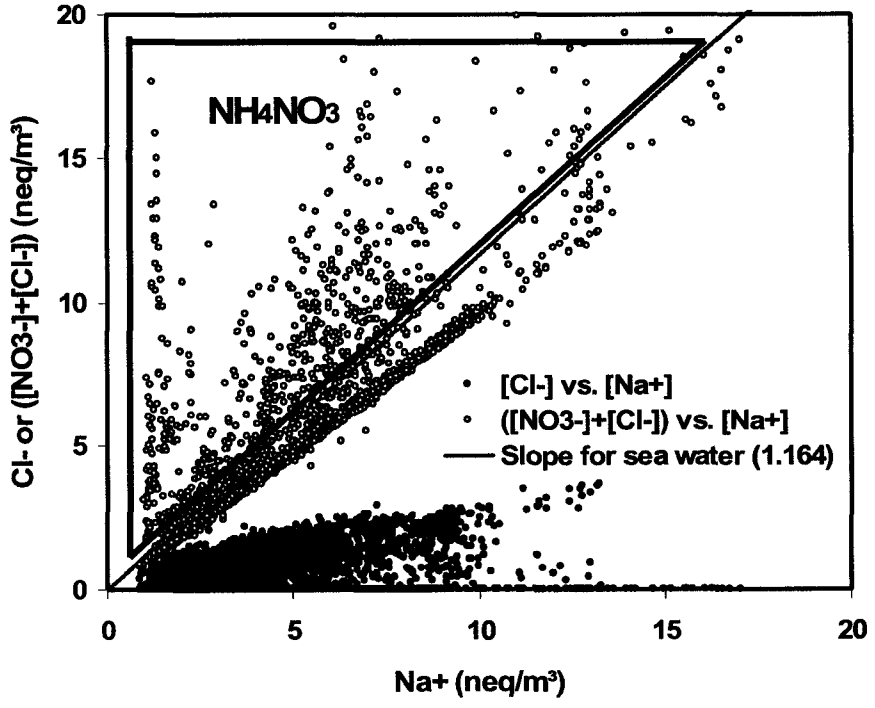

Figure 1.7 Relationship between $[Na^+]$ and the sum of $[NO_3^-]$ and $[Cl^-]$ and between $[Na^+]$ and $[Cl^-]$ measured using PILS

this measurement technique is provided in subsequent chapters. Generally, the PILS nitrate concentration trends were similar to sodium, suggesting an association between these species in the aerosol, consistent with displacement of chloride from sea salt by reaction with nitric acid or its precursors. If one looks closer, one sees that when the nitrate concentration exceeds the concentration of Na^+, the chloride is typically fully depleted from the aerosol; when the Na^+ concentration exceeds the NO_3^- concentration, residual Cl^- is present (Figure 1.6). Figure 1.7 shows ratios of Cl^- or the sum of NO_3^- and Cl^- concentrations to Na^+ concentrations for the 15 min PILS measurement points. Here one again sees a significant depletion of chloride from the aerosol. When the nitrate and chloride are summed, their ratio against Na^+ defines an envelope of points with a lower bound similar to the expected sea water Cl^-/Na^+ ratio, consistent with stoichiometric replacement of chloride by nitrate in the aerosol. Points well above this ratio in this case are mainly accounted for by formation of ammonium nitrate, which was occasionally observed to be an important contributor to the local aerosol. Particle ion size distribution measurements at Yosemite also provide evidence of the importance of reaction of nitric acid or its precursors with sea salt. The observed importance of coarse nitrate at Yosemite came as something of a surprise, given the large ammonia emissions found in California's Central Valley, which typically lies upwind of the park. This finding, however, is consistent with the hot, dry summertime conditions at the park which tend to disfavor formation of ammonium nitrate.

Findings of the importance of coarse particle nitrate at Big Bend and Yosemite National Parks suggested a need to further explore the dominant forms of nitrate at a variety of rural monitoring locations. Knowledge of the prevalence of different forms of

nitrate is important for understanding important properties of nitrate aerosol, including its hygroscopicity, refractive index, dry deposition velocity, and ability to act as cloud condensation nuclei.

1.4 Study Objectives

The observations that $PM_{2.5}$ nitrate at both Big Bend National Park and in summer at Yosemite National Park was not ammonium nitrate but rather consisted of the lower tail of a coarse particle mode of sodium or calcium nitrate raised concerns about the overall importance of fine particle ammonium nitrate across the United States. A general lack of measurements of either gas phase ammonia or particulate phase ammonium in the U.S., especially at non-urban locations, suggests that conventional wisdom about the occurrence of ammonium nitrate in rural and remote environments needs to be carefully examined. The main goal of this research is to answer the question, "What is the dominant form of particulate nitrate?" at a number of rural U.S. locations. The answer to this question bears importantly on the lifetime of nitrate in the atmosphere and the likely effectiveness of potential ambient particle control strategies. It is also important for understanding impacts of particle nitrate on visibility reduction and climate forcing as well as for understanding impacts of various N emissions sources on N deposition in sensitive ecosystems.

As explained below, measurement sites were selected in different parts of the country where significant amounts of particulate nitrate were known, from historical records, to occur. The measurement locations were chosen in consultation with representatives from the IMPROVE program. A series of special measurement

campaigns, each several weeks in length, conducted to characterize the chemical form and size distribution of particulate nitrate.

As part of the overall study objectives, we also examined the adequacy of current protocols for particulate nitrate measurement in the IMPROVE program and the potential for making accurate measurements of particulate ammonium off the same filters currently used for $PM_{2.5}$ anion (nitrate, sulfate, chloride) analysis. The IMPROVE program collects $PM_{2.5}$ aerosol particles on a nylon filter for ion analysis. The sampled air is first drawn through a cyclone, providing the $PM_{2.5}$ size cut, and then through a coated denuder (http://vista.cira.colostate.edu/improve/Publications/IMPROVE_SOPs.htm) to remove nitric acid. Specific issues addressed in our work included quantifying losses of nitrate and ammonium from the nylon filter and the efficiency of deionized water extraction for completely recovering particle nitrate collected on the nylon filter. Further information concerning the motivation for these studies and our findings are reported elsewhere (Yu et al., 2005b; Yu et al., 2006).

2. Experimental description

This chapter outlines details regarding field experiments and laboratory analyses conducted as part of this research project. Discussion begins with a summary of field study locations, followed by descriptions of field equipment, sample collection and handling procedures, laboratory analysis methodologies, and quality assurance/quality control, including the comparisons of major ion concentrations (NO_3^-, SO_4^{2-} and NH_4^+) between the two integrated samplers (URG and MOUDI) and semi-continuous sampler (PILS).

2.1 Field study locations

A series of six intensive field experiments was designed and conducted to investigate aerosol particle concentrations, chemical composition, and size distributions at several IMPROVE sites. Measurements were made in a variety of seasons during 2003 and 2004. Measurements were made at Bondville, IL (February 2003), Brigantine National Seashore, NJ (November 2003), San Gorgonio Wilderness Area, CA (April 2003, July 2003, 2004), Grand Canyon National Park, AZ (May 2003) and Great Smoky Mountains National Park, TN (August 2004). Also included in this report are findings from an aerosol characterization study conducted in Yosemite National Park, CA (July – September, 2002). Each field campaign lasted approximately one month except for the two month project at Yosemite National Park. Most of the campaigns were scheduled to examine time periods when nitrate concentrations were near their annual peak at each study location. Two campaigns were scheduled for the nitrate-rich San Gorgonio, CA

Table 2.1 General information of study locations

Location	State	Longitude	Latitude	Elevation (m)	Study period
Yosemite NP	CA	-119.70	37.71	1615	7/14/2002 to 9/04/2002
Bondville	IL	-88.3719	40.0514	211	2/01/2003 to 2/27/2003
San Gorgonio Wilderness	CA	-116.9013	34.1924	1705	4/04/2003 to 4/26/2003 7/01/2003 to 7/30/2003 6/30/2004 to 7/09/2004
Grand Canyon NP	AZ	-111.9841	35.9731	2267	5/01/2003 to 5/20/2003
Brigantine	NJ	-74.4492	39.465	5	11/4/2003 to 11/30/2003
Great Smoky Mts NP	TN	-83.9416	35.6334	810	7/26/2004 to 8/18/2004

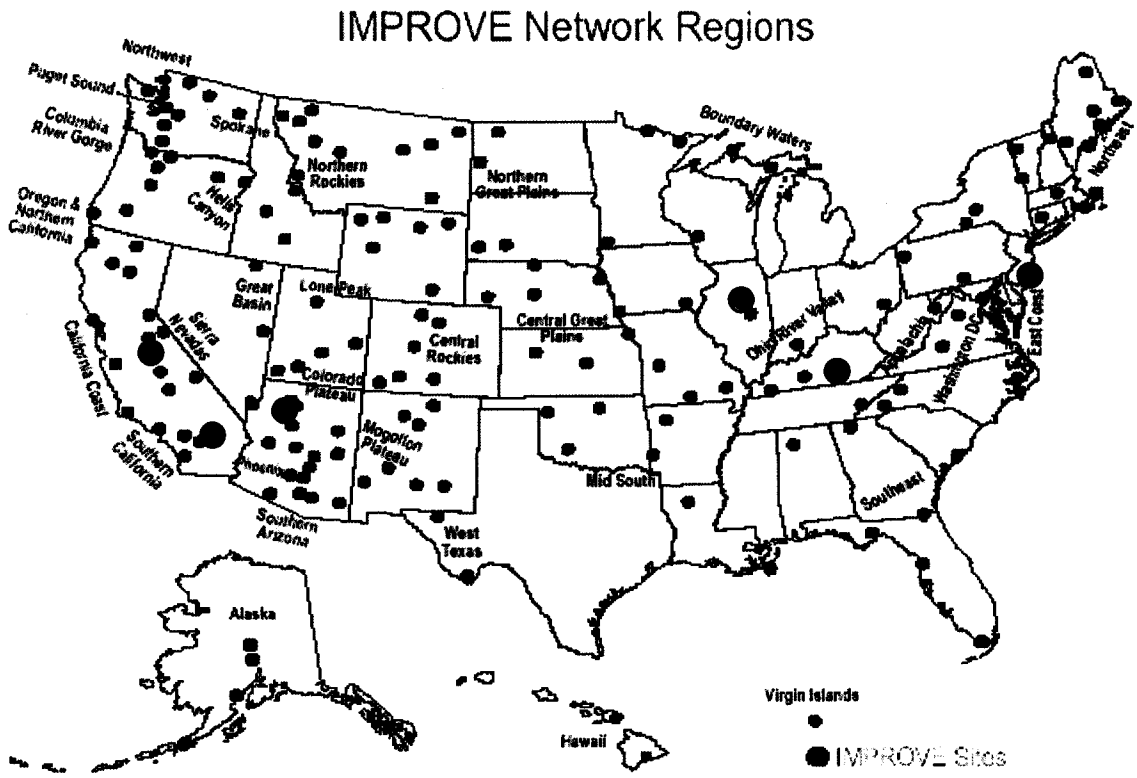

Figure 2.1 Study locations at several IMPROVE sites (study locations in red dot)

site to investigate possible changes in particle composition and gas-particle partitioning with seasonal temperature changes. Table 2.1 and Figure 2.1 summarize location

information and measurement periods of each field campaign (study site pictures in Appendix F).

All but the Yosemite campaign were part of a series of field measurements designed to investigate properties of aerosol nitrate at IMPROVE monitoring locations. The Yosemite study was designed to investigate chemical and physical properties of summertime, smoke-dominated aerosol. As we will see, however, this campaign also provided some interesting insight into summertime aerosol nitrate properties in the central Sierra Nevada. Measurements were made at Bondville in order to examine winter-time, Midwest U.S. aerosol properties. This region experiences high nitrate concentrations during the cooler months of the year. The San Gorgonio site was included because of heavy impacts from the Los Angeles air basin located to the west, which result in the highest $PM_{2.5}$ nitrate concentrations of any IMPROVE site. Grand Canyon was included in the study to investigate aerosol nitrate properties at a site located in the Colorado Plateau. This region is of interest in part because it is home to the so-called *Golden Circle* of National Parks, including Bandelier, Bryce Canyon, Canyonlands, Grand Canyon, Mesa Verde and Petrified Forest. These parks are prized for their scenic vistas, making good visual air quality a high priority. The Brigantine site was included in the study to represent an eastern U.S. coastal location, where mixing of polluted continental and marine air masses might produce interesting aerosol chemistry situations. The final campaign was conducted at Great Smoky Mtns NP in summertime, to characterize aerosol nitrate and potential, associated sampling artifacts, in a highly polluted, acidic, sulfate-dominated environment.

2.2 Setup and Instrumentation

The main $PM_{2.5}$ inorganic ion species (Cl^-, SO_4^{2-}, NO_3^-, Na^+, NH_4^+, K^+, Mg^{2+} and Ca^{2+}) and gas phase concentrations of HNO_3, NH_3, and SO_2 were measured using samples collected by a URG cyclone/annular denuder/filter pack system. Particle species' size distributions were determined using a Micro-Orifice Uniform Deposit Impactor (MOUDI). In addition, a PILS (Particle Into Liquid Sampler)/IC (Ion Chromatography) (Orsini et al., 2003; Weber et al., 2001) semi-continuous particle measurement system was deployed to provide a better understanding of diurnal changes in aerosol concentrations and composition. High time resolution measurement of $PM_{2.5}$ using PILS/IC system allowed quantification of concentrations of major ionic species (Cl^-, SO_4^{2-}, NO_3^-, Na^+, NH_4^+, K^+, Mg^{2+}) with 15-minute time resolution.

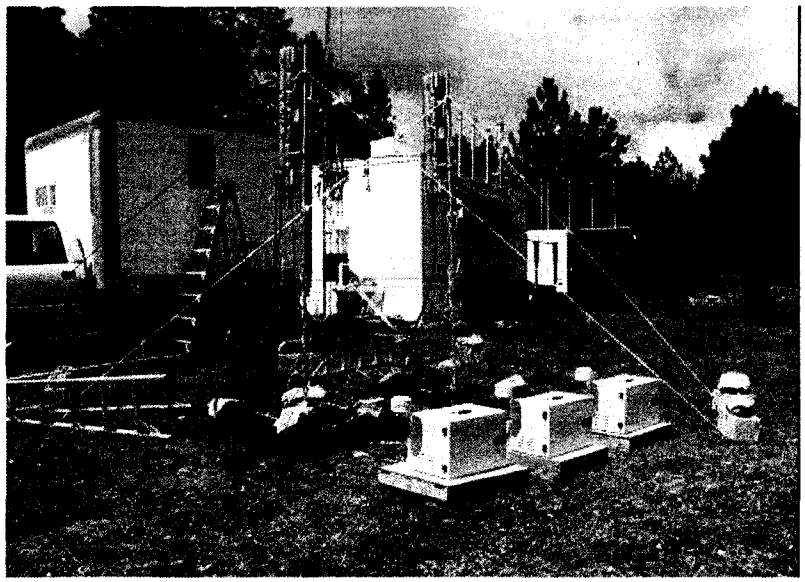

Figure 2.2 Typical study setup (Grand Canyon, AZ) with URG samplers in the foreground and the mobile truck laboratory (containing the MOUDI and PILS/IC system) in the background

Typical site setups are illustrated in Figures 2.2 and 2.3. URG samplers were deployed outside, while the MOUDI sampler and PILS/IC system were housed inside the CSU mobile truck lab.

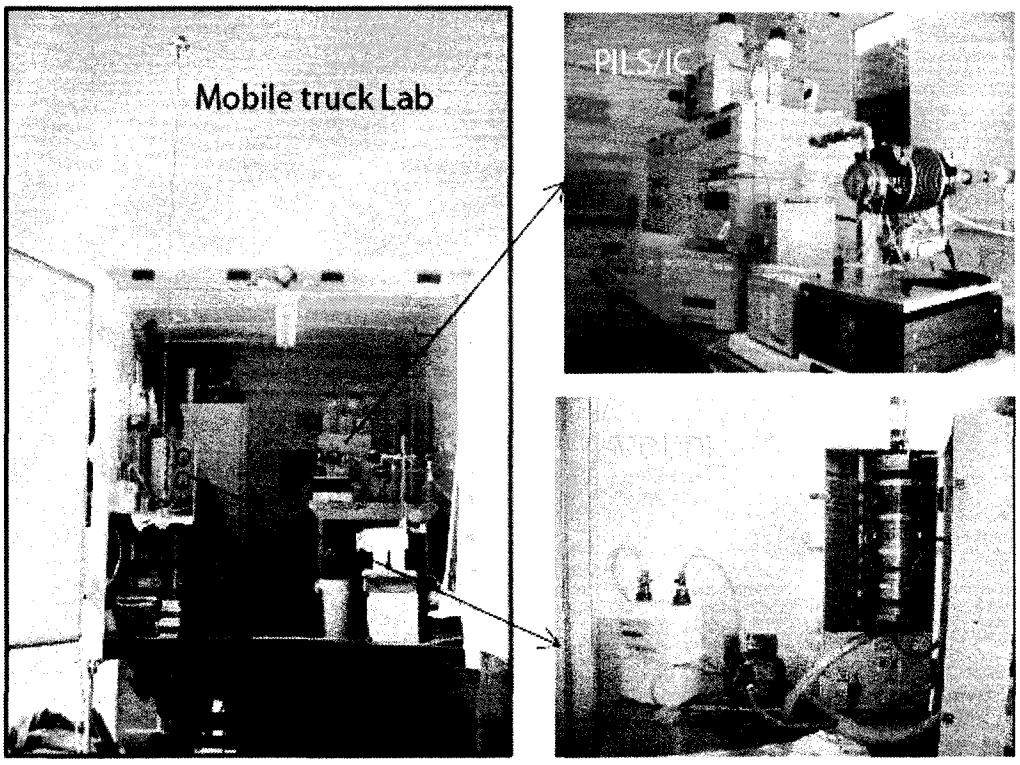

Figure 2.3 Inside setup mobile truck laboratory and PILS/IC and MOUDI

2.2.1 Micro Orifice Uniform Deposition Impactor (MOUDI)

All impactors consist of two basic parts: a nozzle plate and an impaction plate. Multi-stage impactors have multiple stages, often each with multiple nozzles, allowing for particles to be collected in different size ranges. Ambient air enters each impaction stage through the nozzles which direct suspended particles toward an impaction surface. As the airflow is deflected around the impaction surface, particles with sufficient inertia

are collected by impaction on a collection surface; smaller particles with less inertia follow the airstream and proceed onto the next stage where the nozzles are smaller and the flow is accelerated to a greater speed (Figure 2.4). By decreasing nozzle diameter and increasing airstream velocity in subsequent impaction stages, smaller and smaller particles can be collected (Hinds, 1999).

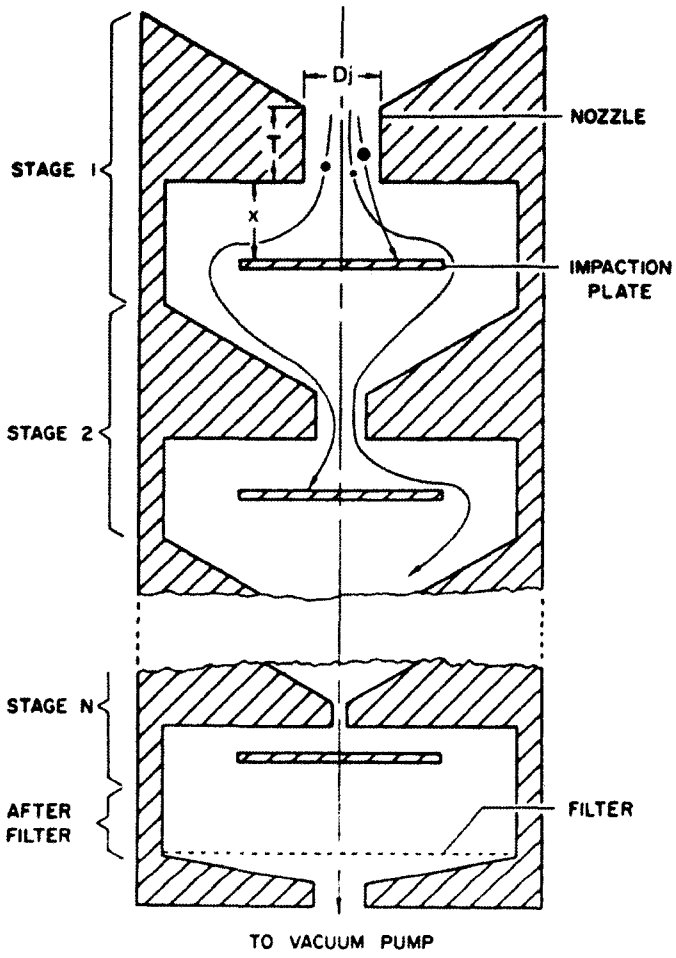

Figure 2.4 Schematic diagram of an impactor
Source: (Hinds, 1999)

A pump pulled the ambient air through the MOUDI inlet, covered with a rain shield and aluminum bug screen, at a nominal flow rate of 30 L/min. Samples were typically collected over 48 hr periods, from approximately 08:00 to 08:00 local time. To reduce particle bounce, grease-coated aluminum foil was used as an impaction substrate except for a 37mm Teflon after-filter (Marple et al., 1991; Marple and Willeke, 1976). The MOUDI (Model 110, MSP Corporation) was operated with 8 stages with aerodynamic diameter size range: D_p >18μm, 18-10μm, 10-5.6μm, 5.6-3.2μm, 3.2-1.8μm, 1.8-1.0μm, 1.0-0.56μm, 0.32-0.18μm and after-filter (D_p<0.18μm).

2.2.2 URG cyclone/annular denuder/filter pack system

A commercially available URG (University Research Glassware) cyclone/annular denuder/filter pack system (model URG-3000C) was used for daily $PM_{2.5}$ sampling. Ambient air is drawn into the sampler through a cyclone (D_{50}=2.5 μm, 10 lpm, URG-2000-30EN) (for more information, Appendix A), and along two 242 mm denuders (URG-2000-30X242-3CSS) (for more information, Appendix A) in series. The denuders are coated with chemicals that absorb the gaseous species of interest. Na_2CO_3 coated the first denuder for collection of HNO_3 and SO_2 (and other acid gases) and the second denuder is coated with phosphorous acid to collect ambient NH_3 (Appel et al., 1981; McCulloch and Shendrikar, 2000; Pang et al., 2002; Shaw et al., 1982; Sickles et al., 1990). The remaining air stream is then filtered through a 37mm 2-stage filter pack (URG-2000-22FB) (detailed description in Appendix A). An additional denuder, coated with phosphorous acid, is used downstream of the filter pack. Two nylon filters (Nylasorb, 37mm Pall Gelman, 1.0μm pore size) or Teflon filter (Teflo 37 mm Pall

Gelman, 2.0 μm pore size) and nylon filter are used in the 2 stage filter pack, depending on the sampling train configuration (Figure 2.5). The downstream nylon filter and ammonia denuder are used to capture nitric acid and ammonia, respectively, which may be volatilized from particulate matter on the first particle collection filter. Volatilization

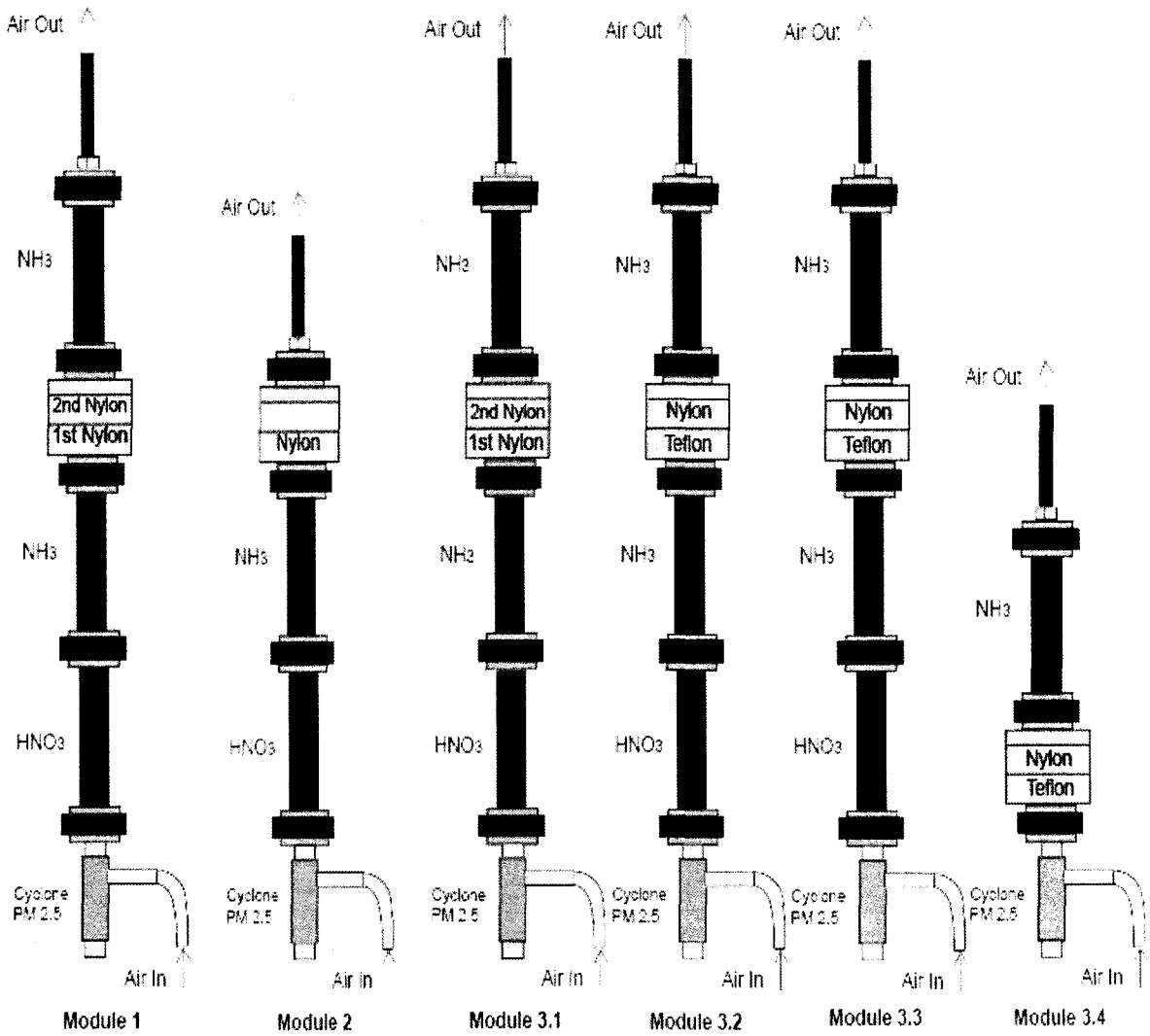

Figure 2.5 URG annular denuder/filter pack setup (Modules 1, 2, and 3.1 to 3.4)

of ammonia and nitric acid is especially problematic during sampling of aerosols containing ammonium nitrate (Appel and Tokiwa, 1981; Appel et al., 1981; Appel et al., 1984; Highsmith et al., 1986; Perrino et al., 1988; Spicer et al., 1985).

The URG denuder/filter-pack assembly was used to collect daily, 24hr samples. Samples were collected from 08:00 – 08:00 (next day) local time. Three different denuder/filter pack-sampling trains were used in parallel to examine the effects of different $PM_{2.5}$ sampling and extraction approaches (Figure 2.5). The first two sampling trains (module 1 and 2) were operated each day in most of the campaigns. Up to four different configurations were utilized on different days in the last sampling train (module 3) to investigate changes on shorter timescales, effects of different denuder/filter configurations, and to determine measurement precision via replicate sampling.

The module 1 configuration consists of a $PM_{2.5}$ cyclone, Na_2CO_3 coated denuder, a phosphorous acid coated denuder, nylon filter for particle collection, a second nylon filter, and a second phosphorous acid coated denuder in series (Figure 2.5). All components of module 1 were extracted and analyzed. Module 1 was designed to address the following issues:

- Daily concentrations of gaseous nitric acid, ammonia, and sulfur dioxide
- Daily concentrations of inorganic aerosol species (from the first nylon filter)
- Retention of nitric acid from particle collected on the first nylon filter

The configuration of module 2 is similar to module 1 except for the absence of the second nylon filter and the final ammonia denuder (Figure 2.5). Module 2 denuders were extracted but not analyzed except to verify suspicious values from the module 1 results.

While the nylon particle collection filter in module 1 was extracted with deionized water, the nylon particle collection filter in module 2 was extracted with a basic carbonate/bicarbonate solution to test whether deionized water adequately recovers collected particle nitrate and recaptured, volatilized nitric acid.

Module 3 was switched between four different configurations (Module 3.1, 3.2, 3.3, and 3.4) (Figure 2.5). Module 3, including the 3.1, 3.2, and 3.3 configurations, consists of a $PM_{2.5}$ cyclone, Na_2CO_3 coated denuder, a phosphorous acid coated denuder, nylon filter (or Teflon filter) for particle collection, a second nylon filter, and a second phosphorous acid coated denuder in series, while module 3.4 consists a $PM_{2.5}$ cyclone, un-denuded Teflon filter for particle collection, a second nylon filter and a final downstream ammonia denuder. The four different configurations in module 3 were designed to examine the following several issues.

1. Module 3.1: This is a duplicate of module 1. Together modules 1 and 3.1 provide measurement precision for our standard sampling approach.
2. Module 3.2: The Teflon filter was extracted using a perchloric acid solution to permit measurement of $PM_{2.5}$ aerosol acidity (EPA, 1992; EPA, 2003; EPA, 1999; Lee, 1992b; Lee and Kang, 2001; Lee et al., 1993) on-site. Analysis of the nylon filter and the final ammonia denuder downstream of the Teflon filter allow comparison of ammonium nitrate volatilization artifacts from particles on Teflon vs. nylon filters.
3. Module 3.3: A Teflon filter was used. Module 3.3 was operated during day and night 12 hr sampling periods to examine diurnal variations in species

concentrations, as well as any sampling artifacts affected by diurnal changes in air mass composition, temperature, and humidity.

4. Module 3.4: An undenuded Teflon filter followed by a nylon filter was used to examine the magnitude of nitrate sampling artifacts of this sampling approach, also used by the CASTNET program.

2.2.3 Particle-Into-Liquid Sampler /Ion Chromatogram (PILS/IC)

To improve understanding of the chemical characteristics of aerosol particles and their temporal variability, high time resolution measurement of $PM_{2.5}$ using a PILS/IC system (DIONEX DX-500) was used for quantification of concentrations of major ionic species (Cl^-, SO_4^{2-}, NO_3^-, Na^+, NH_4^+, K^+, Mg^{2+} and Ca^{2+}) with 15-minute time resolution. The Particle-Into-Liquid sampler has 3 components: the saturated vapor generator, the growth chamber, and the droplet collector (impactor). The overall approach of PILS/IC is to collect particles that comprise the $PM_{2.5}$ aerosol mass into a small continuous flow of high purity water. This is accomplished by generating supersaturated water vapor and mixing it with the ambient sample air. All particles (D_p>50 nm) reach sizes between approximately 3 to 7 μm in the saturated water vapor of the growth chamber by the time the drops exit (Orsini et al., 2003; Sorooshian et al., 2006; Weber et al., 2003; Weber et al., 2001). The liquid stream containing samples is then continually drawn into two ion chromatographs for measurement of aerosol anions and cations (Figure 2.6). A LiBr internal standard (8μN or 15μN) is used to monitor dilution of a liquid carrier stream resulting from water vapor condensation on collected particles. URG annular denuders (URG-2000-30X242-3CSS) and a $PM_{2.5}$ cyclone (16.7 LPM, URG-2000-30EH) were

used upstream of the PILS/IC. The first denuder was coated with Na_2CO_3 for removal of acidic gases and the second denuder was coated with phosphorous acid to remove basic gases. Denuders of PILS/IC were exchanged every 5-6 days after a calibration check standard and blanks. The PILS/IC was set up inside the CSU mobile laboratory.

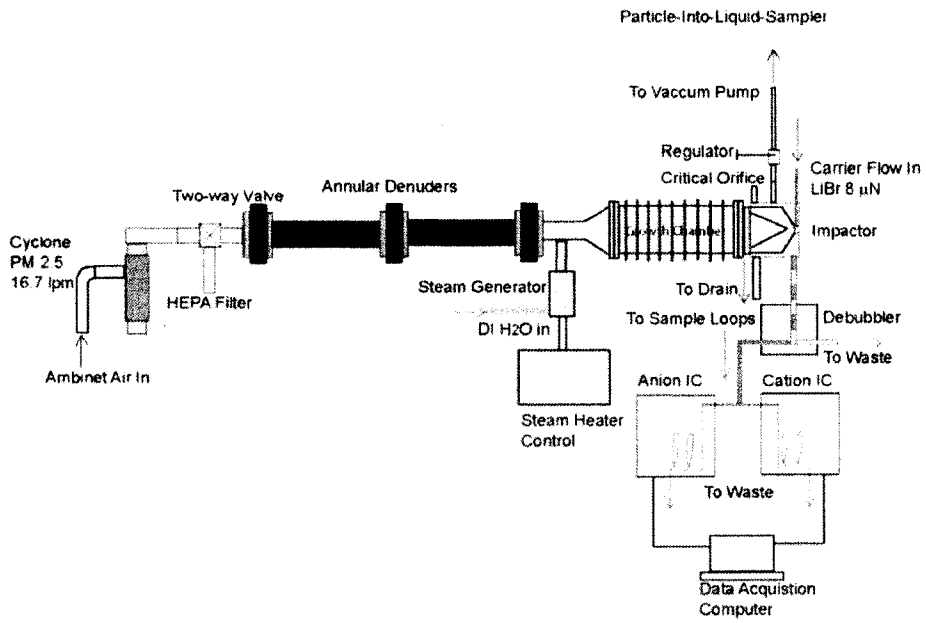

Figure 2.6 PILS/IC schematic and flow diagram

2.2.4 Statistical Analysis

Multivariate statistical analysis has been previously used to identify possible sources of pollutants by several investigators.(Cheng and Tsai, 2000; Cheng et al., 2000; Currie et al., 1984; Herckes et al., 2002; Hopke, 1988; Kaiser, 1958; Lee, 1992a). Correlation and factor analysis were performed to suggest possible sources of major $PM_{2.5}$ ions. For the factor analysis calculation, the factors were rotated by the VARIMAX

method (Kaiser, 1958) which attempts to maximize differences between resulting eigenvectors (factors). The principal component factoring (PCF) method was applied for the factors analyzed.

2.2.5 Trajectory Analysis

HYSPLIT (Hybird Single-particle Lagrangian Intergrated Trajectory v 4.7) was used to compute air mass back-trajectories (Draxler, 2003). HYSPLIT was run interactively on the web (http://www.arl.noaa.gov/ready/open/hysplit4.html) through the READY system. Two-day (48 hr) backward trajectories were run for ending heights of 100 m AGL (above ground level).

2.3 Methodology

Detailed procedures for aerosol and trace gas sampling (URG, MOUDI, and PILS) are described in Appendix B, Standard Operating Procedures (SOP). Discussion here focuses on analytical methodologies used for chemical analysis of collected samples along with sample handling and extraction procedures.

2.3.1 Sample analysis

The inorganic ion analysis for URG annular denuder/filter and MOUDI was completed using two DIONEX DX-500 series ion chromatography at Colorado State University. A DIONEX AG4A-SC column, AS4A-SC separation column and a self-regenerating anion suppressor (ASRS-ULTRA II) were used to quantify concentrations of major anions (Cl^-, SO_4^{2-}, NO_3^-). The cation setup used to find concentrations of major

cations (Na^+, NH_4^+, K^+, Mg^{2+} and Ca^{2+}) has a CG12A guard column and a CS12A separation column and a self-regenerating cation suppressor (CSRS-ULTRA II). The cation and anion systems were operated at flow rates of 1.0 mL/min (20mM methanesulfonic acid (MSA), 50uL sample injection volume) and 2.0 mL/min (1.8mM Na_2CO_3/1.7mM $NaHCO_3$, 25uL sample injection volume), respectively.

Two DIONEX DX-500 series ion chromatographs were also used with the PILS system. Each system consisted of a 6-port valve injector (Alltech, #85525, Fluid Processor 6-Port) fitted with a 200μL sample loop, a pump (DIONEX GP40 or IP20), DIONEX CD20 conductivity detector, an analytical separation column, and a suppressor. The cation eluent was 20mM MSA at a flow rate of 1.0mL/min (CG12A/CS12A column and CSRS-ULTRA II suppressor). The anion system used either an AS4A-SC/AG4A-SC column pair (1.8mM Na_2CO_3/1.7mM $NaHCO_3$ eluent) or an AS14A column (8mM Na_2CO_3/ 7mM $NaHCO_3$ eluent) with an ASRS-ULTRA II suppressor.

Laboratory IC calibrations were performed daily using anion and cation standards prepared from stock solutions made from analytical grade salts. Calibration of the PILS IC systems was performed approximately every 10 days in the field. Dilutions of NIST traceable ion standards from DIONEX were used to evaluate calibration accuracy. Deionized water (>18 Megohm-cm) freshly prepared was used in the field and laboratory for standard preparation. Measurement precision for laboratory analyses was determined based on replicate injections. Detailed quality assurance/quality control procedures are described in section 2.3.

2.3.2 Denuder and filter handling

Denuders are soaked and cleaned with deionized water before coating. The first denuder was coated with 10mL of ~ 1% (W/V) Na_2CO_3 solution (10g of Na_2CO_3 and glycerol in 500mL of deionized and 500mL of methanol) to collect nitric acid (HNO_3) and sulfur dioxide (SO_2). The second denuder was coated with 10mL of 1% (W/V) phosphorous acid in 1:9 water/methanol to collect ammonia (NH_3). After coating, the denuders were dried with clean N_2 gas or clean air scrubbed of interfering contaminants at a flow rate of ~2-3 mL/min for about 5-10 minutes. The clean air was generated by passing air through silica gel (removing moisture), an ammonia scrubber column (Phosphoric acid coating media, AS-200-08-E, Perma Pure Inc.), Purafil column (potassium permanganate on alumina, #7075, Perma Pure Inc.) which oxidizes NO to NO_2, a column of activated charcoal to remove NO_2, SO_2, O_2 and hydrocarbons, and a HEPA capsule filter (12144, Pall Life Sciences). Denuder blanks were found to be very low in both N_2 and clean air drying systems (see Appendix D). Each denuder was extracted using deionized water immediately on-site after sampling. Extracts were refrigerated at 5°C until completion of anion and cation analyses in the laboratory.

The substrate used in the MOUDI was a grease coated aluminum foil (47mm). After an oil containing silicone was applied onto the substrate, it is necessary to bake the substrates in an oven at 65°C for 90 minutes. Grease coated and baked substrates were prepared at CSU and transported to the field. Preparation of URG filter packs was performed in a clean, ammonia-free glove box (a Plexiglas box with a column of a phosphoric acid ammonia scrubber) to prevent contamination by NH_3. After sampling, MOUDI and URG filter samples were stored in filter extract tubes (16mL Polystyrene,

Falcon). Sample tubes were kept in a freezer in sealed plastic bags containing ammonia removal towels soaked with 10% phosphoric acid solution during the field study and later in the laboratory prior to anion and cation analyses.

2.3.3 Denuder and filter extraction and aliquots

Each denuder was extracted with 10mL of deionized water for 10 minutes. The extracts from the ammonia denuders were stored in 5mL cryovials (Nalgene) and 600μL polypropylene IC vials (Sun-Sri, #700-025). 10μL of 30% H_2O_2 was added to 5mL extracts of the nitric acid denuders in 5mL cryovials to fully convert dissolved SO_2 to SO_4^{2-} and 600μL of extract was transferred to an IC vial. 1.4mL of residual extract from the nitric acid denuders was stored in a 1.5mL glass vial with 50μL of chloroform for possible later organic acid analysis. All extracts were refrigerated at 5 °C until anion and cation analyses in the laboratory.

The Nylon filters (Nylasorb, pore size 1.0μm, 37mm (or 47mm), Pall Life Sciences) were extracted either with 5mL (or 6mL) deionized water or with 5mL (or 6mL) anion IC eluent (1.8mM Na_2CO_3/1.7mM $NaHCO_3$). The Teflon filters (Teflo, pore size 2.0μm, 37mm (or 47mm), Pall Life Sciences) were extract with 4.95mL (or 5.9mL) of deionized water with 50μL (or 100μL) of ethanol added first to help wet the hydrophobic filter surface. Filters were extracted in screw-top 16mL polystyrene tubes (Falcon) in an ultrasonic bath (Branson, 5210) for 40-45 minutes. MOUDI impaction substrates and Teflon after-filters were extracted in screw-top 16mL polystyrene tubes with 5mL of deionized water and 4.95mL/50μL of deionized water/ethanol, respectively, also in the ultrasonic bath for 40-45 minutes. 600μL of extract from both nylon and Teflon filters and MOUDI substrates were refrigerated in IC vials for anion and cation

analyses. Remaining extract in a 5mL cryovial was refrigerated for possible future use. Table 2.2 shows the summary of each chemical coating and extract solution and the volumes used for each denuder and filter type.

2.4 Quality assurance and control

In order to both improve and validate the quality of data generated as part of this project, a quality assurance (QA) program was designed and implemented. Included in this QA program were a variety of quality control (QC) procedures. An explanation of these steps is provided below, along with an explanation of key calculations and a summary of key information regarding measurement precision and accuracy.

2.4.1 Sample blanks and replicates

Denuder/filter pack blanks were taken several times during each field campaign, leaving them in the URG sampling housing box (URG-2000-01A) without flow for ~24hr, and then retrieving and processing them the same way as samples. Replicate samples were collected 4-5 times during each field study from the module 3.1 configuration.

MOUDI blanks were taken for all impactor stages at the beginning and end of each field campaign. An additional blank set was taken once in the middle of each field campaign before a MOUDI cleaning procedure was performed. There are no replicate MOUDI samples, except for the Yosemite National Park campaign, due to the lack of a second sampler in other campaigns.

Table 2.2 Chemical solution and volume for coating and extracting of denuders/filters

Denuder Yosemite/Nitrate special study		Coating Na_2CO_3*	Coating Phosphoric acid**	Extracting DI water	Measuring Species
HNO_3 Denuder		10mL		10mL	HNO_3, SO_2
NH_3 Denuder			10mL	10mL	NH_3
					NH_4^+ for backup NH_3 denuder
Filter pack/MOUDI Yosemite		**Ethanol**	**Extracting DI water**	**IC eleunt**	
URG Filter pack	Teflon (47mm)	100μL	5.9mL		Anions[1] and Cations[2]
	nylon (47mm)			6mL	NO_3^-
MOUDI	Teflon (37mm)	50μL	4.95mL		Anions[1] and Cations[2]
	Substrate (47mm)		6mL		Anions[1] and Cations[2]
Filter pack/MOUDI Nitrate Special Study		**Ethanol**	**Extracting DI water**	**IC eleunt**	
Module 1	1st nylon(37mm)		5mL		Anions[1] and Cations[2]
	2nd nylon(37mm)			5mL	NO_3^-
Module 2	1st nylon(37mm)			5mL	Anions[1]
Module 3.1	1st nylon (37mm)		5mL		Anions[1] and Cations[2]
	2nd nylon (37mm)			5mL	NO_3^-
Module 3.2,3, and 4	Teflon(37mm)	50μL	4.95mL		Anions[1] and Cations[2]
	nylon(37mm)			5mL	NO_3^- Except for [HNO3]+[NO3-] in Module 3.4
MOUDI	Teflon(37mm)	50μL	4.95mL		Anions[1] and Cations[2]
	Substrate(47mm)		5mL		Anions[1] and Cations[2]

* : 10g of Na_2CO_3 and glycerol in 500mL of deionized and 500mL of methanol
** : 1% (W/V) phosphorous acid in 1:9 water/methanol
1 : Cl^-, SO_4^{2-}, NO_3^-
2 : Na^+, NH_4^+, K^+, Mg^{2+} and Ca^{2+}

PILS/IC blanks were taken every 5-6 days after a calibration check standard was injected. Blanks were taken by sampling particle-free air, drawn through a HEPA capsule filter (12144, Pall Life Sciences), through PILS/IC system. Every 10 days the PILS/IC was cleaned and the ion chromatographs recalibrated.

Procedures for laboratory analytical blanks, calibrations, and replicate analyses were described above.

2.4.2 Flow determination and concentration calculations

A dry gas meter (Gallus 2000, URG-3000-02C) was installed in-line between the URG filter pack (or MOUDI) and vacuum pump in order to provide an integrated measure of total sample flow. The sample volume measured by the dry gas meter was corrected to ambient conditions by correcting for the measured pressure drop through the sampler. Flows for the PILS/IC and the MOUDI were provided by vacuum pumps and controlled by a critical orifice (O'keefe Controls Co., Metal Orifice #60) with a vacuum regulator (Coast Pneumatics Inc., VR1000-NO1) and a flow controller valve, respectively. Flow for the PILS was verified by use of an independent flow calibration check (Sensidyne Gilibrator). Flow for the URG sampler was provided by a vacuum pump and a mass flow controller. The mass flow rate of the URG (Pump, URG-3000-02BA) was corrected for typical temperature and pressure conditions at Yosemite National Park. For the later studies, on-line temperature and pressure corrections were made to maintain a constant volumetric flow rate of the URG (Pump, URG-300-02BAM) sampler. Table 2.3 shows calculations for the corrections of the flow and the sample

volume (Wight, 1994). The concentrations of all species were calculated using the procedures described in Table 2.4.

2.4.3 Accuracy, Precision, and MDL

Measurement precision was determined by replicate measurements and/or sample analyses. Measurement accuracy of sample analyses was determined by measurement of independent calibration check solutions. Accuracy and precision results are expressed as relative error (%) and CV (Coefficient of Variation), respectively (Skoog et al., 1992).

Table 2.3 Calculation of the corrected flow rate and actual sampling volume

Instrument	Corrected flow rate	Actual sampling volume
URG	Q_v (LPM) = Q_s(SLPM) · (P_s/P_I)·(T_I/T_s)	$V_{air}(m^3) = (F_v\text{-}I_v) \cdot \left(1 - \left(\frac{(Fp - Ip)/2}{Pa}\right)\right)$
MOUDI	The upper magnehelic (magnehelic 1) →20.7 inches of water	
PILS/IC	Vacuum regulator set → 9.5 - 10 inches of Hg Actual flow rate was measured by Gilibrator (Sendidyne Inc.) at each site Orifice #60 : Flow range from 14.6 to 18.2 SLPM between 5 and 10 inches of Hg V_{air} (m^3) = 16.7 l/min × time (min)	

Q_s : the flow rate at standard conditions in SLPM
Q_v : the desired ambient volumetric flow rate (LPM)
P_s : the standard condition pressure (mm Hg)
P_I : the ambient pressure (mm Hg)
T_s : the standard condition temperature (294.18 K)
T_I : the ambient temperature (K)
I_v and F_v : Dry gas meter reading at the start and end, respectively (m^3)
I_p and F_p : pressure drop reading at the start and end, respectively (either inches of Hg(water) or PSI)
P_a : the ambient pressure (either inches of Hg(water) or PSI)

Table 2.4 Calculation of the concentration for all species

Species ($\mu g/m^3$)	Equation*	Comments
HNO_3, NH_3, SO_2 (URG & MOUDI)	$\frac{C_f \times C_s(\mu N) \times E_v(L) \times MW_s(\mu g)}{Vair(m^3)}$	Ion Conversion Factor HNO_3 : 1.016 NH_3 : 0.994 SO_2 : 0.667
Cl^-, SO_4^{2-}, NO_3^- Na^+, NH_4^+, K^+, Mg^{2+} and Ca^{2+} (URG & MOUDI)	$\frac{C_s(\mu N) \times E_v(L) \times MW_s(\mu g)}{Vair(m^3)}$	
Cl^-, SO_4^{2-}, NO_3^- Na^+, NH_4^+, K^+, Mg^{2+} and Ca^{2+} (PILS)	$\frac{R \times C_s(\mu N) \times Q_v(L) \times MW_s(\mu g)}{Vair(m^3)}$	R > 1.0
H^+ ($\mu eq/m^3$) (URG)	$([H^+](\mu N) \times E_V(L))/V_{air}(m^3)$	

* : C_f (conversion factor), C_S (the concentration of species measured by IC, μN), E_V (or Q_V)(the extract volume, L), MW_S (the molecular weight of species), R (dilution factor, The ratio of the internal Li^+ (or Br^-) standard concentration to the Li^+ (or Br^-) concentration measured by the PILS/IC), and V_{air} (actual sampling volume, Table 2.3)

Calibration standards for the IC were prepared from stock solutions made using known concentrations of analytical grade salts. The accuracy of determined major ion concentrations was verified by analysis of dilutions of independent, NIST-traceable ion standards from Dionex (Dionex calibration checks, Table 2.5). IC measurement precision was verified using repetitive analysis of calibration standards. A standard was analyzed once for every 10 sample analyses and several standards were analyzed at the end of each IC run in the laboratory or every 5 days of PILS operation in the field.

Measurement precision for concentrations measured using the URG sampler were determined based on periodic collection and analysis of replicate samples, as described above. Measurement precision for MOUDI samples was based on replicate sampling in Yosemite, but only on replicate sample analysis for the other studies where only one MOUDI sampler was available. Measurement precision ia presented as a RSD (Relative Standard Deviation, %) (Skoog et al., 1992).

Table 2.5 Concentrations of Dionex check standards

Anion	Stock (μN)*	Dionex check 1 1:100 (μN)	Dionex check 2 1:20 (μN)	
Chloride	846.19	8.46	42.30	
Bromide	1251.50	12.52	62.58	
Nitrate	1611.21	16.11	80.56	
Sulfate	3123.13	31.21	156.15	
Cation	**Stock (μN)***	**Dionex check 1 0.075:100(μN)**	**Dionex check 2 0.15:100 (μN)**	**Dionex check 2 1:100 (μN)**
Lithium	7217.98	5.41	10.83	72.18
Sodium	8699.51	6.52	13.05	86.99
Ammonium	13859.28	10.39	20.79	138.59
Potassium	12788.28	9.59	19.18	127.88
Magnesium	20571.90	15.43	30.86	205.72
Calcium	24950.10	18.71	37.43	249.50

*** : Dionex provides the concentrations as ppm**

The MDL (Minimum Detection Limit at the 95% confidence limit) was determined for URG, MOUDI, and PILS measurements. To determine the MDL for each measured species, collection and analysis of blank samples was used. In cases where analyte was not detected in collected blanks, the MDL was calculated using the variability of the lowest analytical standard concentration.

Table 2.6 shows the equations used for calculations of accuracy, precision, and MDL (Skoog et al., 1992). Results are described in the following sections.

Analytical accuracy and precision

Table 2.7 summarizes the accuracy and precision of IC analyses based on Dionex calibration checks (accuracy) and repetitive calibration standard analysis (precision). Most ion concentrations exhibited good accuracy (in the range of - 4 to + 8.5 %) and a high precision (generally a few percent RSD, except for the lowest calibration standard).

Minimum Detection Limits (MDL)

MDL values at the 95% confidence limit of the major ionic species are summarized in Table 2.8. The MDL of each species measured in URG samples was calculated separately for nylon and Teflon filter blanks. Calculated detection limits were generally low compared to concentrations of these species in ambient samples.

Overall measurement precision

Using samples collected and analyzed in duplicate, we are able to determine the overall measurement precision for individual methods and species. This precision incorporates uncertainty associated with media preparation, sampler flow rate, sample handling, sample extraction, and sample analysis. Measurement precision expressed as RSD (%) ranged from 5 to 9 % for the major measured aerosol and gas species (Tables 2.9 and 2.10). Trace aerosol species (Cl^-, Na^+, K^+, Mg^{2+}, and Ca^{2+}) had higher RSDs, ranging from 12 – 27%. Lower measurement precision is expected as concentrations approach MDL.

MOUDI measurement precision was calculated separately using replicate MOUDI measurements from Yosemite National Park and replicate sample analyses from other independently (Table 2.10). Measurement precisions determined by both approaches are in the range of 2-7% (RSD) for the three major aerosol components (nitrate, sulfate, and ammonium), with somewhat larger RSDs for trace species.

Table 2.6 The equations for the accuracy, precision, uncertainties, and MDL

Quality control	Data used	Equation
Accuracy	Dionex Calibration checks	Absolute Error, $E = X_i - X_t$ or Relative Error, $E_r(\%)=((X_i-X_t)/X_t) \times 100\%$ (Where X_i is the measurement of a quantity and X_t is true value)
Analytical Precision	Periodic analyses of calibration standards	CV = (Standard Deviation/ $\overline{X}$) × 100%
Overall Measurement Precision	Replicate sample results or replicate analyses of samples	RSD (Relative Standard Deviation) $= \frac{Spooled^*}{\overline{X}} \times 100\%$ Where $\overline{X}$ represents the average of all replicate data points
MDL @95% Confidence limit	Method blanks (or replicate analysis of low concentration standards)	$MDL \geq t \times S_b \times \sqrt{\frac{N_1+N_2}{N_1 \times N_2}}$ t value given at the 95% confidence level for the appropriate of degrees of freedom S_b is the blank standard deviation N_1 and N_2 is the number of sample measurements (single measurement, N_1=1), the number of analyzed blanks.

Source: (Skoog et al., 1998; Skoog et al., 1992)

$$* : S_{pooled} = \sqrt{\frac{\sum_{i=1}^{N1}\left(X_i-\overline{X_1}\right)^2+\sum_{j=1}^{N2}\left(X_j-\overline{X_2}\right)^2+\sum_{k=1}^{N3}\left(X_k-\overline{X_3}\right)^2+\bullet\bullet\bullet}{N_1+N_2+N_3+\bullet\bullet\bullet-Ns}}$$

Where N_i and N_s represent the number of replicated data points in set "i" and the total number of data sets pooled, respectively. $\overline{X_1}$ and $\overline{X_2}$ are the average concentrations of replicates in set 1 and set 2, respectively, and so forth.

Table 2.7 Accuracy and precision of standard analyses for ion species

Species		Nominal (μN)	$\overline{X}$ (μN)	Standard Deviation	Accuracy (%)	Precision (%)	# of samples
Cl^-	Dionex 1:100	8.462	8.42	0.196	-0.6	2.3	49
	Dionex 1:20	42.31	43.70	0.889	3.3	2.0	49
	Standard 1	1	1.21	0.210		17.4	49
	Standard 3	10	9.74	0.300		3.1	49
	Standard 4	20	19.49	0.738		3.7	194
	Standard 5	50	49.56	0.833		1.7	49
NO_3^-	Dionex 1:100	16.13	16.36	0.724	1.5	4.4	49
	Dionex 1:20	80.64	80.18	1.824	-0.6	2.3	49
	Standard 1	2	2.07	0.246		11.9	49
	Standard 3	20	19.90	0.735		3.7	49
	Standard 4	40	39.02	0.907		2.3	194
	Standard 5	100	98.78	1.207		1.2	49
SO_4^{2-}	Dionex 1:100	31.23	31.76	0.684	1.7	2.2	49
	Dionex 1:20	156.15	158.63	3.323	1.6	2.1	49
	Standard 1	2	2.11	0.400		18.9	49
	Standard 3	20	19.63	0.851		4.3	49
	Standard 4	40	39.31	0.977		2.4	194
	Standard 5	100	98.52	1.166		1.2	49
Na^+	Dionex 0.075:100	6.56	6.73	0.446	2.7	6.6	46
	Dionex 0.15:100	13.12	13.42	0.440	2.3	3.3	46
	Dionex 1:100	87.43	87.20	6.011	-0.3	6.9	46
	Standard 1	1	1.13	0.192		17.0	46
	Standard 3	10	9.99	0.322		3.2	46
	Standard 4	20	20.13	0.701		3.5	164
	Standard 5	50	49.90	0.965		1.9	46
NH_4^+	Dionex 0.075:100	10.52	11.37	0.954	8.1	8.4	46
	Dionex 0.15:100	21.04	21.56	0.859	2.5	4.0	46
	Dionex 1:100	140.25	144.51	5.008	3.0	3.5	46
	Standard 1	2	2.24	0.375		6.7	46
	Standard 3	20	19.76	1.051		5.3	46
	Standard 4	40	39.42	1.951		5.0	164
	Standard 5	100	99.83	5.335		5.3	46
K^+	Dionex 0.075:100	9.65	9.98	0.360	3.5	3.6	46
	Dionex 0.15:100	19.30	19.76	0.651	2.4	3.3	46
	Dionex 1:100	128.65	123.59	6.909	-3.9	5.6	46
	Standard 1	1	1.18	0.157		13.3	46
	Standard 3	10	9.08	0.346		3.5	46
	Standard 4	20	19.95	0.593		3.0	164
	Standard 5	50	49.88	1.767		3.5	46
Mg^{2+}	Dionex 0.075:100	15.43	16.72	2.569	8.4	15.4	46
	Dionex 0.15:100	30.86	32.40	1.720	5.0	5.3	46
	Standard 1	1	1.25	0.211		16.8	46
	Standard 3	10	8.01	0.433		5.4	46
	Standard 4	20	20.09	1.882		9.4	164
	Standard 5	50	49.87	1.539		3.1	46
Ca^{2+}	Dionex 0.075:100	18.96	18.93	2.854	-0.1	15.1	46
	Dionex 0.15:100	37.88	38.58	2.974	1.8	7.7	46
	Standard 1	1	1.23	0.140		11.3	46
	Standard 3	10	8.68	0.692		8.0	46
	Standard 4	20	20.48	1.859		9.1	164
	Standard 5	50	50.22	2.913		5.8	46

Table 2.8 Minimum Detection Limit (MDL) for URG, MODUI, and PILS/IC

Species	S_b(μN)	N_1	N_2	t (Degrees of Freedom)	MDL (μN)	MDL[a] (μg/m^3)
URG annular denuder/filter pack (nylon filters from Module 1)[b]						
Cl^-	0.618	1	24	1.96 (23)	1.24	0.018
NO_3^-	1.364	1	24	1.96 (23)	2.73	0.068
SO_4^{2-}	1.196	1	24	1.96 (23)	2.39	0.046
Na^+	0.458	1	24	1.96 (23)	0.92	0.009
NH_4^+	2.092	1	24	1.96 (23)	4.18	0.030
K^+	0.471	1	24	1.96 (23)	0.94	0.015
Mg^{2+}	1.137	1	24	1.96 (23)	2.28	0.022
Ca^{2+}	1.213	1	24	1.96 (23)	2.43	0.039
HNO_3	0.581	1	45	1.96 (23)	1.15	0.058
NH_3	2.913	1	45	1.96 (23)	5.74	0.084
SO_2	0.719	1	45	1.96 (23)	1.42	0.037
URG annular denuder/filter pack (Teflon filters from all sites)[c]						
Cl^-	0.603	1	13	1.96 (12)	1.23	0.017
NO_3^-	1.272	1	13	1.96 (12)	2.59	0.064
SO_4^{2-}	3.176	1	13	1.96 (12)	6.46	0.124
Na^+	1.734	1	13	1.96 (12)	3.53	0.032
NH_4^+	3.511	1	13	1.96 (12)	7.14	0.051
K^+	0.635	1	13	1.96 (12)	1.29	0.020
Mg^{2+}	1.883	1	13	1.96 (12)	3.83	0.037
Ca^{2+}	1.817	1	13	1.96 (12)	3.70	0.007
PILS (all sites)[d]						
Cl^-	0.285	1	55	1.96 (54)	0.56	0.082
NO_3^-	0.169	1	55	1.96 (54)	0.33	0.085
SO_4^{2-}	0.158	1	55	1.96 (54)	0.31	0.061
Na^+	0.144	1	55	1.96 (54)	0.28	0.027
NH_4^+	0.193	1	55	1.96 (54)	0.38	0.028
K^+	0.185	1	55	1.96 (54)	0.37	0.059
Mg^{2+}	0.088	1	55	1.96 (54)	0.17	0.017
Ca^{2+}	0.415	1	55	1.96 (54)	0.82	0.135
	MOUDI[e] /MOUDI (Yosemite NP)					**ng/m^3**
Cl^-	0.699/0.619	1/1	171/70	1.96 (170/69)	1.23/1.22	5.45/6.94
NO_3^-	0.795/9.425	1/1	171/70	1.96 (170/69)	2.54/0.84	11.1/8.33
SO_4^{2-}	0.472/0.241	1/1	171/70	1.96 (170/69)	1.43/0.48	4.54/3.65
Na^+	0.896/0.237	1/1	171/70	1.96 (170/69)	2.39/0.47	3.87/1.72
NH_4^+	0.557/0.173	1/1	171/70	1.96 (170/69)	1.78/0.44	2.26/0.99
K^+	1.053/0.215	1/1	171/70	1.96 (170/69)	2.33/0.43	6.41/2.66
Mg^{2+}	0.916/0.223	1/1	171/70	1.96 (170/69)	3.52/0.44	3.01/0.86
Ca^{2+}	1.181/0.362	1/1	171/70	1.96 (170/69)	5.23/0.72	7.38/2.29

a: to express MDL as μg/m^3, the average 24hr and 48 hr sampling volume set were used for URG and MOUDI (24 hr sampling volume was applied for Yosemite NP MOUDI), respectively

b: nylon filters and denuders from module 1 of all sites except for Yosemite National Park

c: Teflon filters from all sites, Bondville, Brigantine, Grand Canyon NP, San Gorgonio, Great Smoky Mts. NP

d: Bondville, Brigantine, Grand Canyon NP, San Gorgonio, Great Smoky Mts. NP and Yosemite NP

e: Bondville, Brigantine, Grand Canyon NP, San Gorgonio, and Great Smoky Mts. NP

Table 2.9 URG uncertainties [RSD (%)] of measured aerosol species

Species	$\overline{X}$ ($\mu g/m^3$)	Std. Dev. Pooled ($\mu g/m^3$)	# of data set (N_s)	# of samples (N)	RSD (%)
URG annular denuder/filter pack (Teflon filter from Yosemite NP)					
Cl^-	0.008	0.002	14	24	25.0
NO_3^-	0.304	0.023	14	24	7.5
SO_4^{2-}	1.147	0.034	14	24	2.9
Na^+	0.085	0.003	14	24	3.8
NH_4^+	0.453	0.011	14	24	2.5
K^+	0.047	0.002	14	24	4.7
Mg^{2+}	0.012	0.001	14	24	8.4
Ca^{2+}	0.028	0.003	14	24	11.9
HNO_3	1.824	0.074	14	24	4.1
NH_3	1.529	0.046	14	24	3.0
SO_2	0.644	0.024	14	24	3.7
URG annular denuder/filter pack (nylon filter from module 1 and 2)*					
Cl^-	0.07	0.016	30	60	22.2
NO_3^-	2.36	0.133	31	62	5.6
SO_4^{2-}	1.75	0.114	31	62	6.5
Na^+	0.07	0.007	31	62	9.8
NH_4^+	1.07	0.053	31	62	4.9
K^+	0.07	0.016	31	62	21.8
Mg^{2+}	0.02	0.003	31	62	10.7
Ca^{2+}	0.12	0.009	31	62	7.3
HNO_3	0.56	0.046	26	52	8.3
NH_3	2.13	0.062	26	52	4.0
SO_2	0.99	0.085	31	62	6.3

* : Bondville, Brigantine, Grand Canyon NP, San Gorgonio, and Great Smoky Mts NP.

Table 2.10 MOUDI uncertainties [RSD (%)] of measured aerosol species using the replicate samples and analyses.

Species	$\overline{X}$ ($\mu g/m^3$)	Std. Dev. Pooled ($\mu g/m^3$)	# of data sets (N_s)	# of samples (N)	RSD (%)
MOUDI (using the replicate samples at Yosemite NP)					
Cl^-	0.005	0.001	6	12	22.9
NO_3^-	0.073	0.005	6	12	6.2
SO_4^{2-}	0.1	0.004	6	12	4.2
Na^+	0.022	0.003	6	12	13.0
NH_4^+	0.047	0.003	6	12	6.4
K^+	0.014	0.003	6	12	21.6
Mg^{2+}	0.002	0.001	6	12	27.4
Ca^{2+}	0.005	0.001	6	12	24.9
MOUDI (using the replicate analyses at other sites)*					
Cl^-	0.009	0.001	73	146	9.4
NO_3^-	0.453	0.018	73	146	3.9
SO_4^{2-}	1.108	0.030	74	148	2.7
Na^+	0.013	0.001	72	144	3.4
NH_4^+	0.348	0.008	75	150	2.4
K^+	0.018	0.001	73	146	6.2
Mg^{2+}	0.006	0.001	74	148	7.4
Ca^{2+}	0.019	0.001	77	154	7.6

*: Bondville, Brigantine, Grand Canyon NP, San Gorgonio, and Great Smoky Mts NP

2.5 Data quality

2.5.1 Comparison of $PM_{2.5}$ URG and size-resolved aerosol MOUDI

Ratios of anions to cations should follow the 1:1 line, if all ionic species in a sample were measured accurately. Charge neutrality (the sum of anions = the sum of cations) was investigated in $PM_{2.5}$ URG samples for each site shown in Figure 2.7. The average charge balance ratio was observed as 1.19 (anions/cations), with a standard deviation of 0.12, based on observations in Bondville, San Gorgonio (April and July) and Brigantine, indicating most major anion and cation species were measured accurately, while the charge balance averaged 0.76 (range of 0.66 – 1.16), determined in Grand Canyon N.P., suggests missing minor anion species, such as organic acid species (Carrico et al., 2004), [CO_3^{2-}] and/or [HCO_3^-] associated with mineral dust (which had not been measured in that study). On the other hand, the charge balances were close to the expected slope value of 1.04 from 0.52 when [H^+] was included during the Great Smoky Mountains N.P. study, indicating that measuring H^+ is important for a complete understanding of ionic species contributions in an acidic environment (Lee et al., 1993; Lee et al., 2004).

To validate the MOUDI chemical analysis results, the ionic concentrations of $PM_{2.5}$ URG samples were compared to the sum of aerosol concentrations from stage 4 to the after filter of the MOUDI sampler (i.e., the sum from zero to 3.2 μm aerodynamic diameter) for the major ionic species (SO_4^{2-}, NO_3^- and NH_4^+). Figures 2.8, 2.9 and 2.10 show concentrations averaged over two days of the major ionic species measured with the URG sampler plotted against those from the MOUDI sampler. The concentrations of sulfate show a good correlation between URG and MOUDI data with R^2 values ranging

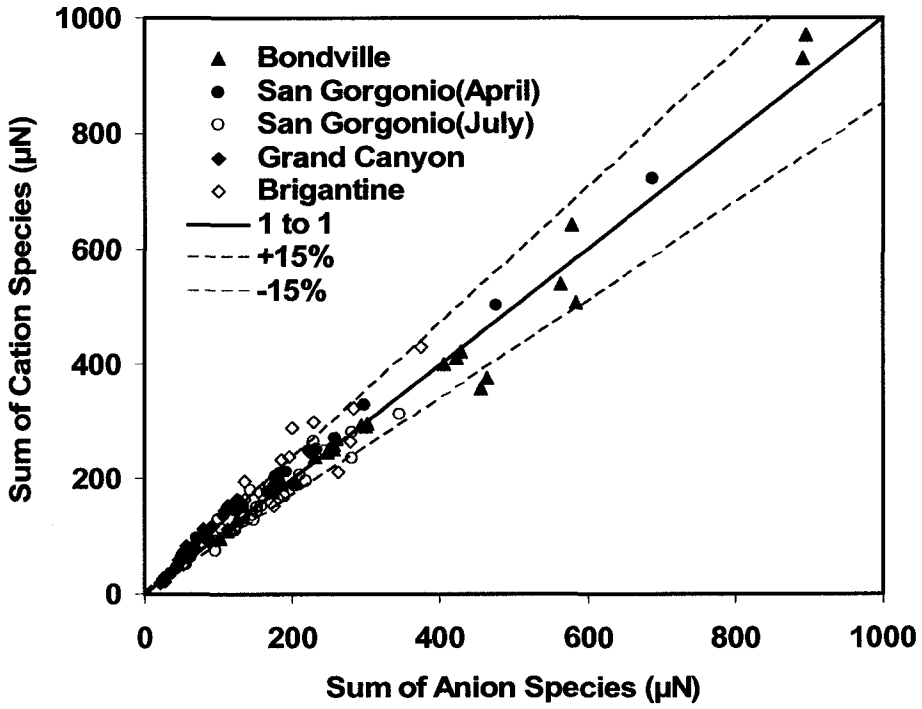

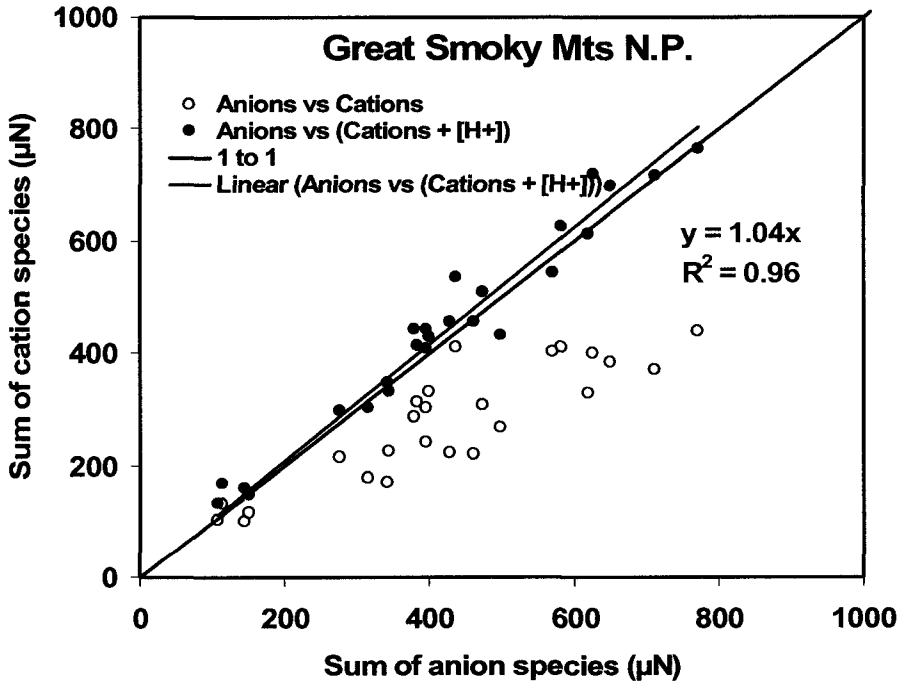

Figure 2.7 Ion charge balance for $PM_{2.5}$ samples

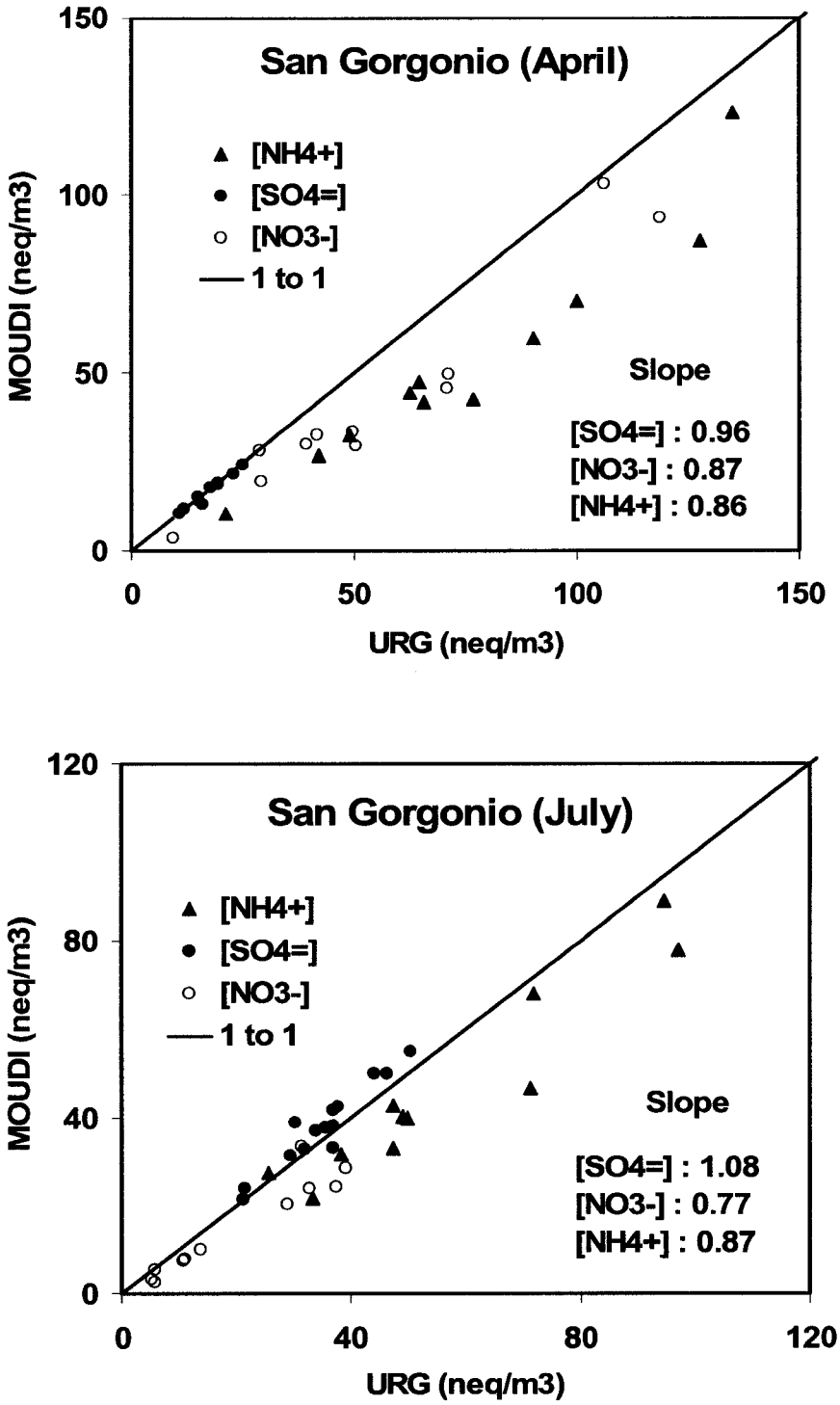

Figure 2.8 Comparisons of concentrations of ammonium, sulfate and nitrate in $PM_{2.5}$ URG versus MOUDI samples (San Gorgonio (April and July))

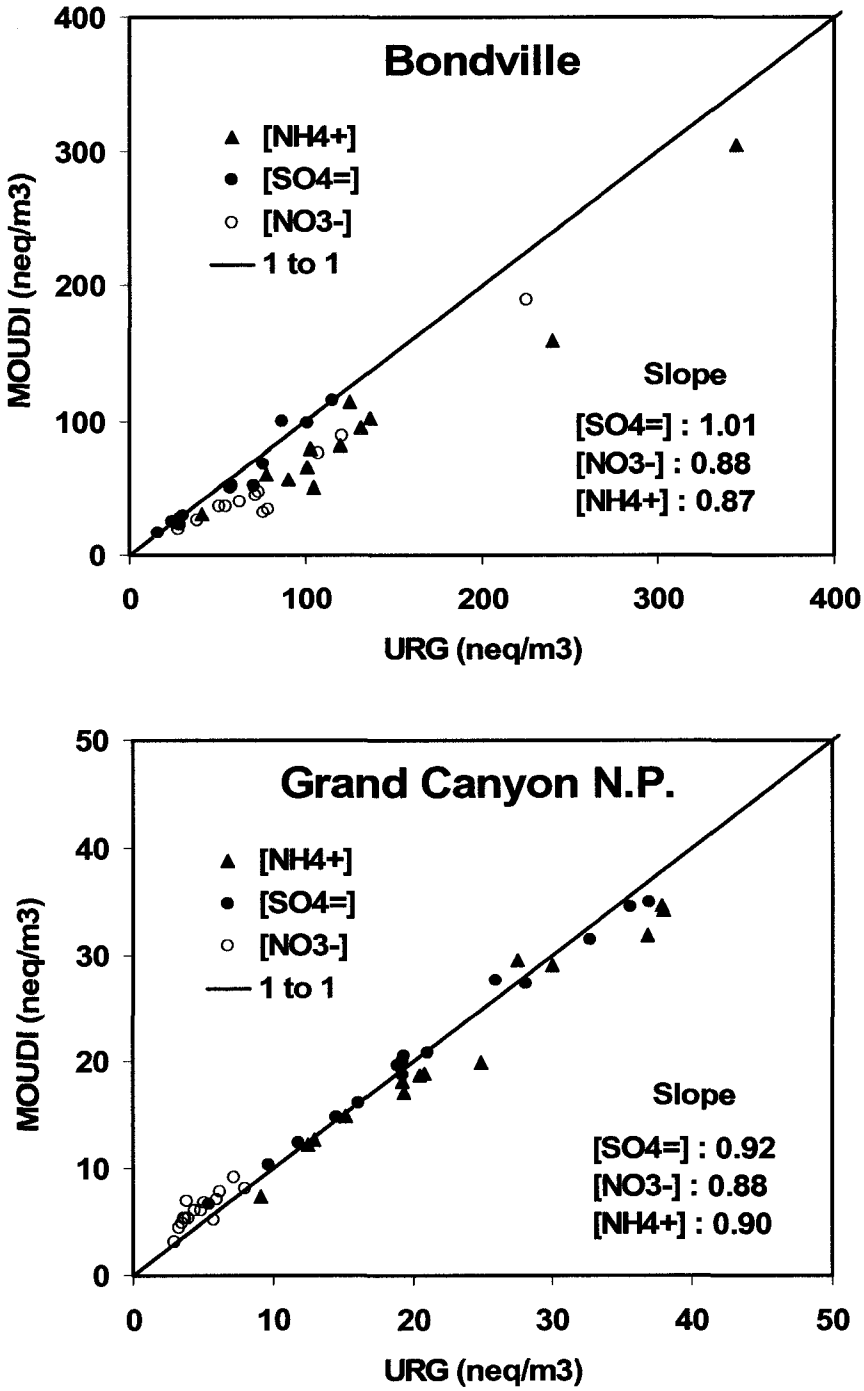

Figure 2.9 Comparisons of concentrations of ammonium, sulfate and nitrate in $PM_{2.5}$ URG versus MOUDI samples (Bondville and Grand Canyon N.P.)

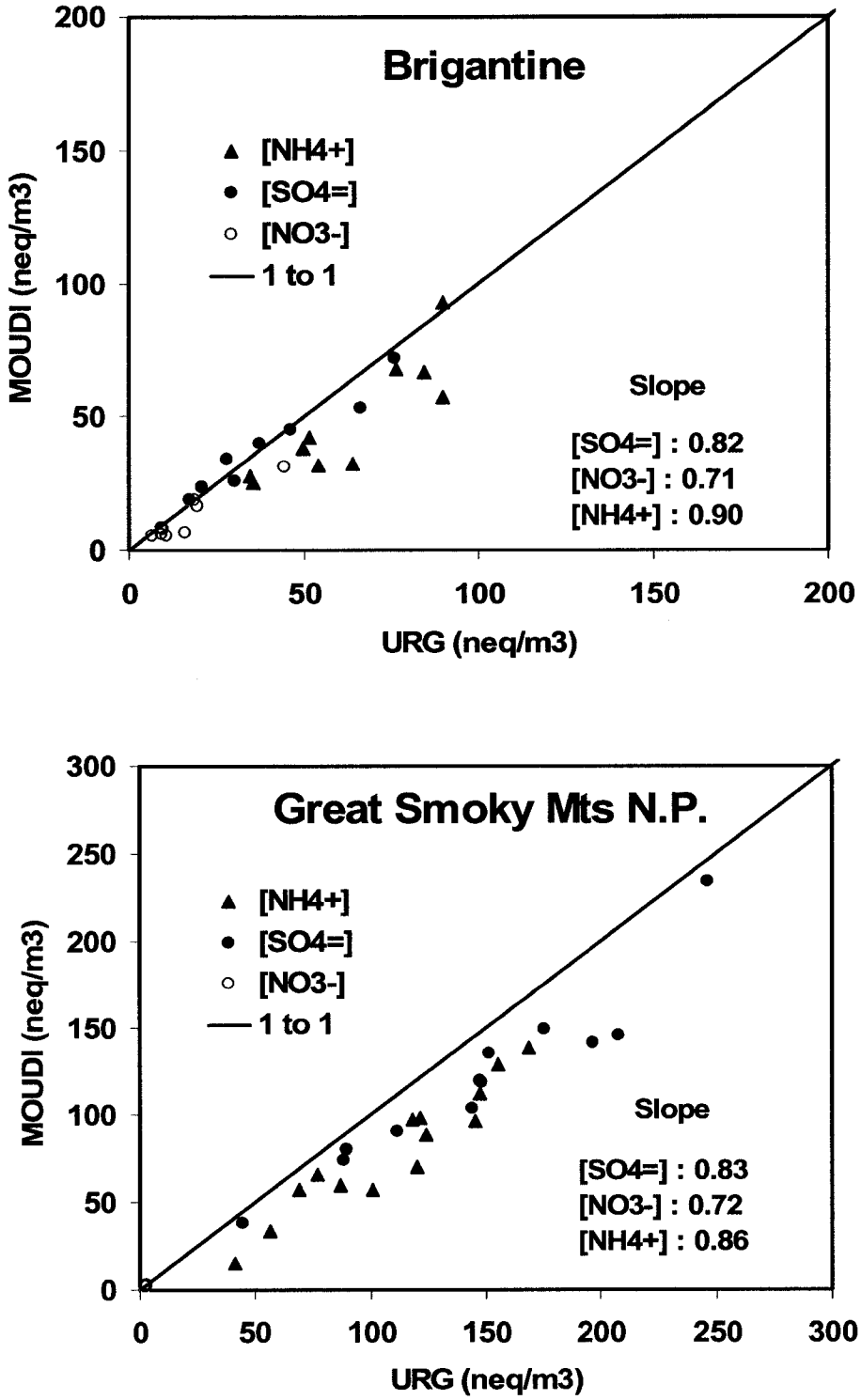

Figure 2.10 Comparisons of concentrations of ammonium, sulfate and nitrate in $PM_{2.5}$ URG versus MOUDI samples (Brigantine and Great Smoky Mts N.P.)

from 0.86 to 1.08, while relatively low correlations (ranging from $R^2 = 0.72$ to $R^2 = 0.90$) were observed for nitrate and ammonium, likely because the lower tail of coarse mode nitrate often appears to be a fraction of $PM_{2.5}$ nitrate measurements and also due to the mismatch in measured size ranges. In addition, relatively longer time-integrated sampling might lead to greater errors in the impactor sampler such as possible ammonium and nitrate loss by thermodynamic dissociation of NH_4NO_3 in the impactor sampler, resulting in the discrepancies of the particulate concentration between impactor sampler and URG sampler corrected by artifacts(Chang et al., 2000; Kerminen et al., 2001; Sioutas et al., 1997; Zhang and McMurry, 1987; Zhang and McMurry, 1992).

2.5.2 Comparison of $PM_{2.5}$ URG and semi-continuous PILS

Filter-based sampling has traditionally been the standard technique for measuring aerosol chemical properties. The concentrations averaged over 24-hr of major ionic species (of sulfate, nitrate and ammonium) from PILS were directly compared against those from URG 24-hr integrated filter measurements. The selected days where the PILS data covered more than 90% of the filter sampling time were used for the comparison between URG and PILS data. The data from Bondville and Brigantine combined to attain enough number of days for the comparisons between PILS and URG filters. Generally, the results are in good agreement with some scatter for sulfate, nitrate and ammonium from all sites as shown in Figure 2.11. The overall slopes were 1.03, 0.97 and 1.00 for sulfate, nitrate and ammonium, respectively, with the intercepts of 0.02, 0.07 and 0.14 $\mu g/m^3$ ranging from $R^2 = 0.94$ to R^2=0.98 between URG and PILS data.

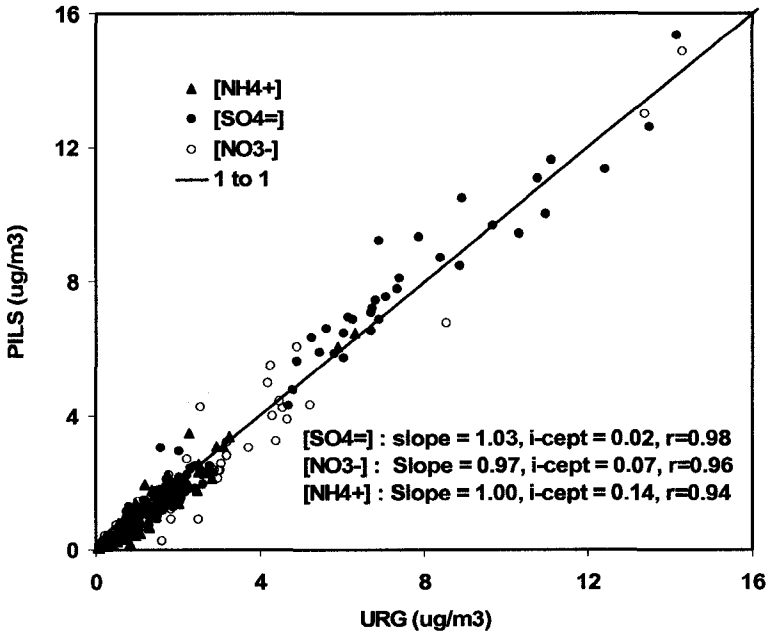

Figure 2.11 Comparison of concentrations of ammonium, sulfate and nitrate in URG filter versus PILS samples

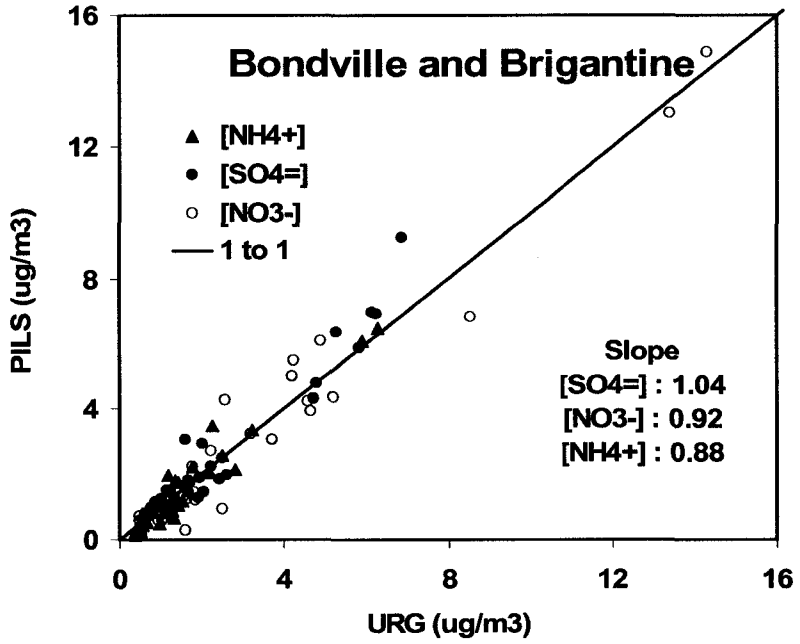

Figure 2.12 Comparison of concentrations of ammonium, sulfate and nitrate in URG filter versus PILS samples (Bondville (Feb., 2003) and Brigantine (Nov., 2003)

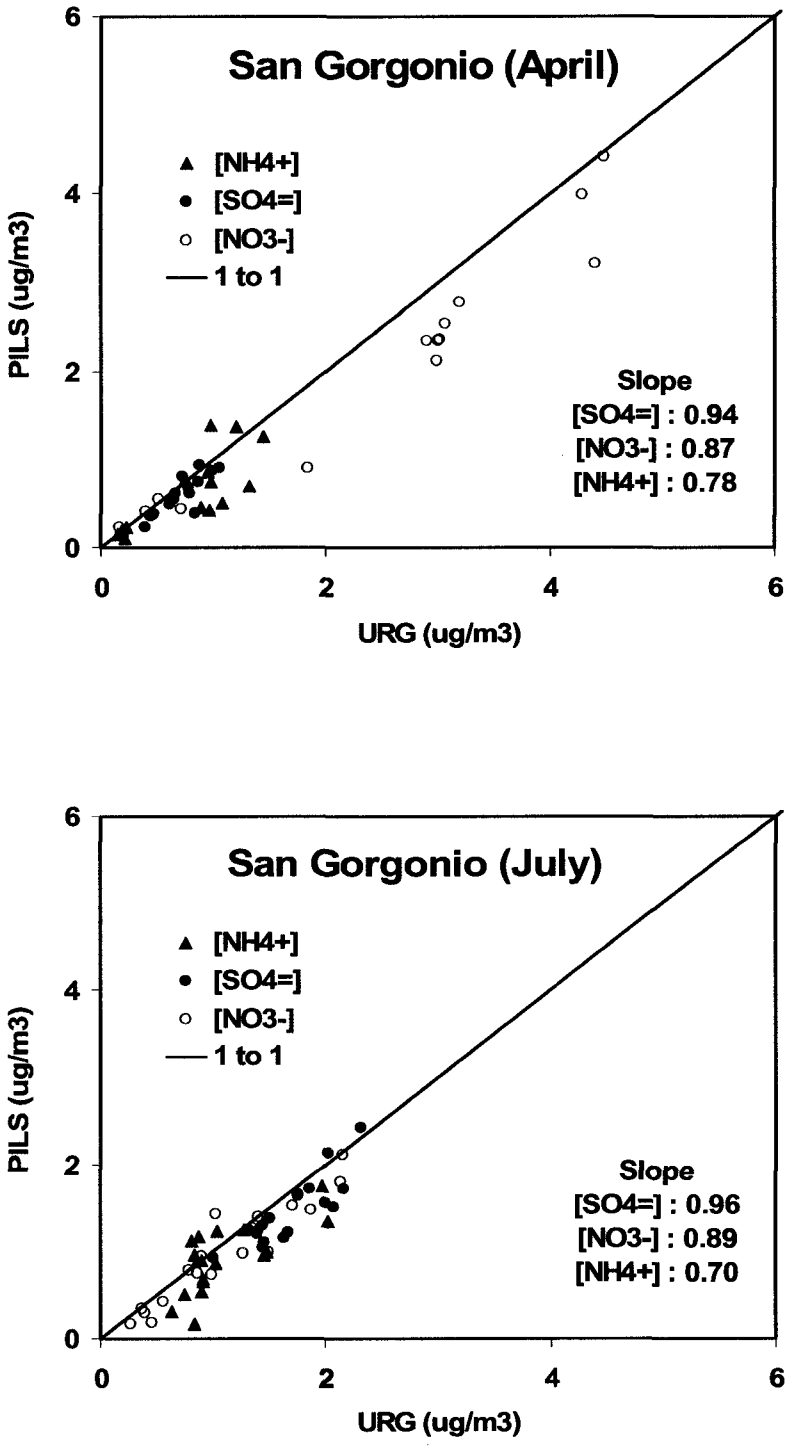

Figure 2.13 Comparison of concentrations of ammonium, sulfate and nitrate in URG filter versus PILS samples (San Gorgonio (April and July))

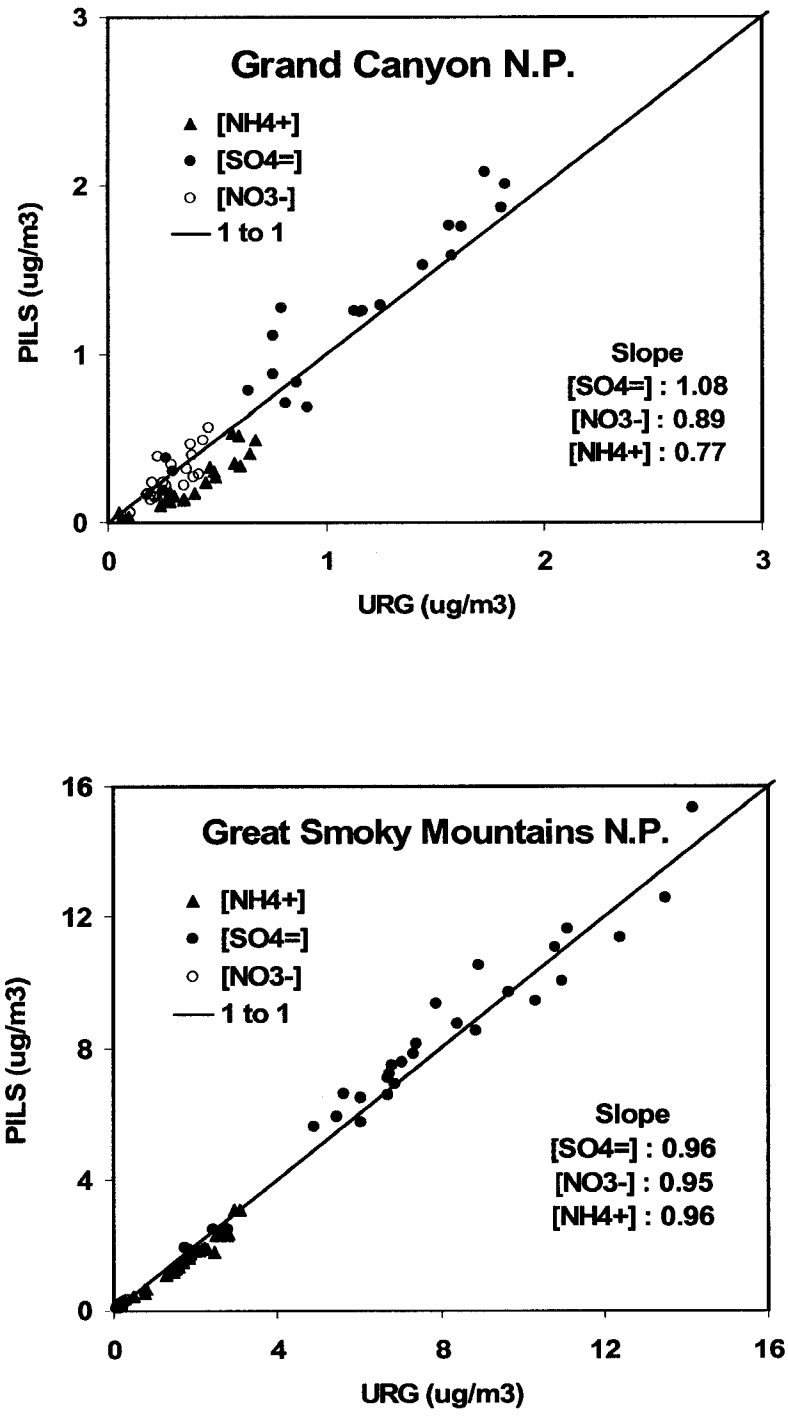

Figure 2.14 Comparison of concentrations of ammonium, sulfate and nitrate in URG filter versus PILS samples (Grand Canyon N.P. (May, 2003) and Great Smoky Mountains N.P.(July/Aug, 2004))

The comparisons of sulfate, nitrate and ammonium between URG and PILS for each site are shown in Figures 2.12, 2.13 and 2.14. Sulfate for most of sites shows good agreement between the PILS and URG filter with the linear regression slopes ranging from 0.94 to 1.08, while the results for ammonium and nitrate are in fairly good agreement with the slope ranging from 0.70 to 0.96 and from 0.87 to 0.95, respectively, with the PILS measurement biased high. It is likely that the relatively poor agreement for ammonium at San Gorgonio (July) and Grand Canyon N.P. are due to difficulties in accurately measuring concentrations approaching the detection limit in the PILS sampler (Orsini et al., 2003; Sorooshian et al., 2006).

3. Ionic composition of $PM_{2.5}$ and size-resolved aerosol

This chapter provides an overview of the chemical properties of aerosol measured in the various field campaigns described in chapter 2. For each campaign timelines of daily $PM_{2.5}$ composition and key trace gas concentrations, measured using the URG denuder/filter-pack sampler, are provided (URG data tables in Appendix C). The average size distribution of each major ion species, measured in 48 hr MOUDI samples, is also presented by campaign. Select individual MOUDI ion size distributions are also presented to aid the discussion of aerosol properties at each study site. All ion size distributions measured with the MOUDI sampler are included in Appendix E. The primary goals of this chapter are to

- Examine general features of $PM_{2.5}$ aerosol composition during each field campaign and how they vary from day to day. Examine relationships between various $PM_{2.5}$ constituents.
- Examine particle size distributions of the major ion species in each field campaign, paying particular attention to the presence of various species in fine and/or coarse particle modes. Examine similarities in size distributions between individual aerosol species.
- Examine the concentrations of key gas phase species, including HNO_3, NH_3, and SO_2, with special emphasis on the gas/particle distributions for ammonia/ammonium and nitric acid/nitrate.

Further discussion of the results presented in this chapter, along with results from semi-continuous aerosol composition (PILS) measurements presented in Chapter 4, can

be found in Chapter 5, which focuses on using all available information to determine the importance of various forms of aerosol nitrate in the environments studied.

3.1 San Gorgonio Wilderness Area (April and July, 2003), CA

Figure 3.1 shows the daily $PM_{2.5}$ sulfate, nitrate, and ammonium concentrations measured in April and July, 2003 in the San Gorgonio Wilderness Area, California. Lower concentrations of sulfate were observed in April with an average of 0.8 $\mu g/m^3$, compared to an average sulfate concentration of 1.7 $\mu g/m^3$ in July. The highest 24 hr average concentrations of nitrate were measured on 4/9 and 4/16 with 14.5 $\mu g/m^3$ and 10.2 $\mu g/m^3$, respectively. Lower concentrations of nitrate were observed in July with a range of 0.3-4.9 $\mu g/m^3$.

Ammonium was the dominant cation species measured in the $PM_{2.5}$ samples in April and July. Other cation species (Na^+, K^+, Mg^{2+} and Ca^{2+}) and Cl^- were found to be minor contributors to total concentrations in $PM_{2.5}$ as shown in Figure 3.2. The maximum concentrations of ammonium were 4.3 $\mu g/m^3$ and 2.0 $\mu g/m^3$ on 4/9 and 7/30, respectively. Concentrations of ammonium ranged from 0.2 to 4.3 $\mu g/m^3$ during April and from 0.5 to 2.0 $\mu g/m^3$ during July in San Gorgonio.

Relatively higher contributions of minor cation species (Na^+, K^+) were observed in July, compared to April. Concentrations of Na^+ in April and July averaged 0.06 $\mu g/m^3$ (range 0.01 – 0.18 $\mu g/m^3$) and 0.16 $\mu g/m^3$ (range 0.05 – 0.48 $\mu g/m^3$). The highest concentration of K^+ was approximately 0.64 $\mu g/m^3$ on 7/5 with a range from below detection limit to 0.64 $\mu g/m^3$ in July. K^+ concentrations were close to the detection limit (0.02 $\mu g/m^3$) on many days in April. The relatively high concentrations of K^+ observed in July were attributed to local and/or regional biomass burning, a known source of water

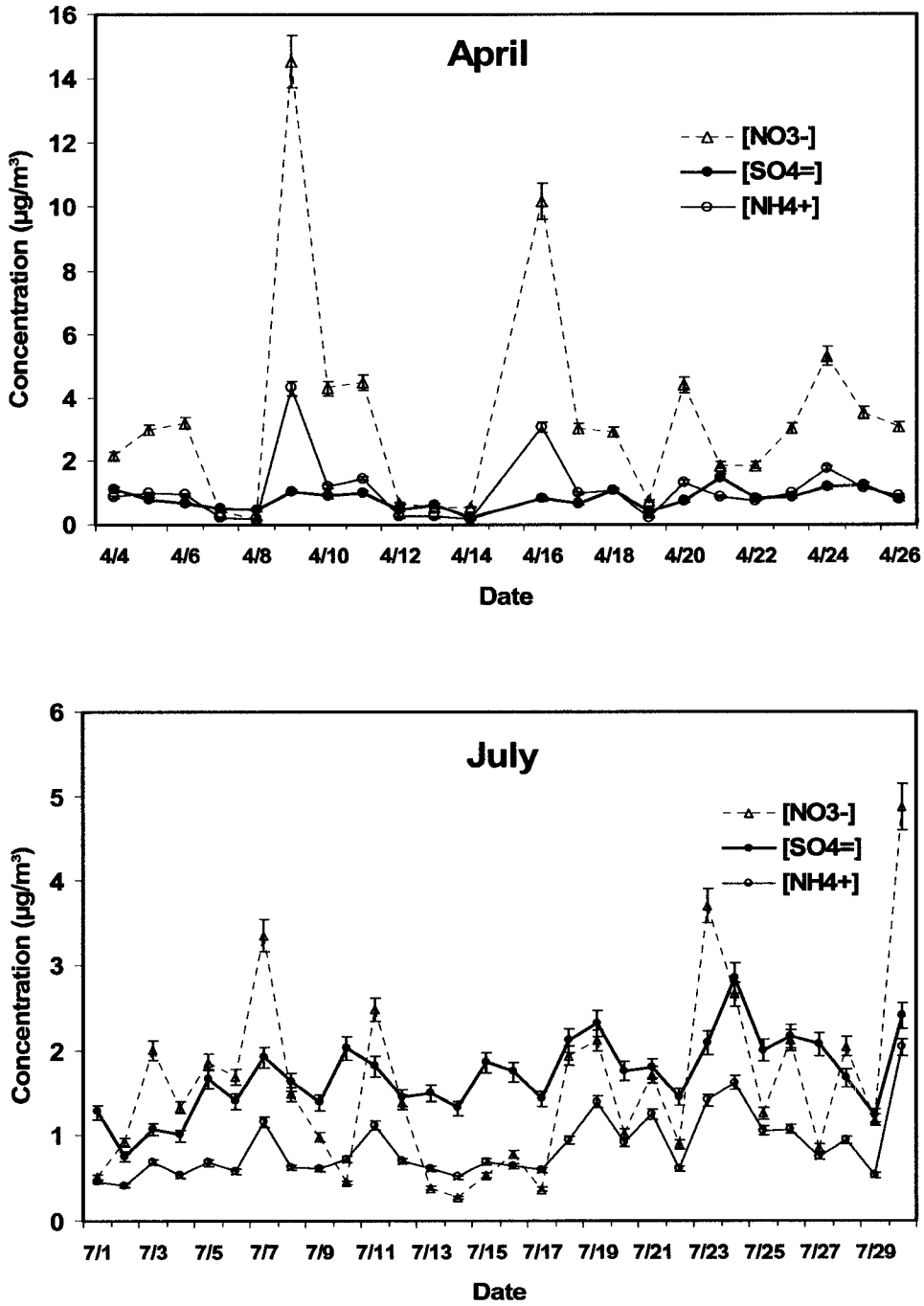

Figure 3.1 Timelines of URG $PM_{2.5}$ SO_4^{2-}, NO_3^- and NH_4^+ concentrations (San Gorgonio (April and July))
(Error bars represent measurement precision (1 standard deviation))

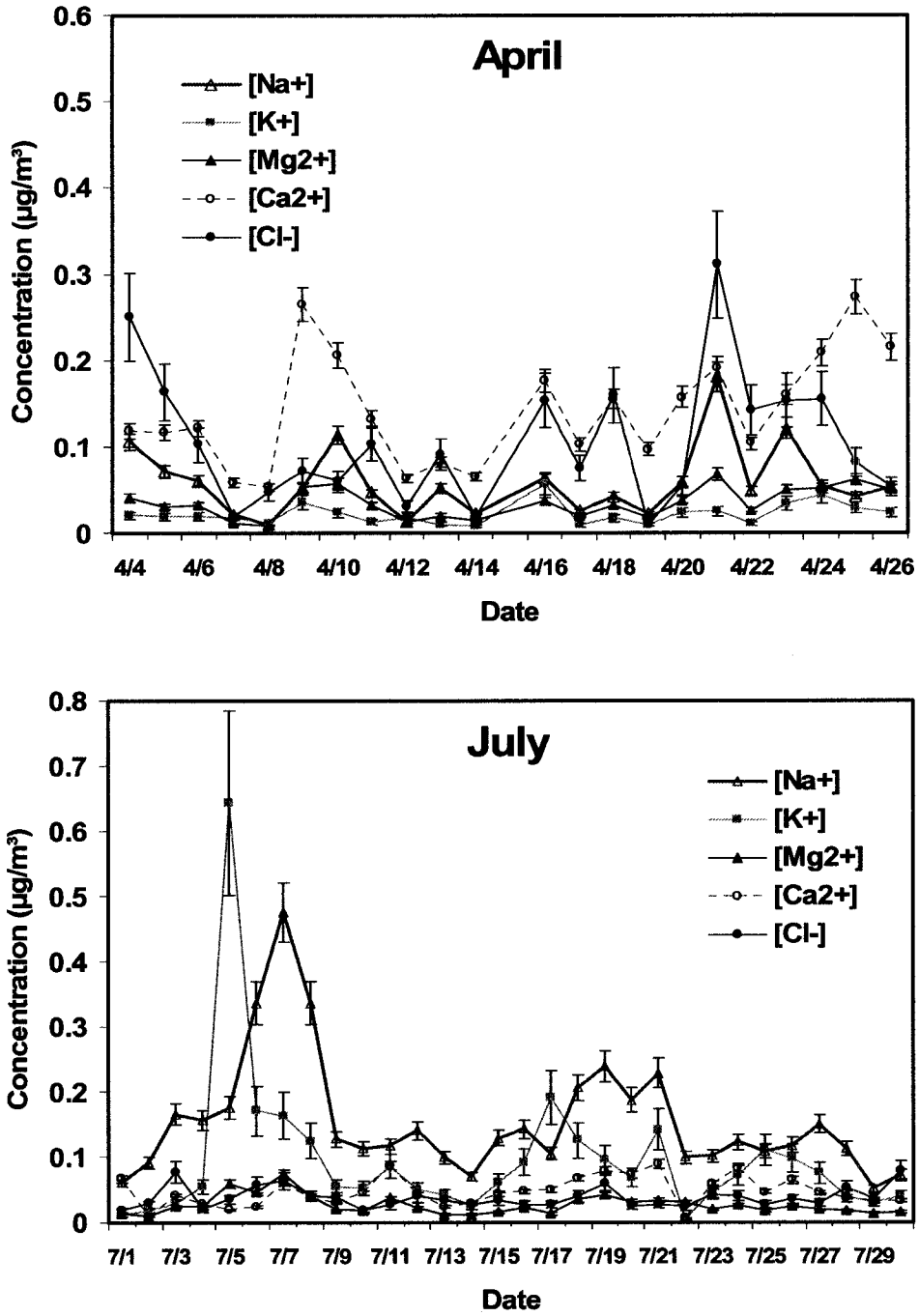

Figure 3.2 Timelines of URG $PM_{2.5}$ Na^+, K^+, Mg^{2+}, Ca^{2+} and Cl^- concentrations (San Gorgonio (April and July)) (Error bars represent measurement precision (1 standard deviation))

soluble potassium (Carrico et al., 2004; Engling, 2006; McMeeking et al., 2005; McMeeking et al., 2006). High K^+ concentrations were also periodically measured in July with the PILS (see chapter 4 for details).

Mg^{2+} and Ca^{2+} were found to be minor contributors to total cation concentrations in the $PM_{2.5}$ samples. Mg^{2+} concentrations ranged from zero (below detection limits) to 0.06 $\mu g/m^3$ and 0.07 $\mu g/m^3$ in April and July, while Ca^{2+} concentrations ranged from 0.05 $\mu g/m^3$ to 0.26 $\mu g/m^3$ and zero to 0.1 $\mu g/m^3$ in April and July, respectively. .

Higher concentrations of chloride were observed in April. The mean chloride concentrations in April and July were 0.11 (range of 0.01 – 0.31) $\mu g/m^3$ and 0.04 (range of 0.02 – 0.08) $\mu g/m^3$, respectively. Because sodium concentrations were higher in July, presumably reflecting greater sea salt concentrations at San Gorgonio during this time period, the decrease in chloride might reflect greater loss of chloride from sea salt aerosol due to reaction with other atmospheric acids (De Haan and Finlayson-Pitts, 1997; Evans et al., 2004; Hoffman et al., 2004; Laskin et al., 2002; Lee et al., 2004; Ro et al., 2001; Spurny, 2000; ten Brink, 1998). We return to this issue in Chapters 4 and 5.

Figure 3.3 presents timelines of San Gorgonio gaseous HNO_3, NH_3 and SO_2 concentrations in April and July. The average concentration of nitric acid was substantially higher in July at 4.26 $\mu g/m^3$ (range of 2.01 – 7.2 $\mu g/m^3$) than observed in April (0.42 $\mu g/m^3$ on average with a range of 0.19 – 1.62 $\mu g/m^3$). Furthermore, the average concentration of gaseous ammonia in July was also higher than in April. Higher concentrations of these two gas phase species in summer are consistent with a shift in their equilibrium with particulate ammonium nitrate that favors the gas phase constituents when conditions are hot and dry. Concentrations of gaseous SO_2 were fairly low

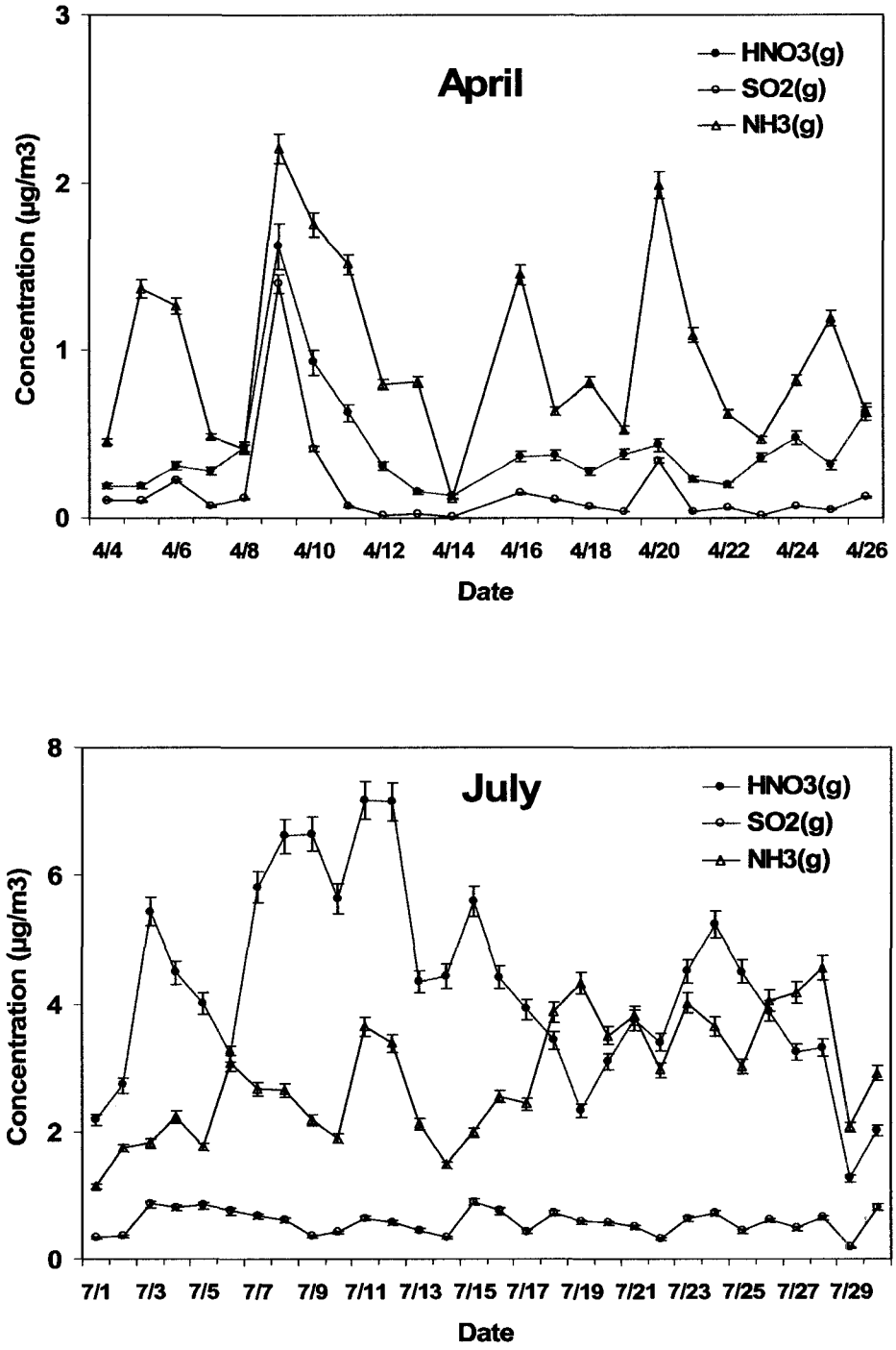

Figure 3.3 Timelines of $HNO_3(g)$, $SO_2(g)$ and $NH_3(g)$ concentrations from URG (San Gorgonio (April and July))
(Error bars represent measurement precision (1 standard deviation))

throughout most of April and July with average values of 0.16 $\mu g/m^3$ and 0.57 $\mu g/m^3$, respectively.

Figure 3.4 depicts timelines of $PM_{2.5}$ SO_4^{2-}, NO_3^- and NH_4^+ concentrations in units of nanoequivalents per cubic meter (neq/m^3). In contrast to the mass concentration units utilized in the preceding figures, these chemically based units, which account for the charge on each species, permit ready analysis of the charge balance of measured species in the aerosol. In April, ammonium and nitrate concentrations typically tracked each other, suggesting an aerosol dominated by ammonium nitrate. A slight deficit of nitrate, relative to ammonium, is accounted for by the presence of a much smaller amount of sulfate, suggesting some ammonium sulfate is also present in $PM_{2.5}$ at the site. The predominance of ammonium nitrate in April at this site is not surprising, given the large sources of NO_x and NH_3 emissions in the Los Angeles Air Basin upwind. The relatively cool conditions of spring at this mountain site also are conducive to formation of ammonium nitrate from its nitric acid and ammonia precursors.

The situation in July is somewhat different, with a relatively larger contribution from sulfate. It is likely that sulfate concentrations increased with enhanced oxidation of SO_2 to SO_4^{2-} in the more oxidant rich conditions typical of summer (Dutkiewicz et al., 2000; Gupta et al., 2003; Husain et al., 2004b). Greater transport of polluted air masses to this mountain site by daily upslope flow (see discussion in Chapter 4), might also be a contributor to higher sulfate concentrations. The hot, dry conditions typical in July at this site, however, do not favor formation of semivolatile particulate ammonium nitrate (Lee et al., 2004; Seinfeld and Pandis, 1998). The decreases in daily average ammonium nitrate concentrations at San Gorgonio from April to July are consistent with the increase

in concentrations of gaseous HNO_3 and NH_3 discussed above.

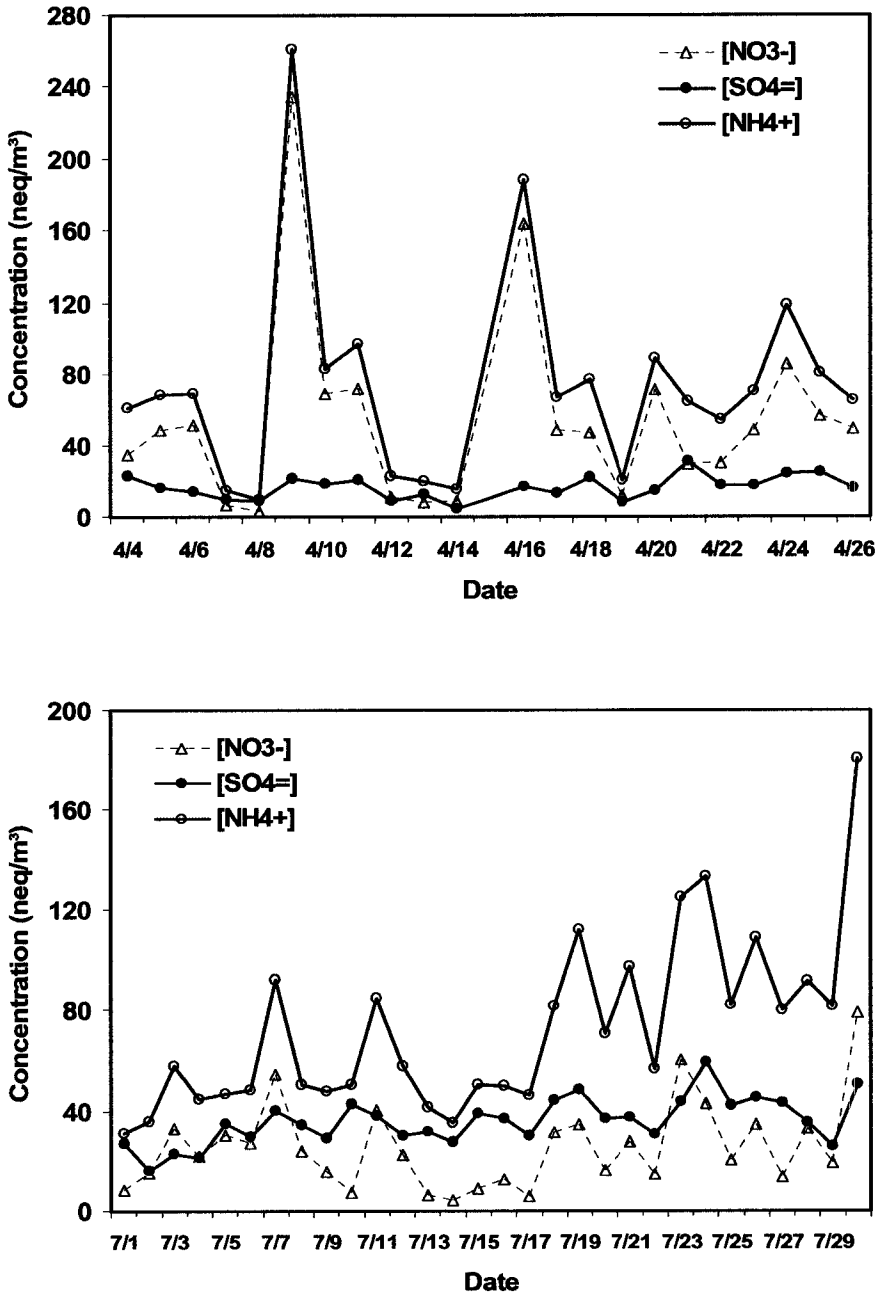

Figure 3.4 Timelines of SO_4^{2-}, NH_4^+ and NO_3^- concentrations in $PM_{2.5}$ (San Gorgonio, April and July, 2003) (Note : units as neq/m^3)

Figure 3.5 shows timelines of the ratio of $HNO_3(g)/N(V)$, $NH_3(g)/N(-III)$ and $SO_2(g)/([SO_4^{2-}(p)]+[SO_2(g)])$ in April and July depicting the fractions of these key nitrogen and sulfur species residing in the gas phase. The sum of gaseous HNO_3 and $PM_{2.5}$ NO_3^- comprises N(V). Similarly, N(-III) represents the sum of gaseous NH_3 and $PM_{2.5}$ NH_4^+. April ratios of $HNO_3(g)/N(V)$ ranged approximately from 0.29 to 0.71 with an average ratio of 0.17 and April ratios of $NH_3(g)/N(-III)$ ranged from 0.03 to 0.52 with an average of 0.46. Ratios were typically much higher during July, ranging from 0.31 to 0.94 (average 0.72) and from 0.47 to 0.78 (average 0.69) for $HNO_3(g)/N(V)$ and $NH_3(g)/N(-III)$, respectively. During April most available N(V) has been taken up into particles, yielding similar amounts of $PM_{2.5}$ ammonium and gaseous ammonia. In July more than two-thirds of both N(-III) and N(V), on average, remained in the gas phase.

In contrast to the nitrogen species, Figure 3.5 shows that total sulfur was present mostly as particle SO_4^{2-}, with average ratios of 0.14 and 0.23 for $[SO_2(g)]/([SO_4^{2-}] + [SO_2(g)])$ in April and July, respectively. A scatter plot of $PM_{2.5}$ sulfate vs. gas phase sulfur dioxide is included in Figure 3.6. Sulfate is mainly formed by SO_2 oxidation in the gas phase and in clouds (Bari et al., 2003; Dutkiewicz et al., 2000; Gupta et al., 2003; Husain et al., 2004a; Husain et al., 2004b; Moore, 2002; Rattigan et al., 2001; Reilly et al., 2001). On average both sulfate and sulfur dioxide concentrations increased from April to July, consistent with stronger transport of polluted air masses to this mountain site. Interestingly, the relative fraction of sulfur dioxide increases in summer, despite the higher oxidant concentrations prevalent at this time of year. Lower conversion of sulfur dioxide to sulfate in July might reflect a decrease in the importance of oxidation in clouds during this warmer, drier season.

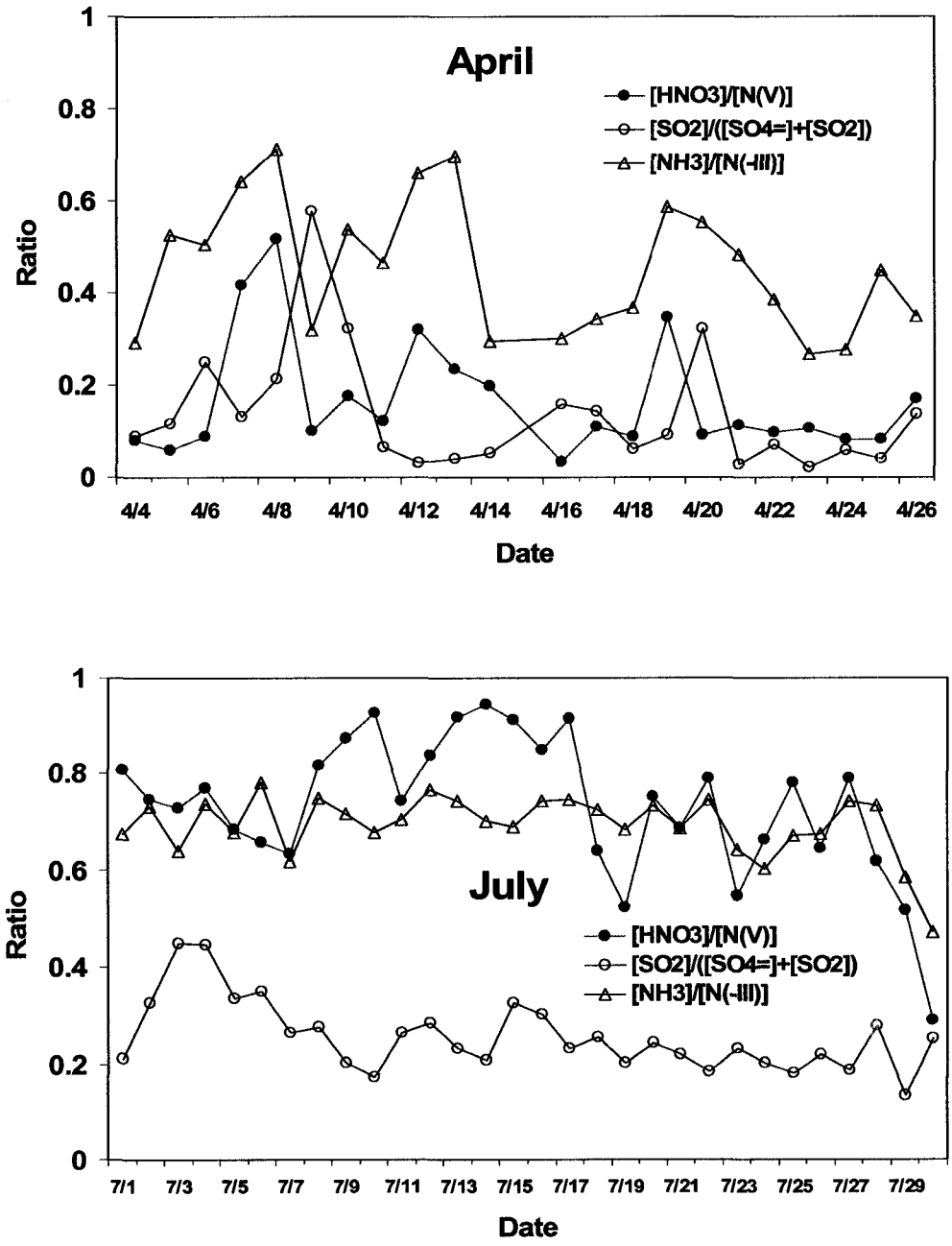

Figure 3.5 Timelines of HNO_3/N(V), NH_3/N(-III) and $SO_2/([SO_4^{2-}]+[SO_2])$ from URG (San Gorgonio (April and July))

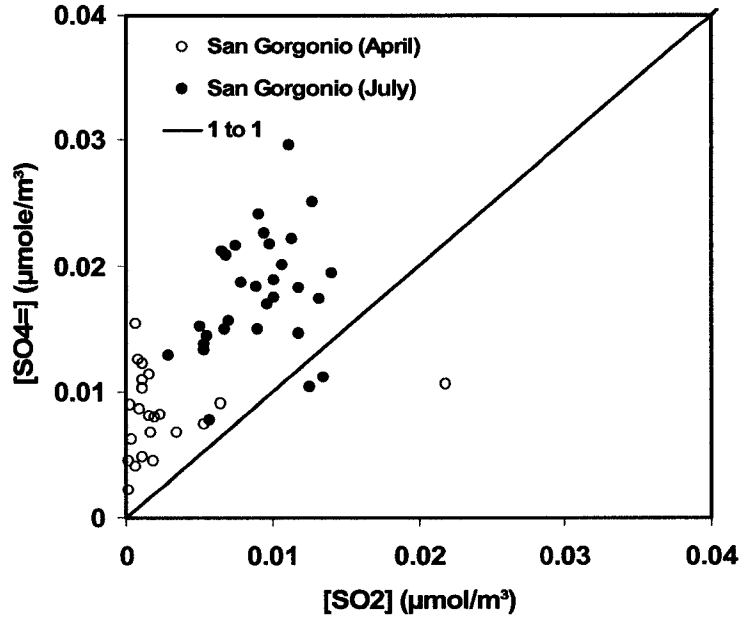

Figure 3.6 Comparison of SO_4^{2-}(p) and SO_2(g) concentrations (San Gorgonio (April and July))

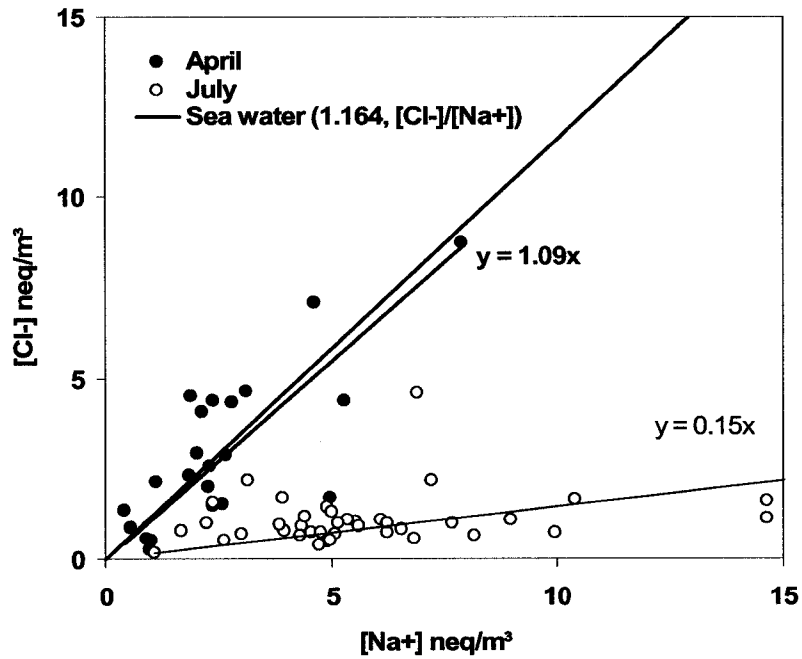

Figure 3.7 Relationship between Na^+ and Cl^- concentrations (April and July)

Figure 3.7 shows Cl^- concentrations plotted against Na^+ concentrations in $PM_{2.5}$ during April and July. Comparison of Na^+ and Cl^- concentrations in April reveals that the observed Cl^-/Na^+ equivalent ratio (average ~1.09) is close to the expected ratio of $[Cl^-]$ to $[Na^+]$ in sea water (~1.164). However, the ratio of $[Cl^-]/[Na^+]$ in July (~ 0.15) is much lower than the sea salt ratio, suggesting significant loss of Cl^- from sea salt as the result of reaction with HNO_3 and/or H_2SO_4. This topic will be discussed further in Chapters 4 and 5. A slight correlation in April (R^2= 0.32) and a moderate correlation in July (R^2= 0.57) between NO_3^- and the sum of $[Ca^{2+}]$ and $[Mg^{2+}]$ (Figure 3.8) suggests nitric acid reaction with soil dust might also be a contributor to particulate NO_3^- formation, especially during summer, at San Gorgonio. Because changes in pollutant concentrations at the site are so strongly tied to local meteorology, however, we must be cautious not to read too much into correlations between various species concentrations.

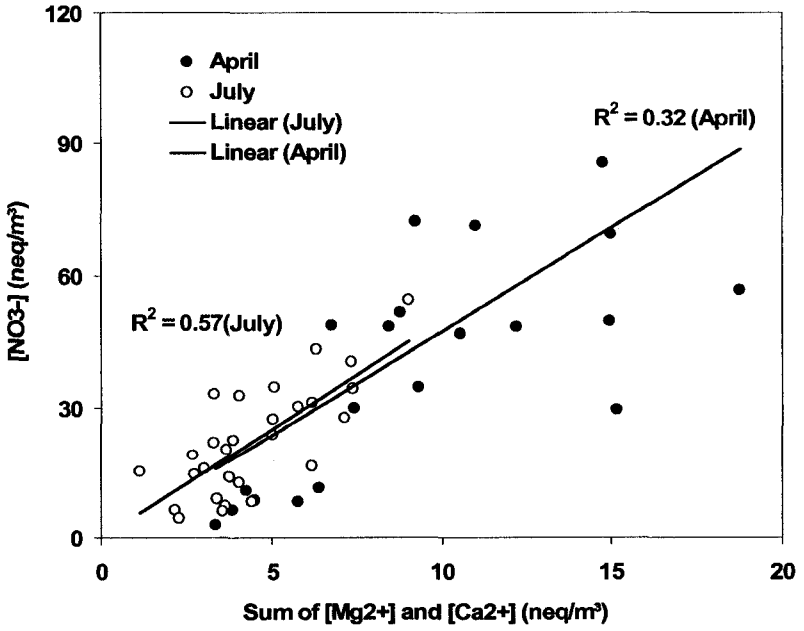

Figure 3.8 Relationship of $[NO_3^-]$ and sum of $[Mg^{2+}]$ and $[Ca^{2+}]$

Further insight into the chemical properties of the aerosol at San Gorgonio is provided by observation of the MOUDI measurements. Figure 3.9 shows size distributions of the monthly averaged inorganic ion concentrations measured in 48-hr MOUDI samples at San Gorgonio in April and July. Generally, inorganic ions are separated into supermicron (mass distribution peaks at approximately 4 -5 μm diameter) and submicron (mass distribution peaks at approximately 0.4 – 0.5 μm diameter) modes, with individual species illustrating either uni-modal or bimodal distributions.

The sulfate and ammonium size distributions were very similar in April and July with a dominant peak in the range from 0.4 – 0.5 μm aerodynamic diameter. However, a small coarse mode was also observed for sulfate with a characteristic mode diameter of approximately 4 – 5 μm, indicating aged sea salt and soil dust may contain some sulfate in the coarse mode through reaction with gaseous SO_2 or H_2SO_4 (Bauer and Koch, 2005; Carmichael et al., 1996; Dentener et al., 1996; Fan et al., 2004; Finlayson-Pitts and Pitts, 2000; Hien et al., 2005; Hwang and Ro, 2005; Liao et al., 2003; Seinfeld and Pandis, 1998).

The average nitrate size distribution in April has a shape very similar to the size distribution of ammonium, with a submicron mode peak at 0.4 – 0.5 μm aerodynamic diameter, consistent with the formation of ammonium nitrate by reaction of gaseous HNO_3 and gaseous NH_3 (Finlayson-Pitts and Pitts, 2000; Seinfeld and Pandis, 1998). The MOUDI nitrate size distribution in July, however, is dominated by a coarse mode, similar to size distributions measured for Na^+, Mg^{2+} and Ca^{2+} which typically are associated with mechanically generated sea salt and soil dust. Na^+, Cl^-, Ca^{2+} and Mg^{2+} exhibit similar size distributions, with a dominant coarse mode peak at 4 - 5 μm in April

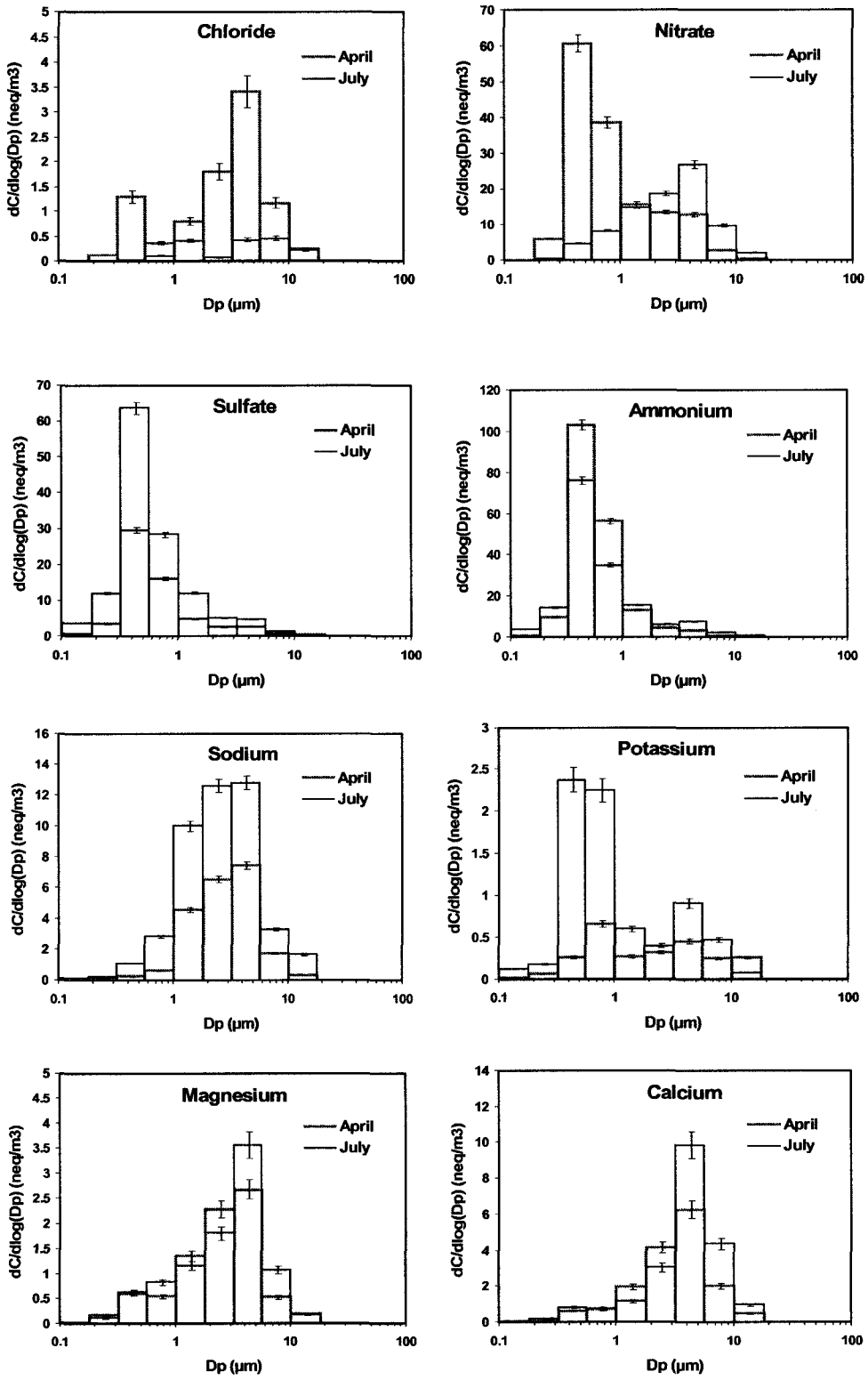

Figure 3.9 Size distributions of average inorganic ion concentrations (San Gorgonio (April and July))
(Error bars represent measurement precision (1 standard deviation))

and July. While these observations again suggest the importance of coarse particle nitrate formation during summer at San Gorgonio, a comparison with $PM_{2.5}$ nitrate measured by the URG sampler and by the PILS/IC system reveals substantial loss of semi-volatile ammonium nitrate from the MOUDI impaction surfaces during July. These losses are not surprising given the substantial daily swings in temperature and relative humidity of sampled air experienced by the MOUDI at this site during 48 hr sample collection periods.

Figure 3.9 also demonstrates an interesting bimodal size distribution for San Gorgonio K^+, especially in July, with a fine mode peaked in the range 0.4 – 0.5 μm and a coarse mode peaked in the range 4 – 5 μm. As discussed in more detail in Chapter 4, the presence of fine mode K^+ is an indicator of smoke plumes intercepting the San Gorgonio measurement site. K^+ is an important contributor to the inorganic fraction of biomass combustion particles (Li et al., 2003; Liu et al., 2000; Posfai et al., 2003).

3.2 Grand Canyon National Park (May, 2003), AZ

Figure 3.10 presents timelines of $PM_{2.5}$ SO_4^{2-}, NO_3^- and NH_4^+ concentrations in May 2003, measured in Grand Canyon National Park. SO_4^{2-} and NH_4^+ concentrations ranged from 0.25 to 1.8 μg/m^3 and from 0.05 to 0.67 μg/m^3, respectively, as the dominant ionic species in $PM_{2.5}$, while NO_3^- concentrations were rather low, ranging from 0.1 to 0.57 μg/m^3. Periods of relatively higher sulfate and ammonium concentrations were observed in the end of May with the highest concentrations on 5/25 and 5/26 with approximately 1.8 μg/m^3 and 0.67 μg/m^3 of sulfate and ammonium, respectively.

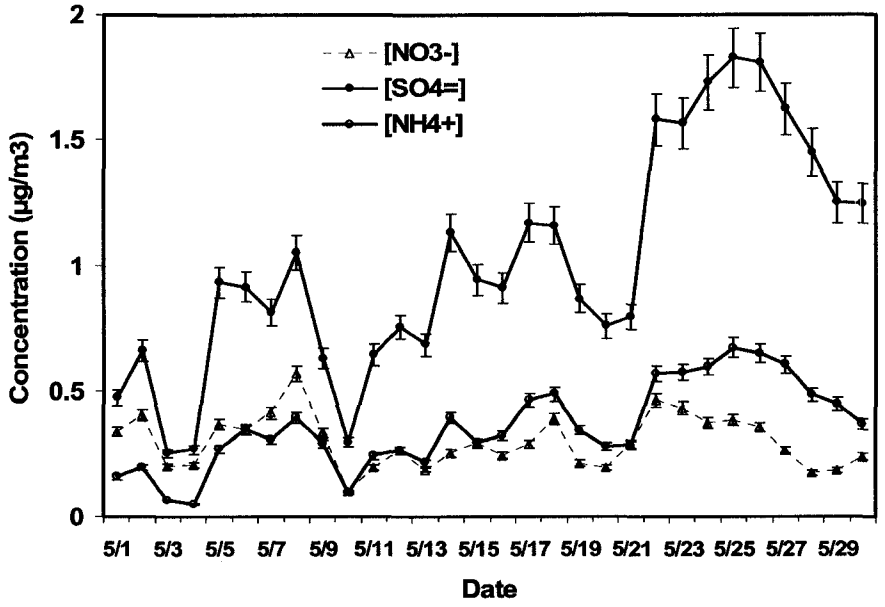

Figure 3.10 Timelines of SO_4^{2-}, NH_4^+ and NO_3^- concentrations in URG $PM_{2.5}$ (Grand Canyon N.P., May, 2003)
(Error bars represent measurement precision (1 standard deviation))

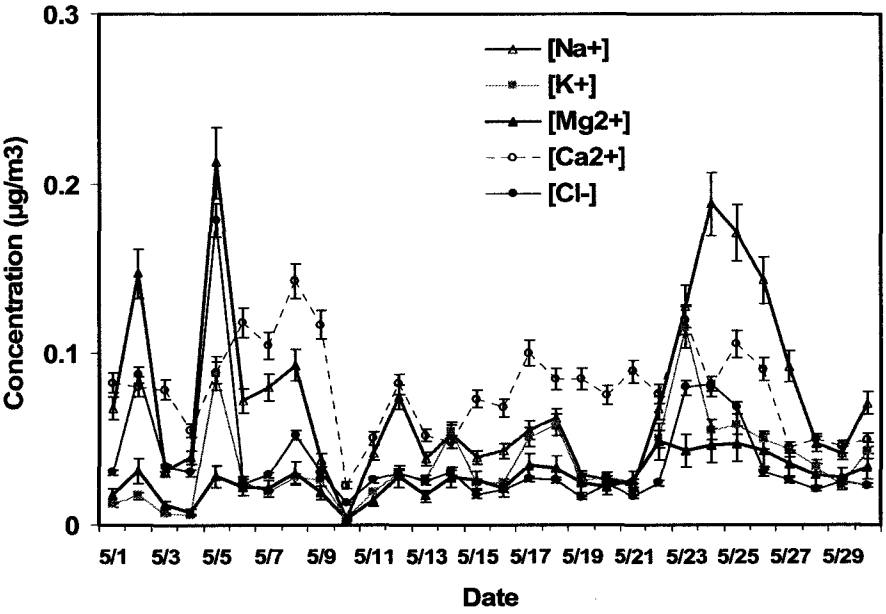

Figure 3.11 Timelines of Cl^-, Na^+, Ca^{2+}, Mg^{2+} and K^+ concentrations in URG $PM_{2.5}$ (Grand Canyon N.P., 2003)
(Error bars represent measurement precision (1 standard deviation))

The variations of concentrations of other cation species and chloride are shown in Figure 3.11. Concentrations of the minor cation species (Na^+, Ca^{2+}, $Mg^{2+}$and K^+) ranged from 3 ng/m^3 to 0.31 μg/m^3 during the Grand Canyon N.P. study. Mg^{2+} and K^+ were found to be minor contributors to total cation concentrations in the $PM_{2.5}$ samples, with average Mg^{2+} concentration of 0.03 μg/m^3 and K^+ concentrations of 0.04 μg/m^3. The highest concentrations of Na^+ were measured on 5/2, 5/5 and 5/23 with 0.15 μg/m^3, 0.21 μg/m^3 and 0.19 μg/m^3, respectively. During the entire campaign Na^+ concentrations averaged 0.07 μg/m^3. Peak concentrations of Cl^-, 0.09 μg/m^3, 0.18 μg/m^3 and 0.08 μg/m^3, coincided with high concentrations of Na^+. Concentrations of $PM_{2.5}$ Ca^{2+} ranged from 0.02 μg/m^3 to 0.15 μg/m^3 with an average of 0.08 μg/m^3, somewhat higher than other trace cation species.

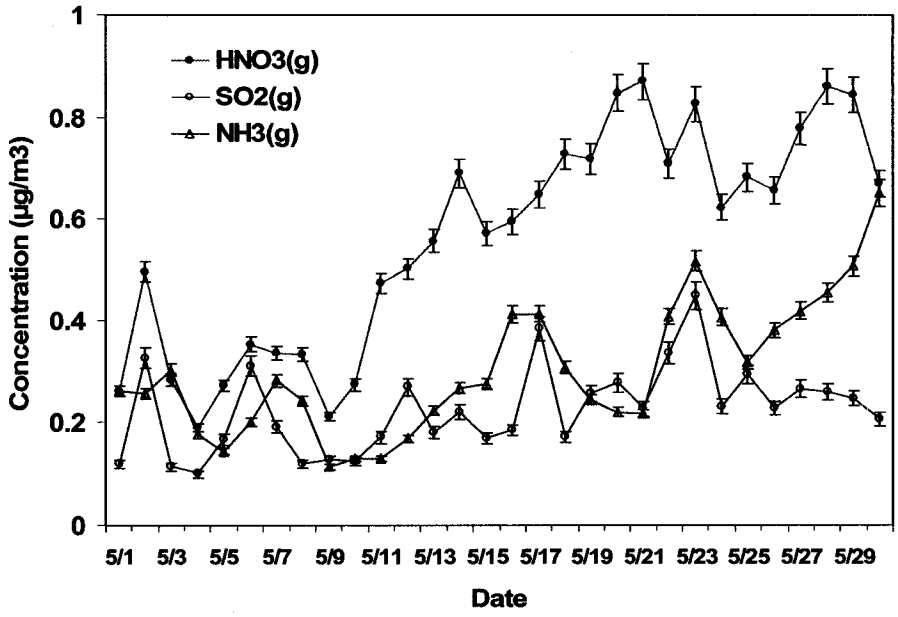

Figure 3.12 Timelines of HNO_3(g), SO_2(g) and NH_3(g) concentrations from URG (Error bars represent measurement precision (1 standard deviation))

The variations of HNO_3 (g), NH_3 (g) and SO_2 (g) concentrations are shown in Figure 3.12. Concentrations of HNO_3 (g) were typically between 0.2 and 0.4 μg/m3 in early May. Periods of higher HNO_3 (g) concentrations started in the middle of May with the highest concentrations observed on 5/21 and 5/28 with 0.87 $\mu g/m^3$ and 0.86 $\mu g/m^3$, respectively. SO_2 (g) and NH_3 (g) concentrations ranged from 0.1 to 0.45 $\mu g/m^3$ and from 0.11 to 0.65 $\mu g/m^3$, respectively. Concentration of SO_2 (g) were generally below 0.4 $\mu g/m^3$ with only modest day to day variability, while NH_3 (g) concentrations increased from approximately 0.2 $\mu g/m^3$ early in May to 0.6 $\mu g/m^3$ at the end of the study.

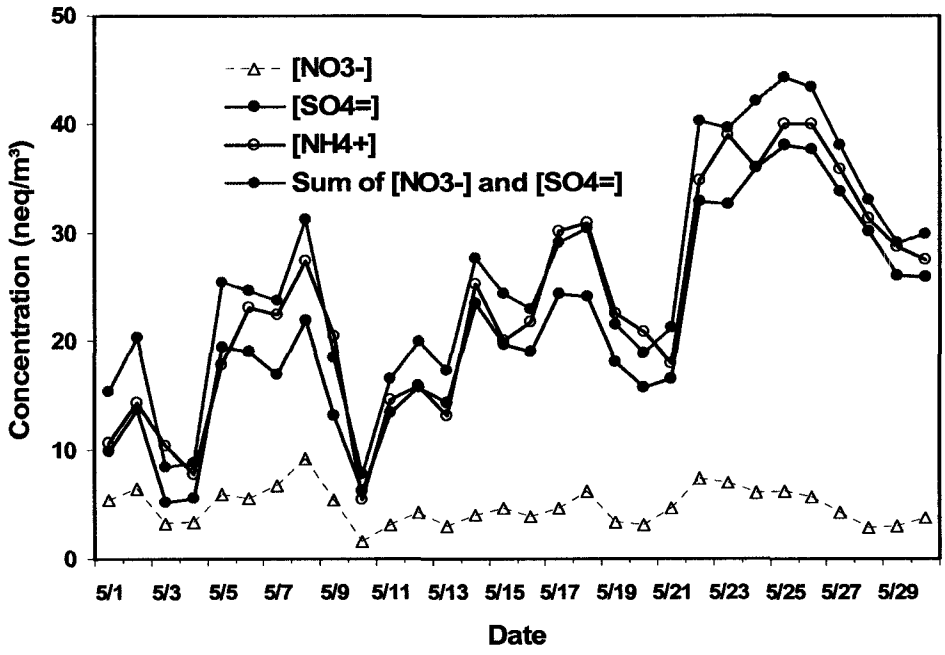

Figure 3.13 Timelines of SO_4^{2-}, NH_4^+, NO_3^- concentrations and sum of [SO_4^{2-}] and [NO_3^-] in URG $PM_{2.5}$ (Grand Canyon N.P., May, 2003) (Note : units as neq/m^3)

Figure 3.13 depicts timelines of $PM_{2.5}$ SO_4^{2-}, NO_3^- and NH_4^+ concentrations in units of nanoequivalents per cubic meter (neq/m^3) permitting ready analysis of the ion balance in the aerosol. Ammonium was measured as the dominant cation species in $PM_{2.5}$ samples, closely followed by sulfate, suggesting that most of the ammonium is associated with sulfate, while nitrate concentrations were observed to range approximately from 1.6 to 9.2 neq/m^3. However, it is clear that there is often insufficient ammonium present to balance the sum of nitrate and sulfate as shown in Figure 3.13. This finding suggests that other forms of nitrate may be present. $PM_{2.5}$ Ca^{2+} and Mg^{2+} concentration trends were somewhat similar to nitrate trends, as shown in Figure 3.14. Together with the observation of insufficient ammonium to balance the sum of nitrate and sulfate, these observations suggest a possible contribution to particulate nitrate formation through reaction with soil dust.

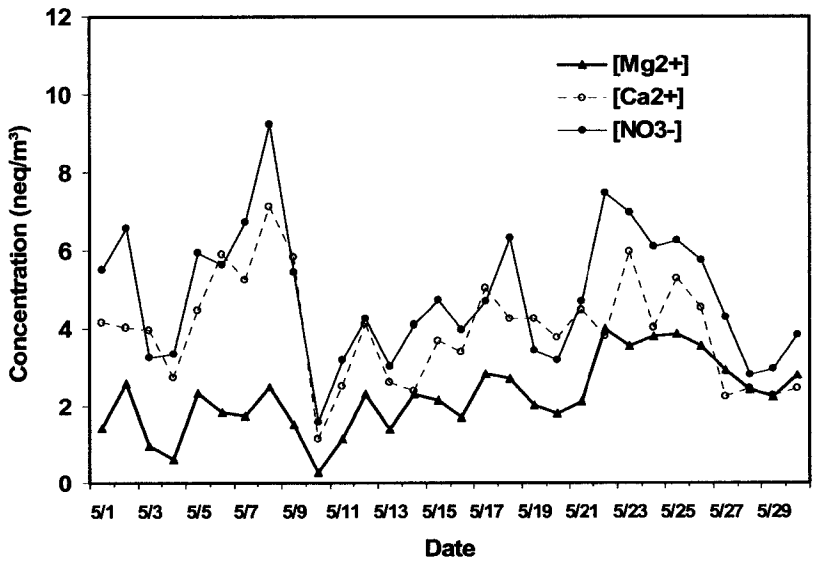

Figure 3.14 Timelines of NO_3^-, Ca^{2+} and Mg^{2+}concentrations in URG $PM_{2.5}$ (Grand Canyon N.P., 2003) (Note : units as neq/m^3)

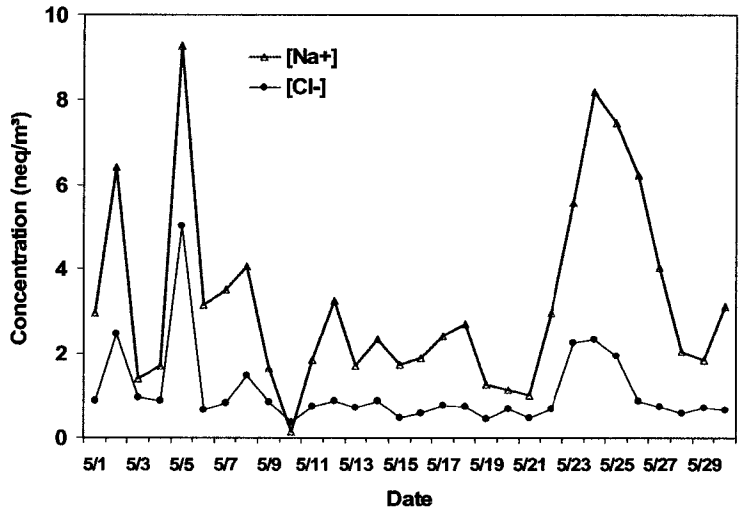

Figure 3.15 Timelines of Na^+ and Cl^- concentrations in URG $PM_{2.5}$ (Grand Canyon N.P., 2003) (Note : units as neq/m^3)

Figure 3.15 shows some tracking of concentrations of $PM_{2.5}$ Na^+ and Cl^-, suggesting possible sea salt transport to this site. Other inland sources of salt (e.g., Owens Lake, California), could also contribute to observed concentrations of these species. The ratio of Cl^- to Na^+ (slope = 0.34) observed in the $PM_{2.5}$ aerosol falls well below the sea water ratio (1.164) (Figure 3.16), suggesting significant loss of Cl^- from sea salt particles (NaCl) by reaction with nitric or sulfuric acid or their precursors (see chapter 5 for details). $PM_{2.5}$ nitrate concentrations were correlated with Na^+ concentrations ($R^2 = 0.37$) and the sum of Ca^{2+} and Mg^{2+} concentrations ($R^2 = 0.74$) as shown in Figure 3.17. Again, the strong correlation of $[NO_3^-]$ and the sum of $[Ca^{2+}]$ and $[Mg^{2+}]$ suggest reaction of nitric acid with soil dust might be important in Grand Canyon NP. This is consistent with observations from the MOUDI measurements of ion size distributions.

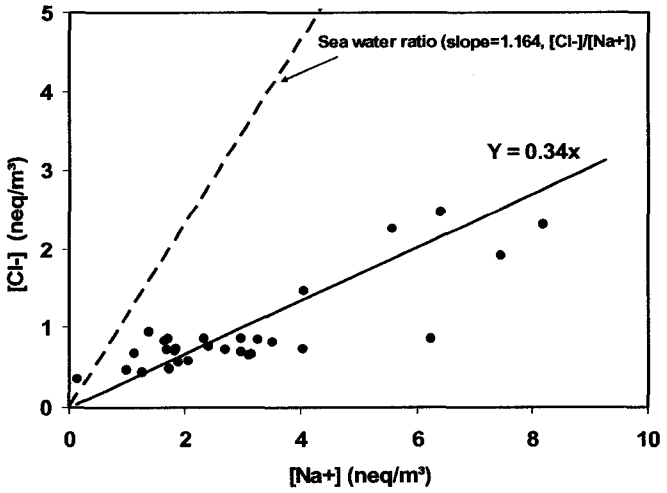

Figure 3.16 Relationship between Na^+ and Cl^- concentration

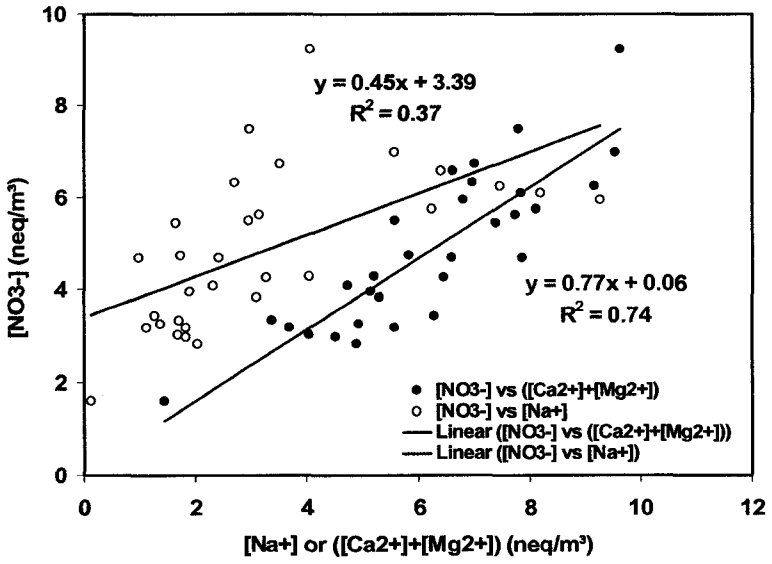

Figure 3.17 Correlation between $PM_{2.5}$ $[NO_3^-]$ and $[Na^+]$ or the sum of $[Ca^{2+}]$ and $[Mg^{2+}]$ (Grand Canyon N. P., May, 2003)

Figure 3.18 depicts study average particle size distributions of the anions and cations as measured in 48 hr MOUDI impactor samples. Similar size distributions for $[NO_3^-]$ and for $[Na^+]$, $[Ca^{2+}]$ and $[Mg^{2+}]$ were observed in the MOUDI measurements,

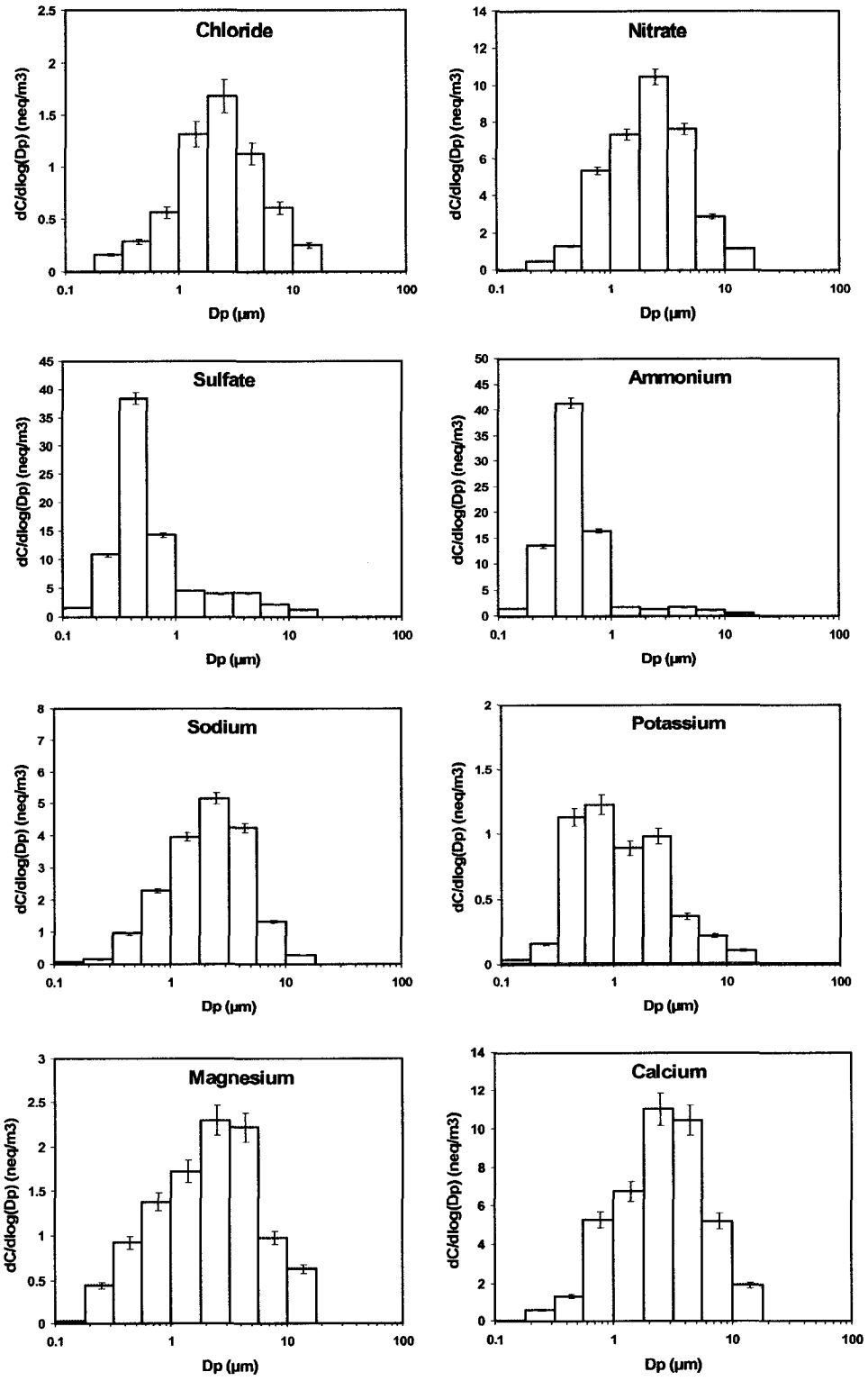

Figure 3.18 Particle size distributions of average inorganic ion concentrations (Grand Canyon National Park (May, 2003)) (Error bars represent measurement precision (1 standard deviation))

consistent with suggestions about the importance of mineral forms of nitrate provided by the URG measurements. Note that Cl^- and Na^+ have similar size distribution shapes, but that significantly less chloride is present in the aerosol, again suggesting loss of chloride during aging of sea salt particles transported inland.

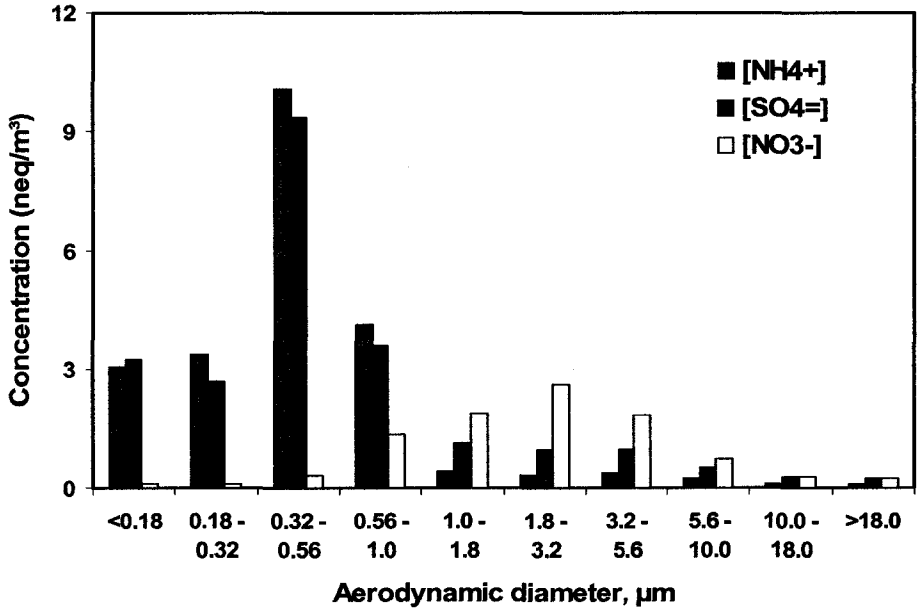

Figure 3.19 Size distributions of averaged ammonium, sulfate and nitrate concentrations (Grand Canyon National Park (May, 2003))

Both sulfate and ammonium are found mainly in the fine particle mode, with a submicron mode typically peaked at 0.4 – 0.5 µm aerodynamic diameter. Note that sufficient ammonium is present in the submicron particle size range to fully neutralize measured sulfate, suggesting the prevalence of $(NH_4)_2SO_4$ at this location. Study average particle size distributions for nitrate, sulfate and ammonium are plotted together in Figure 3.19. Here one readily sees the external mixture of submicron ammonium sulfate aerosol

and a coarse mode of particle nitrate. One also sees some evidence of a modest amount of coarse particle sulfate. The importance of mineral forms of coarse particle sulfate and nitrate are clear in individual MOUDI sampling periods as well. Figure 3.20, for example, shows that insufficient ammonium is present in coarse particles to balance either nitrate or sulfate. Other soil and sea salt cations are present at high enough concentrations, however, to balance observed nitrate and sulfate.

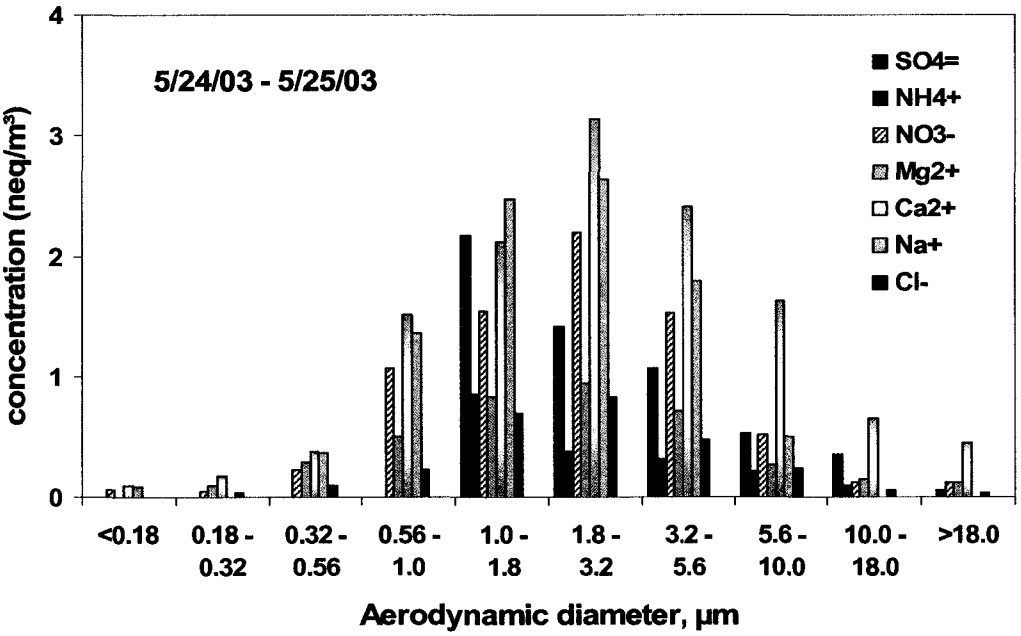

Figure 3.20 Size distributions of major ions measured on 5/24 – 25 at Grand Canyon NP using the MOUDI impactor (Note : SO_4^{2-} and NH_4^+ in fine mode (not shown))

3.3 Bondville, IL (February, 2003)

Figure 3.21 shows the daily $PM_{2.5}$ sulfate, nitrate and ammonium concentrations measured in February, 2003 at the study site near Bondville, IL. Generally,

concentrations of major ion species increase from the middle of the study and higher concentrations are observed in the second half of the month. Concentrations of $PM_{2.5}$ sulfate observed at Bondville averaged 2.87 $\mu g/m^3$, ranging from 0.55 to 6.89 $\mu g/m^3$; nitrate concentrations ranged from 1.63 $\mu g/m^3$ to 14.5 $\mu g/m^3$ with an average concentration of 4.85 $\mu g/m^3$. Based on the URG $PM_{2.5}$ observations it is clear that ammonium nitrate is a dominant contributor to wintertime fine particle composition at this site, although on some days sulfate concentrations exceeded nitrate.

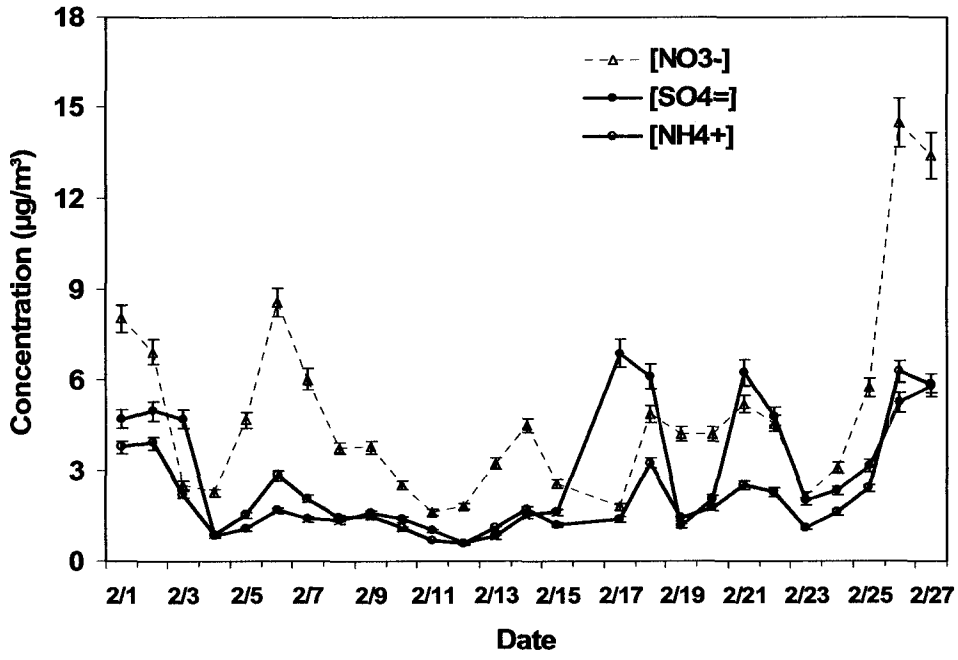

Figure 3.21 Timelines of URG $PM_{2.5}$ SO_4^{2-}, NO_3^- and NH_4^+ concentrations (Bondville, Feb 2003)
(Error bars represent measurement precision (1 standard deviation))

The maximum concentration of ammonium was 6.29 $\mu g/m^3$, observed on 2/26/03. Concentrations ranged from 0.55 $\mu g/m^3$ to 6.29 $\mu g/m^3$, with an average of 2.16 $\mu g/m^3$. As

shown in more detail in chapters 4 and 5, ammonium at this site is paired with both nitrate and sulfate. During some periods, there is insufficient ammonium to neutralize sulfate acidity in the aerosol.

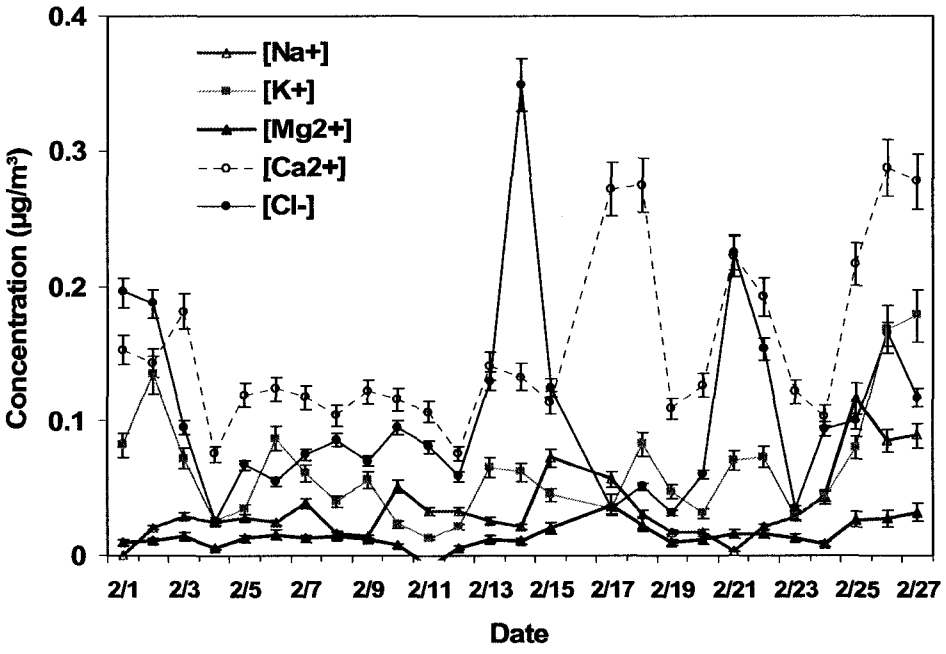

Figure 3.22 Timelines of Cl^-, Na^+, Ca^{2+}, Mg^{2+} and K^+ concentrations in URG $PM_{2.5}$ (Bondville, Feb 2003)
(Error bars represent measurement precision (1 standard deviation))

Na^+ and Mg^{2+} were found to be minor contributors to total cation concentrations in the Bondville $PM_{2.5}$ samples (Figure 3.22). Concentrations of Na^+ and Mg^{2+} ranged from zero (below detection limit) to 0.12 µg/m^3 (an average concentration of 0.04 µg/m^3) and to 0.03 µg/m^3 (an average concentration of 0.02 µg/m^3), respectively. Ca^{2+} was observed to be a more substantial contributor to total cation concentrations. Ca^{2+}

concentrations ranged from 0.08 μg/m^3 to 0.29 μg/m^3 with an average concentration of 0.16 μg/m^3.

Figure 3.23 presents timelines of the mass concentrations of gaseous SO_2, NH_3, and HNO_3 measured using URG annular denuders. Gaseous SO_2 concentrations ranged from 1.01 to 26.1 μg/m^3.The highest concentrations of SO_2 were measured on

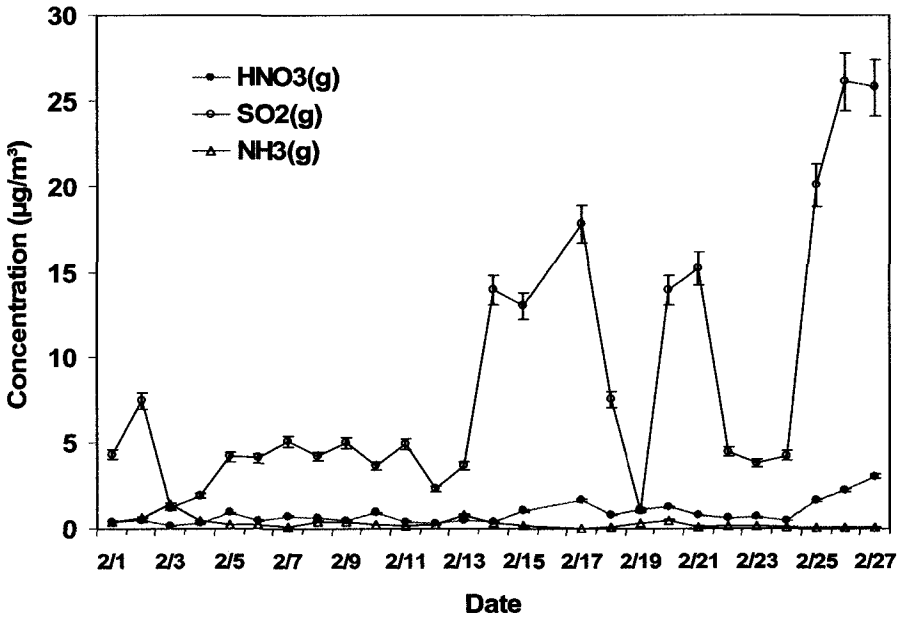

Figure 3.23 Timelines of HNO_3(g), SO_2(g) and NH_3(g) concentrations from URG (Bondville, Feb 2003)
(Error bars represent measurement precision (1 standard deviation))

2/17, 2/20, 2/21, 2/26 and 2/27 with 17.8 μg/m^3, 14.0 μg/m^3, 15.2 μg/m^3, 26.1μg/m^3 and 25.8 μg/m^3. These high SO_2 concentrations likely reflect both the proximity of important sources (coal fired power plants in Illinois and adjoining states) and slow oxidation to sulfate due to lower concentrations of oxidizing species resulting from lower

photochemical activity in winter when temperatures and solar radiation are at a minimum (Bari et al., 2003; Danalatos and Glavas, 1999; Day et al., 1997; Dutkiewicz et al., 2000; Gupta et al., 2003; Husain et al., 2004b; Kasper and Puxbaum, 1998; Shaw and Paur, 1983).

Concentrations of gaseous NH_3 and HNO_3 were much lower than SO_2 concentrations at this site. As illustrated in Figure 3.24, most N(-III) and N(V) at this sites has partitioned to the particle phase, consistent with thermodynamic expectations favoring particulate ammonium nitrate formation at lower temperatures. The average ratio for HNO_3(g)/N(V) was 0.16 and for NH_3(g)/N(-III) was 0.13. Figure 3.24 also demonstrates the relatively small fraction (29% on average) of sulfur found in the particle phase on many days throughout the campaign.

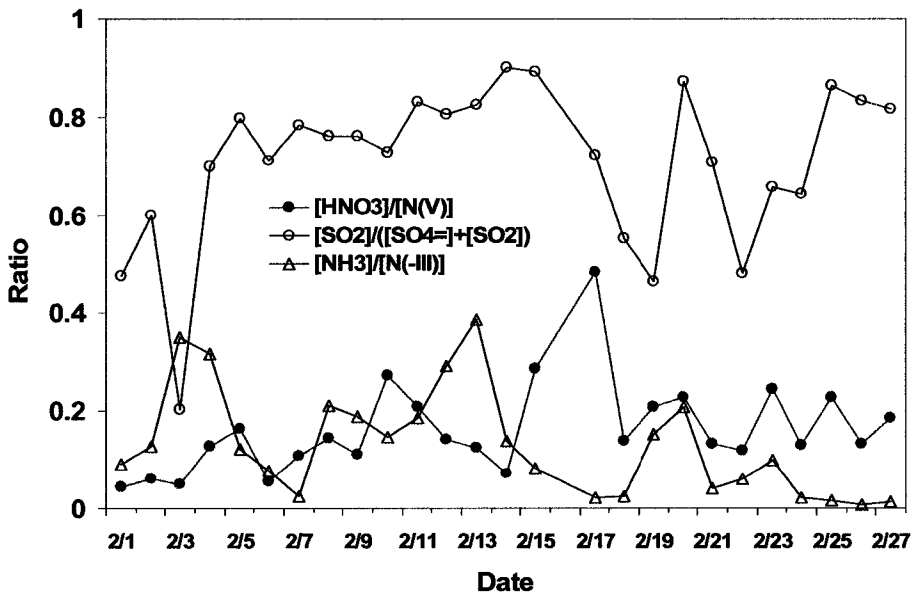

Figure 3.24 Timelines of HNO_3/N(V), NH_3/N(-III) and $SO_2/([SO_4^{2-}]+[SO_2])$ from URG (Bondville, Feb 2003)

Another interesting observation is that the concentrations of K^+ and NO_3^- track each other closely at Bondville (Figure 3.25). Because concentration levels of these species are so different, it is unlikely that we are observing potassium nitrate. More likely, the covariance of these species concentrations reflect similar source types and/or regions or similarities in meteorological conditions (e.g., boundary layer depth) that affect concentrations of multiple aerosol species.

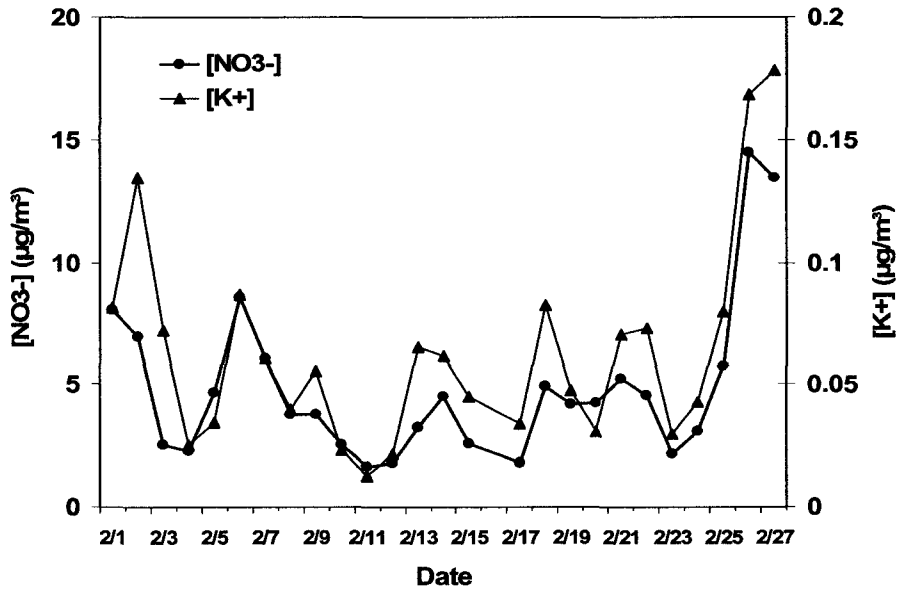

Figure 3.25 Timelines of NO_3^- and K^+ concentrations in URG $PM_{2.5}$ (Bondville, Feb 2003)

The study average particle size distributions of major anion and cation species observed using the MOUDI are shown in Figure 3.26. Cl^- and Mg^{2+} were observed to have broad, perhaps even bimodal size distributions, with fine mode peaks in the range of 0.3 – 0.5 µm and coarse mode peaks in the range 4 – 5 µm. While K^+ was mainly observed in fine particles, Na^+ and Ca^{2+} were clearly enriched in the coarse mode.

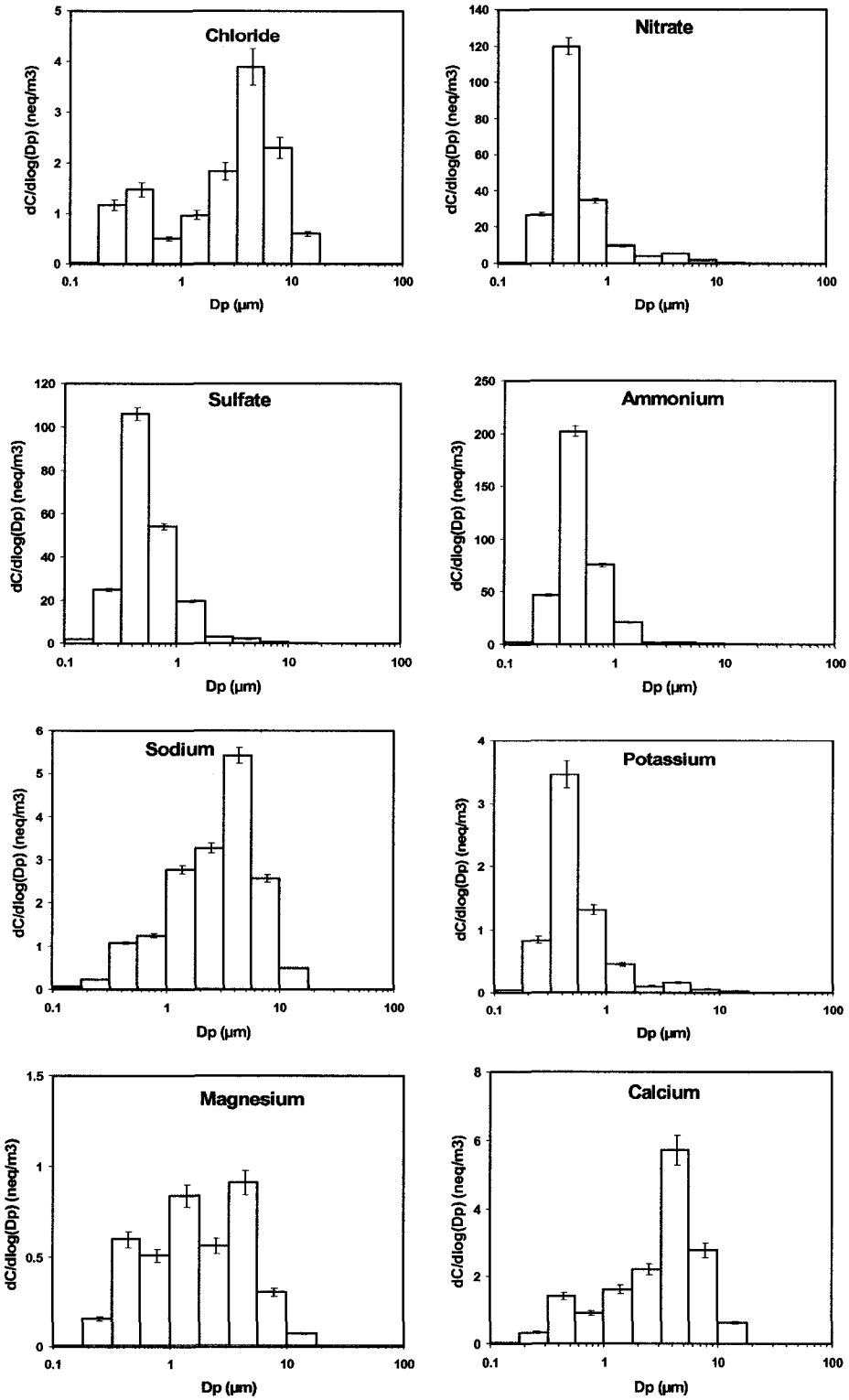

Figure 3.26 Size distributions of average inorganic concentrations (Bondville, IL (February, 2003)) (Error bars represent measurement precision (1 standard deviation))

Occurrence of Cl^-, Na^+, Mg^{2+} and Ca^{2+} in coarse particles is consistent with their presence in mechanically generated sea salt or soil dust particles. Fine mode K^+ may reflect a biomass combustion sources. Fine mode Cl^- is not as easily explained, but could reflect a combustion source associated with power plants or municipal waste incineration.

The particle size distributions of nitrate, sulfate and ammonium exhibit a clear maximum peak in the 0.3 – 0.5 μm in fine mode size range. A small coarse mode was sometimes observed for nitrate as well. Na^+, Mg^{2+} and Ca^{2+} from soil and/or sea salt particle may be associated with coarse mode nitrate. Examples of daily size distributions (e.g., Figure 3.27) provide strong evidences of the formation of coarse mode nitrate associated with reacted salt (sea salt or road salt) or soil dust.

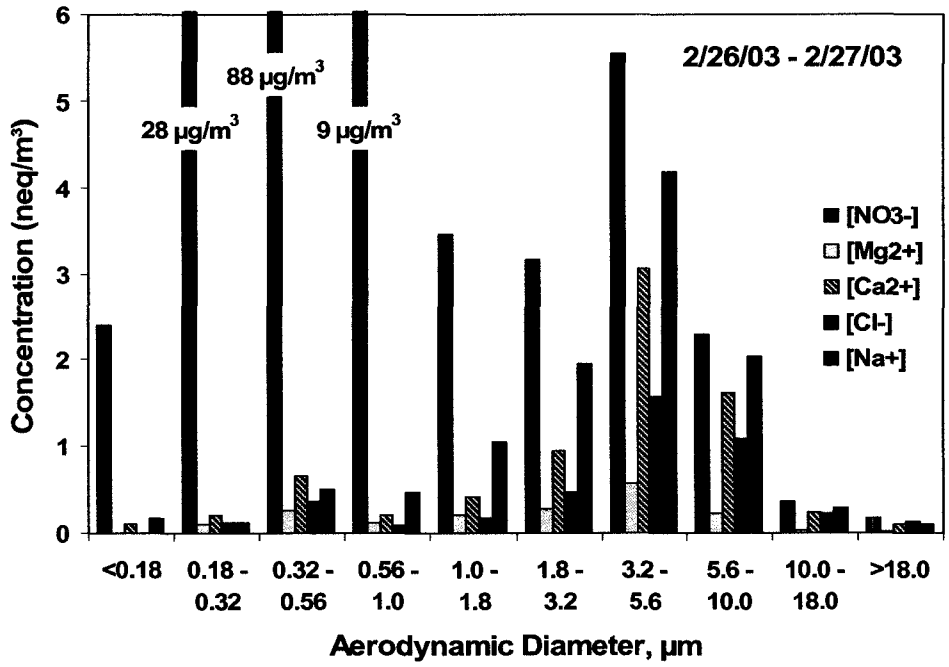

Figure 3.27 Size distributions of NO_3^-, Cl^-, Mg^{2+}, Ca^{2+} and Na^+ concentrations measured on 2/26/03 – 2/27/03 at Bondville using the MOUDI impactor

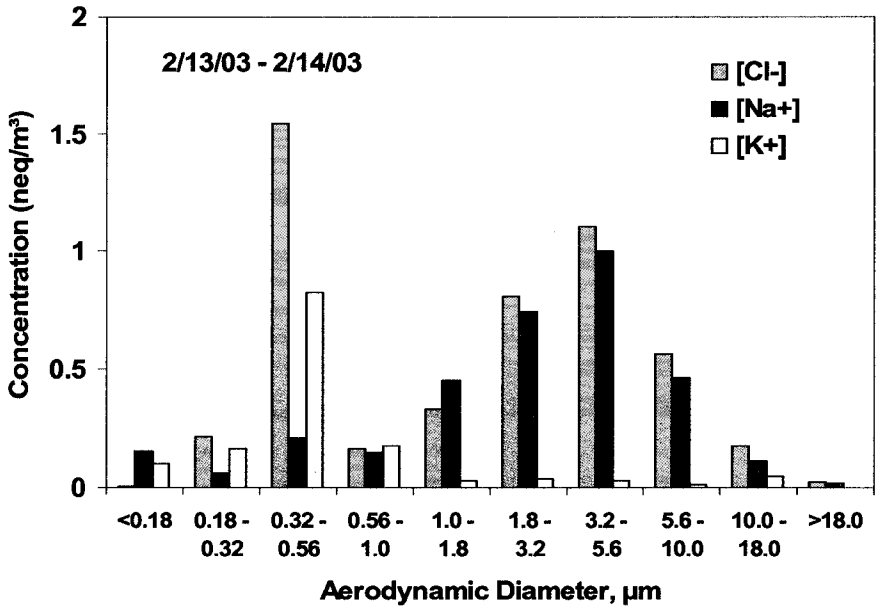

Figure 3.28 Size distributions of Cl^-, Na^+ and K^+ concentrations measured on 2/13/03 – 2/14/03 at Bondville using the MOUDI impactor

The highest fine mode chloride concentration was observed in the sample collected during 2/13/03 – 2/14/03. Figure 3.28 compares particle size distributions of Cl^-, Na^+ and K^+ on 2/13 – 2/14 during Bondville study. Fine particle modes are clearly seen for Cl^- and K^+ but not for Na^+. KCl was one of the most abundant inorganic particle constituents in smoke measured in other field studies (Li et al., 2003; Liu et al., 2000; Niemi et al., 2004; Niemi et al., 2005; Posfai et al., 2003). Local fire burning in wintertime at this site may also be associated with fine mode Cl^- and K^+ observed in MOUDI samples.

3.4 Brigantine National Wildlife Refuge, NJ (November, 2003)

Study timelines of major $PM_{2.5}$ ions measured at Brigantine NWR are presented in Figures 3.29 and 3.30. Sulfate, nitrate and ammonium were typically the dominant

ionic species in daily $PM_{2.5}$ with occasionally significant contributions from Na^+ and Cl^- and smaller contributions from K^+, Mg^{2+} and Ca^{2+}. Concentrations of sulfate and nitrate were highest in the second half of the November study period, with peak values of 4.7 $\mu g/m^3$ and 3.7 $\mu g/m^3$, respectively, on 11/17/03. Average sulfate and nitrate concentrations of 2.98 $\mu g/m^3$ and 4.8 $\mu g/m^3$ were measured with ranges of 0.63 – 4.7 $\mu g/m^3$ and 0.49 – 3.7 $\mu g/m^3$, respectively. Sufficient ammonium was typically present to neutralize nitrate and sulfate particles with an ammonium $PM_{2.5}$ concentration range of 0.38 – 2.85 $\mu g/m^3$ and an average of 2.16 $\mu g/m^3$.

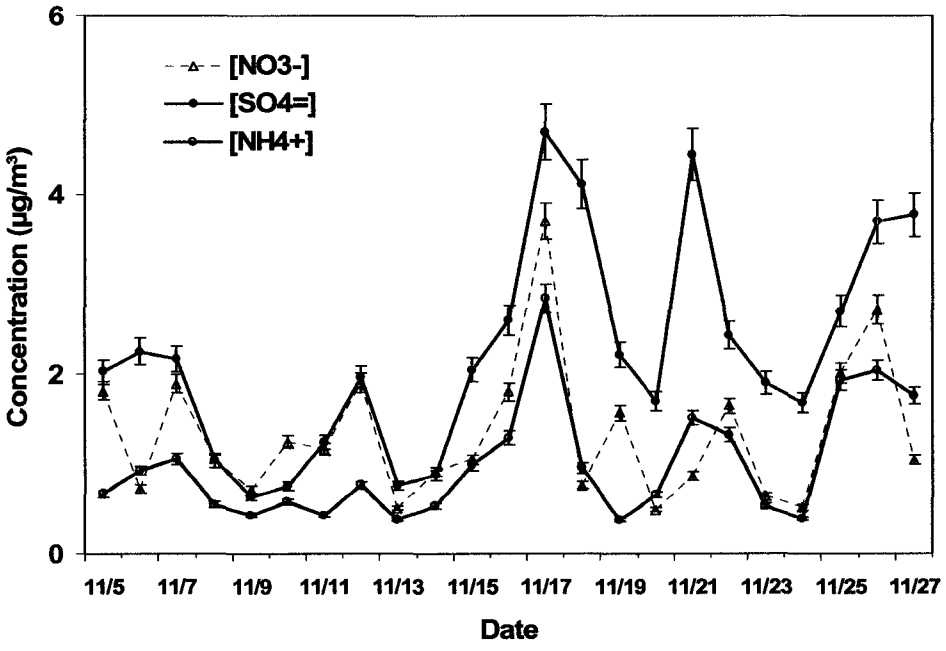

Figure 3.29 Timelines of URG $PM_{2.5}$ SO_4^{2-}, NO_3^- and NH_4^+ concentrations (Brigantine, Nov 2003)
(Error bars represent measurement precision (1 standard deviation))

$PM_{2.5}$ Na^+ and Cl^- concentrations are observed to track each other as shown in Figure 3.30, consistent with substantial contributions from a local sea salt source at this

coastal location. The highest concentrations of Na^+ and Cl^- were measured on 11/19 with 0.88 $\mu g/m^3$ and 1.51 $\mu g/m^3$; study average concentrations were 0.15 $\mu g/m^3$ and 0.23 $\mu g/m^3$, respectively. Concentrations of Ca^{2+} increase from an average of 0.03 $\mu g/m^3$ at the beginning of November to an average of 0.29 $\mu g/m^3$ at the end of study. Concentrations of Mg^{2+} were observed to be close to the detection limit on many days, increasing somewhat during periods of stronger sea salt influence. K^+ concentrations were low throughout the study.

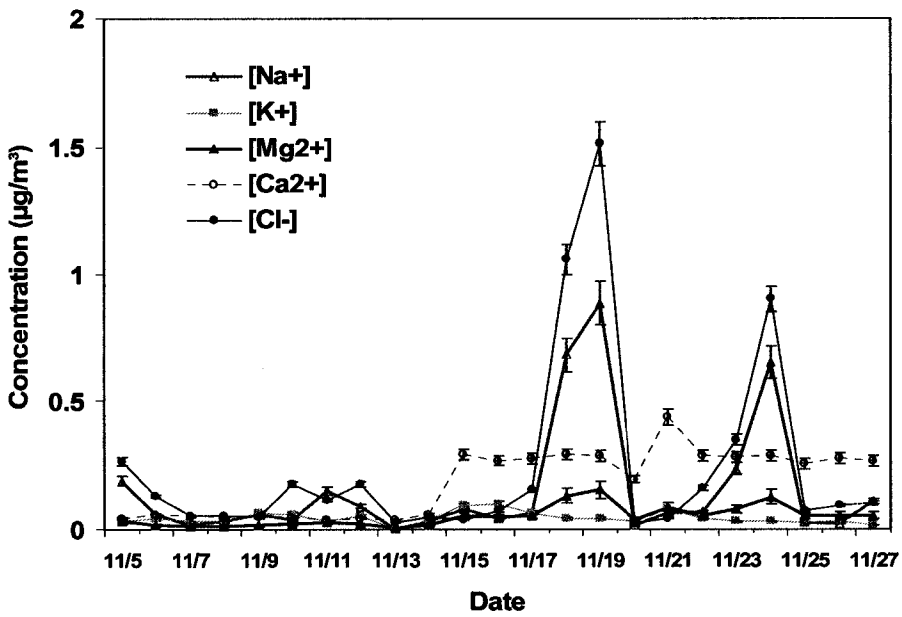

Figure 3.30 Timelines of Cl^-, Na^+, Ca^{2+}, Mg^{2+} and K^+ concentrations in URG $PM_{2.5}$ (Brigantine, Nov 2003)
(Error bars represent measurement precision (1 standard deviation))

Figure 3.31 presents timelines of the concentrations of gaseous SO_2, NH_3 and HNO_3 measured using URG denuders during the Brigantine study. Concentrations of HNO_3 and NH_3 ranged from 0.26 to 1.9 $\mu g/m^3$ and from 0.12 to 0.76 $\mu g/m^3$, with

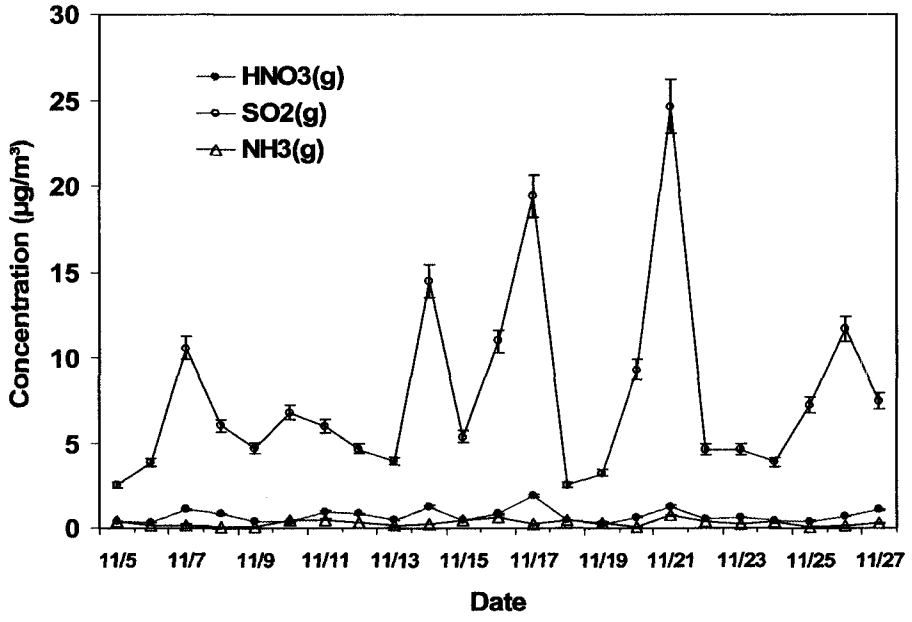

Figure 3.31 Timelines of HNO_3(g), SO_2(g) and NH_3(g) concentrations from URG (Brigantine, Nov 2003)
(Error bars represent measurement precision (1 standard deviation))

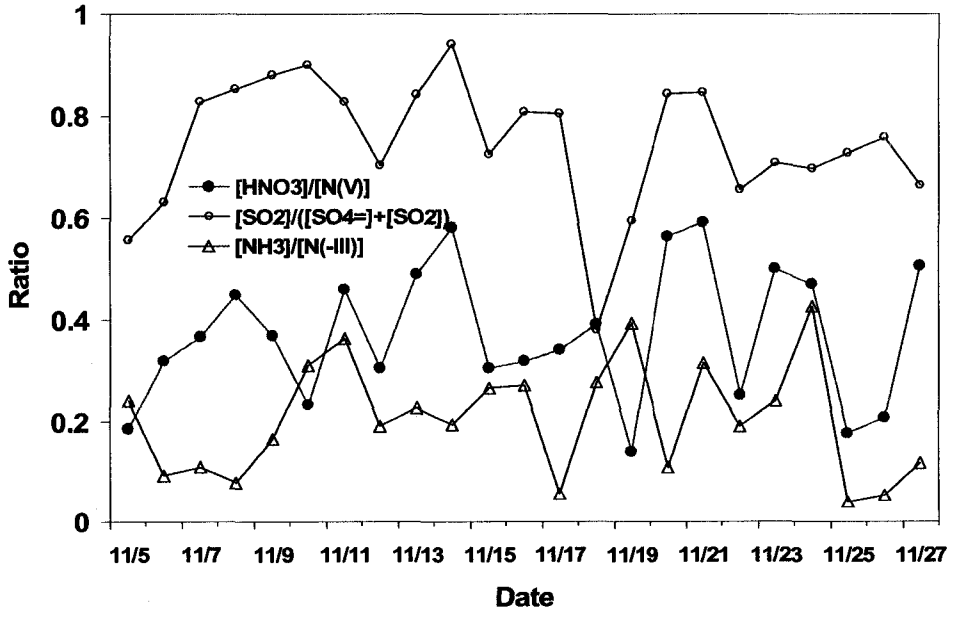

Figure 3.32 Timelines of HNO_3/N(V), NH_3/N(-III) and $SO_2/([SO_4^{2-}]+[SO_2])$ from URG (Brigantine, Nov 2003)

averages of 0.75 and 0.29 $\mu g/m^3$, respectively. Much more sulfur dioxide was observed, with SO_2 concentrations ranging from 1.0 to 26.2 $\mu g/m^3$ with an average of 8.2 $\mu g/m^3$. Similar to observations at Bondville, gaseous SO_2 concentrations here are much higher than concentrations of particle sulfate (see Figure 3.32). The average ratio for $SO_2(g)/([SO_2(g) + [SO_4^{2-}])$ was 0.75. Ammonium and nitrate concentrations were higher than concentrations of gaseous NH_3 and HNO_3. The average ratio for $HNO_3(g)/N(V)$ was 0.4 and for $NH_3(g)/N(-III)$ was 0.19.

The chemical compositions of the size-resolved MOUDI aerosol samples were examined for further insight into the properties of aerosol at Brigantine. Figure 3.33 depicts study average particle size distributions of the major inorganic anions and cations. Sulfate and ammonium exhibit very similar size distributions, with a submicron mode peaked in the 0.32 – 0.56 μm size bin. Generally, the excess ammonium concentrations in the fine mode, the amount of ammonium present beyond that required for neutralizing sulfate, were consistent with observed nitrate concentrations in these same submicron particle size ranges. The study average nitrate particle size distribution is bimodal in nature (Figure 3.33), with peaks in the 0.32 – 0.56 μm and 3.2 – 5.6 μm size bins. Individual MOUDI samples (48 hr) collected at Brigantine reveal that the nitrate is sometimes found either predominantly in a coarse particle mode or as a mix of fine and coarse mode particles. Figure 3.34 shows several example nitrate size distributions. A mix of fine and coarse mode nitrate was found in samples taken on 11/16-17 and on 11/25-26, while nitrate on 11/18-19 and 11/23-24 was observed primarily in supermicron particles. On 11/18, 11/19, 11/23 and 11/24 we measured some of the highest concentrations of Na^+ and Cl^- in URG samples.

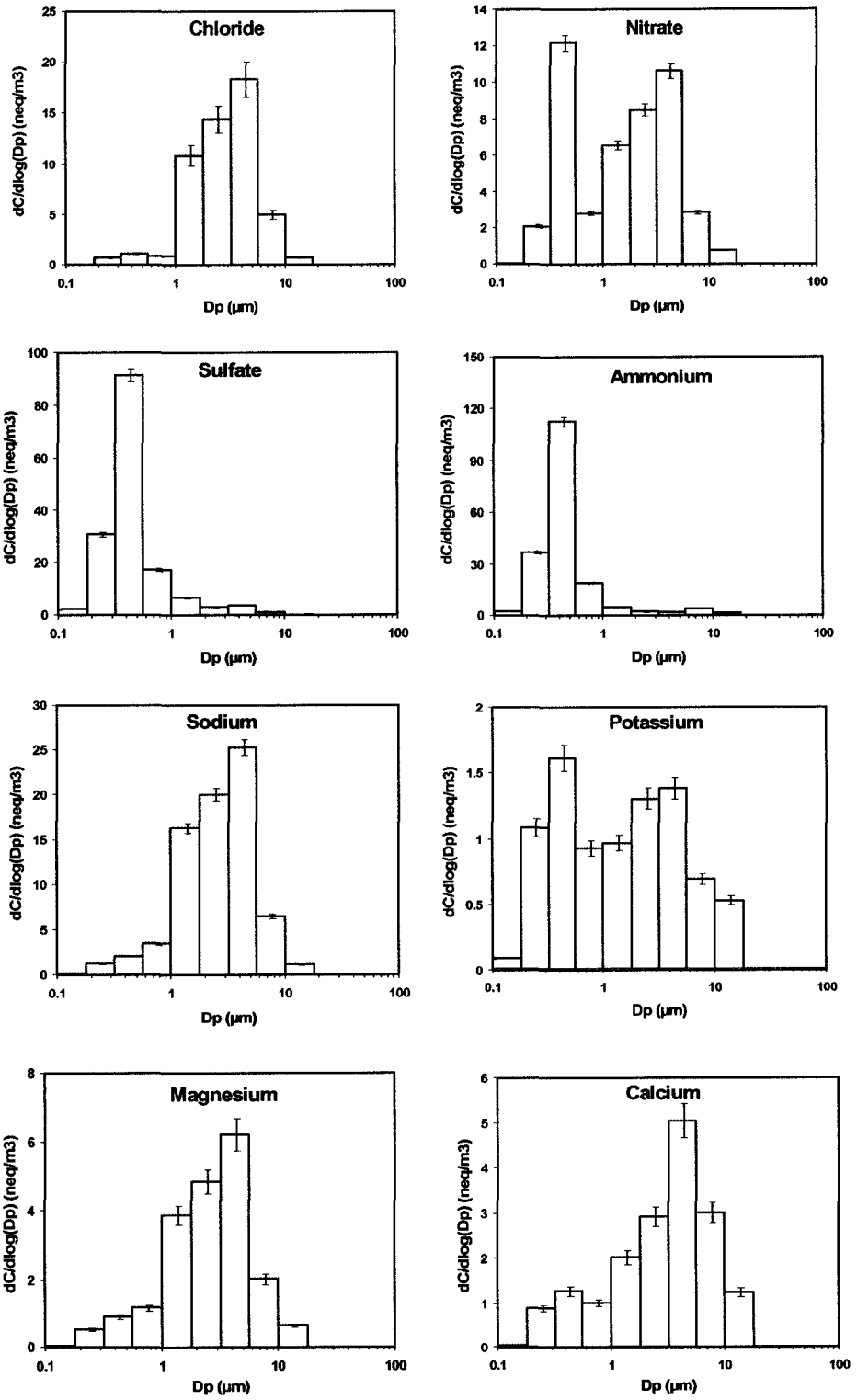

Figure 3.33 Size distributions of average inorganic concentrations (Brigantine , NJ (November, 2003)) (Error bars represent measurement precision (1 standard deviation))

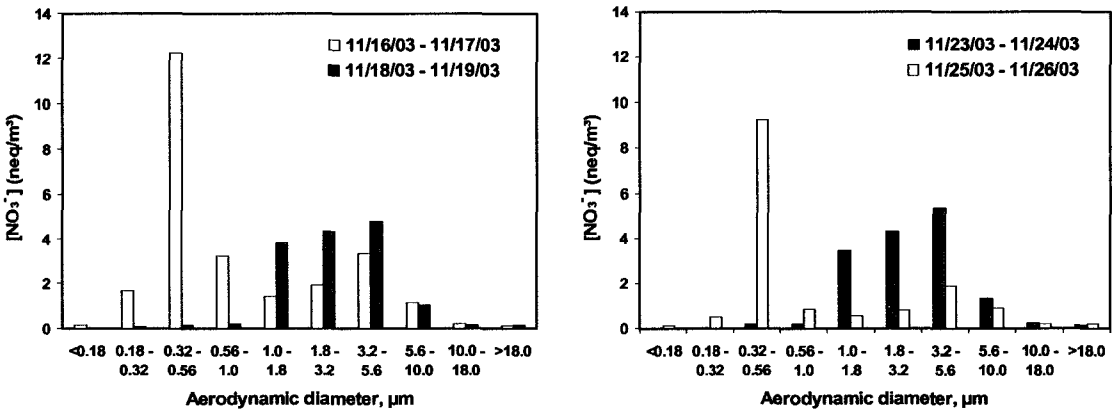

Figure 3.34 Size distributions of nitrate concentrations from 11/16, 11/18, 11/23 and 11/25 (Brigantine , NJ)

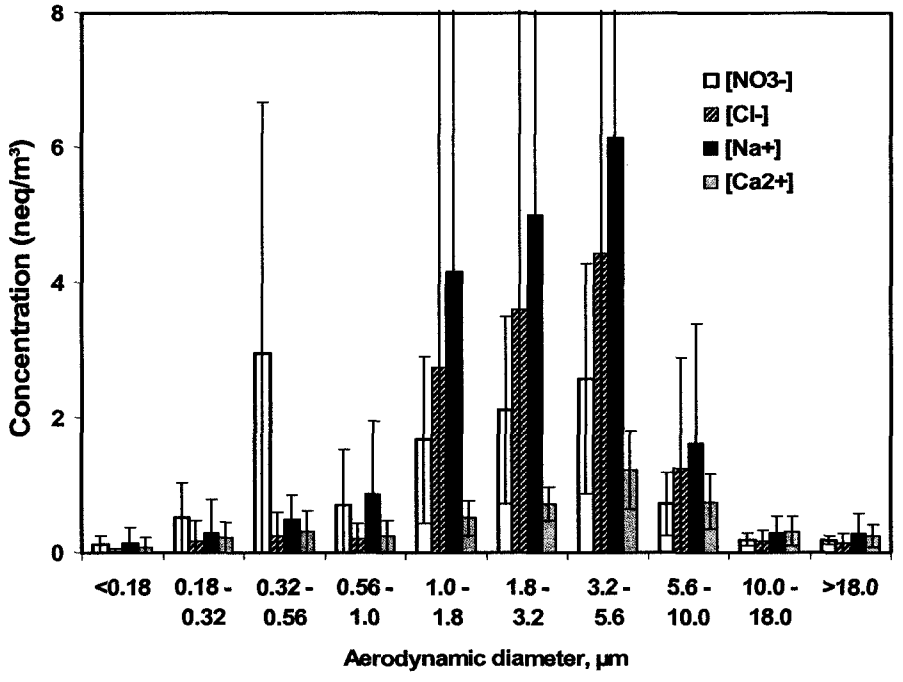

Figure 3.35 Study average size distributions of NO_3^-, Cl^-, Na^+ and Ca^{2+} concentrations (Brigantine , NJ (November, 2003)) (Error bars represent measurement precision (1 standard deviation))

The study average MOUDI Na^+ and Cl^- size distributions (see Figure 3.35) are similar in shape and magnitude to the coarse nitrate mode, suggesting that reaction of nitric acid (or its precursors) with sea salt may be an important mechanism for particle nitrate formation in this environment.

3.5 Great Smoky Mountains NP, TN (July/Aug, 2004)

Figure 3.36 depicts the daily $PM_{2.5}$ sulfate, nitrate and ammonium concentrations measured in July and August, 2004 in Great Smoky Mountains National Park. Sulfate and ammonium were the main ionic species in daily $PM_{2.5}$ samples with small contributions of NO_3^-. The highest sulfate concentrations were measured on 8/3/04, 8/10/04, and 8/17/04 with 13.6 $\mu g/m^3$, 11.5 $\mu g/m^3$ and 13.8 $\mu g/m^3$, respectively. Concentrations of sulfate ranged from 1.7 to 13.6 $\mu g/m^3$. Ammonium was the dominant cation species with an average concentration of 1.6 $\mu g/m^3$, ranging from 0.5 to 2.7 $\mu g/m^3$. Low concentrations of K^+, Mg^{2+}, Na^+ and Ca^{2+} (ranging from 7.5 ng/m^3 to 0.15 $\mu g/m^3$) indicate these species to be minor contributors to total cation concentrations as shown in Figure 3.37.

Figure 3.38 shows that ammonium concentration trends were similar to sulfate, when plotted in terms of equivalents. However, there is generally insufficient ammonium to fully neutralize sulfate particles. The shortage of ammonium in the aerosol produced an acidic aerosol with an average H^+ concentration of 63 neq/m^3, ranging from 12.8 to 129.8 neq/m^3 (Figure 3.38). Figure 3.38 shows that the highest H^+ concentrations were measured during periods with high sulfate concentration on 7/24, 8/5, 8/10, 8/16 and 8/17. Low aerosol acidity was observed on 7/26, 7/30 and 8/12.

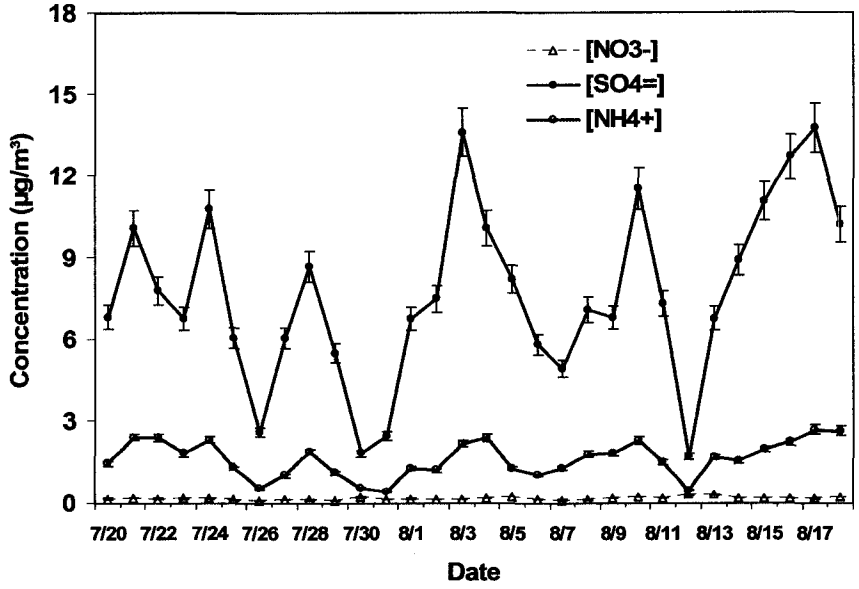

Figure 3.36 Timelines of NH_4^+, SO_4^{2-} and NO_3^- concentrations in URG $PM_{2.5}$ (Great Smoky Mountains NP, July/Aug, 2004) (Error bars represent measurement precision (1 standard deviation))

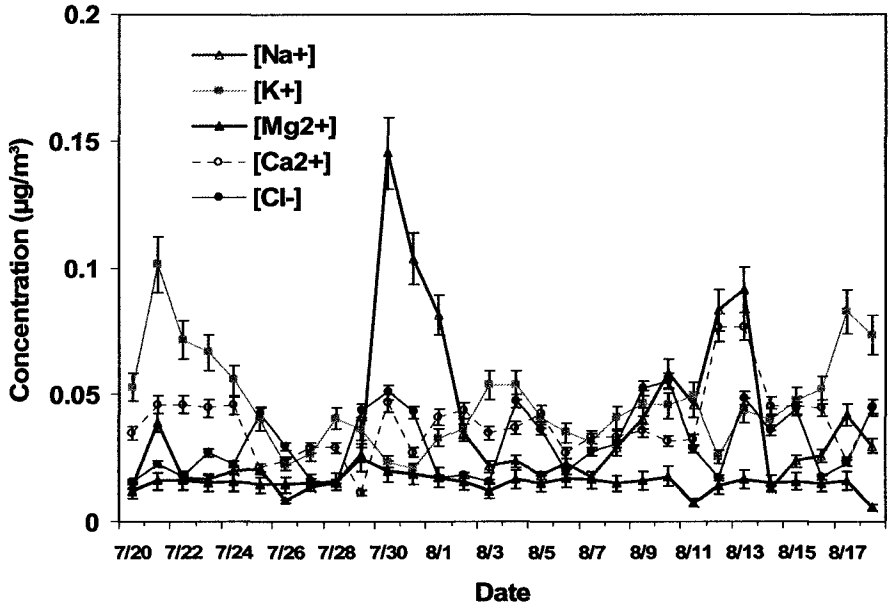

Figure 3.37 Timelines of Cl^-, Na^+, Ca^{2+}, Mg^{2+} and K^+ concentrations in URG $PM_{2.5}$ (Great Smoky Mountains NP, July/Aug, 2004) (Error bars represent measurement precision (1 standard deviation))

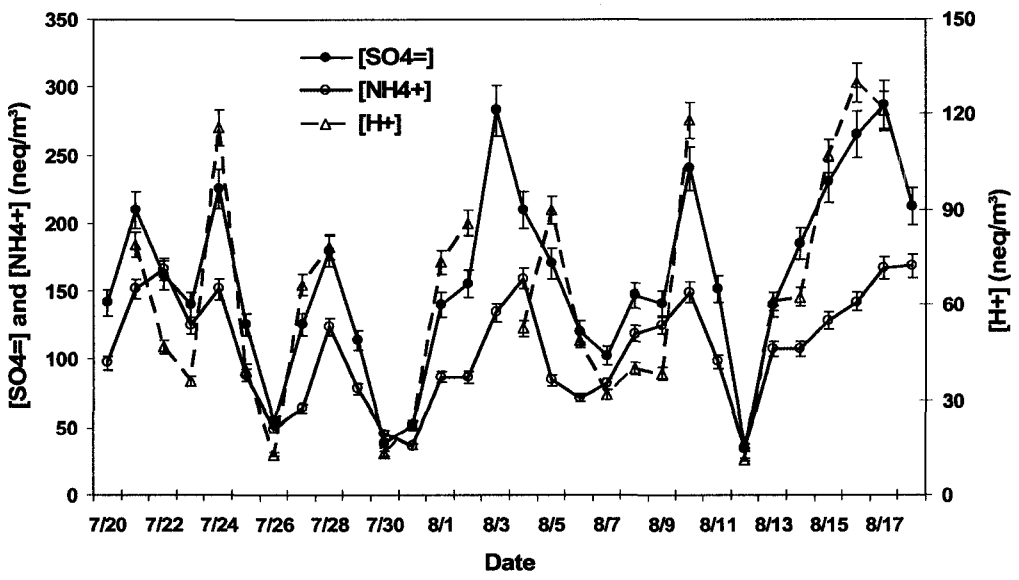

Figure 3.38 Timelines of SO_4^{2-}, NH_4^+ and H^+ concentrations in URG $PM_{2.5}$ (Great Smoky Mountains NP, July/Aug, 2004) (Note : units as neq/m^3) (Error bars represent measurement precision (1 standard deviation))

Ammonium and sulfate can combine in various ratios to yield a variety of compounds, including H_2SO_4 (sulfuric acid), NH_4HSO_4 (ammonium bisulfate), $[NH_4]_3H[SO_4]_2$ (letovicite), and $[NH_4]_2SO_4$(ammonium sulfate) with molar ratios of $[NH_4^+]/[SO_4^{2-}]$ of 0, 1, 1.5 and 2 (Day et al., 1997; Lee et al., 2004). Figure 3.39 shows variations in the ratio of $[NH_4^+]/[SO_4^{2-}]$ during the Great Smoky Mountains NP study. The molar ratios of ammonium to sulfate suggest that sulfate in the Great Smoky Mountains NP ranges from an average composition equivalent to NH_4HSO_4(ammonium bisulfate) up to $[NH_4]_2SO_4$ (ammonium sulfate) with an average ratio of 1.44 (standard deviation of 0.33). The observed aerosol acidity is also consistent with the relationships between gaseous species and particle concentrations (Figures 3.40 and 3.41). Figures 3.40 and 3.41 show low concentrations of NH_3 (g) (0.21 $\mu g/m^3$ on average with a range

from 0.11 to 0.34 $\mu g/m^3$) with N(-III) associated mainly with particles (NH_3 (g)/N(-III) ratio ranging from 0.05 to 0.27). By contrast, appreciable sulfur is still observed in the gas phase, with concentrations of SO_2 (g) ranging from 0.2 to 6.9 $\mu g/m^3$. Concentrations of HNO_3(g) ranged from 0.34 to 1.99 $\mu g/m^3$ (Figure 3.40) with an average ratio of HNO_3 (g)/N(V) of 0.84 (Figure 3.41). The tendency for most nitrate to stay in the gas phase is consistent with the strongly acidic nature of the observed fine particles. Formation of nitrate is not favored in the absence of sufficient ammonia to neutralize fine particle sulfate.

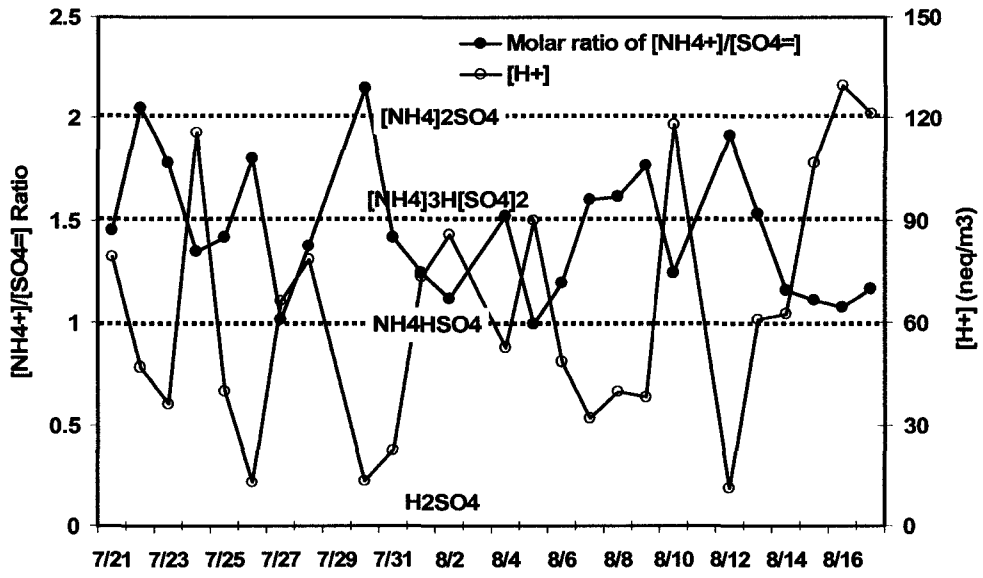

Figure 3.39 Timelines of molar ratio of $[NH_4^+]/[SO_4^{2-}]$ and H^+ concentration in $PM_{2.5}$ (Great Smoky Mountains NP, July/Aug, 2004)

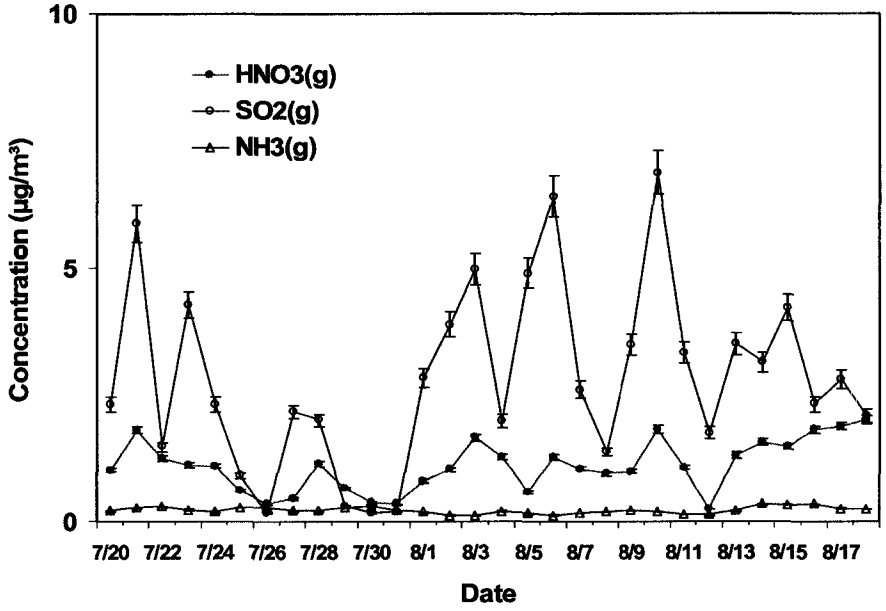

Figure 3.40 Timelines of HNO_3(g), SO_2(g) and NH_3(g) concentrations from URG (Great Smoky Mountains NP, July/Aug, 2004) (Error bars represent measurement precision (1 standard deviation))

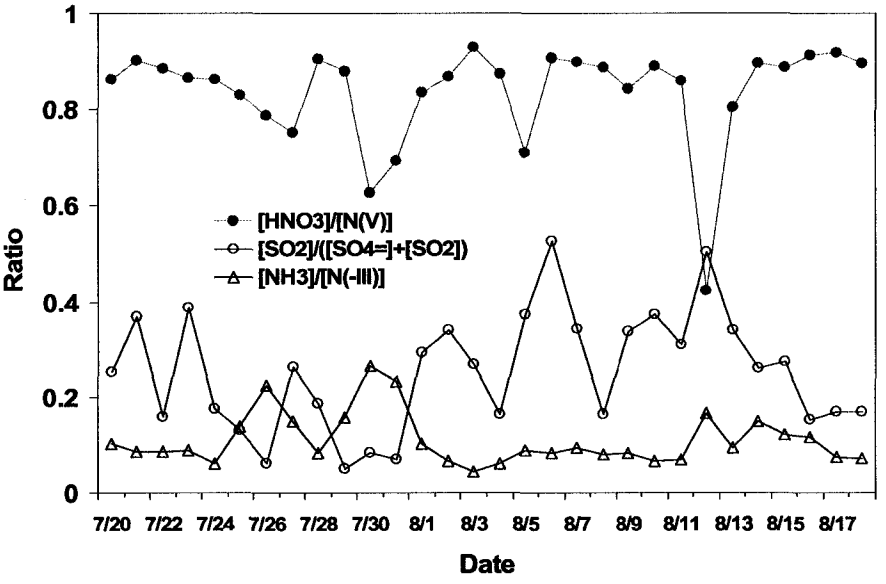

Figure 3.41 Timelines of HNO_3/N(V), NH_3/N(-III) and $SO_2/([SO_4^{2-}]+[SO_2])$ from URG (Great Smoky Mountains NP, July/Aug, 2004)

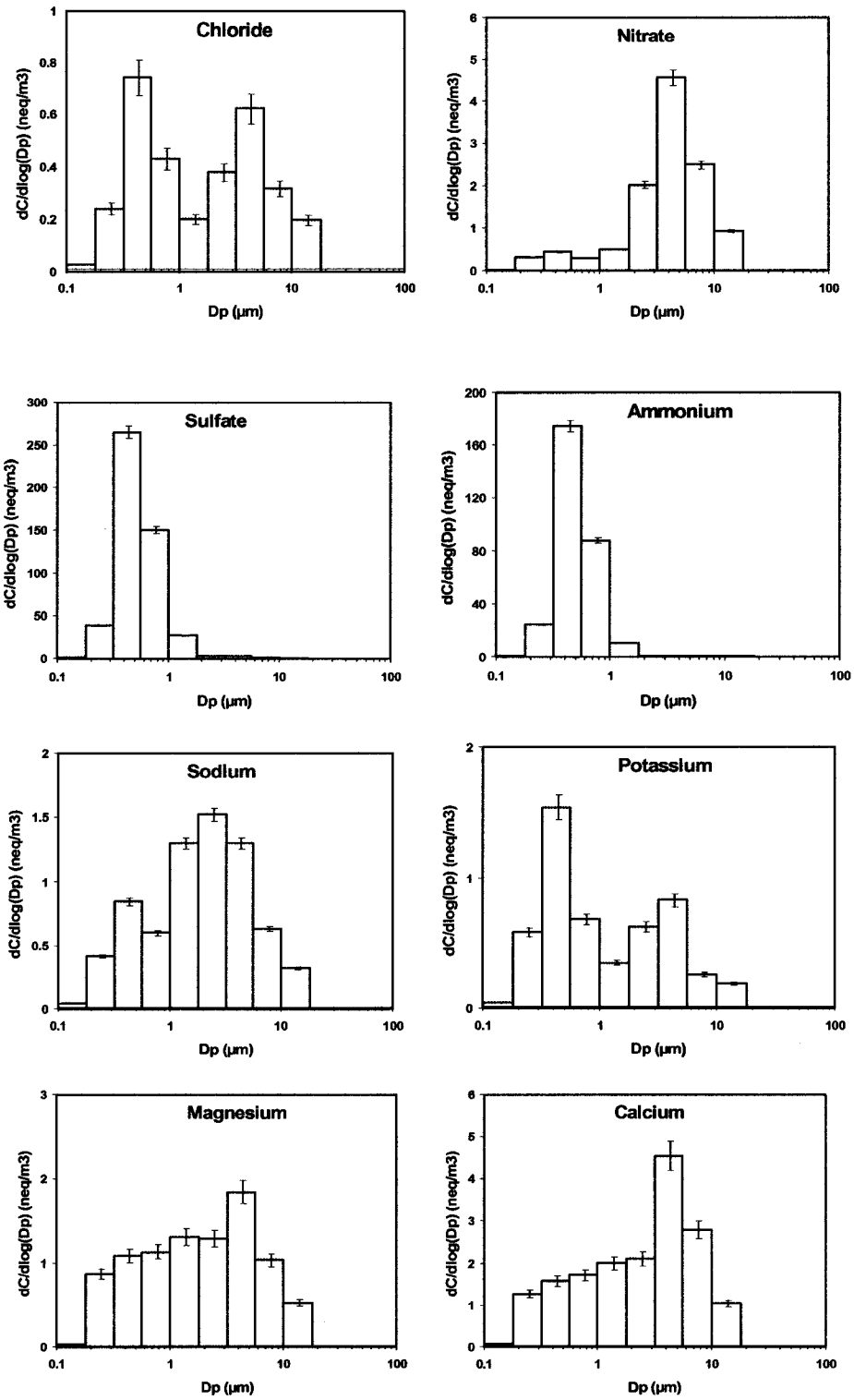

Figure 3.42 Study average particle size distributions of key inorganic ions (Great Smoky Mountains National Park (July/Aug, 2004))
(Error bars represent measurement precision (1 standard deviation))

Figure 3.42 depicts the study average particle size distributions observed at Great Smoky Mountains NP for major anions (Cl^-, NO_3^-, and SO_4^{2-}) and cations (Na^+, NH_4^+, K^+, Mg^{2+} and Ca^{2+}). Sulfate and ammonium are found in a fine particle mode. Here, too, we see that insufficient ammonium is present to neutralize measured sulfate. NO_3^-, Na^+, Ca^{2+} and Mg^{2+} are mainly contained in a coarse particle mode, although a fine particle mode of Na^+ is apparent. Interestingly, the study average K^+ and Cl^- size distributions are bimodal in nature, with fine and coarse particle modes peaked at 0.3 – 0.5 μm and 3 – 5 μm aerodynamic diameter, respectively. The amount of Na^+, Ca^{2+} and Mg^{2+} measured in the coarse mode is roughly sufficient to balance observed nitrate concentrations, suggesting that nitric acid reactions with both sea salt and soil dust contribute to the formation of particle nitrate at this location. As will be discussed in chapters 4 and 5, the main factor controlling formation of particulate nitrate in this location appears to be the availability of sea salt and/or soil dust particles to provide sites for heterogeneous reaction with gaseous nitric acid.

3.6 Summary and conclusions

Annular denuder/filter-pack (URG) and MOUDI samplers were used to collect 24-hr daily $PM_{2.5}$ ions (Cl^-, SO_4^{2-}, NO_3^-, Na^+, NH_4^+, K^+, Mg^{2+}, and Ca^{2+}) and trace gas (HNO_3, NH_3 and SO_2) concentrations and 48-hr size-resolved particle samples, respectively, at several IMPROVE monitoring sites during a series of month-long field studies. Study sites included Bondville, Illinois (February 2003), San Gorgonio Wilderness Area, California (April and July 2003), Grand Canyon N.P. (May 2003),

Brigantine National Wildlife Refuge, New Jersey (November 2003) and Great Smoky Mountains N.P. (July/August, 2004).

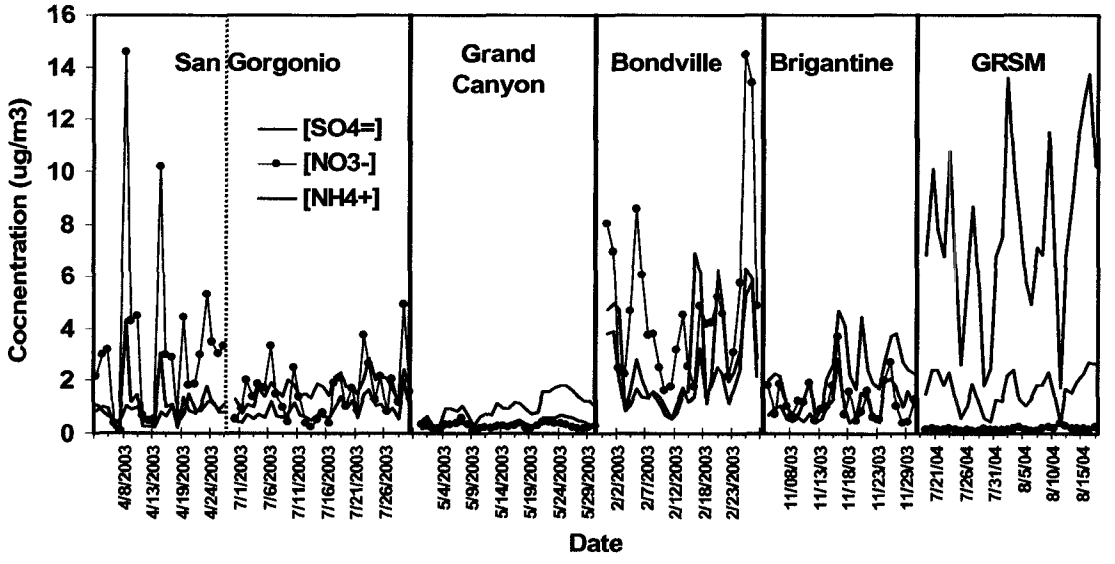

Figure 3.43 Timelines of $[SO_4^{2-}]$, $[NO_3^-]$ and $[NH_4^+]$ at all sites URG $PM_{2.5}$

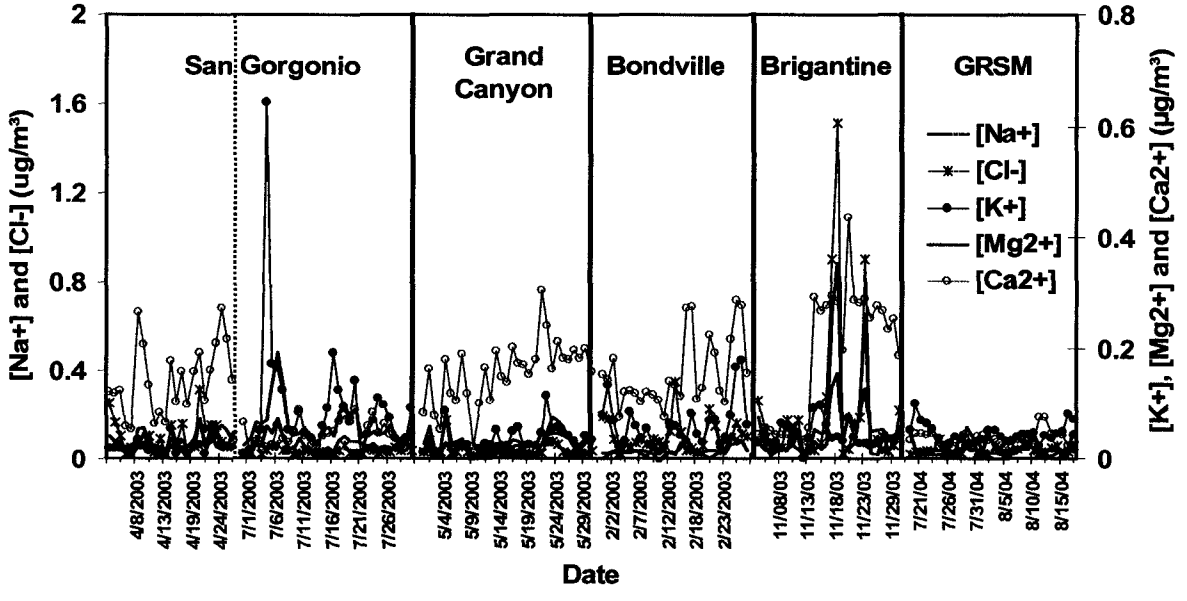

Figure 3.44 Timelines of $[Na^+]$, $[K^+]$, $[Mg^{2+}]$, $[Ca^{2+}]$, and $[Cl^-]$ at all sites URG $PM_{2.5}$

Figure 3.43 shows timelines of the major ionic species (SO_4^{2-}, NO_3^- and NH_4^+) of $PM_{2.5}$ measured in each of the studies. Ammonium and sulfate were observed as predominant species in $PM_{2.5}$ at Great Smoky Mountains N.P. (July/August, 2004) with minor contributions by nitrate, while ammonium, sulfate and nitrate were found in various proportions at the other study sites. Generally, the sulfate contribution to $PM_{2.5}$ increased in moving across the country from west to east, corresponding to more abundant SO_2 sources in the eastern US. By contrast, the lowest concentrations of nitrate were observed in Great Smoky Mountains N.P. where the acidic nature of the aerosol precludes much formation of fine particle ammonium nitrate. Ammonium nitrate concentrations were much higher at sites with relatively greater availability of ammonia and during seasons where temperatures were cooler.

Figure 3.44 presents timelines of the minor $PM_{2.5}$ cation species (plus Cl^-) measured in each of the studies. Relatively higher Ca^{2+} concentrations were observed at San Gorgonio in April, Grand Canyon NP, Bondville, and Brigantine. Higher concentrations of Na^+ and Cl^- at Brigantine reflect the proximity of this study site to the Atlantic Ocean.

Figure 3.45 shows timelines of SO_2, HNO_3 and NH_3 concentrations measured at all sites. The highest average concentrations of HNO_3 and NH_3 were found at San Gorgonio under warm, dry conditions in July, reflecting the low thermodynamic potential for particulate ammonium nitrate formation under these conditions. High concentrations of SO_2 were observed at Bondville and Brigantine, indicating the potential for significant additional particulate SO_4^{2-} formation as the sulfur dioxide is further oxidized in the gas phase or in clouds. Lower concentrations of SO_2 at Great Smoky Mtns. NP reflect, in

part, greater conversion of sulfur dioxide to sulfate in the more oxidant rich conditions typical of summer.

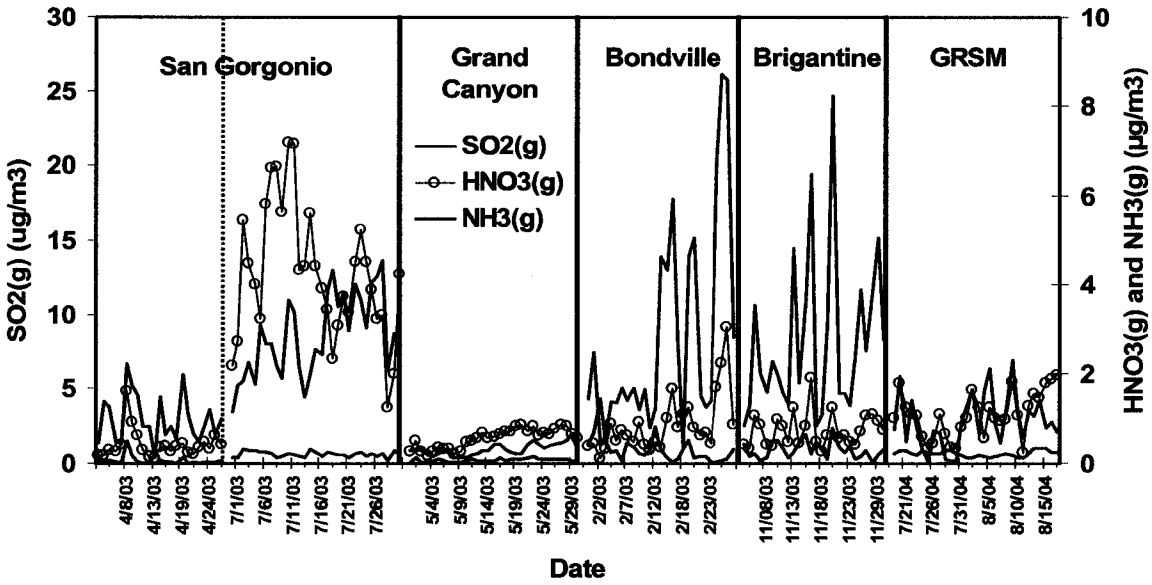

Figure 3.45 Timelines of [SO_2], [HNO_3] and [NH_3] at all sites

Figure 3.46 shows the timelines of ratios of gaseous nitric acid, ammonia and sulfur dioxide to total N(V), N(-III) and total S ([SO_2(g)] + [SO_4^{2-}(p)]), respectively. Here we see evidence of the greater conversion of sulfur dioxide to sulfate in summer at Great Smokies vs. in fall/winter at Bondville and Brigantine. We also see that most of the available N(V) was in the gas phase at San Gorgonio (July), Grand Canyon NP and Great Smoky Mountains NP due to relatively high temperatures (all three sites) and the acidic nature of the aerosol (Great Smoky Mountains NP). More than half of the N(-III) is in the gas phase during the July measurements at San Gorgonio; N(-III) was distributed roughly equally between the particle and gas phases during the spring measurements at

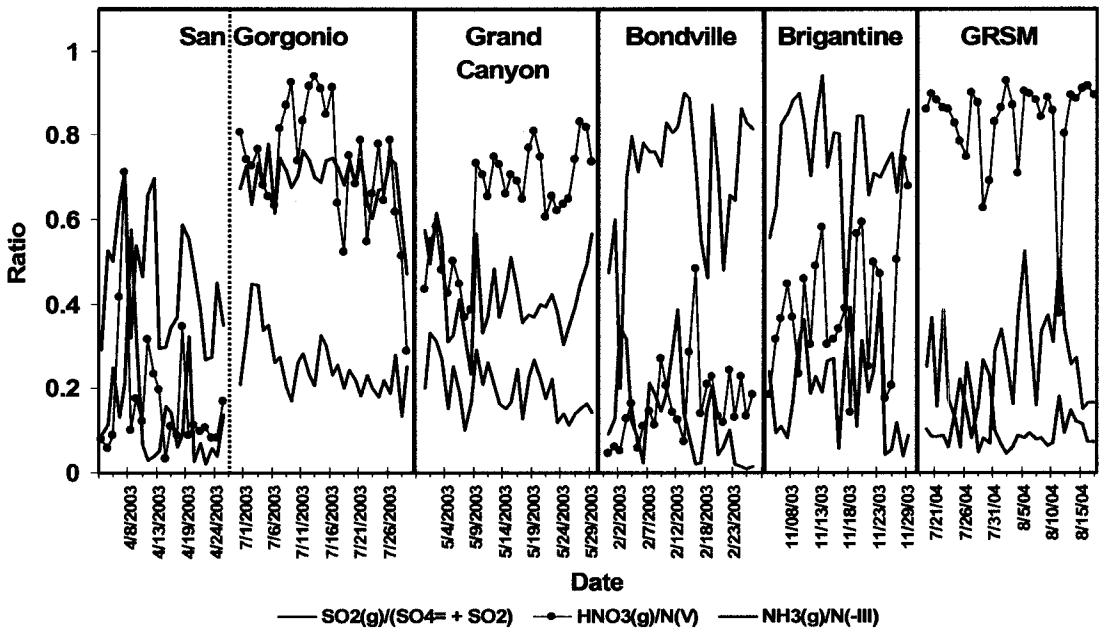

Figure 3.46 Timelines of HNO_3/N(V), NH_3/N(-III) and $SO_2/([SO_4^{2-}]+[SO_2])$ at all sites

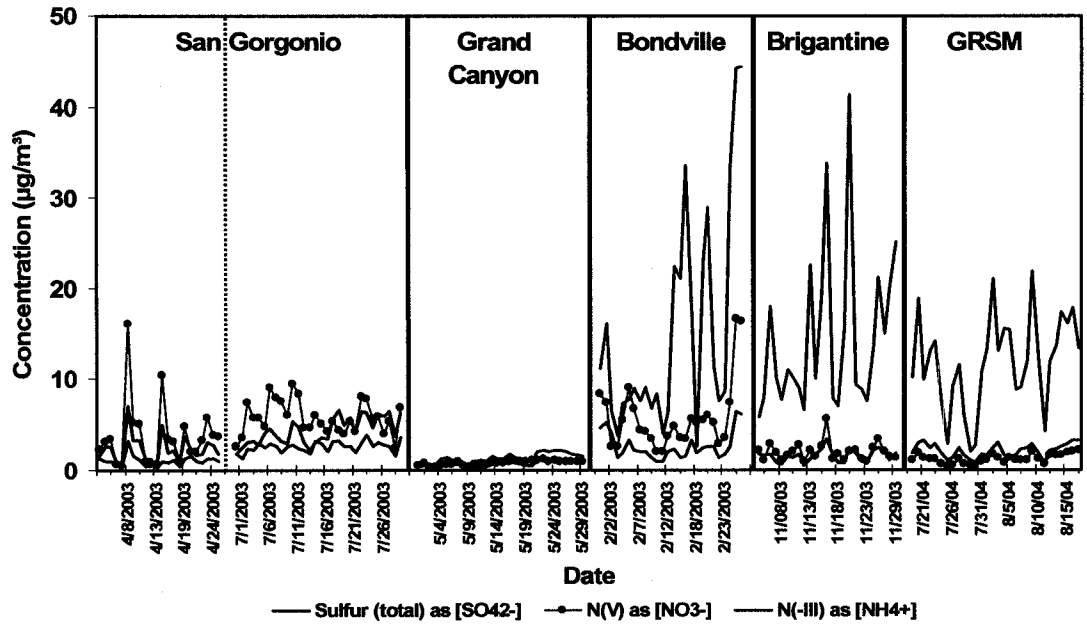

Figure 3.47 Timelines of N(V) as $[NO_3^-]$, N(-III) as $[NH_4^+]$ and total S as $[SO_4^{2-}]$ at all sites

San Gorgonio and Grand Canyon. Most N(-III) was found in the particle phase during the fall/winter studies at Brigantine and Bondville. We also observed most N(-III) in particles during summer at Great Smoky Mtns, consistent with the strong sink for ammonia provided there by acidic sulfate particles.

Figure 3.47 shows the timelines of concentrations in $\mu g/m^3$ of N(V), N(-III) and total sulfur expressed as equivalent $[NO_3^-]$, $[NH_4^+]$ and $[SO_4^{2-}]$, respectively, for all sites. Generally, the highest concentrations of total sulfur were observed in the eastern US, consistent with more abundant SO_2 sources in this region. By contrast, relatively low concentrations of N(V) and N(-III) were observed at the sites in the eastern US, including Brigantine and Great Smoky Mtns NP. The concentrations of N(V), N(-III) and total sulfur were similar during the spring and summer measurements at San Gorgonio, although partitioning between the gas and particle phases differed between spring and summer (Fig. 3.46). Another interesting observation is that the lowest concentrations of N(V), N(-III), and total sulfur were observed in Grand Canyon NP, consistent with lower emissions in this region of the country.

MOUDI size-resolved aerosol

The MOUDI samples collected during all the field campaigns revealed similar size distributions for sulfate and ammonium, with a fine particle mode peaked in the size range from 0.4 to 0.5 μm aerodynamic diameter. A small sulfate coarse mode was also observed at San Gorgonio, Grand Canyon, Bondville, and Brigantine, with a characteristic mode diameter of approximately 4 – 5 μm, suggesting some reaction of gaseous SO_2 or H_2SO_4 with sea salt and soil dust may have occurred at these locations (Bauer and Koch, 2005; Carmichael et al., 1996; Dentener et al., 1996; Fan et al., 2004;

Finlayson-Pitts and Pitts, 2000; Hien et al., 2005; Hwang and Ro, 2005; Liao et al., 2003; Seinfeld and Pandis, 1998).

Nitrate size distributions varied significantly between locations. A dominant fine particle mode, similar in shape to the ammonium size distribution with a mode peak at 0.4 – 0.5 μm aerodynamic diameter, was observed at San Gorgonio (April) and Bondville (February). These observations indicate the importance of formation of fine particle ammonium nitrate by reaction of gaseous HNO_3 with gaseous NH_3 (Finlayson-Pitts and Pitts, 2000; Seinfeld and Pandis, 1998) during these studies. The MOUDI samples collected at San Gorgonio in July reveal nitrate mainly in a coarse mode, associated with Na^+, Mg^{2+} and Ca^{2+}. The absence of coarse mode nitrate in these samples, however, appears to be an artifact resulting from loss of semivolatile fine particle ammonium nitrate during the 48 hr sampling period. A dominant nitrate coarse mode was observed at Grand Canyon N.P. and Great Smoky Mountains N.P. At Brigantine, we often observed a bimodal nitrate particle size distribution. In general, coarse mode nitrate was observed to peak in the size range of ~ 4 - 5 μm, although the coarse mode nitrate in Great Smoky Mountains N.P. typically peaked at approximately 2 – 3 μm.

Generally, Na^+ and Cl^- (sea salt components) and Ca^{2+} and Mg^{2+} (from soil dust) exhibited similarly shaped size distributions at most sites, with a coarse mode peak at 2-3 μm and 4-5 μm in Grand Canyon N.P and at other sites, respectively. The similarity of these cation particle size distributions with observed coarse mode nitrate peaks is consistent with the apparent importance of particle nitrate formation by HNO_3 reaction with sea salt and/or soil dust particles at some locations. Interestingly, a fine mode (0.4 –

0.5 μm) of Cl^- was also observed in San Gorgonio and Bondville, and fine modes (0.4 – 0.5 μm) of Cl^- and Na^+ were observed in Great Smoky Mountains N.P.

The chemical properties of the ambient aerosol (e.g. particle acidity, the chemical forms of nitrate and sulfate) are very important to understand impacts of these particles on light extinction and associated visibility degradation. Extinction efficiencies vary with (1) particle composition and (2) changes in ambient relative humidity that lead to hygroscopic growth of some particle types (Hand and Malm, 2006; Malm et al., 2005b; Watson, 2002). Particle hygroscopicity, in turn, depends on particle composition.

Phase transitions, between particle and gas phases, and the sizes of particles in which individual species are contained also exert an important influence on the atmospheric lifetimes of these species. For example, both HNO_3 and NH_3 in the gas phase have high deposition velocities, meaning their lifetimes in air masses in contact with the surface will be limited to hours/days. Reaction of ammonia and nitric acid to form fine particle ammonium nitrate, however, can drastically increase the lifetimes of these species by significantly reducing dry deposition velocities. Lifetimes of submicron particles tend to be on the order of a week and are controlled mainly by wet removal processes. The increase in species lifetimes as a result of fine particle formation will greatly enhance the distance over which these species may be transported through the atmosphere. In cases where nitric acid enters coarse particles, however, the increase in nitrate's atmospheric lifetime will be less given the much higher dry deposition velocities associated with coarse particles. Several model calculations predict that approximately half of HNO_3 (g) could be removed by sea-salt and/or soil dust and the resulting high dry-deposition velocities associated with supermicron size particles (Erickson et al., 1999;

Spokes et al., 2000). Coarse particles are also removed more efficiently by wet deposition processes than are accumulation mode particles.

In order to understand how future changes in emissions might affect aerosol concentrations, it is necessary to understand the concentrations and forms of various chemical species currently in the atmosphere. In particular we need to consider concentrations of aerosol species, including the relative availability of ammonium, sulfate and nitrate, aerosol acidity, the current distribution of nitrate between ammonium nitrate and mineral forms of nitrate, and concentrations of the key gas phase species HNO_3, NH_3 and SO_2. In the inorganic aerosol system dominated by sulfate-nitrate-ammonium-precursor gas species, nitrate partitioning will favor the gas phase when the aerosol is acidic (sulfate > ammonium). Formation of ammonium nitrate is more favored when sulfate concentrations are low and more gaseous ammonia is available to react with nitric acid. Several model simulations show that reductions of SO_2 emissions are expected to lower average ambient particulate SO_4^{2-} concentrations in the eastern United States (Blanchard and Hidy, 2005; West et al., 1999). Under conditions where sulfate concentrations are lowered (e.g., by reducing SO_2 emissions), it is possible that nitrate may end up replacing sulfate in the aerosol. This is of considerable concern, in terms of impacts on regulated fine particle mass concentrations, because two molecules of NH_4NO_3 can replace a single molecule of $(NH_4)_2SO_4$, resulting in an overall particulate mass increase. The extent of new ammonium nitrate formation, of course, also depends on availability of nitric acid and the environmental conditions (T, RH) that govern the gas-particle equilibrium for ammonium nitrate. If ammonia and nitric acid are present at substantial levels, ammonium nitrate is more likely to form. The biggest impacts are

likely at night, when temperature decreases and humidity increases, and during cooler seasons of the year.

Among the situations studied here, one might expect the most effective emissions reduction strategies to differ depending on location and season. At Bondville and Brigantine in fall/winter, one might expect reductions in SO_2 emissions, if they translate into reductions in particle sulfate concentrations, to be fairly effective at reducing overall particle mass. This is because most N(V) in these environments is already contained in particles. A similar situation is observed at San Gorgonio in spring. In these three environments, one might also expect reductions in NO_x emissions to translate into reductions in particle nitrate. The effectiveness of both SO_2 and NO_x reductions, of course, depends on whether similar decreases in the oxidation products (sulfuric and nitric acids) occurs, or whether an oxidant limited situation prevails under which production of sulfuric and nitric acids is limited more by oxidant availability than by SO_2 or NO_x concentrations. The situation is somewhat different at Great Smoky Mtns. NP. Here, reductions in sulfate would make the aerosol less acidic. If sulfate concentrations were reduced far enough (beyond the aerosol neutrality point), excess ammonia would become available to react with the available nitric acid. Because nitric acid concentrations at this site were modest (~1-2 $\mu g/m^3$) and summertime temperatures at this location are high, formation of additional ammonium nitrate, however, is likely to be small. At San Gorgonio (July) and Grand Canyon (May), reductions in upwind sulfur emissions are also expected to be effective at reducing fine particle concentrations. Most sulfur at these locations is found in the particle phase, suggesting an absence of oxidant limitations for sulfate production. Further, the warm temperatures and low humidities

prevailing during these study periods result in most N(V) remaining in the gas phase. That is unlikely to change significantly even if sulfate is eliminated from the aerosol.

4. Semi-continuous measurement of $PM_{2.5}$

Aerosol chemical composition provides insight into aerosol sources and atmospheric processes. Many processes influence the temporal evolution of fine aerosol mass and chemical composition. Aerosol composition can change on short timescales as a result of changes in meteorological conditions, atmospheric transport, chemical reactions, and gas-particle partitioning.

While traditional filter measurement methods of aerosol composition are still commonly used, a number of semi-continuous measurements have been developed recently to allow aerosol chemical composition measurement on much faster time-scales (Buhr et al., 1995; Karlsson et al., 1997; Khlystov et al., 1995; Oms et al., 1996; Orsini et al., 2003; Simon and Dasgupta, 1993; Simon and Dasgupta, 1995; Slanina et al., 2001; Stolzenburg and Hering, 2000; Trebs et al., 2004; Weber et al., 2001; Zellweger et al., 1999).

Measurements in 15-minute intervals by PILS/IC (Particle Into Liquid Sampler (PILS) coupled to two DIONEX ion chromatographs) (Orsini et al., 2003; Weber et al., 2001) have enhanced our understanding of the chemical forms of ions present in fine particles and provided new information about the variability of fine particle composition on diurnal, and shorter, timescales at the studied locations.

An overview of $PM_{2.5}$ composition, and its temporal variations, measured by PILS/IC at the study locations will be discussed in this chapter. This will include an examination of changes in species concentrations and relationships between individual ionic components that provide insight into the chemical forms of the major ion species.

4.1 San Gorgonio Wilderness Area (April and July, 2003)

Figure 4.1 shows timelines of the major ion concentrations (sulfate, nitrate and ammonium) measured in April and July, 2003 in the San Gorgonio Wilderness Area.

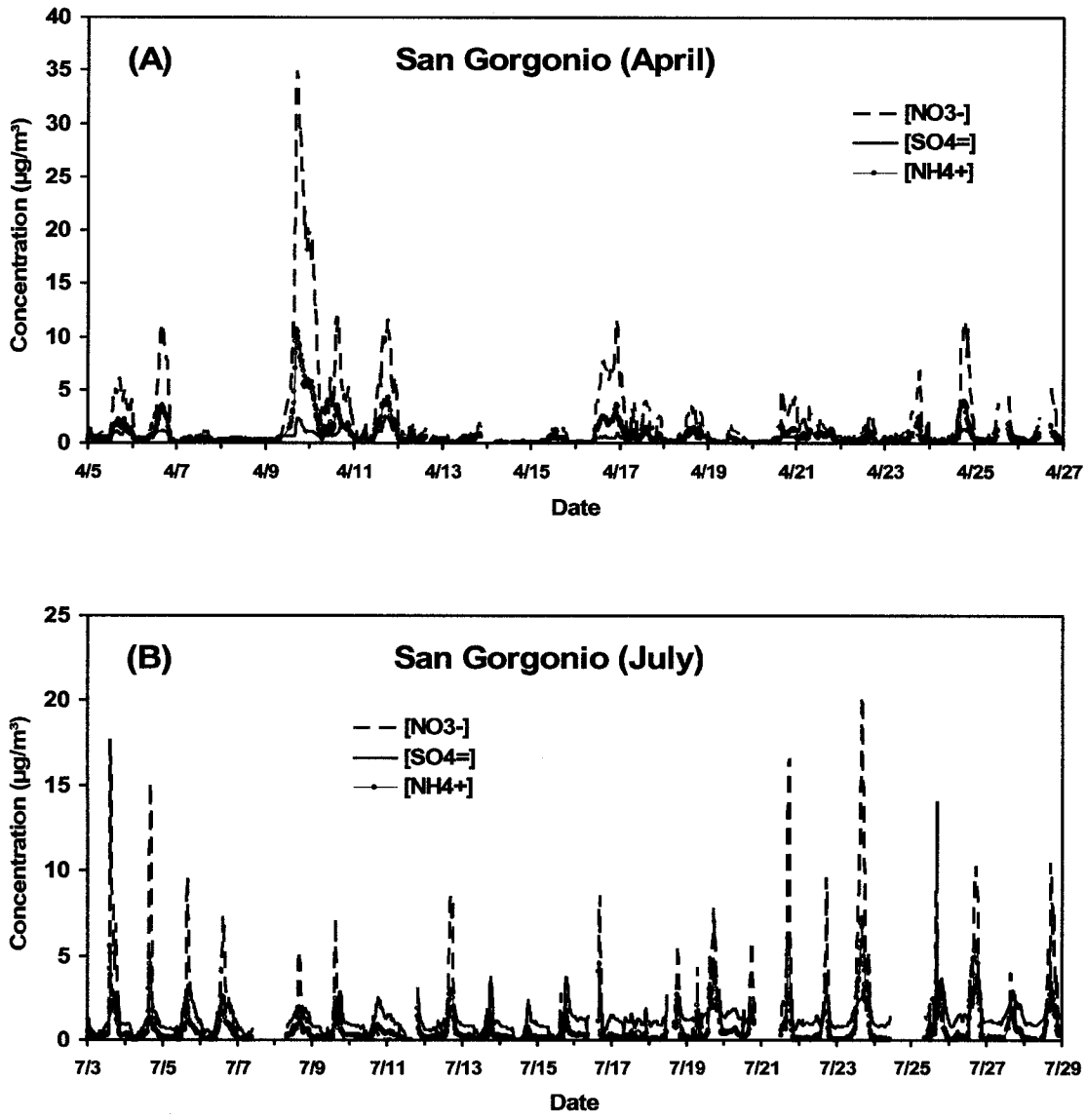

Figure 4.1 Timelines of PILS $PM_{2.5}$ major ionic species (NO_3^-, SO_4^{2-} and NH_4^+) concentrations (San Gorgonio (April and July, 2003))

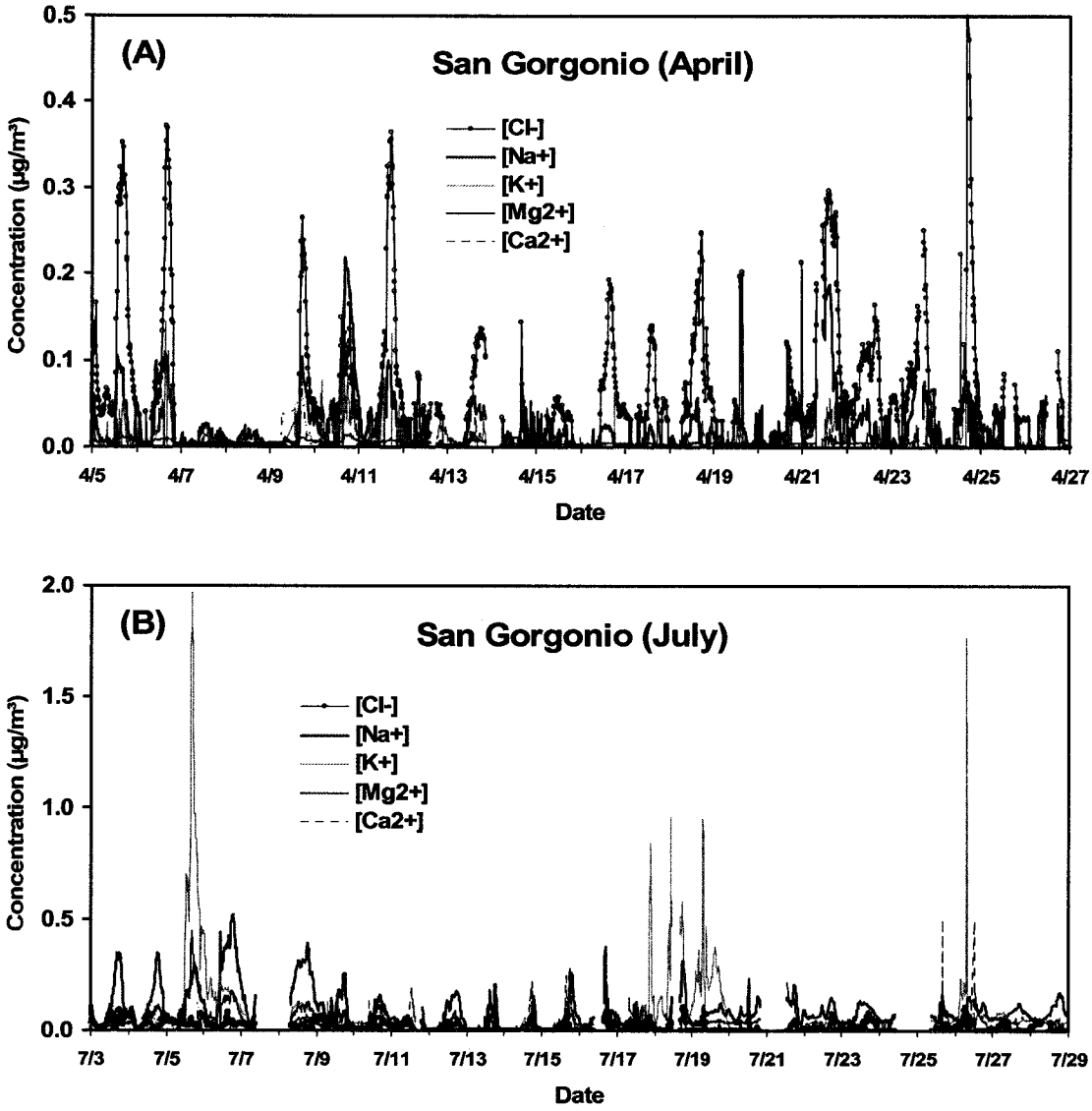

Figure 4.2 Timelines of PILS $PM_{2.5}$ minor ionic species (Cl^-, Na^+, K^+, Mg^{2+} and Ca^{2+}) concentrations (San Gorgonio (April and July, 2003))

Sulfate was a relatively small contributor to $PM_{2.5}$ at San Gorgonio in April, with formation of ammonium nitrate favored during the relatively low temperature and high humidity environment at this time. While lower concentrations of the major ions were observed in the middle of April and July during the San Gorgonio studies, periods of higher concentrations occurred in early April and in early and late July. The highest

concentration of sulfate, observed on 7/23, was 3.26 $\mu g/m^3$. The highest concentrations of nitrate and ammonium were observed on 4/9 (34.9 $\mu g/m^3$ and 10.4 $\mu g/m^3$), with high concentrations also measured on 7/23 (20.2 $\mu g/m^3$ and 7.2 $\mu g/m^3$).

Variations of cation species' (Na^+, K^+, Ca^{2+} and Mg^{2+}) concentrations as well as the anion Cl^- are shown in Figure 4.2. Cl^-, Na^+, K^+, Ca^{2+} and Mg^{2+} were found to be minor contributors to total ion concentrations. The highest concentration of Ca^{2+} and Mg^{2+} were observed at 0.08 $\mu g/m^3$ and 0.01 $\mu g/m^3$ in April and 0.58 $\mu g/m^3$ and 0.45 $\mu g/m^3$ in July, respectively. The maximum concentration of Na^+ was approximately 0.51 $\mu g/m^3$ on 4/24 and again on 7/6.

Periods with the highest concentrations of K^+ occurred on 7/5 - 7/6 and 7/17 - 7/19, and large spikes of K^+ concentrations were measured on 7/5 and 7/26 in July at San Gorgonio, as illustrated in Figure 4.2. Biomass burning releases a large of amount of potassium in submicron particles and thus non sea salt potassium is regarded as a good tracer for biomass burning (Carrico et al., 2004; Engling, 2006; Li et al., 2003; Liu et al., 2000; McMeeking et al., 2006; Posfai et al., 2003).

PILS data from San Gorgonio showed diurnal concentration trends for many species, likely related to changes in atmospheric transport associated with mountain-valley winds as shown in Figure 4.3 (A) and (B). Stronger, more regular diurnal trends were observed in July (Figure 4.3 (B)), when large concentration peaks were registered daily during the afternoon after approximately 2:00 PM. The more regular pattern in July was presumably due to strengthening of the mountain-valley wind circulation and deeper boundary layer development associated with more intense solar activity than occurred in April.

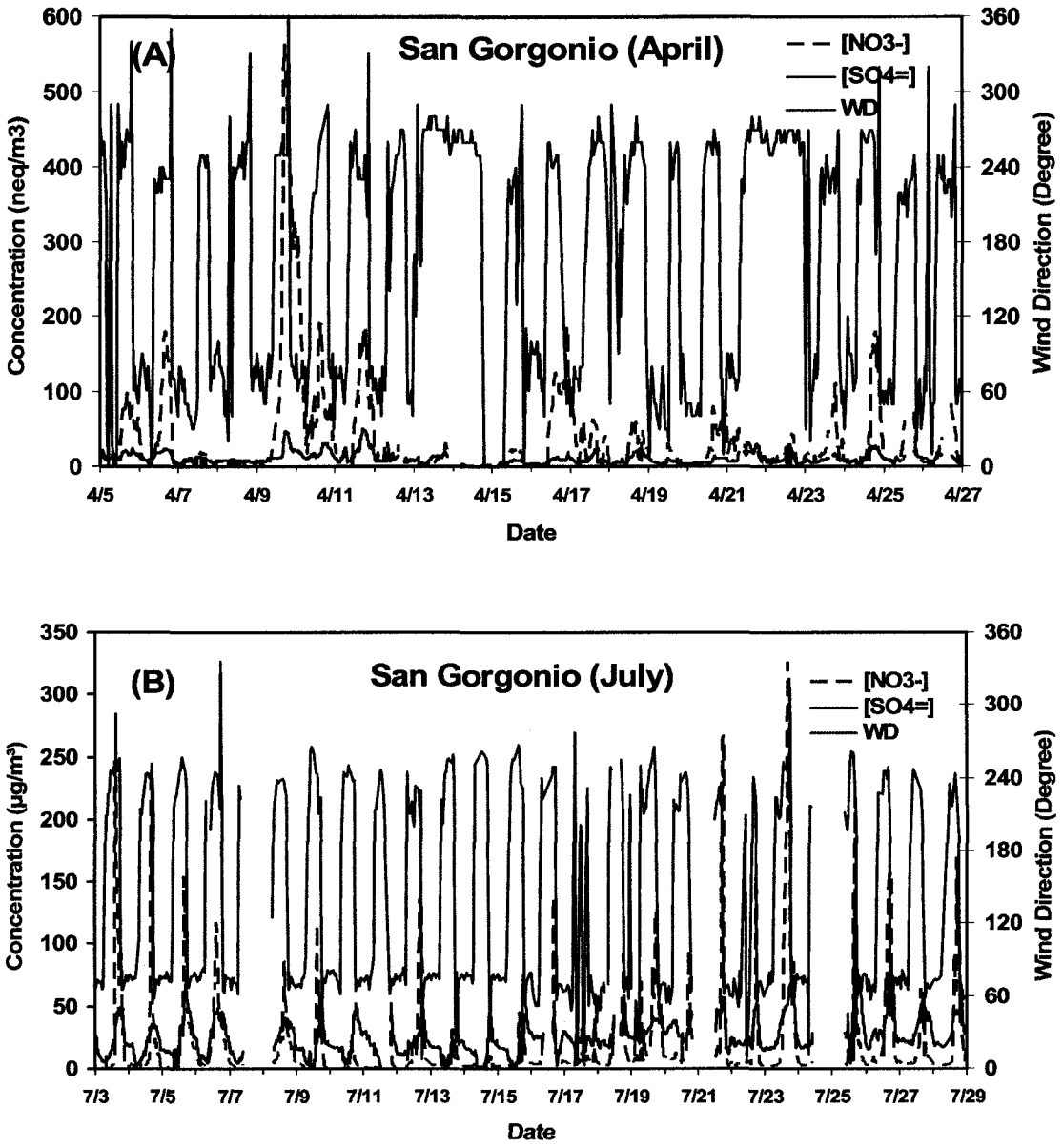

Figure 4.3 Timelines of PILS $PM_{2.5}$ NO_3^-, SO_4^{2-} and wind direction (San Gorgonio (April and July, 2003)) Upslope flow is from the west and downslope flow from the east

The theoretical non sea salt (nss) soluble K^+ for July was calculated from Equation 4.1, with a $[K^+]/[Na^+]$ ratio of 0.0128 in sea water as shown in Table 1.1. Figure 4.4 depicts the timelines of nss-K^+ concentration over the course of the study. These observations suggest that fires significantly impacted the sampling site on 7/5 -6,

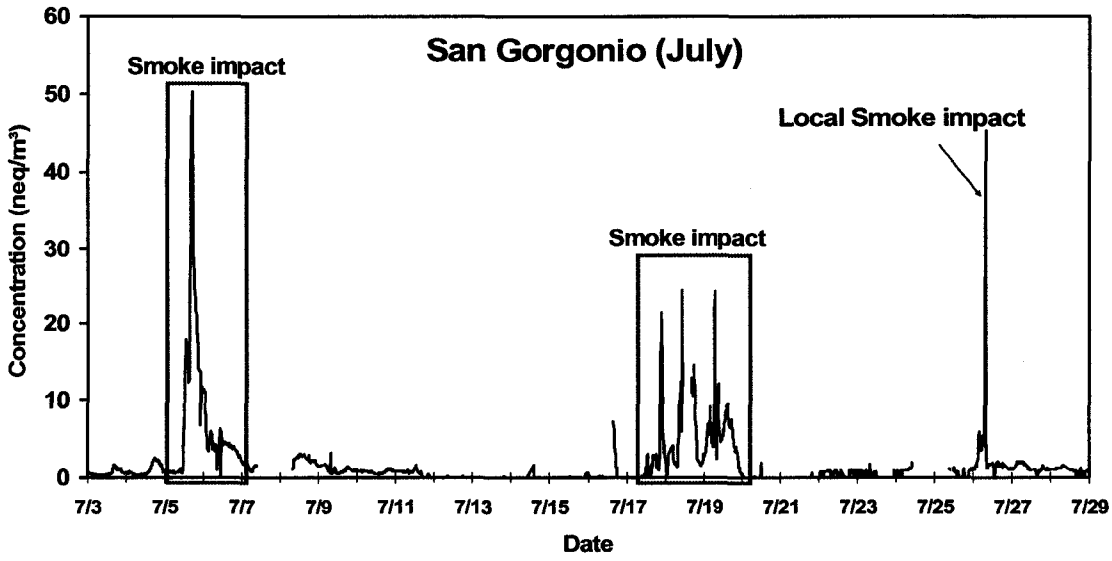

Figure 4.4 Timeline of $PM_{2.5}$ nss-$[K^+]$ ion concentration measured using PILS (San Gorgonio(July))

$$\text{nss-}[K^+] = [K^+]_{measured} - 0.0218 \times [Na^+]_{measured} \quad \textbf{(Eqn. 4.1)}$$

(Cheng et al., 2000; Finlayson-Pitts and Pitts, 2000; Wilson, 1975)

7/17 – 19, and 7/26. The PILS K^+ spikes are consistent with high concentrations of K^+ also observed in URG filter samples on 7/5, 7/17, 7/18 and 7/19 (see chapter 3 for URG data). The K^+ concentration spike observed on 7/26 at San Gorgonio demonstrates, for example, how highly time-resolved measurements can provide insight into even brief plumes of aerosol advected to the site. July is wildfire season in southern California and fires were burning in the region during the study. No smoke impacts were evident in April.

Figure 4.5 shows timelines of Cl^- and Na^+ concentrations at San Gorgonio in April and July. Concentrations are shown in nanoequivalents (neq/m^3).

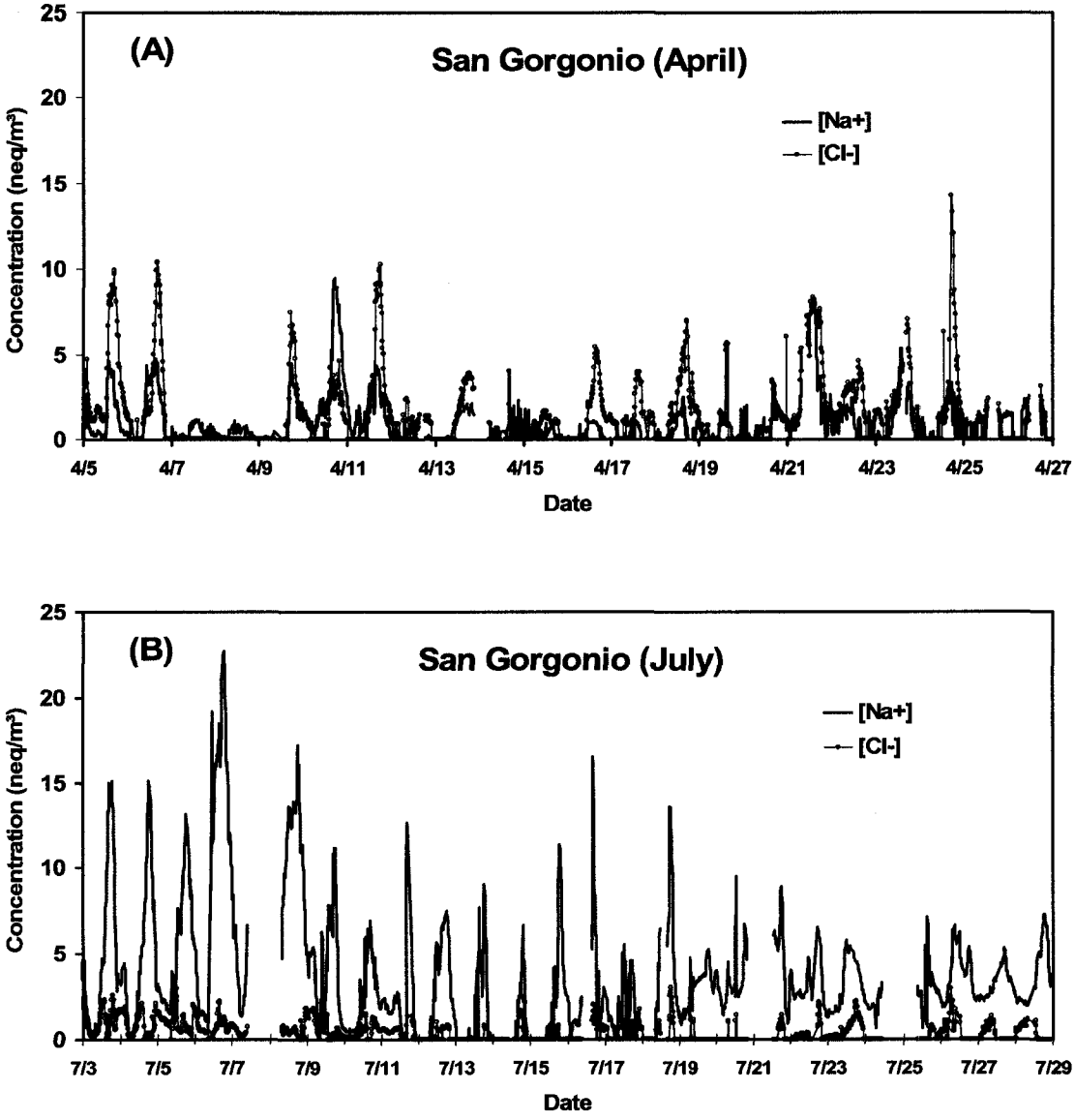

Figure 4.5 Timelines of PILS $PM_{2.5}$ Na^+ and Cl^- concentrations (San Gorgonio (April and July, 2003))

While Na^+ and Cl^- concentrations are similar most days in April, Cl^- concentrations are much lower than Na^+ concentrations in July. One possible explanation of the change in July is that displacement of Cl^- in sea salt particles (NaCl) has occurred by reaction between nitric acid (HNO_3) and sea salt, as shown in Equation 4.2. The PILS data shown

$$HNO_3(g) + NaCl \rightarrow NaNO_3 + HCl\,(g) \quad \textbf{(Eqn. 4.2)}$$

in Figure 4.6 demonstrate how concentrations of "excess" NO_3^- and Na^+ often track each other closely, consistent with displacement of Cl^- from sea salt. Excess NO_3^- is defined as $PM_{2.5}$ nitrate minus the amount of ammonium present beyond that required to neutralize sulfate. In some case excess NO_3^- exceeds Na^+ significantly (e.g. on the afternoon of 7/5), suggesting that other mineral forms of nitrate may be present.

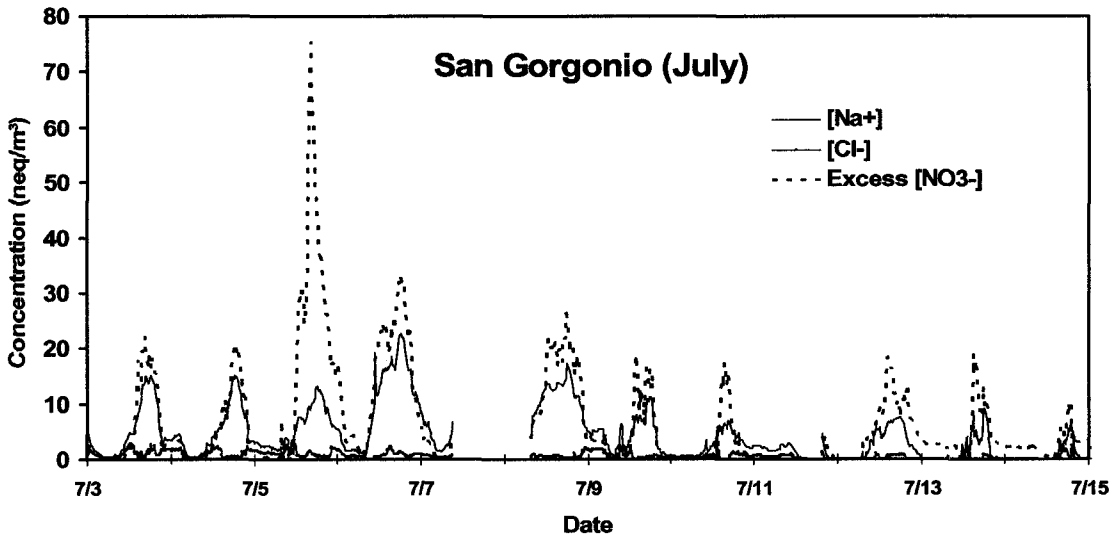

Figure 4.6 Timelines of PILS $PM_{2.5}$ Na^+, Cl^- and "Excess" NO_3^- ion concentrations measured from July 3 – 15 (San Gorgonio, 2003)

Figure 4.7 shows comparisons of PILS $PM_{2.5}$ Cl^- (or the sum of NO_3^- and Cl^-) vs. Na^+ concentrations for April and July. The observed Cl^-/Na^+ equivalent ratio (average ~1.11) in April is close to that expected for sea salt (approximately 1.16), suggesting that sea salt

aerosol is often observed unreacted at the site in April. However, the $[Cl^-]/[Na^+]$ ratio in July (~ 0.07) is much lower, indicating apparent loss of Cl^- from sea salt aerosol. When the sum of NO_3^- and Cl^- concentrations are plotted against Na^+ concentrations in July, the $[NO_3^- + Cl^-]/[Na^+]$ ratios generally meet or exceed the sea salt ratio. If the only nitrate present in the aerosol is the result of HNO_3 displacement of chloride from sea salt, the ratio of nitrate plus chloride to Na^+ should equal the sea salt Cl^-/Na^+ ratio. Larger ratios of the sum of $[NO_3^-]$ and $[Cl^-]$ to $[Na^+]$ indicate the presence of particulate ammonium nitrate or mineral NO_3^-. The importance of various forms of nitrate at this site will be further discussed in chapter 5.

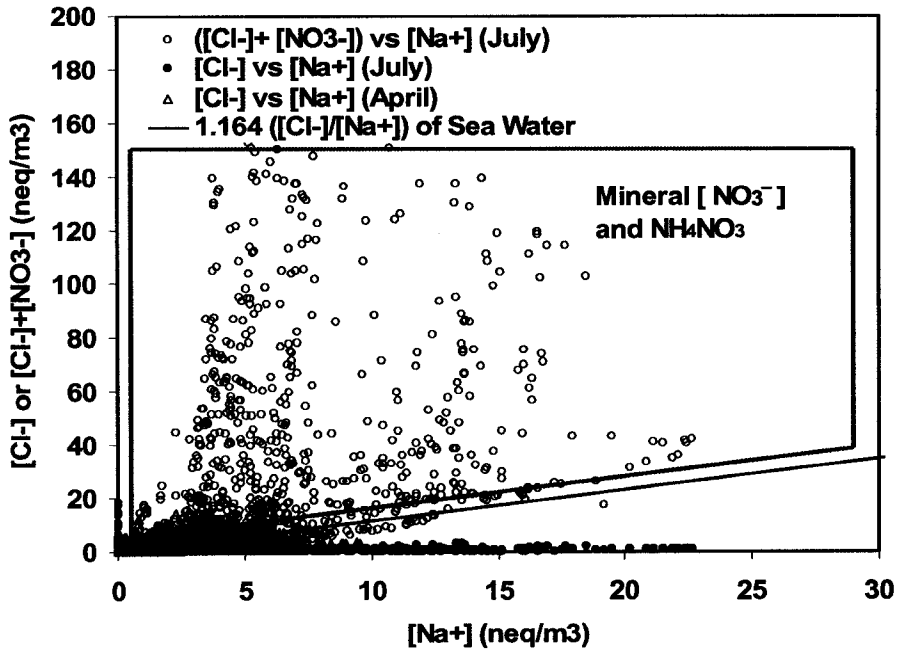

Figure 4.7 Relationship between $[Na^+]$ and the sum of $[NO_3^-]$ and $[Cl^-]$ and between $[Na^+]$ and $[Cl^-]$ measured using PILS data (San Gorgonio (April and July, 2003))

4.2 Grand Canyon National Park (May, 2003)

Figure 4.8 depicts timelines of ion concentrations of $PM_{2.5}$ SO_4^{2-}, NO_3^- and NH_4^+ measured using a PILS sampler during the Grand Canyon National Park study. Generally, lower concentrations of the major ion species were observed in early May. A period of higher concentrations of the major ionic species started in the middle of May and lasted until the end of the study. Concentrations ranged from zero (below detection limits) to 1.46 $\mu g/m^3$ and 1.41 $\mu g/m^3$ for NO_3^- and NH_4^+, respectively, and from 0.01 to 2.94 $\mu g/m^3$ for SO_4^{2-}.

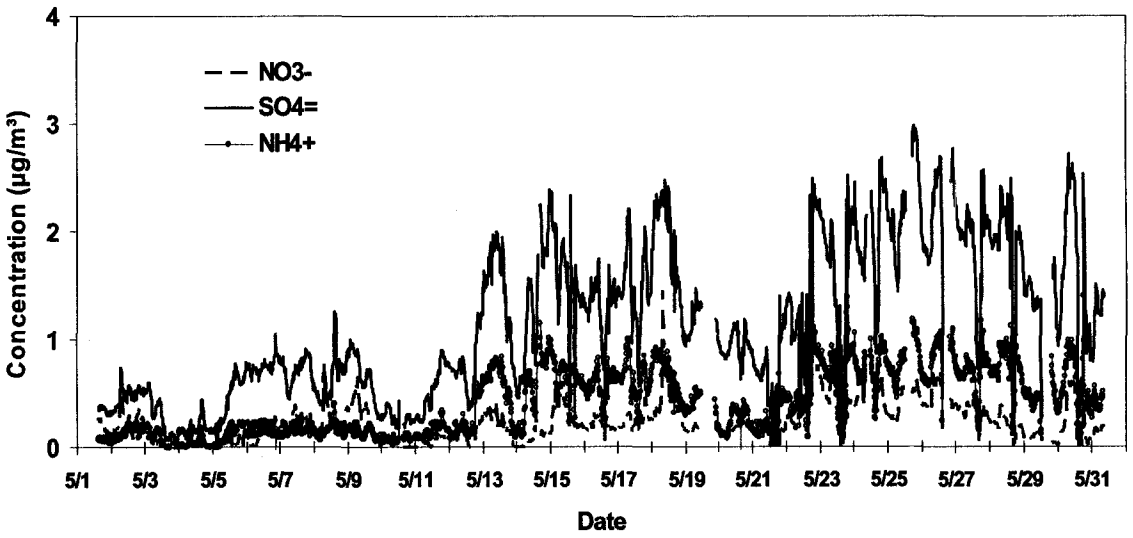

Figure 4.8 Timelines of PILS $PM_{2.5}$ NO_3^-, SO_4^{2-} and NH_4^+ concentrations (Grand Canyon N.P. (May, 2003))

Timelines of Cl^- and trace cations are shown in Figure 4.9. K^+ and Cl^- were generally found to be minor contributors to $PM_{2.5}$, although a period of higher K^+ concentrations was observed at the end of May. Mg^{2+} and Ca^{2+} concentrations ranged from zero up to 0.11 $\mu g/m^3$ and 0.77 $\mu g/m^3$, respectively.

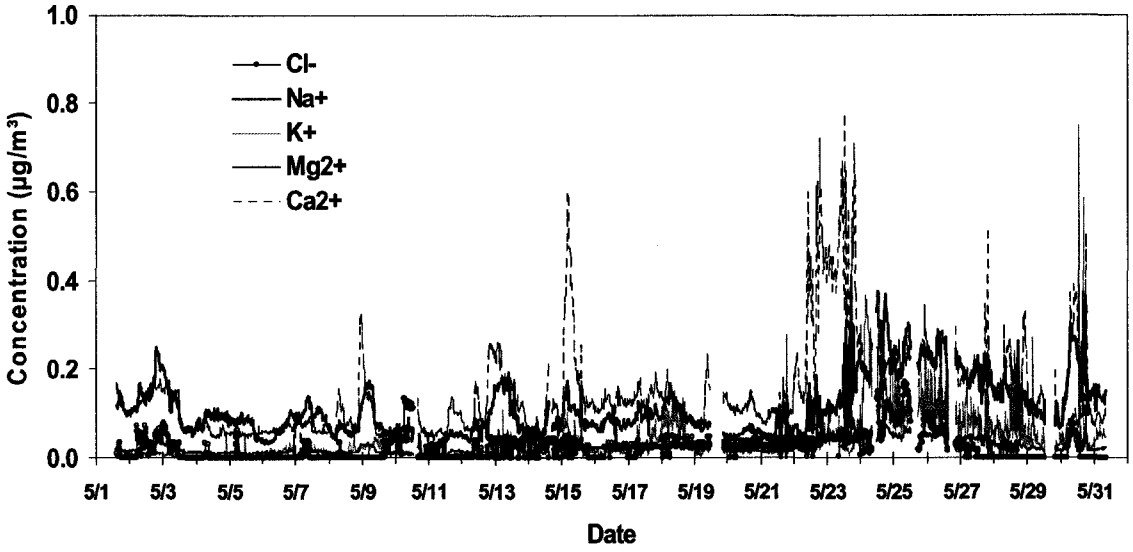

Figure 4.9 Timelines of PILS $PM_{2.5}$ Na^+, K^+, Mg^{2+}, Ca^{2+} and Cl^- concentrations (Grand Canyon N.P. (May, 2003))

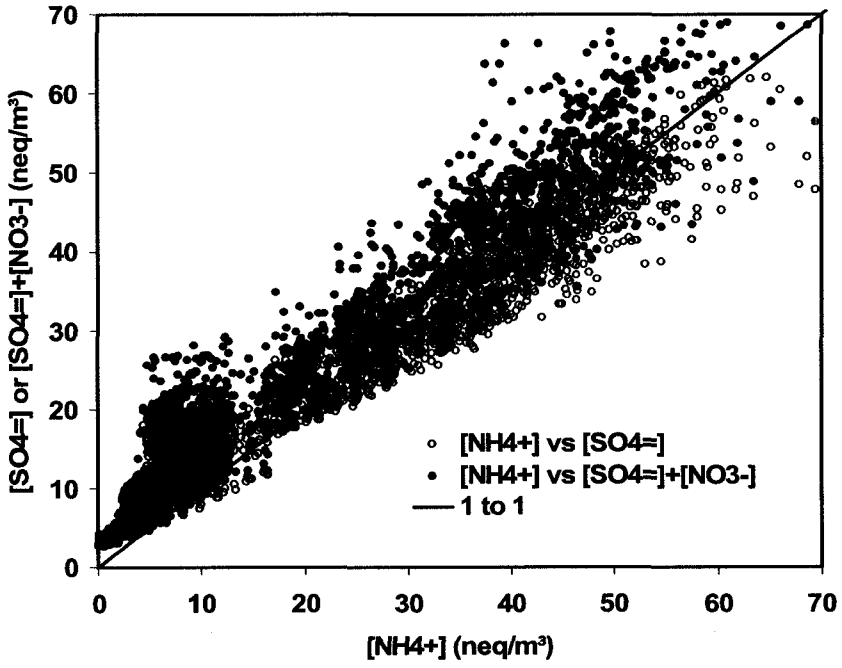

Figure 4.10 Relationship of PILS $PM_{2.5}$ concentrations of sulfate, nitrate and ammonium (Grand Canyon N.P. (May, 2003))

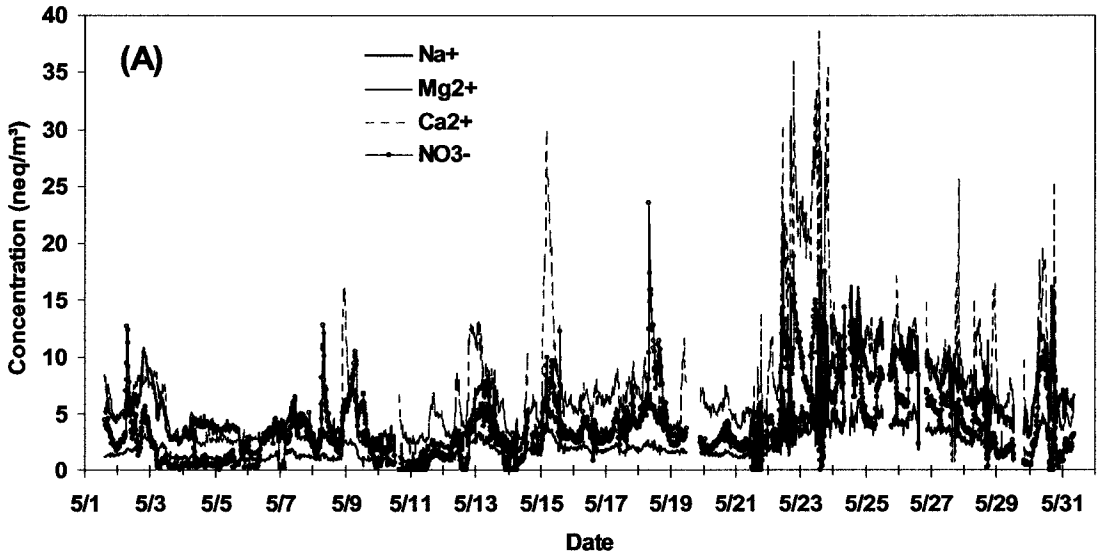

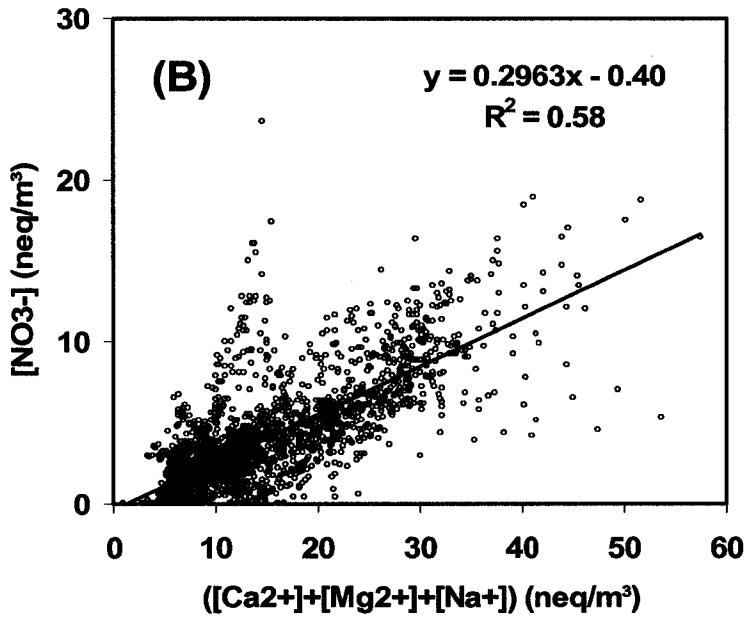

Figure 4.11 (A) Timelines of PILS $PM_{2.5}$ K^+, Mg^{2+} and Ca^{2+} concentrations and (B) relationship of PILS $PM_{2.5}$ concentrations of NO_3^- and sum of Ca^{2+}, Mg^{2+} and Na^+ (Grand Canyon N.P. (May, 2003))

Most of the ammonium at the site appears to be associated with sulfate, with a sulfate to ammonium ratio close to 1 on a charge equivalent concentration basis (See Figure 4.10). There is sufficient ammonium available to neutralize sulfate but not sulfate and nitrate simultaneously (see Figure 4.10), implying another formation pathway of particulate nitrate may be important in this environment. Nitric acid reaction with soil dust and/or sea salt particles is a possibility. Figures 4.11 show timelines (A) and the correlations (B) of $PM_{2.5}$ NO_3^- with Na^+, Ca^{2+} and Mg^{2+}, which typically are associated with sea salt and soil dust. Close tracking of NO_3^- with Na^+, Ca^{2+} and Mg^{2+} provides evidence of the importance of nitric acid reaction with sea salt and/or soil dust.

4.3 Bondville, Illinois (February, 2003)

Figures 4.12 and 4.13 show that sulfate, nitrate and ammonium were the dominant ionic species during the Bondville campaign in February, 2003, with minor contributions from Mg^{2+} and Ca^{2+}. Concentrations of sulfate, nitrate and ammonium ranged from 0.02 to 20.4 $\mu g/m^3$, 0.01 to 37.7 $\mu g/m^3$, and 0.01 to 13.7 $\mu g/m^3$, respectively, with the highest concentrations occurring at the end of study. Figure 4.13 shows timelines of the concentrations of the minor cations and Cl^-. Very low concentrations of Mg^{2+} and Ca^{2+} were observed with maximum values of 0.16 $\mu g/m^3$ and 0.17 $\mu g/m^3$, respectively. The highest Cl^- concentration measured was 2.64 $\mu g/m^3$ on 2/14. Periods of higher Na^+ and K^+ concentrations started at the end of February with maximum concentrations observed on 2/25 and 2/27 at 0.55 $\mu g/m^3$ and 0.56 $\mu g/m^3$.

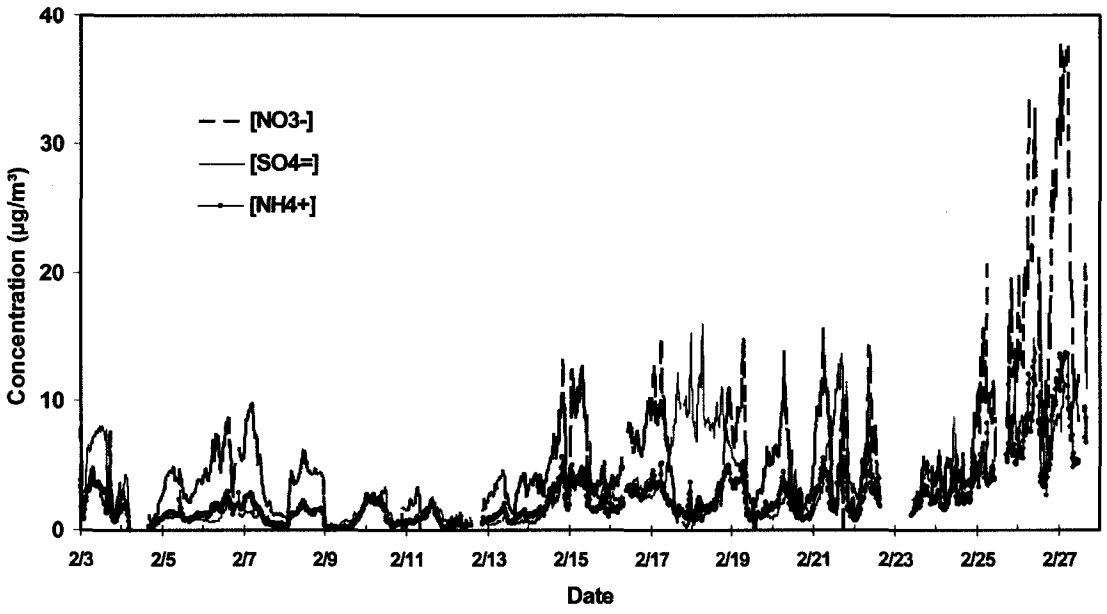

Figure 4.12 Timelines of PILS $PM_{2.5}$ NO_3^-, SO_4^{2-} and NH_4^+ concentrations (Bondville (February, 2003))

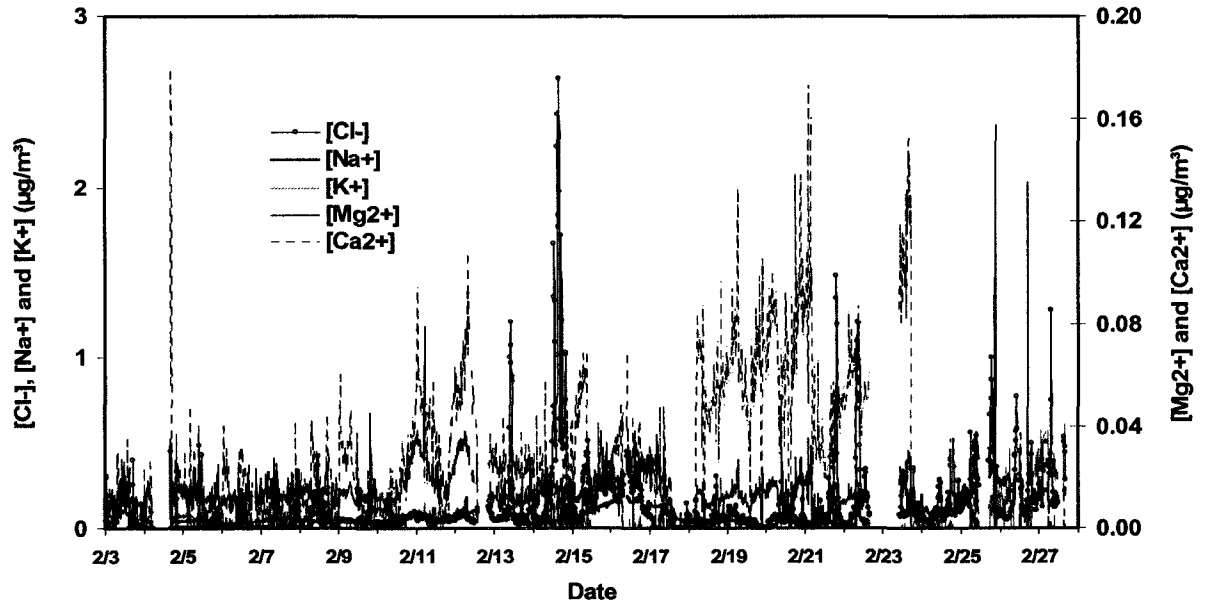

Figure 4.13 Timelines of PILS $PM_{2.5}$ minor ionic species Cl^-, Na^+, K^+, Mg^{2+} and Ca^{2+} concentrations (Bondville (February, 2003))

The high time resolution nitrate and sulfate measurements at Bondville give interesting insights into ambient aerosol processes. Figures 4.14 and 4.15 show timelines of NO_3^- and SO_4^{2-}, the $[NH_4^+]/[SO_4^{2-}]$ molar ratio, and temperature (°F) and wind direction (degrees). The meteorological data were measured at the same site by the Clean Air Status and Trends Network (CASTNET) (http://www.epa.gov/castnet/site.html). Observations from noon on 2/17 to midnight on 2/18, and again during the afternoon of 2/21, revealed rapid transitions between nitrate and sulfate dominated aerosols. These rapid transitions appear to be associated with changes in wind direction. During this same time period we also see large changes in the aerosol acidity, as reflected in the ammonium to sulfate ratio (Fig. 4.15).

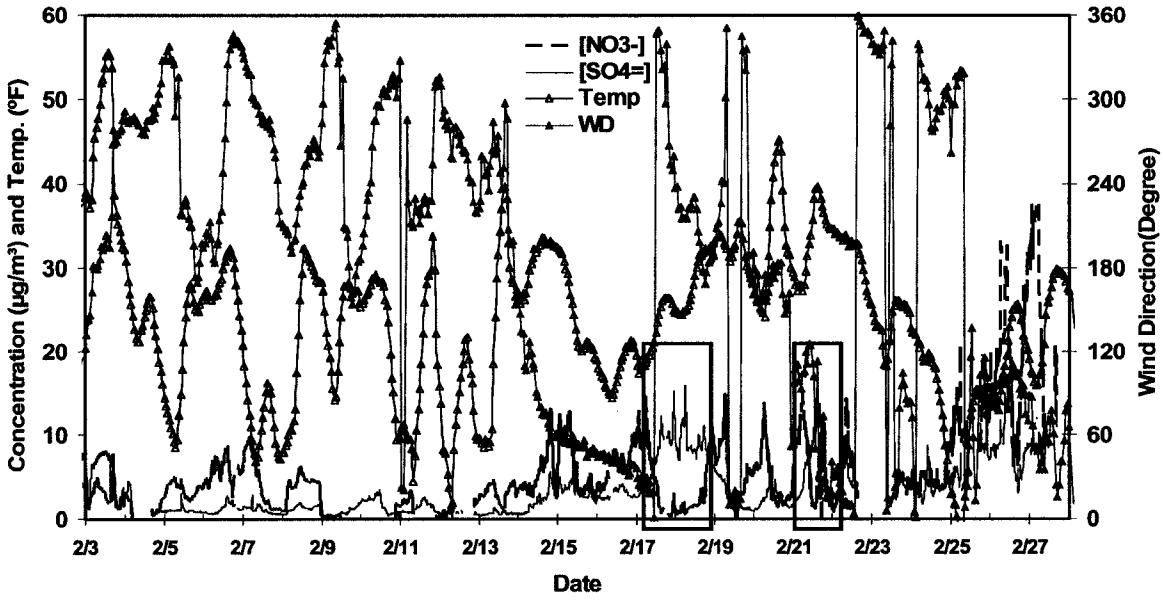

Figure 4.14 Timelines of PILS $PM_{2.5}$ NO_3^-, SO_4^{2-}, wind direction and temperature (Bondville (February, 2003))

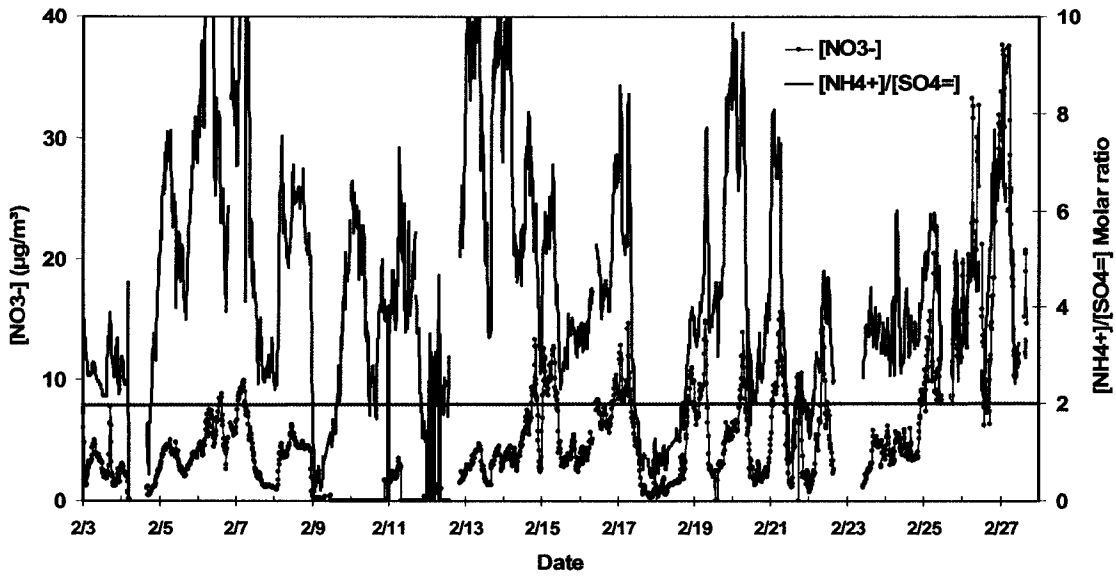

Figure 4.15 Timelines of PILS $PM_{2.5}$ NO_3^- and $[NH_4^+]/[SO_4^{2-}]$ molar ratio (Bondville (February, 2003))

Figure 2.16 shows a closer inspection of the transient sulfate episodes in the 2/17 – 2/20 period. A sulfate rich air mass passed over the sampling site when the wind pattern shifted from approximately 50 ° (northeast) to 350 ° (northwest). As sulfate concentrations rose, they reached a point where insufficient ammonia was available to neutralize the aerosol and nitrate concentrations decreased as nitric acid was forced back to the gas phase. Later, on 2/18, the $[NH_4^+]/[SO_4^{2-}]$ ratio rose allowing NH_4NO_3 aerosol to form once again.

Another interesting observation is the variation of the nitrate concentrations with changes in ambient temperature at the Bondville site. Figure 4.17 shows timelines of temperature (°C), sulfate and nitrate during a 10 day period, 2/18 – 2/28, at Bondville. Nitrate is frequently observed to reach its daily peak when temperature reaches its daily minimum. This supports the theory that temperature and RH have an

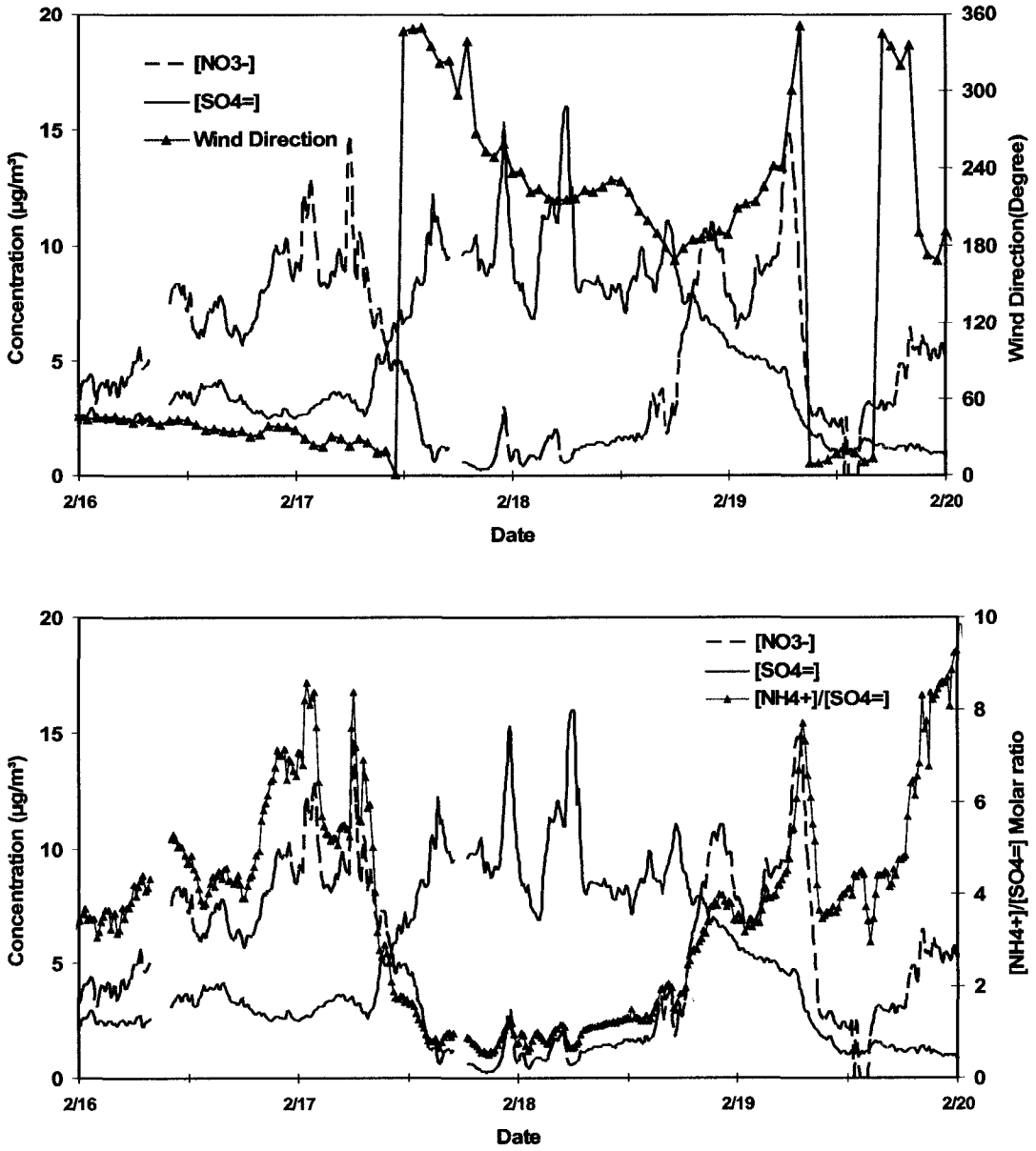

Figure 4.16 Timelines of PILS $PM_{2.5}$ NO_3^- and SO_4^{2-} concentrations, wind direction and molar ratio of $[NH_4^+]/[SO_4^{2-}]$ at the Bondville site from February 16 to February 20

impact on gas-particle partitioning of nitric acid and NH_4NO_3 dissociation (Appel, 1993; Chang et al., 2000; Cheng and Tsai, 1997; Chow et al., 2005; Finlayson-Pitts and Pitts, 2000; Mozurkewich, 1993; Olszyna et al., 2005; Stelson and Seinfeld, 1982; Yu et al.,

2006; Zhang and McMurry, 1992). Sulfate concentrations don't always follow the same pattern, suggesting that the nitrate peaks don't simply reflect increased pollutant concentrations under a nocturnal inversion, although this possibility can't be ruled out entirely.

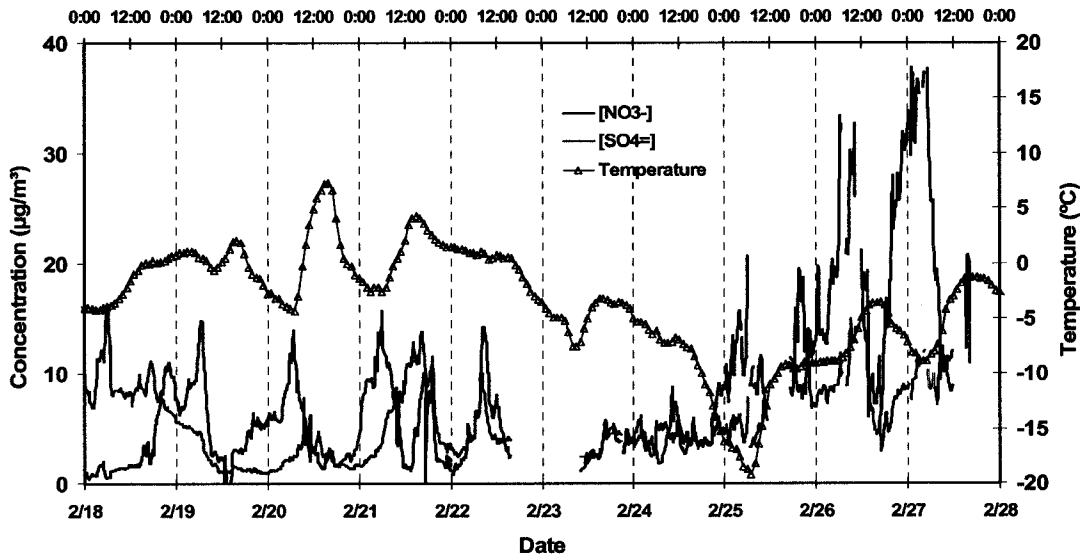

Figure 4.17 Timelines of PILS $PM_{2.5}$ NO_3^- and SO_4^{2-} concentrations and ambient temperature at the Bondville site from February 18 to February 28, 2003

The amount of non sea salt-[Cl^-] (nss-[Cl^-]) in Bondville aerosol was calculated by subtracting the Cl^- amount associated with sea water from the total measured Cl^- concentrations in the PILS $PM_{2.5}$ using the ratio of Cl^-/Na^+ (ratio = 1.164, Table 1.2) for sea water as shown in equation 4.2. Figure 4.18 depicts timelines of $PM_{2.5}$ Na^+, Cl^- and nss-Cl^- concentrations. The large fraction of chloride comprised by nss-[Cl^-] suggests that

$$\textbf{nss-}[Cl^-] = [Cl^-]_{measured} - 1.164 \times [Na^+]_{measured} \quad \textbf{(Eqn. 4.2)}$$

the particulate chloride comes mainly from anthropogenic sources rather than sea salt. Road salt, automobile emissions and coal combustion/local fires are all possible sources of Cl^- in the atmosphere (Godwin et al., 2003; Kang et al., 2006; Pakkanen et al., 2003; Virtanen et al., 2006). In order to examine possible road salt contribution to the nss-Cl^- at Bondville, precipitation data (mostly snow in wintertime at Bondville) measured by CASTNET were considered due to the fact that road salt used as deicer contains sodium chloride, magnesium chloride and/or potassium chloride (Fischel, 2001; Wegner and Yaggi, 2001; Williams and Stensland, 2006).

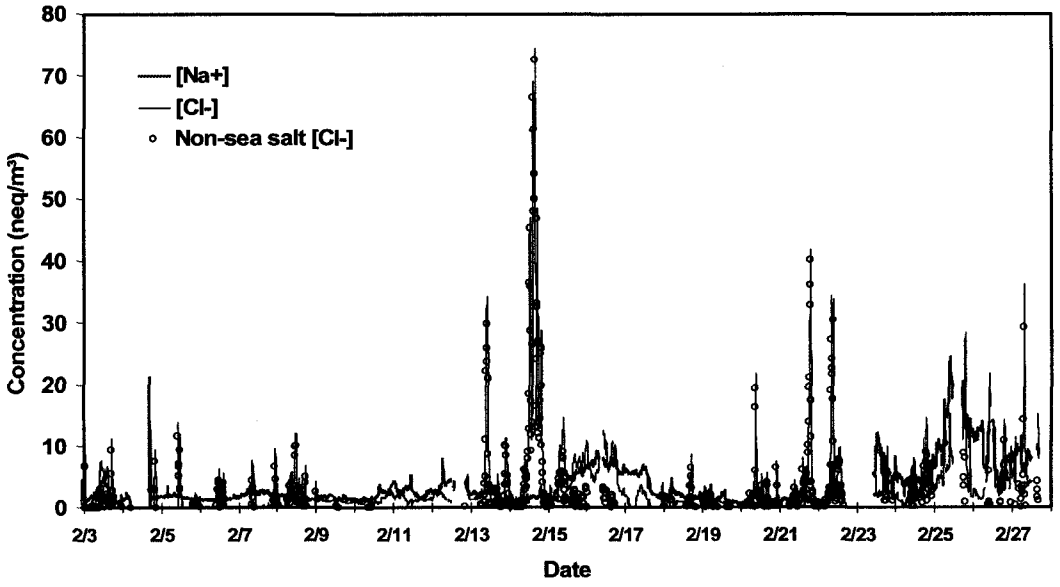

Figure 4.18 Timelines of PILS $PM_{2.5}$ Na^+, Cl^- and non sea salt-Cl^- (Bondville (February, 2003))

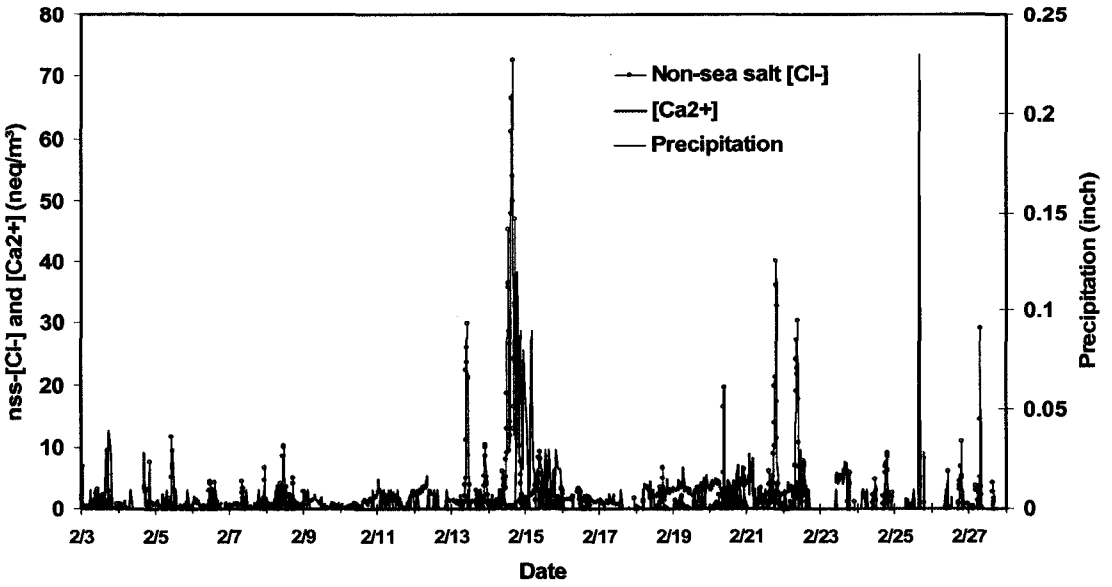

Figure 4.19 Timelines of PILS $PM_{2.5}$ non-sea salt Cl^-, Ca^{2+} and precipitation (Bondville, February, 2003)

Sodium chloride and calcium chloride are used as the primary and secondary deicers in Illinois (Fischel, 2001). Figure 4.19 presents timelines of nss-[Cl^-], [Ca^{2+}] and precipitation during the Bondville study. Although nss-[Cl^-], [Ca^{2+}] and precipitation events do not correlate on all days, generally events of precipitation coincide with spikes in nss-[Cl^-], suggesting road salt may be an important source of nss-[Cl^-] during winter at the Bondville site.

4.4 Brigantine National Wildlife Refuge, NJ (November, 2003)

Figure 4.20 shows timelines of the major ion species (NO_3^-, SO_4^{2-} and NH_4^+) measured by PILS at the Brigantine National Wildlife Refuge, New Jersey in November, 2003. NO_3^-, SO_4^{2-} and NH_4^+ were found to be major contributors to the total ion

concentrations in $PM_{2.5}$. The concentrations of sulfate, nitrate and ammonium ranged from zero (below detection limits) to 4.31, 6.16 and 2.95 $\mu g/m^3$, respectively. K^+, Mg^{2+} and Ca^{2+} were found to be present at very low concentrations (close to the detection limits) on most days, as shown in Figure 4.21.

Figure 4.21 shows Na^+ and Cl^- present at relatively high concentrations during the Brigantine study. The maximum concentrations of Na^+ and Cl^- were 2.03 $\mu g/m^3$ and 0.86 $\mu g/m^3$ on 11/19, with periods of high Na^+ and Cl^- concentrations in the middle and the end of November and spikes of Cl^- also on 11/10 and 11/23. The majority of Na^+ was associated with Cl^- at Brigantine, reflecting the local sea salt source.

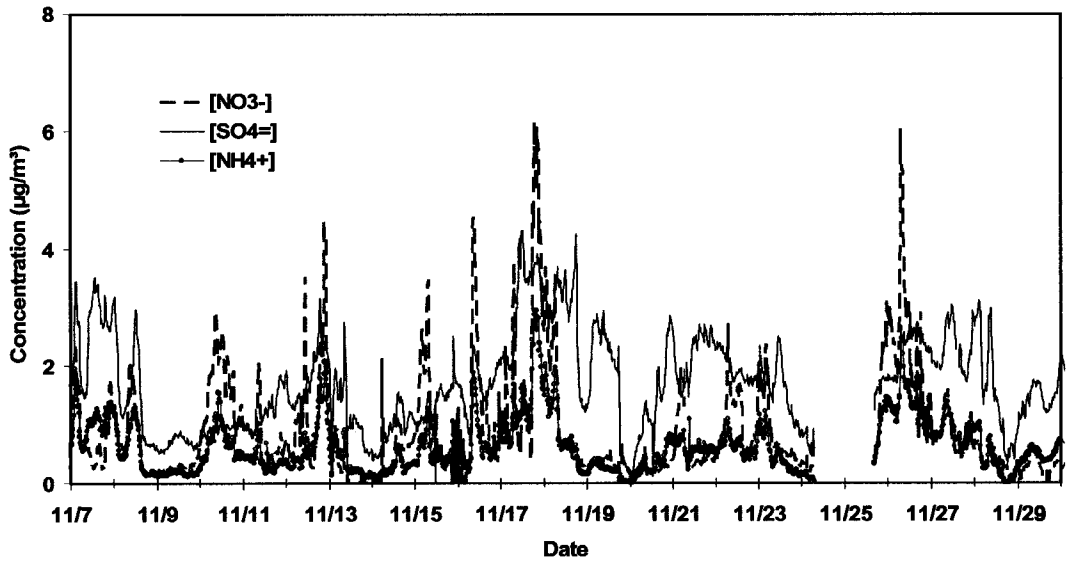

Figure 4.20 Timelines of PILS $PM_{2.5}$ NO_3^-, SO_4^{2-} and NH_4^+ concentrations (Brigantine (November, 2003))

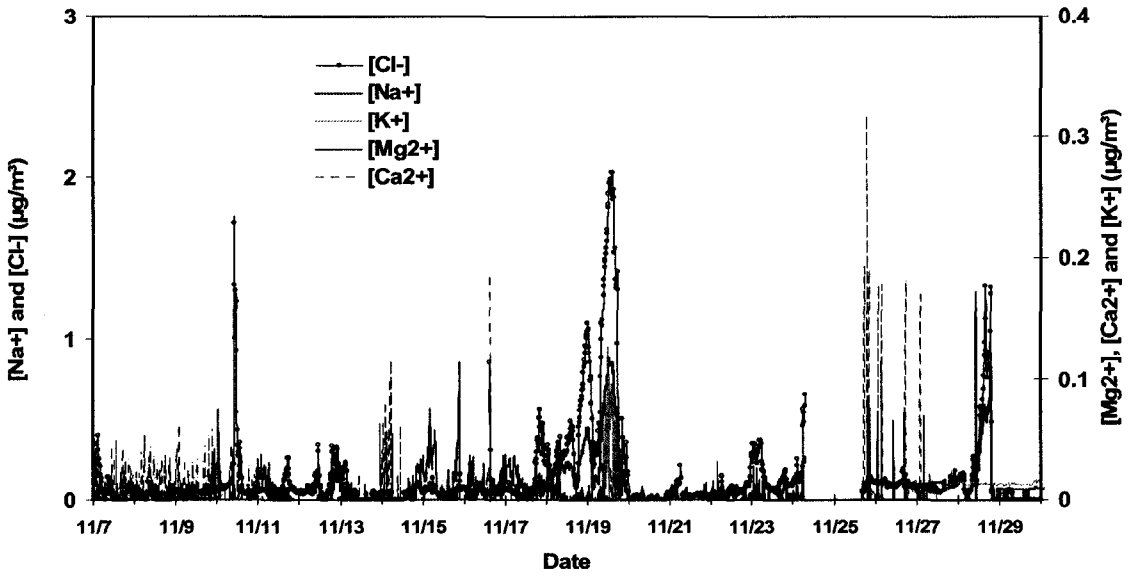

Figure 4.21 Timelines of PILS $PM_{2.5}$ minor ionic species Cl^-, Na^+, K^+, Mg^{2+} and Ca^{2+} concentrations (Brigantine (November, 2003))

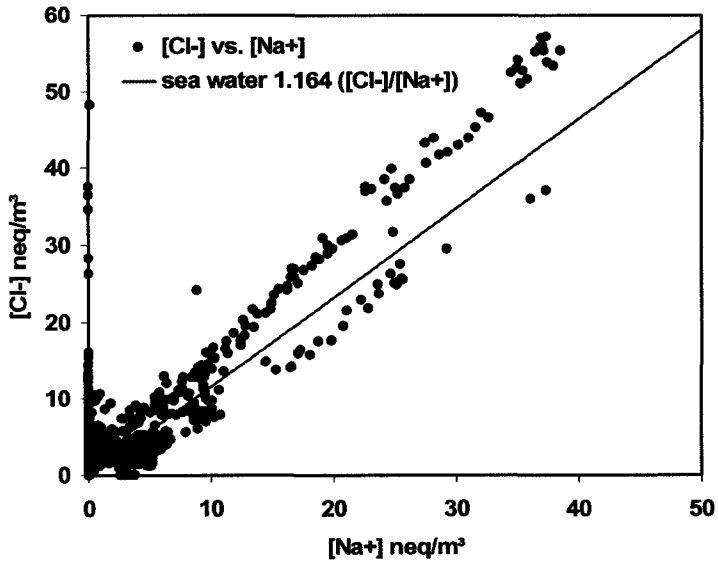

Figure 4.22 Relationship between $[Na^+]$ and $[Cl^-]$ measured using PILS (Brigantine (November, 2003))

Figure 4.22 shows Cl^- concentrations plotted against Na^+ concentrations measured by PILS at Brigantine. The ratios of $[Cl^-]$ to $[Na^+]$ are close to the expected value of 1.164 for the sea water $[Cl^-]/[Na^+]$ ratio on most days. However, during some periods more Cl^- was observed than expected for sea water, with ratios of $[Cl^-]/[Na^+]$ above the sea water $[Cl^-]/[Na^+]$ ratio, suggesting additional non-marine sources of Cl^-, such as coal burning, automobile/industrial emission or incinerator emissions where chlorine is emitted as elemental Cl or gaseous Cl_2 (Lee et al., 2002; Pakkanen et al., 2003; Song et al., 2001; Wang et al., 2006). Non sea salt Cl^- was estimated using Equation 4.2 and the sea water $[Cl^-]/[Na^+]$ ratio of 1.164 to compare non sea salt-$[Cl^-]$ and total Cl^- concentrations.

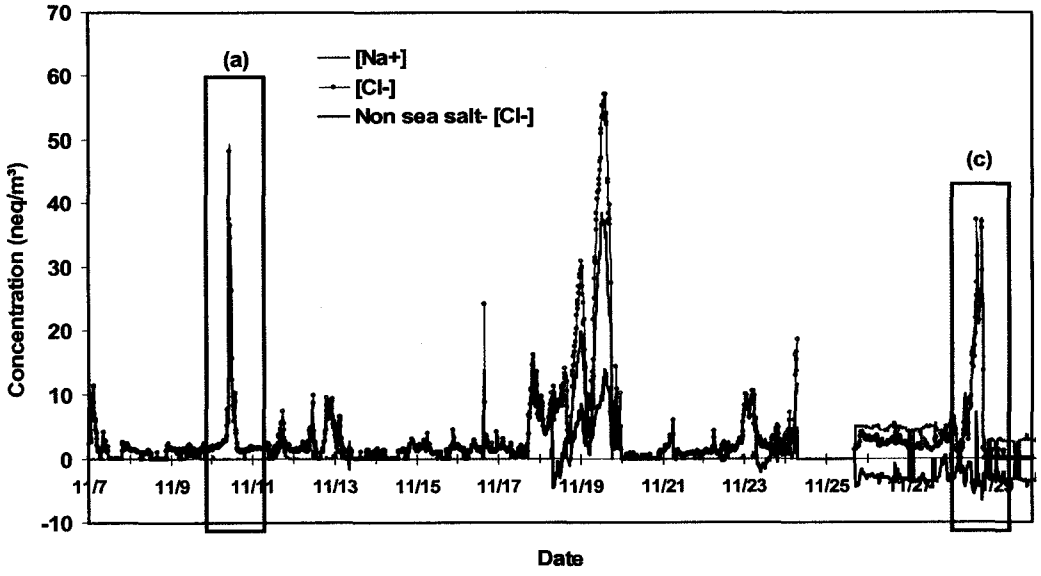

Figure 4.23 Timelines of PILS $PM_{2.5}$ Na^+, Cl^- and non sea salt-Cl^- (Brigantine (Novembery, 2003))

Figure 4.23 shows different periods of significant non sea salt chloride (period(a)) and sea salt chloride (period(c)). Period (a) on 11/10 is the most interesting and was characterized mainly by non-marine sources of Cl^-. Emissions from waste incinerators located in southwestern New Jersey and southeastern Pennsylvania may be contributing non-marine sources of Cl^- (Lee et al., 2002; Song et al., 2001). Air mass trajectories in Figure 4.24 show that most of the air masses on 11/10 spent time over land before arriving at the Brigantine site. On the other hand, air masses passed over the sea on 11/28 (Period (c)) when Cl^- had mainly a sea salt source, as shown in Figures 4.23 and 4.24.

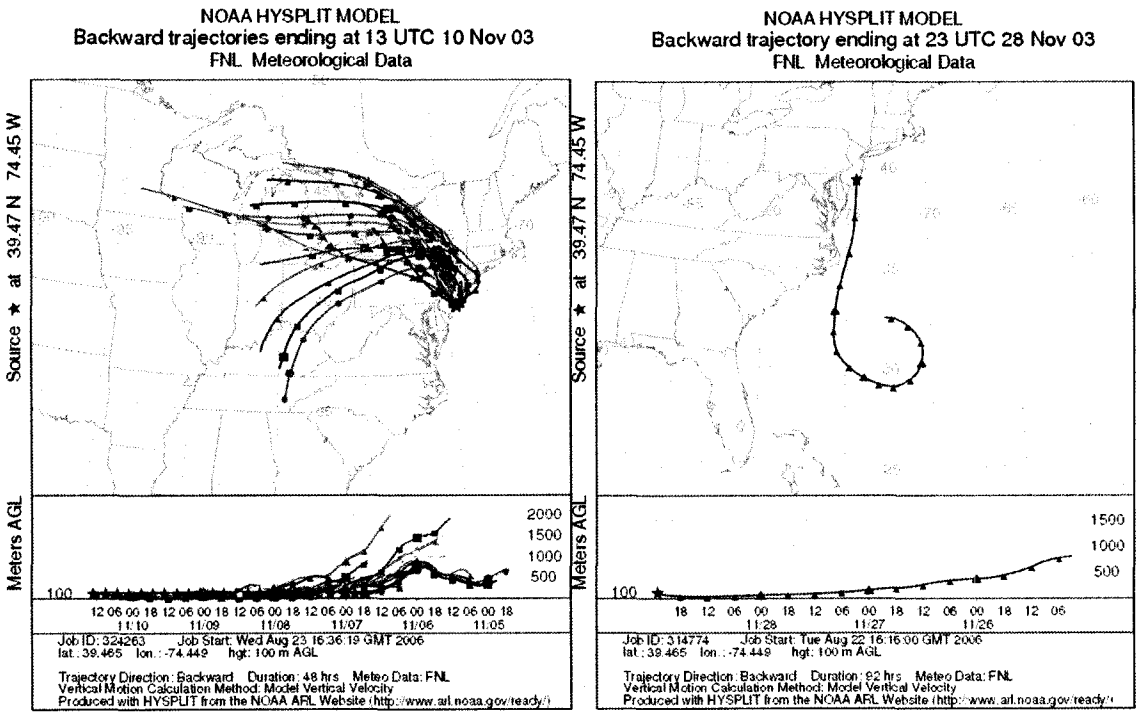

Figure 4.24 Air mass trajectories for 11/10/03 (left panel) and 11/28/03 (right panel) (Brigantine, 2003)

4.5 Great Smoky Mountains National Park (July/Aug, 2004)

Figure 4.25 shows timelines of PILS $PM_{2.5}$ sulfate, nitrate and ammonium concentrations measured from 7/20 to 8/19 in Great Smoky Mountains National Park. Lower concentrations of sulfate were observed on 7/26 – 27, 7/30 – 8/1 and 8/12. The highest sulfate concentrations were measured on 7/22, 7/24, 8/3, 8/11 and 8/17 with peaks of 14.0 $\mu g/m^3$, 14.3 $\mu g/m^3$, 19.5 $\mu g/m^3$, 15.1 $\mu g/m^3$ and 15.7 $\mu g/m^3$, respectively. Generally, the ammonium concentration trends were similar to sulfate, ranging from zero to 3.80 $\mu g/m^3$. Nitrate concentrations were almost always well below 1 $\mu g/m^3$.

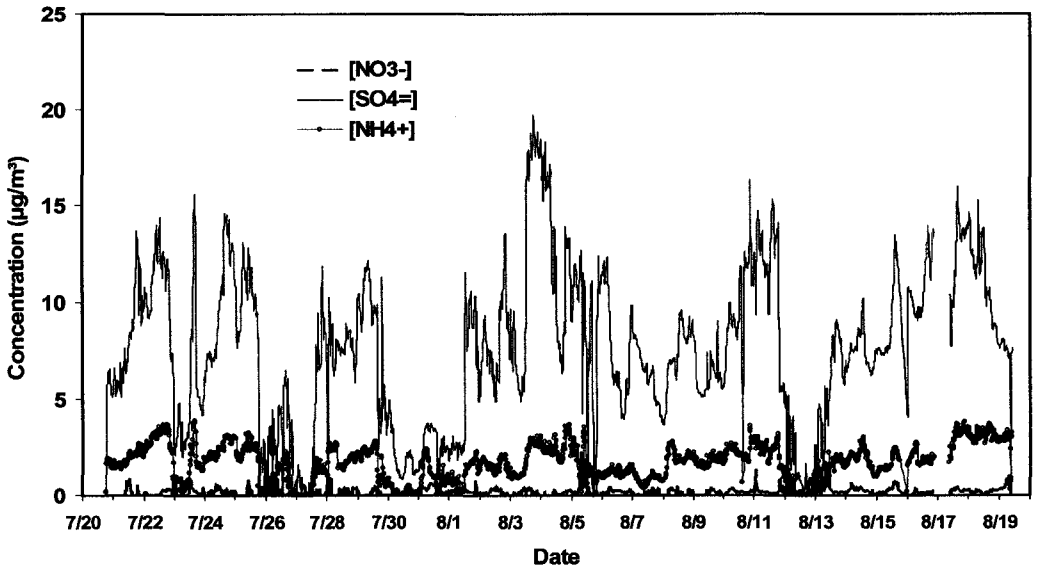

Figure 4.25 Timelines of PILS $PM_{2.5}$ NO_3^-, SO_4^{2-} and NH_4^+ concentrations (Great Smoky Mtns N.P.(July/Aug, 2004))

The variation of minor cation species and Cl^- concentrations is shown in Figure 4.26. The maximum concentration of K^+ was 1.08 $\mu g/m^3$ on 7/27. Concentrations ranged from zero to 1.08 $\mu g/m^3$ during this study. Na^+, Mg^{2+}, Ca^{2+} and Cl^- were found to

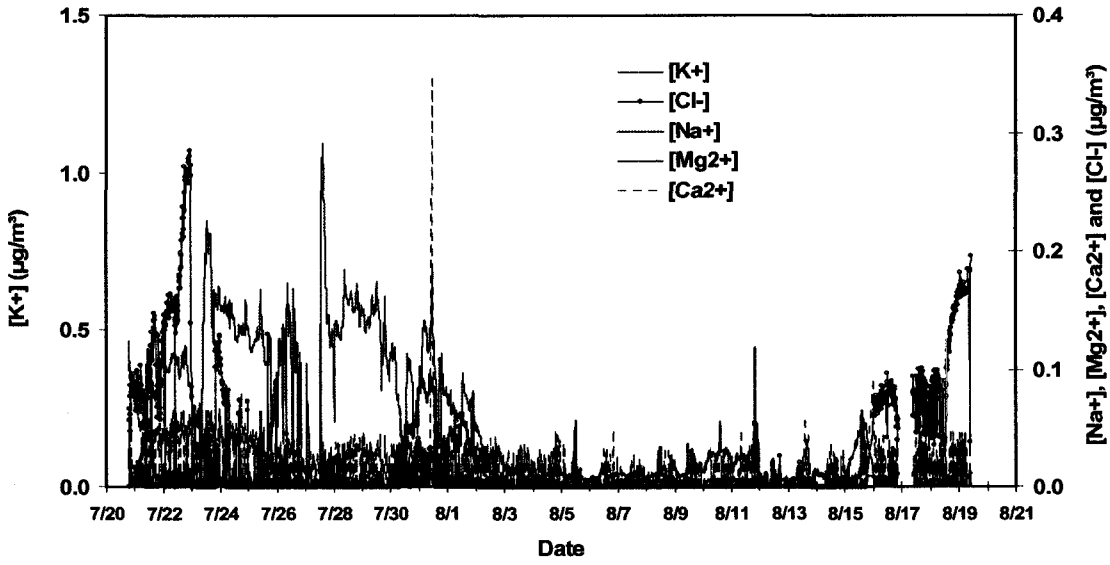

Figure 4.26 Timelines of PILS $PM_{2.5}$ minor ionic species (Cl^-, Na^+, K^+, Mg^{2+} and Ca^{2+}) concentrations (Great Smoky Mtns N.P.(July/Aug, 2004))

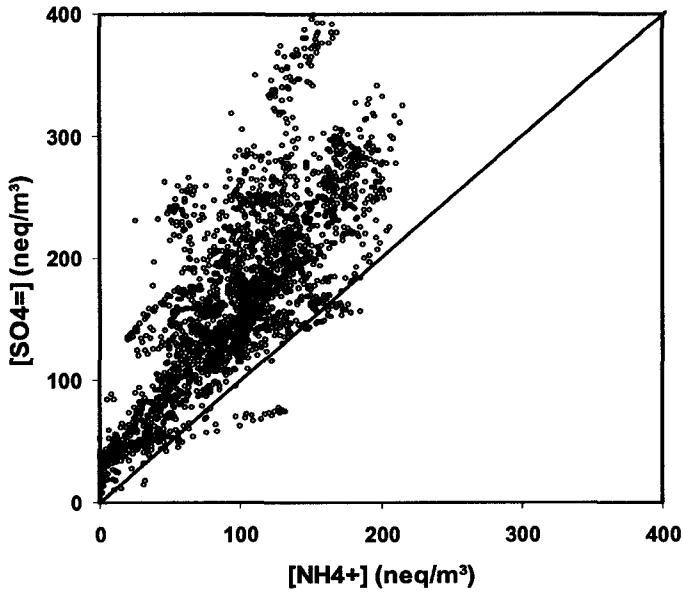

Figure 4.27 Relationship between SO_4^{2-} and NH_4^+ concentrations (Great Smoky Mtns N.P.(July/Aug, 2004))

be minor contributors to $PM_{2.5}$. The highest concentrations of Cl^- and Na^+ were approximately 0.29 $\mu g/m^3$ on 7/22 and 0.12 $\mu g/m^3$ on 8/11, respectively, with concentrations of Na^+, Mg^{2+}, Ca^{2+} and Cl^- close to the detection limit on most days.

Figure 4.27 shows SO_4^{2-} concentrations plotted against NH_4^+ concentrations, indicating a typically acidic aerosol with insufficient ammonium to fully neutralize sulfate particles. This is consistent with URG measurements presented in chapter 3. Molar ratios of $[NH_4^+]/[SO_4^{2-}]$ are presented as a timeline in Figure 4.28. The ratio shows considerable variability during the study, but only rarely reached 2.0, the aerosol neutral point. Molar ratios ranged from 0.05 to 3.56 with an average of 1.19. Generally, molar ratios dropped from 2 to below 1 during large increases in sulfate concentrations. Figure 4.29 shows sulfate concentrations plotted against molar ratios of $[NH_4^+]/[SO_4^{2-}]$.

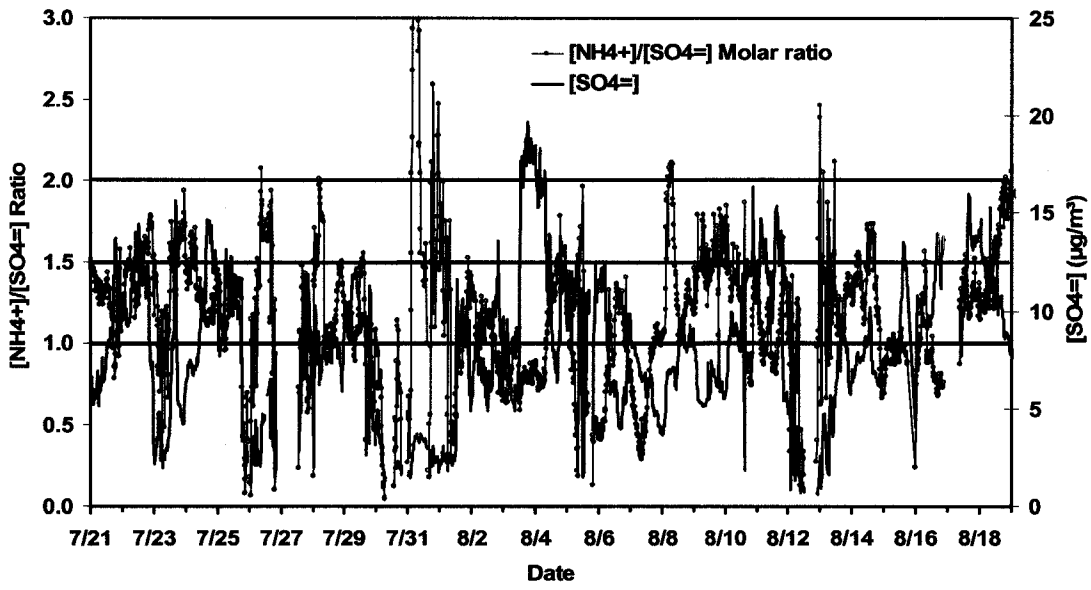

Figure 4.28 Timeline of PILS $PM_{2.5}$ molar ratios of $[NH_4^+]/[SO_4^{2-}]$ (Great Smoky Mtns N.P.(July/Aug, 2004))

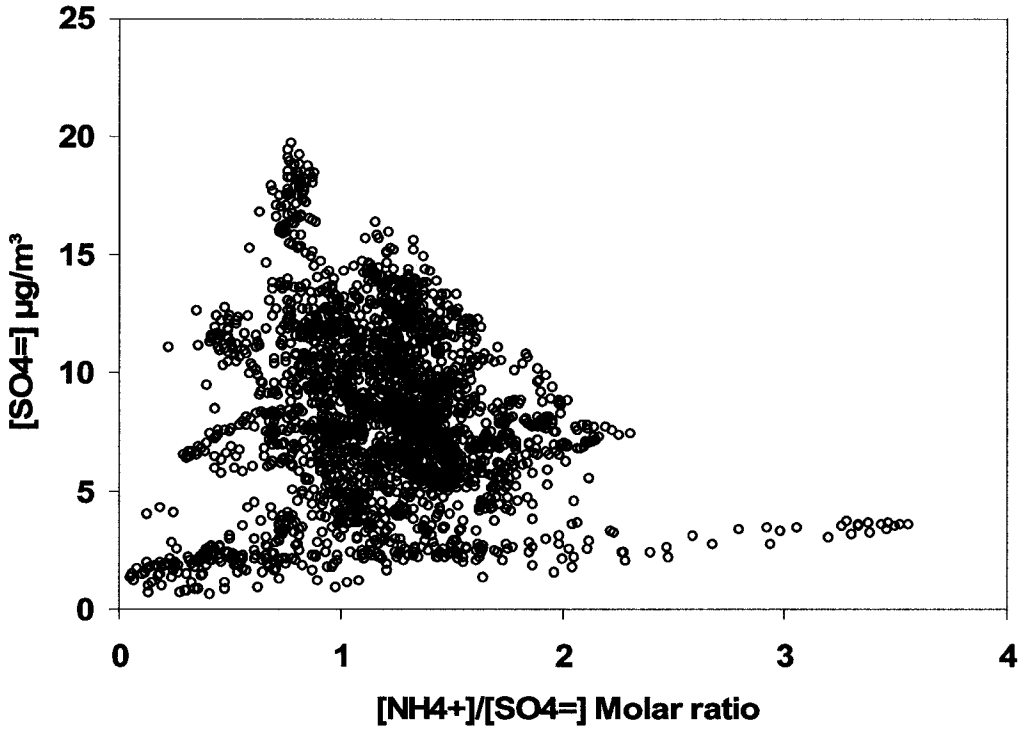

Figure 4.29 Relationship between molar ratio of $[NH_4^+]/[SO_4^{2-}]$ and SO_4^{2-} (Great Smoky Mtns N.P.(July/Aug, 2004))

Generally one sees a trend toward lower $[NH_4^+]/[SO_4^{2-}]$ molar ratios at higher sulfate concentrations, suggesting that aerosol acidity at the site typically increases with the amount of sulfate.

The relationship between sulfate concentration and local transport at the site is examined in Figure 4.30. Figure 4.30 shows that sulfate temporal trends are correlated with the wind pattern at the site. Boundary layer breakup (or growth) starts in the early morning and reaches the site in the early afternoon, leading to increases in sulfate concentration typically between the hours of 2 and 4 in the afternoon. Generally, winds shifted from northerly and/or northwesterly (up-slope) to southerly and/or southeasterly (down-slope) around sunset, along with a decrease in sulfate concentrations, indicating

meteorological changes at the site are important in driving changes in aerosol characteristics (see also Hand and Kreidenweis, 1997; Sherman et al., 1997).

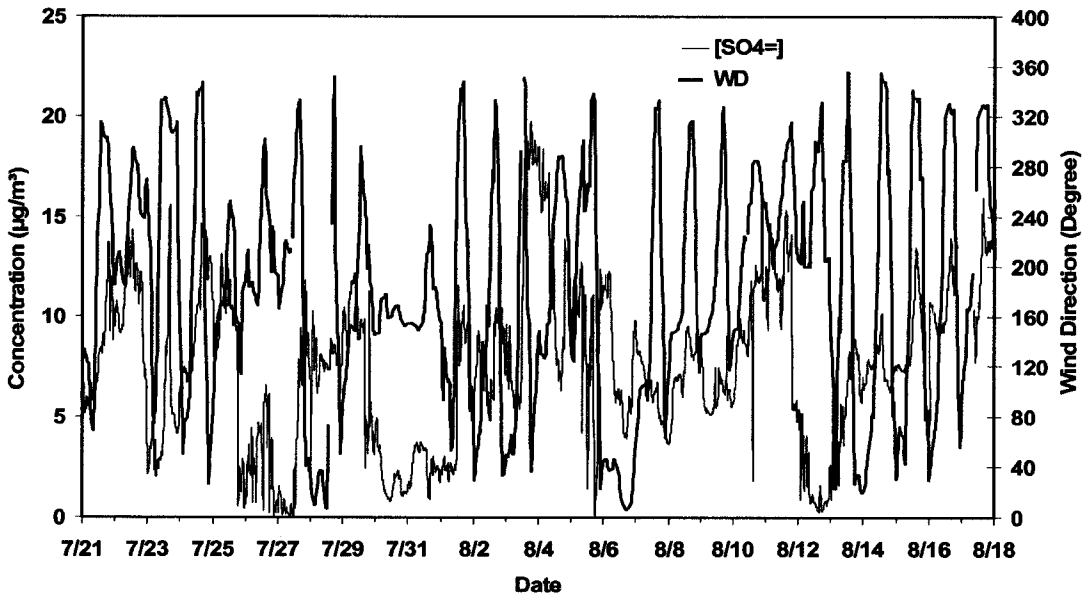

Figure 4.30 Timelines of PILS $PM_{2.5}$ SO_4^{2-} and wind direction (Great Smoky Mtns N.P. (July/Aug, 2004))

4.6 Summary and conclusions

To improve understanding of the chemical characteristics of aerosol particles and their temporal variability, high time resolution measurements of $PM_{2.5}$ composition are of great value. $PM_{2.5}$ ion composition was measured at 15 minutes intervals using a Particle Into Liquid Sampler (PILS) coupled to two DIONEX ion chromatographs. Study sites included Bondville, Illinois (February 2003), San Gorgonio Wilderness Area, California (April and July 2003), Grand Canyon National Park (May 2003), Brigantine National

Wildlife Refuge, New Jersey (November 2003) and Great Smoky Mountains National Park (July/Aug 2004).

PILS data provide addition insight into correlations between ion species and temporal variations in ion concentrations. Strong diurnal concentration trends of many ionic species were clearly correlated with upslope transport due to mountain-valley winds, bringing polluted air masses to the site at San Gorgonio, California, located in the mountains north of San Bernadino, downwind of Los Angeles. PILS data from Grand Canyon National Park, Arizona clearly suggested an association between nitrate and sodium/calcium/magnesium due to reaction of nitric acid with soil dust and/or sea salt. Observations from Bondville, Illinois, revealed rapid transitions between nitrate and sulfate dominated aerosols, and demonstrated that particle nitrate formation depends on temperature and RH. While sulfate and nitrate, fully neutralized by ammonium, were the dominant ionic species at Brigantine National Wildlife Refuge, New Jersey, very acidic sulfate aerosol was observed at Great Smoky Mountains National Park, Tennessee.

Semi-continuous measurements of aerosol composition provide additional insights into processes and factors controlling ambient aerosol concentrations. First, ammonium and sulfate were founded as predominant species in $PM_{2.5}$ at Great Smoky Mountains N.P., while ammonium, sulfate and nitrate were observed as the major ionic species at other sites. Second, the PILS data provided very useful, high time resolution measurements of K^+ which serves as an indicator of periods when the sampling site was impacted by smoke from local and/or distant fire (i.e. San Gorgonio (July)). Third, the nitrate observed in San Gorgonio (July) and Grand Canyon N.P. suggested reaction of nitric acid or its precursors with sea salt and/or soil dust. Fourth, the variation of Cl^- with

Na^+ concentrations and non sea salt-[Cl^-] from PILS measurements shows the displacement of chloride from sea salt by reaction with nitric acid or its precursors and possible different sources of chloride, such as sea salt, road salts, combustion and emissions from industrial sources and incinerators.

High time resolved data by PILS/IC provide insights into aerosol chemical properties not afforded by traditional time-integrated, off-line measurements. The detailed associations of various chemical constituents and the chemical forms of aerosol observed by PILS/IC allow better understanding of aerosol contributions to visibility degradation and aerosol effects on the local environment through wet and dry deposition. Nitrate may exist in several different chemical forms (e.g., NH_4NO_3, $NaNO_3$ and/or $Ca(NO_3)_2$ (and/or $Mg(NO_3)_2$) and in coarse or fine particles, as we have seen. Particle light scattering efficiencies depend on both particle size and on particle hygroscopicity. The humidity at which deliquescence occurs varies from 74.3 % to 39.2 % at 298 K for mixtures of $Ca(NO_3)_2$ and $NaNO_3$ to pure $NaNO_3$ (Kelly and Wexler, 2006; Tang and Munkelwitz, 1993), an important factor in how particulate nitrate can impact visibility under various humidity conditions. Deposition rates for airborne nitrate also vary strongly between species. Evans et al. (2004) showed the local total nitrogen deposition decreased as particle concentrations increased (Evans, 2003). Particles have lower deposition velocities and longer residence times than HNO_3 (Evans et al., 2004; Pryor and Sorensen, 2000). As a results when HNO_3 is transferred to the particle phase as NH_4NO_3, $NaNO_3$, $Ca(NO_3)_2$ or ($Mg(NO_3)_2$), it is subject to greater transport horizontally instead of being quickly deposited as HNO_3. Among the various particle nitrate forms, those occurring as coarse particles will deposit more quickly than fine particle nitrate.

5. Characterization of particulate nitrate

Nitrate comprises an important part of aerosol mass at many locations during at least some times of the year, as discussed in Chapter 1. Although particulate nitrate is generally assumed to consist mainly of fine particle NH_4NO_3, we have already seen that both $NaNO_3$, and $Ca(NO_3)_2$), products from the reactions of gaseous of HNO_3 with sea salt or soil dust, can be important components of $PM_{2.5}$ nitrate at some locations (e.g., Big Bend and Yosemite National Parks).

Properties of aerosol nitrate were characterized at several IMPROVE monitoring sites during a series of field studies. Study sites include Bondville, Illinois (February 2003), San Gorgonio Wilderness Area, California (April and July 2003), Grand Canyon N.P. (May 2003), Brigantine National Wildlife Refuge, New Jersey (November 2003) and Great Smoky Mountains N.P. (Aug 2004). Details of measurements at these sites were provided in Chapter 2. Briefly, 24 hour average $PM_{2.5}$ ion concentrations and concentrations of key gases (HNO_3, SO_2, NH_3) were determined by annular denuder/filter-pack measurements. Ion size distributions were measured using a Micro-Orifice Uniform Deposit Impactor (MOUDI). $PM_{2.5}$ ion concentrations were also measured using a semi-continuous PILS (Particle-Into-Liquid –Sampler) with 15-minute time resolution.

An overview of aerosol composition and its temporal variations at these locations was provided already in Chapters 3 and 4. In this chapter we use these observations to ascertain the dominant forms of particulate nitrate in the various campaigns and summarize factors that control the occurrence of fine vs. coarse particle nitrate.

5.1 San Gorgonio Wilderness Area (April and July, 2003), CA

Measurements at San Gorgonio Wilderness Area (Longitude:-116.901, Latitude: 34.19, 1705 m elevation), California were made during two campaigns in April and July 2003. These time periods were chosen for investigating possible seasonal changes in the form of aerosol nitrate in moving from cooler spring to hot summer temperatures in this nitrogen rich environment (see Fig 1.1).

Figure 5.1 depicts correlations of the concentrations of nitrate, sulfate and ammonium (expressed in nanoequivalents per cubic meter (neq/m^3)). Low correlations ($R^2 \sim 0.2$) between $PM_{2.5}$ ammonium and sulfate were found in both April and July. Much stronger correlations (R^2=0.997 and 0.91 for April and July, respectively) between ammonium and the sum of nitrate and sulfate concentrations were observed, indicating the important contributions of ammonium nitrate at this site. Clustering of these ratios around the 1:1 line in April demonstrates that the aerosol is neutral, with sufficient inputs of ammonia accounting for the inputs of sulfuric and nitric acids. A similar picture is seen on many days in July, although a few points falling significant above the line indicate the possible importance of another cation in the aerosol.

Figure 5.2 shows timelines of the ratios of gaseous nitric acid to total N(V) (the sum of gaseous nitric acid and $PM_{2.5}$ nitrate) and of gaseous ammonia to total N(-III) (the sum of gaseous ammonia and $PM_{2.5}$ ammonium). The average ratios for $HNO_3(g)/N(V)$ and $NH_3/N(-III)$ were 0.17 and 0.46 for April, indicating the low temperature and relatively high humidities during April favor significant particulate ammonium nitrate formation. During July, much higher ratios are observed (0.72 and 0.69 for $HNO_3(g)/N(V)$ and $NH_3/N(-III)$, respectively) consisted with the expected tendency for

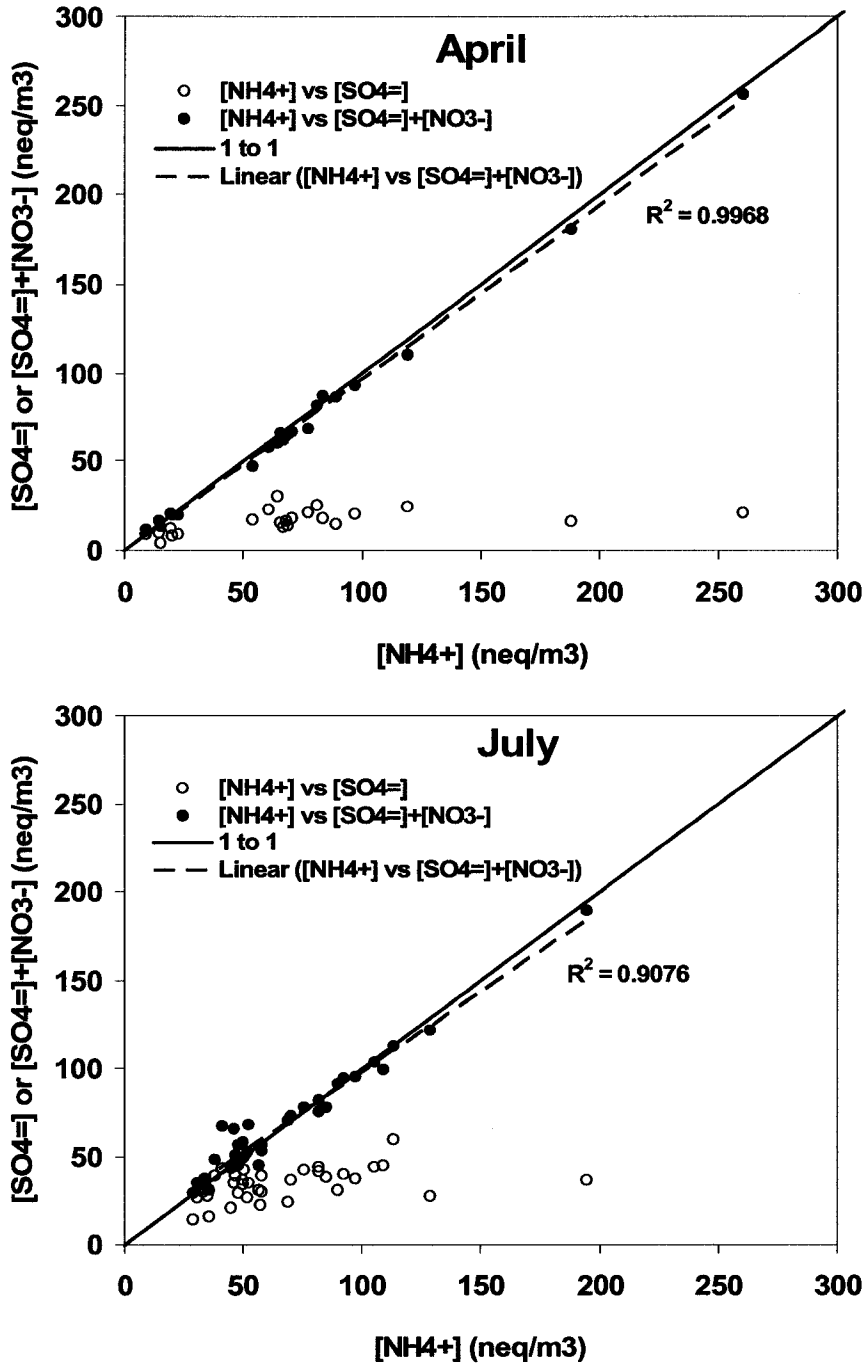

Figure 5.1 Relationship of URG $PM_{2.5}$ concentrations of sulfate, nitrate, and ammonium (San Gorgonio (April and July))

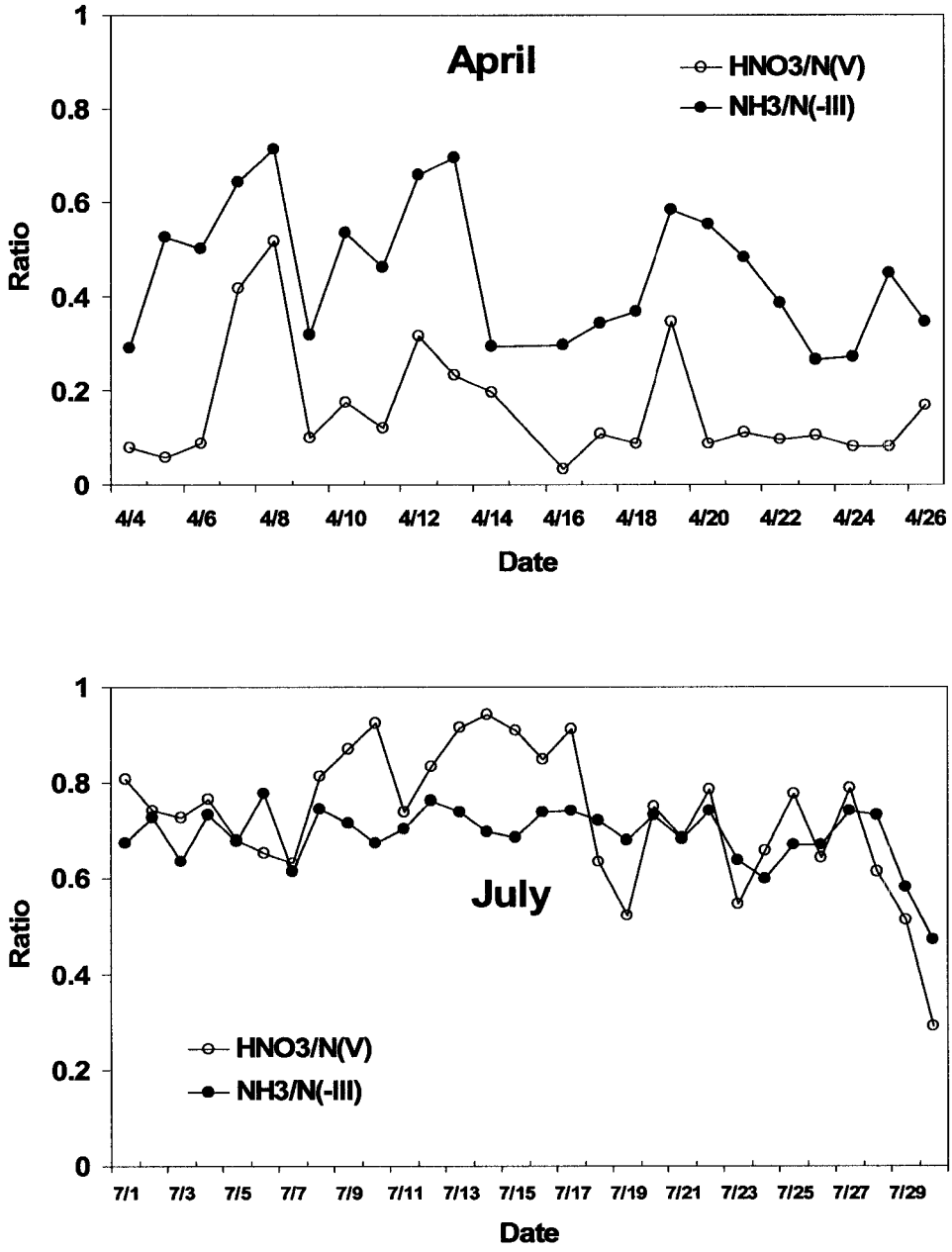

Figure 5.2 Timelines of ratio of [HNO_3]/[N(V)] and [NH_3]/[N(-III)] from URG (San Gorgonio (April and July))

this system to thermodynamically favor the gas phase components over semivolatile ammonium nitrate formation at high temperatures and lower humidities.

Figure 5.3 shows Na^+ concentrations plotted against $[Cl^-]$ as well as the sum of $[NO_3^-]$ and $[Cl^-]$ for April and July. The observed $[Cl^-]/[Na^+]$ equivalent ratio in April is close to the ratio of $[Cl^-]$ to $[Na^+]$ in sea water (1.164), indicating a lack of sea salt reaction. This picture changes significantly in July, however, when the $[Cl^-]/[Na^+]$ ratio falls far below the sea water ratio, indicating loss of chloride from sea salt aerosol transported to San Gorgonio. Ratios of the sum of $[Cl^-]$ and $[NO_3^-]$ to $[Na^+]$ in July, by contrast, fall at or above the sea water ratio of $[Cl^-]/[Na^+]$. This pattern indicates likely replacement of sea salt aerosol chloride by nitrate, reflecting reaction of sea salt with nitric acid or its precursors as shown in equations 1.4, 1.5 and 4.2. Formation of $NaNO_3$ is also consistent with the observation that insufficient ammonium was present to balance the sum of nitrate and sulfate on some days in July (Figure 5.1). Occurrence of ratios of $[Cl^-] + [NO_3^-]$ to $[Na^+]$ greater than the sea water $[Cl^-]/[Na^+]$ ratio simply reflects the presence of $PM_{2.5}$ NH_4NO_3.

Further insight into the properties of San Gorgonio particulate NO_3^- is possible through examination of the MOUDI and PILS results. Figure 5.4 depicts the campaign-averaged measured size distributions for major ions SO_4^{2-}, NH_4^+, NO_3^-, and Na^+. The MOUDI SO_4^{2-} and NO_3^- size distributions are very similar to the shape of the ammonium size distribution in April, with a submicron mode peaked at 0.4 – 0.5 μm aerodynamic diameter. Some nitrate is seen in supermicron particles. On the other hand, NO_3^- and Na^+ size distributions mainly cover the coarse mode in July, with an aerodynamic mode

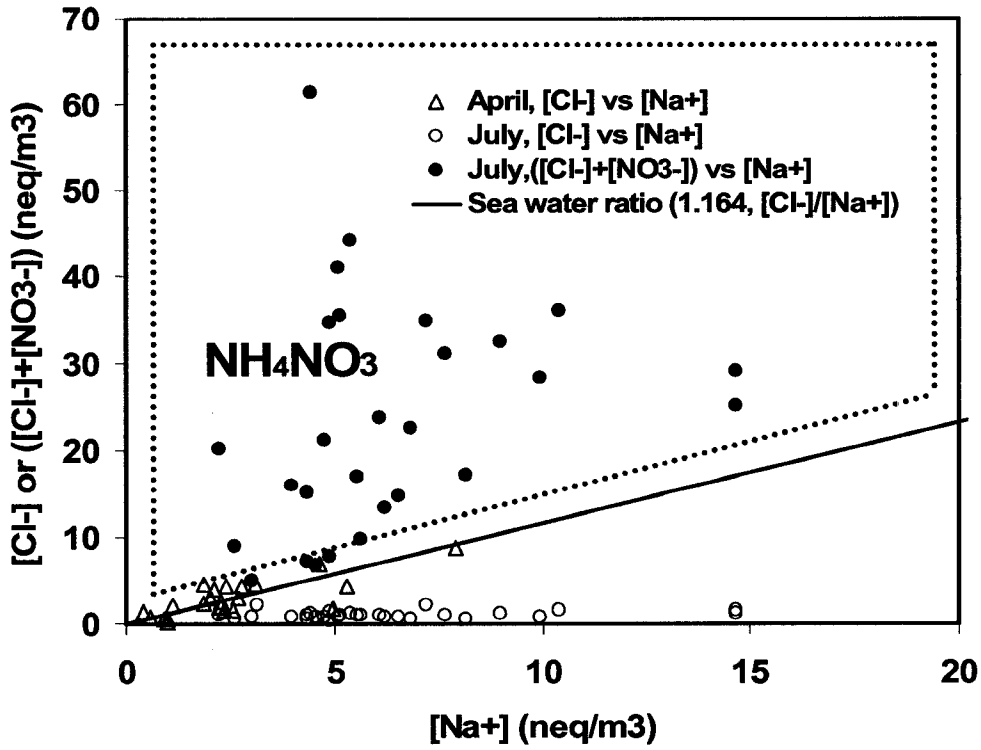

Figure 5.3 Relationship between Na^+ and Cl^- and between Na^+ and the sum of NO_3^- and Cl^- from URG (San Gorgonio (April and July))

diameter of ~ 4 μm. The similarity of the size distributions for these two species further supports the interpretation above that significant particle NO_3^- in July was formed by sea salt particle reaction with gaseous nitric acid or its precursors. Higher temperatures at this time do not favor ammonium nitrate formation, leaving more nitric acid available to react with sea salt or soil dust. The apparent absence of significant submicron particulate nitrate in July, however, may reflect a negative sampling bias associated with 48 hr sampling of semivolatile ammonium nitrate by the MOUDI. The July San Gorgonio comparison of $PM_{2.5}$ nitrate included in Chapter 3 reveals that generally less nitrate was measured by the MOUDI than by the URG denuder/filter-pack sampler.

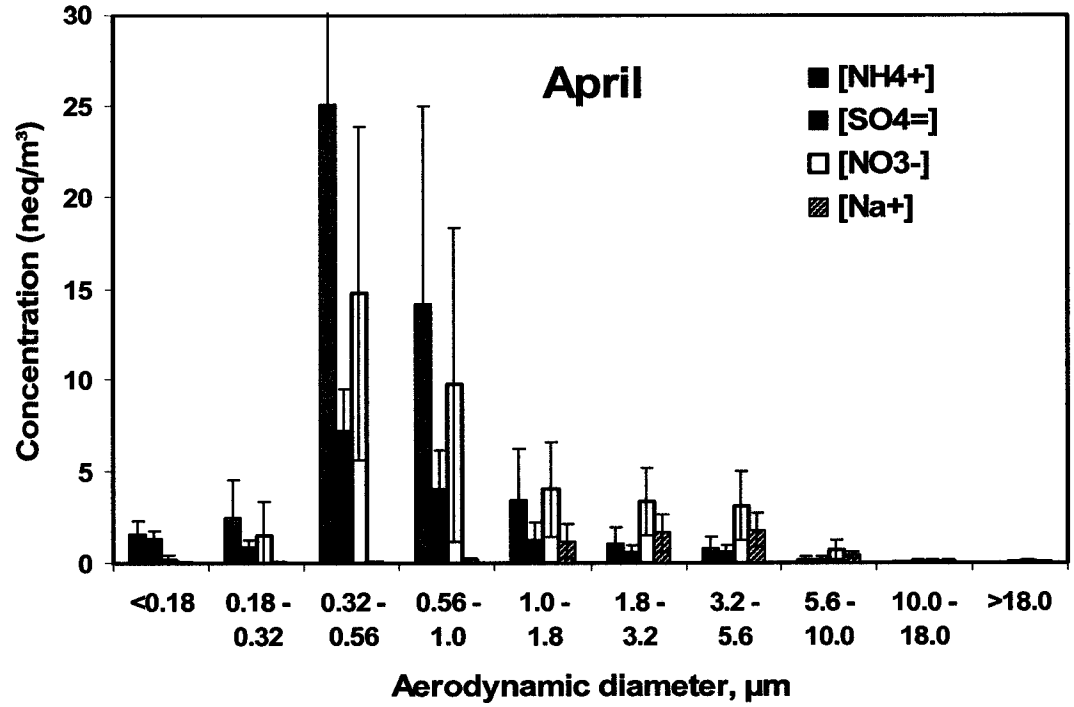

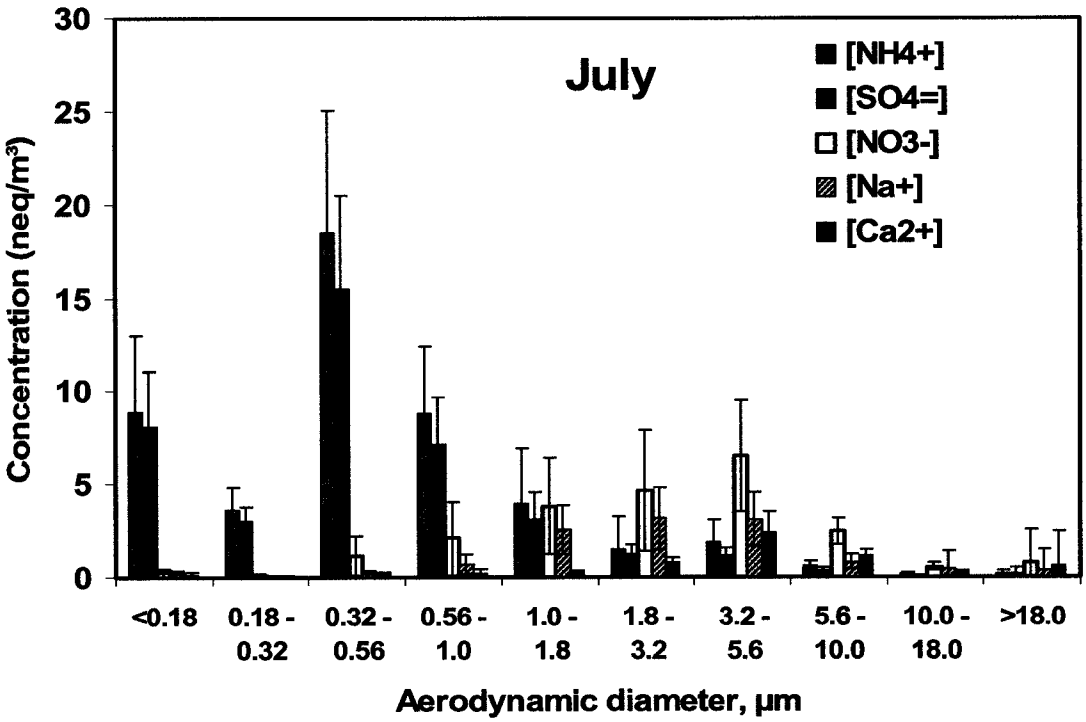

Figure 5.4 The size distribution of averaged ammonium, sulfate, nitrate, sodium and calcium concentrations (San Gorgonio (April and July)) (Error bar represent standard deviation of all samples)

Because the URG sampler configuration was designed to retain any volatilized nitrate, we interpret the difference between these two measurements as an indication of nitrate volatilization loss from the MOUDI. Such loss is not unexpected in a 48 hr sampling cycle during hot times of year featuring large diurnal swings in temperature and relative humidity. The correlation between particulate NO_3^- and Na^+ (or soil dust, Ca^{2+} and Mg^{2+}) and the dissociation of ammonium nitrate by temperature all become clearer in PILS observations as shown in Figures 5.5, 5.6 and 5.7.

In Figure 5.5 (note two vertical scales used) one can see simultaneous changes in NO_3^- and Na^+ concentrations. The diurnal variability is driven largely by mountain-valley wind patterns. During upslope flow pollution is brought up to the site and decreases again during night-time drainage flow. Concentrations of NO_3^- and Na^+ are often similar during the early part of the daily concentration rise, but as seen in Fig. 5.5 far more nitrate is present in the peak maximum than can be balanced by Na^+. Looking at the relative amounts of Cl^- and Na^+, one also sees that much of the Cl^- was lost from the precursor sea salt aerosol much of the time, consistent with nitric acid reaction with these particles. It is likely that some nitric acid also reacted with soil dust. Indeed, if we look at the PILS timeline for Ca^{2+} and Mg^{2+} in Fig. 5.5, we also see a spike in these species' concentrations often accompanying the afternoon nitrate spike. Again, however, there is insufficient Ca^{2+} or Mg^{2+} to fully balance the NO_3^- observed. Looking back at the full PILS timeline in Chapter 4, one sees that much of the nitrate during the concentration spikes is still NH_4NO_3.

A closer look at the San Gorgonio PILS timeline in July provides interesting insight into factors controlling the timing of the nitrate peak. An example in July is

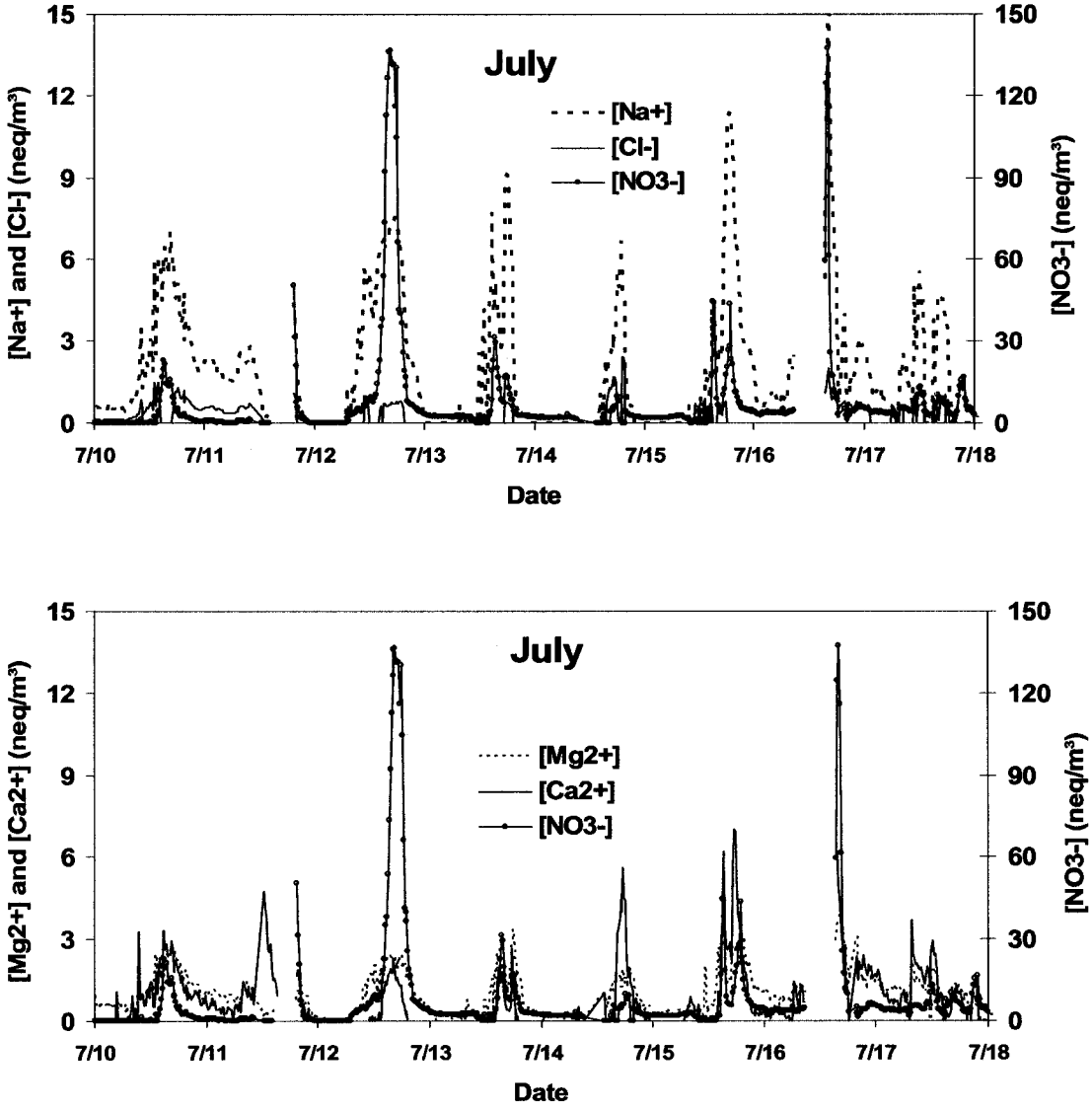

Figure 5.5 Timelines of PILS $PM_{2.5}$ NO_3^-, Na^+, Ca^{2+} and Mg^{2+} ion concentration measured from July 10–18

shown in Figure 5.6, where peaks in the nitrate and sulfate concentrations were observed during the afternoon with upslope transport of air to the site. Following the return to downslope flow around 18:00, a lag is seen before the sulfate concentration drops off. Using sulfate as a tracer for the polluted air mass, we interpret this lag as the time

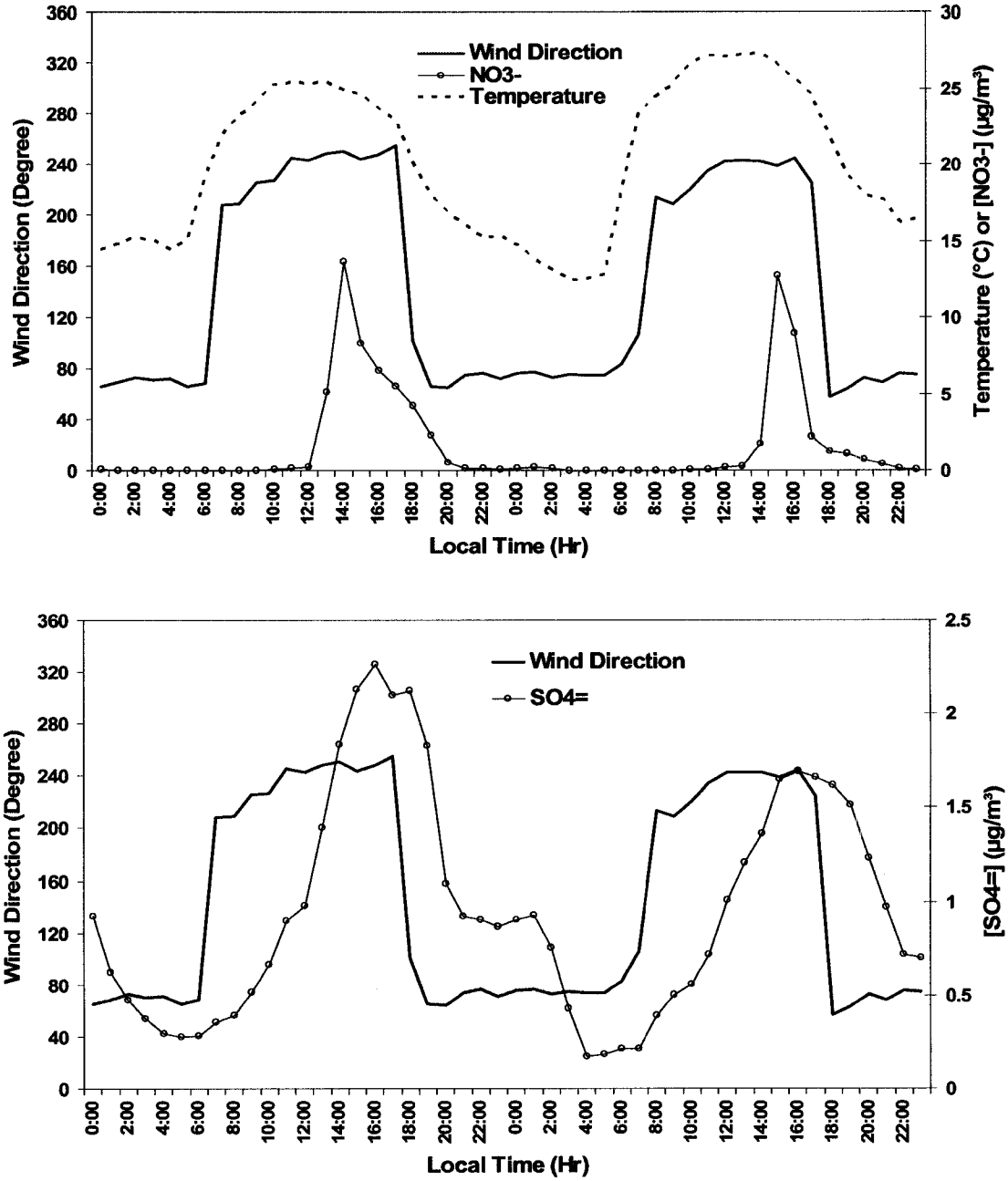

Figure 5.6 Example PILS NO_3^- and SO_4^{2-} timeline with wind direction and temperature in July.

required for the downslope flow to carry the pollution "front" back past the site to lower elevations. The nitrate concentration, by contrast, already decreases before the wind changes from upslope to downslope. This is consistent with loss of particulate

ammonium nitrate to the gas phase as afternoon temperatures warm. Some of the particulate nitrate loss likely occurs at lower altitude, where temperatures are even warmer.

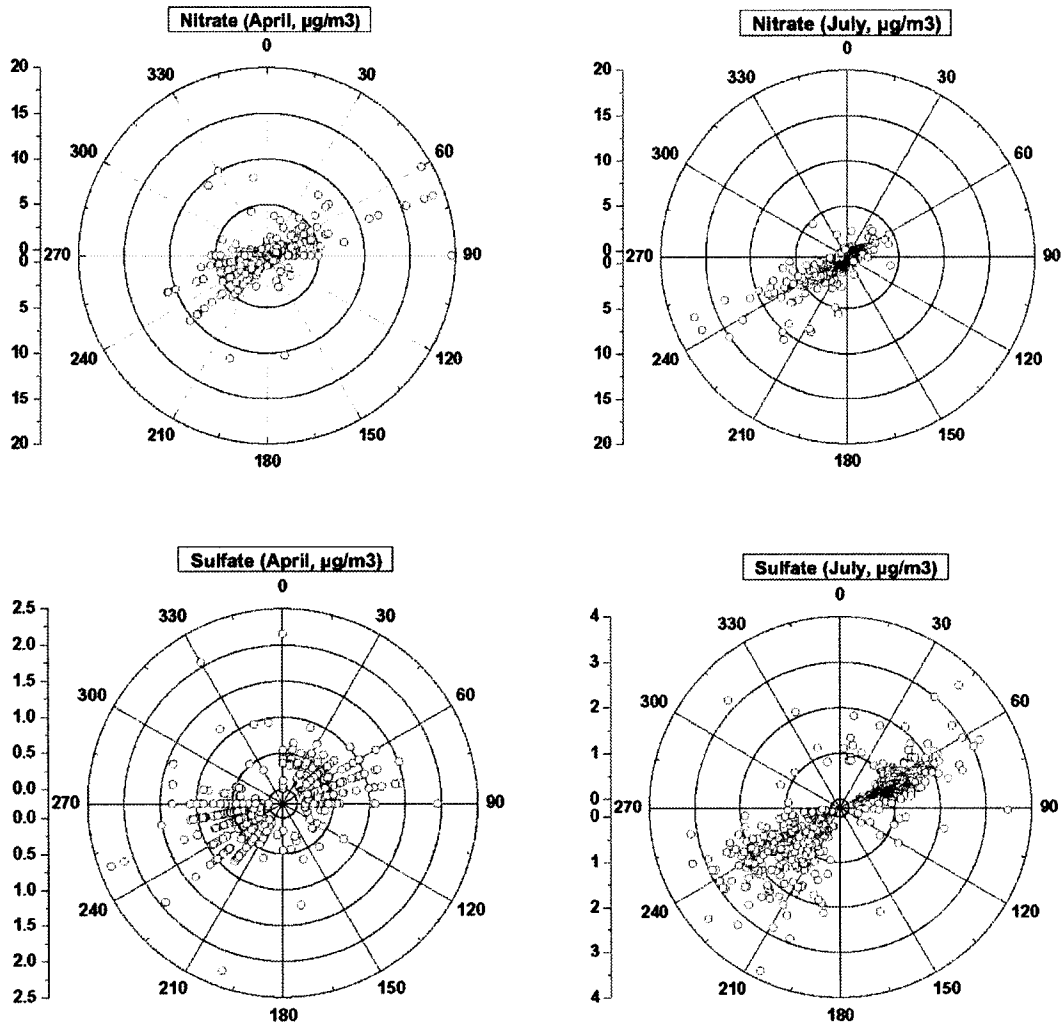

Figure 5.7 PILS NO_3^- and SO_4^{2-} concentrations by wind directions (April and July, San Gorgonio)

Figure 5.7 illustrates variations of $PM_{2.5}$ sulfate and nitrate concentration with wind direction during the April and July San Gorgonio campaigns. A variety of sulfate concentrations are observed during both upslope and downslope flow in both April and July, consistent with the transport of a polluted air mass past the site and back again on many days. During April we see a similar pattern for nitrate. This changes, however, in July, when high nitrate concentrations are generally observed in the upslope (SW) flow. Again, this is consistent with the loss of substantial particulate nitrate to the gas phase during the upslope flow phase as temperatures rise, likely followed by significant deposition of nitric acid to vegetation surfaces. During this period only the less volatile forms of nitrate associated with reacted sea salt and soil dust are likely present.

5.2 Grand Canyon National Park, Arizona

Measurements at Grand Canyon National Park (Logitude:-111.984, Latitude: 35.973, and 2267 m of elevation), Arizona were performed in May, 2003. This period was chosen because IMPROVE data indicate the park historically has experienced the highest particulate nitrate concentration in the spring (http://vista.cira.colostate.edu/improve/data/graphicViewer/seasonal.htm) and may be increasing with time (Malm et al., 2000; Malm et al., 2004).

Figure 5.8 shows a comparison of ammonium concentration and sulfate concentration and the sum of sulfate and nitrate concentrations. The observations indicate that sufficient ammonium is typically present to fully neutralize the $PM_{2.5}$ sulfate but not to balance both sulfate and nitrate. The implication is once again that other forms of nitrate may be important in this environment.

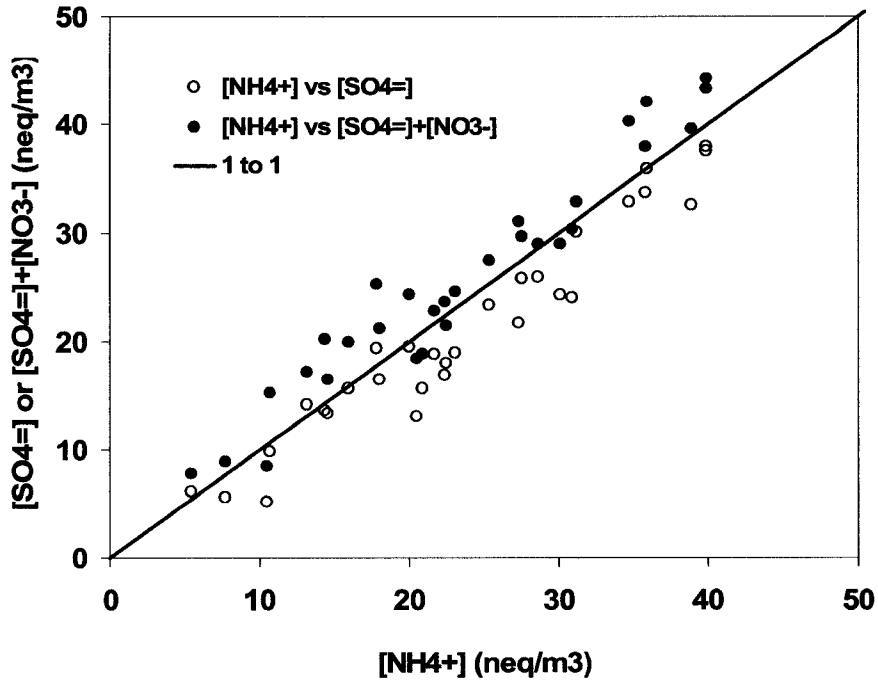

Figure 5.8 Relationship of URG $PM_{2.5}$ concentrations of sulfate, nitrate and ammonium (Grand Canyon National Park, May 2003)

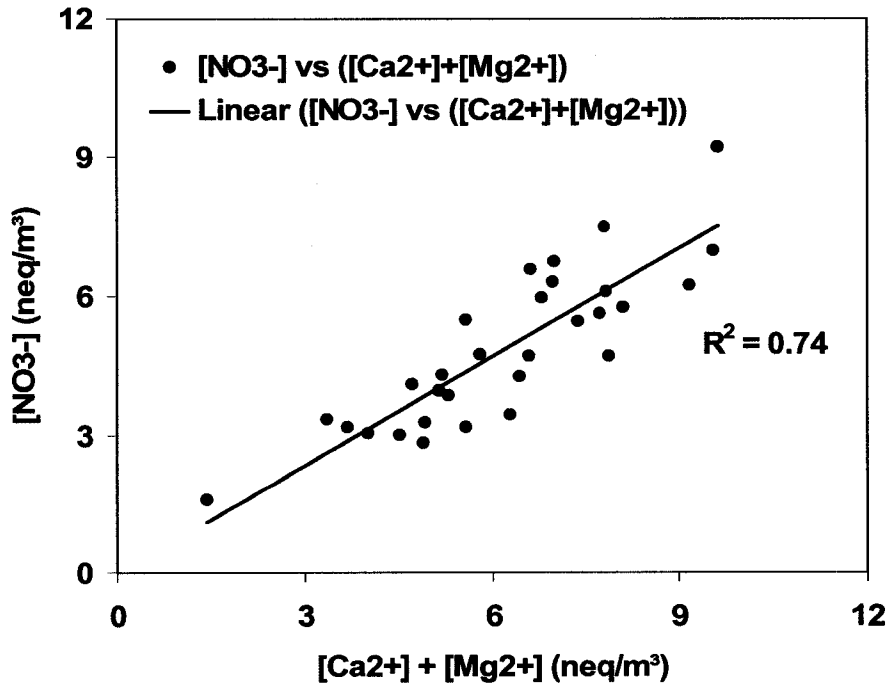

Figure 5.9 Relationship of $[NO_3^-]$ and sum of $[Ca^{2+}]$ and $[Mg^{2+}]$ from URG

Figure 5.9 shows the correlation of particulate nitrate with Ca^{2+} and Mg^{2+}, which typically are associated with soil dust (Table 1.2 and 1.3) (Cheng et al., 2000; Evans et al., 2004; Finlayson-Pitts and Pitts, 2000; Goodman et al., 2000; Grassian, 2002; Hanisch and Crowley, 2001a; Hanisch and Crowley, 2001b; Hanisch and Crowley, 2003; Ooki and Uematsu, 2005; Pakkanen, 1996; Underwood et al., 2001). Particulate nitrate concentrations were strongly correlated with the sum of Ca^{2+} and Mg^{2+} (R^2=0.85), suggesting soil particles are likely sinks for gas phase nitric acid to form particulate nitrate. The PILS observations of $PM_{2.5}$ composition provide further support for this idea as illustrated in Figure 5.10. Although the time trends are complex and

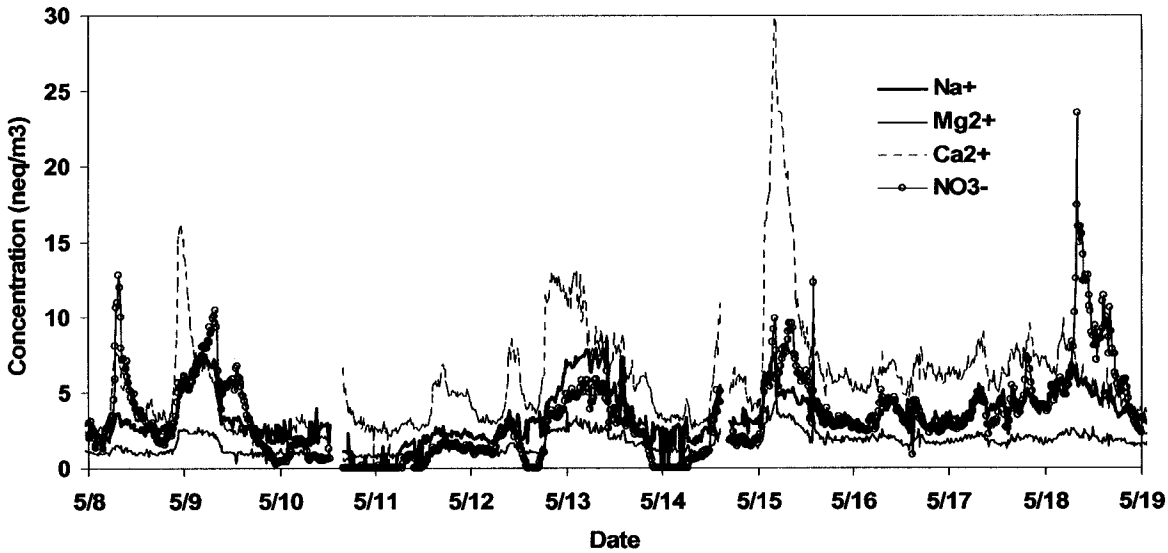

Figure 5.10 PILS NO_3^-, Mg^{2+}, Ca^{2+} and Na^+ timelines measured from May 8 – 19 (Grand Canyon National Park)

concentrations generally low (hence somewhat noisy due to increased measurement uncertainty), NO_3^- concentration changes appear to track changes in Ca^{2+} and Mg^{2+}

concentrations in many periods. Some tracking of NO_3^- and Na^+ is apparent as well (Figure 5.10), indicating the possible role of sea salt and/or other sodium salts (e.g. Na_2CO_3) for formation of particulate nitrate as well.

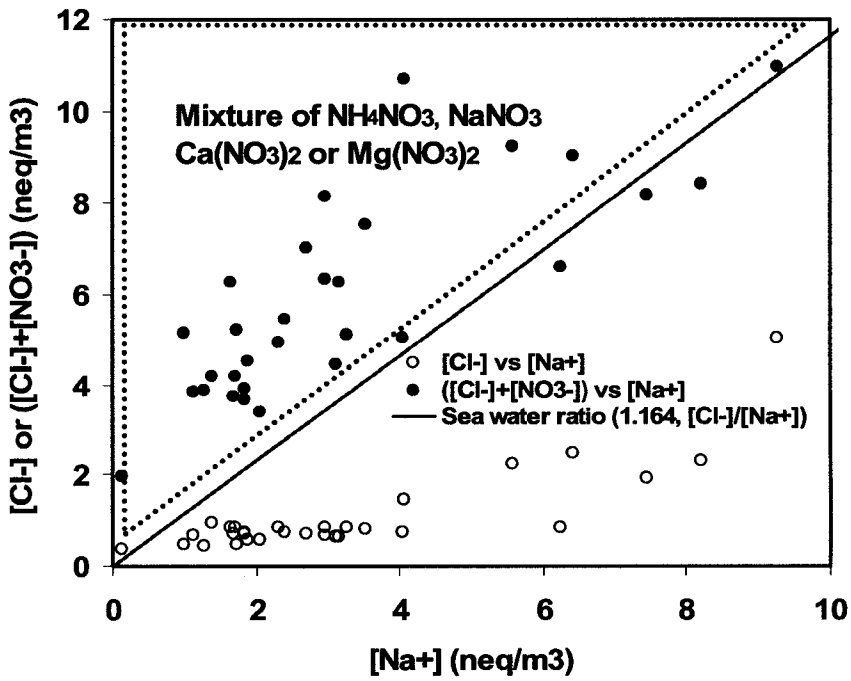

Figure 5.11 Relationship between Na^+ and Cl^- and between Na^+ and the sum of NO_3^- and Cl^- (Grand Canyon NP)

Cl^- loss from sea salt is evident in the data plotted in Figure 5.11, where the ratio of $[Cl^-]$ to $[Na^+]$ falls well below the sea water ratio of $[Cl^-]/[Na^+]$ on nearly every day. When sodium concentrations are compared to the sum of nitrate and chloride, however, there is more nitrate than can be explained by nitric acid displacement of sea salt Cl^- alone, consistent with the importance of other forms of nitrate as discussed above.

The strong correlations between sulfate and ammonium and particulate nitrate associated with $[Na^+]$, $[Ca^{2+}]$ and $[Mg^{2+}]$ were observed as a function of particle size in the MOUDI measurements as well (Figure 5.12). The MOUDI sulfate and ammonium size distributions exhibit very similar shapes, with a submicron mode typically peaked at 0.4 – 0.5 μm aerodynamic diameter. Nitrate, calcium, magnesium, and sodium size distributions, by contrast, peaked in the coarse mode with a mode diameter in the 2-4 μm size range. The similarity of these size distributions lends further support to the conclusion above that particle nitrate at this site depends largely on reaction of nitric acid or its precursors with soil dust or sea salt.

Table 5.1 shows additional information regarding correlations of particulate nitrate and cation concentrations (Na^+ and the sum of Ca^{2+} and Mg^{2+}) measured by the URG sampler, the MOUDI, and the PILS. Stronger correlations of $[NO_3^-]$ were observed with the sum of $[Ca^{2+}]$ and $[Mg^{2+}]$ than with $[Na^+]$. This suggests that the reaction of nitric acid with soil dust might be more important than that with sea salt particles in this environment. This conclusion is not surprising given the substantial distance of this site from sea salt sources.

Table 5.1 Summary of correlation (R^2) between $[NO_3^-]$ and $[Na^+]$ or the sum of $[Ca^{2+}]$ and $[Mg^{2+}]$

		$[Na^+]$	$[Ca^{2+}] + [Mg^{2+}]$
URG	$[NO_3^-]$	0.36	0.74
PILS	$[NO_3^-]$	0.36	0.59
MOUDI (All stage)	$[NO_3^-]$	0.69	0.83

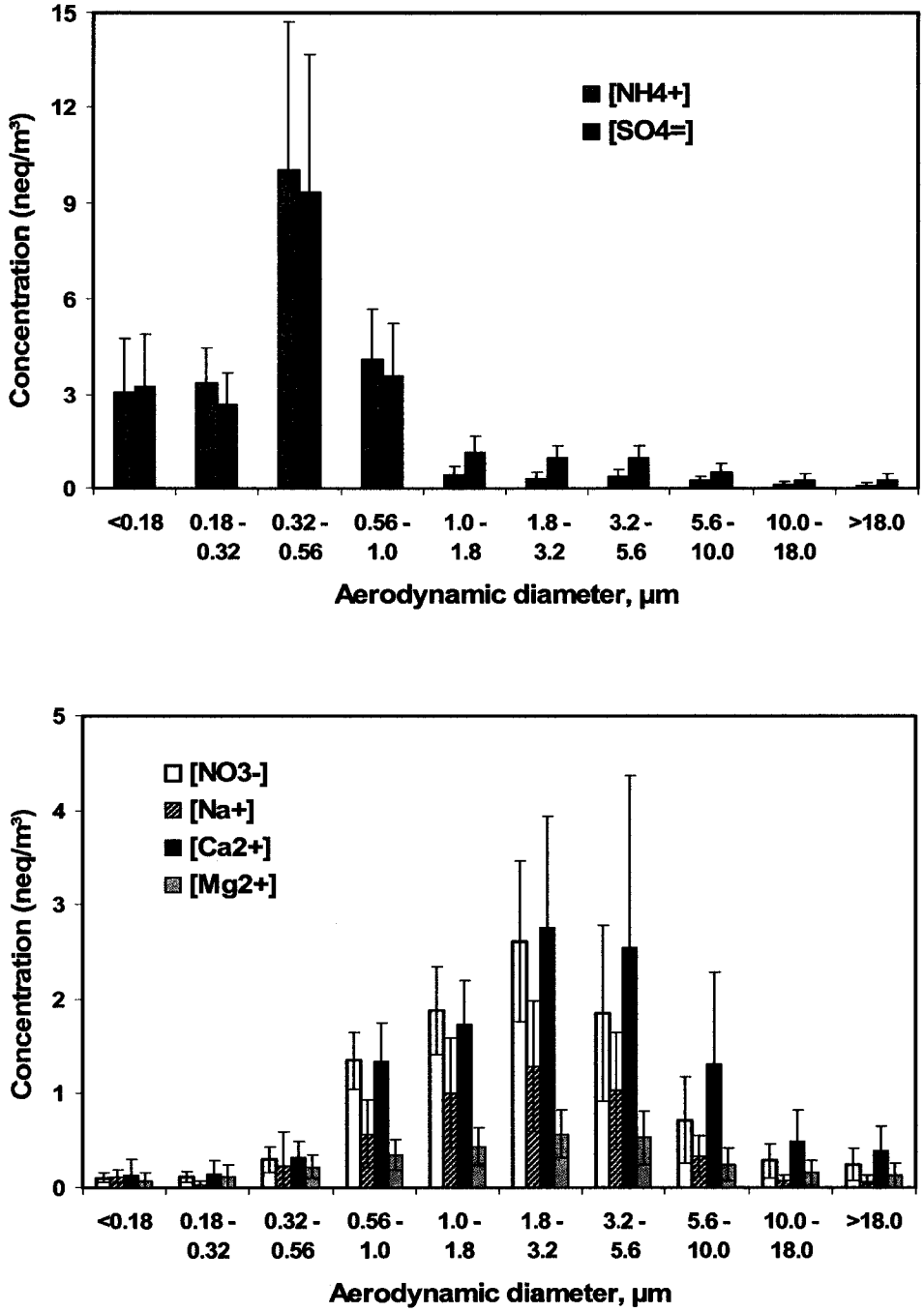

Figure 5.12 The size distribution of averaged ammonium, sulfate, nitrate, sodium, calcium, and magnesium concentrations in May, Grand Canyon N.P. (Error bar represent standard deviation of all samples)

In order to investigate the potential for formation of additional particulate nitrate, the available reservoirs of gaseous nitric acid and ammonia were considered. Figure 5.13 illustrates timelines of the ratios of [NH3]/[N(-III)] and [HNO_3]/[N(V)]. On average, 42% of the total ammonia+ammonium was present in the gas phase. An average of 65% of the total nitric acid + nitrate was present as gas phase nitric acid. This indicates a significant potential for increasing particulate nitrate with increased aerosol dust or sea salt loads or during periods when lower temperature and higher humidity favor particulate ammonium nitrate formation.

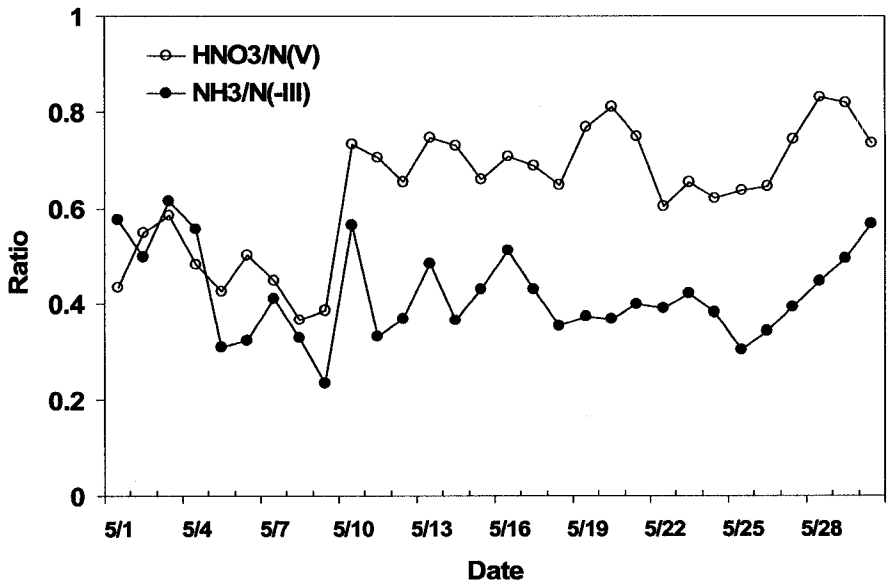

Figure 5.13 Timelines of ratio of [HNO_3]/[N(V) and [NH_3]/[N(-III)] (May 2003, Grand Canyon)

5.3 Bondville, IL and Brigantine National Wildlife Refuge, NJ

Two campaigns in February and November, 2003 were performed at Bondville, Illinois (Longitude: -88.3719, Latitude: 40.05 and 211 m of elevation) and Brigantine

National Wildlife Refuge, New Jersey (Longitude: -74.449, Latitude: 39.46 and 5 m of elevation), respectively.

Sulfate, nitrate and ammonium were the dominant ionic species in daily $PM_{2.5}$ both at Bondville, IL and Brigantine, NJ with important contributions also from sea salt (Cl^- and Na^+) at Brigantine, NJ. Figures 5.14 and 5.15 show the ammonium concentrations plotted against sulfate and the sum of sulfate and nitrate in $PM_{2.5}$ from URG and PILS for Bondville and Brigantine, respectively. Modest correlations of R^2 = 0.43 (0.47) and R^2 = 0.56 (0.51) between ammonium and sulfate were observed in the URG and PILS observations, respectively, at Bondville (Brigantine). When nitrate concentrations were added to sulfate concentrations to compare to ammonium concentrations, the correlations improved substantially, reaching 0.91 and 0.94 at Bondville and 0.72 and 0.86 at Brigantine for URG and PILS measurements. The slope of these latter correlations are also close to 1, indicating sufficient ammonia was generally present to neutralize the aerosol nitrate and sulfate.

An external mixture of aerosol chemical composition was evident in MOUDI data from both Bondville and Brigantine (Figure 5.16 and Figure 5.17, respectively). The majority of ammonium, sulfate and nitrate were observed, on average, in submicron particles at Bondville, with an aerodynamic mode diameter ~0.4 μm (Figure 5.16). Sulfate and ammonium exhibit very similar size distributions at Brigantine, with an aerodynamic mode diameter ~0.4 μm, with a slight excess of ammonium appearing to balance nitrate concentrations in submicron particles (Figure 5.17). In contrast to Bondville, however, study average MOUDI observations reveal a bimodal nature to the

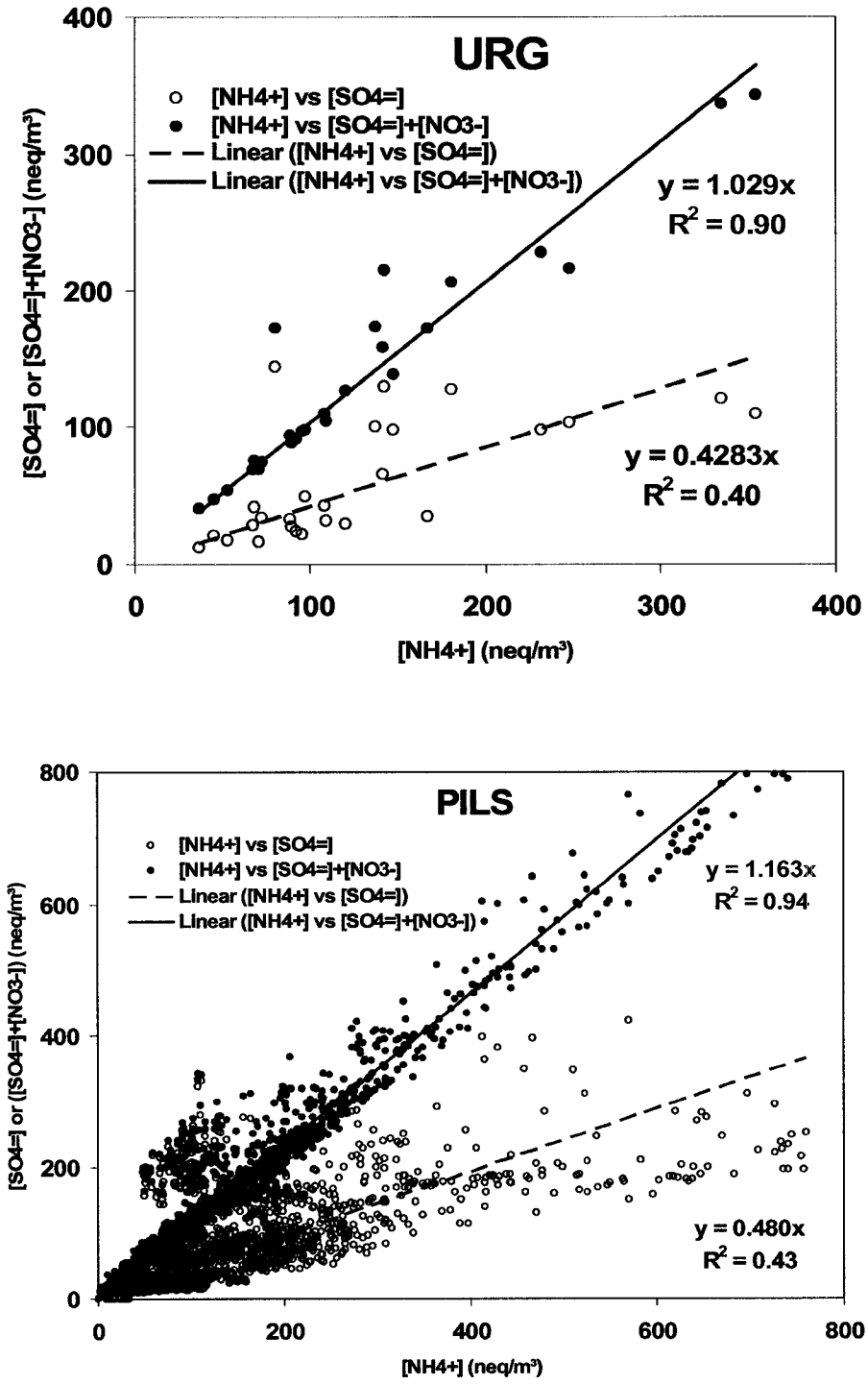

Figure 5.14 Relationship of $PM_{2.5}$ concentrations of sulfate, nitrate and ammonium from URG and PILS (Bondville, February 2003)

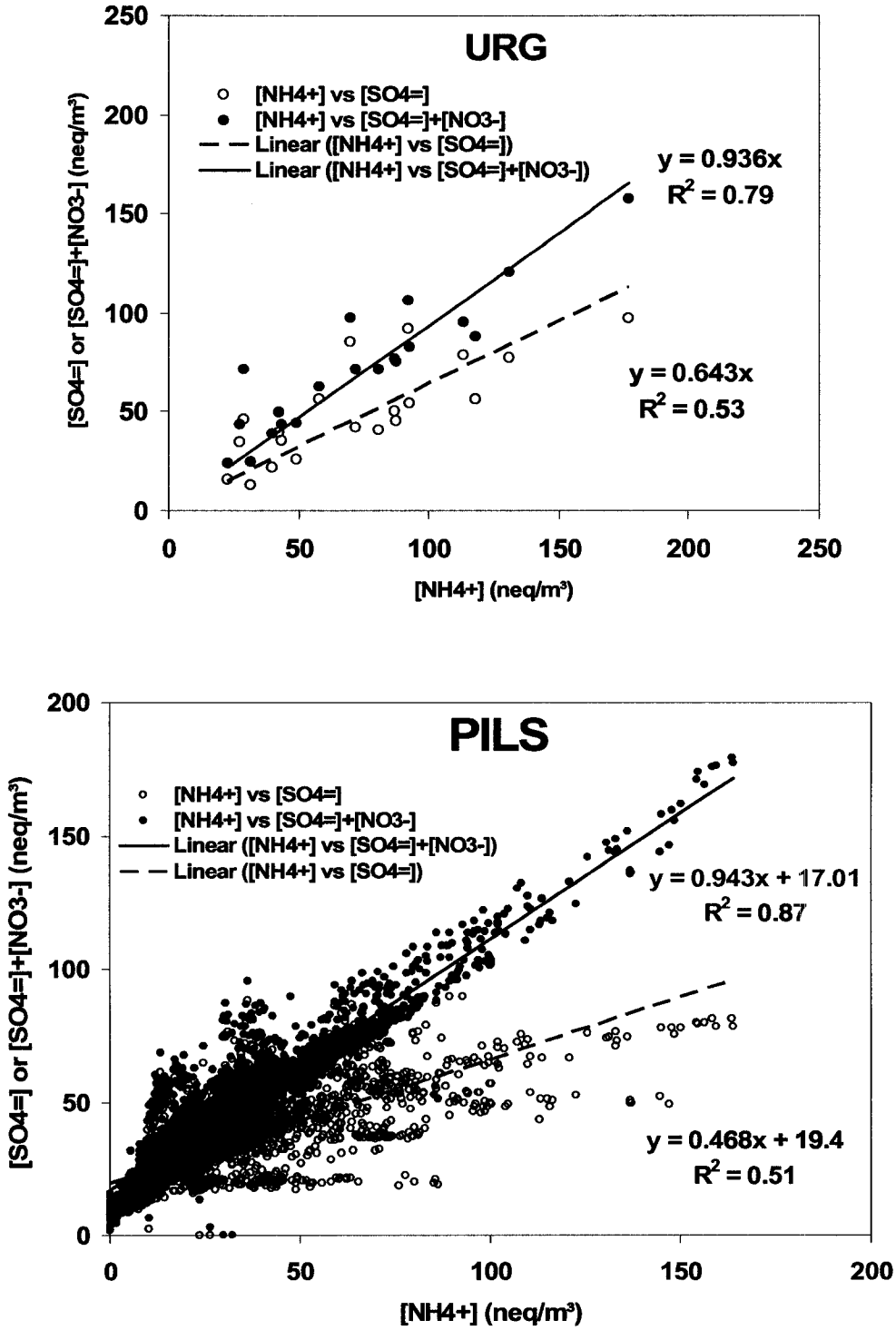

Figure 5.15 Relationship of $PM_{2.5}$ concentrations of sulfate, nitrate and ammonium from URG and PILS (Brigantine, November 2003)

nitrate size distribution (Figure 5.17). As shown in Figure 5.17, study average Brigantine Na^+ and Cl^- size distributions exhibit very similar shapes with coarse modes peaked at 4-5 μm, reflecting the local sea salt source. Another interesting size distribution is K^+ at Bondville. Soluble K^+ is sometimes regarded as a good smoke marker for biomass burning (Carrico et al., 2004; Li et al., 2003; Liu et al., 2000; McMeeking et al., 2006; Niemi et al., 2005; Posfai et al., 2003).

If one compares the amount of ammonium in each particle size category with the amounts of sulfate and nitrate, one can define "excess nitrate:" the amount of nitrate present beyond that which can be neutralized by ammonium (after first pairing ammonium with sulfate). Figure 5.18 compares Bondville study average particle size distributions of excess nitrate, K^+, Mg^{2+}, and Ca^{2+}. At supermicron particle sizes, there is sufficient Mg^{2+} and Ca^{2+} to balance the measured excess nitrate. In submicron particles,

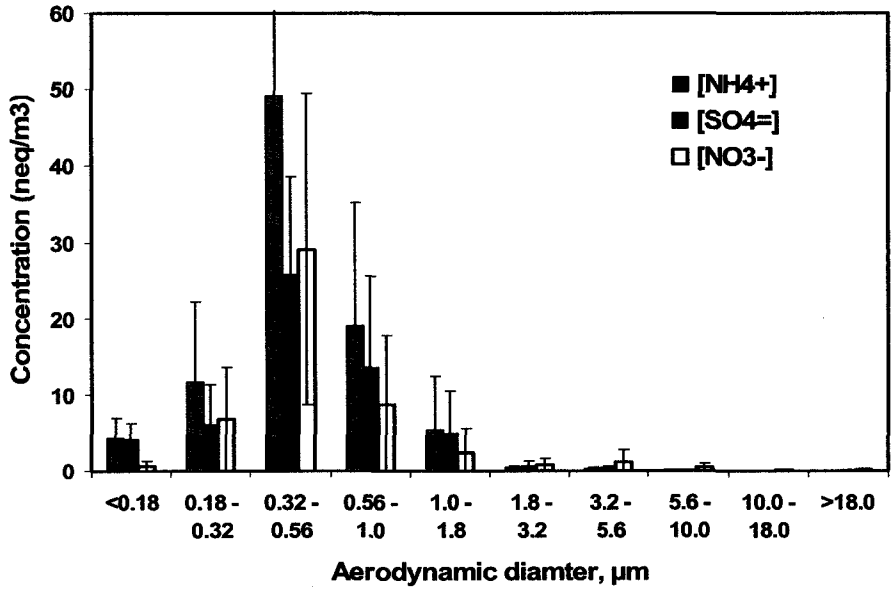

Figure 5.16 The study average particle size distribution of major inorganic ion concentrations (February 2003, Bondville, IL)
(Error bars represent the standard deviation of all sample observations)

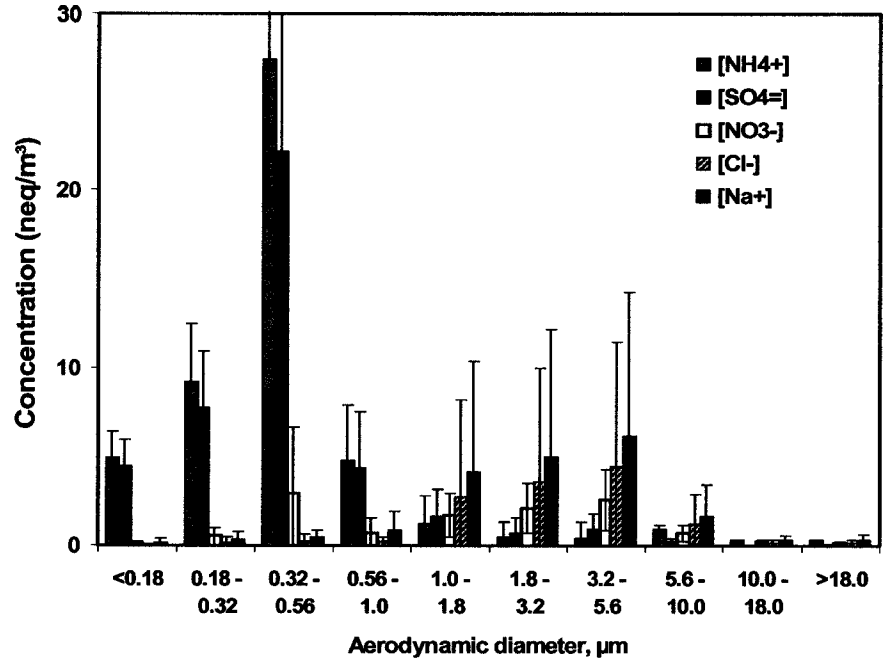

Figure 5.17 The study average particle size distribution of major inorganic ion concentrations (November 2003, Brigantine, NJ).
(Error bars represent the standard deviation of all sample observations)

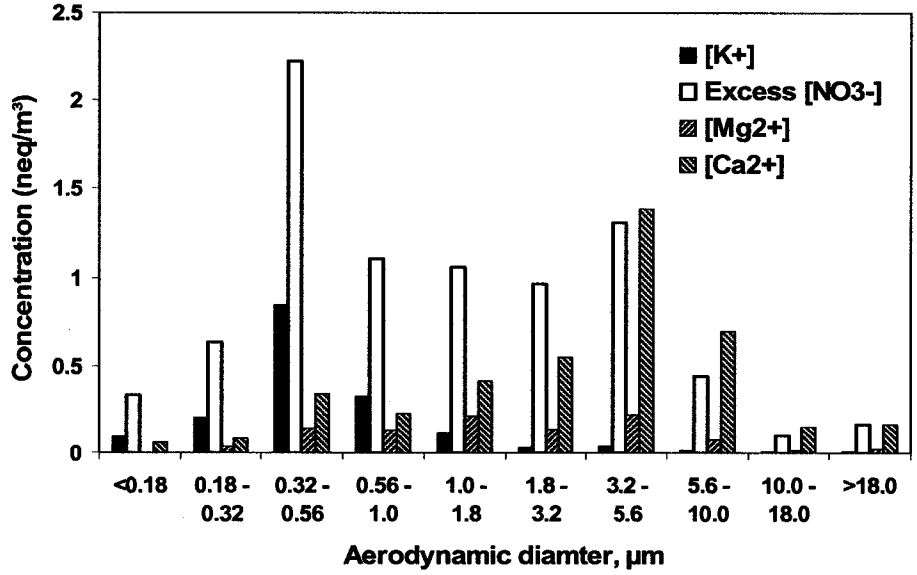

Figure 5.18 Study average particle size distributions of K^+, Mg^{2+}, Ca^{2+} and Excess NO_3^- concentrations (February. 2003, Bondville, IL).

it appears that nearly enough K^+, Mg^{2+}, and Ca^{2+} are present to balance the excess nitrate, although it is possible that the excess nitrate apparent in this fine particle mode may be only the result of errors in differences of the much higher fine particle concentrations of sulfate+nitrate and ammonium.

Table 5.2 presents a statistical correlation matrix between measured aerosol chemical species. Ammonium has strong positive correlations with SO_4^{2-} and NO_3^- in both the MOUDI and URG observations, as seen already above. While minor cation species (Na^+, Ca^{2+} and Mg^{2+}) have modest positive correlations with NO_3^- there is, interestingly, a much stronger correlation between NO_3^- and K^+ in both the URG filter and MOUDI impaction stage results. One possible explanation would be a similarity of source types or locations for K^+ and NO_x emissions. As indicated in Chapter 3, for example, it is likely that one ore more coal-fired power plants influence air pollution concentrations at the Bondville site. These plants are major sources of NO_x and may also emit fine particle K^+ in conjunction with fly ash.

Timelines of ratios of $[HNO_3]/[N(V)]$ and $[NH_3]/[N(-III)]$ are shown in Figure 5. 19. The average ratios for $HNO_3(g)/N(V)$ were 0.16 and 0.39 and for $NH_3(g)/N(-III)$ were 0.13 and 0.19 at Bondville and Brigantine, respectively, implying that most available N(V) and N(-III) was already taken up into particles at both locations. Under these conditions, significant increases in particle nitrate would be most likely with significant increases in NO_x emissions or, perhaps, increases in the efficiency of NO_x oxidation to nitric acid.

While the average percentage of N(V) in the gas phase at Bondville is modest, there are periods where it climbs to appreciable levels. Analysis of PILS observations

Table 5.2 Spearman's correlation matrix of ionic species in URG and MOUDI samples (February 2003 Bondville).

	Cl^-	NO_3^-	SO_4^{2-}	Na^+	NH_4^+	K^+	Mg^{2+}	
NO_3^-	.139							URG
	.439	**1.00**						MOUDI
SO_4^{2-}	-.180	**.806**						URG
	.307	.452	**1.00**					MOUDI
Na^+	**.701**	.195	.063					URG
	-.065	-.115	.110	**1.00**				MOUDI
NH_4^+	-.132	**.862**	**.976**	.055				URG
	.456	**.869**	**.726**	-.056	**1.00**			MOUDI
K^+	-.114	**.821**	**.631**	.066	**.647**			URG
	.506	**.838**	**.623**	-.023	**.612**	**1.00**		MOUDI
Mg^{2+}	**.580**	**.517**	.348	**.741**	.347	.378		URG
	.119	**.404**	**.672**	.335	**.509**	**.558**	**1.00**	MOUDI
Ca^{2+}	**.741**	**.116**	.-.052	**.816**	-.067	-.011	**.792**	URG
	.408	**.554**	**.818**	.130	**.729**	**.737**	**.723**	MOUDI

can help understand why this might occur. An example is shown in Figure 5.20, where rapid transitions between nitrate and sulfate dominated aerosol were observed in Bondville $PM_{2.5}$. During the period late on Feb. 17th and through much of the 18th, for example, we see a period of elevated sulfate and almost no nitrate. During this period there is insufficient ammonium to fully neutralize the sulfate. Under these conditions, no ammonia is available to react with gas phase nitric acid to form fine particle nitrate, since the aerosol thermodynamics dictate that ammonia will first pair with sulfate.

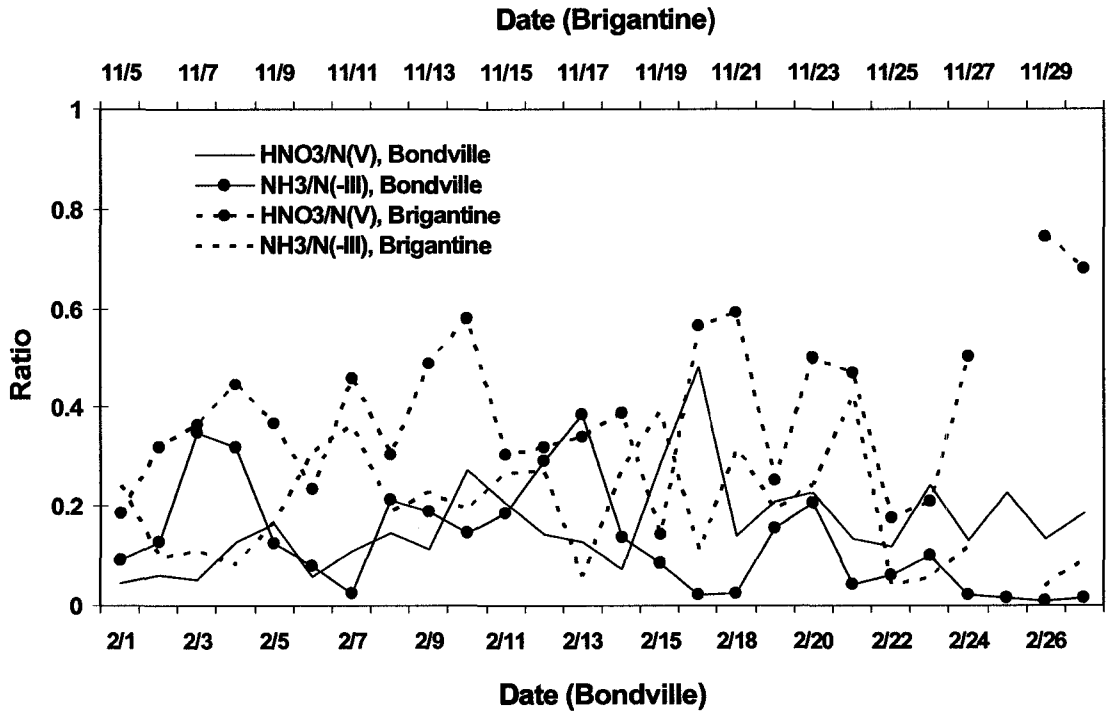

Figure 5.19 Timelines of ratio of $[HNO_3]/[N(V)]$ and $[NH_3]/[N(-III)]$ (Bondville, IL and Brigantine, NJ)

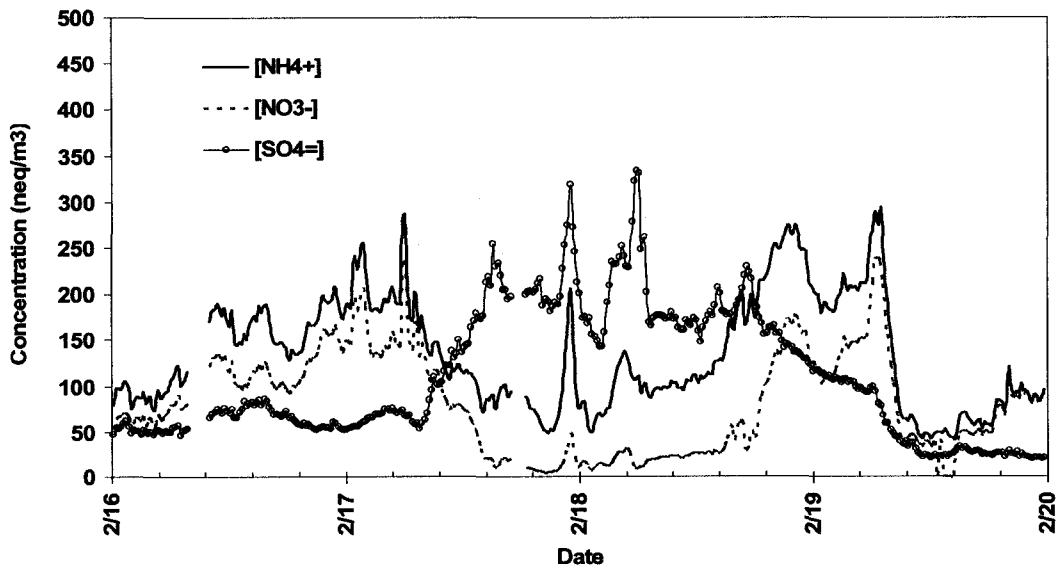

Figure 5.20 Major PILS $PM_{2.5}$ ion concentrations measured from Feb 16 – 20, 2002 (Bondville, IL).

5.4 Great Smoky Mountains National Park, Tennessee

The Great Smoky Mountains National Park (GSMNP) is located approximately 25 miles south of Knoxville, Tennessee on the border between Tennessee and North Carolina. Previous work in GSMNP has demonstrated that transport of fossil fuel combustion emissions leads to extremely high aerosol concentrations and severe visibility degradation (Ames and Kreidenweis, 1996; Hand and Kreidenweis, 1997; Tanner et al., 2004; Yu et al., 2005a). Major aerosol constituents observed in past measurements include sulfate, nitrate, and carbonaceous material (Cheng and Tanner, 2002; Malm et al., 2004; Malm et al., 1994; Olszyna et al., 2005; Tanner et al., 2005; Tanner et al., 2004; Tong et al., 2005; Yu et al., 2005a). Sampling during this study, located at the Look Rock site (Longitude: -83.941, Latitude: 35.633 and 810 m of elevation) near the park boundary, was focused on examining aerosol nitrate formation in highly acidic atmospheres. In addition to measurements performed in the other field campaigns, aerosol acidity was also measured in daily URG $PM_{2.5}$ samples. Measurements were conducted in July and August 2004.

Significant acidity was present in the GSMNP fine aerosol throughout the study period. The average aerosol acidity in the study was determined to be 63.3 nmole H^+/m^3 with a range of 12.8 to 129.8 nmole/m^3. These values are high compared to average urban and non-urban aerosol acidities measured in other studies (Figure 5.21) (Brauer et al., 1991; Koutrakis et al., 1988a; Koutrakis et al., 1988b; Lee et al., 1993; Lee et al., 2004; Spengler et al., 1990; Spengler et al., 1989; Tsai et al., 2000).

Sulfate and ammonium were the dominant ionic species in daily $PM_{2.5}$ with smaller contributions from NO_3^- and Na^+. Figure 5.22 shows sulfate concentrations

Figure 5.21 Averaged $PM_{2.5}$ H^+ concentrations measured in various locations including measurements from this study at Great Smoky Mountains National Park.

plotted against ammonium concentrations in $PM_{2.5}$. Consistent with the aerosol acidity observations, there clearly is insufficient ammonium present to neutralize the sulfate acidity. One consequence of this is that formation of particulate ammonium nitrate is not favored thermodynamically (Karlsson and Ljungstrom, 1998; Lee et al., 2004; Seinfeld and Pandis, 1998)

Observed gas/particle partitioning of N(-III) and N(V) at GSMNP are consistent with the observations discussed above. Timelines of the ratios of gaseous nitric acid and ammonia to total N(V) and N(-III), respectively, are shown in Figure 5.23. While approximately 11% of the N(-III) was found, on average, as gaseous NH_3, an average

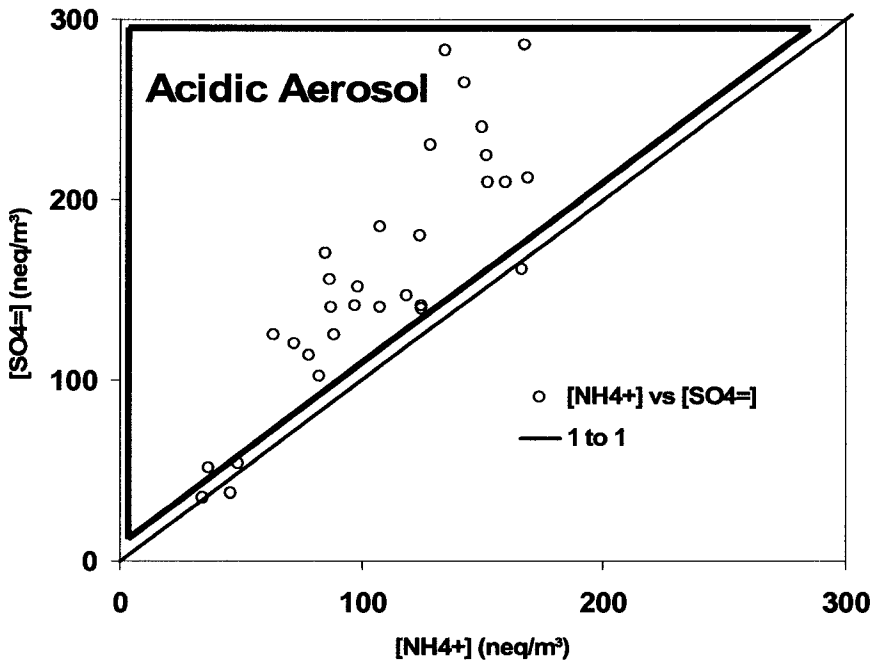

Figure 5.22 Relationship of $PM_{2.5}$ concentrations of sulfate and ammonium (July-August 2004, Great Smoky Mountains N.P.)

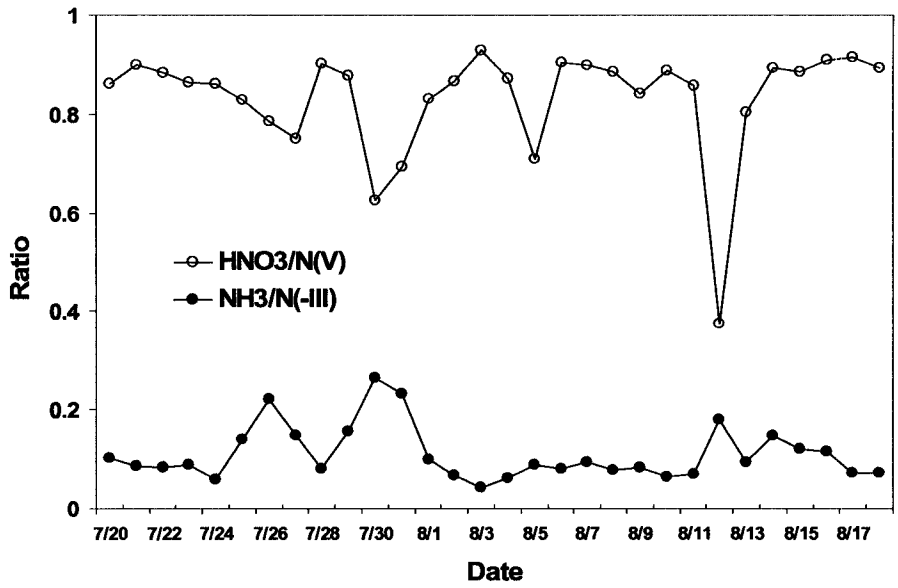

Figure 5.23 Timelines of ratio of $[HNO_3]/[N(V)]$ and $[NH_3]/[N(-III)]$ (Great Smoky Mountains N. P., TN)

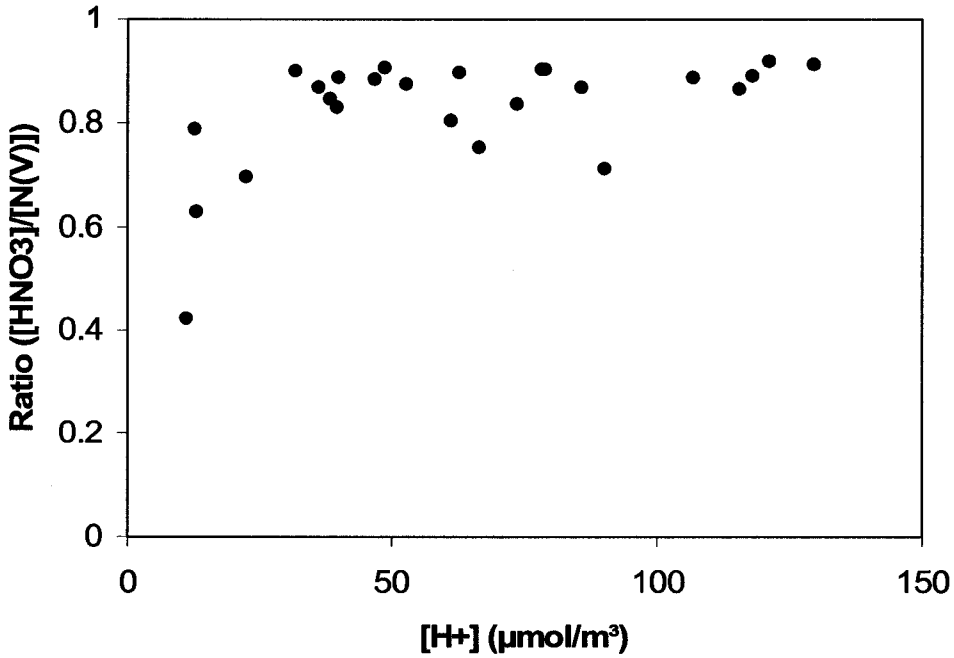

Figure 5.24 Relationship of H^+ concentration vs. ratio of $[HNO_3]/[N(V)]$ (Great Smoky Mountains N. P., TN)

83% of the total N(V) was present as HNO_3 during the study. As illustrated in Figure 5.24, the fraction of N(V) in the gas phase increases as a function of observed aerosol acidity.

Figure 5.25 depicts MOUDI particle size distributions for NH_4^+, SO_4^{2-}, Na^+, and NO_3^-. Both ammonium and sulfate are observed in a fine particle mode, with nearly all material present in submicron particles. It is also apparent that insufficient ammonium is present to fully neutralize the sulfate, consistent with the other study measurements of an acidic aerosol. Na^+ and NO_3^- are contained primarily in a coarse particle mode, although the average mode diameters during the study period appear to differ slightly. There is also more NO_3^- than Na^+, suggesting another cation must be present in coarse particles to balance nitrate. The fact that nitrate is contained almost exclusively in coarse particles

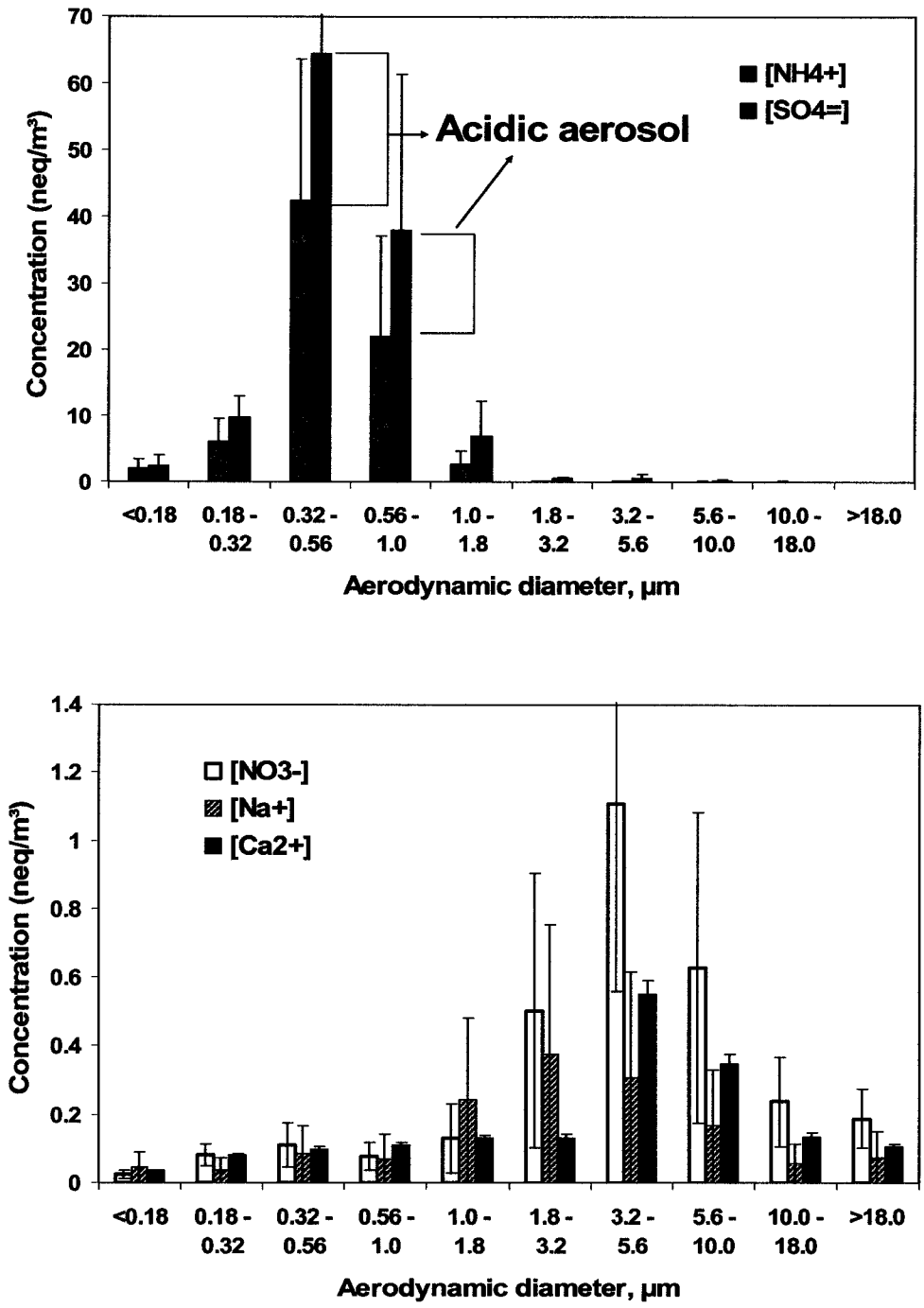

Figure 5.25 The size distribution of averaged NH_4^+, SO_4^{2-}, NO_3^- and Na^+concentrations (July – Aug 2004, Great Smoky Mountains N.P.) (Error bar represent standard deviation of all samples)

is consistent with the presence of acidic fine particles evident from both URG and MOUDI samples. The main factor controlling the formation of particulate nitrate in this environment appears to be the availability of sea salt and soil dust particles that gaseous HNO_3 can deposit on and react with.

5.5 Particulate nitrate formation under ammonia-limited conditions

In order to examine the potential for formation of particulate nitrate by HNO_3 reaction with sea salt and/or soil dust, it is useful to consider four possible scenarios using a gas ratio parameter suggested by Ansari and Pandis (1998). This parameter defines the ratio of free ammonia to total nitrate as shown Equation 5.1. Equations 5.2 and 5.3 define free ammonia and total nitrate. Free ammonia is defined as the sum of gaseous ammonia and particulate ammonium, minus the particulate sulfate concentration (all expressed in equivalents). Total nitrate is the sum of gaseous nitric acid and particulate nitrate.

$$\textbf{Gas Ratio} = [NH_{3(Free)}]/[HNO_{3(Total)}] \qquad \textbf{(Eqn. 5.1)}$$

$$[NH_{3(Free)}] = [NH_3(g)] + [NH_4^+(p)] - 2 \times [SO_4^{2-}(p)] \qquad \textbf{(Eqn. 5.2)}$$

$$[HNO_{3(Total)}] = [NO_3^-(p)] + [HNO_3(g)] \qquad \textbf{(Eqn. 5.3)}$$

(Ansari and Pandis, 1998; Blanchard and Hidy, 2005)

A gas ratio of 1 indicates no excess ammonia is available, beyond that required to neutralize all sulfate plus all nitric acid and nitrate. A negative ratio (GR < 0) corresponds to an acidic aerosol, where insufficient ammonia is present to neutralize sulfate. Under

this scenario particulate ammonium nitrate tends to be absent or present only at very low concentrations. At low gas ratios (0<GR<0.4) the aerosol is no longer acidic but little excess ammonia is available. Under these conditions particulate NO_3^- does not readily decrease in response to HNO_3 reductions. When the gas ratio is 0.4<GR<1.5, particulate NO_3^- generally responds nonlinearly to HNO_3 changes and changes are not limited by NH_3. It is likely that temperature and RH are the main factors controlling formation of particulate NO_3^- in this situation. At high gas ratios (GR > 1.5), particulate NO_3^- decreases in response to HNO_3 reductions (Ansari and Pandis, 1998; Blanchard and Hidy, 2002; Blanchard and Tanenbaum, 2003).

In order to examine the relationship between particulate NO_3^- concentration and the presence of sea salt and soil dust, in conjunction with changing gas ratios, MOUDI and URG data from our seven measurement locations (Big Bend, Yosemite, San Gorgonio, Grand Canyon, Bondville, Great Smoky Mtns and Brigantine) were utilized. Changes in particle nitrate were examined as a function of the sum of particle soil dust and sea salt cations ($Na^+ + Ca^{2+} + Mg^{2+}$) for periods when the aerosol was acidic (GR < 0) or the system was NH_3 limited (0 < GR < 0.4). Results are plotted in Figure 5.26.

At negative gas ratios (acidic aerosol), we see a weak correlation ($R^2 = 0.28$) between $PM_{2.5}$ nitrate and the sum of the three $PM_{2.5}$ sea salt and soil dust cations. The slope of a least squares linear regression line suggests an average 12 % increase in $PM_{2.5}$ nitrate for a 100 % increase in the $PM_{2.5}$ sum of the three cations. This relatively low value is somewhat surprising, given the general availability of nitric acid at Great Smoky Mtns, where most of the negative gas ratios were measured (84 % of Great Smoky Mtns

gas ratios were negative; see Fig. 5.27). A stronger relation might exist at larger particle sizes, where much of the nitrate, sea salt, and soil dust were observed.

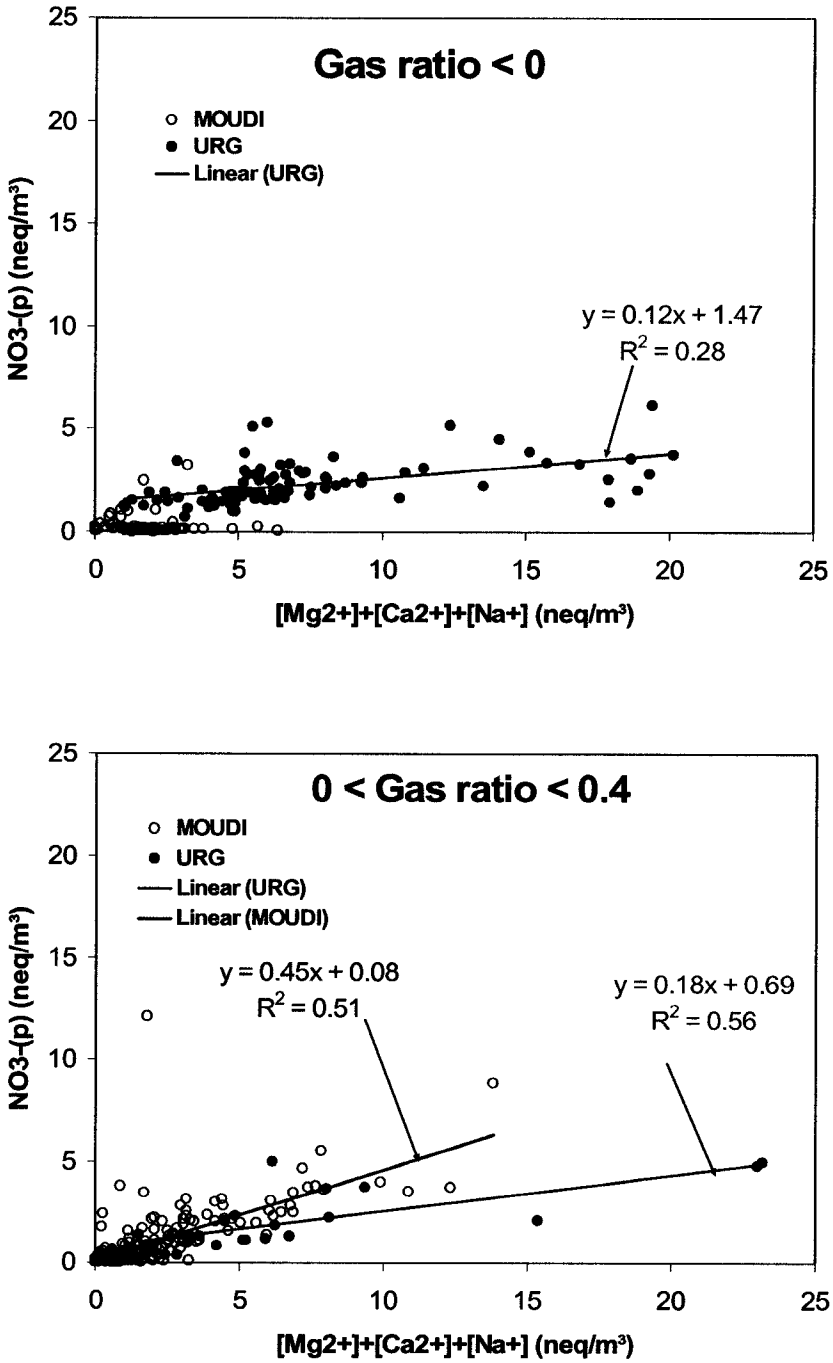

Figure 5.26 Relationship between particulate NO_3^- and soil dust/sea salt for negative gas ratios and for small positive gas ratios

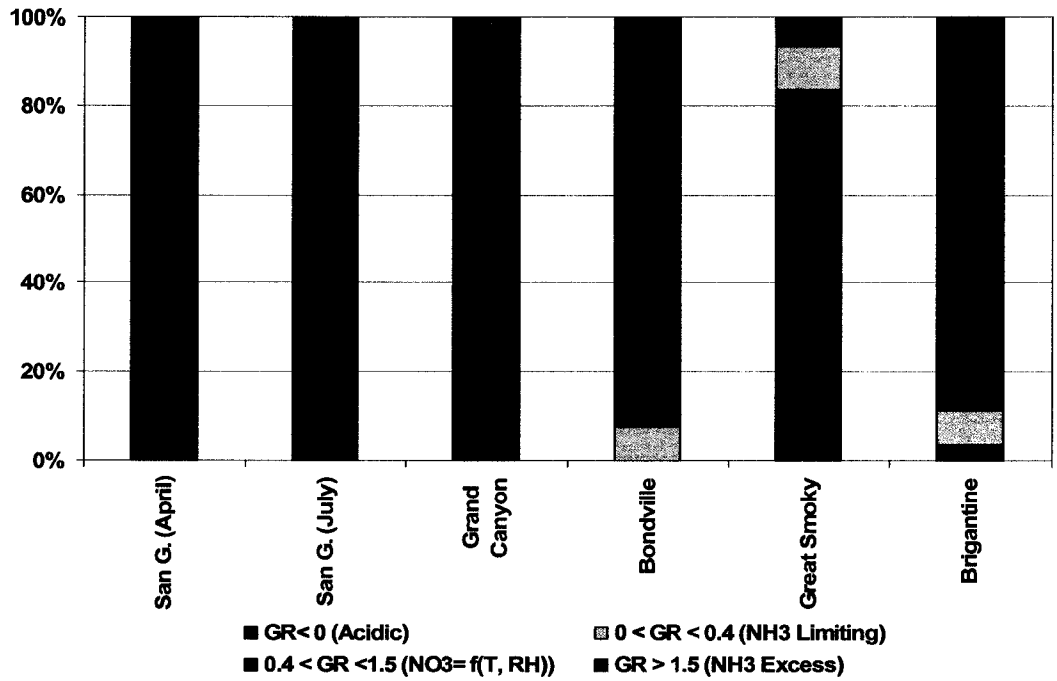

Figure 5.27 Distribution of measured gas ratios in $PM_{2.5}$ URG samples

At low positive gas ratios (0< GR < 0.4, aerosol not acidic but system NH_3 limited) the correlation of nitrate with the sum of sea salt and soil dust cation increases, with values of R^2=0.51 for MOUDI samples and R^2=0.56 for URG $PM_{2.5}$ results. The regression slope for the MOUDI samples (0.45), interestingly, is higher than for the URG $PM_{2.5}$ samples (0.18), likely reflecting the fact that increases in sea salt and soil dust nitrate occur mostly at particle sizes larger than 2.5 μm aerodynamic diameter.

5.6 Summary and Conclusions

Properties of aerosol nitrate were characterized at several IMPROVE monitoring sites during a series of 1-month field studies. Study sites included Bondville, Illinois

(February 2003), San Gorgonio Wilderness Area, California (April and July 2003), Grand Canyon N.P. (May 2003), Brigantine National Wildlife Refuge, New Jersey (November 2003) and Great Smoky Mountains N.P. (July/Aug 2004). 24 hour average concentrations of $PM_{2.5}$ nitrate, gaseous nitric acid, and other species were determined by annular denuder/filter-pack measurements. Nitrate and other key ion size distributions were also measured using a Micro-Orifice Uniform Deposit Impactor (MOUDI). Concentrations of key $PM_{2.5}$ inorganic ions were also measured using a semi-continuous Particle-Into-Liquid-Sampler (PILS). Observations at many locations revealed the presence of coarse particle nitrate which appeared to have formed as a result of reactions of nitric acid or its precursors with sea salt and/or soil dust.

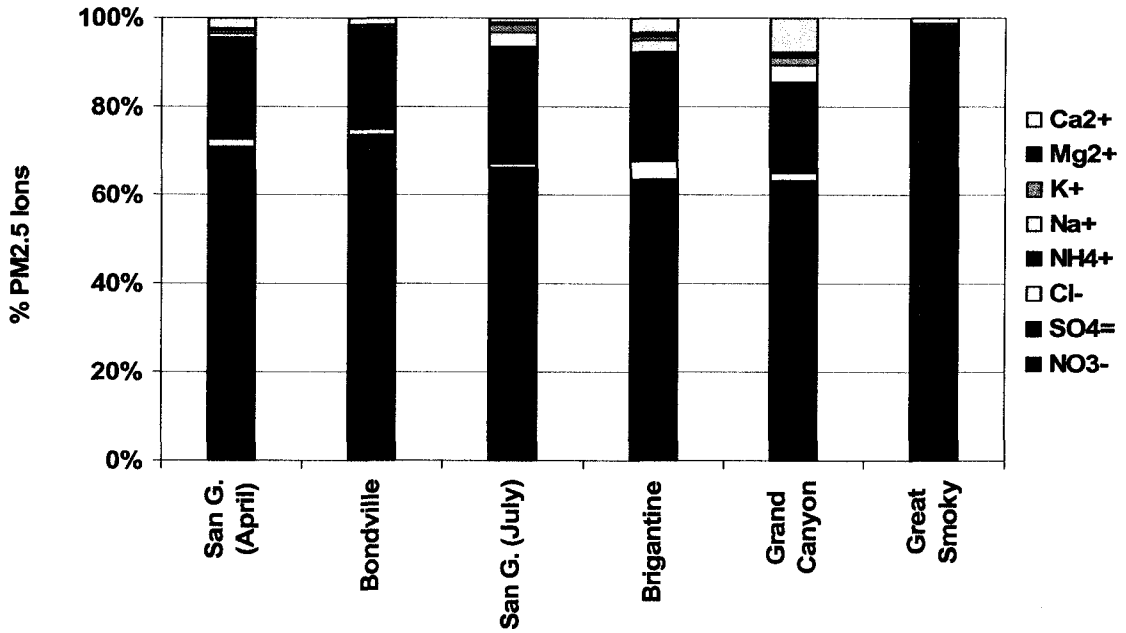

Figure 5.28 Percent contribution of individual ionic chemical species to measured URG $PM_{2.5}$ by mass.

Figure 5.28 shows the study average percent contribution of individual ionic chemical species to $PM_{2.5}$ measured in each of the field campaigns. Nitrate, sulfate, and ammonium were major components of the measured $PM_{2.5}$ in all six campaigns, with the exception of the summer 2004 study in Great Smoky Mtns NP when little $PM_{2.5}$ nitrate was measured. The nitrate fraction was also below 25 % at Grand Canyon and at Brigantine. Sulfate was a relatively small contributor to $PM_{2.5}$ at San Gorgonio in April and at Bondville. It was a major contributor to measured $PM_{2.5}$ during the Great Smoky Mtns summer campaign and the spring campaign in Grand Canyon. The relative importance of sulfate increased at San Gorgonio in July when ammonium nitrate formation was less favored thermodynamically by higher temperatures and lower relative humidities.

Observations of aerosol composition from each field campaign were analyzed to summarize the fractions of fine and coarse particle nitrate present in the form of ammonium nitrate or in other mineral forms. This was done by examining ammonium, sulfate, and nitrate concentrations for different particle size ranges, measured with the URG or MOUDI sampler. The amount of ammonium nitrate was estimated by first pairing ammonium with sulfate (as $(NH_4)_2SO_4$) and pairing any additional ammonium with nitrate. Remaining particle nitrate was then assumed to be present as the result of reaction with sea salt or soil dust. This fraction was termed mineral nitrate. The fraction of nitrate in this "mineral" form is listed by field campaign in Table 5.3 for $PM_{2.5}$ (URG samples), fine particles (MOUDI $D < 1.8$ μm) and coarse particles (MOUDI $D > 1.8$ μm). Focusing on the results for fine and coarse particles as measured by the MOUDI, we see that between 81 and 99% of the coarse particle nitrate appears to be in mineral

form in the various studies. Not surprisingly, more variability is seen in fine particle nitrate composition. At San Gorgonio (April), Bondville, and Brigantine, two-thirds or more of the nitrate is present as ammonium nitrate. At the other extreme, 99% of the fine particle nitrate at Great Smoky Mtns NP appears to be present in mineral form, consistent with the acidic nature of fine particles at this location.

Table 5.3 Summary of the chemical forms of NO_3^- in coarse and fine aerosol particles for each field campaign

	Mineral NO_3^- fraction		
Site	**URG***	**MOUDI fine mode ****	**MOUDI coarse mode *****
San Gorgonio (April)	3 %	6 %	92 %
San Gorgonio (July)	6 %	15 %	91 %
Grand Canyon N.P.	50 %	75 %	99 %
Bondville	15 %	25 %	99 %
Great Smoky Mts N.P	93 %	99 %	98 %
Brigantine	15 %	33 %	81 %

* **< 2.5 μm aerodynamic diameter**
** **< 1.8 μm aerodynamic diameter**
*** **> 1.8 μm aerodynamic diameter**

Using additional MOUDI ion measurements we estimated the fraction of particle nitrate at each study location in the form of ammonium nitrate, reacted sea salt nitrate, and reacted soil dust nitrate. This was done by first pairing nitrate with excess ammonium

(beyond that needed to neutralize sulfate, as above), then pairing nitrate with chloride deficient Na^+ (total Na^+ minus Cl^- multiplied by the sea water ratio of Na^+/Cl^-), then assuming remaining nitrate is present as calcium nitrate. Although it has been suggested that nitric acid reacts more quickly with soil dust than with sea salt (Evans, 2003; Evans et al., 2004), we made the assignment of $NaNO_3$ first in this analysis because additional information about the extent of sea salt reaction was available from measured chloride deficiencies. Results of these calculations are shown in Fig. 5.29 for the six studies presented in this dissertation and for our earlier measurements at Big Bend and Yosemite National Parks. As discussed above, ammonium nitrate comprises half or more of total particle nitrate at Bondville in winter, at San Gorgonio in spring, at Brigantine in fall, and at Yosemite in the summer. The smallest contributions of ammonium nitrate are seen at the two sites with strongly acidic aerosol: Great Smoky Mtns and Big Bend. By our estimates, sea salt nitrate is generally more prevalent than nitrate associated with reacted soil dust. $NaNO_3$ is estimated to comprise 39% or more of total particle nitrate at Yosemite (summer), San Gorgonio (summer but not spring), Grand Canyon (spring), Big Bend (summer and fall), Great Smoky Mountains (summer), and Brigantine (fall). 25% or more of particle nitrate is estimated to be associated with reacted soil dust at three locations: Grand Canyon (spring), Big Bend (summer + fall), and Great Smoky Mtns (fall). The importance of soil dust nitrate at Grand Canyon and Big Bend is not surprising, given the arid regions that reside upwind of these parks. In looking at all these patterns, it is important to keep in mind the relative importance of nitrate to total aerosol at these sites. Referring back to Fig. 5.29, one is reminded that nitrate is a small contributor to aerosol composition particularly at Great Smoky Mtns. NP.

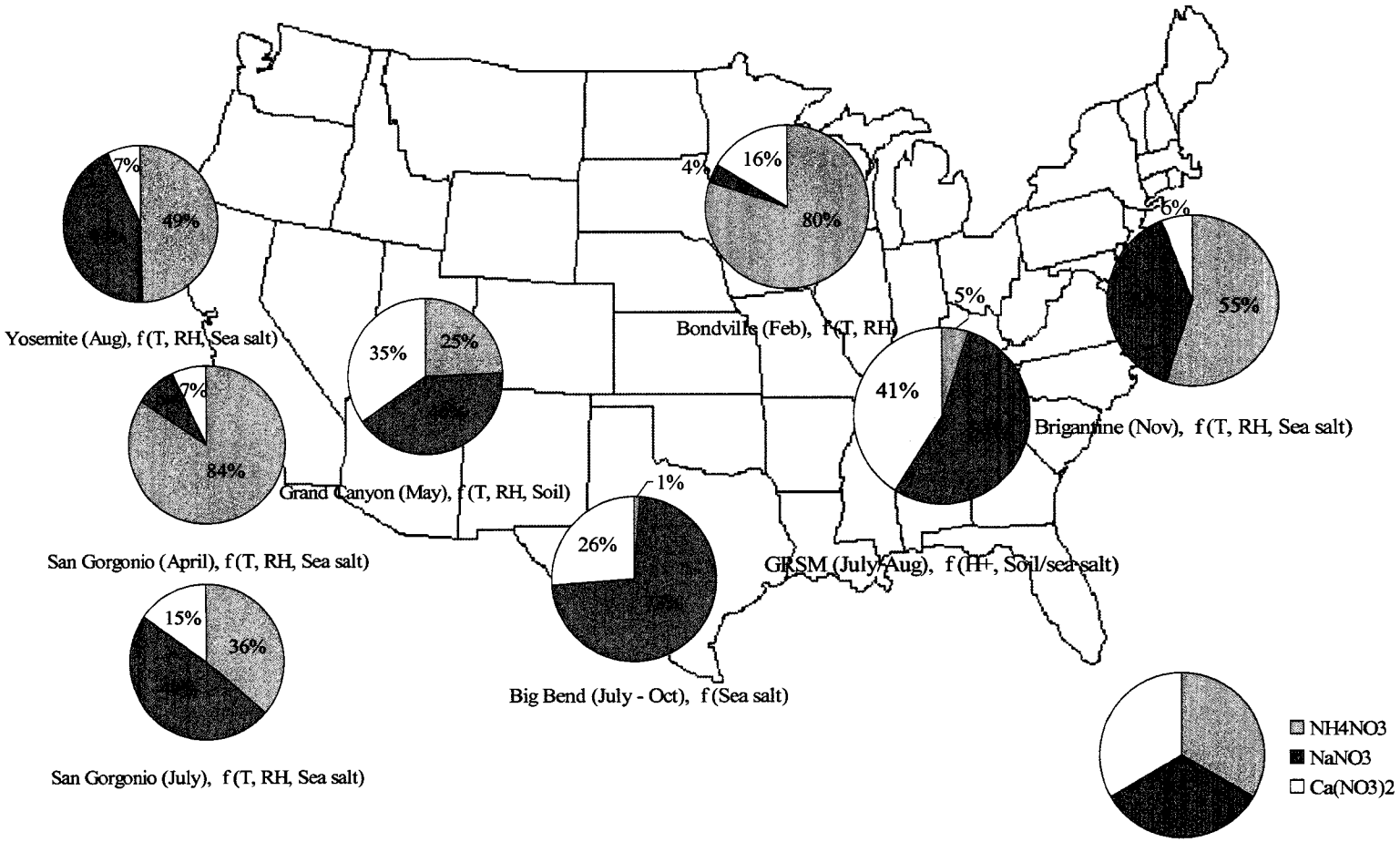

Figure 5.29 Estimated contributions of different forms of nitrate to total particle nitrate measured with the MOUDI sampler during eight field campaigns. See text for an explanation of the method used to assign nitrate to different forms.

In order to understand the potential for further particle nitrate formation with additions of nitric acid, key precursor species in the gas phase have to be considered. Figure 5.30 shows the average ratios of gaseous nitric acid and ammonia to total N(V) and N(-III), respectively, measured in each field study. Most of the available N(V) was taken up into particles at San Gorgonio (April) and Bondville (February) due to thermodynamically favored conditions for ammonium nitrate formation, including approximately 50% of N(-III) present in the gas phase and cold to moderate temperatures. Under these conditions, addition of gaseous nitric acid should result in significant increases in ammonium nitrate formation. Under warmer, drier conditions, large fractions of both N(V) and N(-III), however, were found in the gas phase at San Gorgonio (July) and Grand Canyon N.P (May), reflecting the tendency for ammonium nitrate dissociation under these conditions. Changes in nitric acid concentrations in these cases are unlikely to significantly affect ammonium nitrate formation. The relative abundance of nitric acid at these sites also suggests that nitric acid is probably not the limiting ingredient in the formation of mineral nitrate. In the more acidic aerosols at Great Smoky Mtns NP and at Brigantine, we observed some dependence of mineral nitrate content on mineral cation availability (see Fig. 5.26). The relative abundance of gaseous nitric acid at this location, however, suggests that mineral nitrate formation at this site may be less affected by increases in nitric acid concentrations.

Although it is common to assume that particulate nitrate is present as fine particle NH_4NO_3, our work here has demonstrated this is often not the case. The observation of important contributions from coarse particle nitrate, first at Big Bend National Park and later at Yosemite National Park, prompted a more widespread investigation of the forms

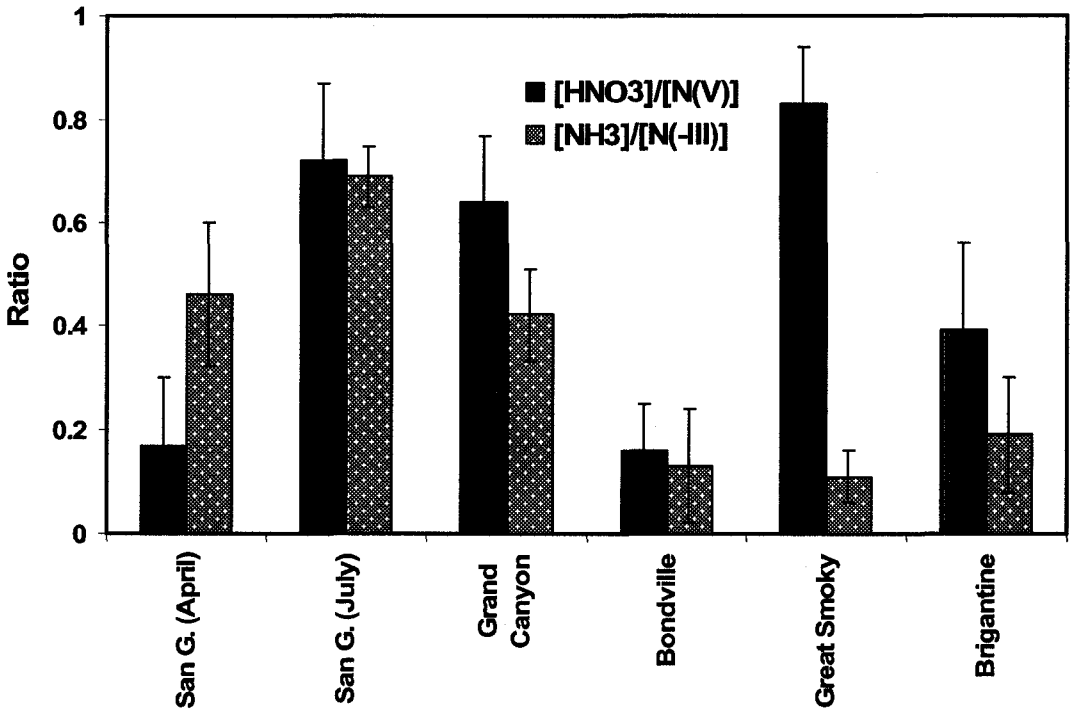

Figure 5.30 Averaged ratios of $[HNO_3]/[N(V)]$ and $[NH_3]/[N(-III)]$ for each field campaign.
(Error bars represent standard deviations of all sample values in a campaign)

of particulate nitrate in a variety of environments across the U.S. As noted in the preceding discussion, the presence of coarse particle nitrate is common when fine aerosol particles are acidic and when temperatures are high and relative humidities low. All of these factors act to prevent formation of NH_4NO_3, leaving greater amounts of nitric acid in the gas phase to react with available sea salt or soil dust.

Findings from this work have several important implications for IMPROVE network monitoring of aerosol composition and its effects on visibility degradation. First, the $PM_{2.5}$ size cut used in the IMPROVE sampler often captures a significant part of the coarse particle mineral nitrate mode. MOUDI size distributions from most of our

study sites show that a 1 μm size cut would provide a much better division of the coarse and fine particle modes. Understanding and modeling of $PM_{2.5}$ speciation is confounded by the external mixture of aerosol types that results from making the "fine particle" size cut part way through the coarse particle mode. Second, the differing particle sizes, refractive index, and hygrosopicity of sodium and calcium nitrate vs. ammonium nitrate affect the ability of measured nitrate to scatter solar radiation and impact visibility. For example, the deliquescence point of NH_4NO_3 at 25 °C is 61.8%, significantly lower than the deliquescence points of $NaNO_3$ (74.3%) or a mixture of NaCl and $NaNO_3$ (68.0%) (Finlayson-Pitts and Pitts, 2000; Seinfeld and Pandis, 1998). Third, while IMPROVE assumes that atmospheric coarse particles are comprised of soil dust, our findings suggest contributions from reacted soil dust and sea salt can be important. In its most recent review of regulatory methods for computing aerosol-derived light extinction (Hand and Malm, 2006), the IMPROVE program reviewed findings of this work and discussed their implications. In the end, however, the absence of cation measurements in IMPROVE fine particle samples and the absence of any speciation of coarse particles led them, for extinction calculation purposes, to continue to treat $PM_{2.5}$ nitrate in network samples as ammonium nitrate.

6. Summary and Conclusions

6.1 Summary

Nitrate comprises a significant fraction of airborne particulate matter in many environments. Knowledge about the chemical forms and size distributions of particle nitrate and gas-particle partitioning between nitrate and nitric acid is important for understanding its atmospheric lifetime and its impacts on visibility degradation, human health, climate, and nitrogen deposition fluxes to sensitive ecosystems. Such knowledge is also crucial to designing effective strategies to reduce particulate nitrate concentrations.

The chemical characteristics of the inorganic ions in atmospheric aerosol, specifically particulate nitrate and its size distribution, were investigated at several non-urban locations during a series of field studies. Aerosol measurements included trace gases and $PM_{2.5}$ (URG annular denuder/filter-pack sampler), size-resolved particle composition (MOUDI impactor), and semi-continuous $PM_{2.5}$ composition (PILS/IC system). Measurements were made during fall/winter at Bondville, IL (February, 2003) and Brigantine National Wildlife Refuge, NJ (November, 2003), during spring at San Gorgonio Wilderness Area, CA (April, 2003) and Grand Canyon NP, AZ (May, 2003), and during summer at Great Smoky Mountains NP, TN (July/August, 2004) and San Gorgonio (July, 2003).

The two campaigns at the nitrate-rich San Gorgonio site were designed to investigate possible seasonal changes in aerosol chemical composition, including the predominant form of nitrate, during the transition from cooler spring to hotter summer conditions. Measurements were made in May, 2003 at Grand Canyon NP because the

park historically has the highest $PM_{2.5}$ nitrate concentrations during that time based on IMPROVE data. Two campaigns at Bondville and Brigantine were performed during fall/winter, when nitrate concentrations tend to peak at these locations. The Great Smoky Mountains NP study was scheduled for summertime in order to examine the amount and form of nitrate present during periods of strong aerosol acidity. Key findings from these field campaigns are summarized below.

San Gorgonio Wilderness Area, California (April and July, 2003)

Ammonium, nitrate and sulfate were the dominant ionic species in $PM_{2.5}$ samples at San Gorgonio in July. Sulfate was a less significant contributor during April. Sulfate and ammonium were found predominantly in fine particles during both measurement campaigns. Nitrate was found mainly in fine particles in April. A mix of fine and coarse particle nitrate was observed in July. Large diurnal concentration trends were observed for many species during both study periods. Concentrations typically increased in the afternoon during thermally driven upslope flow and decreased at night during drainage flow. During the cooler conditions of April, 80 – 90 % of total N(V) and approximately half the total N(-III) was associated with particles. The nitrogen phase partitioning shifted substantially in July when approximately 70% of the total N(V) and N(-III) were present as HNO_3 (g) and NH_3(g). This change between seasons is consistent with the thermodynamics of the ammonia-nitric acid-ammonium nitrate system, which favor particle formation at cooler temperatures (and higher RH).

The amount of chloride lost from sea salt during transport inland to San Gorgonio was substantially larger during summer than spring, with an average of 87 % Cl^-

depletion in July, compared with 7 % in April. Much of the chloride loss appears to have resulted from sea salt reaction with nitric acid. A moderate correlation ($R^2 = 0.57$) between NO_3^- and the sum of $[Ca^{2+}]$ and $[Mg^{2+}]$ was also observed in July, suggesting some reaction of nitric acid with soil dust may also have occurred. While ammonium nitrate was still observed at substantial levels during July, it often disappeared during warmer times of the day, making sea salt and soil dust important nitric acid sinks for particulate nitrate formation.

Grand Canyon National Park, Arizona (May, 2003)

Measurements of ionic composition at Grand Canyon National Park (May, 2003) reveal that the inorganic ionic fraction of the aerosol there is comprised of a mixture of submicron ammonium sulfate (0.4 – 0.5 μm mode peak) and supermicron nitrate and sulfate (2 – 3 μm mode peak) particles mixed with Mg^{2+}, Ca^{2+}, Na^+ and Cl^-. Correlations between NO_3^- and Na^+ ($R^2 = 0.37$), as well as the sum of Ca^{2+} and Mg^{2+} ($R^2 = 0.74$), indicate that reactions of nitric acid or its precursors with soil dust and/or sea salt are important for formation of particulate nitrate in this region. Close tracking of concentrations of NO_3^- with Na^+, Ca^{2+} and Mg^{2+} in semi-continuous $PM_{2.5}$ measurements further support this hypothesis.

Concentrations of SO_2 were generally low during the Grand Canyon study, while 40 – 60 % of the total N(-III) typically resided in the gas phase. The fraction of N(V) in the gas phase increased from ~ 40 % early in May to ~ 80 % at the end of the study. The significant amount of gas phase nitric acid at this location reveals a potential for increases

in particle nitrate if additional ammonia or larger quantities of soil dust and/or sea salt particles were present in the environment.

Bondville, Illinois (February, 2003)

Ammonium, nitrate and sulfate were the primary ionic species in $PM_{2.5}$ measured in winter at Bondville. Ammonium nitrate and ammonium sulfate particles were the dominant aerosol components most of the time, except for occasional periods when the aerosol was strongly acidic and fine particle nitrate disappeared. Size distributions for aerosol ammonium, nitrate, and sulfate were clearly dominated by submicron particles, with mass modes peaked in the 0.3 – 0.5 μm aerodynamic diameter size range. A small coarse mode of nitrate (4 – 5 μm mode peak) was also apparent.

Approximately 80 % of the total N(V) and N(-III) was typically found in the particle phase. This is consistent with the relative abundance of both N(V) and N(-III) at this location and the strong tendency to form particulate ammonium nitrate at low temperatures and high humidities. In contrast to the nitrogen species, the majority of measured sulfur ($[SO_2(g)] + [SO_4^{2-}]$) (70 – 80%) was typically observed in the gas phase, representing considerable potential for formation of additional particulate sulfate as the air mass ages.

Brigantine National Wildlife Refuge, New Jersey (November, 2003)

Fully neutralized ammonium sulfate and nitrate were the dominant contributors to the ionic fraction of $PM_{2.5}$ samples during November 2003 at Brigantine. The SO_4^{2-} and NH_4^+ size distributions exhibited very similar shapes, with a submicron uni-modal size

distribution typically peaking at 0.32 – 0.56 μm aerodynamic diameter. Nitrate, by contrast, was found in both fine (0.32 – 0.56 μm) and coarse (4 -5 μm) particles at this coastal site. Fine mode nitrate was associated with ammonium, while coarse mode nitrate appears to have formed mainly as the result of reactions with sea salt.

Most N(-III) and approximately half of the N(V) is in the particle phase due to preferential formation of ammonium nitrate under relatively cold temperatures during the wintertime. Most of the available total sulfur, by contrast, is in the gas phase, representing significant potential for formation of additional particulate SO_4^{2-}.

Great Smoky Mountains National Park, Tennessee (July/August, 2004)

Ammoniated sulfate was the main component of ambient $PM_{2.5}$ aerosol measured in summer in Great Smoky Mountains National Park. The aerosol was typically acidic with an average $PM_{2.5}$ ammonium to sulfate molar ratio of 1.44 and a range of 1.0 – 2.1. Ammonium nitrate formation was suppressed by the lack of ammonia which results in the predominance of acidic particles in this region. The acidic, ammoniated sulfate particles were contained in a fine particle mode typically peaked at 0.3 – 0.5 μm; NO_3^-, Ca^{2+}, Mg^{2+} and Na^+ were contained in similar coarse particle modes peaked at 3 – 5 μm. The observations at Great Smoky Mtns NP, along with our earlier findings from Big Bend NP, clearly reveal the importance of sea salt and/or soil dust for formation of particulate nitrate in environments characterized by acidic submicron particles.

The observed partitioning of N(V) and N(-III) between the gas and particle phases is consistent with the acidic nature of the submicron sulfate aerosol. Most N(V) (typically ~80%) was observed in the gas phase. N(-III), by contrast, was observed

mostly in the particles, reflecting the strong sink for basic, gas phase ammonia presented by the acidic submicron aerosol fraction. The amount of sulfur present in sulfate particles was also typically much higher than the amount of gaseous sulfur dioxide, reflecting the chemically aged nature of most air masses encountered at the site and the conducive nature of the summertime, oxidant-rich atmosphere in the SE US for sulfur oxidation.

6.2 Conclusions

The findings of the measurements conducted as part of this research outline a number of common themes governing aerosol composition at rural environments, especially in regards to aerosol nitrate. These are outlined below:

- The common assumption that NH_4NO_3 is the main form of particle nitrate is frequently inappropriate in the kinds of rural environments studied here. Our observations reveal significant contributions by mineral forms of nitrate, including $NaNO_3$, $Ca(NO_3)_2$ and $Mg(NO_3)_2$. These mineral nitrate particles are typically several micrometers in diameter, quite different from the typical submicron particle sizes observed for ammonium nitrate. The prevalence of mineral nitrate depends on several factors. Greater mineral nitrate formation is favored when temperatures are hot, relative humidities are low, insufficient ammonia is present to fully neutralize acidic sulfuric acid contained in submicron aerosol particles. The presence of a substantial quantity of alkaline particles to react with nitric acid or its precursors is also a prerequisite to significant coarse particle nitrate formation. The chemical form and size distribution of aerosol nitrate are important factors influencing its atmospheric lifetime and effects. For

example, the relative humidity of deliquescence varies from approximately 40% to 74% for mixtures of $Ca(NO_3)_2$ and $NaNO_3$ to $NaNO_3$, including approximately 62% of NH_4NO_3. Hygroscopicity is an important factor influencing changes in a particle's impact on light scattering with changing environmental conditions. Changes in refractive index and particle size, between submicron ammonium nitrate and supermicron mineral forms of nitrate, also have important consequences for nitrate's impacts on haze formation.

- Particle species size distributions observed at all of the study sites reveal limitations to the current operational definition of 2.5 μm aerodynamic diameter as the split between fine and coarse particles for regulatory purposes (USEPA, IMPROVE). A 1 μm size cut would provide a more natural division between coarse and fine mode particles and better reflect the different origins and formation mechanisms for these two particle size classes. Use of a $PM_{2.5}$ size cut leads to the inclusion of a significant fraction of the lower tail of coarse mode particles in a "fine" particle sample. This mixing of particle classes makes interpretation of aerosol particle composition unnecessarily difficult and can create problems when using observational $PM_{2.5}$ data as the basis for numerical simulation of aerosol properties. Particularly problematic is application of aerosol thermodynamic models which utilize measured gas phase and $PM_{2.5}$ components, along with environmental conditions (T, RH) to simulate expected particle composition. Such models do not correctly predict the formation of $PM_{2.5}$ nitrate in the presence of acidic, submicron sulfate particles, because the fine particle fraction is assumed to be internally mixed.

- High time resolution measurements of particle composition are of great value in providing better insights into the chemical characteristic of aerosol particles, their temporal variability and relationships to transport conditions, and their role in visibility degradation, than are possible with traditional time-integrated filter measurements. For example;
    - Concentration changes of many species measured at high time resolution clearly illustrate changes in aerosol composition and amount associated with changing transport conditions, including mountain-valley winds, land-sea breeze systems, and larger scale forcing. Data of this type are also much more useful in identifying aerosol and aerosol precursor source regions and determining how changing environmental conditions (e.g., T and RH) influence the partitioning of semi-volatile components between the gas and particle phases.
    - Close tracking of concentrations between individual species can greatly aid determination of the chemical compositions of key aerosol components. In some cases, for example, closely tracking balances between ammonium and the sum of nitrate and sulfate concentrations reveals the presence of fully neutralized ammonium sulfate and ammonium nitrate in the aerosol. In other cases, clear evidence is provided of the extent of nitric acid reaction with sea salt and resulting displacement of chloride. Clearly the measurement technology developed with PILS (and probably other similar instruments) has advanced to the

stage where accurate measurements even of trace level components in fairly remote environments is possible and quite useful.

- Short term spikes of some components seen in the time resolved measurements also provide insight into transient influences from some source types. For example, spikes of acidic sulfate might signal interception of a power plant plume while spikes of can K^+ indicate impacts from smoke from biomass combustion.

- In order to understand both current aerosol composition, and ways in which it might be influenced by changes in future emissions, it is critical to accurately observe both gas and particle phase components. Predicting how $PM_{2.5}$ mass and composition will change in response to reductions in sulfur dioxide emissions, for example, requires an understanding of the amount of ammonia currently in both particles and the gas phase and the amount of gas phase nitric acid. Knowledge about gas phase components is also key to verifying regional and global scale air quality model simulations and to understanding both dry and wet deposition of sulfur and nitrogen species to the environment. Too often, current regulatory networks focus only on measuring particle phase components and even those measurements have some major omissions (e.g., ammonium is not measured in the IMPROVE network).

We hope that the measurement approaches tested and utilized in these studies will provide a useful guide to future investigators hoping to address similar scientific questions in other environments. Moreover, we hope that the detailed information about

the chemical characteristics of atmospheric aerosols and associated gaseous species presented here will improve the scientific community's understanding of the nature of aerosols in rural environments and aid air quality regulators and policymakers in designing and implementing effective new strategies for improving air quality.

7. Recommendations for further study

Although the field, laboratory and data analysis efforts reported here provide considerable new insight into the properties of aerosol particles at several IMPROVE monitoring sites, there are many possibilities for enhancing our understanding of aerosol chemistry and its impacts on visibility degradation even further. Several possibilities for future research efforts are suggested here.

- Extending the length of the study periods for each site would provide additional interesting data. Summer time studies in Bondville, Brigantine, and Grand Canyon would be interesting because of possible changes in the behavior of the NO_3^- $HNO_3/NH_4^+/SO_4^{2-}/SO_2$ system under warmer, drier, and more photochemically active conditions than experienced in fall/winter/spring. Understanding such changes would be facilitated by additional gas phase measurements (e.g., NO_X and ozone) to better investigate photochemical production of pollutants and formation of secondary aerosol.
- Aerosol thermodynamic equilibrium model studies could be conducted for each site to see if model predictions match observations and to elucidate how changes in inputs of various chemical species might alter aerosol properties. For example, the model could be applied to examine predicted equilibrium composition changes of $PM_{2.5}$ aerosol as a result of decreases in sulfate concentrations resulting from sulfur dioxide emissions reductions. This might be most interesting in the acidic, sulfate-dominated environment at Great Smoky Mountains National Park and at the Bondville and Brigantine sites where sulfate is also a major aerosol component.

- Simulations of changes in aerosol composition, and amount, resulting from increases or decreases in ammonia emissions might also be interesting. Although ammonia is not currently a regulated ambient air pollutant, agricultural emissions of ammonia are receiving increasing scrutiny as awareness grows about the important role ammonia plays in particle formation and its apparently growing contribution to nitrogen deposition.
- The real-time data obtained in this project with the PILS/IC system was an extremely valuable tool for figuring out the form of nitrate present at each field site and for examining rapid changes in aerosol amount and composition. The PILS could also be coupled to other analytical instruments to provide insight into aerosol components beyond the inorganic ion species measured here. Coupling organic measuring systems to PILS, for example, would provide useful new information regarding carbonaceous aerosol contributions from different source types and give a better understanding of the hygroscopic nature of the aerosols and their effects on visibility degradation. For instance, levoglucosan and water soluble organic carbon from PILS/HPAEC-PAD (High Performance Anion Exchange Chromatography-Pulsed Amperometric Detection) and PILS/TOC (Total Organic Carbon) could provide high time resolution measurements of biomass smoke tracers (levoglucosan and related anhydrosugars) and general organic contributions to aerosol mass, respectively.
- Although the high time resolution PILS measurements of $PM_{2.5}$ ions have proven very useful, our ability to understand gas-particle partitioning of both sulfur and nitrogen species is limited by the lack of gas phase measurements of HNO_3, NH_3 and SO_2 at the same time resolution. High time resolution measurements of both aerosol

and gas phase components would improve our understanding of changes in aerosol concentrations and composition and permit better evaluation of aerosol thermodynamic model (e.g. ISORROPIA and SCAPE 2) predictions. Current evaluations of thermodynamic model predictions, typically based on 24-hr time integrated samples, suffer from the large variations in temperature, relative humidity, and aerosol composition that occur on diurnal time scales.

- Further improvement of PILS operation is also desirable to provide increasingly accurate and useful measurement products.
    - Switching from a peristaltic pump to a computer controlled syringe pump for filling the sample loop of an IC system could improve measurement precision. Sample loss presently associated with debubbling of the peristaltic flow could also be minimized. Feedback between observed analyte concentrations and sample injection volume/sampling time would also be facilitated by a syringe driven injection system. Finally, the system detection limit could be lowered by using a concentrator column rather than a sample loop between the syringe pump and the IC.
    - Faster measurement is important and preferable for some applications (e.g., for airborne studies). By exploring different IC columns, separation times could be shortened and thus the measurement time resolution would be increased. Coupling the PILS to a capillary electrophoresis (CE) analytical system could also increase time resolution due to the inherently more efficient (and faster) separations associated with CE.

- Further steps might also be possible to improve the accuracy of PILS measurements. Verification that that all sample droplets are entrained into the stream of carrier solution upon impaction and accurately transferred between the PILS and the analytical instrument (e.g., by using minimum lengths of sample transport tubing) could be fruitful areas for further testing and development. Possible losses of volatile species during sampling within the PILS system due to high temperatures (for steam generation) should also be investigated in more detail.

8. References

Abbatt, J.P.D., 1997. Interaction of HNO_3 with water-ice surfaces at temperatures of the free troposphere. Geophysical Research Letters, 24(12): 1479-1482.

Abbatt, J.P.D. and Waschewsky, G.C.G., 1998. Heterogeneous interactions of HOBr, HNO_3, O_3, and NO_2 with deliquescent NaCl aerosols at room temperature. Journal of Physical Chemistry A, 102(21): 3719-3725.

Adams, P.J., Seinfeld, J.H., Koch, D., Mickley, L. and Jacob, D., 2001. General circulation model assessment of direct radiative forcing by the sulfate-nitrate-ammonium-water inorganic aerosol system. Journal of Geophysical Research-Atmospheres, 106(D1): 1097-1111.

Adams, P.J., Seinfeld, J.H. and Koch, D.M., 1999. Global concentrations of tropospheric sulfate, nitrate, and ammonium aerosol simulated in a general circulation model. Journal of Geophysical Research, [Atmospheres], 104(D11): 13791-13823.

Allegrini, I., Febo, A., Perrino, C. and Masia, P., 1994. Measurement of Atmospheric Nitric-Acid in Gas-Phase and Nitrate in Particulate Matter by Means of Annular Denuders. International Journal of Environmental Analytical Chemistry, 54(3): 183-201.

Allen, A.G., Nemitz, E., Shi, J.P., Harrison, J.P. and Greenwood, J.C., 2001. Size distributions of trace metals in atmospheric aerosols in the United Kingdom. Atmospheric Environment, 35(27): 4581-4591.

Allen, H.C., Laux, J.M. and Vogt, R., 1996. Water-induced reorganization of ultrathin nitrate fims on NaCl: Implications for the tropospheric chemistry of sea salt particles. Journal of Physical Chemistry, 100: 6371-6375.

Ames, R.B. and Kreidenweis, S.M., 1996. Optical Measurements of Aerosol Size Distribution in Great Smoky Mountains National Park: Particle Hygroscopicity and its impact on Visibility. ISSN 0737-5352-33, CIRA, Colorado State University, Fort Collins.

Anderson, T.L., Charlson, R.J., Schwartz, S.E., Knutti, R., Boucher, O., Rodhe, H. and Heintzenberg, J., 2003. Climate forcing by aerosols - a hazy picture. Science, 300(5622): 1103-1104.

Aneja, V.P., Chauhan, J.P. and Walker, J.T., 2000. Characterization of atmospheric ammonia emissions from swine waste storage and treatment lagoons. Journal of Geophysical Research, 105: 11535-11545.

Aneja, V.P., Roelle, P.A., Murray, G.C., Southerland, J., Eristman, J.W., Fowler, D., Asman, W.A.H. and Patni, N., 2001. Atmospheric nitrogen compounds II: emissions, transport, transformation, deposition and assessment. Atmospheric Environment, 35: 1903-1911.

Ansari, A.S. and Pandis, S.N., 1998. Response of inorganic PM to precursor concentrations. Environmental Science & Technology, 32: 2706-2714.

Appel, B.R., 1993. Sampling of Selected Labile Atmospheric Pollutants. Advances in Chemistry Series(232): 1-40.

Appel, B.R. and Tokiwa, Y., 1981. Atmospheric particulate nitrate sampling errors deu to reactions with particulate and gaseous strong acids. Atmospheric Environment, 15: 1087-1089.

Appel, B.R., Tokiwa, Y. and Haik, M., 1981. Sampling of Nitrates in Ambient Air. Atmospheric Environment, 15(3): 283-289.

Appel, B.R., Tokiwa, Y., Haik, M. and Kothny, E.L., 1984. Artifact Particulate Sulfate and Nitrate Formation on Filter Media. Atmospheric Environment, 18(2): 409-416.

Arimoto, R., Kim, Y.J., Kim, Y.P., Quinn, P.K., Bates, T.S., Anderson, T.L., Gong, S., Uno, I., Chin, M., Huebert, B.J., Clarke, A.D., Shinozuka, Y., Weber, R.J., Anderson, J.R., Guazzotti, S.A., Sullivan, R.C., Sodeman, D.A., Prather, K.A. and Sokolik, I.N., 2006.

Characterization of Asian Dust during ACE-Asia. Global and Planetary Change, 52(1-4): 23-56.

Aymoz, G., Jaffrezo, J.L., Jacob, V., Colomb, A. and George, C., 2004. Evolution of organic and inorganic components of aerosol during a Saharan dust episode observed in the French Alps. Atmospheric Chemistry And Physics, 4: 2499-2512.

Bari, A., Ferraro, V., Wilson, L.R., Luttinger, D. and Husain, L., 2003. Measurements of gaseous HONO, HNO_3, SO_2, HCl, NH_3, particulate sulfate and $PM_{2.5}$ in New York, NY. Atmospheric Environment, 37(20): 2825-2835.

Bauer, S.E. and Koch, D., 2005. Impact of heterogeneous sulfate formation at mineral dust surfaces on aerosol loads and radiative forcing in the Goddard Institute for Space Studies general circulation model. Journal of Geophysical Research-Atmospheres, 110(D17).

Beichert, P. and FinlaysonPitts, B.J., 1996. Knudsen cell studies of the uptake of gaseous HNO_3 and other oxides of nitrogen on solid NaCl: The role of surface-adsorbed water. Journal Of Physical Chemistry, 100(37): 15218-15228.

Berresheim, H., Elste, T., Tremmel, H.G., Allen, A.G., Hansson, H.C., Rosman, K., Dal Maso, M., Maekelae, J.M., Kulmala, M. and O'Dowd, C.D., 2002. Gas-aerosol relationships of H_2SO_4, MSA, and OH: observations in the coastal marine boundary layer at Mace Head, Ireland. Journal of Geophysical Research, [Atmospheres], 107(D19): PAR5/1-PAR5/12.

Berresheim, H., Wine, P.H. and Davis, D.D., 1995. Sulfur in the atmosphere, in Compostion, Chemistry, and Climate of the Atmosphere. Van Nostrand Reinhold, 251-307 pp.

Blanchard, C.L. and Hidy, G.M., 2002. Effects of changes in sulfate, ammonia, and nitric acid on particle composition in the southeastern United States. Proceedings of the Air & Waste Management Association's Annual Conference & Exhibition, 95th, Baltimore, MD, United States, June 23-27, 2002: 132-147.

Blanchard, C.L. and Hidy, G.M., 2005. Effects of SO_2 and NO_x emission reductions on $PM_{2.5}$ mass concentrations in the Southeastern United States. Journal of The Air & Waste Management Association, 55(3): 265-272.

Blanchard, C.L. and Tanenbaum, S., 2003. Trends in ambient NOx and particulate nitrate concentrations in California, 1980-2000. CRC Project No. A-43C, Coordinating Research Council, INC, Albany, California 94706.

Borensen, C., Kirchner, U., Scheer, V., Vogt, R. and Zellner, R., 2000. Mechanism and kinetics of the reactions of NO_2 or HNO_3 with alumina as a mineral dust model compound. Journal of Physical Chemistry A, 104(21): 5036-5045.

Brauer, M., Koutrakis, P., Keeler, G.J. and Spengler, J.D., 1991. Indoor and outdoor concentration of inorganic acidic aerosols and gases. Journal of Air & Waste Management Association, 41(2): 171-181.

Buhr, S.M., Buhr, M.P., Fehsenfeld, F.C., Holloway, J.S., Karst, U., Norton, R.B., Parrish, D.D. and Sievers, R.E., 1995. Development of A Semicontinuous Method For The Measurement of Nitric-Acid Vapor And Particulate Nitrate And Sulfate. Atmospheric Environment, 29(19): 2609-2624.

Cabada, J.C., Rees, S., Takahama, S., Khlystov, A., Pandis, S.N., Davidson, C.I. and Robinson, A.L., 2004. Mass size distributions and size resolved chemical composition of fine particulate matter at the Pittsburgh supersite. Atmospheric Environment, 38(20): 3127-3141.

Carmichael, G.R., Zhang, Y., Chen, L.L., Hong, M.S. and Ueda, H., 1996. Seasonal variation of aerosol composition at Cheju Island, Korea. Atmospheric Environment, 30(13): 2407-2416.

Carrico, C.M., Malm, W.C., Kreidenweis, S.M., Collett, J.L., Day, D., McMeeking, G.R., Hand, J.L., Herckes, P., Engling, G., Lee, T. and Carrillo, J., 2004. The Yosemite

Aerosol Characterization Study of 2002, CIRA, Colorado State University, Fort Collins, CO 80523.

Chang, M.C., Sioutas, C., Kim, S., Gong, H. and Linn, W.S., 2000. Reduction of nitrate losses from filter and impactor samplers by means of concentration enrichment. Atmospheric Environment, 34(1): 85-98.

Charlson, R.J., Schwartz, S.E., Hales, J.M., Cess, R.D., Coakley, J.A., Hansen, J.E. and Hofmann, D.J., 1992. Climate Forcing By Anthropogenic Aerosols. Science, 255(5043): 423-430.

Chen, S.J., Hsieh, L.T., Kao, M.J., Lin, W.Y., Huang, K.L. and Lin, C.C., 2004. Characteristics of particles sampled in southern Taiwan during the Asian dust storm periods in 2000 and 2001. Atmospheric Environment, 38(35): 5925-5934.

Cheng, M.D. and Tanner, R.L., 2002. Characterization of ultrafine and fine particles at a site near the Great Smoky Mountains National Park. Atmospheric Environment, 36(38): 5795-5806.

Cheng, M.T. and Tsai, Y.I., 2000. Characterization of visibility and atmospheric aerosols in urban, suburban, and remote areas. Science of the Total Environment, 263(1-3): 101-114.

Cheng, Y.H. and Tsai, C.J., 1997. Evaporation loss of ammonium nitrate particles during filter sampling. Journal of Aerosol Science, 28(8): 1553-1567.

Cheng, Z.L., Lam, K.S., Chan, L.Y., Wang, T. and Cheng, K.K., 2000. Chemical characteristics of aerosols at coastal station in Hong Kong. I. Seasonal variation of major ions, halogens and mineral dusts between 1995 and 1996. Atmospheric Environment, 34: 2771-2783.

Choi, J., Lee, M., Chun, Y., Kim, J. and Oh, S., 2001. Chemical composition and source signature of spring aerosol in Seoul, Korea. Journal of Geophysical Research-Atmospheres, 106 (D16): 18067-18074.

Chow, J.C., Watson, J.G., Lowenthal, D.H. and Magliano, K.L., 2005. Loss of $PM_{2.5}$ nitrate from filter samples in central California. Journal of the Air & Waste Management Association, 55(8): 1158-1168.

Chun, Y., Boo, K., Kim, J., Park, S. and Lee, M., 2001. Synopsis, transport, and physical characteristics of Asian dust in Korea. Journal of Geophysical Research-Atmospheres, 106 (D16): 18461-18469.

Currie, L.A., Gelach, C.W., Lewis, W.D., Balfour, J.A., Copper, S.L., Dattner, R.T., De Cesar, G.E., Gordon, S.L., Heiser, P.K., Hopke, J.J., Shah, G.D., Thurston and Williamson, H.J., 1984. Interlaboratory comparison of source apportionment procedures: result for simulated data sets. Atmospheric Environment, 18: 1517-1537.

Danalatos, D. and Glavas, S., 1999. Gas phase nitric acid, ammonia and related particulate matter at a Mediterranean coastal site, Patras, Greece. Atmospheric Environment, 33(20): 3417-3425.

Day, D.E., Malm, W.C. and Kreidenweis, S.M., 1997. Seasonal variations in aerosol composition and acidity at Shenandoah and Great Smoky Mountains National Parks. Journal of the Air & Waste Management Association, 47(3): 411-418.

De Haan, D.O. and Finlayson-Pitts, B.J., 1997. Knudsen cell studies of the reaction of gaseous nitric acid with synthetic sea salt at 298 K. Journal of Physical Chemistry A, 101(51): 9993-9999.

de Leeuw, G., Cohen, L., Frohn, L.M., Geernaert, G., Hertel, O., Jensen, B., Jickells, T., Klein, L., Kunz, G.J., Lund, S., Moerman, M., Muller, F., Pedersen, B., von Salzen, K., Schlunzen, K.H., Schulz, M., Skjoth, C.A., Sorensen, L.L., Spokes, L., Tamm, S. and Vignati, E., 2001. Atmospheric input of nitrogen into the North Sea: ANICE project overview. Continental Shelf Research, 21(18-19): 2073-2094.

Dentener, F.J., Carmichael, G.R., Zhang, Y., Lelieveld, J. and Crutzen, P.J., 1996. Role of mineral aerosol as a reactive surface in the global troposphere. Journal of Geophysical Research, 101: 22869 - 22889.

Draxler, R.R., 2003. HYSPLIT 4 User's Guide, Technical Memorandum #ERL ARL-224. NOAA Air Resources Laboratory, NOAA.

Dutkiewicz, V.A., Das, M. and Husain, L., 2000. The relationship between regional SO_2 emissions and downwind aerosol sulfate concentrations in the northeastern US. Atmospheric Environment, 34(11): 1821-1832.

Engling, G., 2006. Characterizing Biomass Combustion Emission Contributions to Ambient Aerosol Concentrations, Colorado State University, Fort Collins, CO 80523.

Engling, G., Herckes, P., Kreidenweis, S.M., Malm, W.C. and Collett, J.L., 2006. Composition of the fine organic aerosol in Yosemite National Park during the 2002 Yosemite Aerosol Characterization Study. Atmospheric Environment, 40(16): 2959-2972.

EPA, 1992. Determination of the strong acidity of atmospheric fine particles (<2.5 μm) using annular denuder technology. 600/R-93-037, Environmental Protection Agency, Washington D.C.

EPA, 2003. $PM_{2.5}$ Chemical Speciation Laboratory Services Standard Operating Procedures. Technology Transfer Network - Ambient Monitoring Technology Information Center.

EPA, U.S., 1999. Compendium of methods for the determination of inorganic compounds in ambient air. EPA/625/R-96/010a: Method IO-4.2.

Erickson, D.J., III, Seuzaret, C., Keene, W.C. and Gong, S.L., 1999. A general circulation model based calculation of HCl and $ClNO_2$ production from sea salt dechlorination: Reactive Chlorine Emissions Inventory. J. Geophys. Res., 104(D7): 8347-8372.

Evans, M.C.F., 2003. Characterization and Formation of Particulate Nitrate in a Coastal Area. Ph. D. Thesis, University of South Florida.

Evans, M.S.C., Campbell, S.W., Bhethanabotla, V. and Poor, N.D., 2004. Effect of sea salt and calcium carbonate interactions with nitric acid on the direct dry deposition of nitrogen to Tampa Bay, Florida. Atmospheric Environment, 38(29): 4847-4858.

Fan, S.M., Horowitz, L.W., Levy, H. and Moxim, W.J., 2004. Impact of air pollution on wet deposition of mineral dust aerosols. Geophysical Research Letters, 31(2).

Finlayson-Pitts, B.J. and Pitts, J.N.J., 2000. Chemistry of the Upper and Lower Atmosphere. Academic Press.

Fischel, M., 2001. Evaluation of selected deicers based on a review of the literature, Colorado Department of Transportation, Denver, CO.

Gard, E.E., Kleeman, M.J., Gross, D.S., Hughes, L.S., Allen, J.O., Morrical, B.D., Fergenson, D.P., Dienes, T., Galli, M.E., Johnson, R.J., Cass, G.R. and Prather, K.A., 1998. Direct observation of heterogeneous chemistry in the atmosphere. Science, 279(5354): 1184-1187.

Godwin, K.S., Hafner, S.D. and Buff, M.F., 2003. Long-term trends in sodium and chloride in the Mohawk River, New York: the effect of fifty years of road-salt application. Environmental Pollution, 124(2): 273-281.

Goodman, A.L., Underwood, G.M. and Grassian, V.H., 2000. A laboratory study of the heterogenous reaction of nitric acid on calcium carbonate particles. Journal of Geophysical Research, 105: 29053-29064.

Grassian, V.H., 2002. Chemical reactions of nitrogen oxides on the surface of oxide, carbonate, soot, and mineral dust particles: Implications for the chemical balance of the troposphere. Journal of Physical Chemistry A, 106(6): 860-877.

Guimbaud, C., Arens, F., Gutzwiller, L., Gaggeler, H.W. and Ammann, M., 2002. Uptake of HNO_3 to deliquescent sea-salt particles: a study using the short-lived radioactive isotope tracer N-13. Atmospheric Chemistry and Physics, 2: 249-257.

Gupta, A., Kumar, R., Kumari, K.M. and Srivastava, S.S., 2003. Measurement of NO_2, HNO_3, NH_3 and SO_2 and related particulate matter at a rural site in Rampur, India. Atmospheric Environment, 37(34): 4837-4846.

Hand, J.L. and Kreidenweis, S.M., 1997. Aerosol Hygroscopicity and Visibility estimates in the Great Smoky Mountains National Park. ISSN No. 0737-5352-35, CIRA, Colorado State University, Fort Collins.

Hand, J.L. and Malm, W.C., 2006. Review of the IMPROVE Equation for Estimating Ambient Light Extinction Coefficients. ISSN 0737-5352-71, CIRA, Colorado State University, Fort Collins.

Hand, J.L., Malm, W.C., Laskin, A., Day, D., Lee, T., Wang, C., Carrico, C., Carrillo, J., Cowin, J.P., Collett, J.L. and Iedema, M.J., 2005. Optical, physical, and chemical properties of tar balls observed during the Yosemite Aerosol Characterization Study. Journal Of Geophysical Research-Atmospheres, 110(D21).

Hanisch, F. and Crowley, J.N., 2001a. Heterogeneous reactivity of gaseous nitric acid on Al_2O_3, $CaCO_3$, and atmospheric dust samples: A Knudsen cell study. Journal of Physical Chemistry A, 105(13): 3096-3106.

Hanisch, F. and Crowley, J.N., 2001b. The heterogeneous reactivity of gaseous nitric acid on authentic mineral dust samples, and on individual mineral and clay mineral components. Physical Chemistry Chemical Physics, 3(12): 2474-2482.

Hanisch, F. and Crowley, J.N., 2001c. Heterogenous reactivity of gaseous nitric acid on Al_2O_3, $CaCO_3$, and atmospheric dust samples: A Knudsen cell study. Journal of physical Chemistry A, 105: 3096-3106.

Hanisch, F. and Crowley, J.N., 2003. Heterogeneous reactivity of NO and HNO_3 on mineral dust in the presence of ozone. Physical Chemistry Chemical Physics, 5(5): 883-887.

Haywood, J. and Boucher, O., 2000. Estimates of the direct and indirect radiative forcing due to tropospheric aerosols: A review. Reviews of Geophysics, 38(4): 513-543.

Herckes, P., Wendling, R., Sauret, N., Mirabel, P. and Wortham, H., 2002. Cloudwater studies at a high elevation site in the Vosges Mountains. Environmental pollution, 117: 169-177.

Hien, P.D., Bac, V.T. and Thinh, N.T.H., 2005. Investigation of sulfate and nitrate formation on mineral dust particles by receptor modeling. Atmospheric Environment, 39(38): 7231-7239.

Highsmith, V.R., Bond, A.E. and Howes, J.E., 1986. Particle and Substrate Losses from Teflon and Quartz Filters. Atmospheric Environment, 20(7): 1413-1417.

Hinds, W.C., 1999. Aerosol Technology. JOHN WILEYS & SONS, INC.

Hodzic, A., Bessagnet, B. and Vautard, R., 2006a. A model evaluation of coarse-mode nitrate heterogeneous formation on dust particles. Atmopheric Environment, 40: 4158-4171.

Hodzic, A., Vautard, R., Chazette, P., Menut, L. and Bessagnet, B., 2006b. Aerosol chemical and optical properties over the Paris area within ESQUIF project. Atmospheric Chemistry and Physics, 6: 3257-3280.

Hoffman, R.C., Laskin, A. and Finlayson-Pitts, B.J., 2004. Sodium nitrate particles: physical and chemical properties during hydration and dehydration, and implications for aged sea salt aerosols. Journal of Aerosol Science, 35(7): 869-887.

Hopke, P.K., 1988. Target transformation factor analysis as an aerosol mass apportionment method: a review and sensitivity study. Atmospheric Environment, 22: 1777-1792.

Husain, L., Ghauri, B., Yang, K., Khan, A.R. and Rattigan, O.V., 2004a. Application of the SO_4^{2-}/Se tracer technique to study SO_2 oxidation in cloud and fog on a time scale of minutes. Chemosphere, 54(2): 177-183.

Husain, L., Parekh, P.P., Dutkiewicz, V.A., Khan, A.R., Yang, K. and Swami, K., 2004b. Long-term trends in atmospheric concentrations of sulfate, total sulfur, and trace elements in the northeastern United States. Journal of Geophysical Research-Atmospheres, 109(D18).

Hwang, H.J. and Ro, C.U., 2005. Single-particle characterization of four aerosol samples collected in ChunCheon, Korea, during Asian dust storm events in 2002. Journal of Geophysical Research-Atmospheres, 110(D23).

Jacobson, M.Z., 2001. Global direct radiative forcing due to multicomponent anthropogenic and natural aerosols. Journal of Geophysical Research-Atmospheres, 106(D2): 1551-1568.
John, W., Wall, S.M., Ondo, J.L. and Winklmayr, W., 1990. Modes in the size distributions of atmospheric inorganic aerosol. Atmospheric Environment, 24A(9): 2349-2359.
Jordan, C.E., Dibb, J.E., Anderson, B.E. and Fuelberg, H.E., 2003. Uptake of nitrate and sulfate on dust aerosols during TRACE-P. Journal of Geophysical Research-Atmospheres, 108(D21): 1-10.
Kaiser, H.F., 1958. The Varimax criterion for analytic rotation in factor analysis. Psychometrika, 23: 187-200.
Kang, C.M., Kang, B.W. and Lee, H.S., 2006. Source identification and trends in concentrations of gaseous and fine particulate principal species in Seoul, South Korea. Journal of The Air & Waste Management Association, 56(7): 911-921.
Karlsson, A., Irgum, K. and Hansson, H.C., 1997. Single-stage flowing liquid film impactor for continuous on-line particle analysis. Journal of Aerosol Science, 28(8): 1539-1551.
Karlsson, R. and Ljungstrom, E., 1998. A laboratory study of the interaction of NH_3 and NO_2 with sea salt particles. Water Air and Soil Pollution, 103(1-4): 55-70.
Kasper, A. and Puxbaum, H., 1998. Seasonal variation of SO_2, HNO_3, NH_3 and selected aerosol components at Sonnblick (3106 m asl). Atmospheric Environment, 32(23): 3925-3939.
Kelly, J.T. and Wexler, A.S., 2006. Water uptake by aerosol: Water activity in supersaturated potassium solutions and deliquescence as a function of temperature. Atmospheric Environment, 40(24): 4450-4468.
Kerminen, V.-M., Pakkanen, T.A. and Hillamo, R.E., 1997. Interactions between inorganic trace gases and supermicrometer particles at a coastal site. Atmospheric Environment, 31(17): 2753-2765.
Kerminen, V.M., Hillamo, R., Teinila, K., Pakkanen, T., Allegrini, I. and Sparapani, R., 2001. Ion balances of size-resolved tropospheric aerosol samples: implications for the acidity and atmospheric processing of aerosols. Atmospheric Environment, 35(31): 5255-5265.
Khlystov, A., Wyers, G.P. and Slanina, J., 1995. The Steam-Jet Aerosol Collector. Atmospheric Environment, 29(17): 2229-2234.
Koutrakis, P., Wolfson, J.M., Slater, J.L., Brauer, M., Spengler, J.D., Stevens, R.K. and Stone, C.L., 1988a. Evaluation of an annular denuder/filter pack system to collect acidic aerosols and gases. Environmental Science & Technology, 22(12): 1463-8.
Koutrakis, P., Wolfson, J.M. and Spengler, J.D., 1988b. An Improved Method for Measuring Aerosol Strong Acidity - Results from a 9-Month Study in St-Louis, Missouri and Kingston, Tennessee. Atmospheric Environment, 22(1): 157-162.
Krueger, B.J., Grassian, V.H., Cowin, J.P. and Laskin, A., 2004. Heterogeneous chemistry of individual mineral dust particles from different dust source regions: the importance of particle mineralogy. Atmospheric Environment, 38(36): 6253-6261.
Laskin, A., Iedema, M.J. and Cowin, J.P., 2002. Quantitative time-resolved monitoring of nitrate formation in sea salt particles using a CCSEM/EDX single particle analysis. Environmental Science & Technology, 36(23): 4948-4955.
Laskin, A., Wietsma, T.W., Krueger, B.J. and Grassian, V.H., 2005. Heterogeneous chemistry of individual mineral dust particles with nitric acid: A combined CCSEM/EDX, ESEM, and ICP-MS study. Journal of Geophysical Research-Atmospheres, 110(D10): D10208, doi:10.1029/2004JD005206.
Laux, J.M., Hemminger, J.C. and Finlaysonpitts, B.J., 1994. X-Ray Photoelectron Spectroscopic Studies of The Heterogenous Reaction Of Gaseous Nitric-Acid With Sodium-Chloride - Kinetics And Contribution To The Chemistry Of The Marine Troposphere. Geophysical Research Letters, 21(15): 1623-1626.
Lee, G., 1992a. The variation of nitric acid vapor and nitrate aerosol concentrations near the Island of Hawaii. Ph. D. Thesis, University of Rhode Island.

Lee, H.S., 1992b. Measurement and evaluation of acid air pollutions in Chicago using an annular denuder system. The Degree of Doctor of Philosophy Thesis, University of Illinois at Chicago.

Lee, H.S. and Kang, B.-W., 2001. Chemical characteristics of principal $PM_{2.5}$ species in Chongju, South Korea. Atmospheric Environment, 35: 739-746.

Lee, H.S., Wadden, R.A. and Scheff, P.A., 1993. Measurement and evaluation of acid air pollutants in Chicago using an annular denuder system. Atmospheric Environment, 27A: 543-553.

Lee, J.H., Yoshida, Y., Turpin, B.J., Hopke, P.K., Poirot, R.L., Lioy, P.J. and Oxley, J.C., 2002. Identification of sources contributing to Mid-Atlantic regional aerosol. Journal of The Air & Waste Management Association, 52(10): 1186-1205.

Lee, T. and Collett, J.L., 2002. The ionic composition of aerosol in Big Band National Park. Master Thesis, Colorado State University, Fort Collins, CO, 220 pp.

Lee, T., Kreidenweis, S.M. and Collett, J.L., 2004. Aerosol Ion Characteristics during the Big Bend Regional Aerosol and Visibility Observational Study. Journal of Air & Waste Management Association, 54: 585-592.

Li, J., Posfai, M., Hobbs, P.V. and Buseck, P.R., 2003. Individual aerosol particles from biomass burning in southern Africa: 2, Compositions and aging of inorganic particles. Journal Of Geophysical Research-Atmospheres, 108(D13).

Liao, H., Adams, P.J., Chung, S.H., Seinfeld, J.H., Mickley, L.J. and Jacob, D.J., 2003. Interactions between tropospheric chemistry and aerosols in a unified general circulation model. Journal Of Geophysical Research-Atmospheres, 108(D1).

Liu, X.D., Van Espen, P., Adams, F., Cafmeyer, J. and Maenhaut, W., 2000. Biomass burning in southern Africa: Individual particle characterization of atmospheric aerosols and savanna fire samples. Journal of Atmospheric Chemistry, 36(2): 135-155.

Malm, W.C., Day, D.E., Carrico, C., Kreidenweis, S.M., Collett, J.L., McMeeking, G., Lee, T., Carrillo, J. and Schichtel, B., 2005a. Intercomparison and closure calculations using measurements of aerosol species and optical properties during the Yosemite Aerosol Characterization Study. Journal of Geophysical Research-Atmospheres, 110(D14): D14302, doi:10.1029/2004JD005494.

Malm, W.C., Day, D.E., Kreidenweis, S.M., Collett, J.L., Carrico, C., McMeeking, G. and Lee, T., 2005b. Hygroscopic properties of an organic-laden aerosol. Atmospheric Environment, 39(27): 4969-4982.

Malm, W.C., Pitchford, M.L., Scruggs, M., sisler, J.F., Ames, R., Copeland, S., Gebhart, K.A. and Day, D.E., 2000. Spatial and Seasonal Patterns and Temporal Variability of Haze and its Constituents in the United States. ISSN 0737-5352-47, CIRA, Colorado State University, Fort Collins.

Malm, W.C., Schichtel, B.A., Pitchford, M.L., Ashbaugh, L.L. and Eldred, R.A., 2004. Spatial and monthly trends in speciated fine particle concentration in the United States. Journal Of Geophysical Research-Atmospheres, 109(D3).

Malm, W.C., Sisler, J.F., Huffman, D., Eldred, R.A. and Cahill, D.M., 1994. Spatial and Seasonal Trends in Particle Concentration and Optical Extinction in the United States. Journal of Geophysical Research, 99(D1): 1347-1370.

Marple, V.A., Rubow, K.L. and Behm, S.M., 1991. A Microorifice Uniform Deposit Impactor (MOUDI): Description, Calibration, and Use. Aerosol Science and Technology, 14: 434-446.

Marple, V.A. and Willeke, K., 1976. Impactor Design. Atmospheric Environment, 10(10): 891-896.

Martin, S.T., Hung, H.M., Park, R.J., Jacob, D.J., Spurr, R.J.D., Chance, K.V. and Chin, M., 2004. Effects of the physical state of tropospheric ammonium-sulfate-nitrate particles on global aerosol direct radiative forcing. Atmospheric Chemistry and Physics, 4: 183-214.

Maxwell-Meier, K., Weber, R., Song, C., Orsini, D., Ma, Y., Carmichael, G.R. and Streets, D.G., 2004. Inorganic composition of fine particles in mixed mineral dust-pollution plumes observed from airborne measurements during ACE-Asia. Journal of Geophysical Research-Atmospheres, 109(D19).

McCulloch, R.B. and Shendrikar, A.D., 2000. Concurrent atmospheric ammonia measurements using citric-acid-coated diffusion denuders and a chemiluminescence analyzer. Atmospheric Environment, 34: 4957-4958.

McMeeking, G.R., Kreidenweis, S.M., Carrico, C.M., Collett, J.L., Day, D.E. and Malm, W.C., 2005. Observations of smoke-influenced aerosol during the Yosemite Aerosol Characterization Study: 2. Aerosol scattering and absorbing properties. Journal Of Geophysical Research-Atmospheres, 110(D18).

McMeeking, G.R., Kreidenweis, S.M., Lunden, M., Carrillo, J., Carrico, C.M., Lee, T., Herckes, P., Engling, G., Day, D.E., Hand, J., Brown, N., Malm, W.C. and Collett, J.L., 2006. Smoke-impacted regional haze in California during the summer of 2002. Agricultural and Forest Meteorology, 137(1-2): 25-42.

Michel, A.E., Usher, C.R. and Grassian, V.H., 2003. Reactive uptake of ozone on mineral oxides and mineral dusts. Atmospheric Environment, 37(23): 3201-3211.

Moore, K.F., 2002. Drop Size-dependent Chemical Composition in Clouds and Fogs, Colorado State University, Fort Collins.

Mozurkewich, M., 1993. The Dissociation-Constant of Ammonium-Nitrate and Its Dependence on Temperature, Relative-Humidity and Particle-Size. Atmospheric Environment Part a-General Topics, 27(2): 261-270.

Nel, A., 2005. Air Pollution-Related illness:Effects of Particle. Science, 308: 804 - 806.

Niemi, J.V., Tervahattu, H., Vehkamaki, H., Kulmala, M., Koskentalo, T., Sillanpaa, M. and Rantamaki, M., 2004. Characterization and source identification of a fine particle episode in Finland. Atmospheric Environment, 38(30): 5003-5012.

Niemi, J.V., Tervahattu, H., Vehkamaki, H., Martikainen, J., Laakso, L., Kulmala, M., Aarnio, P., Koskentalo, T., Sillanpaa, M. and Makkonen, U., 2005. Characterization of aerosol particle episodes in Finland caused by wildfires in Eastern Europe. Atmospheric Chemistry And Physics, 5: 2299-2310.

O'Dowd, C.D., Smith, M.H., Consterdine, I.E. and Lowe, J.A., 1997. Marine aerosol, sea-salt, and the marine sulphur cycle: A short review. Atmos. Environ., 31: 73-80.

Odowd, C.D., Lowe, J.A., Smith, M.H., Davison, B., Hewitt, N. and Harrison, R.M., 1997. Biogenic sulphur emissions and inferred non-sea-salt-sulphate cloud condensation nuclei in and around Antarctica. Journal of Geophysical Research-Atmospheres, 102(11D): 12839-12854.

Olszyna, K.J., Bairai, S.T. and Tanner, R.L., 2005. Effect of ambient NH_3 levels on $PM_{2.5}$ composition in the Great Smoky Mountains National Park. Atmospheric Environment, 39(25): 4593-4606.

Oms, M.T., Jongejan, P.A.C., Veltkamp, A.C., Wyers, G.P. and Slanina, J., 1996. Continuous monitoring of atmospheric HCl, HNO_2, HNO_3, and SO_2, by wet-annular denuder air sampling with on-line chromatographic analysis. International Journal of Environmental Analytical Chemistry, 62(3): 207-218.

Ooki, A. and Uematsu, M., 2005. Chemical interactions between mineral dust particles and acid gases during Asian dust events. Journal of Geophysical Research-Atmospheres, 110(D3): D03201, doi:10.1029/2004JD004737.

Orsini, D.A., Ma, Y.L., Sullivan, A., Sierau, B., Baumann, K. and Weber, R.J., 2003. Refinements to the particle-into-liquid sampler (PILS) for ground and airborne measurements of water soluble aerosol composition. Atmospheric Environment, 37(9-10): 1243-1259.

Padgett, P.E. and Bytnerowicz, A., 2001. Deposition and adsorption of the air pollutant HNO_3 vapor to soil surfaces. Atmospheric Environment, 35(13): 2405-2415.

Pakkanen, T.A., 1996. Study of formation of coarse particle nitrate aerosol. Atmospheric Environment, 30(14): 2475-2482.

Pakkanen, T.A., Kerminen, V.-M., Hillamo, R.E., Makinen, M., Makela, T. and Virkkula, A., 1996. Distribution of Nitrate over Sea-salt and Soil derived particles-Implications from a field study. Journal of Atmospheric Chemistry, 24: 189-205.

Pakkanen, T.A., Kerminen, V.M., Loukkola, K., Hillamo, R.E., Aarnio, P., Koskentalo, T. and Maenhaut, W., 2003. Size distributions of mass and chemical components in street-level and rooftop PM1 particles in Helsinki. Atmospheric Environment, 37(12): 1673-1690.

Pang, Y., Eatough, N.L. and Eatough, D.J., 2002. Evaluation of the Performance of Annular Denuder Samplers. Aerosol Sicence & Technology, 36: 790-798.

Perrino, C., Desantis, F. and Febo, A., 1988. Uptake of Nitrous-Acid and Nitrogen-Oxides by Nylon Surfaces - Implications for Nitric-Acid Measurement. Atmospheric Environment, 22(9): 1925-1930.

Posfai, M., Simonics, R., Li, J., Hobbs, P.V. and Buseck, P.R., 2003. Individual aerosol particles from biomass burning in southern Africa: 1. Compositions and size distributions of carbonaceous particles. Journal of Geophysical Research-Atmospheres, 108(D13).

Prospero, J.M. and Savoie, D.L., 1989. Effect of continental sources on nitrate concentration over Pacific Ocean. Nature, 339: 687.

Pryor, S.C. and Sorensen, L.L., 2000. Nitric acid-sea salt reactions: Implications for nitrogen deposition to water surfaces. Journal of Applied Meteorology, 39(5): 725-731.

Raes, F., Van Dingenen, R., Vignati, E., Wilson, J., Putaud, J.P., Seinfeld, J.H. and Adams, P., 2000. Formation and cycling of aerosols in the global troposphere. Atmospheric Environment, 34(25): 4215-4240.

Rattigan, O.V., Reilly, J., Judd, C.D., Moore, K.F., Das, M., Sherman, D.E., Dutkiewicz, V.A., Collett, J.L. and Husain, L., 2001. Sulfur dioxide oxidation in clouds at Whiteface Mountain as a function of drop size. Journal of Geophysical Research, 106(D15): 17347-17358.

Reilly, J.E., Rattigan, O.V., Moore, K.F., Judd, C., Sherman, D.E., Dutkiewicz, V.A., Kreidenweis, S.M., Husain, L. and Collett, J.L., 2001. Drop size-dependent S(IV) oxidation in chemically heterogeneous radiation fogs. Atmospheric Environment, 35(33): 5717-5728.

Ro, C.U., Oh, K.Y., Kim, H., Kim, Y.P., Lee, C.B., Kim, K.H., Kang, C.H., Osan, J., De Hoog, J., Worobiec, A. and Van Grieken, R., 2001. Single-particle analysis of aerosols at Cheju Island, Korea, using low-Z electron probe X-ray microanalysis: A direct proof of nitrate formation from sea salts. Environmental Science & Technology, 35(22): 4487-4494.

Rogaski, C.A., Golden, D.M. and Williams, L.R., 1997. Reactive uptake and hydration experiments on amorphous carbon treated with NO_2, SO_2, O_3, HNO_3, and H_2SO_4. Geophysical Research Letters, 24(4): 381-384.

Roth, B. and Okada, K., 1998. On the modification of sea-salt particles in the coastal atmosphere. Atmospheric Environment, 32(9): 1555-1569.

Savoie, D.L. and Prospero, J.M., 1982. Particle Size Distribution of Nitrate and Sulfate in the Marine Atmosphere. Geophys. Res. Letts., 9(10): 1,207-1,210.

Seinfeld, J.H. and Pandis, S.N., 1998. Atmospehric Chemistry and Physics: From air pollution to climate change. John Wiley & Sons, INC., New York.

Seinfeld, J.H. and Pandis, S.N., 2006. Atmospheric Chemistry and Physics: From Air Pollution to Climate Change. John Wiley & Sons, INC., New York.

Seisel, S., Borensen, C., Vogt, R. and Zellner, R., 2004. The heterogeneous reaction of HNO_3 on mineral dust and gamma-alumina surfaces: a combined Knudsen cell and DRIFTS study. Physical Chemistry Chemical Physics, 6(24): 5498-5508.

Shaw, R.W. and Paur, R.J., 1983. Measurements of Sulfur In Gases And Particles During 16 Months In The Ohio River Valley. Atmospheric Environment, 17(8): 1431-1438.

Shaw, R.W., Stevens, R.K., Bowermaster, J., Tesch, J.W. and Tew, E., 1982. Measurements of Atmospheric Nitrate and Nitric-Acid - the Denuder Difference Experiment. Atmospheric Environment, 16(4): 845-853.

Sherman, D.E., Kreidenweis, S.M. and McKee, T., 1997. The influence of synoptic and local meteorological conditions on ambient particle concentrations during the Southeastern Aerosol and Visibility Study (SEAVS). ISSN No. 0737-5352-34, CIRA, Colorado State University, Fort Collins.

Sickles, J.E., Hodson, L.L., McClenny, W.A., Paur, R.J., Ellestad, T.G., Mulik, J.D., Anlauf, K.G., Wiebe, H.A., Mackay, G.I., Schiff, H.I. and Bubacz, D.K., 1990. Field Comparison of Methods for the Measurement of Gaseous and Particulate Contributors to Acidic Dry Deposition. Atmospheric Environment Part a-General Topics, 24(1): 155-165.

Simon, P.K. and Dasgupta, P.K., 1993. Wet Effluent Denuder Coupled Liquid Ion Chromatography Systems - Annular and Parallel-Plate Denuders. Analytical Chemistry, 65(9): 1134-1139.

Simon, P.K. and Dasgupta, P.K., 1995. Continuous Automated Measurement of Gaseous Nitrous and Nitric- Acids and Particulate Nitrite and Nitrate. Environmental Science & Technology, 29(6): 1534-1541.

Singh, H.B., Herlth, D., Kolyer, R., Salas, L., Bradshaw, J.D., Sandholm, S.T., Davis, D.D., Crawford, J., Kondo, Y., Koike, M., Talbot, R., Gregory, G.L., Sachse, G.W., Browell, E., Blake, D.R., Rowland, F.S., Newell, R., Merrill, J., Heikes, B., Liu, S.C., Crutzen, P.J. and Kanakidou, M., 1996. Reactive nitrogen and ozone over the western Pacific: Distribution, partitioning, and sources. Journal of Geophysical Research-Atmospheres, 101(D1): 1793-1808.

Sioutas, C., Koutrakis, P., Godleski, J.J., Ferguson, S.T., Kim, C.S. and Burton, R.M., 1997. Fine particle concentrators for inhalation exposures - Effect of particle size and composition. Journal of Aerosol Science, 28(6): 1057-1071.

Skoog, D.A., Holler, F.J. and Nieman, T.A., 1998. Principles of Instrumental Anaylysis. Harcourt Brace College Publishers.

Skoog, D.A., West, D.M. and Holler, F.J., 1992. Fundamentals of analytical chemistry. Saunders College Publication, Fort Worth, TX, 6-63 pp.

Slanina, J., ten Brink, H.M., Otjes, R.P., Even, A., Jongejan, P., Khlystov, A., Waijers-Ijpelaan, A. and Hu, M., 2001. The continuous analysis of nitrate and ammonium in aerosols by the steam jet aerosol collector (SJAC): extension and validation of the methodology. Atmospheric Environment, 35(13): 2319-2330.

Song, X.H., Polissar, A.V. and Hopke, P.K., 2001. Sources of fine particle composition in the northeastern US. Atmospheric Environment, 35(31): 5277-5286.

Sorooshian, A., Brechtel, F.J., Ma, Y.L., Weber, R.J., Corless, A., Flagan, R.C. and Seinfeld, J.H., 2006. Modeling and characterization of a particle-into-liquid sampler (PILS). Aerosol Science and Technology, 40(6): 396-409.

Spengler, J.D., Brauer, M. and Koutrakis, P., 1990. Acid air and health. Environmental Science & Technology, 24(7): 946-956.

Spengler, J.D., Keeler, G.J., Koutrakis, P., Ryan, P.B., Raizenne, M. and Franklin, C.A., 1989. Exposures to acidic aerosols. Environmental Health Perspectives, 79: 43-51.

Spicer, C.W., 1977. Photochemical atmospheric pollutants derived from nitrogen oxides. Atmospheric Environment, 11: 1089-95.

Spicer, C.W., Joseph, D.W. and Schumacher, P.M., 1985. Determination of Nitrate in Atmospheric Particulate Matter by Thermal-Decomposition and Chemi-Luminescence. Analytical Chemistry, 57(12): 2338-2341.

Spokes, L.J., Yeatman, S.G., Cornell, S.E. and Jickells, T.D., 2000. Nitrogen deposition to the eastern Atlantic Ocean. The importance of south-easterly flow. Tellus Series B-Chemical And Physical Meteorology, 52(1): 37-49.

Spurny, K.R., 2000. Aerosol chemical processes in the environment. Lewis.

Stelson, A.W. and Seinfeld, J.H., 1982. Relative humidity and temperature dependence of the ammonium nitrate dissociation constant. Atmospheric Environment, 16(5): 983-92.

Stolzenburg, M.R. and Hering, S.V., 2000. Method for the automated measurement of fine particle nitrate in the atmosphere. Environmental Science & Technology, 34(5): 907-914.

Sullivan, R.C., Guazzotti, S.A., Sodeman, D.A. and Prather, K.A., 2006. Direct observations of the atmospheric processing of Asian mineral dust. Atmospheric Chemistry and Physics Discussions, 6: 4109-4170.

Tabazadeh, A., Jacobson, M.Z., Singh, H.B., Toon, O.B., Lin, J.S., Chatfield, R.B., Thakur, A.N., Talbot, R.W. and Dibb, J.E., 1998. Nitric acid scavenging by mineral and biomass burning aerosols. Geophysical Research Letters, 25: 4185-4188.

Tang, I.N. and Munkelwitz, H.R., 1993. Composition and Temperature-Dependence of the Deliquescence Properties of Hygroscopic Aerosols. Atmospheric Environment Part A-General Topics, 27(4): 467-473.

Tanner, R.L., Bairai, S.T., Olszyna, K.J., Valente, M.L. and Valente, R.J., 2005. Diurnal patterns in $PM_{2.5}$ mass and composition at a background, complex terrain site. Atmospheric Environment, 39(21): 3865-3875.

Tanner, R.L., Parkhurst, W.J. and McNichol, A.P., 2004. Fossil sources of ambient aerosol carbon based on C-14 measurements. Aerosol Science and Technology, 38: 133-139.

Tegen, I., Koch, D., Lacis, A.A. and Sato, M., 2000. Trends in tropospheric aerosol loads and corresponding impact on direct radiative forcing between 1950 and 1990: A model study. Journal of Geophysical Research, [Atmospheres], 105(D22): 26971-26989.

ten Brink, H.M., 1998. Reactive uptake of HNO_3 and H_2SO_4 in sea-salt (NaCl) particles. Journal of Aerosol Science, 29(1-2): 57-64.

Tong, D.Q., Kang, D.W., Aneja, V.P. and Ray, J.D., 2005. Reactive nitrogen oxides in the southeast United States national parks: source identification, origin, and process budget. Atmospheric Environment, 39(2): 315-327.

Trebs, I., Meixner, F.X., Slanina, J., Otjes, R., Jongejan, P. and Andreae, M.O., 2004. Real-time measurements of ammonia, acidic trace gases and water-soluble inorganic aerosol species at a rural site in the Amazon Basin. Atmospheric Chemistry and Physics, 4: 967-987.

Tsai, C.J., Perng, S.B. and Chiou, S.F., 2000. Use of two different acidic aerosol samplers to measure acidic aerosols in Hsinchu, Taiwan. Journal of the Air & Waste Management Association, 50(12): 2120-2128.

Umann, B., Arnold, F., Schaal, C., Hanke, M., Uecker, J., Aufmhoff, H., Balkanski, Y. and Van Dingenen, R., 2005. Interaction of mineral dust with gas phase nitric acid and sulfur dioxide during the MINATROC II field campaign: First estimate of the uptake coefficient gamma(HNO_3) from atmospheric data. Journal of Geophysical Research-Atmospheres, 110(D22): D22306, doi:10.1029/2005JD005906.

Underwood, G.M., Li, P., Usher, C.R. and Grassian, V.H., 2000. Determining accurate kinetic parameters of potentially important heterogeneous atmospheric reactions on solid particle surfaces with a Knudsen cell reactor. Journal of Physical Chemistry A, 104(4): 819-829.

Underwood, G.M., Song, C.H., Phadnis, M., Carmichael, G.R. and Grassian, V.H., 2001. Heterogeneous reactions of NO_2 and HNO_3 on oxides and mineral dust: A combined

laboratory and modeling study. Journal of Geophysical Research-Atmospheres, 106(D16): 18055-18066.

Usher, C.R., Al-Hosney, H., Carlos-Cuellar, S. and Grassian, V.H., 2002. A laboratory study of the heterogeneous uptake and oxidation of sulfur dioxide on mineral dust particles. Journal of Geophysical Research-Atmospheres, 107(D23).

Usher, C.R., Michel, A.E., Stec, D. and Grassian, V.H., 2003. Laboratory studies of ozone uptake on processed mineral dust. Atmospheric Environment, 37(38): 5337-5347.

Virtanen, A., Ronkko, T., Kannosto, J., Ristimaki, J., Makela, J.M., Keskinen, J., Pakkanen, T., Hillamo, R., Pirjola, L. and Hameri, K., 2006. Winter and summer time size distributions and densities of traffic-related aerosol particles at a busy highway in Helsinki. Atmospheric Chemistry and Physics, 6: 2411-2421.

Wang, Y., Zhuang, G.S., Zhang, X.Y., Huang, K., Xu, C., Tang, A.H., Chen, J.M. and An, Z.S., 2006. The ion chemistry, seasonal cycle, and sources of $PM_{2.5}$ and TSP aerosol in Shanghai. Atmospheric Environment, 40(16): 2935-2952.

Wang, Y.H., Logan, J.A. and Jacob, D.J., 1998. Global simulation of tropospheric O_3-NO_x-hydrocarbon chemistry 2. Model evaluation and global ozone budget. Journal of Geophysical Research-Atmospheres, 103(D9): 10727-10755.

Watson, J.G., 2002. Visibility: Science and regulation. Journal of The Air & Waste Management Association, 52(6): 628-713.

Wayne, R.P., 2000. Chemistry of Atmospheres. Oxford University Press, New York, NY.

Weber, R., Orsini, D., Duan, Y., Baumann, K., Kiang, C.S., Chameides, W., Lee, Y.N., Brechtel, F., Klotz, P., Jongejan, P., ten Brink, H., Slanina, J., Boring, C.B., Genfa, Z., Dasgupta, P., Hering, S., Stolzenburg, M., Dutcher, D.D., Edgerton, E., Hartsell, B., Solomon, P. and Tanner, R., 2003. Intercomparison of near real time monitors of $PM_{2.5}$ nitrate and sulfate at the US Environmental Protection Agency Atlanta Supersite. Journal of Geophysical Research-Atmospheres, 108(D7): 8421, doi:10.1029/2001JD001220.

Weber, R.J., Orsini, D., Daun, Y., Lee, Y.N., Klotz, P.J. and Brechtel, F., 2001. A particle-into-liquid collector for rapid measurement of aerosol bulk chemical composition. Aerosol Science and Technology, 35(3): 718-727.

Wegner, W. and Yaggi, M., 2001. Environmental Impacts of Road Salt and Alternatives in New York City Watershed. Stormwater, 2(5): 10.

West, J.J., Ansari, A.S. and Pandis, S.N., 1999. Marginal $PM_{2.5}$: Nonlinear aerosol mass response to sulfate reductions in the Eastern United States. Journal of Air & Waste Management Association, 49: 1415-1424.

Wight, G.D., 1994. Fundamental of Air Sampling. Lewis Publishers.

Williams, A.L. and Stensland, G.J., 2006. Atmospheric Dispersion Study of Deicing Salt Applied to Roads, Illinois State Water Survey, Atmospheric Environment Section, Champaign, Illinois.

Wilson, T.R.S., 1975. Salinity and the major elements of sea water. In:Riley, J. P., Skirrow, G. (Eds),Chemical Oceanography (1, 2 Edition). Academic, Orlando FL.

Wolff, G.T., 1984. On the nature of nitrate in coarse continental aerosols. Atmospheric Environment, 18(5): 977-981.

Wu, P.M. and Okada, K., 1994. Nature of Coarse Nitrate Particles In The Atmosphere - A Single, Particle Approach. Atmospheric Environment, 28(12): 2053-2060.

Yu, L.E., Shulman, M.L., Kopperud, R. and Hildemann, L.M., 2005a. Fine organic aerosols collected in a humid, rural location (Great Smoky Mountains, Tennessee, USA): Chemical and temporal characteristics. Atmospheric Environment, 39(33): 6037-6050.

Yu, X.-Y., Lee, T., Ayres, B., Kreidenweis, S.M. and Collett, J.L., 2005b. Particulate nitrate measurement using nylon filters. Journal of the Air & Waste Management Association, 55: 1100 - 1110.

Yu, X.-Y., Lee, T., Ayres, B.R., Kreidenweis, S.M. and Collett, J.L., 2006. Loss of fine particle ammonium from denuded nylon filters. Atmospheric Environment, 40: 4797-4807.

Zellweger, C., Ammann, M., Hofer, P. and Baltensperger, U., 1999. NO_y speciation with a combined wet effluent diffusion denuder-aerosol collector coupled to ion chromatography. Atmospheric Environment, 33(7): 1131-1140.

Zhang, D.Z., Iwasaka, Y., Shi, G.Y., Zang, J.Y., Matsuki, A. and Trochkine, D., 2003. Mixture state and size of Asian dust particles collected at southwestern Japan in spring 2000. Journal of Geophysical Research-Atmospheres, 108(D24).

Zhang, R.J., Arimoto, R., An, J.L., Yabuki, S. and Sun, J.H., 2005. Ground observations of a strong dust storm in Beijing in March 2002. Journal of Geophysical Research-Atmospheres, 110(D18).

Zhang, X. and McMurry, P.H., 1987. Theoretical analysis of evaporative losses from impactor and filter deposits. Atmosperic Environment, 21: 1779-1789.

Zhang, X.Q. and McMurry, P.H., 1992. Evaporative Losses of Fine Particulate Nitrates During Sampling. Atmospheric Environment Part a-General Topics, 26(18): 3305-3312.

Zhuang, H., Chan, C.K., Fang, M. and Wexler, A.S., 1999. Formation of nitrate and non-sea-salt sulfate on coarse particles. Atmospheric Environment, 33(26): 4223-4233.

Zondlo, M.A., Barone, S.B. and Tolbert, M.A., 1997. Uptake of HNO_3 on ice under upper tropospheric conditions. Geophysical Research Letters, 24(11): 1391-1394.

Appendix A:
Detailed instrument schematics and setup information

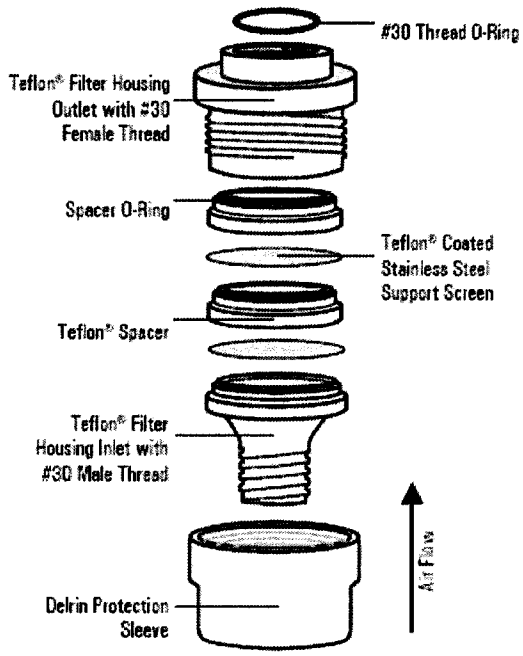

Figure A1 Detailed URG 2-stage filter pack (Adapted from URG catalog)

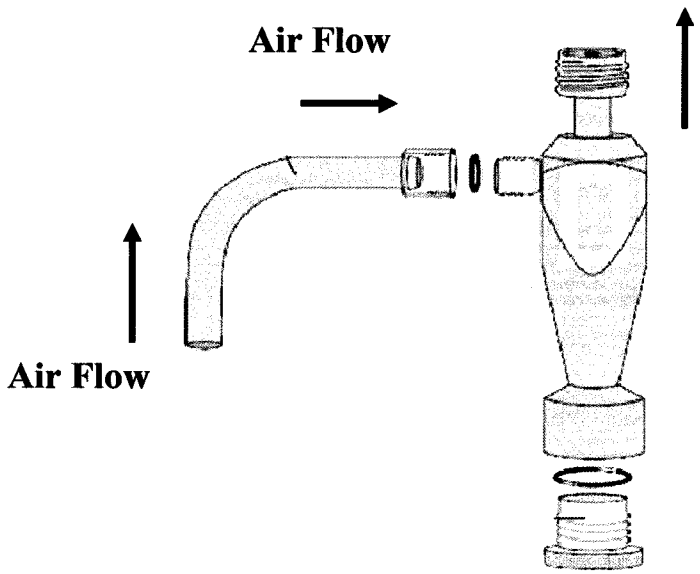

Figure A2 URG cyclone (10 lpm and 16.7 lpm for URG and PILS/IC, respectively) (Adapted from URG catalog)

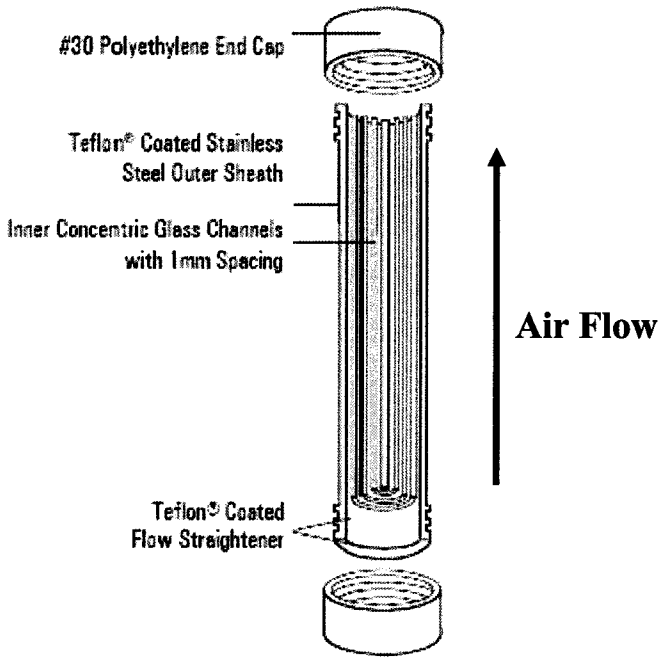

Figure A3 URG annular diffusion denuder for URG sampler and PILS/IC system (Adapted from URG catalog)

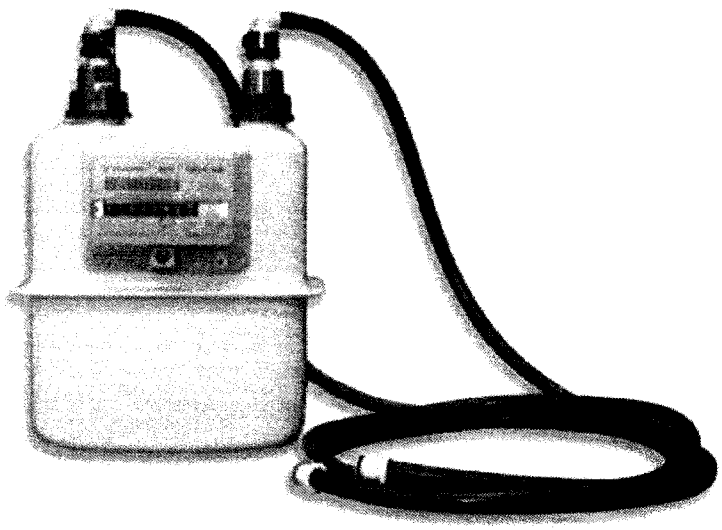

Figure A4 Dry gas meter (Gallus 2000 (ACTARIS), m^3) (Adapted from URG catalog)

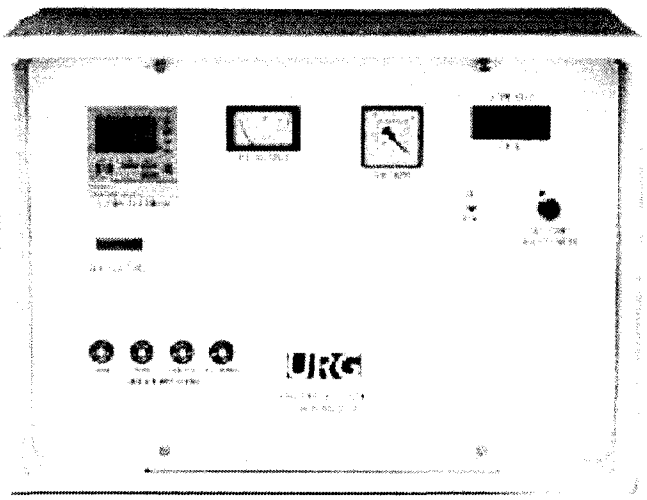

Figure A5 URG pump with mass flow controller and without temperature and pressure sensors (Adapted from URG catalog)

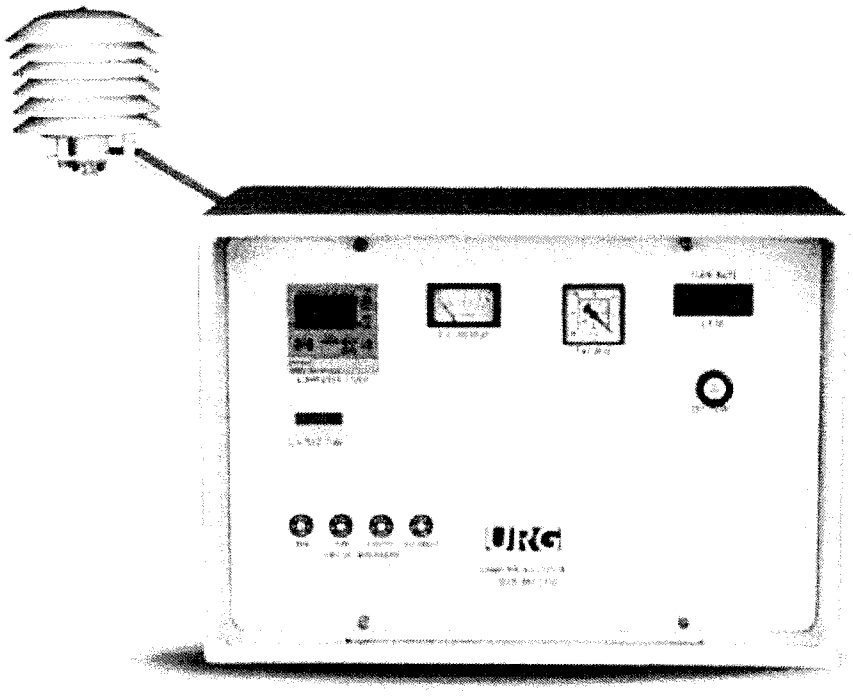

Figure A6 URG pump without mass flow controller and with temperature and pressure sensors (Adapted from URG catalog)

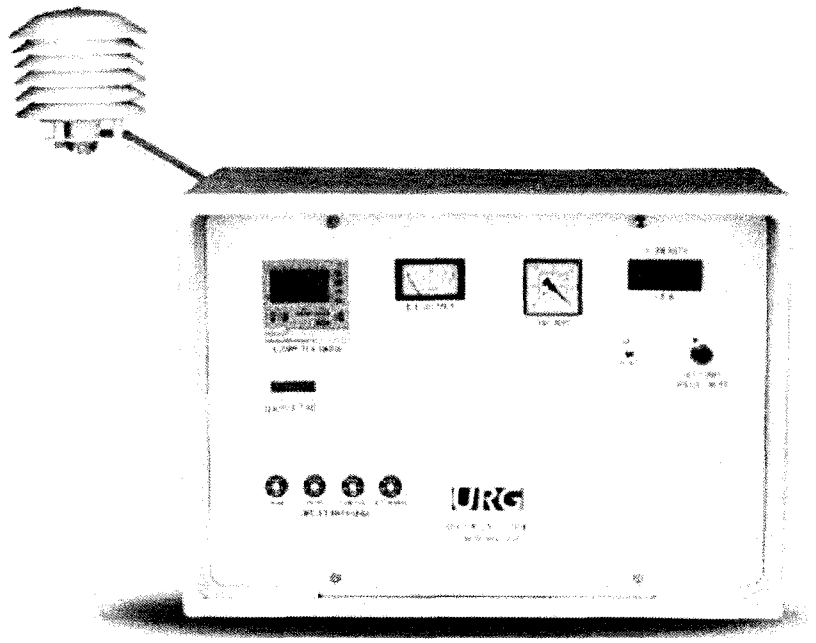

Figure A7 URG pump with mass flow controller and temperature and pressure sensors (Adapted from URG catalog)

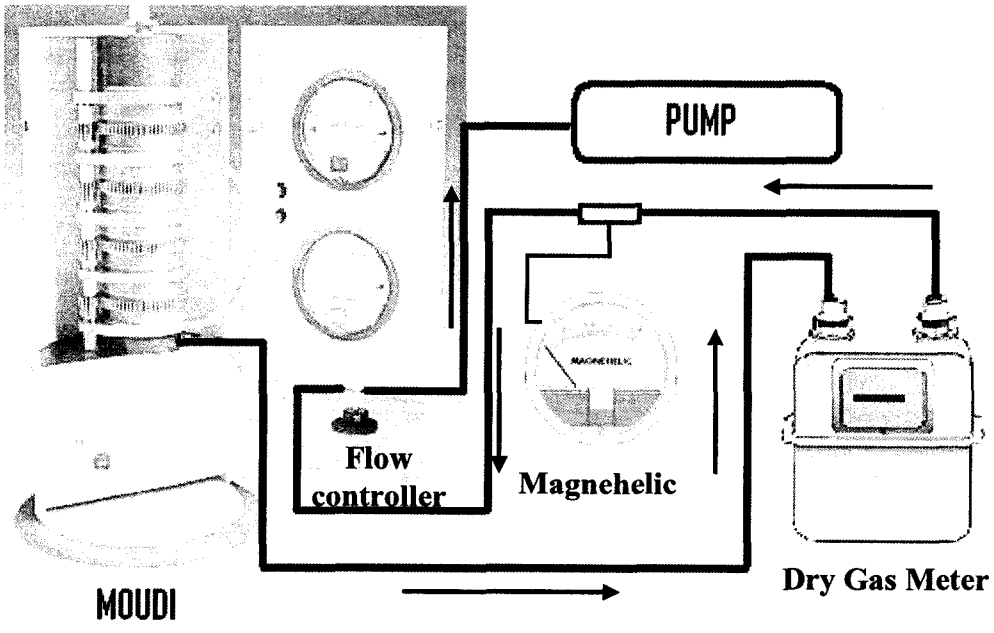

Figure A8 Typical MOUDI setup (MOUDI/dry gas meter/magnehelic/pump)

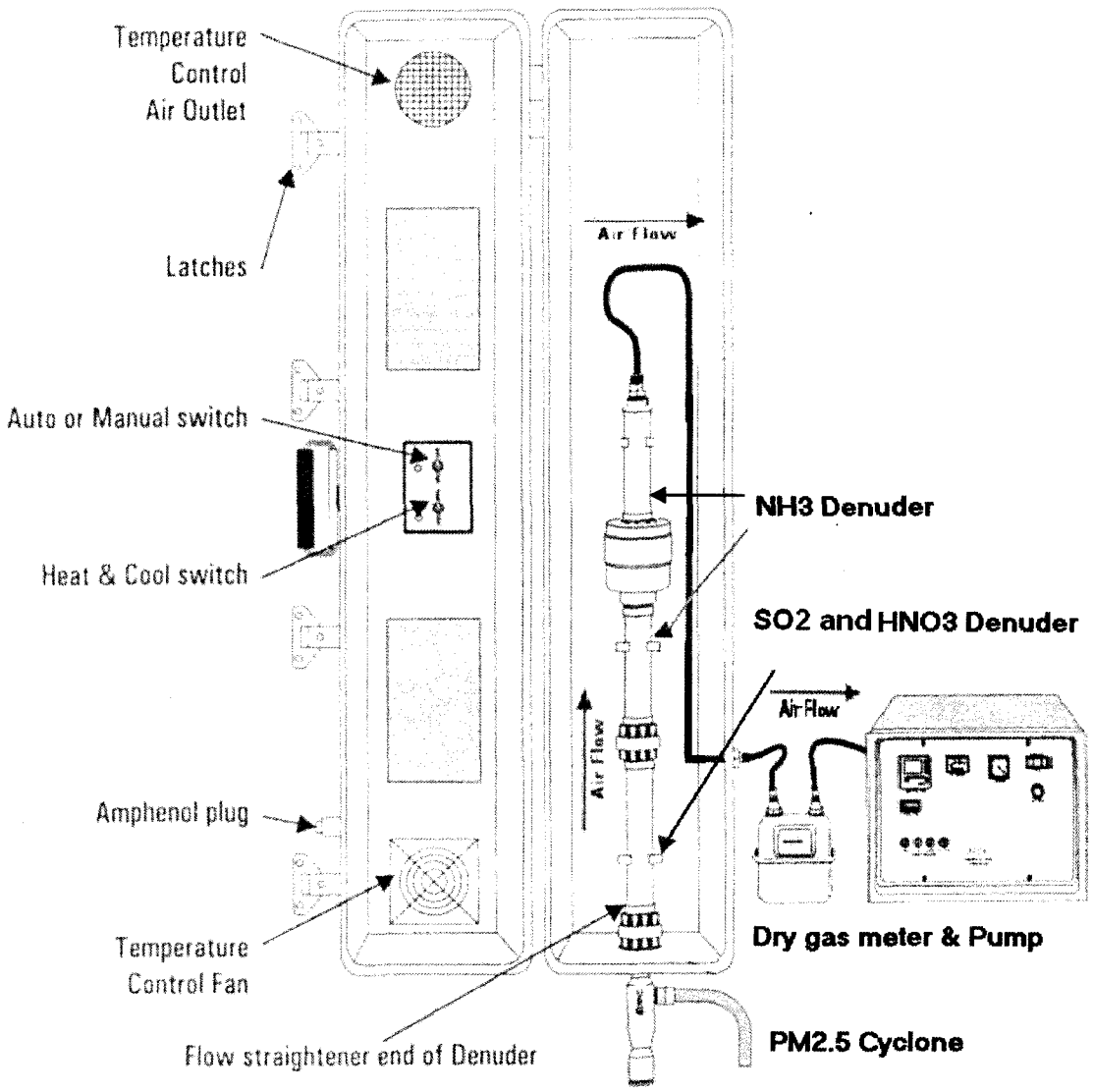

Figure A9 Typical URG sampler (cyclone/annular denuder/filter pack/dry gas meter/pump) setup

Appendix B:

Standard Operating procedures (SOP)

URG cyclone/annular denuder/filter pack sampler
Micro Orifice Uniform Deposition Impactor (MOUDI)
Particle-Into-Liquid Sampler /Ion Chromatograph (PILS/IC)

1. URG cyclone/annular denuder/filter-pack sampler

The URG denuder/filter-pack assembly is used to collect daily, 24-hour samples. Samples are run from 0800-0800 local time. Two parallel sampling trains are used to facilitate a rapid change between samples. Air is drawn through the sample train at a nominal value of 10 lpm (actual volumetric flow) in order to provide the desired 2.5 μm aerodynamic diameter size cut in the URG cyclone.

1.1 Sample train assembly

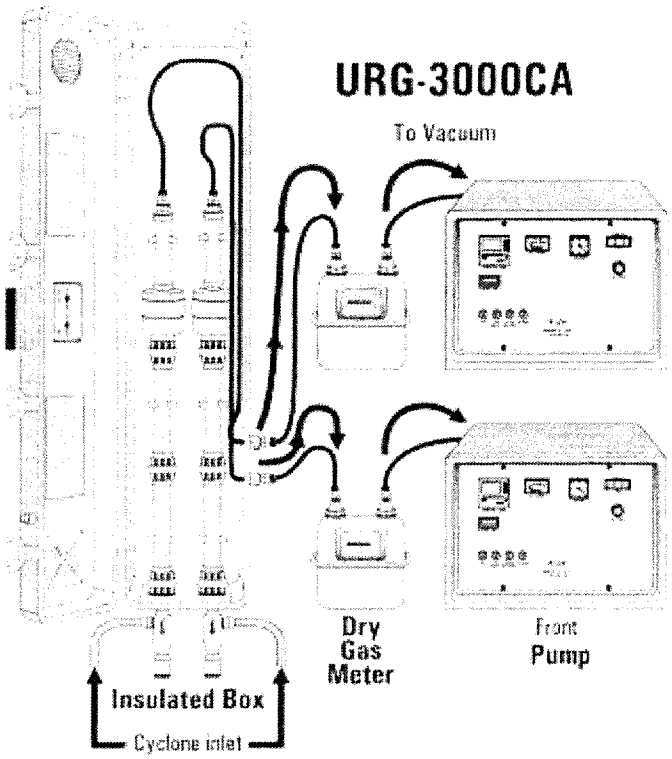

Figure B1 Schematic of the dual channel URG annular denuder/filter pack system

Air is drawn in series through two a cyclone, two 242 mm annular denuders, a 2-stage filter pack, a dry gas meter, a mass flow controller, and a vacuum pump. Figure B1, taken from the URG sampler manual, illustrates the setup except that the figure depicts three denuders in

series and a 2-stage filter pack. The flow is set at 10 actual lpm at ambient conditions using the mass flow controller, with appropriate corrections for atmospheric pressure and temperature deviations from standard conditions if necessary.

The sampling train should be assembled as follows. Clean procedures should be followed to avoid contamination of the denuders or filter pack.

- The cyclone, mounted below the sampling box, is attached to the first denuder (coated with a Na_2CO_3 solution, see below, for collection of HNO_3) using a coupler.
- The 1st denuder is connected to the 2nd denuder (coated with phosphorus acid, see below, for NH_3 collection) using a second coupler.
- The 2nd denuder screws into the bottom of the 2-stage filter pack holder which is loaded with Teflon and nylon filters (or nylon filter only in the 1st stage of the 2-stage filter pack) (in that order, from bottom to top).
- The 3rd denuder (coated with phosphorus acid, see below, for collection of NH_3 volatilized from particulate matter on the first particle collection filter) screws into the top of the 2-stage filter pack
- Tubing is connected at the top of the 3rd denuder with a quick connect. The tube passes through the sampling box and the other end connects to the inlet of the dry gas meter.
- The outlet of the dry gas meter connects to the vacuum port on the URG sampling pump assembly.

Assembly of the two denuders with the filter pack should be completed in the laboratory so that only the cyclone and tubing need to be attached outside.

1.2 Setting the flow rate

Flow is provided by a vacuum pump and controlled by a mass flow controller. A dry gas meter is installed in-line between the filter pack and mass flow controller in order to provide an integrated measure of total sample flow. The sample flow read by the dry gas meter is corrected to ambient conditions by correcting for the pressure drop through the denuders and filters. An inline pressure measurement is used to make this correction.

1.2.1 URG pump <u>with</u> mass flow controller and <u>without</u> temperature and pressure controller (model URG-3000-02BAM or URG-3000-02BBM made by URG until approximately in 2001)

The flow rate is set by adjusting the setpoint on the mass flow controller. The setpoint control is accessed on the front of the URG pump assembly (see the URG manual for details of how to adjust the setting). An estimate of ambient temperature and pressure at the sampling site is needed to choose the mass flow setpoint.

The following equation is used to determine the "Corrected Flow Rate" that should be set on the pump for atmospheric condition other than 21°C (294.18 K) and 760 mm Hg (these are the standard conditions for which the Sierra mass flow controller in the URG pump assembly is calibrated) in order to achieve an actual volumetric flow rate of 10 lpm.

$$Q_V = Q_S \cdot \left(P_s / P_I\right) \cdot \left(T_I / T_S\right) \qquad \textbf{(Eqn. B1)}$$

where

Q_S = the standard flow rate in LPM

Q_V = the desired ambient volumetric flow rate (LPM) at a given temperature, and barometric pressure

P_S = the standard condition barometric pressure (760 mm Hg)

P_I = the indicated (ambient) barometric pressure reading (in mm Hg)

T_S = the standard condition temperature (294.18 K)

T_I = the indicated temperature reading in degree Kelvin at the time of the calibrator flow reading

Table B1 illustrates mass flow setpoints determined for conditions typical of operation at the SimLab and at Big Bend National Park. Pressure differences from standard conditions due to differences in sampling altitude exert the greatest influence on the ratio of standard to actual flow rates.

For example, the mass flow controller setpoint should be adjusted to 8.71 slpm at Big Bend National Park in order to achieve a nominal actual flow rate of 10 lpm. Actual volumetric flow

will vary somewhat with temporal changes in ambient temperature and pressure. The actual sample volume will be determined from readings made with an in-line dry gas meter.

Table B1 Calculation of actual flow for ambient flow of 10 lpm

	Q_V (LPM)	P_S (mmHg)	P_I (mmHg)	T_S (K)	T_I (K)	Q_S (LPM)
Standard Conditions	10	760	760	294.18	294.18	**10**
Fort Collins, CO	10	760	637.7	294.18	300.18	**8.22**
Big Bend N.P., TX	10	760	675.2	294.18	300.18	**8.71**

1.2.2 URG pump without mass flow controller and with temperature and pressure controller (model URG-3000-02BA or URG-3000-02BB made by URG after approximately in 2001)

The differential flow meter regulates a constant differential pressure between the flow inlet and outlet, thereby maintaining a nearly constant flow in a system in which the inlet or discharge pressure is subject to fluctuations. The flow displayed on panel of pump is the actual volumetric flow rate (lpm).

1.2.3 URG pump with mass flow controller, temperature and pressure controller (model URG-3000-02BAM or URG-3000-02BBM made by URG after approximately in 2001)

The flow is set at 10 actual lpm using the mass flow controller, with appropriate corrections automatically for atmospheric pressure and temperature deviations from standard conditions by built-in temperature and pressure sensors in URG pump, thereby maintaining a nearly constant flow in a system without fluctuations during sampling. The flow displayed on panel of pump is the actual volumetric flow rate (lpm).

1.3 Sampler operation

- Before the sample begins, record the initial volume from the dry gas meter on the log sheet and reset the elapsed timer.
- Start the pump at 08:00 local time. Reset the elapsed timer on the front of the pump assembly. Record the start time, your initials, and which denuder channel (1 or 2) is used on the log sheet. Also record the denuder and filter pack serial numbers on the log sheet.
- After the pump has run a few (15-30) minutes record the following items on the log sheet
    - Initial pressure drop through the sampler assembly (read in inches of Hg from the vacuum gauge on the front of the URG pump assembly)
    - The setpoint and actual flow from the mass flow controller (displayed on the pump assembly panel; use the toggle switch to change between the flow setpoint and the actual flow reading) on the log sheet. If the set and read values for the flow differ by more than 10% the pump is having trouble achieving the desired flow. Shut the pump off (be sure to record this action and the time it is taken on the log sheet) and check for clogging of the system upstream of the mass flow controller. The most likely source of clogging is the coated glass fiber filter; try replacing it with a fresh one and restarting the pump (record on log sheet). Clogging should also be evidenced by an abnormally high reading on the vacuum gauge.
- The sample is scheduled to end at 08:00, 24 hours after it starts. A few minutes before 08:00 record the following items on the log sheet:
    - Vacuum gauge reading
    - Flow setpoint and reading from mass flow controller
- At 08:00 turn off the pump. Record the following items on the log sheet
    - Operator initials
    - Sample stop time
    - Elapsed time
    - Final reading on Dry Gas Meter

- The denuder and filter pack assembly should be removed from the sampler as soon as possible. If necessary, however, it may stay up to several hours on the sampler before retrieval. Removal is accomplished by the following steps:
    - Unscrew the coupler at the bottom of the 1st denuder and replace it with a clean cap. Cover the coupler still attached to the cyclone with a piece of clean Parafilm (the side against the paper backing is the clean side).
    - Disconnect the tubing from the filter pack and cap the top of the filter pack or cover with Parafilm.
    - Take the denuder/filter-pack assembly into the lab and place inside the ammonia-free glove box for disassembly and extraction.

Note: This procedure may be modified to automate the stop and start of the samples using the programmable capabilities of the URG pump assembly. If automation is employed, the sampler will automatically start and stop at 08:00. In this event

- the operator must be sure to reset the elapsed timer and record the initial volume from the dry gas meter in advance of the automated sample start
- the operator should note on the log sheet that automated operation is being used
- the initial vacuum gauge and flow readings should be taken as soon as possible after 08:30 and the times of these readings recorded
- the final vacuum gauge and flow readings should be taken as close to (but before!) the end of the sample period as possible and the time of the readings recorded
- the final volume should be read from the dry gas meter when the samples are retrieved

1.4 Preparation of coating and extract solutions, H^+ measurement reagents and IC eluent

1.4.1 Cleaning procedures

The procedures below outline how to clean the different sampling components used in the URG sampler and in sample handling.

- Whenever cleaning with pure water (DDW) is described, this refers to high purity deionized water taken from the Barnstead EasyPure system. The conductivity of this water should be approximately 18 Megohm-cm. If the water conductivity produced by the system drops below 17.5 Megohm-cm, the system cartridges should be replaced with identical new cartridges following the procedure specified in the Barnstead EasyPure manual.

- Whenever rinsing/washing with DDW is called for in these procedures, rinse with DDW 5-10 times.

- In all cases, **"clean" surfaces of items being cleaned should not come in contact with potential contamination sources**, including fingers, Kimwipes, unclean surfaces, etc....

- If an item must be set down, **create a clean surface by using a piece of fresh aluminum foil. Although EPA procedures call for use of Kimwipes as clean surfaces, do not use them!!!** Kimwipes contain high concentrations of soluble ions, especially sulfate!

- **Do not use Kimwipes to dry "clean" surfaces.** Air dry them. A stream of pure nitrogen is used for denuder drying.

- **Don't assume that new latex gloves are clean – they are not!** Touching of "clean" surfaces with gloves should be avoided. If this is necessary, clean the gloves first by rinsing thoroughly with DDW. After touching a clean surface it should be cleaned by thorough rinsing with DDW and allowed to air dry.

Denuder cleaning

- Clean insides of denuder caps with DDW. The inside of the cap should be treated as a "clean" surface and should never contact anything but DDW, clean aluminum foil, or a denuder. The outside of the denuder cap does not need to be extremely clean and can be handled with bare hands or gloves; occasional rinsing of the outside of denuder caps is advised, especially if they are dropped.

- Clean denuders with DDW. Denuder ends and interiors should be treated as "clean" surfaces.
    - With both caps removed, allow water to flow through denuder, alternating ends.
    - Replace bottom cap.
    - Partially fill denuder with DDW, cover open end and shake.
    - Repeat 5 times.
    - Remove bottom cap and run DDW through denuder again.
    - Shake off excess DDW and replace caps.

Cyclone cleaning

Wash cyclone cup every two weeks - more often if residue build-up is noted.

- Pull out bottom cup where large particles accumulate.
- Wash with DDW, tap upside down on clean foil surface to expel water drops, air dry, and replace on cyclone.

Wash entire cyclone once monthly.

- Remove connectors and cup and wash with DDW.
- Shake to remove excess DDW and air dry or dry with clean compressed N_2.

Coupler cleaning

End/attachment surfaces of couplers are "clean" surfaces; sides of couplers are not. Wash couplers with DDW weekly. Tap on clean foil to expel water drops and air dry. Store cleaned couplers in clean Ziploc bags or assembled with denuders.

Tweezer (forceps) cleaning

Ends of tweezers are "clean" surfaces. Clean tweezers with DDW prior to each use. Tap tweezers on clean aluminum foil to expel water drops and air dry. Store clean tweezers by wrapping in clean aluminum foil or inside clean Ziploc bags.

1.4.2 Coating procedures

Denuder coating

Denuder 1 (for HNO_3 and SO_2)

Coating solution:
0.1g Na_2CO_3
0.1g Glycerol
50mL DDW
50mL Methanol

Denuder 2 and 3 (for NH_3)

Coating solution:
0.1 g Phosphorus Acid
10mL DDW
90mL Methanol

Denuder top = labeled end, glass close to outside rim.

Denuder bottom = unlabeled end, glass ~1 inch from outside rim.

Each denuder is labeled for NH_3 or HNO_3.

Use 5 mL of coating solution to wash denuder.

- Remove top cap of clean denuder (leave bottom capped) and set denuder upright on capped end.
- Slowly pipette 5 mL of appropriate coating solution so that it will cover all surfaces.
- Replace cap.
- Hold denuder horizontally and rotate while lifting one end then the other for 1 minute to distribute the coating solution evenly.

- Remove top cap and decant excess coating solution into chemical waste container.
    - Return denuder to upright position, then decant excess coating solution again; repeat until no solution is decanted.

Use 10 mL of coating solution to coat denuder.

- Remove top cap of denuder.
- Pipette 10 mL of coating solution into denuder as described above, then rotate as described above for 1 minute.
- Remove top cap and decant excess solution into chemical waste container.
    - Return denuder to upright position, then decant excess coating solution again; repeat until no solution is decanted.

Dry denuders

NOTE: Drying manifold caps are labeled to match denuders. Each denuder must be attached to matching labeled manifold cap.

- Remove top cap of denuder and place on clean aluminum foil.
- Attach top end of each denuder to appropriately labeled drying manifold port.
- Remove bottom cap of denuder and place on clean aluminum foil.
- It is best to dry 4 denuders at once, but if only two, DO NOT cover vacant manifold ports.
- Open valve on nitrogen tank to 6 PSI flow rate. (Indicator needle on regulator is on 2nd red tick)
- Allow flow to continue for 3-4 minutes.
- Remove each denuder from drying manifold and attach opposite end to same drying manifold port.
- Allow flow from nitrogen tank to continue another 3-4 minutes.
- Close valve on nitrogen tank.
- Remove each denuder and replace top and bottom caps, making sure cap numbers match denuder number.
- Place denuders in ammonia-free hood.

1.4.3 Extraction procedure

Denuder extractions

NH_3 extraction must be done in the glove box; HNO_3 extraction can be done outside of the glove box.

1. Place clean aluminum foil on work surface.
2. Remove top cap of denuder and pipette 10mL of DDW over exposed glass surfaces.
3. Replace cap and agitate denuder for 1 minute by rotating denuder while alternately lifting each end to spread DDW evenly over all interior glass surfaces.
4. Decant extraction solution into 5mL cryovial. Label vial appropriately. Decant additional extract solution into waste container.
5. From the 5ml cryovial, pipette 600 µl into IC vial, cap and label appropriately.
6. Place both vials in appropriate racks for refrigeration.

Filter extractions

After each sampling period, the filter holder is placed in the ammonia-free glove box. Open the holder at each union and, using clean forceps, remove each filter (nylon, and Teflon) individually and place it in screw-top 16mL polystyrene tubes (Falcon), then cap. The tubes are placed in freezer until the next anion/cation extraction.

1. Turn on glove box pump and allow to run for ≥ 60 minutes.
2. Remove filters from freezer; let them sit at room temperature for 30-60 minutes.
3. Teflon and glass fiber filter extractions should be performed in the ammonia-free glove box. Nylon filters may be extracted outside the glove box.

Teflon filter extraction - I

1. Teflon filter must be coated with 50 µl of ethanol before perchloric acid extract solution (for H^+ and ionic species measurements both) or DDW (for ionic species measurement only) can be added (See Table 2.2 in chapter 2 for detail)

- With Teflon filter in tube, pipette 25 µl of ethanol onto inside surface of filter one drop at a time.
- After each drop, angle tube/filter so drop will move across filter to wet as much of surface as possible
- Repeat process one more time, each with another 25 µl of ethanol. Filter should be completely wetted at the end.

NOTE: It is difficult to wet the entire filter with 50 µl of ethanol, because the ethanol does not readily move through the Teflon membrane. Practice may be required to develop a technique that ensures proper wetting of the filter. Also, because ethanol evaporates rapidly, time required to accomplish this step should be kept to a minimum.

2. Add 4.95 ml 0.0001 N perchloric acid ($HClO_4$) (or DDW) by pipette.
   - Pipette 4.0 ml into bottle containing teflon filter, avoiding direct application to the filter.
   - Pipette 950 µL into the bottle, again avoiding direct application to the filter.
   - Replace tube cap and set aside.

Nylon filter extraction - I

1. Remove tube cap and pipette 5.0 ml of IC anion eluent ($NaHCO_3/Na_2CO_3$ aqueous solution) over nylon filter.
2. Replace tube cap and set aside.

Ultrasonic bath

1. Fill bath with water.
2. Place filter tubes into bath and run for 40 – 45 minutes.

Teflon filter extraction - II

1. Pipette 600 µl into IC vial, label and place in appropriate rack and refrigerate.
2. Pipette 1 ml of extract into each 2mL cryovials and place in appropriate rack for use in pH measurements.

3. Pipette 2 ml of extracts into 5mL cryovial, label and place in appropriate rack and refrigerate.

Nylon filter extraction - II

1. Pipette 600 µl into IC vial, label and place in appropriate rack and refrigerate.
2. Pipette 4 ml of extracts into 5mL cryovial, label and place in appropriate rack and refrigerate.

1.4.4 pH measurement

Solution

Three solutions are needed for pH measurement; these must be made daily. DDW refers to deionized water from the Barnstead EasyPure system. In all directions calling for filling a volumetric flask to the fill line, the flask should be filled until the bottom of the meniscus is at the fill line. Adding the last small portion of DDW from a small squirt bottle will enable the line to be matched more easily (thereby avoiding the need to remake solutions in which the flask has been overfilled).

Extract solution(ES)

- Pipette 200µl of 0.1 N $HClO_4$ into a 200ml polypropylene volumetric flask containing 1-2 inches of DDW.
- Fill volumetric flask to 200 ml line with DDW. Cap flask and mix thoroughly by inversion.
- Rinse 125 ml Teflon bottle with three small portions of ES solution, fill Teflon bottle with ES solution, and discard remaining ES solution.

pH Meter (Orion 250) Calibration

1. If electrode has not been stored in storage solution, let stand for 1 hour in vial containing electrode storage solution before use.
2. Prepare two 2mL cryovials each with pH 7 solution and two 2mL cryovials with pH 4 buffer solution. One cryovial will be used to wash the electrode, the other to measure pH.

3. After turning pH meter on, set to room temperature by using the ∧ or ∨ keys. Temperature is displayed after model number (250) disappears from screen.
4. Press the '2nd' key then the 'Cal' key. P1 will appear at bottom of screen.
5. Rinse electrode with DDW from a squirt bottle then place in wash vial containing pH 7 buffer solution.
6. Remove electrode from wash vial and place in pH 7 buffer measure vial.
7. When pH meter 'beeps' and displays 'Ready', record pH reading in log book.
8. Press 'Yes' key one time. P2 will appear at bottom of screen.
9. Rinse electrode with DDW then place in wash vial containing pH 4 buffer solution.
10. Remove electrode from wash vial and place in pH 4 buffer measure vial.
11. When meter 'beeps' and displays 'Ready', record pH reading in log book.
12. Press 'Yes' key two times. 'Slp will appear at bottom of screen, followed by a number. That number is the slope of the calibration line and should be ≥ 0.9. Record the value in the log book. If the slope is < 0.9 try repeating the calibration procedure. If this does not resolve the problem, try a different electrode.
13. The pH meter is now calibrated and ready to measure pH of solutions.

pH of samples

1. Locate 5 ml cryovials containing extracts of Teflon filters which are to be analyzed for pH. For each sample, label one 2 ml cryovial with the sample name and a second with the sample name plus *. Pipette 1 ml of the sample into each vial and cap. Vials labeled with a * will be used for electrode washing, the others for pH measurement.
2. Place 2ml cryovials containing samples from Teflon filter extracts in numerical order in two rows in rack, with vials marked with '*' in one row, vial without '*' in another.
3. Allow all sample vials to come to room temperature.
4. Rinse pH electrode with DDW, place in the first sample wash cryovial (labeled with a *), then place in the first sample measurement vial to measure pH.
5. When pH meter 'beeps' and displays the word 'Ready', record pH on log sheet.
6. Repeat until pH has been measured for each sample.

Checking electrode calibration

1. Using previously prepared wash and measurement buffer vials, measure the pH of the 7 and 4 buffers and record on the log sheet. If these values differ by more than +/- 0.04 from the nominal values, recalibrate the pH electrode and repeat all pH measurements (H_2SO_4 calibration standards and samples). Be sure to note this procedure was followed in the log book, mark the completed log sheet "Invalid due to pH electrode calibration drift" and use a new log sheet for the repeated measurements.
2. When pH measurements are satisfactorily completed, turn off the pH meter, rinse the electrode with DDW, and store it in electrode storage solution.

1.4.5 IC Measurement

Extracts from all the denuders and filters described in this SOP will be analyzed by ion chromatography (IC) on a Dionex Model DX500 IC using standard techniques of ion chromatography. A brief summary of methods is presented here, along with a summary of procedures for IC calibration, analysis of quality control samples, and replicate analyses, is presented here. More detailed descriptions of the operation and use of the IC itself and the accompanying PeakNet software can be found in the Dionex product manuals and in the following three CSU IC lab manuals: Practical Overview of the Ion Chromatograph, Step-by-Step IC, and Troubleshooting and Set-Up of the IC.

Method description

The instrument used for analysis of inorganic ions is a Dionex DX-500 dual channel system. One channel is dedicated to analysis of cations (Sodium, Ammonium, Potassium, Magnesium, Calcium). The other channel is dedicated to anion analysis (Chloride, Nitrate, Sulfate)

The DX-500 ion chromatograph (IC) is attached to an AS3500 autosampler which allows random access to the sampling vials. This allows you to run the same standards at the beginning and end of each run of samples. In addition, the autosampler can be programmed to automatically run duplicate samples.

To make sure that the IC is running properly, periodic duplicates are run as well as standards. At the beginning of each run of samples, regardless of whether they are run for anions or cations a DI water blank and a test standard are run to ensure the method is operating properly. A series of standards are then run from which a calibration curve will be constructed. After the calibration standards are run, samples are run in groups of approximately ten. Within each group of ten, one sample is analyzed in duplicate to gather information about the precision of the measurements. Between sample groups one or more quality control (QC) samples are run to check for drift in instrument response and as independent checks on the instrument calibration. At the end of the run, a series of standards are reanalyzed to ensure significant drift has not occurred over the course of the run. These QC standards and their placement in the analysis sequence are described in more detail in sections below.

Cations are analyzed with a Dionex CS-12 Column preceded by a CG-12 guard column, with a Dionex Cation Self Regenerating Supressor operating in Auto Suppression Recycle Mode. Detection is with a Dionex CD20 conductivity detector. 50 µl sample injections are made by the AS3500 autosampler. The cation eluent is 20 mM methanesulfonic Acid, prepared from concentrated methanesulfonic acid and DI water. 2.6 ml of concentrated MSA is added to a 2-l plastic eluent reservoir. DI water is added to the 2 l mark, and the eluent is then pressurized with helium. The pump is primed and the system is started with a flow rate of 1 ml/minute and left to equilibrate for at least one hour before starting analyses. Note the time, pressure and total conductivity in the DX-500 logbook now and periodically while the instrument is running. Expected background conductivity for the cation analysis is between 1 and 2 µS.

Anions are analyzed with a Dionex AS4A-SC Column and AG4A-SC guard column. Supression is with a Dionex Anion Self Regenerating Suppressor, and detection is by a Dionex CD20 conductivity detector. An AS3500 autosampler is used to introduce the samples into the column. Sample injection volume is 25 µl. The anion eluent is 1.8 mM Na_2CO_3/1.7 mM $NaHCO_3$. The eluent is prepared from a stock solution of 180 mM Na_2CO_3/170 mM $NaHCO_3$ (prepared by adding 19.08 g of Na_2CO_3 and 14.28 g of $NaHCO_3$ to a clean one-liter glass volumetric flask and adding deionized water to the 1 l mark). 20 ml of stock solution is added to a clean plastic 2 l eluent reservoir which is then filled with deionized water (with a conductivity of at least 18 megohm-cm) to the 2 l mark. The eluent is then pressurized with helium. The pump is primed and the system is started with a flow rate of 2 ml/minute and left to equilibrate

for at least one hour before starting analyses. The time, pressure and total conductivity are noted in the DX-500 logbook periodically while the instrument is operating. The expected background conductivity for the anion analysis is ~14 µS.

Previously prepared "IC" vials are loaded into racks of forty for the AS3500 autosampler. If samples have not been previously prepared, 500 µl of each sample is pipetted into a 500 µl sample vial and the top is securely screwed on. Sample vials are polypropylene 500 µL with screw-type polyethylene caps with Teflon/silicon/Teflon septa (supplied by the SUN division of Comar, Inc).

Standards should be loaded in autosampler tray A and samples in tray B. After a run is completed the samples should be refrigerated as soon as possible.

Calibration Standards

Stock solutions of Anions and Cations should be prepared for the analyses. The anion and cation stock solutions can be prepared in advance and stored in polyethylene bottles in the refrigerator for several weeks.

The anion stock solution is prepared as follows:

0.005 N Chloride
0.01 N Nitrate
0.01 N Sulfate

NaCl	(Sodium Chloride)	0.292 grams/liter
$NaNO_3$	(Sodium Nitrate)	0.850 grams/liter
Na_2SO_4	(Sodium Sulfate)	0.710 grams/liter

Weigh out the above chemicals and place them in a clean 1 l flask. Fill the flask half-way full with DI water and gently shake the flask to dissolve the crystals. Then fill the flask to the 1 l mark with DI water and mix by inversion.

The cation stock solution is prepared as follows:

0.005 N Calcium
0.005 N Magnesium
0.01 N Ammonium

0.005 N Sodium
0.005 N Potassium

NH_4Cl	(Ammonium Chloride)	0.535 grams/liter
NaCl	(Sodium Chloride)	0.292 grams/liter
KCl	(Potassium Chloride)	0.373 grams/liter
$MgCl_2 \cdot 6H_2O$	(Magnesium Chloride)	0.508 grams/liter
$CaCl_2 \cdot 2H_2O$	(Calcium Chloride)	0.368 grams/liter

Weigh out the above chemicals and place them in a clean 1 L flask. Fill the flask half-way full with DI water and gently shake the flask to dissolve the crystals. Then fill the flask to the 1 L mark with DI water and mix by inversion.

Preparation of standards from stock solutions

All of these dilutions are prepared in the same way. Wear clean (rinsed) latex examination gloves when preparing the standards to prevent contamination.

Use a clean pipette tip and pipette the appropriate of stock solution into a clean volumetric flask of the specified size. Fill the flask with DI water to the fill line. Mix thoroughly.

Transfer the solution to the appropriately labeled standard solution to two or three polyethylene bottles, using a small portion of standard to rinse the bottle prior to filling them. Leave one bottle in the CSU lab and take one or two bottles to the field for on-site use.

Table B2 and B3 show the standard concentrations of ions and the corresponding dilutions.

Table B2 Concentrations of anion standards

Standard Number	Concentration	Volume of Stock/flask
1	2 μN NO_3^-/ 2 μN $SO4^{2-}$ / 1 μN Cl^-	50 μl/250 ml
2	10/10/5 μN	100 μl/100 ml
3	20/20/10 μN	200 μl/100 ml
4	40/40/20 μN	400 μl/100 ml
5	100/100/50 μN	1000 μl/100 ml
6	200/200/100 μN	2000 μl/100 ml

Table B3 Concentrations of cation standards

Standard Number	Concentration	Volume of Stock/flask
1	2 μN NH_4^+/1 μN Na^+/1 μN K^+/1 μN Ca^{2+}/1 μN Mg^{2+}	50 μl/250 ml
2	4/2/2/2/2 μN	40 μl/100 ml
3	8/4/4/4/4 μN	80 μl/100 ml
4	20/10/10/10/10 μN	200 μl/100 ml
5	30/15/15/15/15 μN	300 μl/100 ml
6	40/20/20/20/20 μN	400 μl/100 ml
7	80/40/40/40/40 μN	800 μl/100 ml
8	120/60/60/60/60 μN	1200 μl/100 ml
9	160/80/80/80/80 μN	1600 μl/100 ml

QC samples and standards

The following types of QC samples/standards are analyzed as part of each IC run.

- 10% of samples are run in duplicate to establish measurement precision.
- Dilutions of NIST-traceable standards purchased from Dionex are analyzed to establish measurement accuracy for each ion.
- Low level standards and blanks/DI water are analyzed to establish analytical detection limits.
- One calibration standard (anion standard 5, cation standard 7) is run after every 10 samples to measure calibration drift within a run and to establish changes in instrument response between runs.
- Several calibration standards are reanalyzed at the end of each IC run as a second check on calibration drift.

Sample analysis schedules

For each IC run, the following analysis schedule should be used. Additional test or control samples may be added at the operator's discretion.

Injection 1:	DI water	DI water
Injection 2:	Anion standard 5	cation standard 7
Injection 3:	DI water	DI water

Injections 4 to n	Anion standards 1-6	Cation standards 1-9
Injection n+1	DI water	DI water
Injection n+2 to n+m	Dionex check standards	Dionex check standards
Injection n+m to n+m+11	Samples 1-10 plus 1 replicate	Samples 1-10 plus 1 replicate
Injection n+m+12	Anion standard 5	Cation standard 7
Injection n+m+13	DI water	DI water

After this continue running groups of 10 samples plus 1 replicate followed by a standard (anion standard 5 or cation standard 7) and DI water. At the end of the run, reanalyze all odd numbered calibration standards.

QC of calibrations and sample chromatograms

This is a brief overview of QC for IC analytical results. The operator should consult the CSU IC lab manuals for further detailed procedures.

- Check all chromatograms to ensure peaks are properly marked and integrated; adjust as needed following procedures in the CSU IC lab manuals.
- Make sure all peaks are identified properly; change component times as needed in the method to correct misidentification problems. See CSU IC lab manuals for details.
- Add the areas marked for all analyses of anion standard 5 or cation standard 7 to a project control chart. Changes in area exceeding 10% warrant further investigation. It is possible they represent a problem with the standard or a change in instrument response. Consult the project PI regarding what action to take.
- Make sure calibration curves for each ion fit closely to the calibration standards. The difference between the nominal and calculated value of each standard's ion concentrations should be less than 10% for concentrations greater than 10 μN.
- Compare the measured and nominal concentrations of the Dionex check standards. They should agree within 10% for concentrations exceeding 10 μN. Consult the project PI if larger discrepancies are observed.
- Make sure all standards > 10 μN analyzed during the run are within 10% of their nominal values. If they are not, response may have drifted warranting reanalysis of the entire run. Consult the project PI for appropriate action.

- Examine concentrations obtained for replicate analyses to ensure they agree within 10% for concentrations > 10 μN. Consult the project PI regarding appropriate action if they do not. Replicate concentrations will be used at the end of the study to establish measurement precision.

Additional QA/QC Procedures and comments

- Blanks should be taken for all filters and denuders at least once per week. Blanks are to be taken by loading denuders and filters into the sampler, leaving them there at least 1 hour, then retrieving them and processing them the same way samples are processed.

- When personnel staffing permits, duplicate denuder/filter setups should be run once per week.

- All actions taken should be recorded in the log book. Entries should include date, time, and operator name.

- All log sheets should be completed fully as actions are taken. Do not wait to make log sheet entries.

- Copies of all log sheets and log book entries should be made on a weekly basis and returned to CSU for safe keeping. All IC data should be backed up weekly to a ZIP disk or CD.

- All IC results and chromatograms and all log sheets should be punched and stored in labeled 3-hole ring binders.

2. Micro Orifice Uniform Deposition Impactor (MOUDI)

The MOUDI (Micro Orifice Uniform Deposition Impactor) sampler is used to collect size-resolved airborne particulate matter. 24 hour samples will be collected at Big Bend National Park, Texas beginning at approximately 08:00 Central Standard Time. The largest 8 stages of the MOUDI are used, corresponding to the following aerodynamic diameter size ranges: (Stage 1A) 18 – 10 μm, (Stage 2A) 10 – 5.6 μm, (Stage 3A) 5.6 – 3.2 μm, (Stage 4A) 3.2 – 1.8 μm, (Stage 5A) 1.8 – 1.0 μm, (Stage 6A) 1.0 – 0.56 μm, (Stage 7A) 0.56- 0.32 μm, (Stage 8A) 0.32 – 0.176 μm. Additionally, there is an initial stage (we will call it Stage 0) that collects particles with diameter > 18 μm and a filter at the very bottom of the MOUDI (called the after-filter) that collects particles < 0.176 μm. Analysis of the collected size-resolved PM will focus on quantification of the primary ionic species, e.g., nitrate, sulfate, ammonium, chloride, sodium, etc... MOUDI samples will be analyzed for a subset of periods when $PM_{2.5}$ aerosol chemistry measurements indicate a significant presence of both sodium and sulfate.

2.1 How does this sampler work?

The MOUDI sampler is a sequential impaction device. It works as follows:

1. A pump pulls the ambient air through an inlet which is on the roof of the CSU chemistry trailer or mobile laboratory truck. This inlet is covered with a rain shield and some aluminum bug screen.
2. The air flow is then pulled into the MOUDI sampler housing, where 9 aluminum foil impaction surfaces and after filter collect 10 size ranges of PM.
3. There are 2 magnehelics in the MOUDI sampler housing. The upper magnehelic (Magnehelic 1) measures the pressure drop across several stages. The manufacturer prescribes setting Magnehelic 1 to 23.5 inches of water, which should correspond to a 30 l/min flow rate through the MOUDI. The lower magnehelic (Magnehelic 2) measures the difference in pressure between the final stage and the ambient environment. Magnehelic 2 should read 30 inches of water when Magnehelic 1 is set to 23.5 inches of water. Magnehelic 2 is designed to be used to determine if there is a problem (clogging or leaking) inside the MOUDI sampler. If Magnehelic 2 increases

from 30, but Magnehelic 1 is still at 23.5, clogging is likely present. A low reading on magnehelic 2 suggests a leak has developed.

4. After air has transited the impaction stages and leaves the MOUDI sampler housing, the air flow is pulled through the "flow determination tubing" that leads to the pump, which is under the trailer. During this stretch, the air flow goes through Magnehelic 3, then a dry gas meter, followed by a flow control valve. Magnehelic 3 and the dry gas meter will be used with an elapsed time meter to determine the total air volume pulled through the MOUDI and to check the manufacturer's 30 l/min flow rate.

****Reminder:** This sampler is used to quantify trace levels of inorganic ionic compounds found in the airborne PM, so it is very important not to contaminate the sampler with inorganic compounds – DO NOT TOUCH the inside of the sampler or the impaction surfaces with your hands! Impaction surfaces need to be handled with clean stainless steel tweezers.

2.2 Sampling scheme

We will be collecting 24 hr (or 48 hr) samples with the MOUDI, so impaction surfaces will be changed once a day (or every other day). Impaction surfaces that are sampling the ambient air will be switched at the specified time – approximately 8 am. We have several extra impaction surface holders, so at 8 am (or as close as possible) we will remove the "used" impaction surface holders from the MOUDI and load the "new" impaction surface holders in the MOUDI. After the new impaction surfaces are readied, the MOUDI is reassembled and sampling is started. Once the MOUDI is running, remove any remaining "used" impaction surfaces from the impaction surface holders and place them into newly labeled petri dishes. At the same time, load new impaction surfaces onto the available impaction surface holders and put these holders in a clean plastic tupperware container– ready to be loaded onto the MOUDI the following day. One day a week (typically Monday), we will not run the MOUDI, but collect blanks and clean.

2.3 How do I operate the MOUDI ?

<u>At 8 am:</u>

1. Deal with the other samplers (URG, organic aerosol, and SEM denuder/filter samplers) 1st, then go to the MOUDI.
2. Take out the MOUDI log sheet and record the final magnehelic readings for all 3 magnehelics.
3. Record the dry gas meter reading.
4. Close the flow control valve.
5. Unplug the MOUDI pump.
6. Record the stop time.
7. Go to the MOUDI pump box and record the elapsed time meter reading.
8. Zero the elapsed time meter – i.e., press the red button on the elapsed time meter.
9. Go back into the trailer, it is now time to change the impaction surface holders.
10. Tear off a new, big piece of aluminum foil. This will be your work surface, and you should make it as long as the piece of tape on the MOUDI table. Set it out right in front of the piece of tape. This piece of tape is labelled "top", "0", "1", "2", …, "8" so that you can easily keep track of the MOUDI stages.
11. Remove the tubing from the MOUDI sampler housing. Get the yellow handled nut wrench out. Loosen the hose clamps at the top and bottom of the MOUDI sampler housing. Gently pull off these tubes. Also pull off the tubes that go to Magnehelics 1 and 2.
12. Briefly flip down the switch at the lower left hand corner of the MOUDI sampler housing. This will cause the MOUDI stages to rotate out of their snug fit into the housing.
13. Once the MOUDI stages are free, with 2 hands pull the stages out and set them on the aluminum foil work surface.
14. Get out and open the tupperware that contains the clean and "new" impaction surface holders.
15. Pull apart the MOUDI stages. Only touch the outside of the stages. Set each stage on the aluminum foil work surface in front of the corresponding stage number that is on the tape, so you would put the top stage in front of the "0", the next stage in front of the "1" and so on.
16. Get out a pair of clean tweezers.

17. Using the tweezers, pull the impaction surface holders off of each stage and place each directly in front of the corresponding stage.
18. Put a pair of new latex gloves on and rinse with DI water from the Barnstead EasyPure system (new latex gloves are not clean). Air dry.
19. Using the tweezers, load a "new" impaction surface holder from the tupperware onto each stage except the bottom one. Unload this surface, place the "used" impaction surface into the appropriate, labeled petri dish, reload the impaction surface holder with a clean impaction surface and load onto the bottom MOUDI stage. Procedures for loading/unloading impaction surfaces are specified below.
20. Put the stages back together in the correct order after installing after-filter on the bottom of MOUDI stage. This should be easy since they are sitting in front of you in descending order.
21. Place the stages back into the housing. Try to make the stacked stages sit against the gears.
22. Reconnect all the tubes. Be sure to snug down the hose clamps.
23. Briefly flip up the switch in the lower left hand corner of the housing. This will cause the stages to rotate together and snug in place firmly.
24. Record the new sample name on the log sheet. The sample name = SSMMDDM where SS stands for study site, MM stands for month (e.g., July = 07), DD stands for the day of the month on which the sample is started (e.g., july 4^{th} = 04), M stands for MOUDI. Individual impaction foils will be named in the same way except the impaction stage number (0-9) will be appended to the end.
25. Record the initial dry gas meter reading.
26. Plug the pump back in.
27. SLOWLY open the flow control valve until Magnehelic 1 is reading 23.5 inches of water. (Note: Magnehelic 2 should be reading 30" H_2O when you do this. If it reads higher you have a problem with one of your impaction surfaces and you need to take the MOUDI apart and realign the impaction surfaces. If an impaction surface has "popped up" it needs to be replaced with a new one. If Magnehelic 2 reads less than 30" it is likely a like has developed and you will need to regrease the MOUDI o-rings as outlined in the cleaning section.)

28. Record the start time.
29. Record the initial magnehelic readings for all 3 magnehelics.
30. Good work, now you are 1/2 way done. You must now load/unload the impaction surfaces from the impaction surface holders that you just removed from the MOUDI. Since these are currently sitting out in the open, you must do this right away.

Load/unloading impaction surfaces from the impaction surface holders:

1. Get out the 8 remaining empty petri dishes that used to contain these aluminum foil impaction plates. Label each with the names of the samples that you are about to remove (or just removed) from the sampler. Sample names= SSMMDDMS where SS stands for study site, MM stands for month (e.g., July = 07), DD stands for the day of the month the sample was started (e.g., july 4^{th} = 04), M stands for MOUDI, and S stands for stage number (which will be 0-9). If you do this early in the morning or the previous day, it is easier.
2. Get 8 new petri dishes with unused impaction sufaces and Teflon filter for after filter stage. Each aluminum foil impaction surface has been sprayed with Silicon grease and baked; it is important to make sure that you do not flip the petri dishes over.
3. Put a pair of clean gloves on, rinse with DI water, and air dry.
4. Time to swap out the "used" impaction surfaces for the "new" impaction surfaces. With the tweezers and the dental pick, pull off the ring that holds the impaction surface onto the impaction surface holder. Using the tweezers, take off the "used" impaction surface and place into the corresponding labelled petri dish. Using the tweezers, place a "new" impaction surface into the impaction surface holder. Using the tweezers and dental pick, place the hold down ring over the impaction surface and press down firmly to seal it in place. Close the petri dishes. This is a rather involved step that takes some tweezer and dental pick practice.
5. Repeat step 5 for each impaction surface holder.
6. Using the tweezers, put the impaction surface holders back into the tupperware container and seal it.
7. Place the dental pick and tweezers into the "dirty utensil tupperware".

8. Put the petri dishes with the "used" impaction surfaces into the MOUDI petri dish box in the refrigerator. Be sure they stay upright. Log these into the inventory sheet that is in the box.
9. Record the actions taken, the time, and your name in the BRAVO Ion Balance log book. If you had any problems during your switch, please write them down both in the log book and on the MOUDI log sheets.
10. Crumple up the just-used aluminum foil surface and dispose.

*** If you drop the new aluminum foil impaction surface on anything but the clean aluminum foil surface, you need to throw it away and start over.

*** If you drop a "used" impaction surface, pick it up as fast and as cleanly as possible. Record exactly what happened on the MOUDI log sheet and in the Ion Balance log book.

Every Monday:

Take a blank. You should do the same thing that you do every other day, but do not plug the MOUDI pump in. Come back to the MOUDI a little later (time delay is up to you), and swap the impaction surfaces out again. Label the blanks that you pull out of the MOUDI as "SSMMDDMSBLK", where SS stands for study site, MM stands for the month (06 = June), DD stands for the day of the month, and MS = S^{th} stage of MOUDI, and BLK = blank. You also will be cleaning, so before you install tomorrow's impaction surfaces, take the MOUDI apart.

➔ Clean the utensils, tupperware, impaction surface holders, and the MOUDI stages.

How to clean (i.e., get rid of the inorganic ionic species):

1. Locate the following items: Aluminum foil, latex gloves, DI water from the Barnstead EasyPure system, a plastic wash tub, dilute Triton X-100 solution, Q-tips, and plastic bags which can be used to cover everything while they dry. All of these items should be under the MOUDI table.
2. Spread out a piece of new aluminum foil to use as a work surface.
3. Put on the latex gloves and rinse with DI.

4. You need to determine how dirty the MOUDI is so you will know if you have to scrub the stages with soap and a Q-tip. Look at the underside of the first and last stage (stages 0 and 8). Do you see dirt around the nozzle holes? If you do, then you need to scrub. If you do not, then don't worry about the soap and Q-tips (i.e., skip ahead to step 7)
5. Fill the wash tub with DI and a small amount of Triton soap. Now scrub the underside each stage with a Q-tip in the soapy water.
6. Rinse the soapy water off completely with DI water.
7. Rinse and fill the wash tub and each tupperware container with DI.
8. Soak all the stages in the tub of DI water, and soak all the items contained in the tupperware in their respective tupperware. Rinse the tupperware a few extra times after finishing with everything else.
9. Rinse each piece thoroughly with DI after you have let them soak for at least 1 hr. Only touch the pieces with clean tweezers or tongs.
10. After rinsing, set each piece out on the aluminum foil to air dry. Place a clean plastic bag over the pieces as they dry.
11. Once dry, reassemble the sampler. Again, remember that you must use tweezers. You can't touch impaction surface holders. You can touch the outside of the stages, this will make it easier to reassemble.
12. Following cleaning, the MOUDI o-rings should be regreased with the silicone grease from the MOUDI accessories box. Remove the double O-rings from the side of each MOUDI stage. Apply a small amount of grease to your fingers and grease each O-ring, getting more grease as needed. Put the O-rings back onto the MOUDI. It is best to remove, grease, and replace O-rings one stage at a time. Disassemble the after-filter stage and grease those O-rings as well.
13. Once it is all put back together, load a new set of impaction surfaces and get ready for sampling at 8 am tomorrow.

When to clean:

Blanks should be taken and cleaning performed. The exact day is unimportant, but Monday generally works best with the rest of the activity schedule. This day can be changed if needed.

If you drop or touch the impaction surface holder, an impaction surface hold down ring, or the inside of the stages, then you need to clean them.

Troubleshooting:

Remember to record any problems and attempts to solve them in both the Ion Balance project log book and on the MOUDI log sheet.

The pump is not working.

Solution: Replace the pump. We brought 1 spare pump. You should be able to unscrew the nuts from underneath the pump box and pull the "dead" pump out of the pump box. The new pump should fit in the pump box as well as the old pump.

The elapsed time meter does not read 24 hrs after the day of sampling (accounting for any difference due to a non-08:00 start or stop time).

Solution: The pump has an automatic thermal shut down – i.e., if the pump gets too hot the pump will automatically shut down until it has cooled down. If this occurs, the elapsed time meter will show an elapsed time less than 24 hrs for the day long sample. Please record this info on the log sheet and in the log book.

The fan is not working.

***Solution*:** Check the wire connections. If they are intact and the fan still isn't working, then you need to replace the fan. Spare fans should be located with the spare pumps.

The elapsed time meter is dead.

Solution: Check the wire connections. If they are intact and the elapsed time meter still isn't working, then you need to replace it. Spare elapsed time meters should be located with the spare pumps.

The magnehelic 2 reading exceeds 30" H_2O when the sample is started.

Solution: It is likely one of the impaction surface holder rings and/or the impaction surface has popped up. Close the flow valve, unplug the pump, and disassemble the MOUDI. Replace any impaction surfaces that have popped up. Reassemble and restart the MOUDI (be sure to SLOWLY open the flow valve when starting), checking to ensure readings are now OK. Record the new start time and all actions on the log sheet and in the log book.

The magnehelic 2 reading is less than ~30" H_2O when the sample is started.

Solution: It is likely a leak has developed between stages or in the after-filter assembly. Close the flow valve, unplug the pump and disassemble the MOUDI. Remove impaction surface holders, regrease O-rings (as outlined above) and reassemble, making sure the after-filter assembly is tightly attached (the two bottom tube attachment points should be aligned). Restart the MOUDI and record the new start time and all actions on the log sheet and in the log book.

The magnehelic reading increased substantially during sampling.

***Solution*:** It is likely a clog developed during sampling or an impaction surface may have popped off. Please note the problem and any observations of possible causes on the log sheet and in the Ion Balance project log book.

3. Particle-Into-Liquid Sampler/Ion Chromatograph (PILS/IC)

PILS/IC system is used for high time resolution measurement of major ionic species of PM2.5 with 15-minute time resolution. Major ionic species include anions such as Cl^-, NO_2^-, NO_3^- and $SO_4^=$, and cations such as Na^+, NH_4^+, K^+, Mg^{2+}, and Ca^{2+}.

The instrument consists of three parts: 1) Denuders upstream of the PILS/IC system to remove gaseous species that could interference with the aerosol measurements (e.g., HNO_3, NH_3 and SO_2). 2) The particle-into-liquid sampler, which collects particles that comprise the $PM_{2.5}$ aerosol mass into a small continuous flow of high purity water. 3) A dual channel ion chromatograph (IC) for quantification of concentrations of major ionic species dissolved in the water generated by the PILS. The Particle-Into-Liquid sampler also has 3 components: the saturated vapor generator, the growth chamber and the droplet collector (impactor).

3.1 Denuder coating

Denuders used are made by URG. The procedures of the preparation and handling for denuders are the same for both the phosphorus acid and sodium carbonate coated denuder as shown in standard operating procedure (SOP) of URG sampler.

3.2 Steam generation and droplet collector (impactor)

The goal of steam generation is to heat just high enough until PILS gets a constant steam jet but not too high so that the PILS has superheated steam. The best temperature for steam generation is just above that at which the steam flow transitions from "spitting" to a steady steam jet with no liquid water.

The left hand readout of heater control box is to control heater temperature. However, the right hand readout reads temperature at the tip of the steam injector only. An appropriate temperature set for the heater (left controller) we have used is around 150 °C with readout temperatures of 90 – 100 °C at tip of steam injector. The steam jet must be centered along axis of PILS. This should be checked if any fitting have been retightened or turned.

All particles grow to droplets from water vapor condensation in the growth chamber. These droplets, which contain the ionic species, are removed by impaction. The impactor inertially collects droplets onto a vertical surface that is contained within a cavity. The impacted liquid-sample is wicked-away by a small strip of stainless steel mesh which lines the outside of the impactor cavity. At the top of the cavity, carrier solution, high purity water containing a known concentration of LiBr (an internal standard with the concentration of 8 μN or 10 μN), is introduced at 0.068 mL/min flow by a peristaltic pump. At the bottom of the cavity, carrier solution plus water from collected droplets are drawn off by peristaltic pump. Following the debubbler, the flow is split and directed to the sample loops (200 μL) of the two ICs. Figure B2 shows the example of PILS coupled with ion chromatographs for online measurements of $PM_{2.5}$ inorganic ion species and the conditions of PILS/IC operations.

3.3 Ion Chromatograph measurement

The inorganic ion analysis was completed using two DIONEX ion chromatographs. A Dionex AG4A-SC (guard column) and AS4A-SC (separation column) (or AS14A-SC) and a self-regenerating anion suppressor (4mm) are used to quantify concentrations of major anions. The setup for concentration of major cations was a CG12A (guard column) and CS12A (separation column) (or CS12A-5μm) and a self-regenerating anion suppressor (4mm) (or a self-

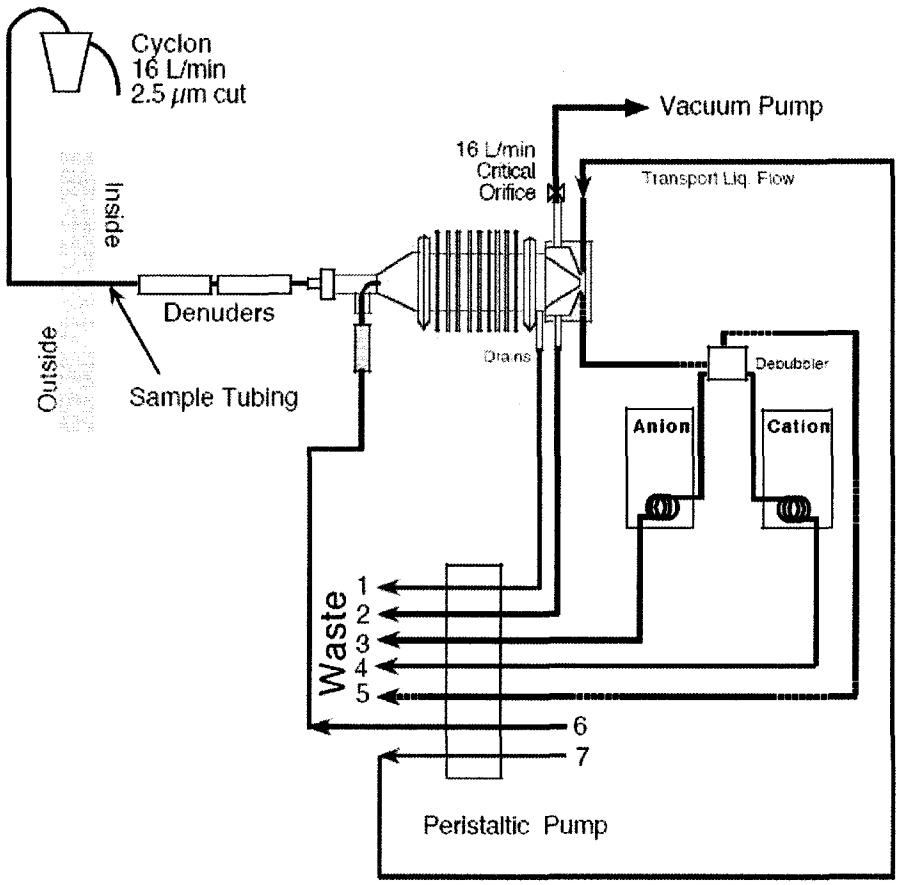

(Source : Rodney Weber)

	Steam generation	Tip of steam injector
Temperature	150 °C	89 – 100 °C
Sample loops (Anion/Cation)	200 μl / 200 μL	
Peristaltic pump	33 speed	
# in peristaltic pump	Flow, mL/min	Tubing bridge color
1 (Growth chamber drain)	1 mL/min	Gray/Gray
2 (Impactor drain)	1 mL/min	Gray/Gray
3 (Anion) (Pulling mode)	270 μL/ 15 min	Orange/Red
4 (Cation) (Pulling mode)	270 μL/ 15 min	Orange/Red
5 (Debubbler)	270 μL/ 15 min	Orange/Red
6 (Steam generation, DI water)	1 mL/min	Gray/Gray
7 (LiBr carrier solution)	0.068 mL/min	Orange/Green

Figure B2 PILS schematic and flow diagram and conditions of PILS/IC operation (Note : 3 and 4 in peristaltic pump were used by pushing mode for filling samples into anion and cation sample loops in this study)

regenerating anion suppressor for CS12A-5μm). See URG SOP in Appendix B and the DIONEX literature supplied with the columns and suppressors for making eluents and the detailed information of their operations.

Calibration Standards

Stock solutions of Anions and Cations should be prepared for the analyses. The anion and cation stock solutions can be prepared in advance and stored in polyethylene bottles in the refrigerator for several weeks.

The anion stock solution is prepared as follows:

0.005 N Chloride
0.005 N Nitrite
0.01 N Nitrate
0.01 N Sulfate
0.01 N Bromide

NaCl	(Sodium Chloride)	0.292 grams/liter
$NaNO_2$	(Sodium Nitrite)	0.345 grams/liter
$NaNO_3$	(Sodium Nitrate)	0.850 grams/liter
Na_2SO_4	(Sodium Sulfate)	0.710 grams/liter
LiBr	(Lithium Bromide)	0.8685 grams/liter

Weigh out the above chemicals and place them in a clean 1 l flask. Fill the flask half-way full with DI water and gently shake the flask to dissolve the crystals. Then fill the flask to the 1 l mark with DI water and mix by inversion.

The cation stock solution is prepared as follows:

0.005 N Calcium
0.005 N Magnesium
0.01 N Ammonium
0.005 N Sodium
0.005 N Potassium
0.01 N Lithium

NH_4Cl	(Ammonium Chloride)	0.535 grams/liter
NaCl	(Sodium Chloride)	0.292 grams/liter
KCl	(Potassium Chloride)	0.373 grams/liter

$MgCl_2 \cdot 6H_2O$	(Magnesium Chloride)	0.508 grams/liter
$CaCl_2 \cdot 2H_2O$	(Calcium Chloride)	0.368 grams/liter
LiBr	(Lithium Bromide)	0.8685 grams/liter

Weigh out the above chemicals and place them in a clean 1 L flask. Fill the flask half-way full with DI water and gently shake the flask to dissolve the crystals. Then fill the flask to the 1 L mark with DI water and mix by inversion.

All of these dilutions are prepared in the same way. Wear clean latex examination gloves when preparing the standards to prevent contaminations and use a clean pipette tip and pipette the appropriate of stock solution into a clean volumetric flask of the specified size. Fill the flask with DI water to the fill line. Mix thoroughly. Table B4 shows the standard concentrations of ions and the corresponding dilutions.

Table B4 Concentrations of anion and cation standards

Standard Number	Anion concentration	Volume of Stock (Stock of Br^-)/flask
1	2 μN NO_3^-/ 1 μN NO_2^-/ 2 μN $SO4^{2-}$ / 1 μN Cl^- / 2 μN Br^-	100 μl (100 μl)/500 ml
2	10/5/10/5/4 μN	500 μl (200 μl)/500 ml
3	20/10/20/10/8 μN	1000 μl (400 μl)/500 ml
4	40/20/40/20/10 μN	2000 μl (500 μl)/500 ml
5	100/50/100/50/20 μN	5000 μl (1000 μl)/500 ml
Standard Number	**Cation concentration**	**Volume of Stock (Stock of Li^+)/flask**
1	2 μN NH_4^+/1 μN Na^+/1 μN K^+/1 μN Ca^{2+}/1 μN Mg^{2+}/2 μN Li^+	100 μl (100 μl)/500 ml
2	10/5/5/5/5/4 μN	500 μl (200 μl)/500 ml
3	20/10/10/10/8 μN	1000 μl (400 μl)/500 ml
4	40/20/20/20/10 μN	2000 μl (500 μl)/500 ml
5	100/50/50/50/20 μN	5000 μl (1000 μl)/500 ml
Standard Number	**Internal LiBr concentration For carrier solution**	**Volume of Stock (Stock of Li^+)/flask**
	10 μN Li^+ and Br^-	1000 μl/1000 ml

Sample injection schedules

For each IC run, the following analysis schedule should be used, based on 10 days cycles. Additional test or control samples may be added at the operator's discretion.

Injection number	Anion system	Cation system
Injection 1:	DI water	DI water
Injection 2 to 6:	Anion standard 5	Cation standard 5
Injection 7:	LiBr (carrier solution)	LiBr (carrier solution)
Injection 8:	1st Blank	1st Blank
Injection 9:	2nd Blank	2nd Blank
Injection 10:	Sample	Sample
Injection 480: (5 days)	Calibration Check (Anion standard 3)	Calibration Check (Cation standard 3)
Injection 481:	1st Blank	1st Blank
Injection 482:	2nd Blank	2nd Blank
Injection 960: (10 days)	Calibration Check (Anion standard 1)	Calibration Check (Cation standard 1)
Injection 961:	Calibration Check (Anion standard 3)	Calibration Check (Cation standard 3)
Injection 962:	Calibration Check (Anion standard 5)	Calibration Check (Cation standard 5)
Injection 963:	LiBr (carrier solution)	LiBr (carrier solution)
Injection 964:	1st Blank	1st Blank
Injection 965:	2nd Blank	2nd Blank

Note : 15 minute interval between injections.

Data Management

Data management include routinely backing up data, checking integration of peaks manually since the automated integrations program can fail at low concentrations, batch processing of data to determine ambient concentrations of aerosol components in the unit of $\mu g/m^3$ and/or neq/m^3.

An excel spreadsheet containing time-resolved ion concentrations is created using the "Batch" program by the Peaknet software (DIONEX). Concentrations of standards, calibration checks, blanks and the LiBr standard are saved in a separate spreadsheet. The background concentration of each ion is subtracted before the final value of each species is reported in the unit of μN. Dilution factors (R) are calculated by the ratio of the Li^+ (or Br^-) concentration from LiBr carrier solution injections to the internal Li^+ (or Br^-) concentration in the flow to the impactor measured by the PILS/IC. PILS sampling air flow rate, PILS carrier flow rate, molecular weight and dilution factor are used to determine ambient concentrations of each species. The equation to calculate ambient aerosol concentrations from IC liquid concentration is as follows:

$$\frac{R \times C_s(\mu N) \times Q_v(L) \times MW_s(\mu g)}{Vair(m^3)} \quad \textbf{(Eqn. B2)}$$

Where:

C_S = The concentration of species measured by IC, μN
Q_V (L) = The extract volume, L (Carrier flow rate (0.068 ml/min) × 15 min)
MW_S = The molecular weight of species
V_{air} = actual sampling volume, M^3 (16.7 L/min × 15 min × 1000 m^3/L)
R (Dilution factor) = The ratio of the internal Li^+ (or Br^-) standard concentration to the Li^+ (or Br^-) concentration measured by the PILS/IC)

QA/QC procedures and comments

This is a brief overview of QC for PILS/IC operations. The following procedure should be performed during routine checks and maintenance of the instrument.

- Check all chromatogram to ensure peaks are properly marked and integrated.
- Make sure LiBr is added in carrier solution.
- Measure and record flow rates (Total flow into cyclone (16.7 L/min) by flow meter (e.g. Gillibrator) and LiBr carrier solution flow to top of impactor measuring gravimetrically)
- Check IC calibration by running standard 3 for anion cation at the beginning and every 5 days.
- Check IC calibration by running standard 3 for anion and cation. Recalibrate IC if the concentrations are off by the more than 10%. This calibration check procedure should be done at the beginning, every few days (usually whenever exchanging denuders) and at the end.
- Clean air PILS/IC blank sample should be taken immediately at the beginning and end and after the denuder change and calibration checks.
- Exchange denuders every 4 to 5 days (exchange 3 to 4 days if necessary).
- Check air flow into cyclone by flow meter at the beginning and end.
- Refill all liquid containers if needed (Eluent, DI water for steam generation and LiBr carrier solution).

Appendix C:URG data tables

Table C1 URG $PM_{2.5}$ data for anion and cation (All samples ran 08:00 – 08:00 local time)

San Gorgonio Start Date	Sampling Vol m^3	$HNO_3(g)$ $\mu g/m^3$	$SO_2(g)$ $\mu g/m^3$	$NH_3(g)$ $\mu g/m^3$	Cl^- $\mu g/m^3$	NO_3^- $\mu g/m^3$	SO_4^{2-} $\mu g/m^3$	Na^+ $\mu g/m^3$	NH_4^+ $\mu g/m^3$	K^+ $\mu g/m^3$	Mg^{2+} $\mu g/m^3$	Ca^{2+} $\mu g/m^3$
4/4/2003	13.5446	0.1885	0.1042	0.4520	0.2510	2.1601	1.0917	0.1067	1.0982	0.0206	0.0410	0.1193
4/5/2003	12.8230	0.1881	0.1013	1.3682	0.1646	2.9932	0.7856	0.0717	1.2306	0.0193	0.0316	0.1174
4/6/2003	13.1717	0.3095	0.2209	1.2643	0.1030	3.1885	0.6612	0.0615	1.2471	0.0198	0.0327	0.1221
4/7/2003	13.0587	0.2787	0.0704	0.4854	0.0195	0.3886	0.4723	0.0207	0.2697	0.0182	0.0110	0.0589
4/8/2003	13.1025	0.4204	0.1186	0.4175	0.0477	0.1694	0.4398	0.0093	0.1688	0.0115	0.0085	0.0534
4/9/2003	13.3235	1.6239	1.3968	2.2029	0.0719	14.5562	1.0233	0.0523	4.7061	0.0366	0.0535	0.2655
4/10/2003	12.6878	0.9275	0.4139	1.7510	0.0603	4.3036	0.8757	0.1142	1.5037	0.0239	0.0572	0.2061
4/11/2003	13.4447	0.6270	0.0691	1.5181	0.1039	4.4880	0.9920	0.0468	1.7482	0.0136	0.0321	0.1322
4/12/2003	13.0870	0.3114	0.0139	0.7950	0.0316	0.6670	0.4357	0.0129	0.4120	0.0184	0.0134	0.0637
4/13/2003	13.2269	0.1556	0.0250	0.8125	0.0920	0.5100	0.6061	0.0528	0.3539	0.0105	0.0204	0.0823
4/14/2003	25.7940	0.1342	0.0115	0.1170	0.0193	0.5416	0.2163	0.0231	0.2797	0.0080	0.0150	0.0661
4/16/2003	12.8897	0.3661	0.1489	1.4533	0.1538	10.1757	0.7952	0.0641	3.3927	0.0568	0.0371	0.1767
4/17/2003	12.9661	0.3743	0.1075	0.6371	0.0752	3.0149	0.6512	0.0255	1.2115	0.0094	0.0195	0.1033
4/18/2003	13.0033	0.2778	0.0695	0.8140	0.1599	2.9067	1.0468	0.0432	1.3983	0.0175	0.0333	0.1565
4/19/2003	13.1544	0.3796	0.0398	0.5265	0.0098	0.7151	0.3979	0.0225	0.3711	0.0097	0.0186	0.0975
4/20/2003	13.2841	0.4359	0.3426	1.9902	0.0550	4.4169	0.7197	0.0595	1.6030	0.0239	0.0380	0.1582
4/21/2003	12.7673	0.2313	0.0395	1.0914	0.3108	1.8364	1.4830	0.1814	1.1668	0.0259	0.0684	0.1911
4/22/2003	12.9616	0.2001	0.0626	0.6183	0.1434	1.8489	0.8323	0.0488	0.9813	0.0108	0.0268	0.1046
4/23/2003	12.9779	0.3603	0.0184	0.4664	0.1544	3.0063	0.8600	0.1217	1.2701	0.0345	0.0507	0.1605
4/24/2003	12.9981	0.4760	0.0725	0.8180	0.1554	5.3111	1.1753	0.0551	2.1501	0.0443	0.0523	0.2094
4/25/2003	13.2768	0.3167	0.0512	1.1955	0.0815	3.5084	1.2103	0.0428	1.4594	0.0302	0.0622	0.2735
4/26/2003	13.4205	0.6299	0.1234	0.6341	0.0534	3.0734	0.7693	0.0544	1.1826	0.0239	0.0511	0.2156
7/1/2003	13.7469	2.1895	0.3427	1.1509	0.0183	0.5190	1.2766	0.0603	0.5556	0.0105	0.0139	0.0663
7/2/2003	8.8454	2.7279	0.3663	1.7352	0.0275	0.9398	0.7514	0.0913	0.6432	0.0175	0.0088	0.0083
7/3/2003	12.8753	5.4426	0.8662	1.8226	0.0772	2.0335	1.0690	0.1657	1.0389	0.0285	0.0244	0.0412

7/4/2003	13.4178	4.4932	0.8044	2.2348	0.0197	1.3570	1.0006	0.1569	0.8062	0.0543	0.0229	0.0291
7/5/2003	13.2334	4.0125	0.8459	1.7583	0.0349	1.8740	1.6661	0.1763	0.8359	0.6436	0.0588	0.0187
7/6/2003	13.5342	3.2226	0.7538	3.0805	0.0574	1.6996	1.4011	0.3368	0.8717	0.1707	0.0467	0.0243
7/7/2003	12.6132	5.8225	0.6852	2.6700	0.0632	3.3701	1.9232	0.4761	1.6614	0.1640	0.0731	0.0604
7/8/2003	12.9607	6.6142	0.6175	2.6607	0.0397	1.4870	1.6254	0.3371	0.9028	0.1249	0.0396	0.0361
7/9/2003	13.5378	6.6521	0.3534	2.1798	0.0377	0.9813	1.3884	0.1274	0.8630	0.0538	0.0186	0.0302
7/10/2003	13.2147	5.6369	0.4204	1.8976	0.0176	0.4546	2.0262	0.1126	0.9081	0.0519	0.0170	0.0455
7/11/2003	13.3702	7.1736	0.6460	3.6562	0.0255	2.5007	1.8132	0.1167	1.5334	0.0859	0.0362	0.0876
7/12/2003	13.5615	7.1497	0.5738	3.3857	0.0384	1.4002	1.4409	0.1403	1.0400	0.0491	0.0216	0.0425
7/13/2003	13.5844	4.3502	0.4509	2.1314	0.0329	0.3918	1.4984	0.0996	0.7421	0.0403	0.0118	0.0240
7/14/2003	13.3733	4.4360	0.3448	1.4775	0.0252	0.2697	1.3186	0.0693	0.6351	0.0257	0.0112	0.0281
7/15/2003	13.5742	5.6080	0.8998	1.9876	0.0330	0.5497	1.8630	0.1292	0.9035	0.0610	0.0158	0.0425
7/16/2003	13.4944	4.4205	0.7554	2.5531	0.0264	0.7797	1.7499	0.1432	0.8949	0.0921	0.0208	0.0473
7/17/2003	13.7251	3.9200	0.4343	2.4323	0.0270	0.3703	1.4344	0.1050	0.8319	0.1908	0.0130	0.0500
7/18/2003	13.2877	3.4309	0.7239	3.8733	0.0392	1.9434	2.1212	0.2063	1.4766	0.1258	0.0341	0.0678
7/19/2003	13.5749	2.3343	0.5843	4.3308	0.0597	2.1303	2.3164	0.2393	2.0254	0.0965	0.0418	0.0791
7/20/2003	13.3333	3.0887	0.5688	3.5060	0.0238	1.0202	1.7580	0.1876	1.2719	0.0683	0.0309	0.0733
7/21/2003	13.5324	3.7498	0.5039	3.8249	0.0260	1.7128	1.7934	0.2289	1.7573	0.1422	0.0330	0.0891
7/22/2003	13.4886	3.3978	0.3253	2.9633	0.0229	0.9026	1.4528	0.0995	1.0183	0.0049	0.0294	0.0062
7/23/2003	13.3815	4.5116	0.6312	4.0200	0.0424	3.7359	2.0842	0.1014	2.2618	0.0468	0.0201	0.0585
7/24/2003	13.5617	5.2446	0.7139	3.6464	0.0394	2.6761	2.8459	0.1235	2.4078	0.0710	0.0264	0.0829
7/25/2003	13.5714	4.5089	0.4401	3.0229	0.0268	1.2668	2.0011	0.1094	1.4802	0.1107	0.0168	0.0461
7/26/2003	13.5427	3.8908	0.6054	4.0503	0.0350	2.1423	2.1622	0.1184	1.9668	0.0977	0.0232	0.0642
7/27/2003	13.1773	3.2455	0.4782	4.1876	0.0288	0.8594	2.0732	0.1508	1.4494	0.0756	0.0186	0.0453
7/28/2003	13.5725	3.3203	0.6482	4.5618	0.0518	2.0572	1.6727	0.1127	1.6550	0.0388	0.0174	0.0380
7/29/2003	10.5250	1.2636	0.1889	2.0704	0.0355	1.1893	1.2343	0.0513	1.4760	0.0312	0.0134	0.0318
7/30/2003	13.0901	2.0117	0.8156	2.9100	0.0776	4.9108	2.4083	0.0726	3.2541	0.0400	0.0151	0.0320
6/30/2004	13.3141	0.7048	0.1401	1.8892	0.1627	9.5118	1.7306	0.1585	3.5098	0.0428	0.0405	0.2006
7/1/2004	13.2414	1.2857	0.3847	1.9527	0.0599	5.8657	1.2926	0.0903	2.3239	0.0285	0.0342	0.2158
7/2/2004	13.2956	1.7559	0.6655	1.4851	0.0335	3.7259	1.4803	0.0888	1.6225	0.0489	0.0319	0.1684
7/3/2004	13.4114	2.0209	0.5535	1.6583	0.0462	2.1706	2.0314	0.1149	1.3623	0.0582	0.0309	0.1512
7/4/2004	13.4965	2.3400	0.6609	1.4684	0.0140	1.0651	1.8564	0.1089	1.0481	0.0841	0.0363	0.1348
7/5/2004	13.5367	2.5977	0.7895	1.7943	0.0350	2.4269	3.5326	0.1437	1.3534	1.1507	0.1513	0.1732

7/6/2004	13.5506	2.2190	0.5153	1.3541	0.0180	0.7473	1.8484	0.1146	0.8493	0.1002	0.0368	0.1452
7/7/2004	13.4379	1.9105	0.2777	1.3539	0.0564	1.5834	1.2580	0.0551	0.9322	0.0296	0.0282	0.1549
7/8/2004	12.9674	1.5520	0.2030	1.5557	0.0274	2.8749	1.1619	0.0385	1.2472	0.0176	0.0252	0.1701
7/9/2004	14.6173	1.8833	0.1913	1.4791	0.0059	0.8975	0.6860	0.0247	0.5231	0.0093	0.0215	0.1233
Grand Canyon NP	**Sampling Vol**	**$HNO_3(g)$**	**$SO_2(g)$**	**$NH_3(g)$**	**Cl^-**	**NO_3^-**	**SO_4^{2-}**	**Na^+**	**NH_4^+**	**K^+**	**Mg^{2+}**	**Ca^{2+}**
Date	**m^3**	**$\mu g/m^3$**	**$\mu g/m^3$**	**$\mu g/m^3$**	**$\mu g/m^3$**	**$\mu g/m^3$**	**$\mu g/m^3$**	**$\mu g/m^3$**	**$\mu g/m^3$**	**$\mu g/m^3$**	**$\mu g/m^3$**	**$\mu g/m^3$**
5/1/2003	13.2016	0.2624	0.1188	0.2615	0.0305	0.3403	0.4761	0.0681	0.1923	0.0117	0.0175	0.0831
5/2/2003	13.2359	0.4953	0.3266	0.2567	0.0877	0.4067	0.6591	0.1475	0.2591	0.0170	0.0315	0.1613
5/3/2003	12.9321	0.2838	0.1135	0.3025	0.0337	0.2015	0.2521	0.0317	0.1889	0.0063	0.0118	0.0793
5/4/2003	13.3267	0.1913	0.1001	0.1764	0.0305	0.2067	0.2675	0.0393	0.1402	0.0058	0.0075	0.0550
5/5/2003	12.9694	0.2721	0.1677	0.1441	0.1786	0.3679	0.9336	0.2130	0.3210	0.0888	0.0285	0.1785
5/6/2003	13.2005	0.3523	0.3108	0.2003	0.0234	0.3484	0.9149	0.0723	0.4166	0.0256	0.0223	0.1183
5/7/2003	13.0729	0.3364	0.1912	0.2820	0.0290	0.4164	0.8134	0.0809	0.4033	0.0187	0.0213	0.1051
5/8/2003	12.9188	0.3332	0.1189	0.2424	0.0523	0.5720	1.0490	0.0932	0.4933	0.0274	0.0304	0.1892
5/9/2003	12.9412	0.2117	0.1281	0.1134	0.0297	0.3367	0.6299	0.0379	0.3690	0.0259	0.0187	0.1172
5/10/2003	12.9497	0.2744	0.1237	0.1292	0.0128	0.0994	0.2979	0.0031	0.0989	0.0036	0.0035	0.0232
5/11/2003	13.1364	0.4729	0.1707	0.1307	0.0262	0.1970	0.6437	0.0421	0.2629	0.0192	0.0141	0.1013
5/12/2003	13.3397	0.5018	0.2688	0.1685	0.0303	0.2635	0.7543	0.0749	0.2874	0.0296	0.0282	0.1653
5/13/2003	13.5118	0.5566	0.1805	0.2228	0.0255	0.1873	0.6853	0.0388	0.2373	0.0261	0.0172	0.1049
5/14/2003	12.9500	0.6893	0.2204	0.2660	0.0308	0.2537	1.1274	0.0533	0.4567	0.0543	0.0280	0.1936
5/15/2003	13.0798	0.5713	0.1698	0.2743	0.0170	0.2931	0.9425	0.0397	0.3613	0.0241	0.0260	0.1474
5/16/2003	13.6465	0.5940	0.1852	0.4116	0.0202	0.2454	0.9110	0.0433	0.3919	0.0242	0.0210	0.1370
5/17/2003	13.2828	0.6486	0.3831	0.4125	0.0270	0.2909	1.1682	0.0553	0.5429	0.0511	0.0346	0.2012
5/18/2003	12.9126	0.7274	0.1710	0.3078	0.0259	0.3910	1.1555	0.0620	0.5569	0.0585	0.0330	0.1709
5/19/2003	12.9703	0.7181	0.2566	0.2441	0.0157	0.2127	0.8664	0.0291	0.4057	0.0254	0.0247	0.1705
5/20/2003	13.2510	0.8477	0.2779	0.2204	0.0239	0.1968	0.7573	0.0257	0.3760	0.0276	0.0219	0.1516
5/21/2003	13.5169	0.8699	0.2270	0.2165	0.0166	0.2900	0.7947	0.0226	0.3247	0.0244	0.0257	0.1793
5/22/2003	13.1949	0.7089	0.3353	0.4068	0.0244	0.4630	1.5767	0.0682	0.6270	0.0503	0.0486	0.3050
5/23/2003	13.4947	0.8249	0.4486	0.5169	0.0802	0.4328	1.5633	0.1282	0.7015	0.1156	0.0432	0.2398
5/24/2003	13.4401	0.6221	0.2314	0.4061	0.0824	0.3769	1.7250	0.1884	0.6486	0.0554	0.0463	0.1615
5/25/2003	13.4140	0.6815	0.2940	0.3168	0.0684	0.3867	1.8246	0.1715	0.7200	0.0588	0.0472	0.2116
5/26/2003	13.4986	0.6567	0.2273	0.3801	0.0305	0.3562	1.8055	0.1434	0.7200	0.0495	0.0433	0.1822

5/27/2003	13.5772	0.7766	0.2656	0.4191	0.0262	0.2663	1.6174	0.0928	0.6458	0.0438	0.0358	0.1800
5/28/2003	13.4870	0.8595	0.2584	0.4546	0.0207	0.1751	1.4448	0.0470	0.5628	0.0342	0.0295	0.1974
5/29/2003	13.3920	0.8449	0.2472	0.5069	0.0253	0.1845	1.2500	0.0420	0.5168	0.0232	0.0273	0.1816
5/30/2003	13.6005	0.6696	0.2066	0.6517	0.0230	0.2377	1.2457	0.0714	0.4967	0.0431	0.0342	0.1989

Bondville Date	Sampling Vol m^3	$HNO_3(g)$ $\mu g/m^3$	$SO_2(g)$ $\mu g/m^3$	$NH_3(g)$ $\mu g/m^3$	Cl^- $\mu g/m^3$	NO_3^- $\mu g/m^3$	SO_4^{2-} $\mu g/m^3$	Na^+ $\mu g/m^3$	NH_4^+ $\mu g/m^3$	K^+ $\mu g/m^3$	Mg^{2+} $\mu g/m^3$	Ca^{2+} $\mu g/m^3$
2/1/2003	8.6826	0.3781	4.2840	0.4249	0.1951	8.0371	4.7089	0.0000	4.1881	0.0815	0.0094	0.1526
2/2/2003	13.0974	0.4416	7.4550	0.6647	0.1869	6.9357	4.9749	0.0204	4.4838	0.1340	0.0107	0.1426
2/3/2003	9.1739	0.1344	1.1909	1.4291	0.0946	2.5109	4.7066	0.0287	2.6691	0.0719	0.0139	0.1809
2/4/2003	11.5811	0.3314	1.9158	0.4465	0.0253	2.2532	0.8263	0.0242	0.9576	0.0248	0.0048	0.0753
2/5/2003	12.4664	0.9116	4.1742	0.2428	0.0668	4.6730	1.0613	0.0275	1.7288	0.0345	0.0121	0.1191
2/6/2003	12.2731	0.5135	4.0796	0.2575	0.0548	8.5638	1.6528	0.0242	3.0161	0.0865	0.0152	0.1236
2/7/2003	11.7163	0.7405	5.0715	0.0526	0.0748	6.0377	1.3927	0.0385	2.1628	0.0607	0.0124	0.1171
2/8/2003	12.8508	0.6343	4.1873	0.4342	0.0854	3.7416	1.3179	0.0159	1.6130	0.0397	0.0141	0.1034
2/9/2003	13.3547	0.4777	5.0104	0.3727	0.0696	3.7848	1.5634	0.0137	1.6046	0.0556	0.0120	0.1213
2/10/2003	12.0884	0.9409	3.6187	0.2071	0.0949	2.5163	1.3588	0.0508	1.2107	0.0228	0.0071	0.1150
2/11/2003	11.4072	0.4278	4.8969	0.1831	0.0804	1.6279	0.9938	0.0326	0.8080	0.0127	-0.0086	0.1063
2/12/2003	12.0764	0.2945	2.3075	0.2753	0.0583	1.7833	0.5522	0.0322	0.6653	0.0213	0.0057	0.0753
2/13/2003	12.8557	0.4655	3.6691	0.8017	0.1296	3.2213	0.7843	0.0257	1.2754	0.0652	0.0117	0.1409
2/14/2003	13.0842	0.3570	13.9220	0.3139	0.3488	4.5070	1.5293	0.0211	1.9673	0.0615	0.0107	0.1327
2/15/2003	11.7964	1.0229	12.9829	0.1209	0.1243	2.5617	1.5969	0.0721	1.3076	0.0449	0.0197	0.1131
2/17/2003	13.1399	1.6665	17.7919	0.0312	0.0350	1.7767	6.8879	0.0564	1.4406	0.0342	0.0371	0.2719
2/18/2003	13.5374	0.7945	7.5580	0.0790	0.0511	4.8854	6.1309	0.0309	3.2667	0.0827	0.0224	0.2750
2/19/2003	13.4223	1.1136	1.0018	0.3026	0.0314	4.1976	1.1563	0.0169	1.6679	0.0474	0.0097	0.1090
2/20/2003	13.1013	1.2457	13.9615	0.5119	0.0596	4.2364	2.0290	0.0170	1.9575	0.0311	0.0112	0.1264
2/21/2003	13.2555	0.7963	15.1887	0.1143	0.2242	5.2085	6.2553	0.0030	2.5617	0.0703	0.0155	0.2226
2/22/2003	13.0349	0.6225	4.4539	0.1639	0.1534	4.5673	4.7926	0.0214	2.4720	0.0729	0.0157	0.1917
2/23/2003	13.2315	0.6913	3.7759	0.1393	0.0351	2.1449	1.9716	0.0279	1.2357	0.0298	0.0129	0.1217
2/24/2003	12.6708	0.4621	4.2282	0.0396	0.0934	3.0787	2.3303	0.0444	1.7497	0.0426	0.0086	0.1033
2/25/2003	13.0877	1.6918	20.1404	0.0397	0.0993	5.7557	3.1401	0.1162	2.5560	0.0801	0.0267	0.2165
2/26/2003	12.8945	2.2359	26.1088	0.0619	0.1644	14.4790	5.2638	0.0848	6.4019	0.1679	0.0275	0.2880
2/27/2003	13.0943	3.0452	25.7842	0.0910	0.1168	13.3966	5.8140	0.0889	6.0393	0.1780	0.0316	0.2778

Brigantine	Sampling Vol	$HNO_3(g)$	$SO_2(g)$	$NH_3(g)$	Cl^-	NO_3^-	SO_4^{2-}	Na^+	NH_4^+	K^+	Mg^{2+}	Ca^{2+}
Date	m^3	$\mu g/m^3$	$\mu g/m^3$	$\mu g/m^3$	$\mu g/m^3$	$\mu g/m^3$	$\mu g/m^3$	$\mu g/m^3$	$\mu g/m^3$	$\mu g/m^3$	$\mu g/m^3$	$\mu g/m^3$
11/5/2003	11.0786	0.4154	2.5487	0.4124	0.2662	1.8073	2.0238	0.1886	1.2998	0.0293	0.0300	0.0440
11/6/2003	10.9060	0.3371	3.8630	0.1522	0.1307	0.7222	2.2531	0.0576	1.4730	0.0395	0.0158	0.0574
11/7/2003	11.2714	1.0893	10.5851	0.1951	0.0527	1.8889	2.1743	0.0134	1.5751	0.0289	0.0123	0.0509
11/8/2003	10.9386	0.8574	6.0337	0.0638	0.0511	1.0568	1.0300	0.0330	0.7181	0.0317	0.0122	0.0447
11/9/2003	10.8577	0.4116	4.7376	0.1128	0.0491	0.7075	0.6326	0.0572	0.5675	0.0651	0.0141	0.0444
11/10/2003	11.2431	0.3788	6.8083	0.4816	0.1789	1.2457	0.7490	0.0351	1.0673	0.0593	0.0183	0.0444
11/11/2003	11.8205	0.9819	5.9724	0.5072	0.1149	1.1582	1.2393	0.1504	0.8863	0.0324	0.0250	0.0357
11/12/2003	11.8745	0.8342	4.6666	0.3402	0.1756	1.9003	1.9603	0.0905	1.4523	0.0503	0.0184	0.0426
11/13/2003	10.5745	0.4894	3.9550	0.1227	0.0275	0.5081	0.7481	0.0019	0.4145	0.0000	0.0062	0.0346
11/14/2003	11.4228	1.2659	14.4951	0.2480	0.0492	0.9132	0.8743	0.0289	1.0394	0.0387	0.0133	0.0569
11/15/2003	11.0847	0.4609	5.3881	0.4622	0.0379	1.0486	2.0437	0.0791	1.2736	0.0931	0.0534	0.2915
11/16/2003	11.4782	0.8378	10.9940	0.6210	0.0739	1.7992	2.6003	0.0411	1.6757	0.0971	0.0457	0.2679
11/17/2003	11.3209	1.9205	19.4316	0.1988	0.2799	3.7030	4.6988	0.0648	3.1935	0.0642	0.0515	0.2783
11/18/2003	11.2400	0.4856	2.5279	0.4814	0.9012	0.7606	4.1229	0.6821	1.2626	0.0402	0.1309	0.2935
11/19/2003	11.4700	0.2604	3.2498	0.3413	1.5126	1.5676	2.2181	0.8844	0.5275	0.0408	0.1548	0.2848
11/20/2003	14.7591	0.6400	9.3174	0.0966	0.0267	0.4911	1.6941	0.0142	0.7855	0.0336	0.0373	0.1953
11/21/2003	7.8008	1.2540	24.6605	0.7662	0.0428	0.8599	4.4527	0.0627	1.6654	0.0762	0.0840	0.4374
11/22/2003	11.3744	0.5564	4.6513	0.3700	0.1628	1.6414	2.4281	0.0676	1.5714	0.0421	0.0533	0.2870
11/23/2003	11.0256	0.6406	4.6364	0.2436	0.1899	0.6396	1.8979	0.2357	0.7646	0.0291	0.0780	0.2831
11/24/2003	11.2333	0.4658	3.9058	0.3631	0.9024	0.5227	1.6792	0.6534	0.4903	0.0298	0.1276	0.2887
11/25/2003	11.0179	0.4291	7.2488	0.0955	0.0724	2.0053	2.6979	0.0256	2.1284	0.0250	0.0509	0.2556
11/26/2003	11.4252	0.7165	11.7029	0.1404	0.0944	2.7174	3.7039	0.0206	2.3610	0.0295	0.0543	0.2775
11/27/2003	11.6645	1.0673	7.5142	0.2769	0.1037	1.0418	3.7780	0.1096	2.0490	0.0148	0.0548	0.2667
11/29/2003	10.9943	1.1025	11.6385	0.0447	0.0327	0.3798	2.6973	0.0326	1.0473	0.0370	0.0425	0.2321
11/30/2003	11.3093	0.9629	15.1494	0.1683	0.0637	0.4540	2.4324	0.0880	1.7048	0.0372	0.0442	0.2517
Great Smoky Mtns NP	**Sampling Vol**	$HNO_3(g)$	$SO_2(g)$	$NH_3(g)$	Cl^-	NO_3^-	SO_4^{2-}	Na^+	NH_4^+	K^+	Mg^{2+}	Ca^{2+}
Date	m^3	$\mu g/m^3$	$\mu g/m^3$	$\mu g/m^3$	$\mu g/m^3$	$\mu g/m^3$	$\mu g/m^3$	$\mu g/m^3$	$\mu g/m^3$	$\mu g/m^3$	$\mu g/m^3$	$\mu g/m^3$
7/20/2004	13.9120	1.0064	2.2890	0.2003	0.0210	0.1607	6.7986	0.0143	1.7566	0.0530	0.0470	0.0350
7/21/2004	13.6217	1.7951	5.8768	0.2591	0.0302	0.1992	10.0738	0.0392	2.7413	0.1013	0.0160	0.0460
7/22/2004	13.1907	1.2425	1.4589	0.2766	0.0234	0.1645	7.7770	0.0170	2.9966	0.0718	0.0161	0.0461

7/23/2004	13.9033	1.0982	4.2473	0.2204	0.0361	0.1713	6.7320	0.0169	2.2518	0.0667	0.0152	0.0447
7/24/2004	13.7078	1.0850	2.2883	0.1767	0.0301	0.1728	10.8024	0.0200	2.7355	0.0558	0.0155	0.0457
7/25/2004	13.3530	0.5994	0.8996	0.2602	0.0925	0.1238	6.0253	0.0208	1.6023	0.0405	0.0146	0.0216
7/26/2004	13.2656	0.3375	0.1693	0.2536	0.0396	0.0913	2.6059	0.0082	0.8817	0.0227	0.0146	0.0240
7/27/2004	13.2950	0.4486	2.1469	0.2029	0.0216	0.1493	6.0265	0.0133	1.1512	0.0269	0.0153	0.0292
7/28/2004	12.9219	1.1226	1.9822	0.2005	0.0192	0.1209	8.6634	0.0152	2.2358	0.0407	0.0157	0.0292
7/29/2004	13.3744	0.6594	0.2883	0.2630	0.0231	0.0907	5.4730	0.0269	1.4131	0.0363	0.0480	0.0115
7/30/2004	13.2245	0.3664	0.1663	0.2994	0.0680	0.2178	1.8197	0.1452	0.8226	0.0237	0.0199	0.0468
7/31/2004	13.0914	0.3368	0.1861	0.1986	0.0757	0.1492	2.4727	0.1035	0.6571	0.0208	0.0190	0.0273
8/1/2004	13.7491	0.7977	2.8032	0.1768	0.0231	0.1601	6.7352	0.0814	1.5715	0.0331	0.0175	0.0413
8/2/2004	13.4748	1.0117	3.8679	0.1138	0.0241	0.1557	7.4813	0.0351	1.5683	0.0366	0.0158	0.0439
8/3/2004	13.2461	1.6410	4.9684	0.1125	0.0211	0.1268	13.5825	0.0217	2.4260	0.0538	0.0487	0.0351
8/4/2004	13.2891	1.2499	1.9705	0.1896	0.0631	0.1826	10.0912	0.0240	2.8784	0.0536	0.0168	0.0371
8/5/2004	13.1456	0.5751	4.8910	0.1485	0.0489	0.2360	8.1997	0.0182	1.5317	0.0414	0.0152	0.0426
8/6/2004	12.7732	1.2622	6.4126	0.1165	0.0268	0.1328	5.7792	0.0230	1.2952	0.0354	0.0171	0.0272
8/7/2004	13.1493	1.0291	2.5853	0.1561	0.0368	0.1163	4.9206	0.0180	1.4829	0.0317	0.0165	0.0335
8/8/2004	13.1994	0.9431	1.3674	0.1844	0.0410	0.1224	7.0671	0.0292	2.1421	0.0412	0.0152	0.0336
8/9/2004	13.1347	0.9790	3.4640	0.2053	0.0700	0.1818	6.7824	0.0495	2.2478	0.0467	0.0162	0.0359
8/10/2004	13.2350	1.8154	6.8896	0.1885	0.0741	0.2250	11.5363	0.0760	2.6993	0.0457	0.0179	0.0319
8/11/2004	13.2864	1.0630	3.3005	0.1341	0.0383	0.1751	7.3157	0.0460	1.7747	0.0497	0.0487	0.0323
8/12/2004	13.0150	0.2367	1.7446	0.1215	0.0232	0.3921	1.7064	0.0128	0.5444	0.0255	0.0143	0.0765
8/13/2004	12.8925	1.2988	3.4858	0.2020	0.0280	0.3167	6.7479	0.0110	1.9420	0.0437	0.0167	0.0769
8/14/2004	13.1477	1.5539	3.1207	0.3403	0.0480	0.1825	8.9006	0.0129	1.9447	0.0402	0.0152	0.0456
8/15/2004	13.2014	1.4645	4.2087	0.3212	0.0593	0.1867	11.0645	0.0239	2.3171	0.0474	0.0159	0.0457
8/16/2004	13.2988	1.8010	2.2999	0.3390	0.0239	0.1772	12.7097	0.0260	2.5691	0.0520	0.0152	0.0449
8/17/2004	13.3230	1.8758	2.7835	0.2429	0.0307	0.1717	13.7556	0.0424	3.0230	0.0828	0.0163	0.0238
8/18/2004	13.2894	1.9895	2.0772	0.2363	0.0608	0.2321	10.2118	0.0300	3.0440	0.0734	0.0513	0.0449

Appendix D:URG, MOUDI and PILS/IC blank data tables

Table D1 URG $PM_{2.5}$ blank data for anion and cation

nylon filter Date	Site Name	Cl- µN	NO_3^- µN	SO_4^{2-} µN	Na^+ µN	NH_4^+ µN	K^+ µN	Mg^{2+} µN	Ca^{2+} µN
2/1/2003	Bondville	1.09	2.11	0.00	1.42	1.75	0.90	4.54	6.16
2/6/2003	Bondville	1.32	3.12	2.09	2.04	2.21	0.00	4.68	8.03
2/10/2003	Bondville	1.01	2.20	0.00	2.10	1.65	0.91	4.29	8.74
2/17/2003	Bondville	2.03	3.48	2.14	2.35	1.65	1.67	3.98	8.05
2/24/2003	Bondville	1.40	3.33	0.00	1.88	2.17	0.89	4.59	7.24
4/4/2003	San Gorgonio	1.33	0.00	0.00	1.60	0.53	0.32	2.62	8.89
4/12/2003	San Gorgonio	0.40	0.00	0.00	1.23	1.46	0.19	2.72	9.52
4/20/2003	San Gorgonio	0.00	0.00	0.00	1.69	1.49	0.00	2.12	8.48
5/1/2003	Grand Canyon NP	0.00	3.30	0.00	1.62	1.20	0.68	3.67	5.15
5/9/2003	Grand Canyon NP	0.00	0.00	0.00	2.15	1.39	0.79	3.36	6.60
5/17/2003	Grand Canyon NP	0.00	3.31	0.00	2.08	1.58	0.70	3.57	6.58
5/25/2003	Grand Canyon NP	1.35	0.00	3.83	2.35	1.25	0.77	3.47	6.21
07/01/03	San Gorgonio	0.60	1.77	1.06	1.25	4.17	1.24	5.63	7.31
07/09/03	San Gorgonio	1.01	1.92	0.00	1.09	1.18	1.07	5.59	6.54
07/17/03	San Gorgonio	0.65	1.80	1.20	2.06	1.23	1.40	5.72	6.71
07/25/03	San Gorgonio	0.61	1.85	0.00	0.89	0.00	0.89	5.52	6.29
11/12/03	Brigantine	0.62	0.25	0.00	0.94	3.84	0.00	1.36	1.18
11/20/03	Brigantine	0.44	0.00	0.00	0.38	0.42	0.00	4.65	4.38
11/29/03	Brigantine	0.67	0.36	0.00	1.55	4.72	0.00	4.25	5.27
07/20/04	Great Smoky Mtns NP	0.23	0.00	0.00	0.47	0.75	0.20	5.68	6.52
07/28/04	Great Smoky Mtns NP	0.21	0.16	0.00	0.38	0.80	0.19	5.56	6.56
08/05/04	Great Smoky Mtns NP	0.19	0.22	0.00	0.68	0.70	0.16	5.96	7.43

08/13/04	Great Smoky Mtns NP	0.36	0.19	0.00	0.71	0.64	0.35	5.35	6.04
08/14/04	Great Smoky Mtns NP	0.29	0.25	0.00	0.35	0.73	0.22	5.11	5.74

Teflon filter Date	Sample name	Cl- µN	NO_3^- µN	SO_4^{2-} µN	Na^+ µN	NH_4^+ µN	K^+ µN	Mg^{2+} µN	Ca^{2+} µN
2/3/2003	Bondville	0.63	0.00	0.81	1.10	1.10	1.33	4.24	5.21
2/8/2003	Bondville	0.00	0.00	1.04	0.94	1.15	1.37	4.29	1.61
2/12/2003	Bondville	0.43	0.00	0.00	0.94	1.10	1.32	4.12	4.38
2/21/2003	Bondville	0.88	1.12	1.28	1.22	1.13	1.33	4.21	4.56
2/26/2003	Bondville	0.50	0.00	0.81	0.80	1.11	1.29	4.07	4.20
4/5/2003	San Gorgonio	0.00	0.00	0.00	0.89	1.45	0.00	0.71	3.27
4/13/2003	San Gorgonio	0.00	0.00	0.00	1.86	0.56	0.00	1.03	4.17
4/21/2003	San Gorgonio	0.00	0.00	0.00	1.83	1.27	0.44	0.00	6.23
5/2/2003	Grand Canyon NP	0.00	0.00	0.00	0.66	0.00	0.00	0.00	2.53
5/10/2003	Grand Canyon NP	0.00	0.00	0.00	0.72	0.00	0.00	0.00	1.84
5/18/2003	Grand Canyon NP	0.00	0.00	0.00	0.90	0.00	0.65	0.00	0.96
5/26/2003	Grand Canyon NP	0.00	0.00	0.00	0.50	0.00	0.00	1.83	2.88
07/02/03	San Gorgonio	0.43	0.00	5.64	2.70	8.29	1.35	7.68	8.84
07/10/03	San Gorgonio	0.48	0.00	6.00	4.47	8.49	0.00	6.99	7.62
07/18/03	San Gorgonio	0.99	0.00	5.93	2.13	8.27	0.00	7.12	8.03
07/26/03	San Gorgonio	0.83	3.11	6.10	1.05	7.97	0.00	6.93	7.35
11/05/03	Brigantine	0.56	0.00	0.00	3.72	0.56	0.00	0.40	1.86
11/13/03	Brigantine	0.00	0.00	0.00	3.12	0.70	0.00	0.43	1.34
11/21/03	Brigantine	0.54	0.43	0.00	1.27	5.64	0.00	0.00	0.61
11/30/03	Brigantine	0.96	0.00	0.40	2.13	1.87	0.24	0.76	1.44
07/21/04	Great Smoky Mtns NP	0.29	0.32	4.13	1.79	1.25	0.46	2.60	8.24
07/28/04	Great Smoky Mtns NP	0.86	0.54	3.95	2.45	1.27	0.63	2.02	5.76
07/29/04	Great Smoky Mtns NP	1.36	0.40	3.20	3.00	2.25	0.83	2.10	6.28
08/03/04	Great Smoky Mtns NP	0.46	0.32	3.91	2.09	1.16	1.11	1.75	8.47
08/06/04	Great Smoky Mtns NP	1.43	0.40	4.26	1.91	1.16	0.57	1.37	8.19

08/17/04	Great Smoky Mtns NP	0.47	1.82	3.97	2.32	2.16	0.39	1.85	5.00
Teflon for pH Date	**Sample name**	**Cl- µN**	**NO_3^- µN**	**SO_4^{2-} µN**	**Na^+ µN**	**NH_4^+ µN**	**K^+ µN**	**Mg^{2+} µN**	**Ca^{2+} µN**
2/3/2003	Bondville	0.00	0.00	3.97	0.53	5.15	1.32	6.26	4.09
2/12/2003	Bondville	0.00	0.00	4.67	0.76	5.12	1.32	4.58	5.23
2/26/2003	Bondville	0.31	0.00	4.44	0.74	5.18	1.36	4.52	7.88
4/13/2003	San Gorgonio	0.00	0.00	0.00	1.53	0.19	0.54	3.06	8.86
4/18/2003	San Gorgonio	0.00	0.00	0.00	1.50	0.00	0.50	3.43	9.62
4/25/2003	San Gorgonio	0.00	0.00	0.00	1.30	0.25	0.30	2.79	8.94
5/14/2003	Grand Canyon NP	0.00	0.00	4.43	1.41	0.00	0.79	4.52	6.65
5/30/2003	Grand Canyon NP	0.00	0.00	0.00	2.67	0.00	1.19	3.05	6.18
07/03/03	Great Smoky Mtns NP	1.81	0.00	6.15	7.01	0.00	2.39	8.05	623
07/15/03	Great Smoky Mtns NP	0.87	0.00	9.46	2.60	0.00	1.26	6.82	8.18
07/26/03	Great Smoky Mtns NP	1.17	4.41	6.05	1.65	8.87	1.26	7.29	8.47
08/13/03	Great Smoky Mtns NP	0.63	0.00	6.80	1.27	8.25	0.00	7.03	7.58
08/10/04	Great Smoky Mtns NP	0.90	0.48	3.95	0.71	1.03	1.78	7.26	0.00

Denuders Date	**Sample name**	**NO_3(g) µN**	**SO_2(g) µN**	**NH_3 (g) µN**	**Backup NH_3 (g) µN**	**Denuders Date**	**Sample name**	**NO_3(g) µN**	**SO_2(g) µN**	**NH_3 (g) µN**	**Backup NH_3 (g) µN**
2/1/2003	Bondville	0.70	0.44	4.14	4.41	07/01/03	San Gorgonio	1.63	2.07	5.84	4.40
2/3/2003	Bondville	0.82	0.85	4.99	5.18	07/02/03	San Gorgonio	1.54	1.44	5.84	4.49
2/6/2003	Bondville	0.83	0.00	4.59	3.20	07/09/03	San Gorgonio	1.86	1.64	5.54	3.79
2/8/2003	Bondville	0.80	0.58	3.50	4.34	07/10/03	San Gorgonio	1.58	2.67	5.86	4.45
2/10/2003	Bondville	0.46	0.31	3.12	3.40	07/17/03	San Gorgonio	1.70	0.00	5.67	3.92
2/12/2003	Bondville	1.13	1.72	2.31	2.41	07/18/03	San Gorgonio	1.62	1.39	4.35	3.57
2/17/2003	Bondville	0.73	0.56	4.34	2.72	07/25/03	San Gorgonio	0.30	0.26	5.30	4.12
2/21/2003	Bondville	0.81	0.00	2.63	3.10	07/26/03	San Gorgonio	1.20	0.61	4.65	3.75
2/24/2003	Bondville	1.07	0.44	2.91	2.94	11/04/03	Brigantine	0.66	0.00	3.74	2.51
2/26/2003	Bondville	0.65	0.39	3.51	2.94	11/05/03	Brigantine	0.00	0.08	2.79	3.20
4/4/2003	San Gorgonio	0.00	0.00	2.53	2.06	11/12/03	Brigantine	0.46	0.00	3.01	2.25

4/5/2003	San Gorgonio	0.41	1.39	2.85	0.77	11/13/03	Brigantine	0.43	0.00	5.18	2.31
4/12/2003	San Gorgonio	0.00	0.00	2.30	0.90	11/20/03	Brigantine	0.37	1.05	3.33	3.27
4/13/2003	San Gorgonio	0.35	1.22	2.41	1.96	11/21/03	Brigantine	0.00	1.43	5.00	3.74
4/20/2003	San Gorgonio	0.34	0.91	2.24	2.77	11/29/03	Brigantine	0.75	0.00	3.03	2.77
4/21/2003	San Gorgonio	0.00	0.00	2.54	2.43	11/30/03	Brigantine	0.00	0.00	3.28	1.71
5/1/2003	Grand Canyon NP	0.00	0.00	3.74	3.01	07/20/04	Great Smoky Mtns NP	0.37	0.00	5.75	2.10
5/2/2003	Grand Canyon NP	0.00	0.00	3.50	3.51	07/21/04	Great Smoky Mtns NP	0.34	0.00	5.90	3.41
5/9/2003	Grand Canyon NP	0.00	0.00	3.74	3.28	07/28/04	Great Smoky Mtns NP	0.53	0.00	5.04	3.62
5/10/2003	Grand Canyon NP	0.00	0.12	3.19	2.26	07/29/04	Great Smoky Mtns NP	0.48	0.00	3.75	3.68
5/17/2003	Grand Canyon NP	0.00	0.00	5.06	3.30	08/05/04	Great Smoky Mtns NP	0.40	0.00	3.21	4.21
5/18/2003	Grand Canyon NP	0.00	0.00	2.84	2.59	08/06/04	Great Smoky Mtns NP	0.43	0.00	3.95	2.13
5/25/2003	Grand Canyon NP	0.00	0.00	5.17	2.53	08/13/04	Great Smoky Mtns NP	0.53	0.00	2.76	3.04
5/26/2003	Grand Canyon NP	0.00	0.00	2.51	2.49	08/14/04	Great Smoky Mtns NP	0.53	0.00	3.73	2.81

Table D2 MOUDI blank data for anion and cation

Bondville	Sample Stage #	Cl^- µN	NO_3^- µN	SO_4^{2-} µN	Na^+ µN	NH_4^+ µN	K^+ µN	Mg^{2+} µN	Ca^{2+} µN
2/15/2003	Stage 9	0.668	0.000	0.249	1.520	0.175	0.101	1.029	2.994
2/15/2003	Stage 8	0.000	0.446	0.000	0.280	0.153	0.000	1.296	2.574
2/15/2003	Stage 7	0.260	1.204	0.432	0.337	0.195	0.000	1.009	3.427
2/15/2003	Stage 6	1.051	0.000	0.354	1.505	0.145	0.082	0.977	3.177
2/15/2003	Stage 5	0.000	0.335	0.379	0.411	0.156	0.082	0.995	3.135
2/15/2003	Stage 4	0.373	0.000	0.304	1.196	0.379	0.155	0.981	2.993
2/15/2003	Stage 3	0.918	0.286	0.285	1.063	0.201	0.091	0.951	2.876
2/15/2003	Stage 2	0.000	0.000	0.316	0.317	0.110	0.000	1.069	2.902
2/15/2003	Stage 1	1.442	0.000	0.000	0.671	0.170	0.042	1.052	3.372
2/15/2003	Stage 0	1.439	0.937	0.417	1.813	0.215	0.331	0.924	3.713
2/15/2003	Stage 0	1.013	0.654	0.461	0.991	0.301	0.116	1.040	3.917
2/28/2003	Stage 9	0.000	0.229	0.000	1.082	0.149	0.144	1.157	3.024

2/28/2003	Stage 8	0.494	0.000	0.362	0.608	0.099	0.149	1.442	3.357
2/28/2003	Stage 7	0.853	0.360	0.372	0.332	0.288	0.251	1.266	2.797
2/28/2003	Stage 6	1.293	0.000	0.237	0.423	0.183	0.092	1.189	3.557
2/28/2003	Stage 5	1.017	0.512	0.434	0.482	0.381	0.090	0.322	3.200
2/28/2003	Stage 4	1.063	0.187	0.210	0.538	0.356	0.112	1.024	3.977
2/28/2003	Stage 3	1.137	0.139	0.097	0.499	0.329	0.137	1.569	2.637
2/28/2003	Stage 2	0.089	0.599	0.000	0.630	0.302	0.000	1.124	2.984
2/28/2003	Stage 1	0.959	0.265	0.000	0.811	0.158	0.155	0.290	2.982
2/28/2003	Stage 1	0.830	0.381	0.283	0.275	0.322	0.086	0.736	4.402
2/28/2003	Stage 0	0.312	0.730	0.556	0.452	0.271	0.000	2.187	2.884

Brigantine	Sample Name	Cl- µN	NO_3^- µN	SO_4^{2-} µN	Na^+ µN	NH_4^+ µN	K^+ µN	Mg^{2+} µN	Ca^{2+} µN
11/3/2003	Stage 0	1.299	2.147	0.000	0.000	0.714	0.000	2.452	3.007
11/3/2003	Stage 1	1.263	1.873	0.000	0.000	0.158	0.000	2.047	2.230
11/3/2003	Stage 2	1.288	1.739	0.606	0.000	0.932	0.000	1.789	1.390
11/3/2003	Stage 3	0.000	1.904	0.000	0.000	0.940	0.000	2.072	1.849
11/3/2003	Stage 4	1.560	1.815	0.000	0.000	0.091	0.000	3.976	2.565
11/3/2003	Stage 5	1.308	1.902	0.000	0.000	0.421	0.000	3.520	1.555
11/3/2003	Stage 6	1.381	2.076	0.000	0.000	1.000	0.000	2.239	2.341
11/3/2003	Stage 7	1.561	1.882	0.000	0.000	0.254	0.000	3.303	2.533
11/3/2003	Stage 8	1.220	1.229	0.000	1.253	0.021	0.000	1.724	2.067
11/3/2003	Stage 9	0.544	1.276	0.000	0.000	0.129	0.000	0.271	1.514
11/3/2003	Stage 9	0.613	1.113	0.000	0.000	0.981	0.000	0.597	1.578
11/20/2003	Stage 0	1.438	3.032	0.000	0.000	0.000	0.000	2.423	2.338
11/20/2003	Stage 1	1.687	2.799	0.000	0.000	1.021	0.000	2.749	2.758
11/20/2003	Stage 2	1.418	2.438	0.000	0.000	0.668	0.000	4.093	2.611
11/20/2003	Stage 3	1.797	3.134	1.189	0.000	0.000	0.000	3.926	2.095
11/20/2003	Stage 4	1.726	2.273	0.000	0.000	0.000	0.000	3.221	3.315
11/20/2003	Stage 5	1.067	2.675	0.000	0.000	0.567	0.000	3.217	2.499
11/20/2003	Stage 6	1.097	2.593	0.000	0.000	0.000	0.000	3.047	2.356
11/20/2003	Stage 7	1.524	3.207	0.000	0.000	0.000	0.000	3.894	2.667
11/20/2003	Stage 8	1.507	2.261	0.000	0.000	0.836	0.000	4.066	3.511
11/20/2003	Stage 9	0.527	1.789	0.000	2.615	0.758	0.011	1.377	1.368

11/20/2003	Stage 9	0.487	1.882	1.060	2.636	0.961	0.165	1.225	1.390
11/30/2003	Stage 0	1.405	1.469	0.000	0.000	0.000	0.000	2.056	2.713
11/30/2003	Stage 1	1.473	1.428	0.000	0.000	0.000	0.000	1.457	3.140
11/30/2003	Stage 2	1.247	1.749	0.000	0.000	0.000	0.000	1.731	2.370
11/30/2003	Stage 3	1.383	1.498	0.000	3.503	0.000	0.000	2.525	4.097
11/30/2003	Stage 4	1.681	1.301	0.000	0.000	0.000	0.000	2.093	2.083
11/30/2003	Stage 5	1.469	1.525	0.000	1.255	0.000	0.000	2.057	2.531
11/30/2003	Stage 6	1.397	1.921	0.000	1.741	0.000	0.000	2.432	2.508
11/30/2003	Stage 7	1.508	1.686	0.000	0.549	0.000	0.000	1.863	2.338
11/30/2003	Stage 8	1.368	1.507	0.000	0.799	0.000	0.000	1.540	4.373
11/30/2003	Stage 9	1.177	1.368	1.142	0.000	0.000	0.000	0.246	0.664
11/30/2003	Stage 9	1.170	1.332	1.299	0.000	0.000	0.000	0.245	0.532
Grand Canyon NP	**Sample Name**	**Cl- µN**	**NO_3^- µN**	**SO_4^{2-} µN**	**Na^+ µN**	**NH_4^+ µN**	**K^+ µN**	**Mg^{2+} µN**	**Ca^{2+} µN**
5/20/2003	Stage 0	0.000	0.881	0.249	0.000	0.000	0.000	2.383	1.823
5/20/2003	Stage 1	0.000	0.885	0.000	0.000	1.737	0.000	2.540	3.776
5/20/2003	Stage 2	0.000	0.000	0.432	0.000	0.000	0.000	2.486	3.387
5/20/2003	Stage 3	0.240	0.000	0.354	0.201	1.778	0.000	3.145	3.170
5/20/2003	Stage 4	0.223	0.000	0.379	0.000	1.830	0.000	2.740	3.429
5/20/2003	Stage 5	0.000	0.000	0.304	0.000	0.000	0.000	0.000	2.226
5/20/2003	Stage 6	0.000	0.000	0.285	0.000	0.000	0.000	2.619	3.260
5/20/2003	Stage 7	0.381	0.000	0.316	0.257	0.000	0.000	2.598	3.399
5/20/2003	Stage 8	0.000	1.009	0.000	0.000	1.776	0.000	2.914	3.256
5/20/2003	Stage 9	0.000	0.000	0.417	3.089	0.000	1.226	0.000	2.063
5/20/2003	Stage 9	0.000	0.000	0.461	2.257	0.000	0.989	0.000	3.240
5/17/2003	Stage 0	0.000	0.985	0.000	0.000	0.000	0.628	2.491	3.549
5/17/2003	Stage 1	0.000	1.318	0.362	0.000	0.000	0.000	2.509	2.167
5/17/2003	Stage 2	0.947	1.344	0.372	1.264	1.789	0.000	3.532	2.613
5/17/2003	Stage 3	1.155	1.537	0.237	0.000	1.757	0.000	3.087	3.097
5/17/2003	Stage 4	0.203	1.203	0.434	0.689	1.798	1.001	2.489	3.678
5/17/2003	Stage 5	0.353	1.254	0.210	0.000	1.734	0.000	2.707	2.831
5/17/2003	Stage 6	0.352	1.510	0.097	0.000	0.000	0.721	3.123	3.638
5/17/2003	Stage 7	0.000	1.343	0.000	0.000	1.742	0.000	2.479	3.699

5/17/2003	Stage 8	0.672	1.290	0.000	0.092	1.788	0.000	2.386	2.684
5/17/2003	Stage 9	1.064	0.000	0.283	1.328	1.257	1.561	2.379	3.520
5/17/2003	Stage 9	0.000	0.000	0.556	1.298	1.098	1.594	0.000	3.928
5/30/2003	Stage 0	0.461	0.000	0.372	0.475	1.757	1.012	0.000	1.745
5/30/2003	Stage 1	0.216	1.096	0.237	0.000	1.813	0.000	2.194	2.798
5/30/2003	Stage 2	1.067	0.000	0.434	1.380	0.000	1.478	2.894	3.516
5/30/2003	Stage 3	0.355	0.000	0.210	0.000	0.000	0.000	3.144	4.063
5/30/2003	Stage 4	0.000	0.000	0.097	0.000	0.000	1.282	2.567	3.480
5/30/2003	Stage 5	0.497	0.000	0.000	0.000	1.758	0.000	2.853	2.266
5/30/2003	Stage 6	0.000	0.000	0.000	0.000	1.736	0.000	3.064	1.398
5/30/2003	Stage 7	0.283	1.334	0.283	0.134	0.000	0.714	2.745	2.701
5/30/2003	Stage 8	0.000	0.000	0.556	0.000	0.000	0.000	2.758	2.135
5/30/2003	Stage 9	0.000	0.000	0.000	0.578	0.000	0.687	0.000	3.093
5/30/2003	Stage 9	0.000	0.000	0.000	0.733	0.000	0.000	0.000	2.840
Great Smoky Mtns NP	**Sample Name**	**Cl- µN**	**NO_3^- µN**	**SO_4^{2-} µN**	**Na^+ µN**	**NH_4^+ µN**	**K^+ µN**	**Mg^{2+} µN**	**Ca^{2+} µN**
7/20/2004	Stage 9	0.380	0.380	0.285	0.616	0.781	1.199	1.377	0.000
7/20/2004	Stage 8	0.727	1.019	0.316	0.350	1.603	1.438	0.235	0.000
7/20/2004	Stage 7	0.370	1.380	0.000	0.488	1.609	0.469	1.864	1.806
7/20/2004	Stage 6	0.250	0.660	0.417	0.293	0.718	0.696	0.709	0.000
7/20/2004	Stage 5	0.360	0.280	0.461	0.308	0.735	0.113	0.625	1.250
7/20/2004	Stage 4	0.320	0.000	0.000	0.404	0.691	0.385	1.190	0.000
7/20/2004	Stage 3	0.748	0.473	0.362	1.017	1.919	0.666	1.492	0.000
7/20/2004	Stage 2	2.150	0.269	0.372	2.928	1.928	0.575	0.735	1.651
7/20/2004	Stage 1	0.480	2.590	0.237	0.279	0.793	0.122	2.718	2.292
7/20/2004	Stage 0	5.826	0.566	0.434	5.416	1.351	1.024	0.961	1.573
8/6/2004	Stage 9	0.650	0.000	0.210	0.811	1.969	0.430	1.158	1.328
8/6/2004	Stage 8	0.620	1.470	0.097	0.954	0.987	0.364	1.865	2.153
8/6/2004	Stage 7	0.290	1.870	0.000	0.482	0.966	0.192	1.574	3.576
8/6/2004	Stage 6	0.840	1.980	0.000	0.414	1.088	0.225	2.585	3.598
8/6/2004	Stage 5	0.730	2.040	0.283	0.509	1.695	0.520	1.305	2.180
8/6/2004	Stage 5	0.730	2.029	0.556	0.441	1.421	0.633	1.136	1.934
8/6/2004	Stage 4	0.630	1.760	0.372	0.819	1.090	0.589	0.186	2.269

8/6/2004	Stage 3	0.491	1.186	0.237	0.593	0.857	0.348	1.373	1.014
8/6/2004	Stage 2	0.380	1.130	0.434	0.563	0.847	0.367	1.527	2.684
8/6/2004	Stage 1	0.600	0.740	0.210	0.837	0.587	0.623	1.556	3.146
8/6/2004	Stage 0	2.270	1.460	0.097	1.886	0.786	1.753	1.237	2.506
8/19/2004	Stage 9	0.367	0.000	0.423	1.011	1.654	0.201	1.875	0.000
8/19/2004	Stage 8	2.135	1.234	0.237	2.996	0.917	0.718	2.753	4.356
8/19/2004	Stage 7	0.693	0.473	0.434	0.655	0.571	1.871	2.961	0.000
8/19/2004	Stage 6	0.211	0.000	0.210	0.516	0.781	0.230	2.032	2.266
8/19/2004	Stage 5	0.724	0.805	0.097	0.377	0.910	0.068	2.449	2.269
8/19/2004	Stage 4	0.446	0.827	0.210	0.682	0.933	0.149	1.567	2.266
8/19/2004	Stage 4	0.400	0.854	0.097	0.733	0.870	0.182	2.506	2.288
8/19/2004	Stage 3	0.260	1.096	0.000	0.473	0.655	0.215	2.114	3.537
8/19/2004	Stage 2	0.400	0.607	0.000	0.807	0.614	2.046	2.509	0.000
8/19/2004	Stage 1	0.811	0.852	0.000	0.819	1.014	0.176	1.781	1.619
8/19/2004	Stage 0	0.884	0.325	0.000	0.862	0.641	0.192	1.565	2.127
San Gorgonio (April and July)	**Sample Name**	**Cl- µN**	**NO_3^- µN**	**SO_4^{2-} µN**	**Na^+ µN**	**NH_4^+ µN**	**K^+ µN**	**Mg^{2+} µN**	**Ca^{2+} µN**
4/27/2003	Stage 0	0.000	0.000	0.776	1.643	0.317	0.279	1.924	5.126
4/27/2003	Stage 1	0.000	0.321	0.500	1.200	0.327	0.112	1.914	5.254
4/27/2003	Stage 2	0.160	0.429	0.790	1.565	0.722	0.998	2.419	4.355
4/27/2003	Stage 3	0.260	0.424	0.746	1.783	0.470	0.551	2.032	4.734
4/27/2003	Stage 4	0.085	0.000	0.784	0.548	0.322	0.092	1.901	5.004
4/27/2003	Stage 5	0.135	0.000	0.480	0.439	0.585	0.137	1.794	4.880
4/27/2003	Stage 6	0.691	0.000	0.674	1.083	0.390	0.216	2.275	4.429
4/27/2003	Stage 6	0.524	0.000	0.325	1.401	0.353	0.211	1.838	4.979
4/27/2003	Stage 7	0.163	0.473	0.000	0.798	0.355	0.090	2.051	4.847
4/27/2003	Stage 8	0.125	0.000	0.000	0.550	0.614	0.073	0.271	3.801
4/27/2003	Stage 9	0.000	0.000	1.464	1.017	0.446	0.188	1.919	4.870
4/16/2003	Stage 0	0.212	0.000	1.259	0.517	0.629	0.095	2.455	5.308
4/16/2003	Stage 1	0.352	0.000	0.000	1.056	0.393	0.359	2.670	5.064
4/16/2003	Stage 2	0.088	0.000	0.000	0.342	0.484	0.025	2.510	4.524
4/16/2003	Stage 3	1.098	0.538	1.710	0.442	0.268	0.032	1.780	3.777
4/16/2003	Stage 4	0.135	0.624	1.210	1.177	0.479	0.204	2.404	4.884

4/16/2003	Stage 5	0.129	0.000	1.034	0.409	0.615	0.065	2.350	4.920
4/16/2003	Stage 6	0.332	0.502	0.000	0.447	0.724	0.012	1.624	4.469
4/16/2003	Stage 7	0.000	0.000	1.055	0.816	0.541	0.162	1.990	4.739
4/16/2003	Stage 7	0.000	0.384	0.000	1.258	0.447	0.031	1.347	4.144
4/16/2003	Stage 8	0.376	0.000	0.000	0.578	0.224	0.033	1.429	4.715
4/16/2003	Stage 9	0.000	0.000	0.000	0.480	0.261	0.050	1.773	4.705
4/4/2003	Stage 0	0.241	0.000	0.000	0.354	0.246	0.040	2.161	5.287
4/4/2003	Stage 1	0.193	0.000	1.705	0.521	0.318	0.036	2.516	5.134
4/4/2003	Stage 2	0.345	0.631	0.000	0.323	0.229	0.021	1.541	3.936
4/4/2003	Stage 3	0.522	0.000	1.474	0.341	0.162	0.000	1.635	4.502
4/4/2003	Stage 4	0.394	0.000	1.901	0.417	0.158	0.048	1.942	4.759
4/4/2003	Stage 5	0.310	0.000	1.980	0.444	0.301	0.070	1.945	4.028
4/4/2003	Stage 6	0.267	0.000	1.566	0.722	0.247	0.091	2.264	4.522
4/4/2003	Stage 7	0.352	0.696	1.149	0.668	0.339	0.185	1.579	4.184
4/4/2003	Stage 8	0.964	0.492	0.000	1.027	0.142	0.043	1.219	4.003
7/1/2003	Stage 0	0.000	0.000	0.478	0.264	0.386	0.000	0.860	2.639
7/1/2003	Stage 1	0.873	0.975	0.693	0.403	1.342	0.000	0.797	2.884
7/1/2003	Stage 2	0.946	1.342	0.982	0.261	1.613	0.000	1.012	2.709
7/1/2003	Stage 3	0.000	1.734	0.938	0.237	1.509	0.000	0.834	2.543
7/1/2003	Stage 4	1.962	1.132	0.976	1.048	0.395	0.302	0.974	2.655
7/1/2003	Stage 5	0.000	0.000	0.672	0.316	0.540	0.000	0.981	3.077
7/1/2003	Stage 6	1.156	0.951	0.867	0.279	0.498	0.000	0.829	4.736
7/1/2003	Stage 7	0.000	0.000	0.517	0.351	0.929	0.000	0.691	2.900
7/1/2003	Stage 8	0.976	0.000	0.000	1.134	0.322	0.000	0.380	2.728
7/1/2003	Stage 9	1.086	0.000	0.000	1.197	0.339	0.103	0.826	2.587
7/3/2003	Stage 0	1.451	0.000	0.656	0.352	1.303	0.000	0.810	2.101
7/3/2003	Stage 1	1.444	0.000	1.451	0.294	0.314	0.000	0.685	2.925
7/3/2003	Stage 2	1.444	0.000	0.000	0.232	1.305	0.067	0.866	2.260
7/3/2003	Stage 3	1.444	0.980	0.000	0.543	0.302	0.054	0.610	2.522
7/3/2003	Stage 4	1.451	0.000	1.903	0.732	0.385	0.172	0.383	2.346
7/3/2003	Stage 5	1.604	0.000	0.402	1.218	0.345	0.229	0.796	2.467
7/3/2003	Stage 6	0.000	0.000	0.227	0.345	0.835	0.000	0.919	2.985
7/3/2003	Stage 7	1.629	0.000	0.000	0.466	1.217	0.089	0.895	2.667

7/3/2003	Stage 8	1.600	0.000	0.247	2.101	1.206	0.324	0.754	2.887
7/3/2003	Stage 9	1.306	0.000	0.000	1.221	0.335	0.113	0.748	2.949
7/3/2003	Stage 9	1.412	0.000	0.000	1.187	0.324	0.095	0.000	2.396
7/18/2003	Stage 0	0.000	0.000	0.000	0.334	0.430	0.000	0.958	2.617
7/18/2003	Stage 1	0.000	1.726	0.000	0.383	0.307	0.000	0.996	2.197
7/18/2003	Stage 2	1.788	1.294	0.898	0.328	0.540	0.000	0.902	3.509
7/18/2003	Stage 3	1.066	1.124	0.000	0.545	0.463	0.094	1.009	3.043
7/18/2003	Stage 4	1.630	1.447	1.666	0.577	1.857	0.236	1.107	3.020
7/18/2003	Stage 5	1.741	1.014	1.093	0.647	0.827	0.000	0.984	2.601
7/18/2003	Stage 6	1.156	1.576	1.173	0.542	0.658	0.000	0.984	2.877
7/18/2003	Stage 7	1.405	1.587	0.758	0.354	0.465	0.091	1.015	3.148
7/18/2003	Stage 8	1.172	1.252	1.341	0.340	0.601	9.736	1.032	2.534
7/18/2003	Stage 9	1.125	0.000	0.000	0.928	0.987	0.100	0.674	2.514
7/18/2003	Stage 9	1.954	0.000	0.000	0.876	0.994	0.000	0.554	2.856

Table D3 PILS/IC blank data for anion and cation

Date and Time	Cl^- µN	NO_2^- µN	NO_3^- µN	SO_4^{2-} µN	Na^+ µN	NH_4^+ µN	K^+ µN	Mg^{2+} µN	Ca^{2+} µN
2/2/03 17:48	0.000	0.000	0.000	0.000	0.000	0.000	0.051	0.207	0.494
2/4/03 15:20	0.000	0.000	0.000	0.000	0.011	0.000	0.157	0.208	0.437
2/6/03 20:16	0.000	0.000	0.000	0.080	0.000	0.000	0.109	0.204	0.108
2/12/03 14:44	0.000	0.000	0.000	0.000	0.026	0.000	0.246	0.207	0.148
2/12/03 19:00	0.000	0.000	0.000	0.000	0.000	0.000	0.000	0.063	0.088
2/17/03 17:34	0.000	0.087	0.203	0.107	0.000	0.123	0.000	0.042	0.000
2/17/03 18:04	0.000	0.000	0.021	0.045	0.000	0.061	0.000	0.035	0.000
2/22/03 16:09	0.000	0.000	0.178	0.051	0.000	0.110	0.000	0.017	0.000
2/22/03 21:57	0.000	0.000	0.000	0.000	0.037	0.000	0.000	0.000	0.000
2/23/03 9:45	0.260	0.000	0.000	0.000	0.058	0.000	0.000	0.000	0.000
2/26/03 7:23	0.000	0.071	0.459	0.105	0.000	0.205	0.000	0.000	0.000
2/27/03 17:50	0.000	0.122	0.256	0.938	0.000	0.000	0.000	0.000	0.000
4/4/03 17:18	0.000	0.000	0.432	0.161	0.000	0.000	0.000	0.091	0.000

4/8/03 14:29	0.000	0.000	0.411	0.000	0.000	0.000	0.000	0.096	0.000
4/8/03 15:15	0.000	0.000	0.000	0.000	0.000	0.000	0.000	0.085	0.000
4/12/03 15:34	0.000	0.000	0.440	0.114	0.000	0.000	0.000	0.067	0.000
4/17/03 18:08	0.000	0.000	0.504	0.000	0.000	0.000	0.000	0.103	0.222
4/17/03 18:54	0.000	0.000	0.442	0.000	0.000	0.000	0.012	0.096	0.000
4/21/03 8:30	0.000	0.000	0.494	0.000	0.000	0.000	0.000	0.085	0.000
4/27/03 7:30	0.000	0.000	0.000	0.040	0.000	0.000	0.023	0.087	0.000
5/1/03 14:20	0.021	0.000	0.000	0.108	0.379	0.150	0.074	0.116	1.006
5/5/03 18:03	0.000	0.000	0.000	0.065	0.338	0.000	0.023	0.099	0.301
5/5/03 18:49	0.000	0.000	0.000	0.026	0.301	0.000	0.049	0.099	0.305
5/10/03 13:08	0.102	0.000	0.000	0.149	0.387	0.000	0.036	0.087	0.290
5/14/03 15:13	1.512	0.000	0.000	0.257	0.000	0.034	0.064	0.105	0.440
5/14/03 16:29	0.939	0.000	0.000	0.042	0.000	0.052	0.033	0.117	0.234
5/19/03 20:58	0.903	0.000	0.026	0.132	0.000	0.281	0.024	0.081	0.391
5/24/03 9:22	0.726	0.000	0.000	0.071	0.000	0.000	0.128	0.317	0.663
5/24/03 11:28	0.000	0.000	0.000	0.127	0.000	0.418	0.392	0.118	1.453
5/24/03 11:43	0.000	0.000	0.000	0.086	0.000	0.338	0.294	0.142	1.273
5/25/03 17:17	0.000	0.000	0.000	0.111	0.000	0.000	0.108	0.171	0.390
5/29/03 18:01	0.000	0.000	0.033	0.303	0.278	0.000	0.117	0.297	1.053
5/29/03 19:16	0.000	0.000	0.000	0.066	0.000	0.000	0.012	0.273	0.792
5/31/03 9:16	0.000	0.000	0.000	0.029	0.000	0.000	0.060	0.000	0.000
7/2/03 15:19	0.000	0.000	0.000	0.000	0.090	0.304	0.090	0.063	0.561
7/7/03 9:38	0.000	0.000	0.000	0.000	0.051	0.118	0.220	0.195	0.000
7/7/03 11:43	0.000	0.000	0.000	0.000	0.070	0.000	0.178	0.124	0.432
7/7/03 11:59	0.000	0.000	0.000	0.000	0.068	0.000	0.146	0.106	0.220
7/11/03 10:42	0.000	0.000	0.000	0.355	0.189	0.000	0.192	0.221	0.310
7/11/03 11:28	0.000	0.143	0.000	0.005	0.000	0.000	0.000	0.000	0.000
7/11/03 11:51	0.110	0.000	0.000	0.000	0.197	0.223	0.236	0.189	1.139
7/11/03 12:06	0.190	0.000	0.000	0.000	0.181	0.126	0.329	0.238	1.503
7/11/03 18:42	0.000	0.000	0.000	0.000	0.000	0.000	0.000	0.000	0.000
7/16/03 9:23	0.000	0.000	0.254	0.000	0.000	0.000	0.000	0.118	0.000
7/16/03 12:13	0.000	0.000	0.000	0.000	0.000	0.000	0.000	0.000	0.000
7/21/03 12:21	0.165	0.000	0.317	0.000	0.149	0.000	0.000	0.000	0.548

7/26/03 10:32	0.000	0.000	0.306	0.583	0.197	0.000	0.308	0.000	0.000
7/26/03 12:03	0.231	0.000	0.000	0.000	0.120	0.000	0.262	0.000	0.929
11/6/03 17:43	0.000	0.000	0.000	0.000	0.000	0.000	0.000	0.000	0.000
11/24/03 7:27	0.226	0.199	0.000	0.000	0.000	0.424	0.000	0.000	0.000
11/25/03 16:14	0.182	0.000	0.000	0.114	0.000	0.000	0.000	0.000	0.000
11/27/03 14:19	0.000	0.299	0.000	0.133	0.000	0.900	0.768	0.000	0.000
11/27/03 15:04	0.000	0.000	0.000	0.000	0.000	0.000	0.000	0.000	0.000
11/30/03 10:01	0.000	0.000	0.000	0.085	0.000	0.631	0.714	0.000	0.000
11/30/03 10:16	0.000	0.000	0.000	0.061	0.761	0.636	0.731	0.000	0.000

Appendix E: MOUDI data table and daily plots

Table E1 Size range for stages of MOUDI

Stage	Stage 0 (Inlet) M 0	Stage 1 M 1	Stage 2 M 2	Stage 3 M 3	Stage 4 M 4	Stage 5 M 5	Stage 6 M 6	Stage 7 M 7	Stage 8 M 8	Stage 9 (After filter) M 9
Size Range	>18 μm	10.0 – 18.0 μm	5.6 – 10.0 μm	3.2 – 5.6 μm	1.8 – 3.2 μm	1.0 – 1.8 μm	0.56 – 1.0 μm	0.32 –0.56 μm	0.18 –0.32 μm	< 0.18 μm

Table E2 MOUDI data for anion and cation

San Gorgonio (April) ng/m^3		Cl^-									
Start Date	Sampling Vol	M 9	M 8	M 7	M 6	M 5	M 4	M 3	M 2	M 1	M 0
4/4/03	78.1	0.18	2.89	52.47	9.51	17.49	40.15	75.95	22.79	3.26	1.31
4/6/03	76.4	2.58	1.52	7.78	1.12	1.28	9.71	29.86	12.85	5.33	0.61
4/8/03	76.7	0.90	1.18	3.96	9.37	1.11	3.66	12.30	10.44	3.89	4.18
4/10/03	76.4	0.32	3.58	3.74	1.91	0.42	3.68	10.50	8.11	2.34	0.69
4/12/03	76.3	0.00	0.00	1.11	0.20	6.71	18.11	21.38	4.30	3.86	0.34
4/14/03	76.1	0.00	0.00	2.02	1.31	0.30	1.00	3.67	1.45	0.71	0.54
4/16/03	75.6	0.00	3.24	4.84	1.86	2.12	6.38	14.20	5.96	0.40	0.72
4/18/03	76.6	0.74	0.00	13.26	0.56	0.34	6.53	20.39	6.18	1.05	2.84

4/20/03	75.4	0.00	1.16	16.45	8.25	42.12	61.10	72.09	13.95	1.67	1.69
4/22/03	74.4	0.00	0.00	19.22	1.78	11.54	28.80	56.25	15.01	3.18	0.31
4/24/03	74.0	0.00	0.69	6.83	1.68	1.65	7.14	20.17	16.90	0.65	1.80
4/26/03	37.4	0.00	0.00	2.74	1.14	2.91	5.69	16.09	7.67	0.75	0.32

NO_3^-										SO_4^{2-}									
M 9	M 8	M 7	M 6	M 5	M 4	M 3	M2	M 1	M 0	M 9	M 8	M 7	M 6	M 5	M 4	M 3	M 2	M 1	M 0
22.62	155.49	1066.33	322.79	239.30	206.77	146.03	22.30	5.87	6.65	77.70	56.05	509.04	205.54	49.11	24.33	29.69	3.09	1.00	0.72
10.82	55.46	555.65	249.13	100.83	159.22	130.87	28.45	6.61	4.18	93.89	40.67	266.61	113.02	20.54	22.30	16.78	2.68	1.62	0.49
63.31	338.34	1854.20	1690.39	455.99	151.45	222.72	98.53	21.05	11.23	91.48	82.14	317.32	110.04	42.72	33.41	44.78	22.82	5.07	1.08
9.84	67.06	1015.70	877.86	500.50	351.11	356.43	83.51	13.84	7.42	63.49	50.53	299.89	280.71	155.21	40.77	41.76	12.33	7.40	1.12
0.38	1.52	91.28	3.50	46.30	66.29	51.59	8.68	3.23	6.22	43.08	28.00	255.60	120.75	36.61	24.68	21.50	5.03	2.92	2.68
0.00	2.68	191.00	8.05	19.78	24.52	18.47	3.57	2.29	9.30	32.55	9.12	137.76	21.98	13.55	10.36	9.81	2.96	1.56	0.64
0.48	298.67	1904.67	1277.90	249.44	173.42	193.48	49.45	9.05	7.09	31.35	58.36	360.77	219.83	47.38	12.41	22.03	3.77	2.98	1.71
6.85	21.29	752.57	230.39	80.87	115.77	96.36	16.50	4.47	2.98	41.56	29.59	411.02	199.58	20.12	24.74	27.90	8.06	2.63	1.11
0.00	39.51	594.65	542.59	383.41	273.54	246.04	44.01	5.99	7.71	78.53	40.17	339.59	289.19	96.36	49.69	45.64	10.75	6.97	1.10
5.24	22.49	958.50	362.16	253.75	246.93	164.51	22.40	5.82	5.68	45.87	42.33	525.27	188.80	35.51	24.49	26.32	3.18	2.09	1.14
0.00	67.08	1255.85	1111.41	341.43	295.54	282.06	73.12	6.63	8.26	72.41	46.97	443.64	401.22	136.66	70.07	59.98	20.51	11.31	4.21
14.88	34.81	737.45	560.36	324.06	413.42	407.37	75.65	10.21	0.66	68.81	24.05	274.58	186.17	49.46	33.11	24.76	15.28	7.96	0.00

Na^+										NH_4^+									
M 9	M 8	M 7	M 6	M 5	M 4	M 3	M 2	M 1	M 0	M 9	M 8	M 7	M 6	M 5	M 4	M 3	M 2	M 1	M 0
0.54	0.08	1.72	4.19	42.96	61.78	65.54	14.97	5.24	0.45	32.49	68.77	533.28	154.42	45.74	17.51	9.71	2.38	0.48	0.24
2.58	0.19	1.77	2.07	10.42	26.38	36.36	9.03	1.44	0.64	34.73	33.47	270.03	105.95	23.11	17.93	10.10	3.31	0.96	0.57
3.28	0.57	3.23	3.14	14.74	16.29	27.34	13.67	3.08	1.38	55.86	129.35	898.17	629.95	124.65	21.32	28.91	12.27	2.88	0.94
2.09	2.31	1.78	4.41	28.77	50.53	58.49	14.57	2.24	0.51	27.88	40.69	435.45	364.42	163.44	43.14	27.74	6.64	1.30	0.36
1.09	0.22	1.22	2.05	18.28	22.03	17.65	2.47	1.93	0.03	17.15	10.55	115.28	38.59	2.68	0.66	0.93	3.20	0.71	0.08
0.33	0.38	1.17	0.43	3.19	4.68	4.97	0.99	0.09	0.32	15.25	5.40	107.78	10.23	1.84	0.92	0.94	0.14	0.04	0.05
0.26	1.78	0.46	1.72	12.95	24.72	37.58	10.39	0.42	0.99	13.62	105.45	897.25	467.22	68.03	18.03	11.75	2.99	0.54	0.15
2.80	0.39	0.38	1.71	14.66	25.02	28.63	6.96	1.09	2.51	19.37	18.68	398.88	138.54	9.84	4.99	5.15	1.79	1.03	0.26
1.05	0.54	0.81	10.24	81.01	82.46	75.84	13.64	0.95	1.37	36.67	30.95	328.10	263.73	84.47	20.99	17.39	3.62	1.77	0.71
1.03	0.83	1.46	5.63	46.47	61.22	58.83	10.60	2.06	0.87	19.30	24.28	529.42	169.80	38.71	17.17	8.19	2.07	1.40	0.03
0.86	0.71	1.56	3.01	24.10	39.55	45.76	13.85	0.45	0.43	26.36	37.91	581.88	495.61	100.16	19.67	12.86	3.10	0.32	0.18
1.33	0.33	0.21	2.08	23.53	35.50	39.74	7.98	2.86	5.65	42.97	25.77	327.32	227.26	76.60	54.54	36.38	5.07	0.38	1.23

K^+										Mg^{2+}									
M 9	M 8	M 7	M 6	M 5	M 4	M 3	M 2	M 1	M 0	M 9	M 8	M 7	M 6	M 5	M 4	M 3	M 2	M 1	M 0
1.30	0.43	3.48	2.66	2.82	3.11	5.23	2.18	19.89	0.52	0.00	0.07	1.32	0.90	3.93	6.62	7.08	1.04	0.38	0.34
2.37	1.02	3.75	50.60	1.02	2.28	4.21	1.75	0.68	1.23	0.00	0.24	1.57	1.69	1.57	4.54	5.47	1.63	0.50	0.56
2.21	0.83	1.09	1.70	4.53	6.08	8.68	5.30	2.25	2.04	0.00	1.06	3.96	2.86	3.17	5.14	10.90	4.58	1.19	0.57
1.11	2.29	2.67	1.80	2.35	3.34	5.29	3.08	1.47	0.78	0.00	0.71	2.17	2.00	5.18	9.49	12.76	2.83	0.65	0.83

1.37	0.16	5.28	2.25	2.13	1.68	1.96	0.74	1.41	0.18	0.00	0.33	0.99	0.80	2.51	3.80	3.75	0.61	0.39	0.47
0.34	0.13	0.35	0.17	0.12	0.17	0.23	0.07	0.36	0.10	0.00	0.31	0.80	0.34	0.40	0.58	0.33	0.39	0.19	0.01
0.38	0.92	0.28	0.77	1.68	2.30	3.35	1.07	0.30	0.33	0.00	0.48	2.19	1.92	2.28	3.44	5.42	1.53	0.60	0.26
1.18	0.04	1.78	1.67	1.35	2.51	4.19	1.81	1.99	0.57	0.00	0.38	1.31	1.27	2.06	4.02	3.94	0.87	0.99	0.00
1.96	0.50	1.92	5.40	5.10	4.32	5.08	1.73	0.15	1.55	0.00	0.68	1.82	2.01	11.07	13.37	13.28	1.34	0.51	0.08
0.75	0.04	2.25	2.40	3.19	3.26	3.87	0.94	0.91	0.06	0.00	1.01	1.48	1.44	4.68	9.49	8.24	0.92	0.43	0.28
1.98	0.77	4.84	5.26	4.95	4.34	4.74	9.41	0.24	0.39	0.00	0.46	1.53	2.78	9.64	14.37	12.92	2.24	0.49	0.00
1.92	0.76	2.60	3.14	3.55	3.81	4.76	1.57	1.47	2.66	0.00	0.32	1.99	1.91	3.94	8.33	10.83	1.41	0.50	0.86

Ca^{2+}									
M 9	**M 8**	**M 7**	**M 6**	**M 5**	**M 4**	**M 3**	**M 2**	**M 1**	**M 0**
0.00	0.46	2.52	2.37	4.58	12.55	19.23	6.08	2.18	2.35
1.37	0.79	2.57	2.83	3.84	16.10	22.05	9.90	1.83	2.57
1.08	1.18	6.79	7.55	14.54	28.28	55.05	34.38	9.07	4.75
1.74	1.33	1.73	4.01	9.83	23.23	41.29	15.98	3.50	2.29
0.00	0.50	2.50	1.51	6.06	14.00	17.33	2.68	0.07	0.07
0.00	0.00	1.12	0.73	0.00	0.68	0.51	0.06	0.28	0.03
0.00	0.00	2.19	1.48	3.55	8.64	17.10	6.56	1.97	0.00
0.00	0.00	1.43	2.27	6.85	17.00	21.87	5.50	0.94	0.00
0.08	0.32	2.92	2.07	12.81	26.14	35.23	8.42	2.24	1.29
0.00	0.78	4.29	4.59	7.41	17.23	22.35	5.59	2.34	0.00
0.21	1.02	2.55	7.88	36.32	54.55	58.58	19.98	2.08	0.60
1.40	0.20	4.19	3.81	14.16	31.11	55.17	6.19	2.90	2.65

San Gorgonio (July) ng/m^3		Cl^-								
Start Date	**Sampling Vol**	**M 9**	**M 8**	**M 7**	**M 6**	**M 5**	**M 4**	**M 3**	**M 2**	**M 1**	**M 0**
7/1/03	77.4	0.00	0.00	0.51	0.28	0.72	0.46	0.37	0.00	0.00	1.50
7/3/03	77.0	0.00	0.16	0.00	0.98	0.00	0.00	1.44	3.24	0.22	2.80
7/5/03	76.8	0.00	0.00	0.65	1.28	2.66	0.65	1.72	3.60	1.37	0.47
7/7/03	75.5	0.00	0.00	1.21	0.13	0.95	1.92	5.63	1.77	0.43	1.66
7/9/03	76.1	0.00	0.00	0.00	0.00	0.00	0.00	0.22	1.17	0.00	0.22
7/11/03	75.8	0.00	0.00	0.00	0.00	9.34	0.77	1.79	3.46	0.29	0.67
7/13/03	75.5	4.22	0.00	0.00	0.00	0.54	0.00	0.24	0.23	0.00	0.33
7/15/03	77.3	0.00	0.00	0.00	0.28	0.00	0.21	1.71	2.43	1.27	0.86
7/18/03	78.5	0.00	0.00	0.00	1.43	32.58	2.55	6.16	14.69	6.26	2.00
7/20/03	77.8	0.61	1.07	1.98	1.86	2.02	1.34	0.39	2.71	0.60	0.37
7/22/03	77.1	0.00	0.00	0.00	1.83	0.00	0.00	0.18	0.46	0.00	0.00

7/24/03	77.0	0.00	0.00	0.00	6.21	1.06	0.00	26.64	19.13	17.73	9.33
7/26/03	77.4	0.00	0.00	0.00	0.00	2.36	0.00	0.67	2.23	0.74	1.88
7/28/03	60.1	0.00	0.00	0.00	0.00	0.00	1.33	5.35	2.35	0.98	58.05

NO_3^-

M 9	M 8	M 7	M 6	M 5	M 4	M 3	M2	M 1	M 0
0.00	2.44	28.30	5.85	36.94	86.37	130.02	65.58	0.00	13.48
30.08	9.36	74.76	93.51	145.67	259.11	357.66	134.86	34.92	21.86
51.50	11.43	126.91	423.70	246.61	396.92	403.17	115.75	23.23	15.20
22.45	10.33	99.51	186.36	598.78	845.37	789.46	202.14	38.27	21.03
6.27	5.42	26.13	24.53	95.78	167.05	288.26	136.79	31.63	11.59
15.10	10.17	71.40	318.62	249.37	177.95	325.70	172.67	45.85	23.49
4.32	3.73	14.18	11.75	48.37	118.22	199.16	91.24	27.29	17.78
10.44	6.12	45.15	24.57	107.30	277.28	307.45	149.69	53.13	43.81
4.75	10.16	269.77	201.41	421.99	560.40	719.70	208.71	40.65	37.44
13.62	9.62	34.91	87.69	177.22	169.25	253.19	125.68	28.41	18.91
14.04	10.72	59.62	141.84	439.58	223.59	432.81	177.54	42.72	22.09
9.23	8.08	53.55	158.41	223.57	169.00	433.89	196.23	42.44	19.46
12.60	6.00	30.96	45.40	249.18	237.11	524.94	204.13	35.72	20.62
3.46	5.88	51.54	74.98	270.86	355.23	514.29	161.60	25.63	415.49

SO_4^{2-}

M 9	M 8	M 7	M 6	M 5	M 4	M 3	M 2	M 1	M 0
250.64	89.80	479.36	169.12	23.39	16.43	18.86	6.92	0.00	0.00
516.46	98.48	282.25	140.25	59.49	43.57	45.27	14.08	1.33	0.00
414.48	99.40	519.27	380.29	101.16	64.30	51.18	14.78	0.93	0.00
278.69	104.39	568.46	342.53	190.09	113.09	87.06	21.09	0.00	0.00
230.49	161.65	867.19	365.58	143.35	49.22	47.13	14.87	0.81	0.00
370.02	115.62	705.49	389.80	142.41	55.02	50.60	20.10	3.73	0.11
235.27	130.30	756.70	278.38	73.31	35.07	33.79	9.35	0.00	0.00
401.51	158.10	923.94	338.99	123.88	81.06	63.60	24.80	6.88	8.66
299.81	192.93	1160.38	451.57	190.97	94.27	82.08	26.12	5.44	12.94
689.23	138.75	594.50	230.35	129.34	51.95	42.87	13.79	2.49	0.04
543.93	182.86	707.68	259.27	247.02	52.42	53.38	17.87	3.57	0.00
505.65	195.31	991.72	592.57	276.84	72.45	79.17	27.17	3.67	0.00
482.54	168.15	940.32	485.15	242.99	74.15	71.17	23.56	2.11	0.00
241.56	177.46	916.39	366.97	113.80	49.40	47.18	9.30	0.00	75.92

Na^+

M 9	M 8	M 7	M 6	M 5	M 4	M 3	M 2	M 1	M 0
3.17	0.02	2.25	5.29	19.82	29.75	29.94	8.84	0.00	1.10
7.44	1.50	2.81	11.82	59.76	80.96	78.67	18.84	2.44	2.98
7.59	1.34	6.38	43.77	76.95	115.78	103.84	22.62	2.16	0.85
9.51	1.92	10.35	27.62	139.06	175.89	152.10	30.59	3.31	2.87
3.79	1.11	4.28	12.76	45.67	46.63	42.72	11.25	1.25	1.21
4.70	0.79	6.16	15.91	48.99	54.05	53.50	15.86	1.91	1.56
6.53	0.34	3.76	11.49	29.40	32.81	31.54	8.06	1.19	1.63
4.34	0.80	8.00	39.10	50.25	56.97	55.17	15.73	4.07	3.13
5.19	1.10	9.60	12.14	100.99	105.85	94.37	26.76	5.83	2.42
9.77	1.24	4.63	9.44	53.85	58.93	47.75	9.84	1.60	2.27
7.22	0.78	5.76	6.41	45.20	56.92	58.68	13.87	1.60	1.05
6.41	3.68	9.02	15.65	48.49	64.48	102.01	39.76	16.33	9.12
7.12	2.08	6.68	9.93	55.05	69.66	84.19	24.67	2.59	2.72
4.41	0.39	4.79	6.05	45.85	63.73	66.15	18.83	90.73	94.16

NH_4^+

M 9	M 8	M 7	M 6	M 5	M 4	M 3	M 2	M 1	M 0
92.15	35.20	194.98	59.89	4.66	1.97	2.90	4.53	0.00	2.15
220.02	40.58	137.68	72.16	13.61	13.67	16.23	8.24	2.68	3.32
159.64	37.22	207.86	143.45	21.85	27.21	22.51	7.41	3.20	1.06
105.26	43.73	254.10	160.92	102.37	103.17	64.43	11.86	2.68	1.25
86.80	65.52	375.36	153.61	36.61	9.46	17.08	9.21	1.94	0.62
136.18	51.67	323.08	232.20	87.83	8.68	18.47	13.06	4.59	1.81
86.38	52.60	315.44	96.31	13.31	5.04	11.67	5.56	2.49	1.14
114.96	61.83	382.94	132.38	18.05	6.77	16.41	10.60	5.15	4.40
131.10	90.61	602.15	216.92	108.46	74.56	69.45	14.34	3.46	4.95
334.11	65.01	278.21	107.36	49.21	6.07	13.40	7.41	2.40	1.45
242.62	91.58	336.87	159.23	163.24	28.71	57.53	20.22	5.38	3.40
232.80	99.13	436.85	288.32	154.85	15.21	36.39	14.19	3.88	1.83
199.11	86.04	410.04	224.11	122.99	23.58	51.57	17.83	3.08	1.04
105.80	84.21	410.62	176.62	95.29	63.12	61.87	10.99	0.63	11.47

K^+

M 9	M 8	M 7	M 6	M 5	M 4	M 3	M 2	M 1	M 0
0.00	0.00	2.04	0.00	0.00	0.00	1.60	1.53	0.00	0.00

Mg^{2+}

M 9	M 8	M 7	M 6	M 5	M 4	M 3	M 2	M 1	M 0
0.00	0.21	0.73	1.10	0.60	1.08	2.28	1.41	0.00	0.24

8.50	0.05	3.45	8.31	4.55	4.01	8.77	5.03	1.02	2.32	0.89	0.17	0.74	1.40	3.05	5.11	8.87	3.13	0.46	0.47
35.85	3.70	77.09	187.57	29.54	8.41	10.09	4.42	0.00	0.00	3.06	0.39	5.61	16.32	4.83	6.47	8.67	1.72	0.48	0.29
12.35	1.96	31.70	27.45	15.92	7.85	12.84	4.95	0.56	0.05	1.11	0.31	2.53	2.90	10.41	13.93	18.24	4.33	0.81	0.44
2.93	1.15	14.86	7.66	3.23	2.42	4.73	2.27	0.00	0.00	0.04	0.48	1.76	1.42	2.57	3.55	6.64	2.33	0.46	0.20
5.83	0.48	17.94	7.93	3.76	3.01	7.77	5.94	0.70	0.00	0.26	0.42	1.82	1.69	3.26	3.87	8.67	3.65	0.88	0.32
1.98	0.00	10.12	2.58	1.32	1.10	3.76	1.54	0.00	0.00	0.06	0.20	1.24	0.93	1.32	2.42	3.79	1.33	0.22	0.32
3.83	1.64	27.85	32.20	2.93	3.63	8.25	4.72	1.87	1.25	-0.03	0.02	2.15	3.91	2.96	4.56	9.11	3.55	0.95	0.76
11.80	4.49	37.03	9.07	8.37	3.71	9.44	7.04	1.60	0.82	-0.10	0.31	1.88	0.88	5.81	10.19	19.80	4.48	0.61	0.57
12.46	0.89	8.25	2.94	1.72	2.86	7.32	5.10	0.44	0.00	1.31	0.41	1.48	0.91	2.66	3.40	7.58	2.45	0.42	0.33
11.18	1.00	9.00	1.85	1.85	3.89	7.79	3.34	0.00	0.00	0.12	0.15	1.15	0.57	3.11	5.01	11.16	3.78	0.42	0.27
14.46	5.64	35.96	10.78	2.80	3.33	16.24	9.27	3.93	1.41	0.44	0.45	1.60	1.27	3.18	5.83	15.10	5.62	0.63	0.61
22.66	3.44	29.26	7.73	4.17	4.47	9.33	4.71	0.00	0.00	0.26	0.00	1.45	0.94	3.54	6.38	16.10	4.56	0.22	0.34
3.79	0.00	11.32	3.80	3.36	5.48	12.09	5.24	0.97	81.51	0.00	0.87	1.96	1.13	2.98	5.20	11.16	3.65	0.79	17.61

Ca^{2+}									
M 9	**M 8**	**M 7**	**M 6**	**M 5**	**M 4**	**M 3**	**M 2**	**M 1**	**M 0**
0.00	1.96	5.29	3.49	2.67	6.82	11.06	10.25	0.00	4.15
3.16	0.63	1.91	2.52	4.68	11.32	31.28	16.77	5.00	3.93
1.45	0.40	1.76	4.03	2.25	7.60	21.82	10.36	2.85	1.79
1.36	0.80	3.81	2.16	8.86	20.29	49.71	23.63	5.13	3.36
0.05	0.64	5.08	3.07	5.76	12.43	42.11	18.60	3.88	0.80
1.49	0.47	3.74	2.84	6.33	13.60	48.76	27.02	5.89	2.75
0.92	1.15	2.30	1.50	4.04	11.56	29.30	12.92	3.97	1.25
0.79	0.12	3.28	21.43	5.84	20.50	59.93	28.43	8.90	6.53
0.75	0.73	4.87	1.21	7.68	27.16	86.15	29.78	6.44	7.16
10.03	0.04	3.59	1.40	4.56	10.46	36.40	15.85	3.72	2.85
2.37	0.51	3.14	0.79	5.79	17.09	60.06	25.14	4.68	3.14
1.46	1.77	7.22	4.04	8.36	17.50	72.51	34.36	7.10	4.02
1.89	1.12	3.88	1.91	7.70	22.02	82.53	35.53	3.56	2.61
1.49	1.41	4.41	3.08	6.67	15.71	38.29	20.05	6.43	140.20

Grand Canyon NP ng/m³		Cl^-								
Start Date	**Sampling Vol**	**M 9**	**M 8**	**M 7**	**M 6**	**M 5**	**M 4**	**M 3**	**M 2**	**M 1**	**M 0**
5/1/03	78.7	0.00	1.02	2.34	11.06	17.92	28.05	28.94	11.36	1.40	0.99
5/3/03	80.4	0.00	1.22	0.00	0.00	7.98	11.56	8.97	2.98	7.27	1.68
5/5/03	79.1	0.00	1.33	1.16	0.90	8.08	9.43	6.25	7.66	1.62	1.15
5/7/03	79.6	0.00	2.73	1.33	3.04	9.89	19.51	26.51	7.16	2.42	3.70

5/9/03	78.8	0.00	1.22	1.81	4.93	8.59	11.90	6.46	3.22	1.57	1.33
5/11/03	77.9	0.00	0.00	1.41	1.26	12.51	12.19	4.22	2.81	0.74	0.81
5/13/03	78.7	0.00	0.26	1.78	1.67	10.29	11.31	5.72	3.21	1.08	1.03
5/15/03	78.5	0.00	0.16	0.71	0.49	6.89	7.70	2.43	1.98	0.79	0.31
5/18/03	78.1	0.00	0.00	1.33	1.07	9.73	8.43	2.36	1.45	0.48	0.29
5/20/03	77.3	0.00	0.00	0.97	14.51	8.11	8.46	4.26	4.10	1.05	0.52
5/22/03	77.1	0.00	1.37	9.06	3.44	15.82	19.78	10.49	6.75	2.46	1.56
5/24/03	77.9	0.00	1.16	3.79	7.92	24.95	29.61	16.97	8.52	2.44	1.26
5/26/03	76.3	0.00	0.54	1.86	16.58	9.57	12.95	6.61	5.30	2.37	2.00
5/28/03	74.6	0.00	3.48	4.16	2.32	9.89	10.76	5.68	5.44	3.25	7.77
5/30/03	37.6	0.00	7.46	4.69	6.21	18.21	21.57	9.76	9.58	5.03	9.18

NO_3^-										SO_4^{2-}									
M 9	**M 8**	**M 7**	**M 6**	**M 5**	**M 4**	**M 3**	**M2**	**M 1**	**M 0**	**M 9**	**M 8**	**M 7**	**M 6**	**M 5**	**M 4**	**M 3**	**M 2**	**M 1**	**M 0**
9.33	10.49	24.76	78.17	132.44	186.58	146.29	41.54	11.49	9.13	71.05	104.14	264.12	62.81	40.22	50.75	53.10	18.03	0.00	0.00
0.00	2.71	3.44	59.00	94.57	113.43	50.15	10.70	6.26	8.76	71.52	59.06	102.90	45.08	19.19	24.32	23.38	13.06	0.00	0.00
3.59	3.30	14.38	66.90	95.99	136.08	95.42	31.92	8.18	7.92	200.12	116.43	397.98	125.38	34.59	28.52	32.23	19.23	11.56	0.00
6.05	4.45	19.78	73.98	163.68	238.25	175.39	47.24	13.60	8.90	156.21	101.63	447.70	174.97	56.20	46.31	43.84	21.62	13.74	13.38
10.08	3.85	18.68	92.20	79.61	95.14	31.80	11.24	6.51	5.51	71.00	67.54	208.98	108.86	19.63	18.07	17.15	0.00	0.00	0.00
7.24	6.78	19.78	81.08	95.20	123.16	67.96	24.95	9.86	6.74	94.60	100.37	298.88	130.11	39.69	41.53	38.24	15.83	11.09	0.00
5.77	5.81	13.88	69.43	96.52	134.24	84.78	32.69	13.39	11.37	127.79	113.29	421.68	167.21	56.31	55.67	58.86	42.07	22.82	18.64
5.33	6.24	10.62	70.40	114.17	171.11	141.75	47.72	16.10	12.36	176.24	115.99	403.64	154.94	59.08	51.84	45.79	26.84	18.22	16.35
9.57	6.36	28.90	102.19	106.17	125.62	77.42	25.07	9.62	7.70	101.13	105.32	428.84	245.46	68.50	46.28	47.91	21.01	13.82	12.11
8.62	8.16	17.87	85.08	92.04	115.78	71.36	30.02	14.41	10.36	108.16	106.43	322.60	149.40	44.48	39.74	44.68	23.59	0.00	14.43
7.46	11.26	40.54	85.99	143.82	277.12	260.74	125.22	44.75	33.84	176.77	197.38	703.58	243.41	93.99	91.89	93.15	52.20	27.05	22.68
9.56	9.36	22.83	100.69	151.97	193.00	122.37	52.92	19.34	14.26	165.69	186.75	839.59	317.51	104.39	68.50	51.78	25.36	16.90	0.00
8.55	7.06	17.63	84.35	124.61	177.39	165.47	66.80	30.45	21.35	224.12	202.21	783.01	300.39	87.65	57.27	60.45	27.75	19.08	21.50
8.95	9.36	11.92	71.43	86.81	123.83	102.03	62.53	32.10	36.04	363.17	179.65	515.91	164.56	47.15	40.19	44.99	33.54	23.64	28.10
0.00	16.35	18.27	134.90	166.41	219.79	129.39	60.01	31.58	37.02	234.65	180.95	588.31	213.74	60.65	49.35	46.90	31.41	26.83	31.44

Na^+										NH_4^+									
M 9	**M 8**	**M 7**	**M 6**	**M 5**	**M 4**	**M 3**	**M 2**	**M 1**	**M 0**	**M 9**	**M 8**	**M 7**	**M 6**	**M 5**	**M 4**	**M 3**	**M 2**	**M 1**	**M 0**
3.54	2.04	6.91	11.98	32.34	49.95	49.02	12.57	0.70	0.91	23.48	50.15	102.55	35.14	4.30	4.89	6.18	4.12	2.32	2.24
1.33	0.00	0.00	4.46	14.70	18.41	11.23	0.52	2.54	0.04	23.27	33.95	48.01	28.78	0.00	0.00	0.58	0.00	0.00	0.00
3.88	2.03	33.95	7.37	13.35	17.27	11.36	3.69	1.59	2.67	68.39	54.26	154.96	55.29	3.24	1.77	3.14	1.25	0.00	0.00
2.24	0.72	1.05	8.04	31.76	44.75	37.46	5.89	0.74	1.32	53.57	48.69	171.88	70.58	7.33	7.37	8.41	2.32	0.12	0.00
2.18	0.00	0.00	6.59	9.44	13.41	7.25	1.96	0.01	0.00	29.44	38.01	95.63	63.17	2.41	1.19	1.08	0.20	0.00	0.00
2.52	0.97	4.20	11.27	17.98	23.27	16.92	6.74	1.49	0.86	31.83	49.59	120.02	55.52	5.78	5.42	5.51	4.54	3.34	3.09
5.57	0.42	3.56	9.27	15.16	21.65	16.84	6.35	1.89	0.99	39.53	50.75	153.11	64.51	9.19	9.46	11.69	9.65	5.39	4.82
3.45	0.78	2.25	8.28	18.28	24.58	20.63	9.77	3.05	1.61	58.22	52.70	151.92	61.80	8.98	6.10	6.44	5.74	3.93	3.53

3.10	0.12	2.03	10.85	17.77	17.92	12.61	4.18	1.50	0.71	36.80	51.90	175.00	106.78	14.08	7.57	8.82	5.49	4.06	3.26
0.00	0.00	0.00	16.03	5.65	7.67	6.21	1.91	0.00	0.00	42.70	52.99	135.50	66.38	5.73	4.46	5.36	3.77	1.49	1.06
3.50	1.61	6.42	14.64	32.42	40.44	31.41	12.75	4.16	2.77	69.16	87.94	285.71	100.57	15.32	15.44	18.50	9.86	3.34	2.03
1.92	0.00	8.55	31.41	56.96	60.65	41.48	11.61	0.00	0.00	59.65	79.00	335.15	121.11	15.61	6.86	5.77	3.87	1.74	1.14
1.13	0.00	3.48	32.04	36.46	41.95	37.53	9.30	0.15	0.00	82.41	87.23	321.01	115.71	12.83	6.03	8.44	4.73	2.50	2.22
4.66	2.72	4.56	9.82	14.40	18.00	15.28	8.97	3.83	6.33	144.44	83.58	214.37	71.69	6.18	4.52	8.93	7.10	3.11	3.79
3.15	0.00	2.74	15.08	31.68	44.60	40.29	18.42	2.46	0.00	72.57	93.26	256.83	103.14	4.13	2.41	4.66	4.67	0.64	1.55
K^+										**Mg^{2+}**									
M 9	**M 8**	**M 7**	**M 6**	**M 5**	**M 4**	**M 3**	**M 2**	**M 1**	**M 0**	**M 9**	**M 8**	**M 7**	**M 6**	**M 5**	**M 4**	**M 3**	**M 2**	**M 1**	**M 0**
0.81	0.78	2.68	8.54	8.14	10.17	3.37	1.81	0.23	0.91	0.75	1.11	1.97	2.72	6.31	9.01	9.22	2.24	1.27	0.84
0.12	0.00	0.00	6.32	6.36	6.76	0.90	0.03	1.27	0.30	0.00	0.60	0.87	1.77	2.53	3.14	2.16	0.97	0.73	0.60
2.16	0.27	5.55	8.11	6.89	7.15	1.27	1.36	0.00	0.00	0.73	0.56	1.45	2.65	2.78	3.92	3.51	1.18	0.79	0.00
1.64	0.21	4.38	9.27	8.44	9.61	4.74	1.55	0.27	0.30	0.60	0.72	1.36	2.88	5.11	9.35	7.96	2.06	1.46	1.00
1.77	0.00	3.96	9.41	6.45	6.86	0.00	0.00	0.00	0.00	0.00	1.05	1.72	2.94	2.28	2.56	1.68	1.08	0.75	0.78
1.60	0.85	6.87	9.83	8.59	8.16	1.89	1.19	0.68	0.72	0.56	0.61	1.78	3.45	3.23	3.76	2.72	1.53	0.93	0.00
6.56	1.89	14.76	11.67	8.28	9.17	3.94	2.66	1.25	0.95	0.78	0.53	2.47	3.19	3.98	5.25	5.75	2.39	1.18	0.91
3.92	1.54	8.65	9.87	8.67	8.93	2.86	1.57	0.73	0.50	1.14	1.08	2.25	2.97	5.49	7.62	8.33	2.14	1.19	0.61
2.83	1.24	11.40	14.23	8.98	8.73	2.49	1.27	0.60	0.39	0.76	0.81	2.08	6.04	4.54	5.09	3.77	1.82	1.04	0.64
1.78	0.06	8.25	12.81	7.13	7.21	1.94	1.04	0.00	0.00	0.00	0.83	2.63	3.97	4.62	6.39	5.99	2.44	1.65	1.26
4.54	5.71	34.41	16.14	11.42	13.39	9.53	6.56	3.43	2.97	3.00	3.30	4.26	5.50	7.39	12.87	13.52	7.60	4.12	3.59
3.17	2.47	20.49	17.61	9.06	9.35	3.04	2.08	0.49	0.00	0.00	1.23	3.63	6.10	10.18	11.52	8.86	3.20	1.90	1.57
3.15	1.64	15.98	19.01	8.97	9.11	5.38	2.29	0.88	1.73	0.91	1.33	3.44	4.96	6.98	8.95	11.01	4.54	2.18	1.87
5.63	2.87	7.90	9.75	8.77	10.03	5.84	4.74	3.57	3.67	3.42	0.00	4.03	4.90	5.18	5.64	5.38	4.62	3.79	3.67
8.16	3.62	15.50	18.19	17.23	19.44	5.37	4.60	2.94	4.13	0.00	6.52	6.95	9.26	9.51	9.70	8.33	7.13	6.21	6.06
Ca^{2+}																			
M 9	**M 8**	**M 7**	**M 6**	**M 5**	**M 4**	**M 3**	**M 2**	**M 1**	**M 0**										
0.99	1.83	6.40	21.08	37.08	59.38	53.26	18.47	4.20	5.01										
0.00	0.07	0.26	16.20	19.82	26.62	17.31	4.41	3.30	0.89										
0.00	0.30	3.23	18.00	20.48	30.66	22.79	8.13	1.58	1.47										
0.88	0.00	2.89	22.57	33.96	60.36	55.88	26.01	9.02	4.53										
0.00	0.79	1.91	20.53	18.54	20.03	5.84	3.85	0.64	2.66										
2.26	0.76	7.49	27.55	32.49	48.66	36.15	10.84	4.07	1.59										
3.01	2.16	7.25	26.72	36.77	63.24	52.55	31.51	12.13	7.98										
4.04	1.54	5.24	22.77	39.45	64.49	56.96	26.41	9.55	6.65										
0.96	2.75	9.59	38.99	42.86	54.83	47.69	19.87	6.44	5.85										
0.31	2.28	10.53	32.13	37.23	60.09	57.22	32.61	9.57	8.41										
5.95	5.48	8.78	26.34	45.38	122.98	170.03	83.27	24.75	15.36										
2.04	3.59	7.52	30.51	42.62	62.97	48.35	32.85	13.35	9.14										

2.28	3.22	7.82	25.34	38.12	59.53	61.99	40.28	17.99	15.38
5.74	5.91	6.70	25.37	26.90	39.24	44.97	33.53	16.86	14.74
12.37	12.02	12.12	47.70	48.98	56.76	34.33	22.97	15.31	16.58

Bondville ng/m^3

Start Date	Sampling Vol	Cl^- M 9	M 8	M 7	M 6	M 5	M 4	M 3	M 2	M 1	M 0
2/1/03	79.0	0.26	1.13	8.53	7.56	3.21	0.95	7.04	0.94	0.20	5.38
2/3/03	80.0	0.64	0.32	9.56	2.55	7.14	9.20	10.75	3.02	2.19	1.28
2/5/03	78.9	0.44	2.95	10.29	1.04	6.04	9.90	18.47	8.80	2.59	6.75
2/7/03	78.7	0.43	9.13	13.72	6.22	7.20	16.08	23.33	12.39	4.17	3.41
2/9/03	77.9	3.20	0.56	6.72	10.48	17.31	29.42	60.30	48.18	13.45	8.04
2/11/03	78.2	1.70	3.11	10.31	8.70	17.00	30.52	50.10	27.85	6.78	16.58
2/13/03	73.6	0.17	7.68	54.74	5.82	11.72	28.66	39.11	20.02	6.24	0.79
2/16/03	68.0	0.19	13.27	2.79	0.77	4.86	9.73	32.02	17.08	3.17	7.50
2/18/03	76.0	2.44	2.80	3.29	2.54	3.77	12.90	20.96	14.21	4.57	1.78
2/20/03	75.7	1.83	0.36	3.40	0.65	1.06	8.97	20.20	11.19	2.73	4.08
2/22/03	67.8	1.81	2.96	22.47	1.86	11.54	6.59	14.05	7.00	0.61	2.21
2/24/03	76.7	0.33	8.53	6.54	6.27	16.88	32.01	84.13	57.30	15.92	9.12
2/26/03	76.9	0.24	4.27	12.59	3.26	6.38	16.37	55.94	38.78	7.71	5.01

NO_3^-										SO_4^{2-}									
M 9	M 8	M 7	M 6	M 5	M 4	M 3	M2	M 1	M 0	M 9	M 8	M 7	M 6	M 5	M 4	M 3	M 2	M 1	M 0
7.52	240.45	2172.49	2239.88	784.02	60.95	62.06	13.00	4.45	40.97	125.11	316.72	1593.97	1772.58	841.50	56.47	38.12	2.52	0.00	11.05
44.33	280.01	886.15	240.20	84.49	35.47	20.05	3.35	1.89	11.89	156.52	178.18	1410.70	563.32	155.30	23.55	12.45	2.56	7.28	9.57
40.00	683.95	3014.76	750.56	178.05	74.95	97.88	27.33	4.89	7.24	102.34	140.57	632.87	278.84	91.16	24.17	20.09	6.47	1.65	3.76
32.61	339.25	1286.27	330.73	71.55	32.92	33.09	9.62	1.46	4.89	122.68	135.91	531.58	187.72	52.60	23.14	20.51	3.84	1.63	0.35
29.29	209.82	1309.97	589.26	92.88	35.84	35.30	15.02	4.41	8.04	131.77	134.86	694.07	349.43	63.94	17.56	14.80	4.97	0.47	3.03
42.30	182.82	693.88	132.10	63.81	46.42	42.75	10.88	2.53	5.81	118.61	96.97	375.24	113.84	36.22	22.44	25.03	7.61	2.56	0.70
7.61	316.21	1805.29	223.14	50.82	31.27	25.17	7.55	4.78	4.11	119.58	177.08	696.16	143.90	32.51	19.00	13.79	3.62	1.14	1.56
10.85	359.78	753.40	10.66	7.09	59.01	125.01	33.46	6.72	9.45	273.45	392.27	1852.51	1087.17	597.77	133.13	52.15	14.66	1.19	3.34
11.23	195.34	1688.58	807.46	177.90	42.79	42.21	12.47	3.41	3.00	242.53	222.34	1469.06	1019.18	292.02	31.40	15.90	1.84	1.38	0.34
4.14	124.31	1284.21	505.04	41.96	27.19	45.02	18.69	11.37	7.20	225.19	390.13	1788.76	1737.61	592.65	26.50	18.31	2.25	0.43	0.08
17.00	187.05	1526.74	418.36	96.66	36.89	28.04	5.50	4.76	9.36	179.65	225.46	1406.19	516.85	137.03	24.25	11.99	1.49	0.11	5.85
109.03	602.19	1575.87	234.59	132.64	96.82	153.91	61.12	10.08	14.79	331.79	452.70	1191.40	311.99	91.53	27.80	24.73	7.99	0.95	8.76
149.37	1736.63	5480.36	572.67	214.42	196.30	343.89	143.12	22.66	10.49	450.75	1021.36	2445.46	427.16	137.57	41.37	36.65	14.37	1.66	0.23

Na^+										NH_4^+									
M 9	M 8	M 7	M 6	M 5	M 4	M 3	M 2	M 1	M 0	M 9	M 8	M 7	M 6	M 5	M 4	M 3	M 2	M 1	M 0
0.00	0.57	3.75	4.77	7.62	5.34	4.82	0.48	0.48	5.13	38.82	167.53	1038.47	1120.05	488.72	22.19	13.54	1.40	0.18	0.60

3.64	0.74	6.02	5.74	14.56	12.55	8.98	1.81	0.00	1.69	66.36	134.87	684.12	239.13	59.59	4.79	2.45	0.24	0.07	0.76
3.98	0.91	6.87	4.66	12.73	11.35	15.19	5.86	2.05	3.81	49.19	233.63	1073.20	288.71	62.84	7.21	8.34	2.72	0.47	0.37
4.81	3.64	5.75	6.78	9.87	14.26	17.98	7.34	1.44	1.31	51.61	137.89	535.36	151.45	26.32	4.61	5.67	1.44	0.35	0.24
4.07	0.51	3.47	9.63	14.75	20.81	37.76	30.71	7.97	4.96	58.68	101.12	596.51	280.05	34.00	3.87	4.76	1.58	0.46	0.64
3.77	1.05	4.68	7.66	17.60	22.66	31.13	16.73	4.01	3.94	55.33	80.78	321.88	67.98	14.41	7.24	6.88	3.44	0.60	0.81
3.53	1.32	4.78	3.28	10.47	17.06	23.00	10.74	2.51	0.34	42.75	141.58	723.65	100.82	10.21	1.90	2.68	0.73	0.65	0.32
4.53	2.14	10.64	13.02	43.02	31.48	30.73	12.01	1.18	1.27	93.47	221.88	690.99	242.55	76.45	12.93	5.55	1.52	0.22	0.68
4.39	1.34	3.09	5.42	11.81	10.31	16.31	7.01	0.96	0.98	84.81	121.62	935.35	549.80	130.20	6.38	3.39	0.67	0.27	0.09
3.12	0.70	3.74	3.43	3.88	7.13	16.52	6.17	0.38	2.17	78.02	163.57	920.29	699.45	187.63	4.64	2.76	0.86	0.28	0.46
3.10	0.48	6.87	5.26	10.57	9.25	11.29	2.18	0.00	0.09	63.46	124.08	889.92	288.69	55.86	5.68	2.88	0.98	0.26	0.85
3.84	1.31	7.68	13.79	30.67	37.40	83.58	45.61	10.49	6.68	147.62	308.62	822.57	157.81	37.83	9.36	9.19	2.95	0.62	1.89
4.09	2.79	11.46	10.59	24.32	44.92	96.34	46.85	6.64	2.28	206.73	811.36	2283.96	286.56	74.24	15.02	12.79	3.80	0.70	0.61
K^+										Mg^{2+}									
M 9	M 8	M 7	M 6	M 5	M 4	M 3	M 2	M 1	M 0	M 9	M 8	M 7	M 6	M 5	M 4	M 3	M 2	M 1	M 0
1.76	4.63	42.47	35.33	14.48	1.28	1.46	0.35	0.27	1.70	0.00	0.29	1.08	1.11	0.69	0.46	0.85	0.00	0.00	0.88
1.83	6.13	27.84	3.69	1.62	0.95	0.91	0.02	0.00	0.45	0.00	0.34	1.24	1.05	0.76	0.87	0.90	0.43	0.17	0.29
1.98	10.23	37.23	11.68	3.37	0.69	1.00	0.89	0.12	0.89	0.00	0.43	1.30	1.09	1.40	1.51	3.20	0.84	0.18	0.06
2.36	6.50	20.19	5.83	1.49	0.85	1.20	0.36	0.28	0.16	0.00	0.28	2.18	0.94	0.70	0.85	2.11	0.75	0.16	0.00
2.75	4.03	24.72	9.15	1.85	0.61	3.17	0.73	0.33	0.16	0.04	0.28	0.81	1.26	0.99	1.76	4.03	2.05	0.15	0.29
1.65	3.34	14.86	4.03	2.00	2.46	3.66	1.25	0.00	0.36	0.00	0.35	1.06	0.83	1.10	2.24	3.50	1.16	0.38	0.38
3.88	6.35	32.33	6.71	1.22	1.41	1.10	0.37	1.75	0.05	0.00	0.40	1.04	0.39	1.18	1.23	1.67	0.00	0.44	0.04
5.45	12.36	40.31	10.42	9.07	1.78	0.94	1.07	0.75	0.24	0.04	1.05	5.22	6.55	17.46	5.27	4.96	1.10	0.19	0.21
4.41	5.74	40.30	23.17	5.79	0.62	0.75	0.22	0.00	0.02	0.00	0.19	1.83	1.69	1.77	0.96	1.16	0.57	0.12	0.07
3.91	8.89	37.50	26.16	7.35	0.34	0.49	0.40	0.00	0.90	0.00	0.37	1.36	1.51	1.66	0.81	1.08	0.38	0.24	0.15
2.22	6.11	36.05	11.22	1.95	0.23	0.25	0.04	0.11	0.07	0.00	0.31	1.24	0.98	1.43	0.95	0.84	0.00	0.12	0.15
6.59	6.68	30.05	7.32	2.86	1.14	2.43	0.89	0.20	0.18	0.00	0.72	1.62	1.37	2.21	2.00	3.84	2.16	0.43	0.29
9.26	25.29	43.69	13.39	4.78	1.55	2.73	1.37	0.06	0.03	0.00	1.25	3.08	1.53	2.54	3.31	6.95	2.72	0.35	0.31
Ca^{2+}																			
M 9	M 8	M 7	M 6	M 5	M 4	M 3	M 2	M 1	M 0										
0.00	0.00	6.00	3.35	5.20	0.00	5.12	2.78	0.00	7.89										
0.00	1.56	3.65	3.73	2.79	5.21	9.86	6.02	1.87	4.86										
0.57	1.52	3.57	2.87	6.21	9.54	23.94	8.88	1.73	1.54										
1.46	0.92	6.23	4.27	5.31	12.87	37.30	20.70	4.96	3.45										
2.19	0.27	2.80	3.98	5.25	14.76	37.20	25.06	5.49	5.27										
0.88	1.60	3.10	3.88	9.49	19.23	45.48	17.75	4.58	4.17										
1.99	2.71	9.11	3.50	6.14	13.17	28.33	13.89	4.59	2.88										
2.07	4.01	18.11	12.07	29.54	20.13	34.32	10.05	2.07	2.91										
2.01	0.94	7.36	6.35	7.67	6.54	11.42	8.11	1.91	0.52										

0.62	1.14	5.98	5.24	7.48	5.35	10.93	6.39	2.67	2.50
0.86	0.73	5.31	3.15	5.03	3.65	6.21	2.38	0.53	1.85
1.01	2.21	5.64	3.53	9.25	14.60	50.37	27.87	5.51	4.48
1.93	4.08	13.11	4.25	8.44	18.92	61.48	32.57	4.76	2.13

Brigantine ng/m^3

Start Date	Sampling Vol	Cl^- M 9	M 8	M 7	M 6	M 5	M 4	M 3	M 2	M 1	M 0
11/4/03	35.4	6.37	38.47	2.42	11.56	62.29	139.18	142.41	30.67	3.25	4.53
11/6/03	73.1	0.01	16.05	30.54	2.49	7.89	45.58	51.66	14.87	6.68	11.13
11/8/03	71.5	0.48	2.40	7.95	15.26	10.30	16.81	37.85	26.30	8.04	5.69
11/10/03	71.5	0.00	13.65	9.19	13.08	13.07	30.83	106.90	48.14	9.02	4.46
11/12/03	69.4	0.00	0.00	8.61	0.19	17.62	36.73	59.49	11.27	2.02	19.91
11/14/03	71.0	0.00	0.00	2.16	0.00	0.00	1.98	5.93	4.43	2.55	0.00
11/16/03	70.5	0.00	5.51	37.15	15.84	6.08	3.03	17.27	14.20	0.00	0.00
11/18/03	69.6	0.00	0.00	0.26	24.06	668.25	783.81	813.10	169.62	19.09	6.48
11/21/03	70.8	0.00	2.38	17.89	6.32	8.77	15.20	61.79	33.21	4.77	0.00
11/23/03	71.2	0.00	0.00	0.00	7.82	268.65	392.25	573.09	173.11	17.88	6.35
11/25/03	71.3	0.00	0.00	0.00	0.00	0.00	0.00	7.65	7.30	0.00	0.05
11/27/03	70.5	0.00	0.00	0.00	2.06	206.42	182.90	163.16	41.08	2.66	4.48
11/29/03	34.5	0.00	0.00	1.31	0.39	2.32	8.51	7.05	2.16	0.00	2.61

NO_3^- M 9	M 8	M 7	M 6	M 5	M 4	M 3	M2	M 1	M 0	SO_4^{2-} M 9	M 8	M 7	M 6	M 5	M 4	M 3	M 2	M 1	M 0
6.76	20.03	44.68	74.81	229.41	219.14	154.22	26.26	20.97	15.38	177.47	339.04	960.32	448.71	258.36	41.03	31.00	4.11	0.00	5.12
7.12	14.91	96.89	30.15	59.85	112.41	85.39	21.59	10.14	13.25	185.84	352.07	1414.58	494.23	147.23	42.54	32.17	6.08	0.78	1.21
33.20	92.43	143.57	31.51	31.98	24.06	26.44	14.05	7.33	7.99	167.51	164.89	476.95	57.74	24.66	10.69	11.27	4.35	0.00	0.00
8.23	43.67	125.76	23.96	100.75	155.14	217.45	56.49	11.31	8.00	209.91	297.08	574.64	116.01	41.29	19.23	40.82	13.30	0.85	0.00
4.00	13.74	136.61	26.54	96.70	118.45	71.41	10.71	3.84	6.43	227.11	328.87	848.83	150.40	50.99	19.59	20.17	0.57	0.00	0.00
10.36	39.82	257.02	26.02	29.02	36.09	57.34	24.88	11.94	7.70	189.01	255.02	707.29	56.56	18.42	8.63	15.40	7.35	0.00	0.00
9.75	103.71	757.87	202.35	88.63	118.88	207.62	72.08	13.82	8.23	303.04	668.35	1525.51	328.49	100.54	38.35	54.21	23.44	1.17	0.00
2.12	5.33	9.35	11.86	237.14	269.62	297.42	64.83	10.64	10.06	87.75	362.43	1538.01	246.60	168.02	141.56	156.68	29.59	0.00	0.00
4.59	37.99	182.03	63.82	108.67	158.81	275.00	84.00	13.94	20.76	368.08	719.76	1005.83	127.65	45.05	16.20	40.48	7.75	0.00	0.00
1.11	3.06	11.64	11.41	213.80	266.57	332.01	84.32	13.93	11.07	189.81	266.84	762.80	69.15	70.02	73.10	101.10	19.55	0.00	0.00
8.58	32.76	572.67	52.42	36.08	50.57	115.68	54.52	12.70	13.54	248.44	355.44	1425.44	231.16	49.00	-0.48	15.49	0.92	0.00	0.00
1.22	6.21	11.25	7.87	108.22	164.56	218.52	63.99	25.52	18.86	162.62	373.40	1381.02	308.66	63.40	42.22	47.07	6.59	0.00	0.00
4.26	6.83	30.58	7.81	12.38	12.98	17.18	4.54	2.95	9.66	276.30	329.61	1231.70	93.43	3.58	-2.61	0.22	0.00	0.00	0.00

Na^+ M 9	M 8	M 7	M 6	M 5	M 4	M 3	M 2	M 1	M 0	NH_4^+ M 9	M 8	M 7	M 6	M 5	M 4	M 3	M 2	M 1	M 0

18.92	38.11	24.87	64.55	141.63	157.40	152.32	41.63	17.03	20.59	54.76	113.84	328.71	165.90	92.65	36.42	15.55	119.62	18.06	20.20
7.15	20.32	26.89	11.05	29.17	60.47	52.34	15.37	10.41	13.49	71.50	197.01	644.80	209.16	57.98	14.45	0.00	39.60	14.04	14.19
7.54	8.60	14.02	17.82	21.69	20.69	30.31	21.80	9.52	9.86	72.49	89.49	221.21	32.28	17.91	22.74	20.53	37.99	12.65	12.77
6.74	16.45	13.55	21.40	48.41	70.58	125.74	47.13	13.17	9.29	75.79	149.22	267.95	48.55	17.03	12.56	22.16	19.03	10.58	10.86
0.00	1.03	4.53	4.24	37.26	53.76	52.19	7.72	0.36	17.28	117.83	146.91	399.77	71.51	21.00	5.00	6.49	2.52	13.12	0.99
0.06	0.97	5.25	0.08	2.85	2.01	3.11	1.43	0.36	0.00	76.76	104.79	372.81	23.00	1.24	0.50	1.63	0.00	5.01	0.00
0.00	0.75	9.65	8.48	14.70	23.61	49.06	19.30	1.01	0.00	122.11	321.88	976.25	196.81	43.68	7.93	9.82	0.23	0.00	0.00
0.00	0.62	20.36	80.06	496.88	577.86	611.09	121.54	11.87	3.28	25.56	153.41	488.01	20.17	0.00	0.00	0.00	0.00	0.00	0.00
0.22	1.96	9.01	5.12	24.02	36.51	83.97	27.96	2.37	4.72	143.71	305.77	474.11	70.85	20.57	10.50	11.07	3.58	1.24	4.35
0.18	0.00	8.49	27.78	232.17	304.30	465.75	122.88	12.92	2.31	68.07	111.35	298.08	13.04	1.01	1.74	0.98	0.00	0.73	0.54
0.64	0.53	3.57	1.26	6.13	8.88	27.50	15.84	2.78	2.62	109.40	161.32	834.70	126.19	22.90	5.69	1.41	1.45	0.00	1.00
0.00	0.31	7.09	19.69	184.54	171.43	173.44	44.70	3.92	5.64	58.09	160.48	597.02	103.78	0.00	0.00	0.00	0.00	0.75	0.00
0.50	0.00	1.87	0.00	3.18	5.73	7.85	1.17	0.00	1.14	152.07	149.34	520.01	39.31	1.68	0.00	5.70	0.00	0.00	9.14
K^+										Mg^{2+}									
M 9	**M 8**	**M 7**	**M 6**	**M 5**	**M 4**	**M 3**	**M 2**	**M 1**	**M 0**	**M 9**	**M 8**	**M 7**	**M 6**	**M 5**	**M 4**	**M 3**	**M 2**	**M 1**	**M 0**
26.59	31.78	28.99	34.40	28.82	48.08	36.60	28.85	25.03	24.04	2.36	7.68	8.84	12.57	17.48	22.58	20.56	10.96	8.79	5.85
13.95	18.15	23.02	15.23	15.25	27.97	21.37	14.39	13.62	15.71	1.20	2.59	3.13	3.02	5.89	8.33	8.82	4.04	3.05	2.77
17.09	20.13	25.63	18.31	14.93	13.59	14.96	14.10	12.95	13.90	1.62	2.40	3.67	3.97	4.76	4.95	5.30	5.12	3.53	3.34
16.83	21.27	23.37	17.54	15.06	16.12	19.82	14.83	13.76	13.21	1.13	3.87	4.13	4.26	7.44	9.41	15.39	6.88	3.22	2.49
2.05	2.48	8.89	0.36	1.15	5.06	5.40	0.99	0.13	5.14	0.00	0.00	0.50	0.51	4.80	6.56	7.43	1.22	0.49	0.11
5.02	8.94	16.33	1.78	0.49	0.88	1.51	0.69	0.20	0.00	0.00	0.00	0.15	0.10	1.08	1.89	4.06	2.16	0.73	0.30
6.50	7.77	24.30	5.81	2.28	2.00	4.18	1.56	0.00	0.00	0.00	0.00	0.00	0.00	2.04	3.62	9.30	3.40	0.11	0.00
0.00	0.57	4.50	9.37	17.34	22.30	26.05	3.22	0.00	0.00	0.00	0.00	1.68	6.96	55.45	62.88	65.29	13.03	0.87	0.23
2.87	8.44	16.94	3.14	2.32	4.60	7.53	0.73	0.00	0.00	0.00	1.49	2.17	1.87	5.60	6.41	13.10	5.09	0.22	0.14
2.27	0.56	4.63	0.52	8.69	9.95	16.43	2.88	0.00	0.00	0.00	0.00	2.38	5.18	28.87	37.64	59.34	16.36	2.54	0.95
5.85	7.99	7.70	3.96	3.33	3.13	4.85	2.70	1.63	2.27	0.00	1.73	2.29	0.56	2.62	4.11	7.85	4.34	0.82	1.89
2.77	3.52	5.85	4.97	15.88	8.86	8.07	3.73	1.47	2.25	0.00	1.29	2.92	3.49	19.09	21.62	19.74	6.41	1.61	2.38
5.15	5.91	8.89	3.37	0.00	3.14	3.92	0.00	0.00	0.00	0.00	0.20	3.36	3.85	0.51	1.06	1.84	0.70	0.60	1.21
Ca^{2+}																			
M 9	**M 8**	**M 7**	**M 6**	**M 5**	**M 4**	**M 3**	**M 2**	**M 1**	**M 0**										
10.06	14.68	24.87	16.06	19.77	17.74	20.86	14.75	14.49	11.76										
4.70	7.32	9.21	12.12	13.44	17.18	24.25	14.93	8.80	7.41										
3.93	5.77	7.09	6.55	9.69	13.01	18.14	15.77	8.37	6.99										
3.64	13.99	6.73	6.95	10.63	16.79	25.23	17.01	9.32	7.20										
0.00	1.31	1.50	0.39	4.94	9.11	15.81	9.69	3.62	5.43										
0.00	0.87	3.67	2.68	8.10	19.80	45.79	31.92	13.61	10.12										
0.00	1.83	2.24	4.35	7.07	12.55	31.00	21.57	4.82	1.13										
0.00	1.88	3.01	5.39	19.52	23.25	26.63	4.56	0.73	1.44										

0.00	2.25	9.00	3.76	12.14	18.94	45.82	27.75	5.78	2.94
0.00	0.00	1.82	1.23	10.02	13.79	22.06	8.20	0.45	0.00
0.00	4.22	3.30	2.75	6.84	11.76	26.60	17.18	6.43	3.12
0.00	2.63	3.61	2.02	9.82	11.31	12.78	5.91	3.09	3.43
0.00	0.81	4.30	1.68	1.86	4.49	4.81	7.83	2.82	4.11

Great Smoky Mtns NP ng/m^3		Cl^-								
Start Date	Sampling Vol	M 9	M 8	M 7	M 6	M 5	M 4	M 3	M 2	M 1	M 0
7/22/04	82.0	2.97	3.77	8.17	7.09	3.10	3.05	3.24	2.96	2.62	5.42
7/24/04	81.4	2.77	0.87	2.63	2.94	5.47	3.16	2.39	1.76	1.70	3.82
7/26/04	79.0	2.06	0.84	1.69	2.04	1.93	1.85	1.82	1.26	0.99	3.47
7/28/04	82.5	1.68	1.39	2.87	1.72	1.22	1.81	3.75	2.04	5.70	5.61
7/30/04	81.3	2.35	3.04	3.23	1.63	3.40	24.63	37.30	11.46	1.88	2.07
8/1/04	82.6	1.82	1.78	3.37	0.89	0.79	2.49	3.20	2.18	1.18	5.30
8/3/04	83.0	1.94	1.75	9.83	7.53	3.49	0.59	2.03	1.94	1.47	1.54
8/6/04	86.4	2.42	1.27	5.02	1.43	0.77	0.82	1.45	1.63	1.03	0.94
8/8/04	83.5	3.76	8.15	26.53	11.04	0.85	1.38	4.64	3.10	1.06	1.85
8/10/04	82.4	1.48	2.02	9.92	7.83	0.81	1.14	3.72	2.35	0.90	1.31
8/12/04	83.3	1.70	0.98	1.17	0.49	0.52	0.55	1.19	1.44	1.16	0.90
8/14/04	84.1	1.07	1.22	3.60	1.33	0.52	1.19	1.93	3.03	1.07	0.94
8/16/04	81.7	0.82	0.41	4.99	3.80	0.59	0.73	2.95	1.51	2.23	0.72
8/18/04	39.6	1.21	2.20	21.69	11.85	0.91	1.34	2.77	4.20	1.79	1.51

NO_3^-										SO_4^{2-}									
M 9	M 8	M 7	M 6	M 5	M 4	M 3	M2	M 1	M 0	M 9	M 8	M 7	M 6	M 5	M 4	M 3	M 2	M 1	M 0
1.77	6.35	16.56	9.49	8.06	29.82	92.95	66.32	21.17	19.05	156.56	514.82	3574.70	2040.36	178.41	22.13	20.03	8.05	2.66	2.17
2.08	6.56	12.29	6.44	8.00	18.45	44.45	24.65	13.77	17.82	73.52	396.14	3372.25	2689.93	611.99	30.67	20.65	8.27	3.30	2.68
0.00	3.06	3.91	2.66	4.99	13.35	22.42	9.22	6.29	6.24	36.57	265.90	1777.20	1329.99	411.07	26.62	16.79	4.77	3.29	0.00
1.01	6.78	1.71	2.74	4.85	17.39	37.50	17.51	23.02	17.10	80.64	327.84	2562.86	2119.02	627.48	30.39	29.29	4.86	0.00	0.00
0.99	2.79	2.97	3.80	29.16	112.47	121.08	26.81	8.63	8.77	38.53	152.81	1128.02	400.38	72.16	39.36	30.77	3.56	0.00	0.00
1.12	5.33	4.13	3.81	4.83	44.86	64.33	22.89	7.69	8.65	73.20	359.85	3152.51	1696.91	360.89	40.28	26.84	6.86	1.80	0.00
1.12	3.18	6.05	8.91	6.35	17.80	64.25	40.71	12.87	8.61	101.77	479.72	3811.07	3626.87	778.14	30.60	23.68	8.08	1.84	0.00
2.80	5.95	5.81	2.73	5.44	24.42	61.24	37.46	11.12	7.68	343.92	729.88	2890.94	343.54	27.80	14.78	16.58	6.39	0.00	1.47
1.89	7.91	10.13	3.01	5.75	26.47	71.93	46.16	12.40	12.02	137.76	662.30	3106.25	982.21	68.55	18.23	19.96	7.09	1.18	0.00
0.87	2.49	5.12	3.84	4.66	32.77	81.48	43.66	12.53	9.52	80.75	478.97	3434.85	2361.75	378.60	32.58	27.95	11.77	2.42	0.47
2.05	7.59	8.67	7.59	7.33	21.22	51.77	44.64	15.33	8.55	193.49	600.15	2275.95	389.17	37.71	43.22	106.01	34.18	3.79	1.80
1.99	4.49	4.49	3.21	6.40	27.82	98.84	64.17	21.63	10.47	137.54	653.14	4233.49	1766.27	175.06	27.37	31.75	10.41	2.96	0.00

1.71	2.92	5.47	2.85	9.00	19.44	80.58	62.29	25.08	17.35	84.18	432.23	4903.76	3906.85	627.74	50.42	38.84	9.58	1.91	0.00
0.78	4.20	7.27	7.12	5.81	41.65	151.75	121.24	35.75	0.00	82.46	422.35	4792.20	2691.28	231.96	24.24	25.69	9.88	0.00	0.00
Na^+										NH_4^+									
M 9	**M 8**	**M 7**	**M 6**	**M 5**	**M 4**	**M 3**	**M 2**	**M 1**	**M 0**	**M 9**	**M 8**	**M 7**	**M 6**	**M 5**	**M 4**	**M 3**	**M 2**	**M 1**	**M 0**
3.12	4.64	4.92	3.03	4.58	4.08	2.55	1.81	2.56	6.53	51.19	135.89	1026.13	493.54	23.75	2.30	1.77	1.39	2.53	2.05
1.90	2.16	5.62	3.18	6.75	4.16	2.51	1.46	1.58	2.30	23.47	61.62	591.75	522.49	62.14	1.95	1.69	2.69	1.91	1.89
1.98	1.89	2.14	2.04	3.62	3.10	2.27	0.83	0.97	4.59	10.20	64.16	294.64	183.54	38.75	4.06	2.85	1.48	0.81	1.79
1.81	1.68	4.77	2.47	6.00	7.81	5.35	1.73	5.95	1.12	29.13	54.94	480.07	382.13	73.76	3.29	2.25	2.28	3.58	1.00
2.11	3.25	2.72	6.02	20.00	28.18	14.71	14.33	2.00	1.31	8.40	23.66	180.40	50.92	2.05	2.04	2.21	0.90	1.25	0.86
1.66	2.14	3.97	4.66	18.03	26.01	19.36	4.76	1.41	0.71	16.26	52.33	652.85	308.23	44.48	2.11	1.36	2.55	1.65	1.61
1.16	1.43	4.03	3.99	4.47	3.10	2.16	1.21	0.92	0.73	26.37	93.81	873.11	896.38	132.77	2.22	2.02	2.35	1.21	1.11
5.15	1.51	3.57	1.62	5.22	4.28	2.25	1.00	0.97	1.17	120.64	203.33	735.60	107.44	9.80	2.08	2.09	1.40	1.41	1.54
3.01	2.59	6.69	4.52	6.20	7.89	12.23	6.34	1.44	2.93	37.27	225.11	1190.37	308.28	15.65	2.11	2.48	1.89	0.90	1.17
1.92	3.02	8.10	4.97	13.07	15.98	22.55	8.48	1.37	0.66	29.61	97.62	861.42	560.49	51.56	2.46	1.43	2.01	1.47	1.34
2.31	2.14	2.47	0.84	1.08	0.80	1.03	0.93	0.89	0.90	58.13	173.47	666.69	121.45	10.71	5.06	8.95	2.76	1.45	1.15
2.06	2.18	4.67	2.98	3.12	2.53	1.79	2.74	1.68	0.75	35.95	166.11	1144.79	385.74	29.43	2.06	1.57	1.27	0.70	0.88
1.31	2.42	7.49	4.74	6.85	5.82	5.53	1.87	2.76	1.17	18.22	86.58	1235.09	861.88	114.85	3.46	1.76	0.91	1.06	1.26
3.35	2.22	7.23	6.27	5.99	5.38	6.52	4.98	1.24	1.67	26.51	138.06	1557.29	745.41	33.56	3.40	3.98	3.27	2.33	1.58
K^+										Mg^{2+}									
M 9	**M 8**	**M 7**	**M 6**	**M 5**	**M 4**	**M 3**	**M 2**	**M 1**	**M 0**	**M 9**	**M 8**	**M 7**	**M 6**	**M 5**	**M 4**	**M 3**	**M 2**	**M 1**	**M 0**
3.22	8.67	30.98	20.09	7.62	7.20	7.16	3.63	2.68	2.56	0.61	2.85	2.28	2.11	3.92	3.01	5.36	3.84	1.35	1.31
1.90	6.11	19.18	9.17	7.15	8.79	8.82	2.54	1.23	0.92	0.47	2.04	2.12	2.19	2.92	2.64	4.39	2.42	1.33	1.09
1.58	4.32	8.04	1.96	1.98	8.20	9.68	1.98	1.09	2.20	0.58	1.67	3.41	2.07	4.78	2.13	3.52	1.74	1.31	1.17
2.09	3.56	9.29	5.49	4.04	8.44	12.68	2.03	6.77	1.24	0.79	3.13	3.51	3.85	4.28	4.81	5.05	2.41	3.20	1.79
1.08	5.06	3.22	0.95	3.17	7.80	7.06	2.13	0.30	0.24	0.61	2.33	5.01	4.34	5.44	7.02	7.90	2.19	1.27	1.02
3.08	3.62	8.88	4.05	3.07	7.72	8.39	1.91	0.24	0.73	0.49	1.72	1.81	2.29	4.09	4.50	3.86	1.97	0.93	0.76
2.99	4.57	14.19	10.72	4.12	4.76	8.82	2.45	1.63	0.71	0.85	1.62	1.99	2.87	3.17	3.23	5.14	2.77	1.30	1.40
6.87	2.53	10.17	2.33	1.47	3.71	6.23	2.24	1.56	1.73	0.84	4.02	4.89	3.41	2.97	3.10	4.88	2.47	0.72	1.27
6.69	11.37	25.69	11.99	2.23	3.83	7.48	4.65	1.12	0.98	0.69	1.54	2.25	3.43	1.74	2.30	4.72	3.61	1.26	0.88
2.72	6.07	17.24	5.80	2.38	3.49	5.21	1.94	1.38	0.59	0.68	3.83	4.56	4.45	3.89	4.90	5.02	2.95	1.41	0.99
5.48	6.03	7.58	2.19	1.33	4.66	6.70	2.34	0.24	0.41	0.58	1.95	1.87	2.27	2.90	3.32	6.47	4.61	1.50	1.61
5.51	5.12	13.35	4.89	2.62	6.07	6.91	3.55	2.48	0.63	1.62	4.02	5.35	5.19	5.72	4.67	7.10	5.07	2.87	1.69
4.57	7.38	22.36	7.96	4.33	4.71	7.34	1.94	3.56	0.21	0.22	3.85	2.77	6.62	7.07	5.37	7.39	5.35	3.05	3.22
5.20	7.57	24.68	10.39	2.06	4.12	5.06	5.33	2.70	0.58	1.45	4.31	5.17	6.28	5.77	5.33	10.56	8.03	4.51	6.03
Ca^{2+}																			
M 9	**M 8**	**M 7**	**M 6**	**M 5**	**M 4**	**M 3**	**M 2**	**M 1**	**M 0**										
0.66	1.12	2.03	2.10	3.31	3.70	18.76	13.20	4.17	2.59										
0.47	2.14	2.49	1.77	3.45	3.19	10.22	6.22	3.36	2.90										

0.57	1.72	0.99	2.11	3.09	1.73	4.12	1.61	1.45	2.47
0.82	0.99	1.25	1.33	2.34	2.44	8.38	3.35	3.44	2.08
0.47	0.56	3.18	2.61	1.05	1.05	3.45	1.49	1.12	1.20
0.72	1.72	1.47	1.76	2.69	2.07	5.66	3.72	1.40	1.43
0.85	1.92	2.30	3.19	3.30	3.34	13.45	9.19	2.71	2.20
1.21	2.01	1.72	1.69	1.12	2.21	10.98	8.12	2.25	1.96
1.02	1.43	2.01	2.23	1.52	1.80	8.70	7.02	2.05	2.28
0.45	2.13	2.15	2.42	3.01	2.77	8.48	6.61	2.65	1.51
0.95	1.94	1.49	2.18	1.38	2.78	17.58	8.91	2.43	1.75
0.39	1.28	1.77	1.96	3.18	3.23	18.06	11.36	3.92	2.15
0.65	1.78	2.38	2.98	3.92	4.01	15.81	10.45	3.99	2.53
1.21	1.83	3.56	6.20	5.16	4.67	24.35	20.32	5.32	6.47

Figure E1 San Gorgonio (April) MOUDI (anion and cation) daily plots

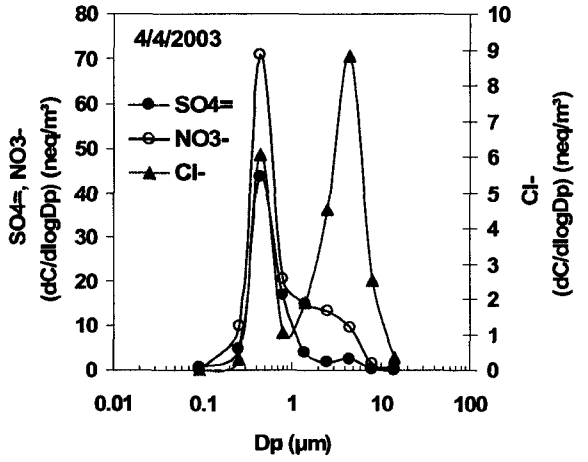

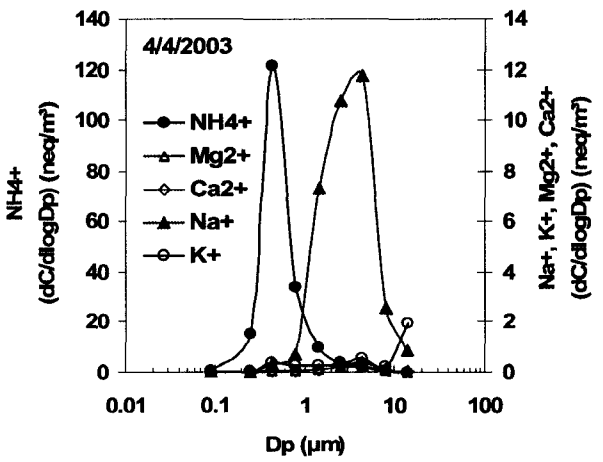

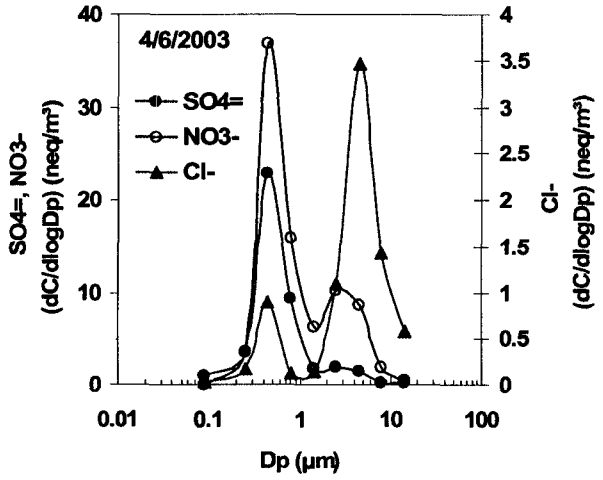

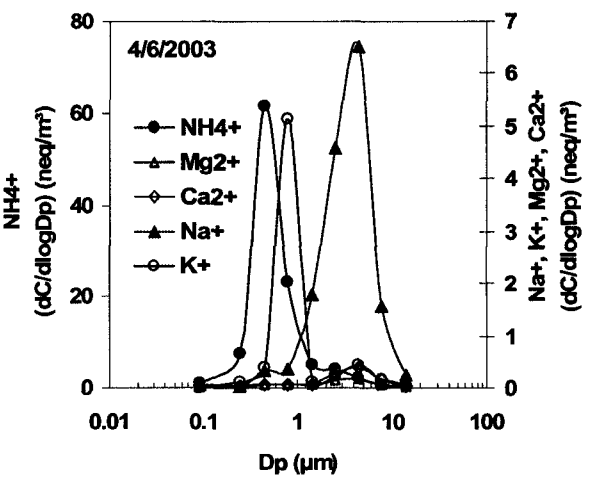

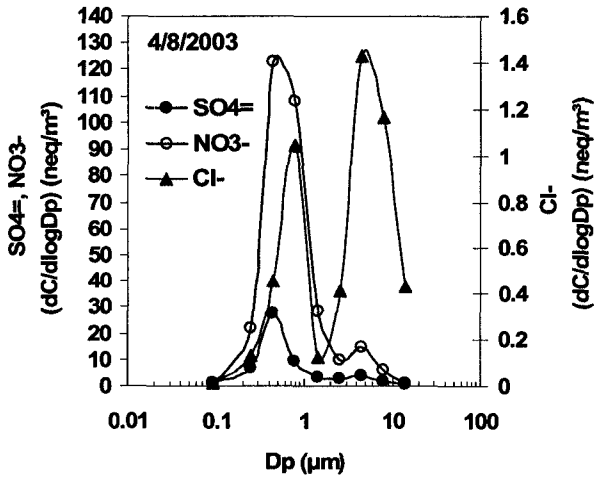

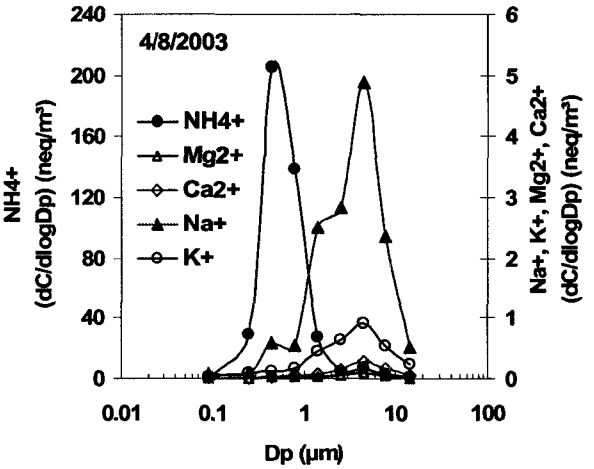

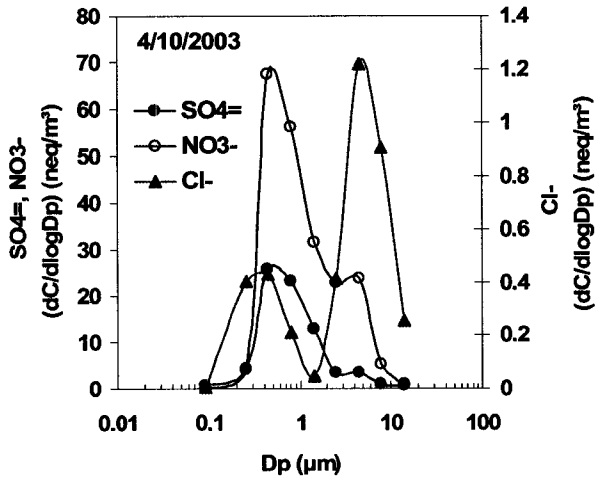

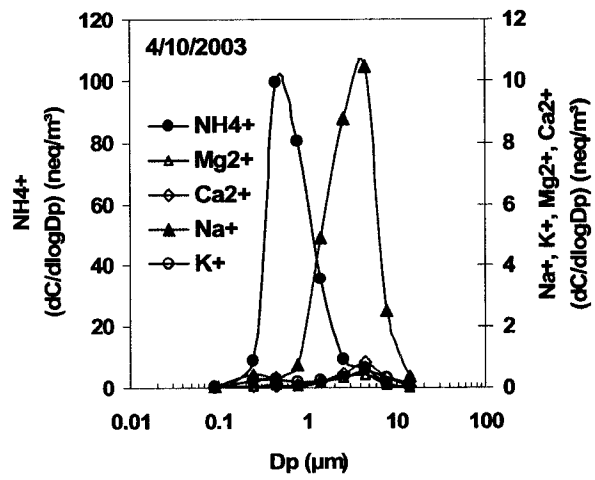

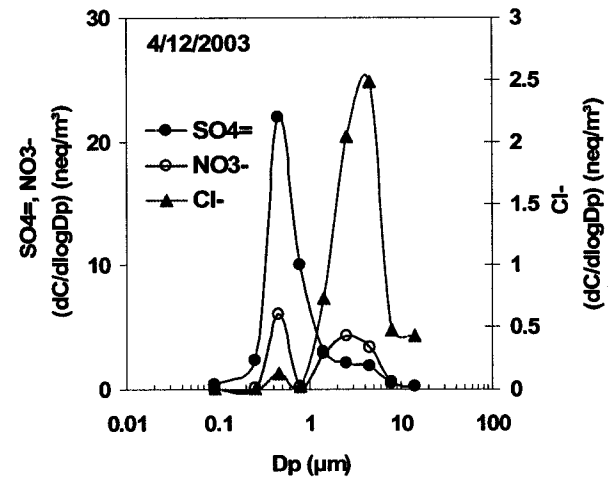

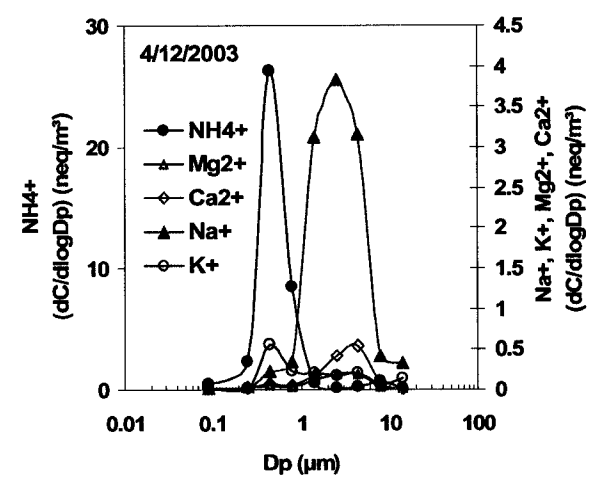

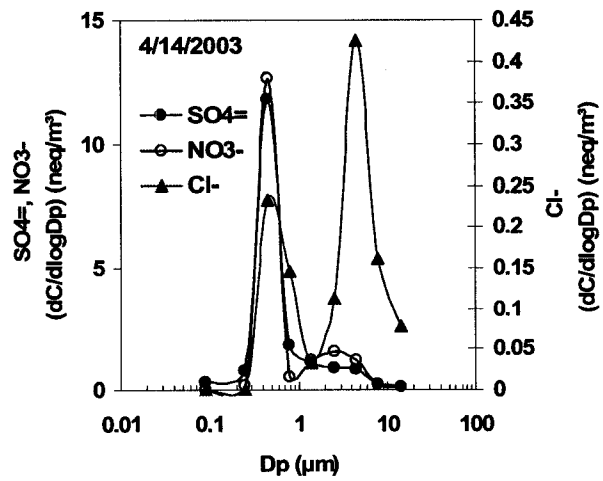

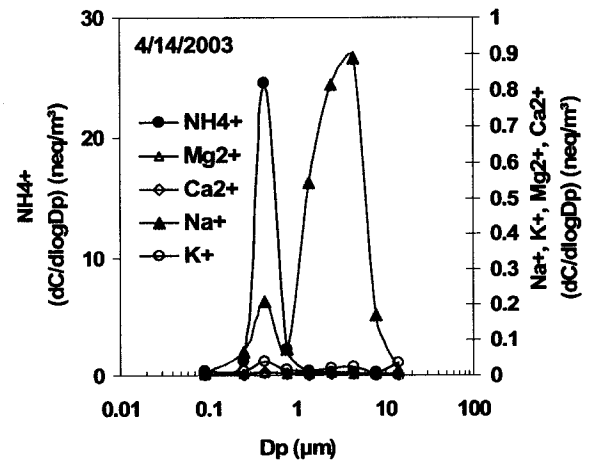

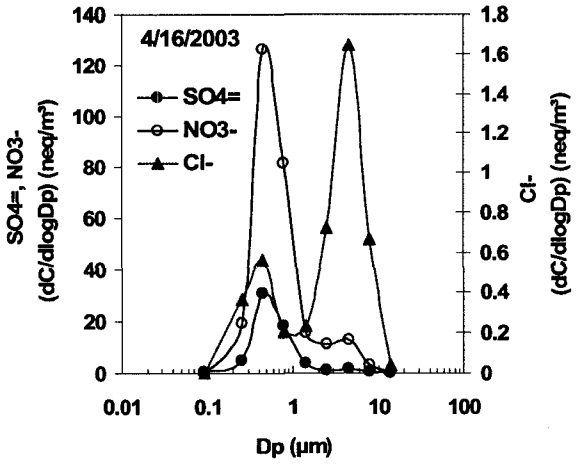

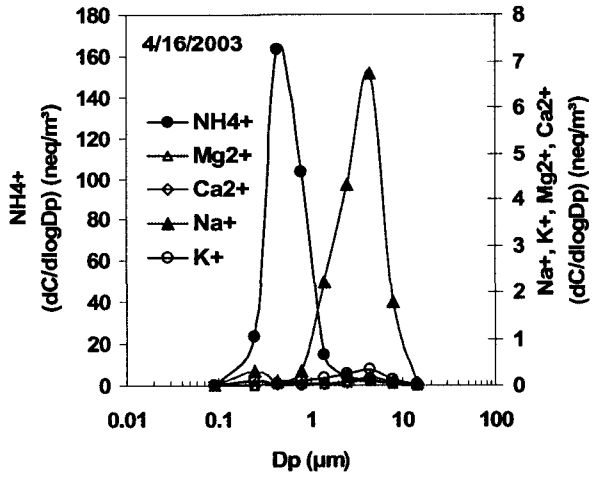

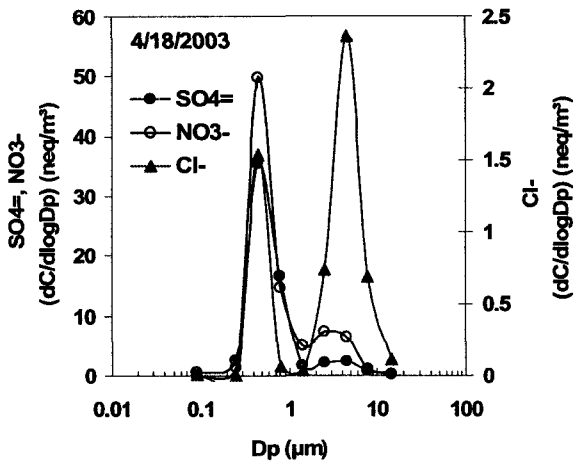

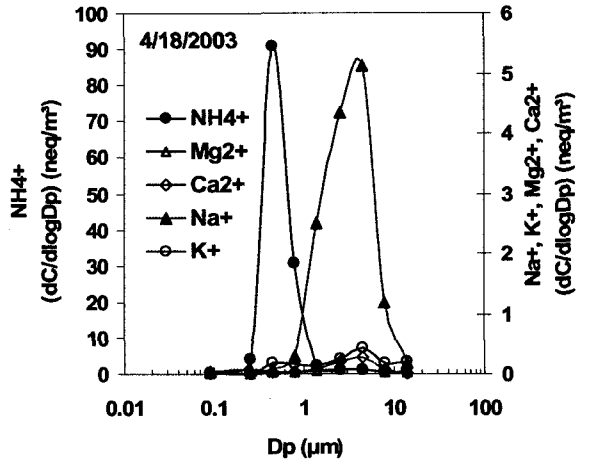

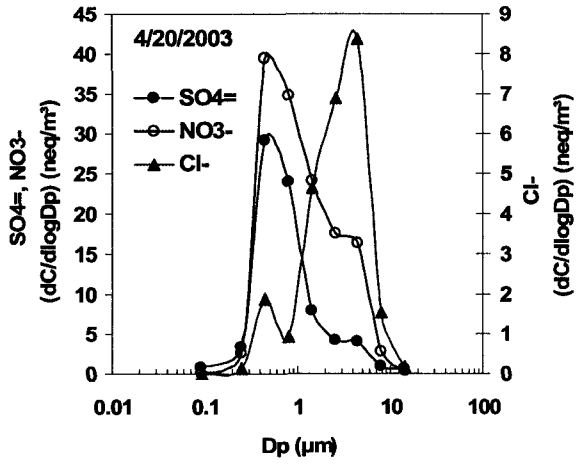

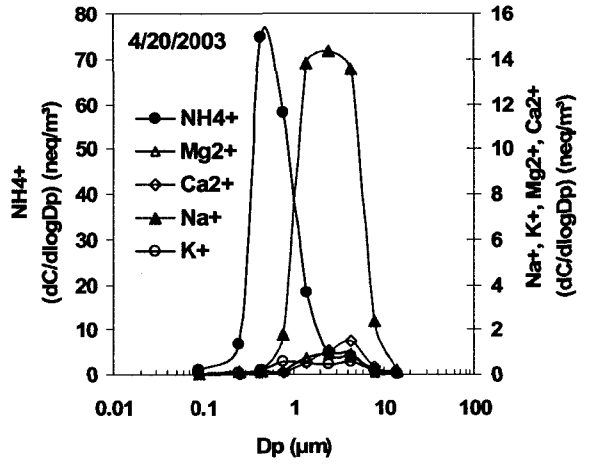

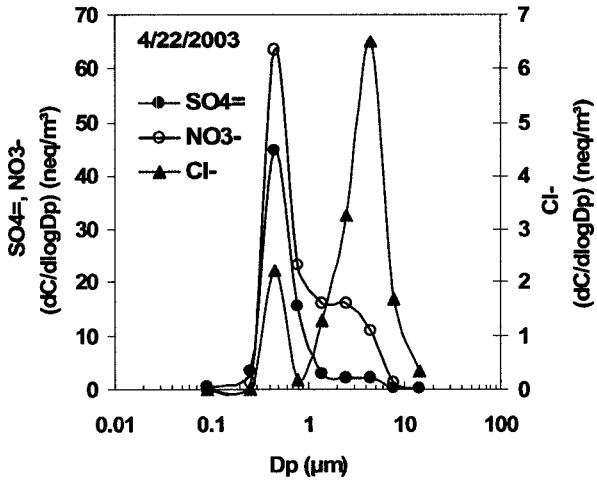

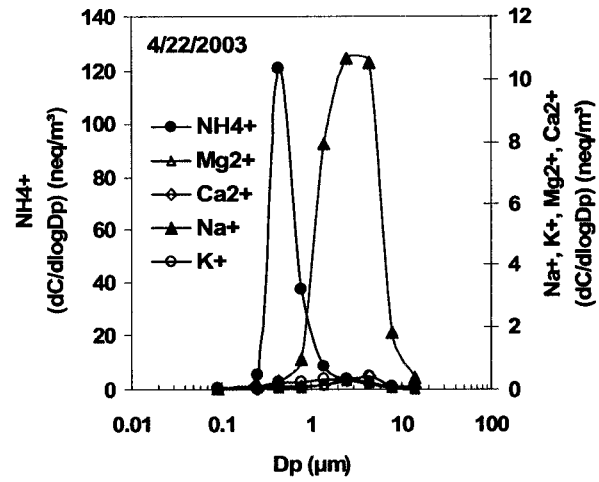

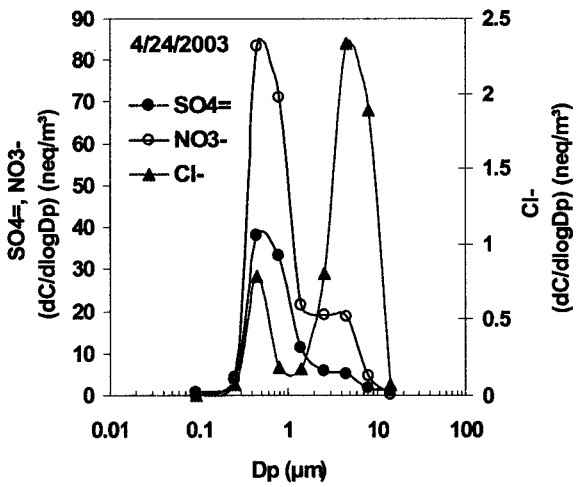

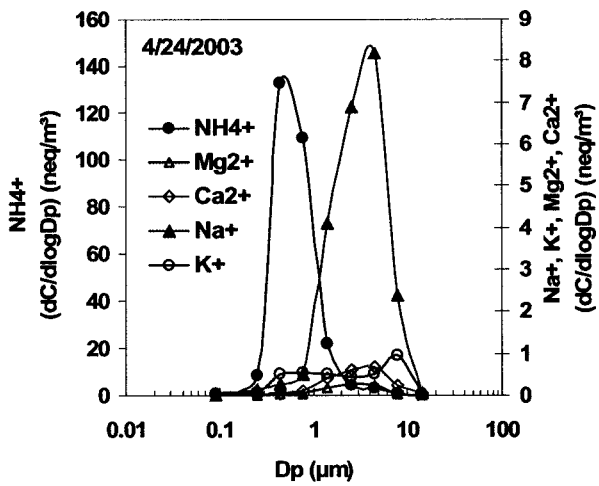

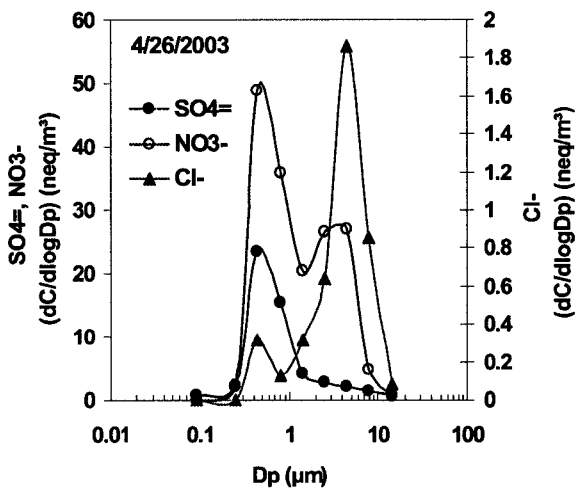

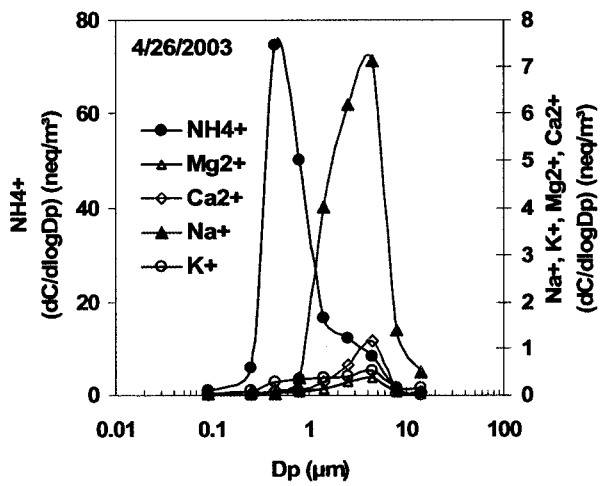

Figure E2 San Gorgonio (July) MOUDI (anion and cation) daily plots

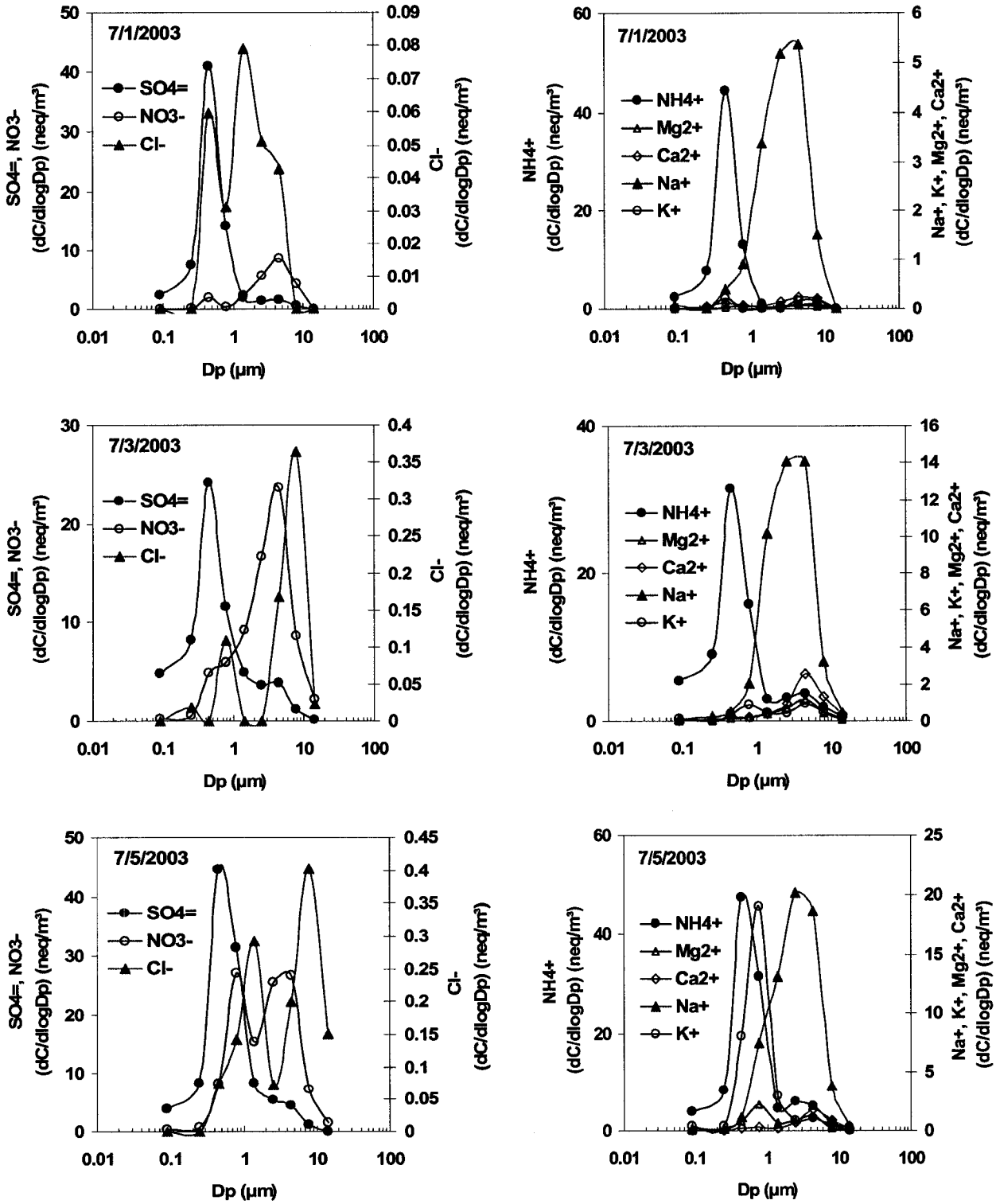

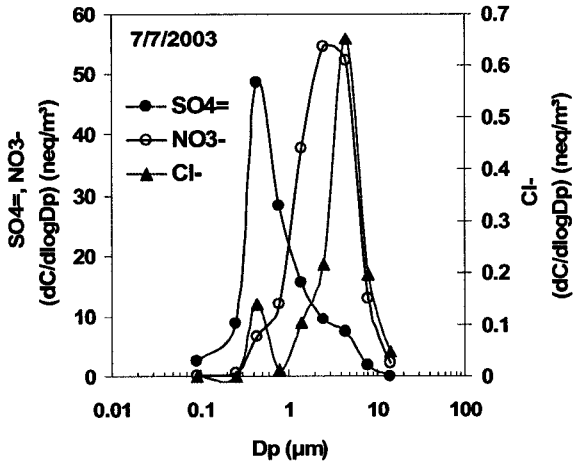

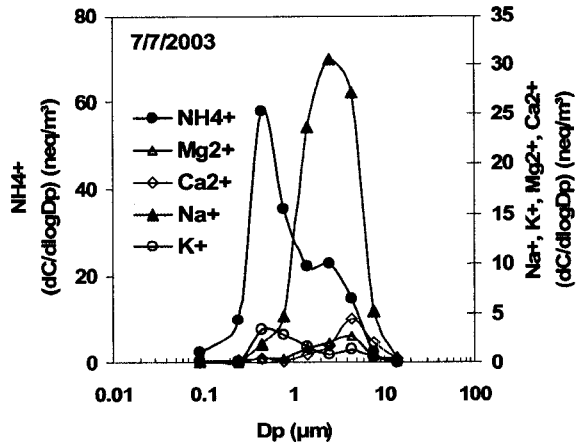

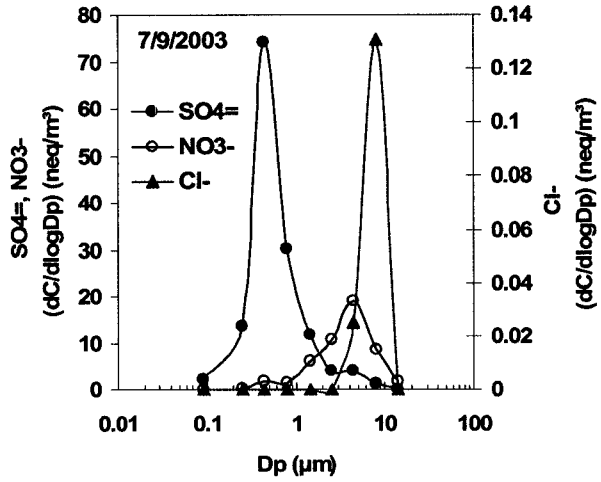

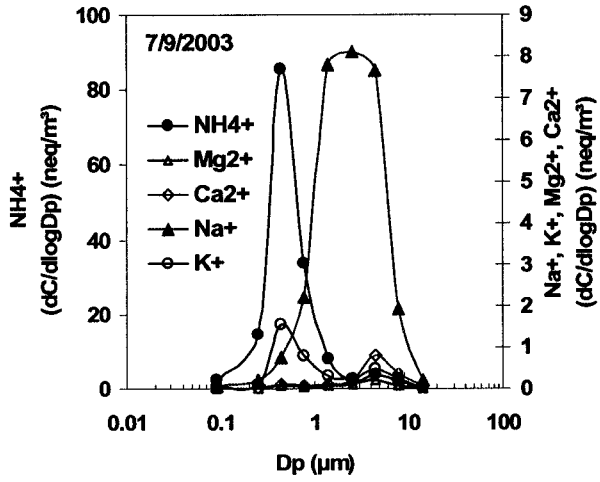

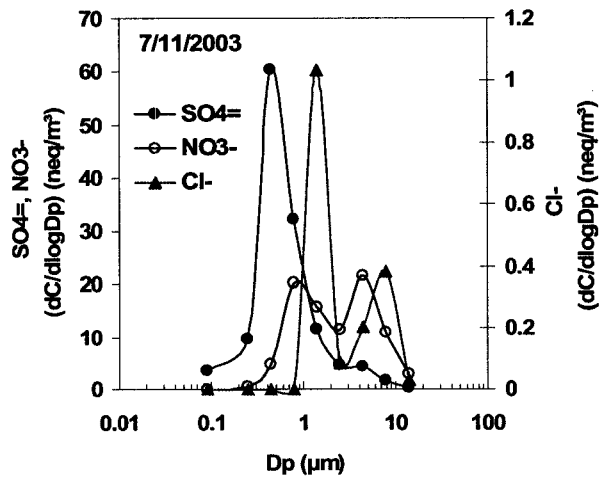

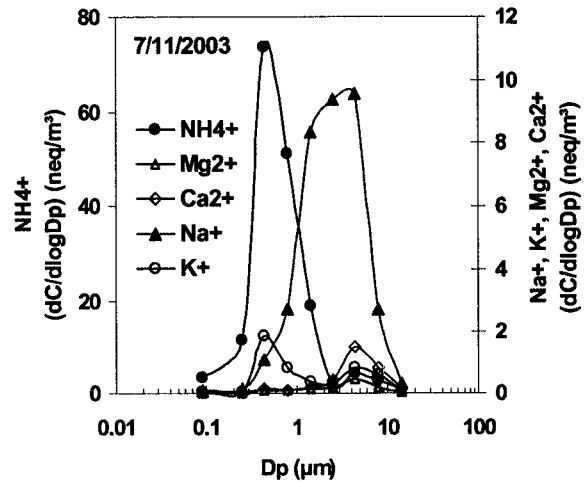

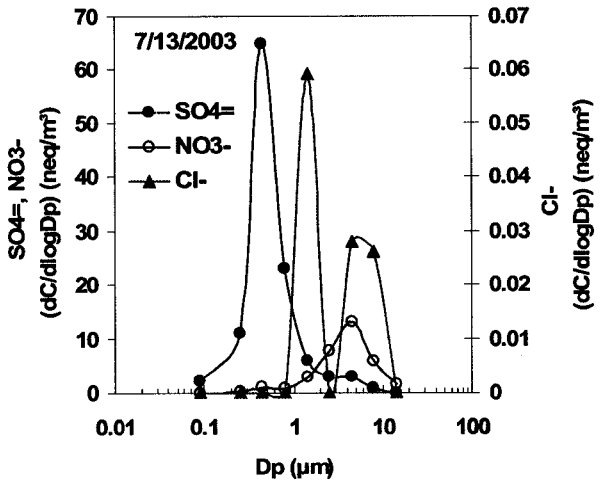

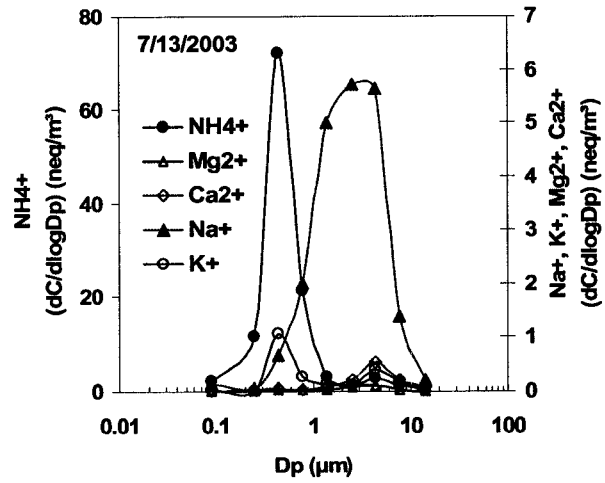

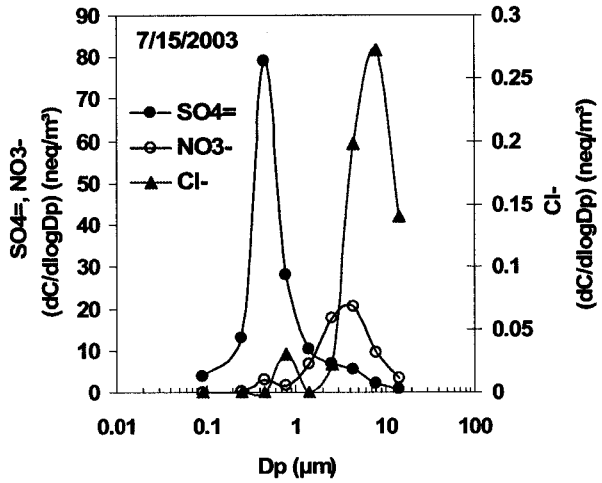

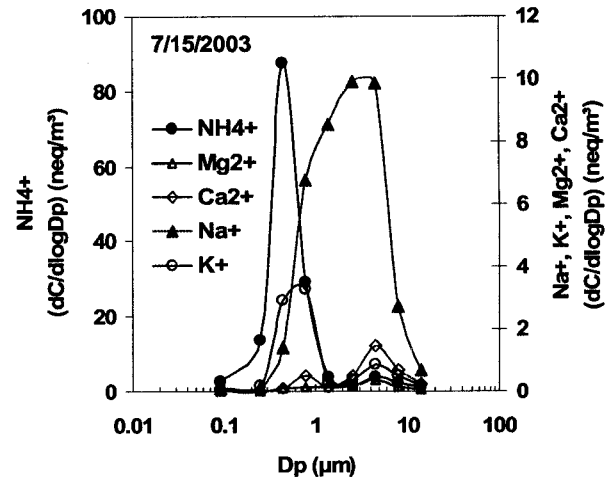

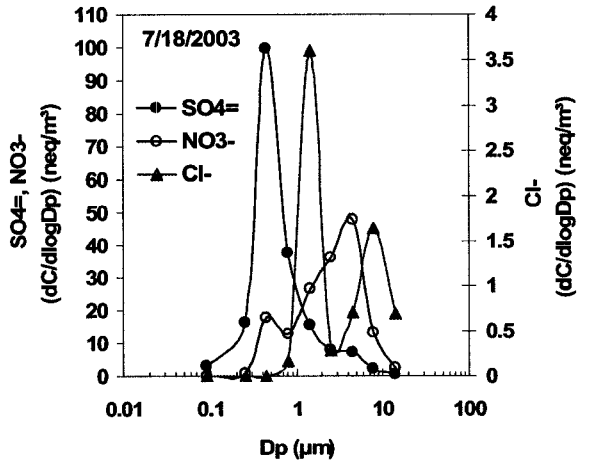

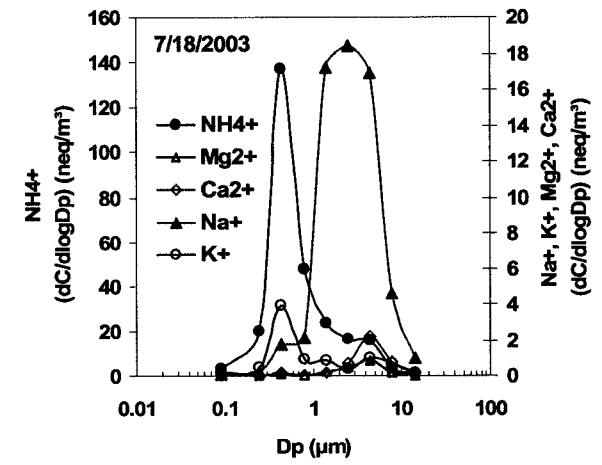

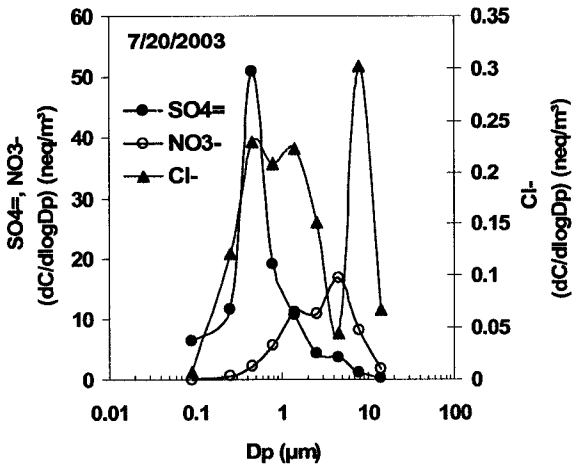

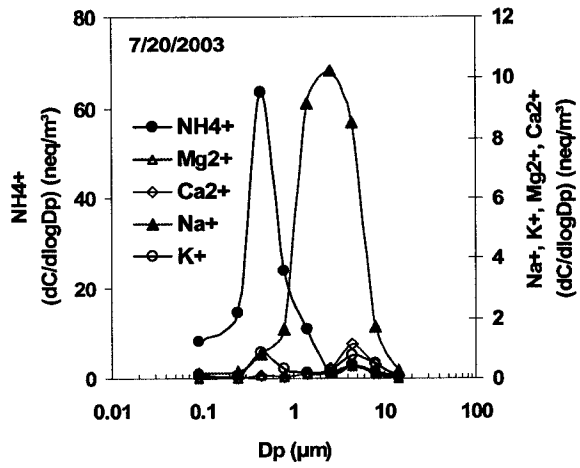

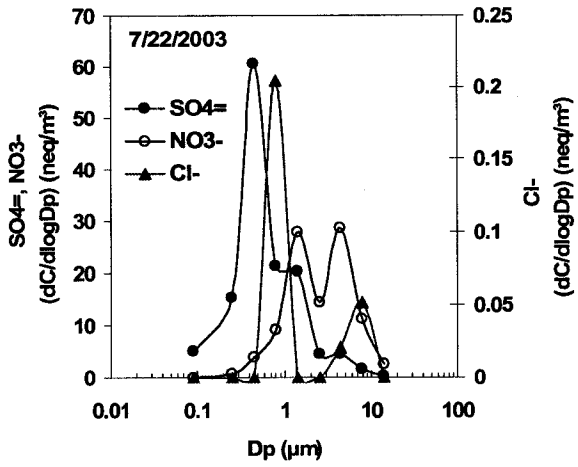

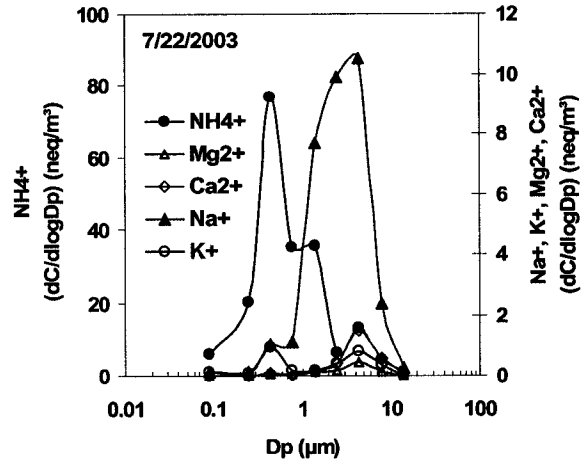

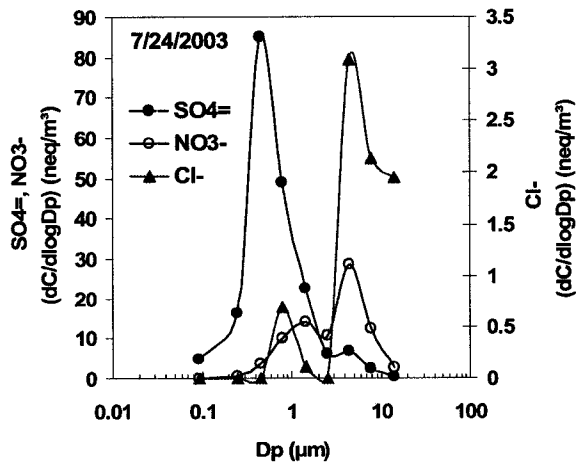

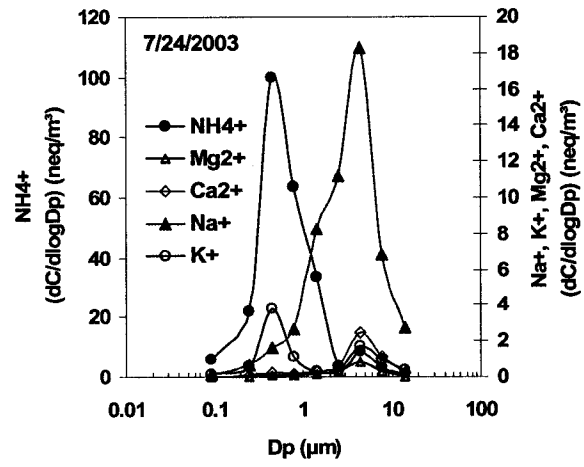

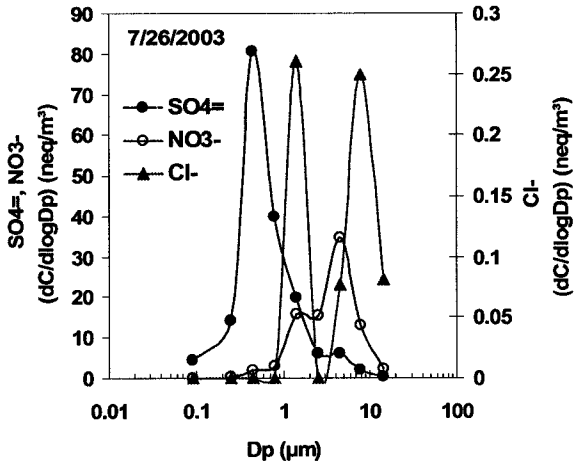

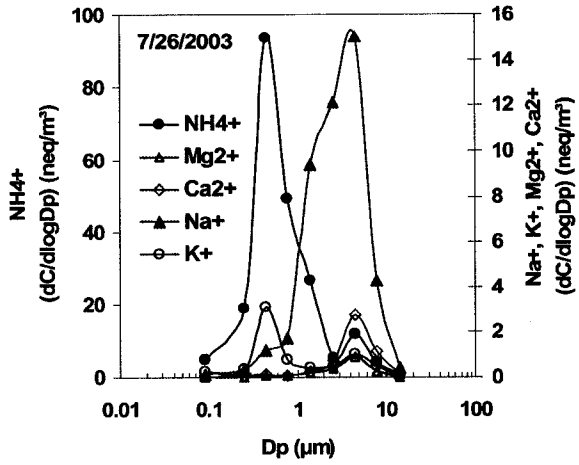

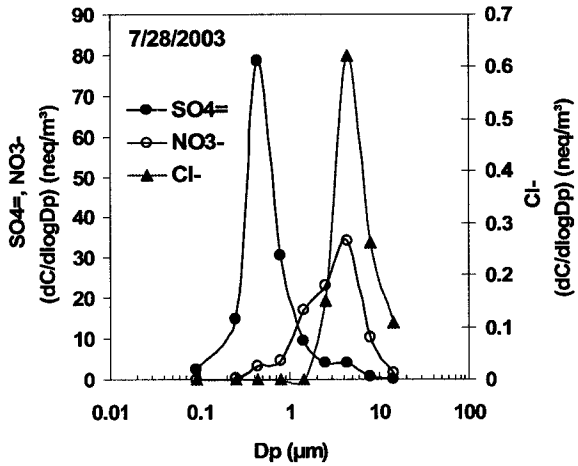

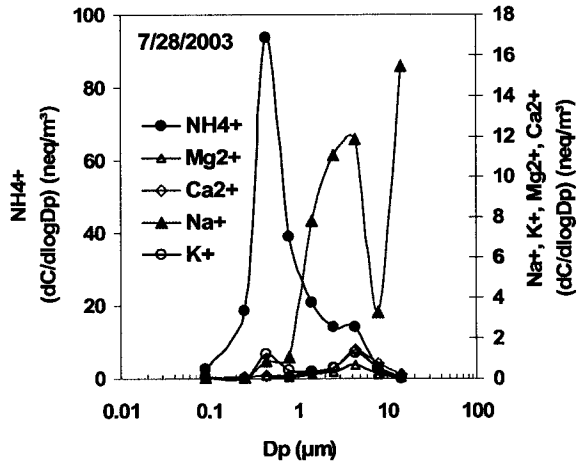

Figure E3 Grand Canyon NP (May) MOUDI (anion and cation) daily plots

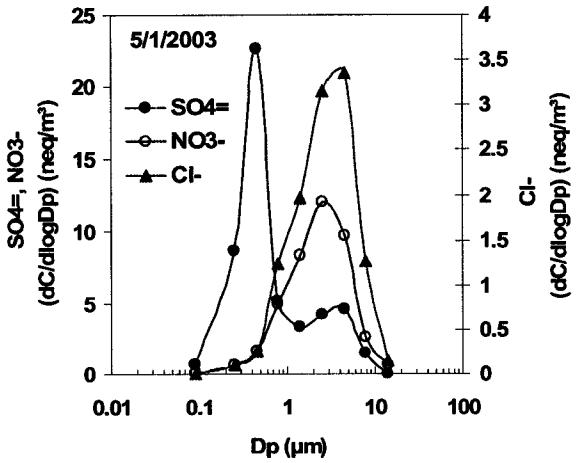

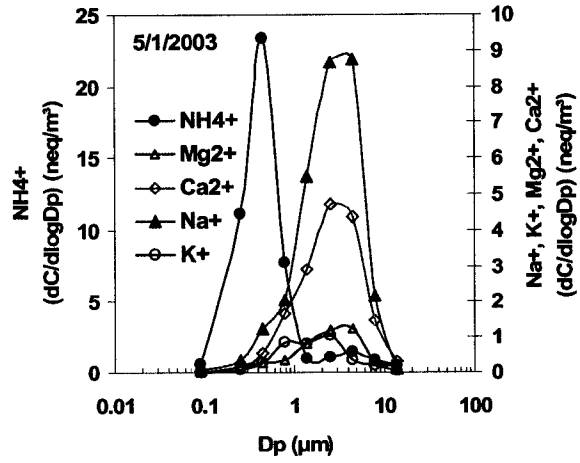

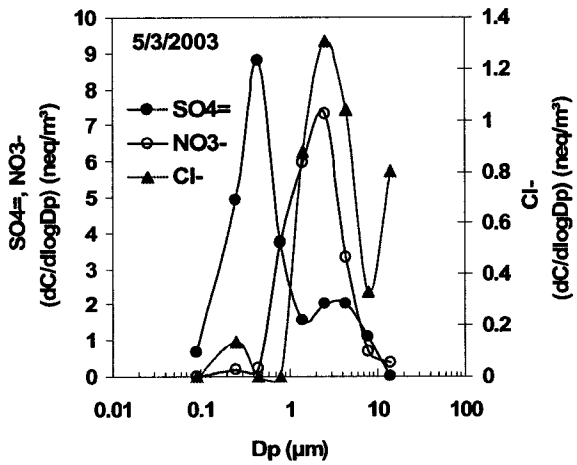

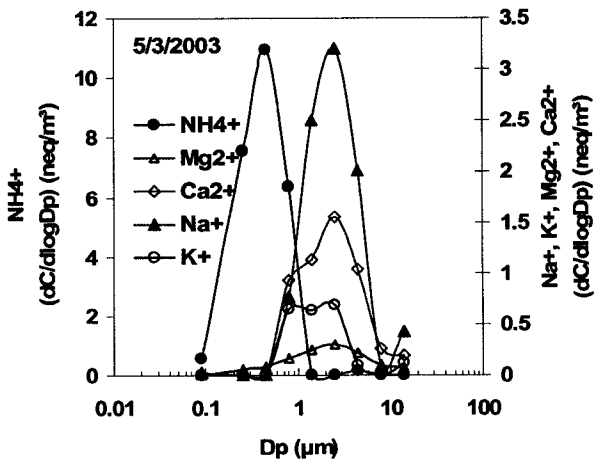

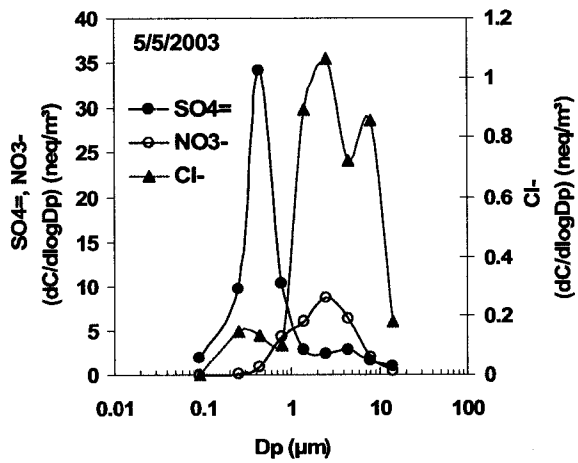

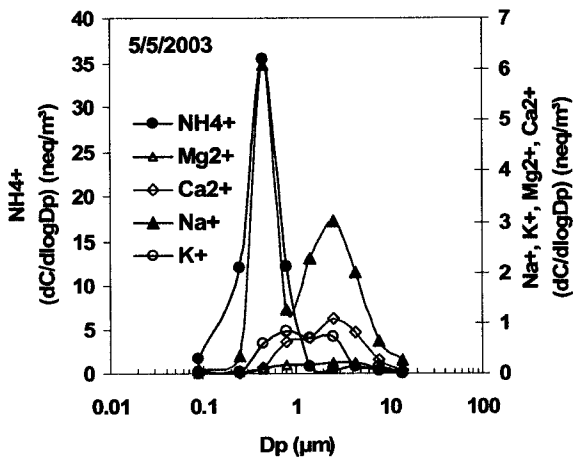

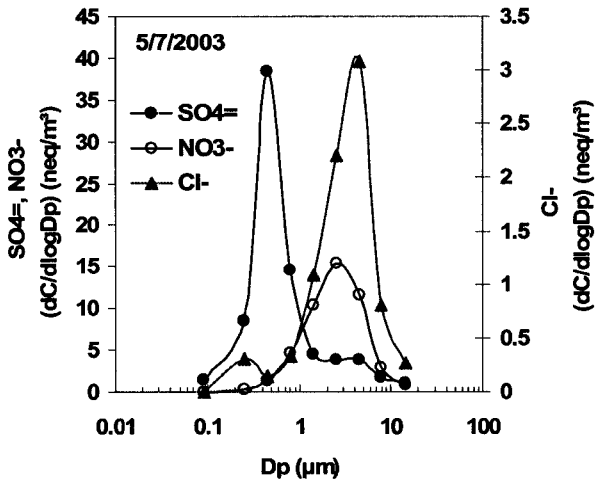

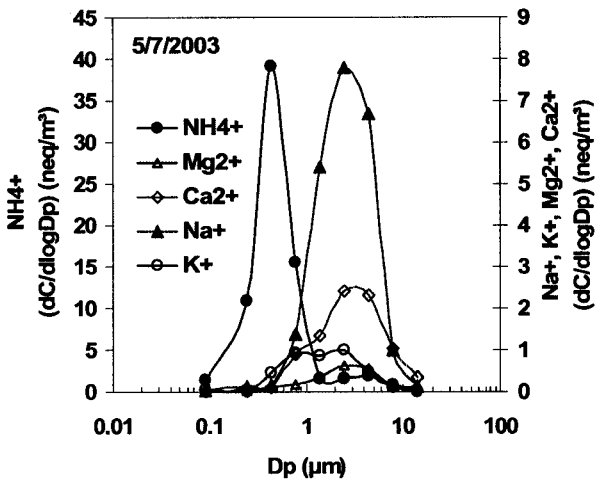

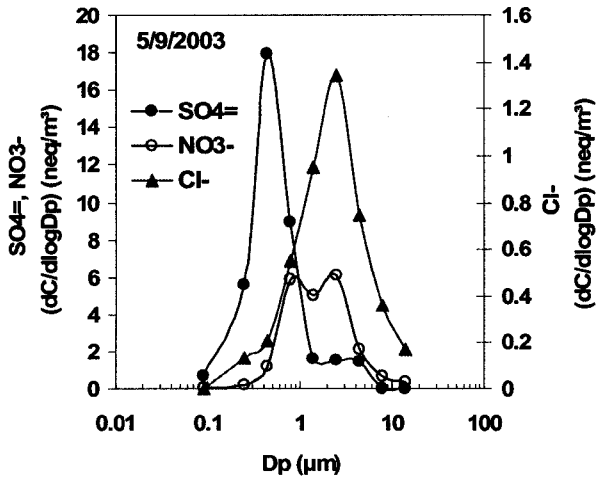

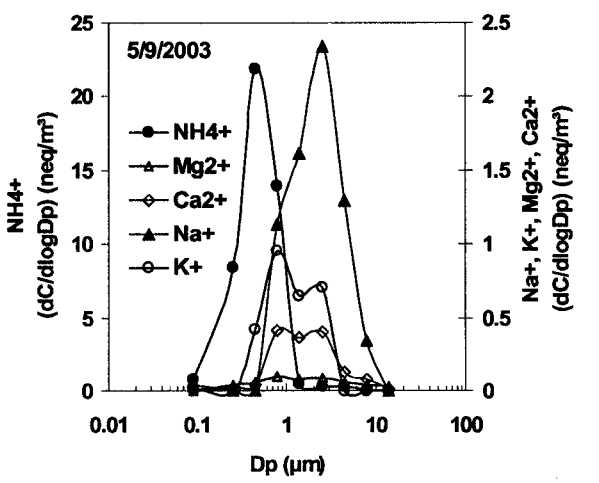

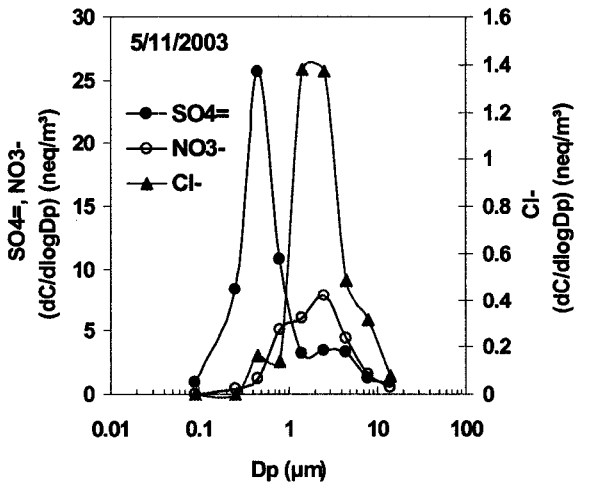

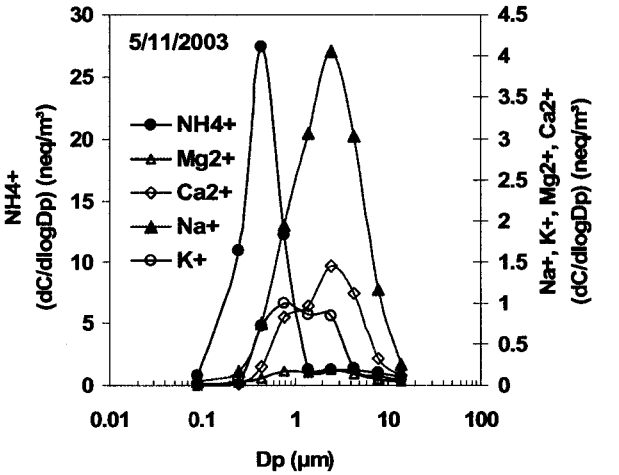

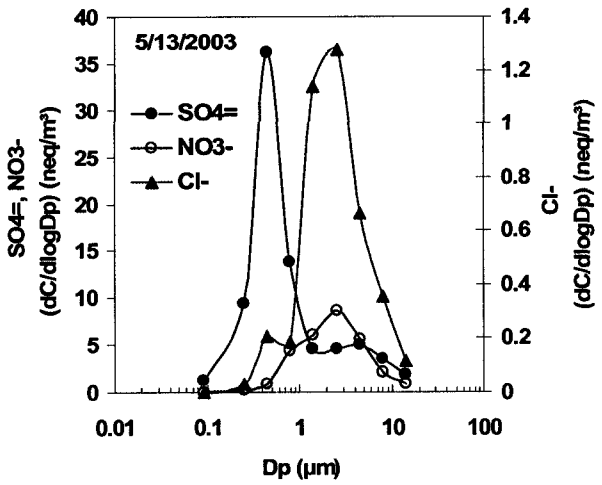

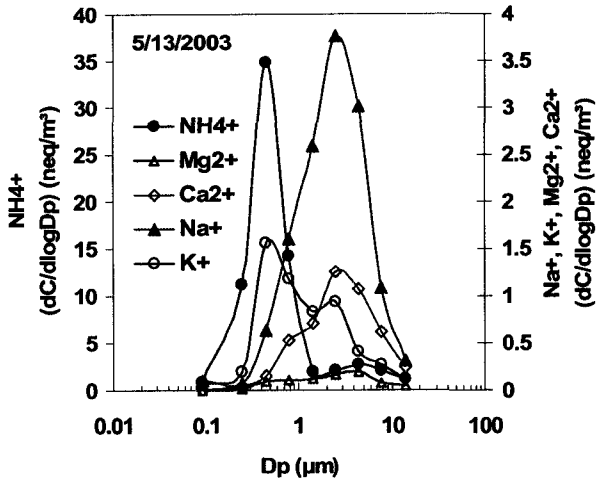

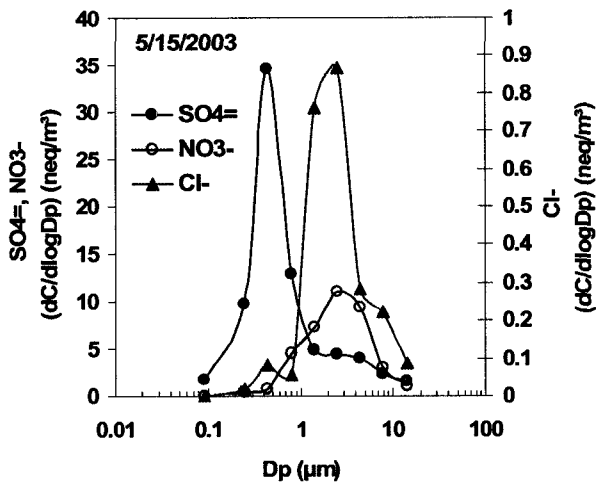

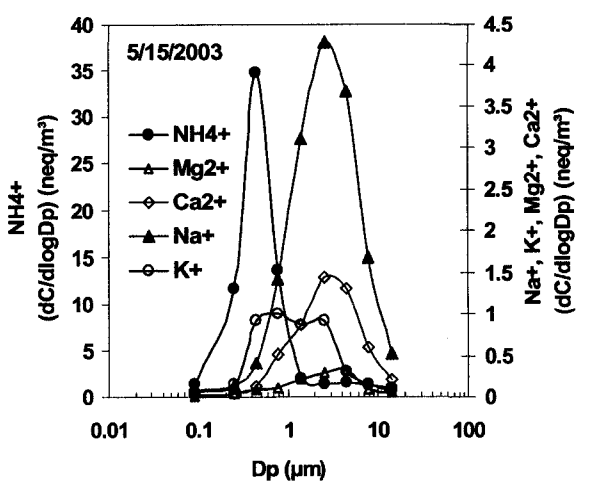

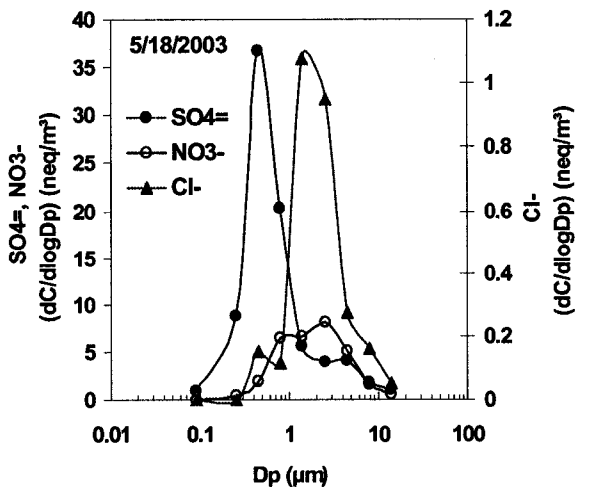

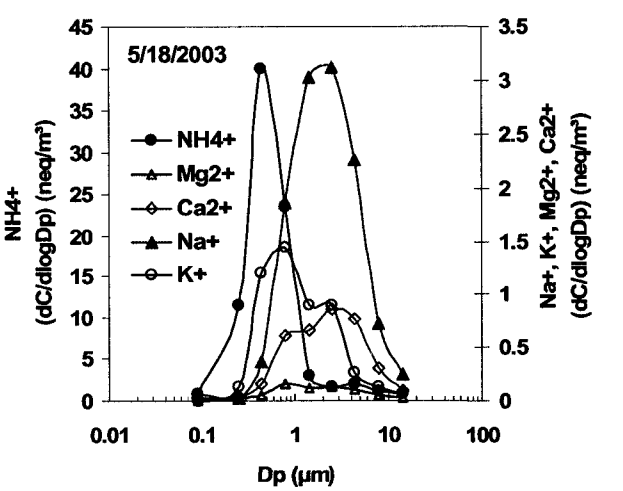

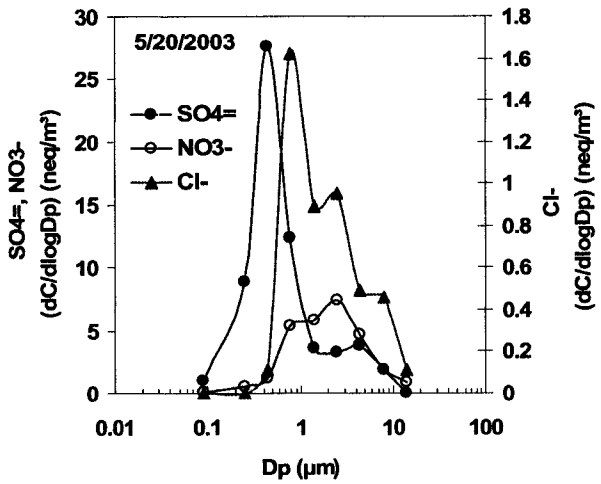

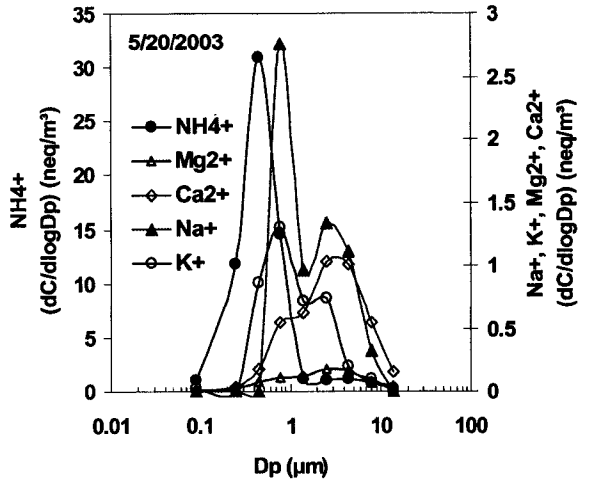

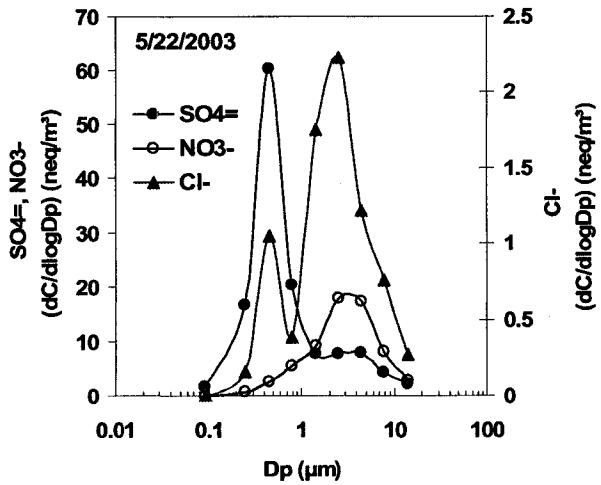

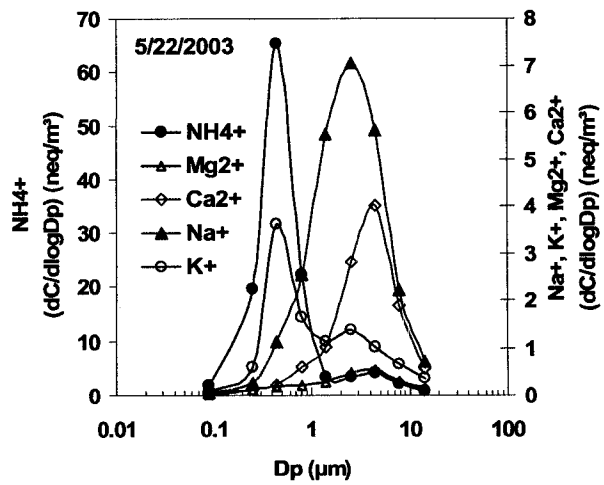

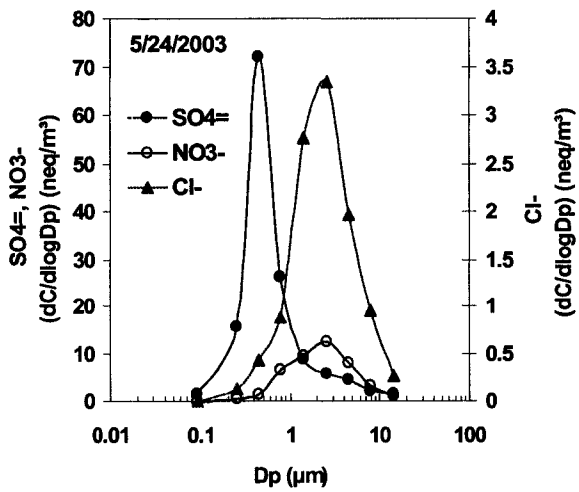

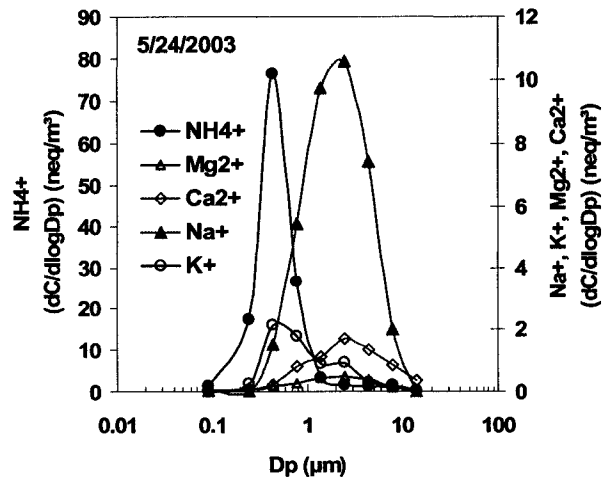

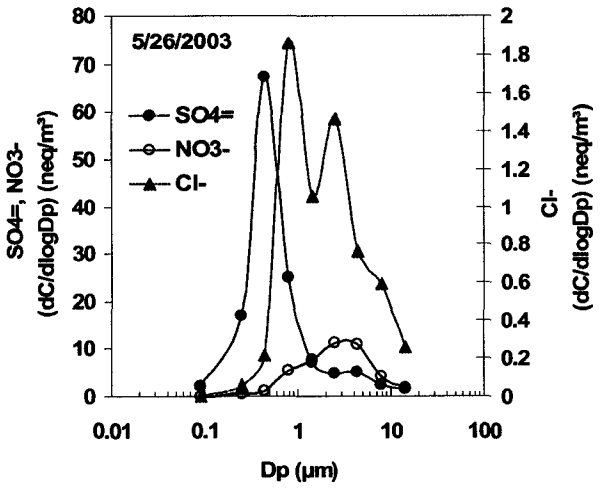

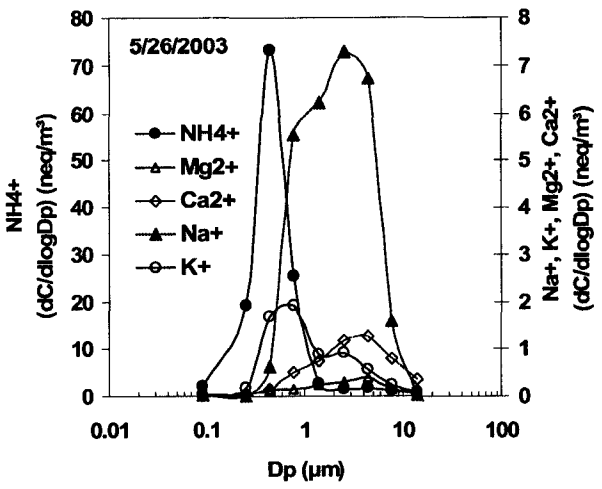

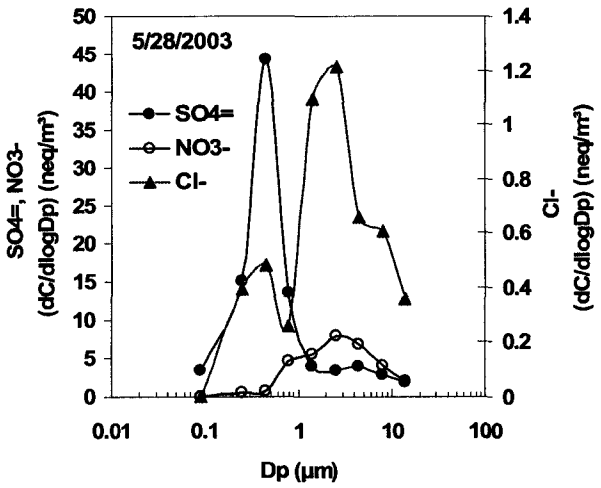

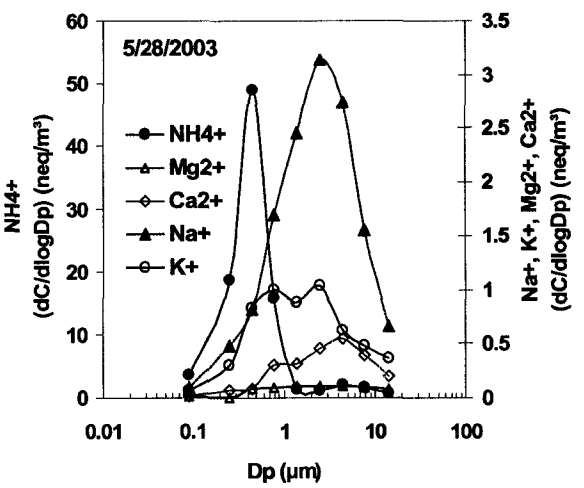

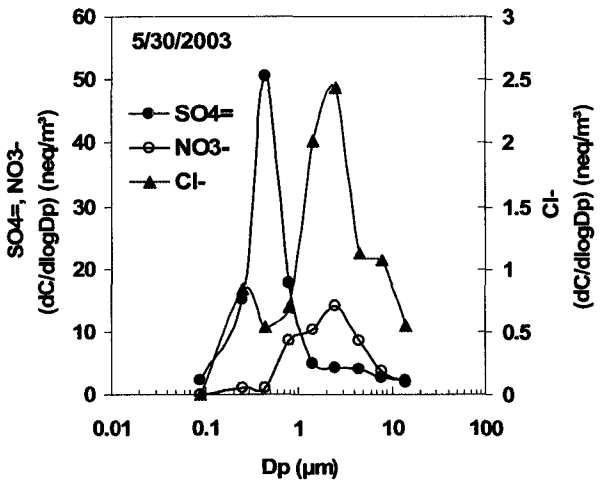

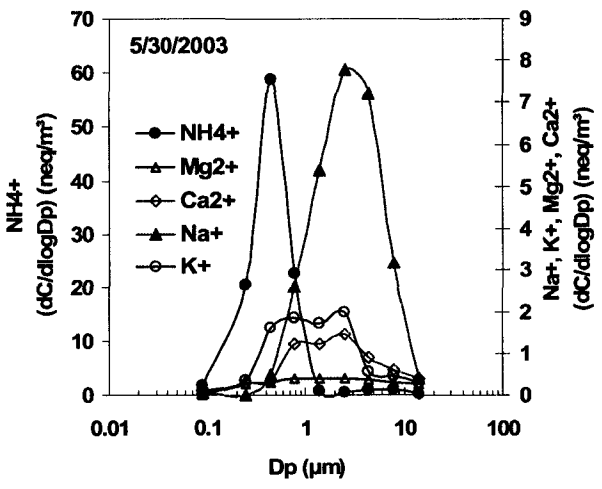

Figure E4 Bondville (Feb) MOUDI (anion and cation) daily plots

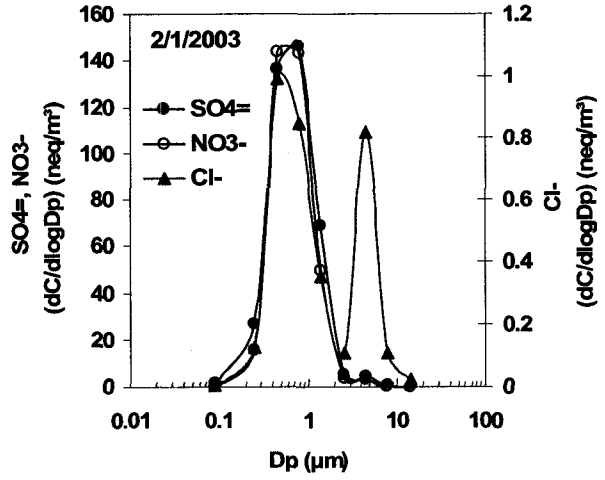

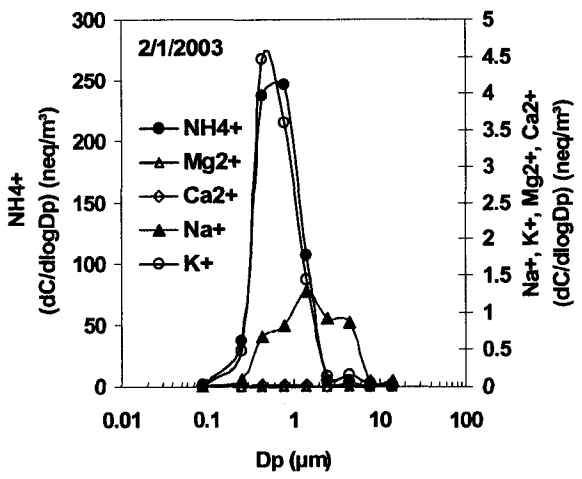

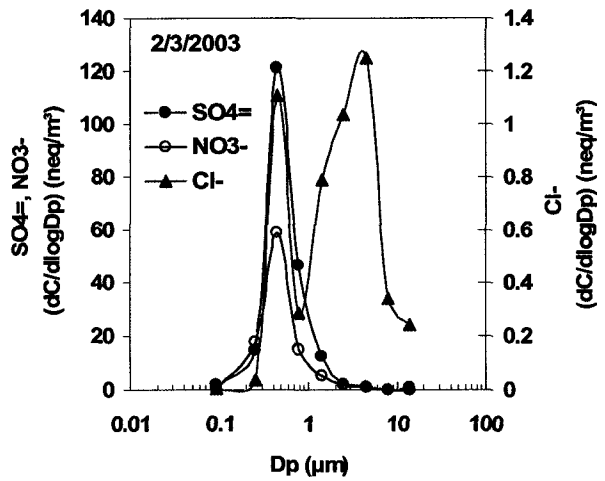

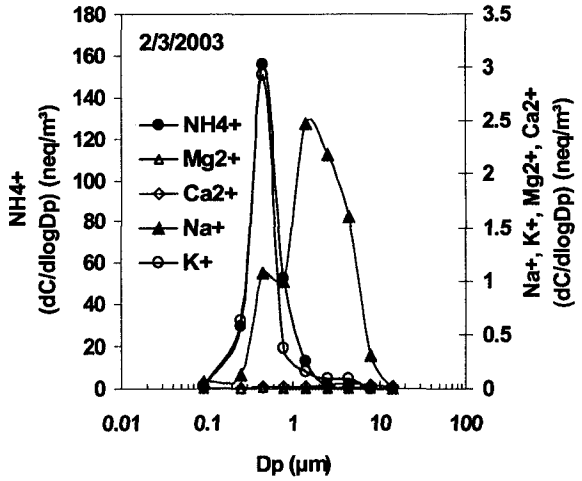

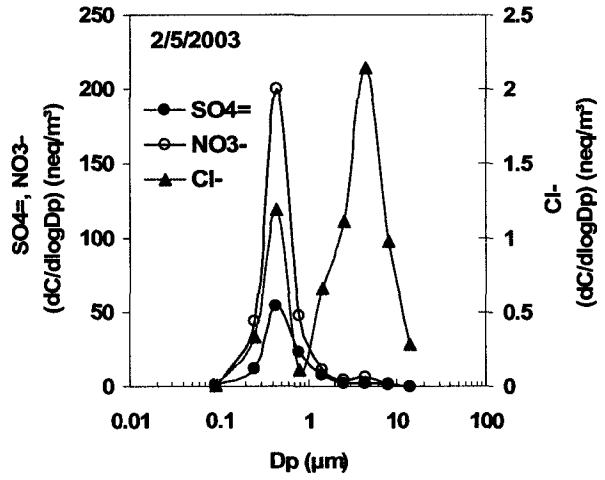

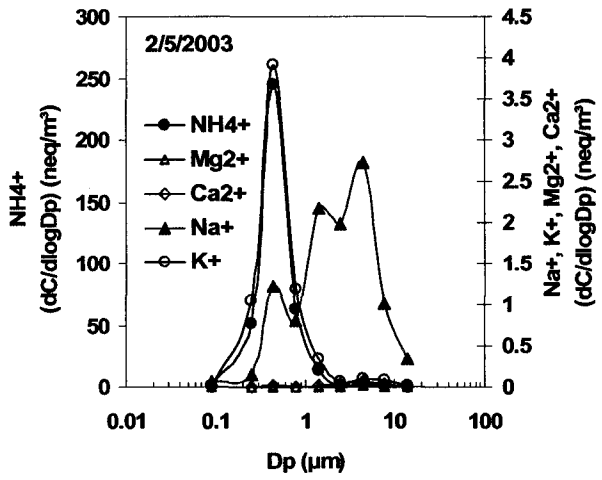

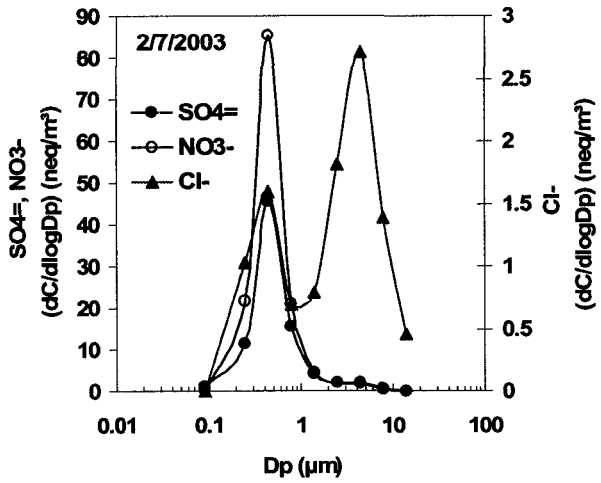

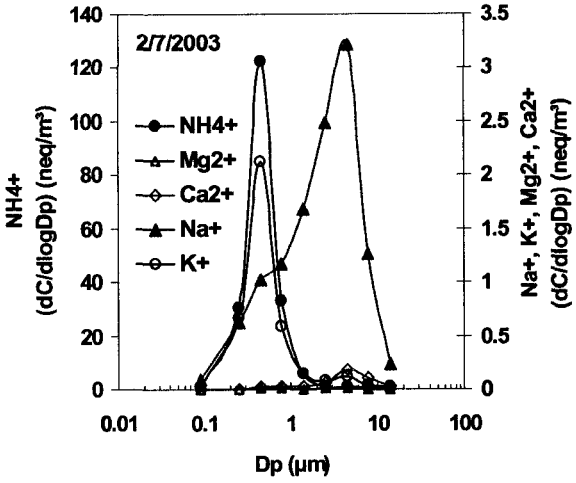

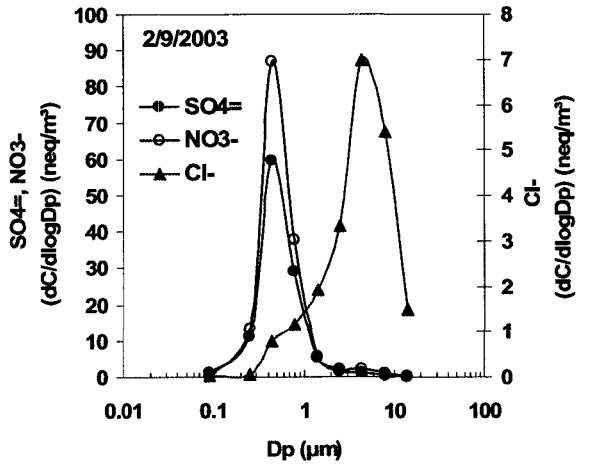

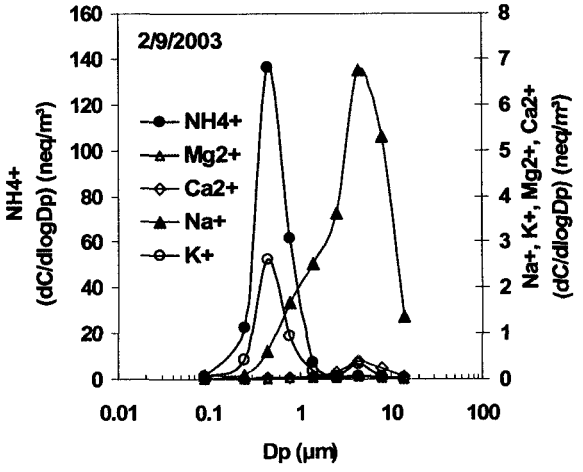

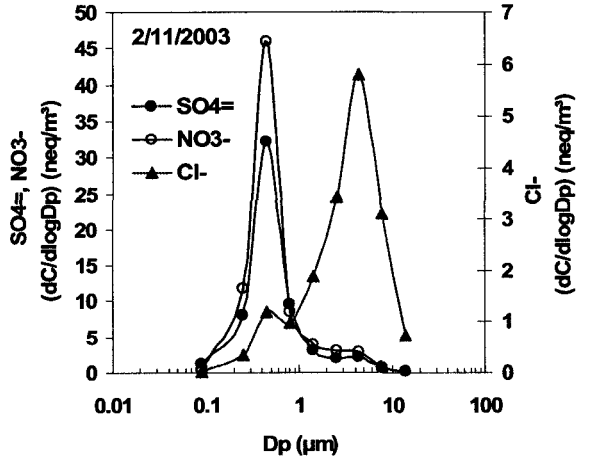

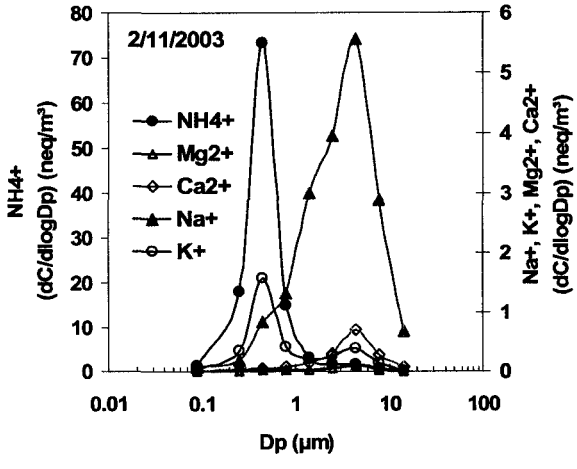

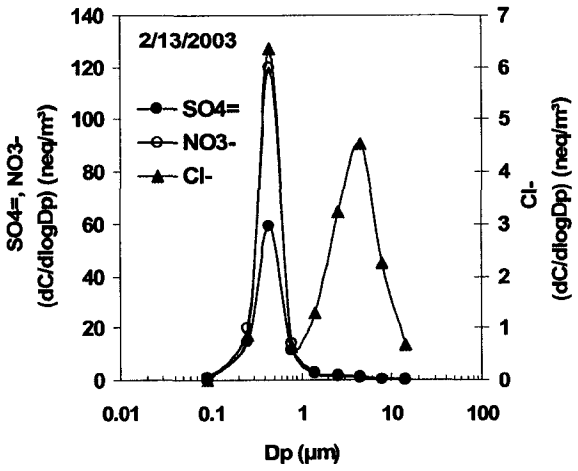

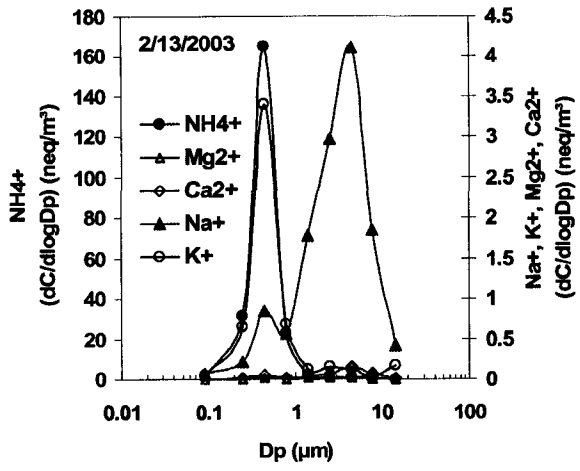

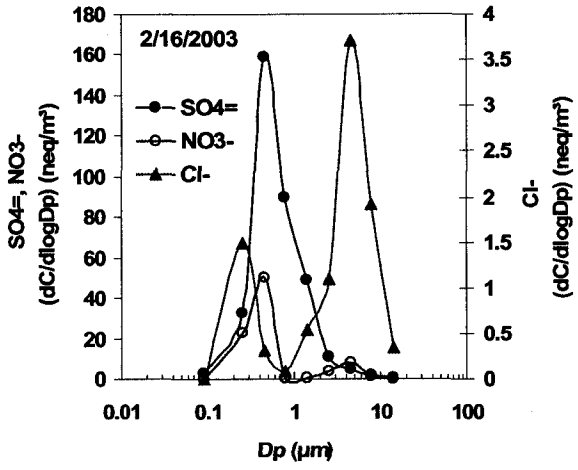

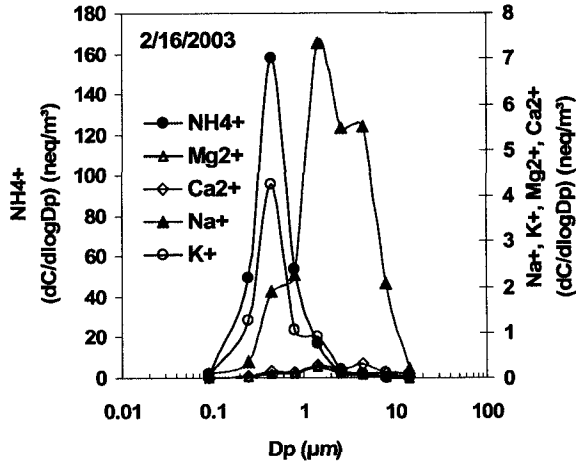

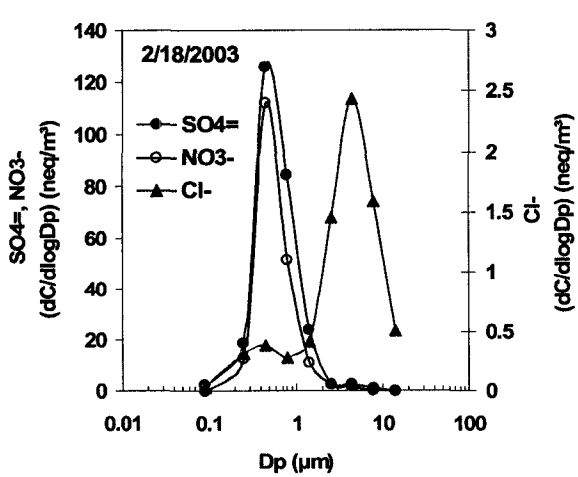

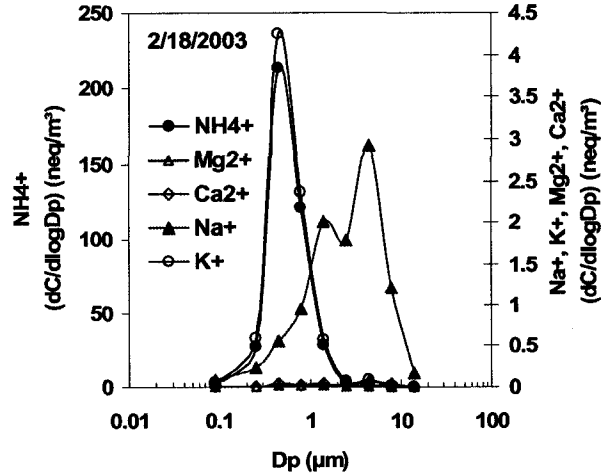

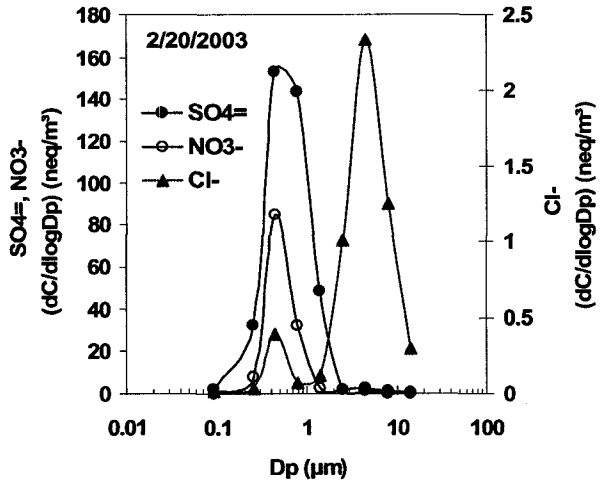

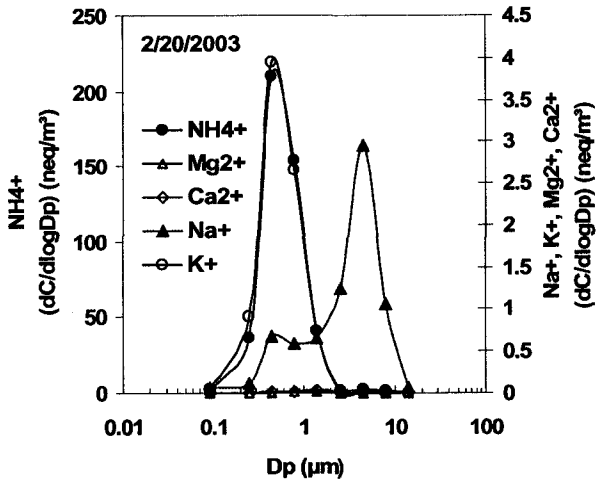

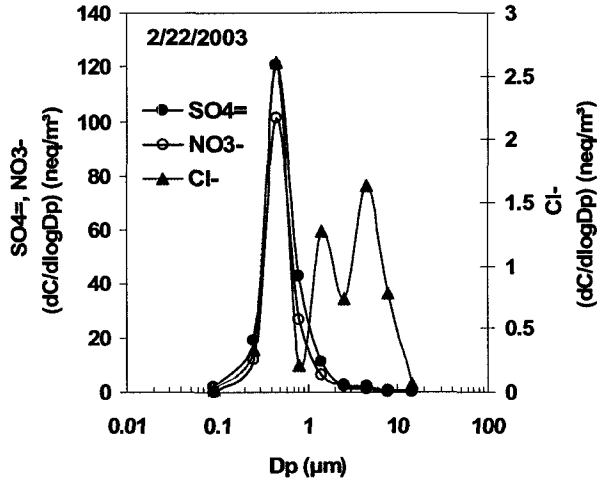

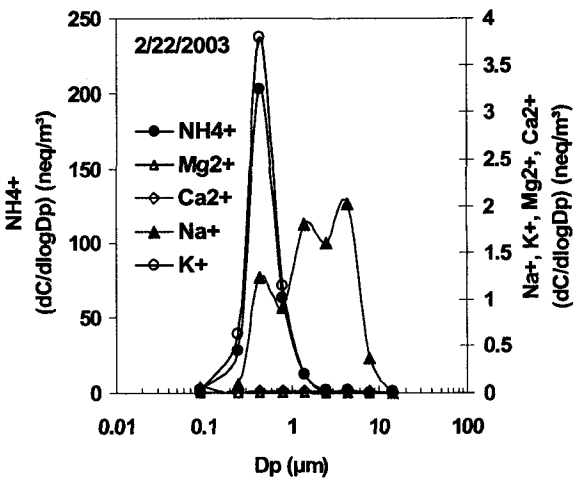

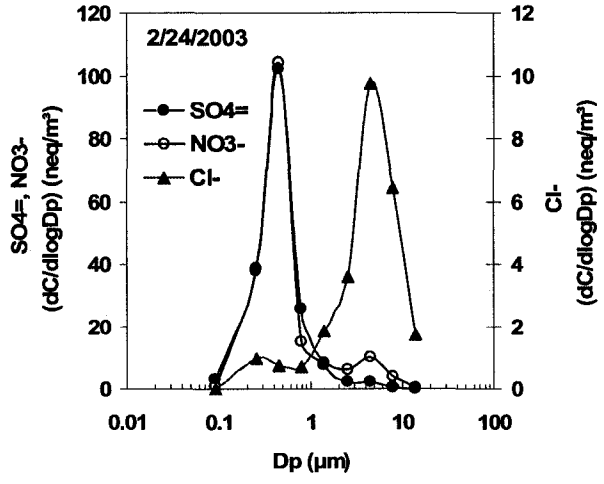

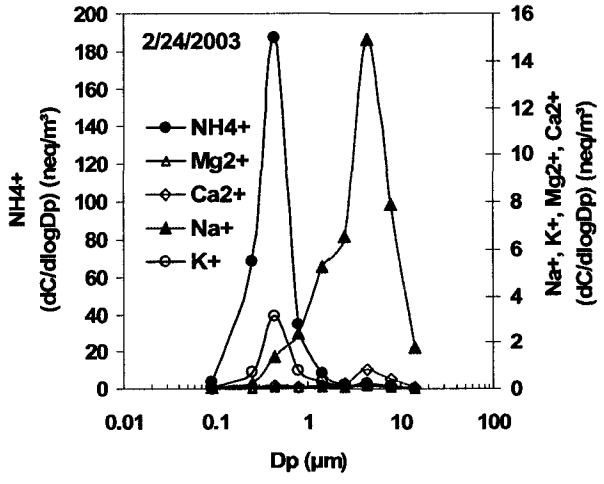

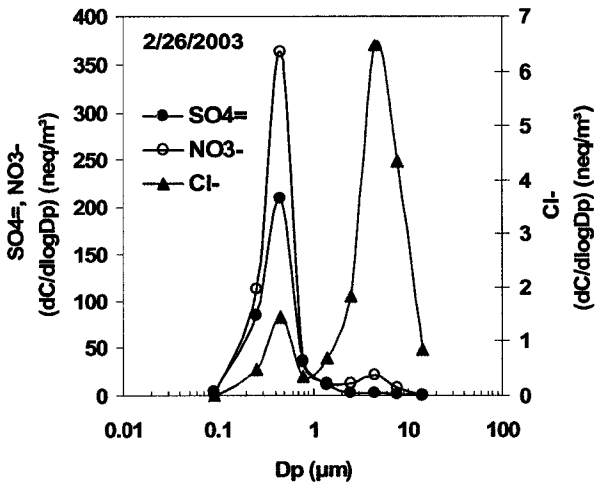

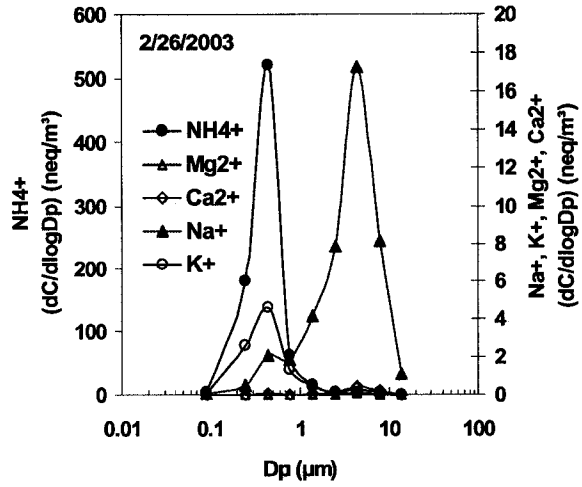

Figure E5 Brigantine (Nov) MOUDI (anion and cation) daily plots

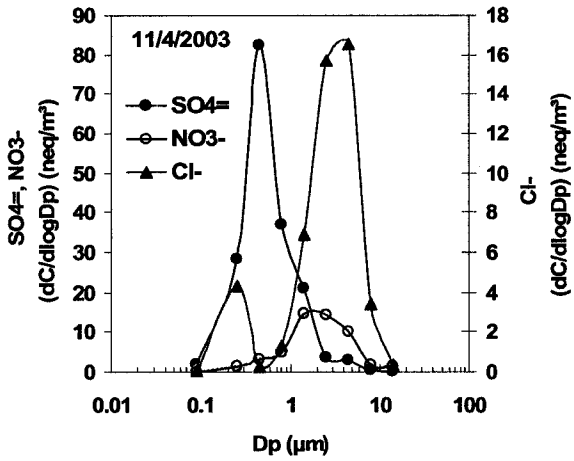

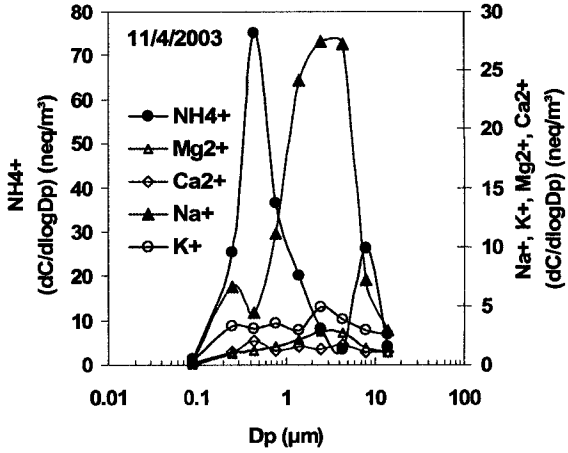

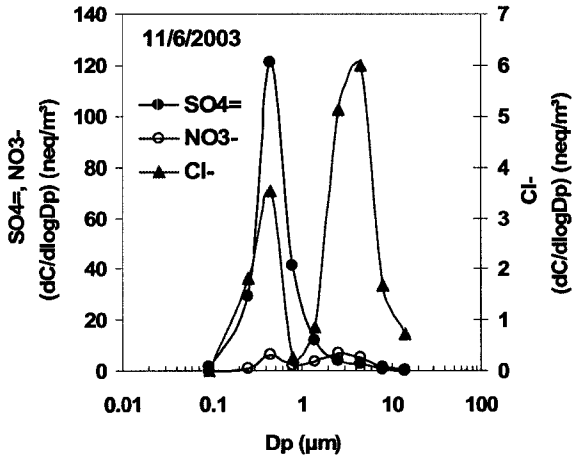

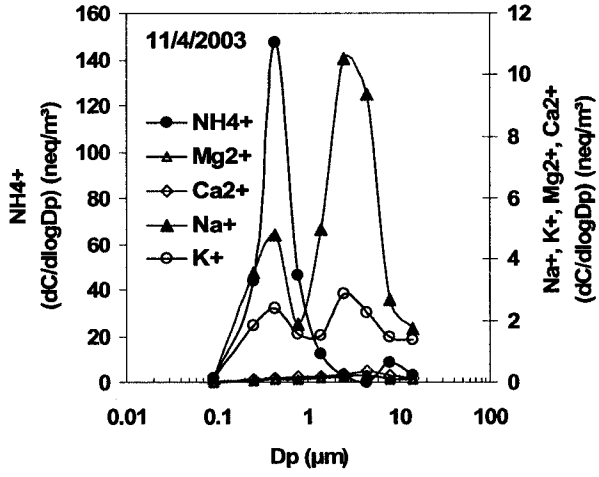

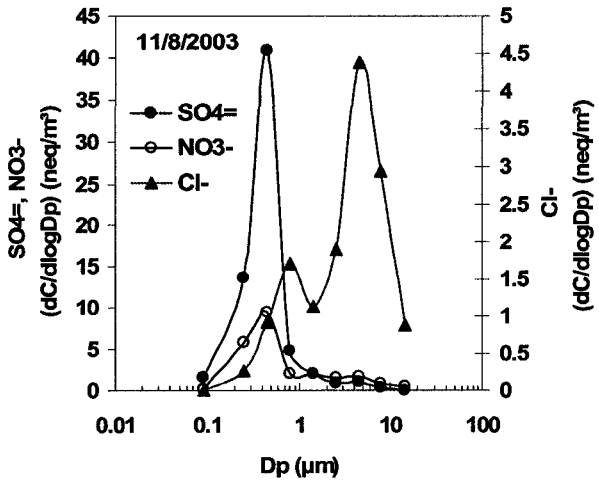

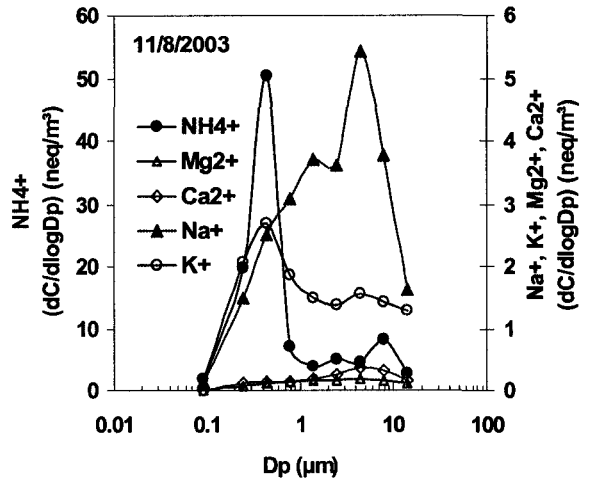

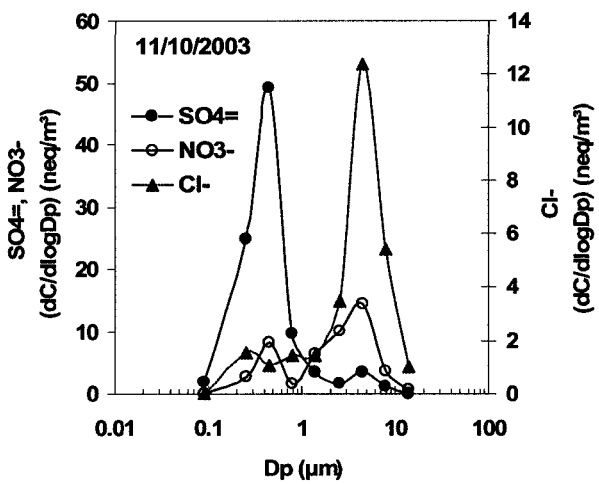

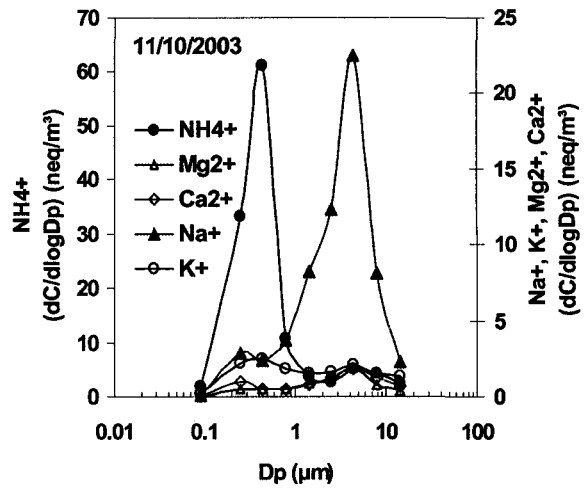

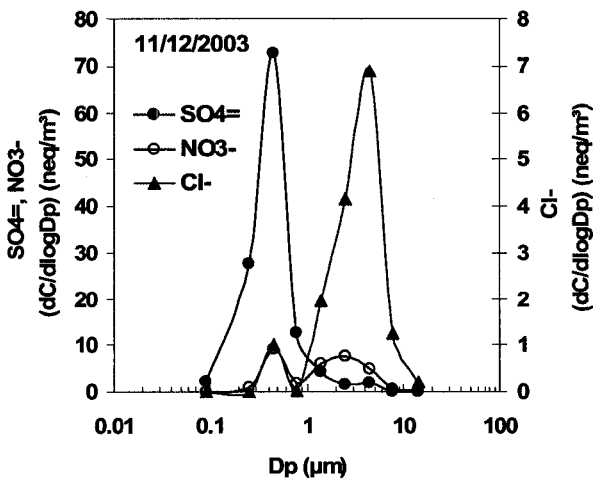

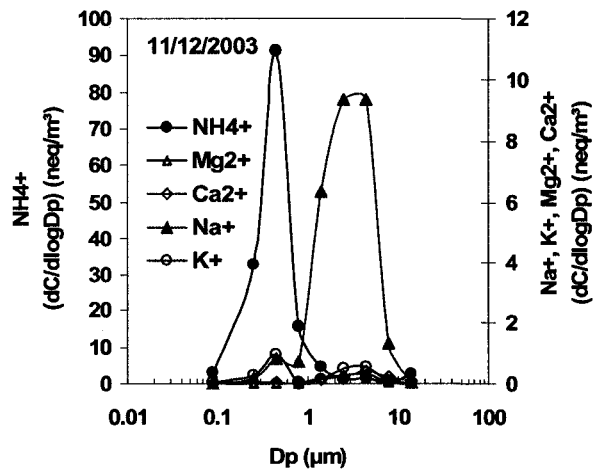

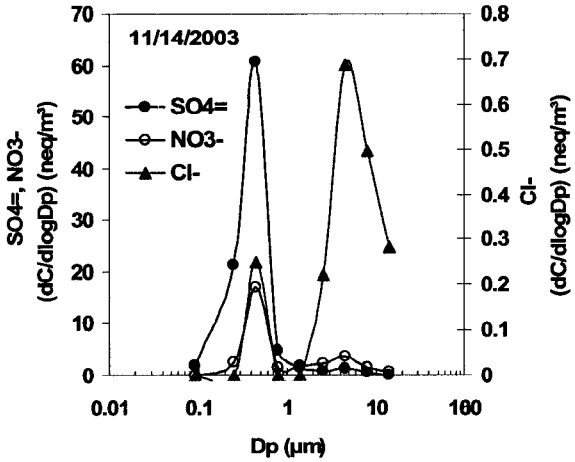

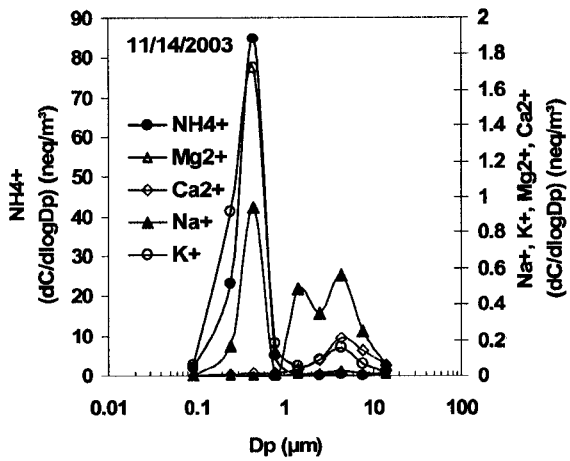

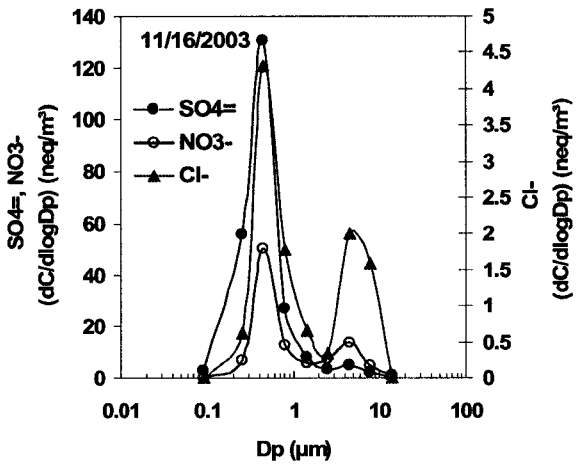

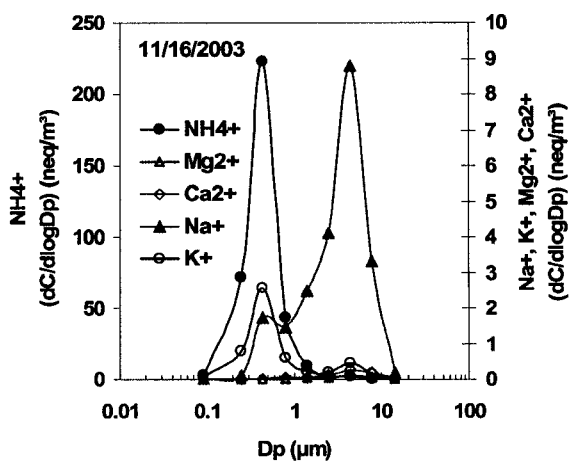

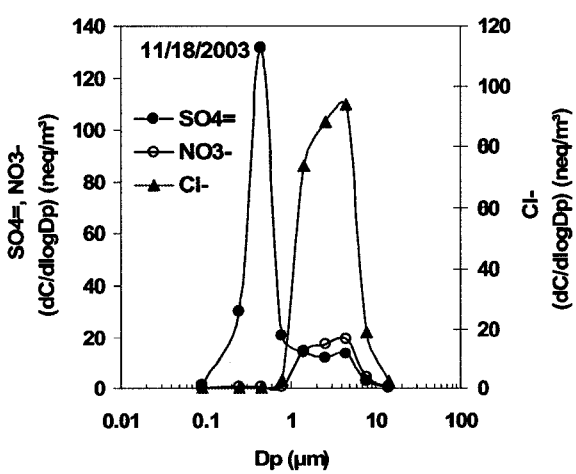

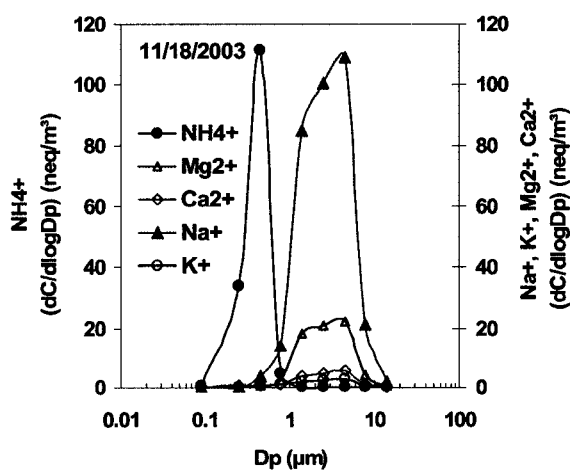

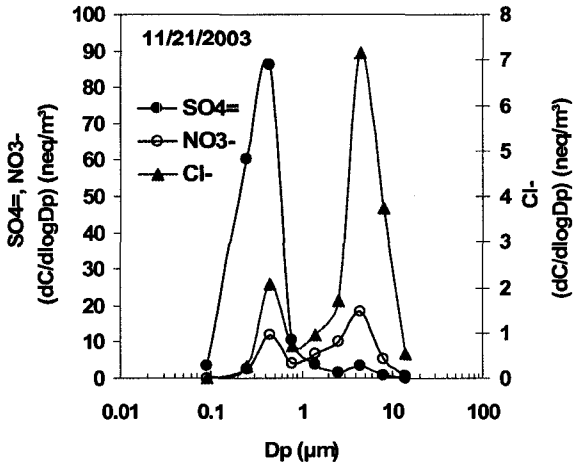

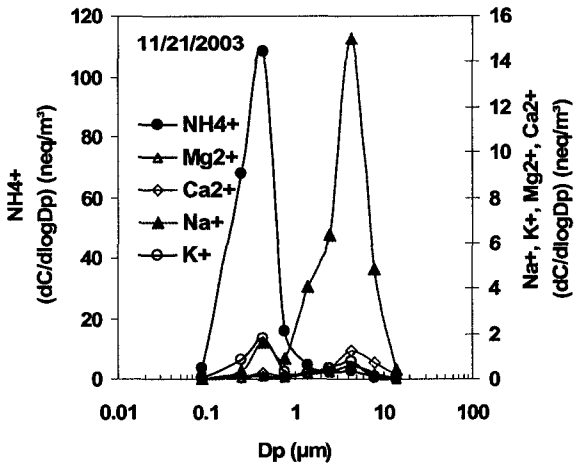

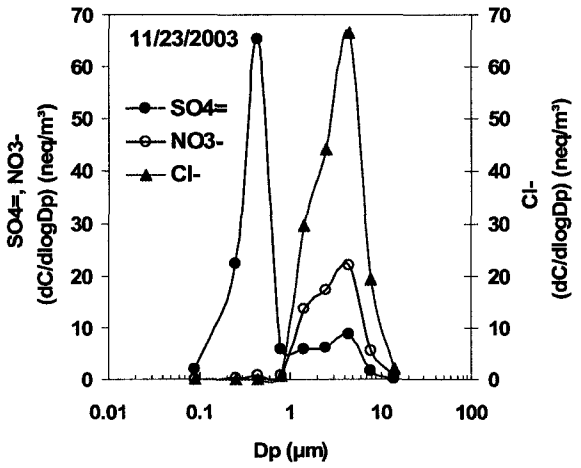

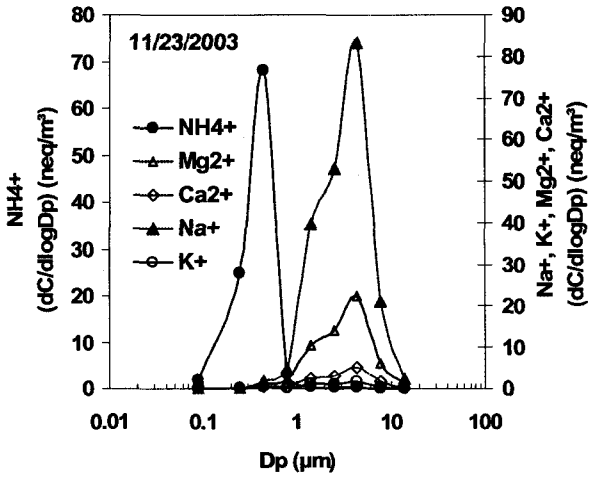

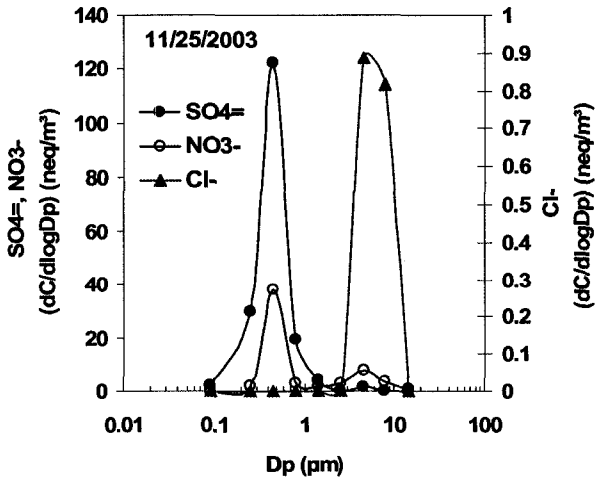

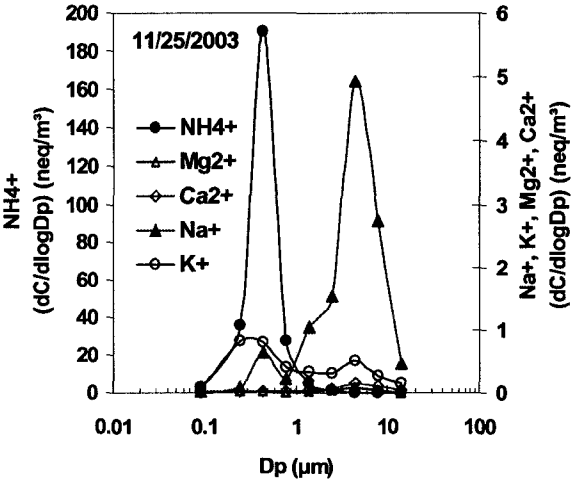

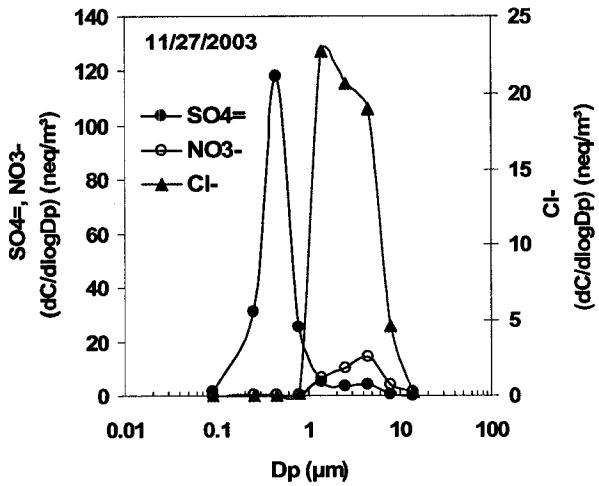

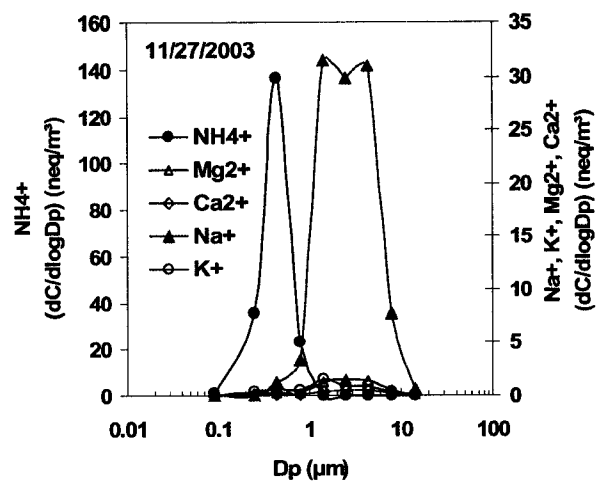

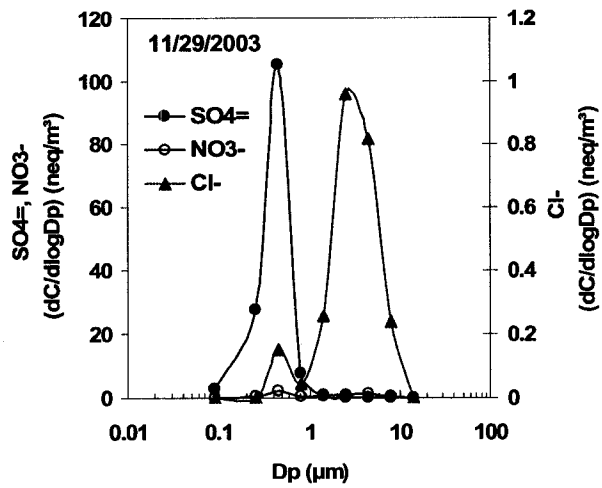

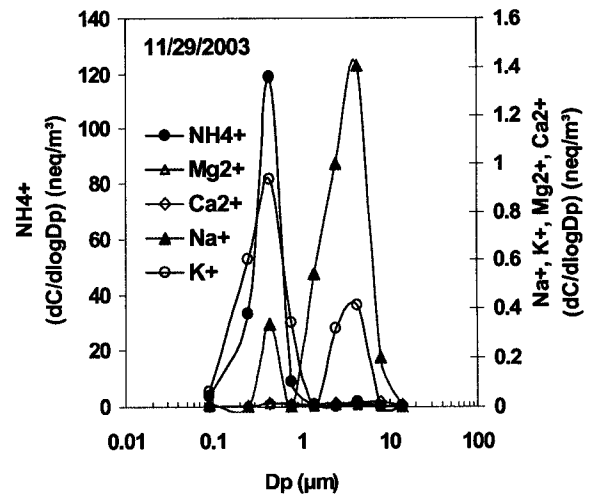

Figure E6 Great Smoky Mountains NP MOUDI (anion and cation) daily plots

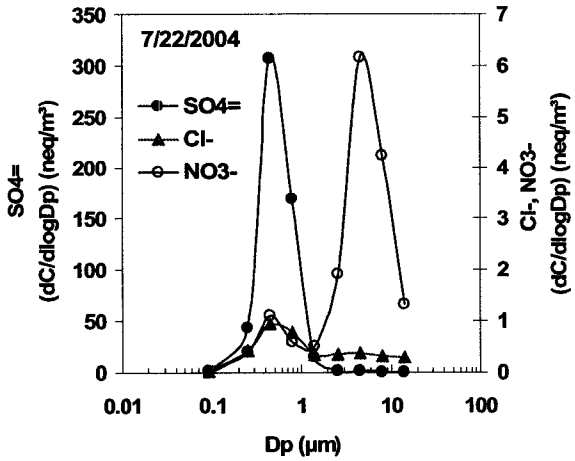

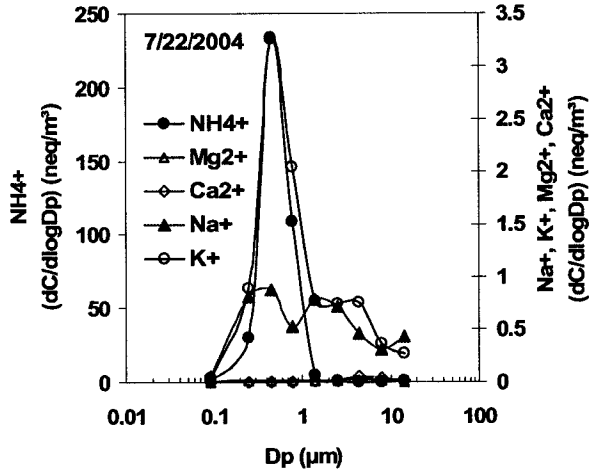

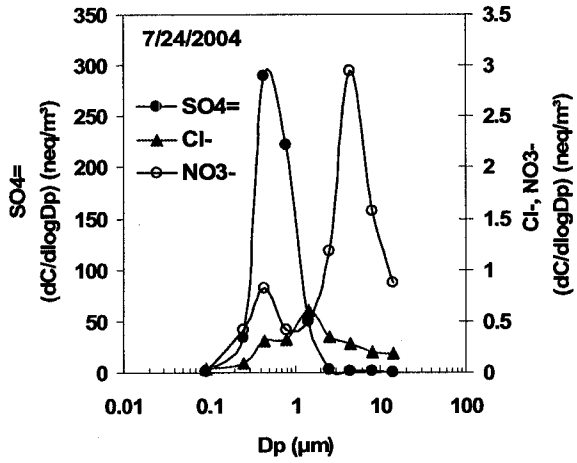

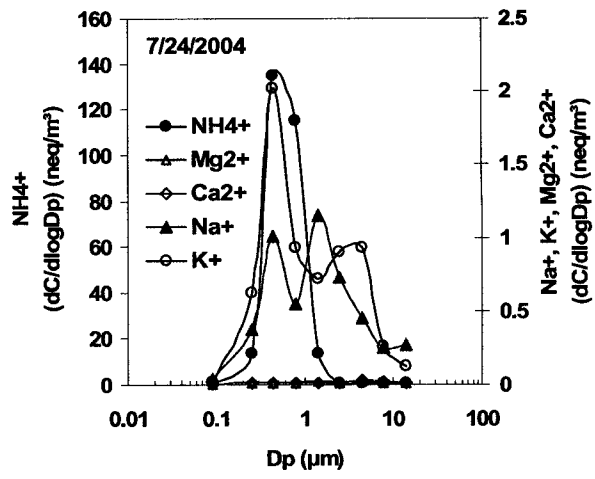

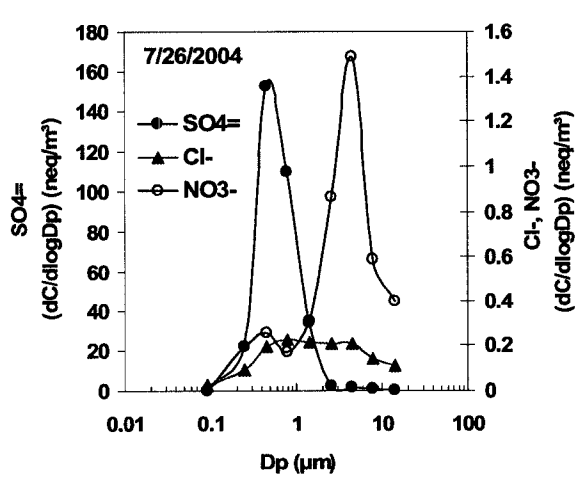

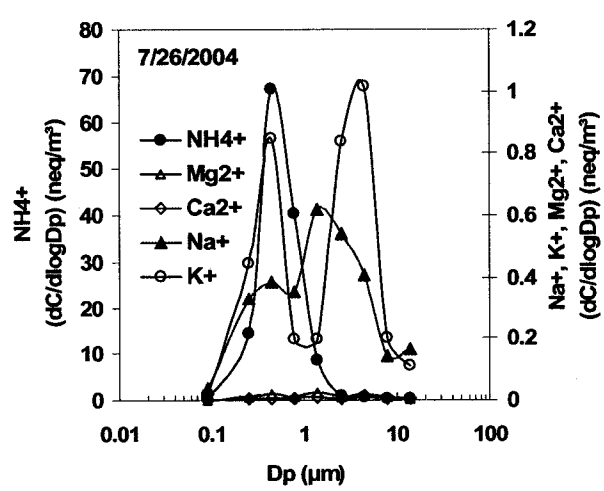

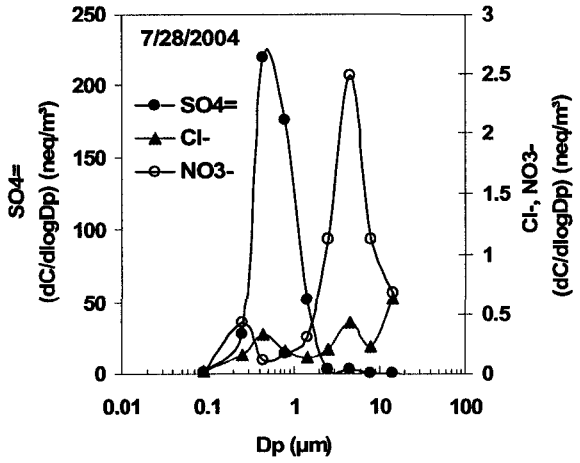

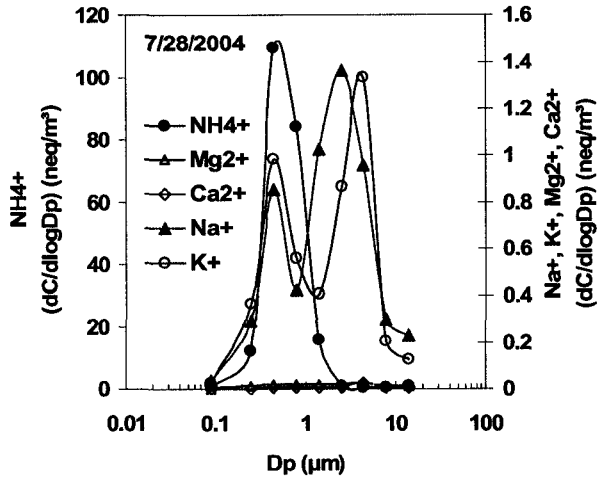

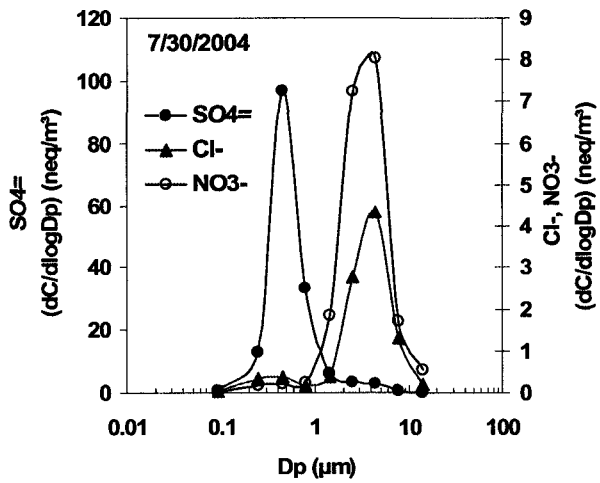

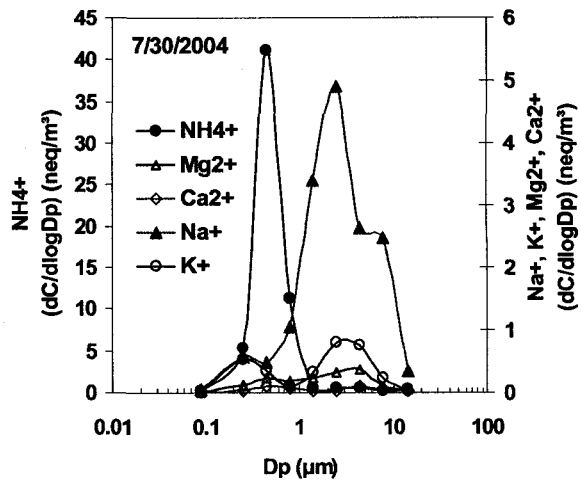

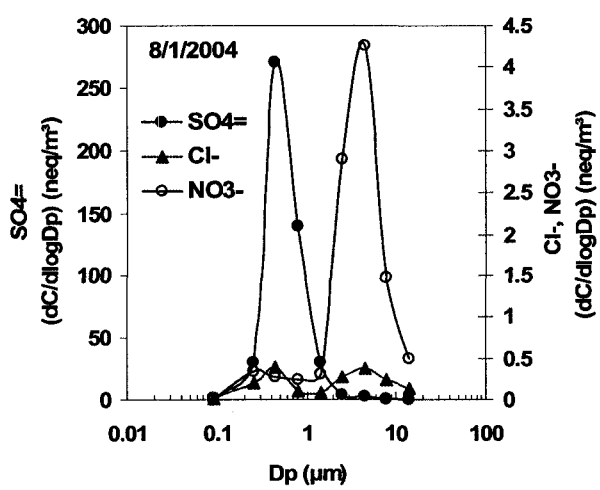

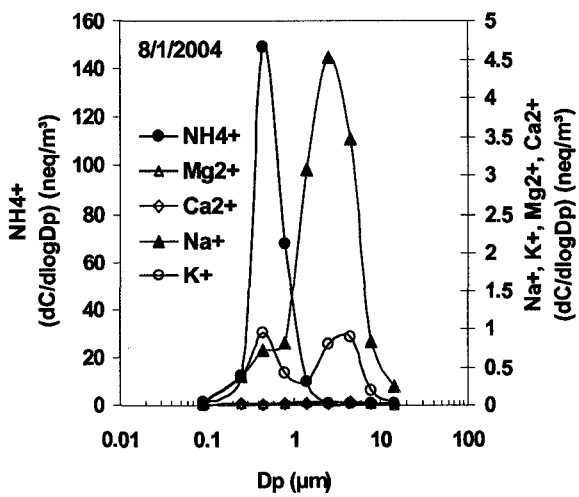

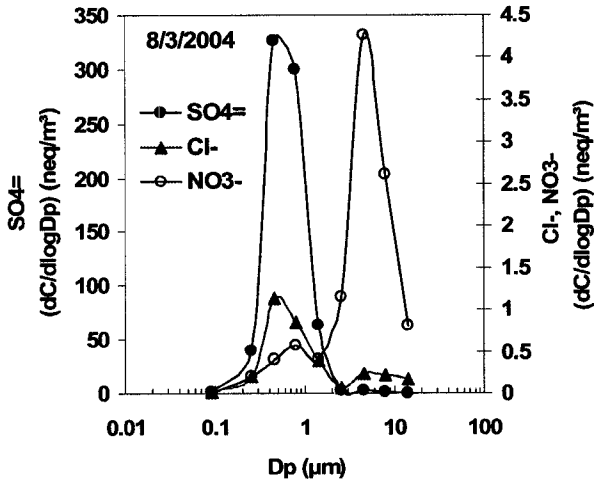

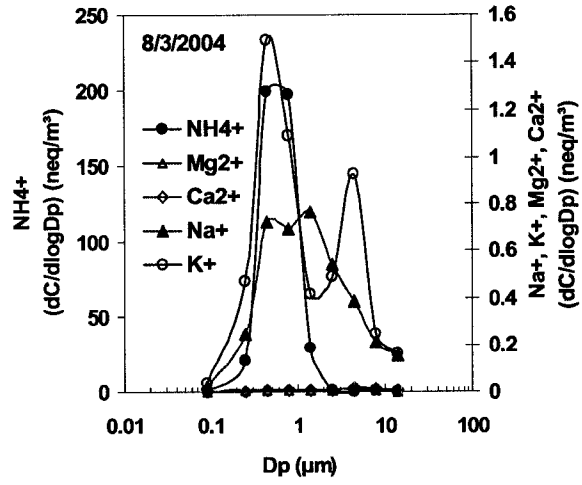

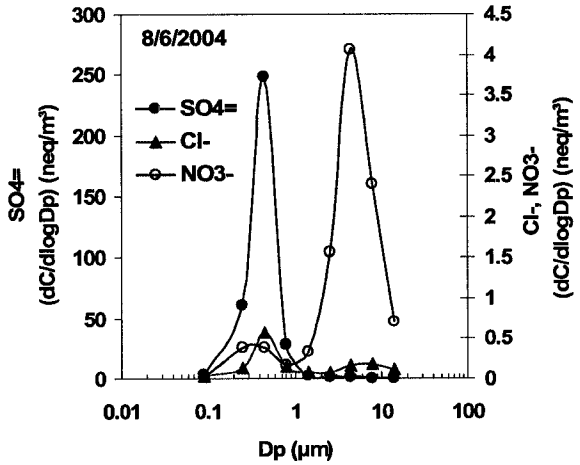

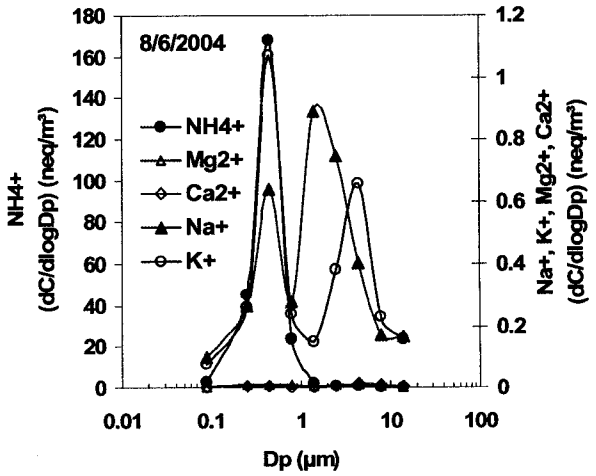

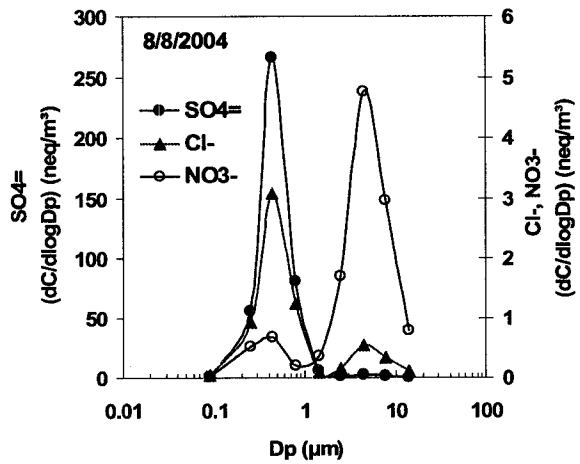

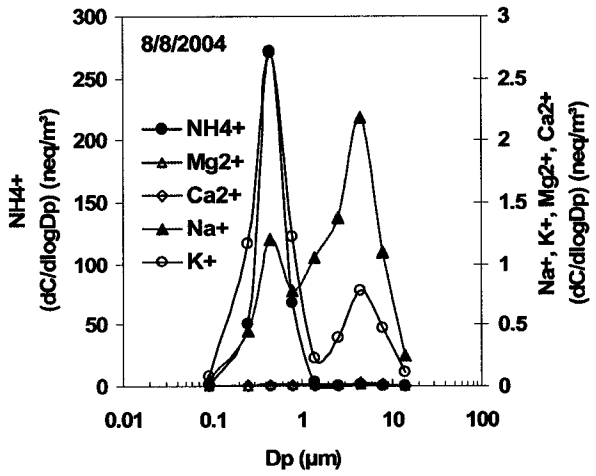

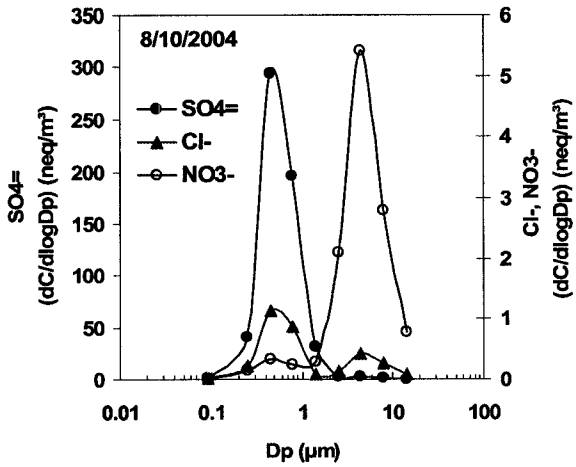

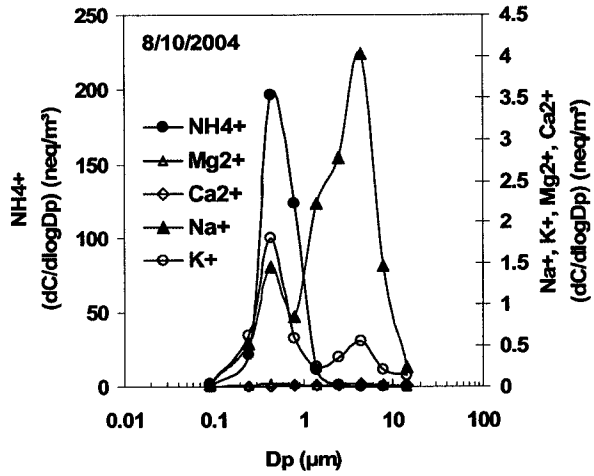

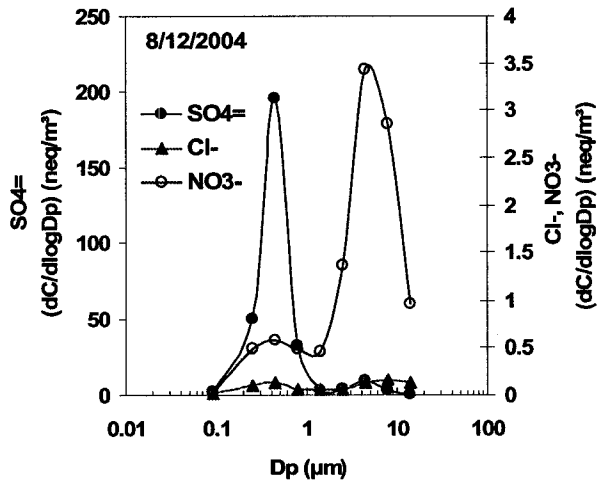

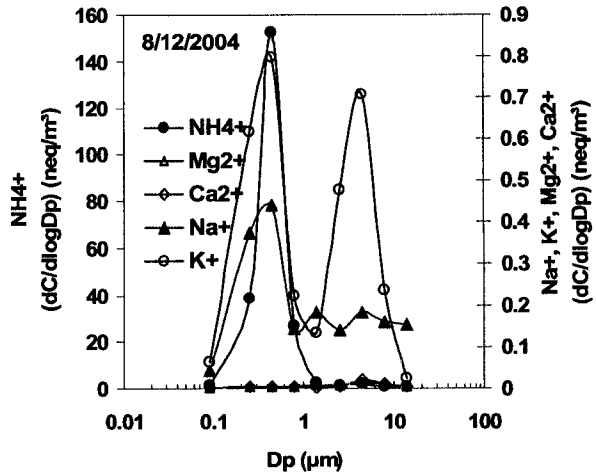

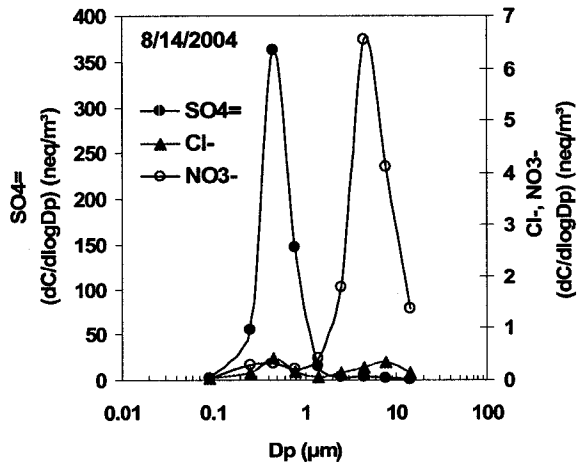

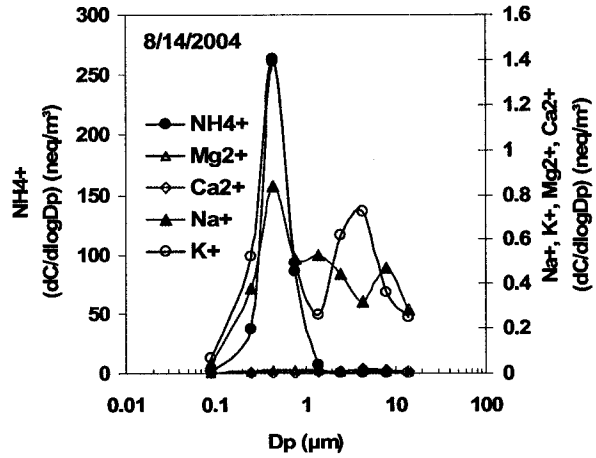

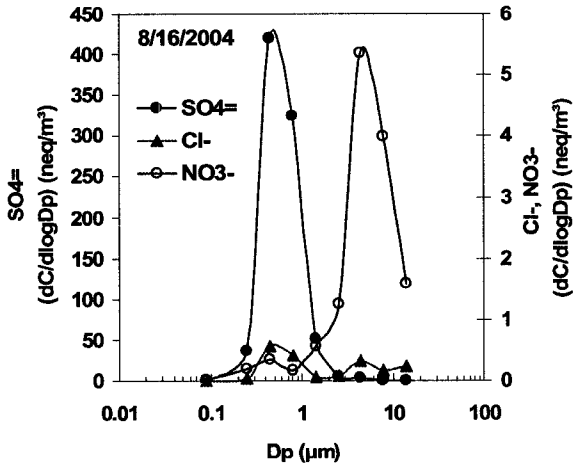

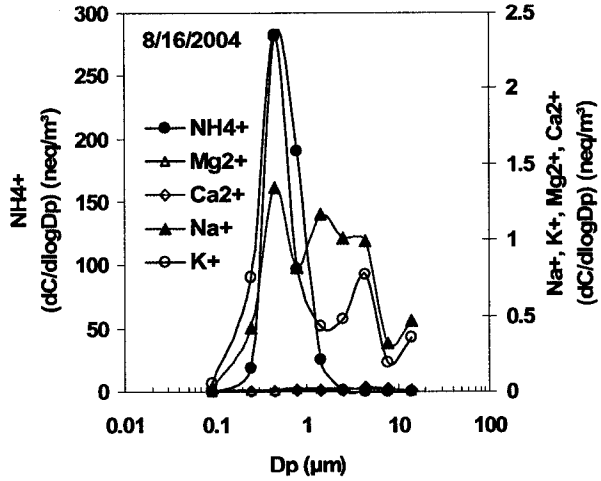

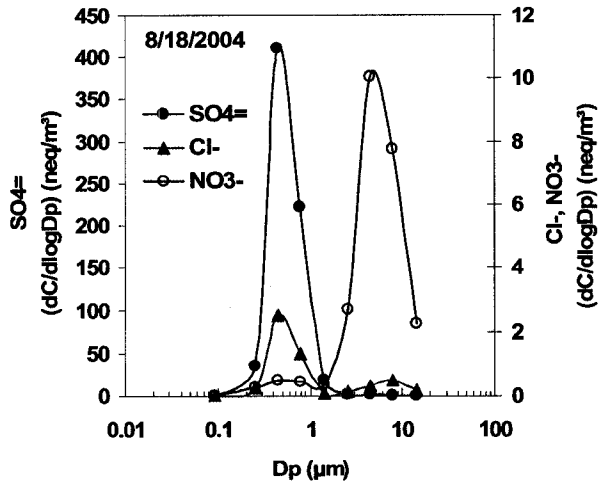

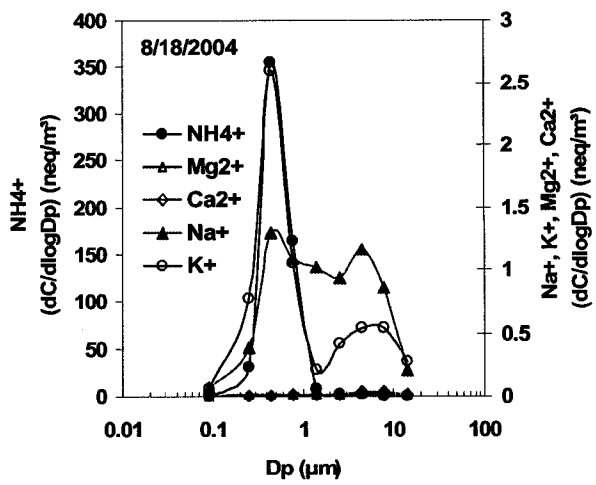

Appendix F: Study site pictures

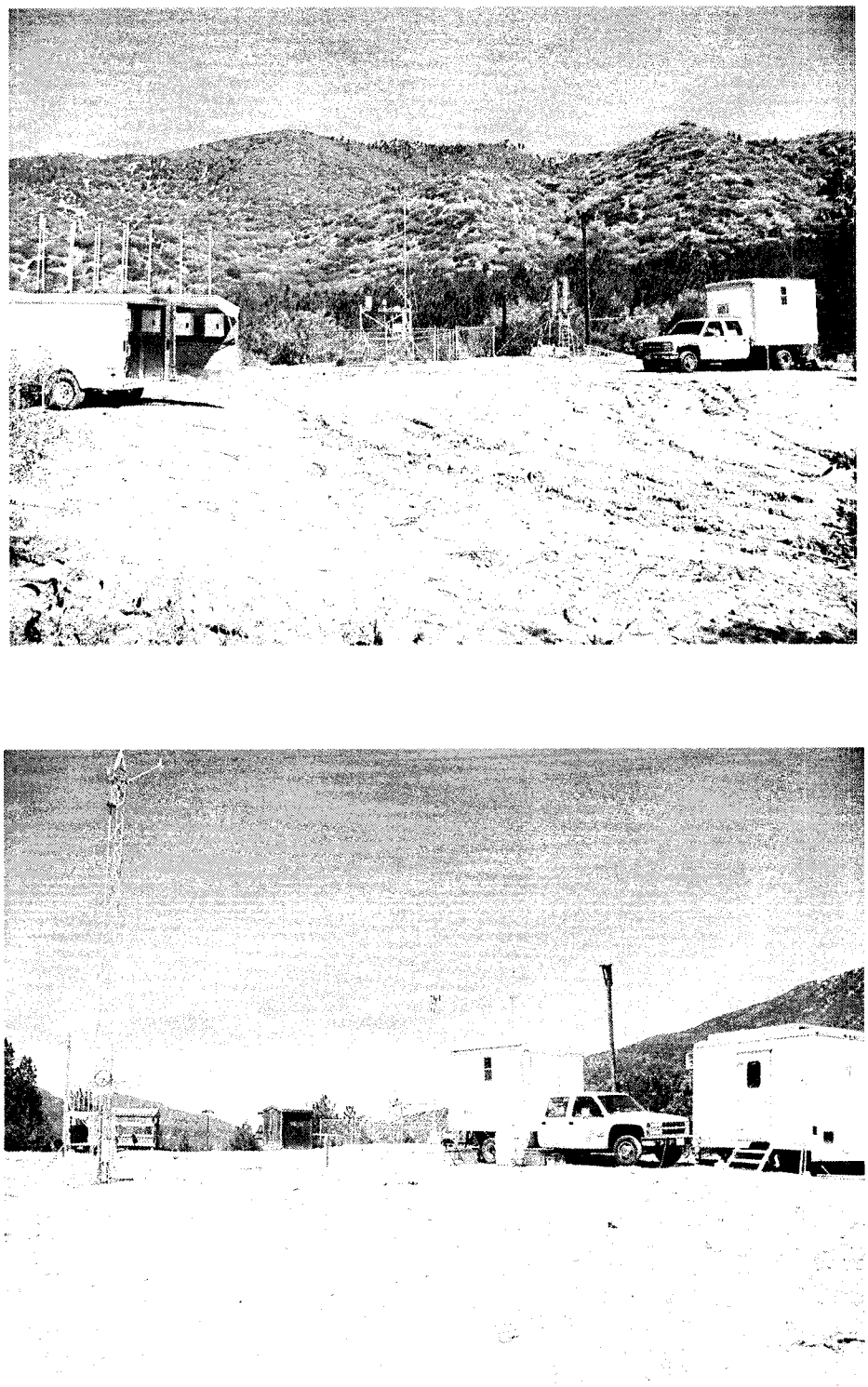

Figure F1 San Gorgonio (California) study site

Figure F2 Grand Canyon National Park (Arizona) study site

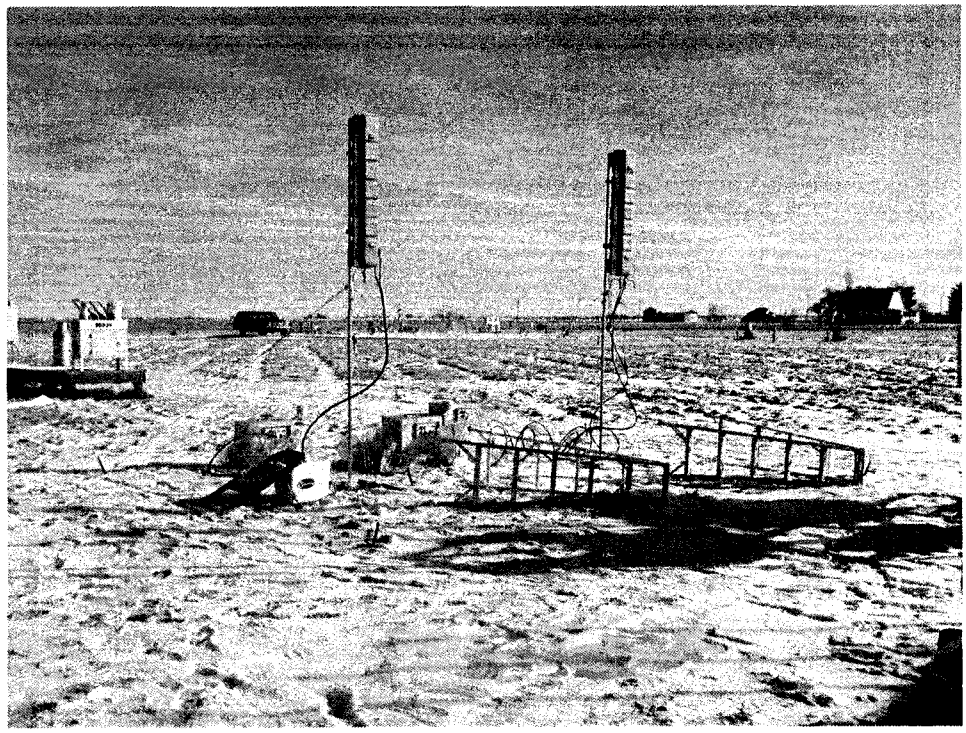

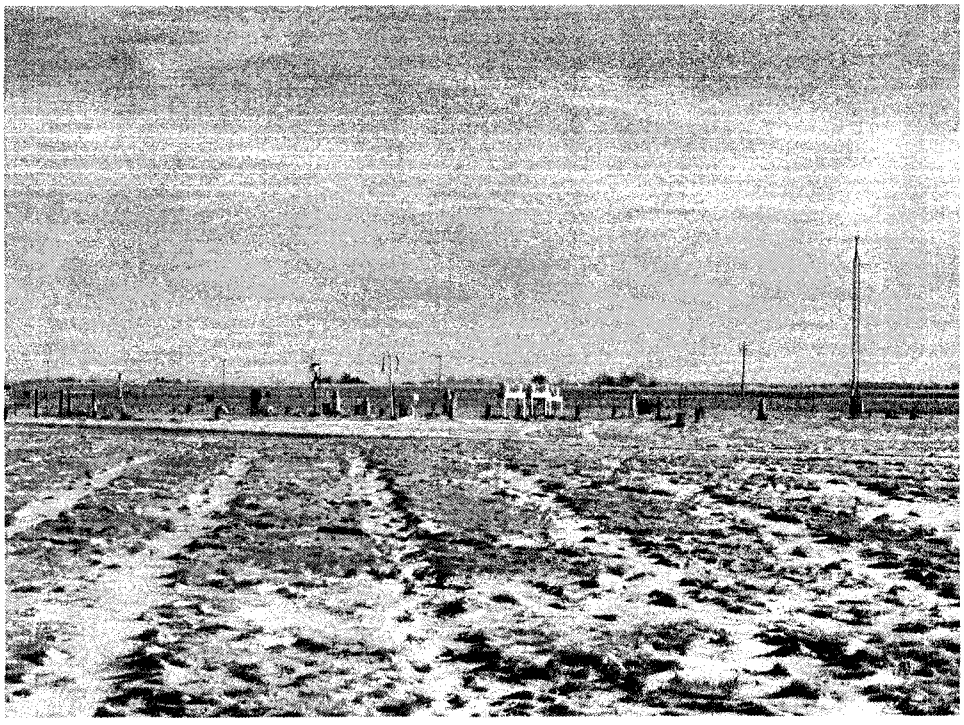

Figure F3 Bondville (Illinois) study site

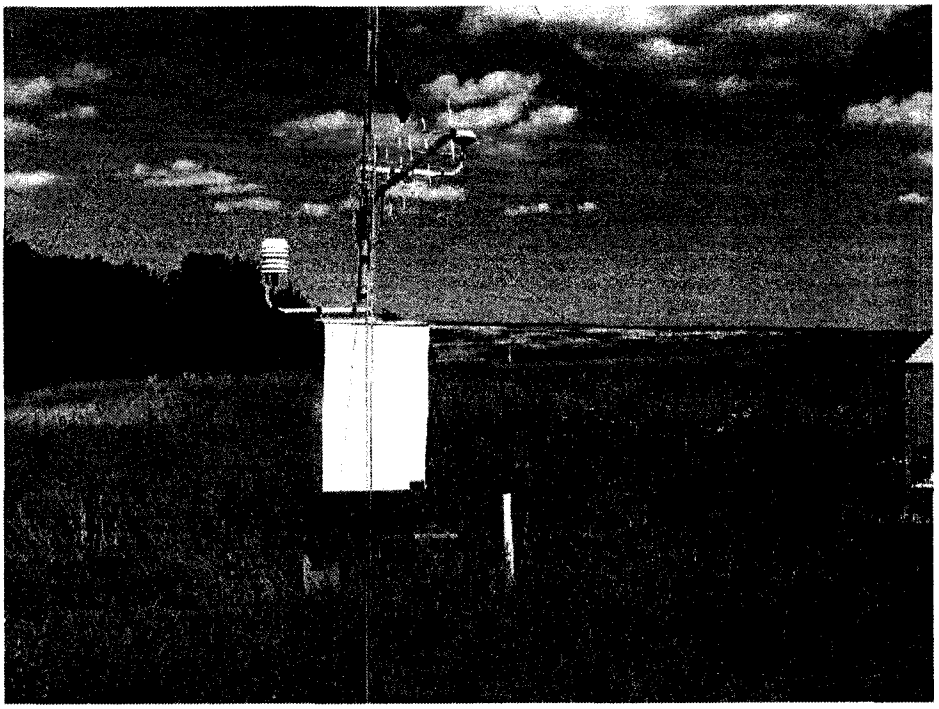

(Source : IMPROVE network aerosol)

Figure F4 Brigantine (New Jersey) study site

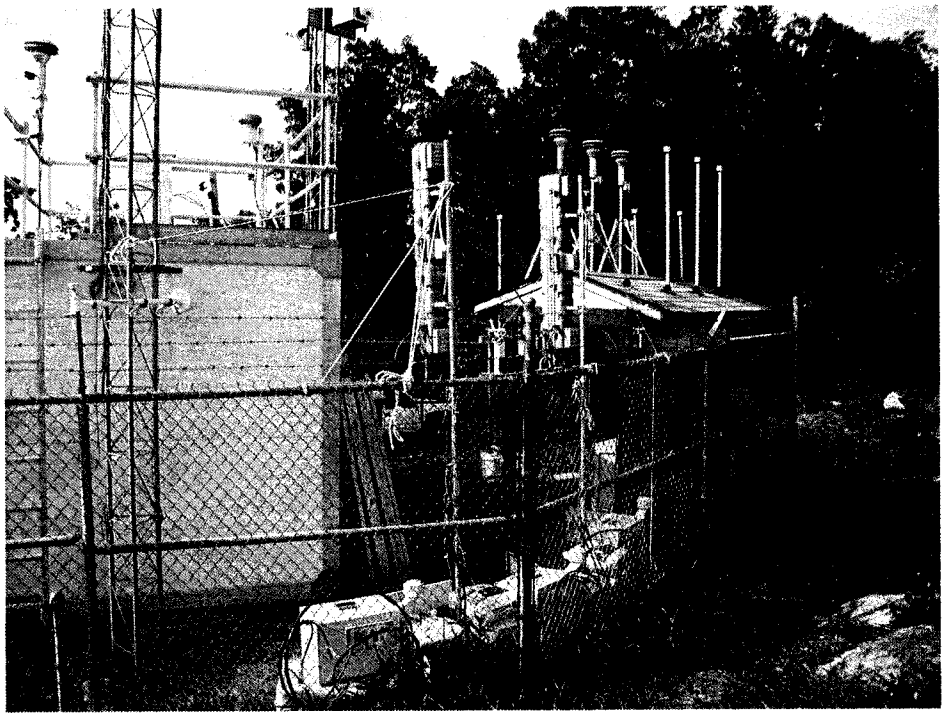

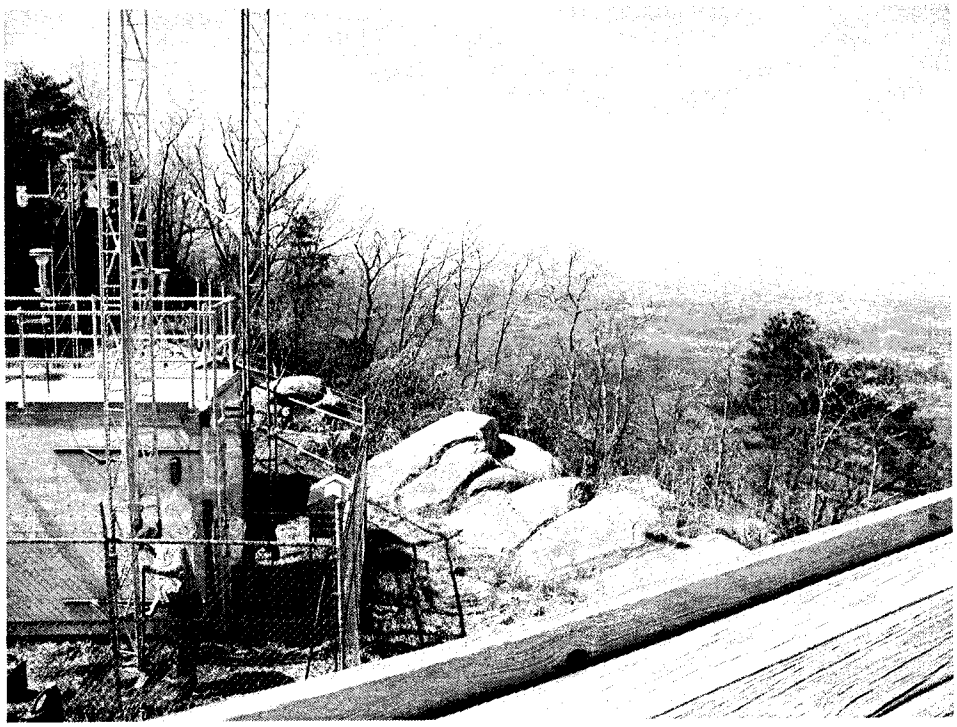

Figure F5 Great Smoky Mountains National Park (Tennessee) study site